

## Durham E-Theses

---

*Lower Cretaceous Ratawi Formation Saudi Arabia-Kuwait Partitioned Neutral Zone : deposition, diagenesis and petroleum geology in the framework of sequence stratigraphy.*

Bushang, Ibrahim Omar

### How to cite:

---

Bushang, Ibrahim Omar (2002) *Lower Cretaceous Ratawi Formation Saudi Arabia-Kuwait Partitioned Neutral Zone : deposition, diagenesis and petroleum geology in the framework of sequence stratigraphy.*, Durham theses, Durham University. Available at Durham E-Theses Online: <http://etheses.dur.ac.uk/1249/>

### Use policy

---

The full-text may be used and/or reproduced, and given to third parties in any format or medium, without prior permission or charge, for personal research or study, educational, or not-for-profit purposes provided that:

- a full bibliographic reference is made to the original source
- a [link](#) is made to the metadata record in Durham E-Theses
- the full-text is not changed in any way

The full-text must not be sold in any format or medium without the formal permission of the copyright holders.

Please consult the [full Durham E-Theses policy](#) for further details.

---

Academic Support Office, Durham University, University Office, Old Elvet, Durham DH1 3HP  
e-mail: [e-theses.admin@dur.ac.uk](mailto:e-theses.admin@dur.ac.uk) Tel: +44 0191 334 6107  
<http://etheses.dur.ac.uk>



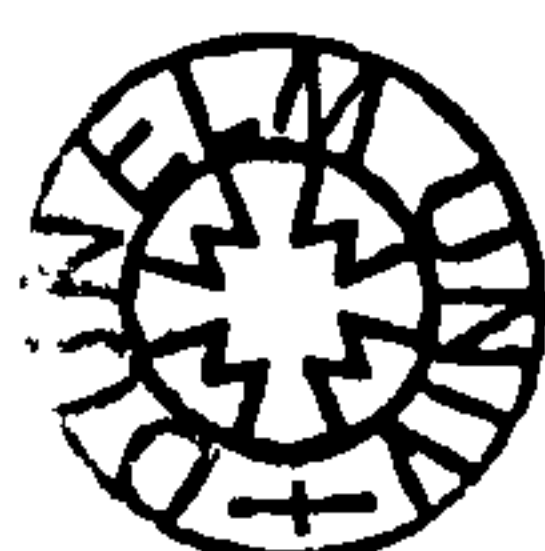
**Lower Cretaceous Ratawi Formation  
Saudi Arabia-Kuwait Partitioned Neutral Zone:  
Deposition, Diagenesis and Petroleum Geology  
in the  
Framework of Sequence Stratigraphy**

**Ibrahim Omar Bushang**

**The copyright of this thesis rests with the author. No quotation from it should be published in any form, including Electronic and the Internet, without the author's prior written consent. All information derived from this thesis must be acknowledged appropriately.**

---

**A thesis submitted in partial fulfillment of the degree of Doctor of Philosophy  
at the Department of Geological Sciences, University of Durham  
2002**



**31 MAY 2002**

No part of this thesis has been previously submitted for a degree in this or any other University. The work described in this thesis is entirely that of the author, except where reference is made to previous published or unpublished work.

Ibrahim Omar Bushang

## Abstract

The richest petroleum system in the world is the Arabian-Iranian basin; the principal oil producing horizons in the region are within Mesozoic and Cenozoic strata. The Wafra oilfield is one giant oilfield, located in the Saudi Arabia-Kuwait Partitioned Neutral Zone. The main reservoir lithofacies in this oilfield is the Lower Cretaceous Ratawi Formation (Ratawi zone), which is also a major hydrocarbon zone in Kuwait and southern Iraq, but only in the northeastern area of Saudi Arabia. The Ratawi Formation is divided into three members: lower Ratawi Oolite, middle Ratawi Limestone and upper Ratawi Shale.

The systematic variations in Ratawi lithofacies in three dimensions (Ratawi facies tract and depositional system) and its reservoir and seal rock characteristics are the product of (1) sedimentological processes <sup>related to</sup> ~~that include~~ the Ratawi platform type (carbonate ramp with moderate energy) and geological age: the Lower Cretaceous greenhouse period, (2) diagenetic processes (marine, subaerial exposure and burial) and (3) stratigraphic processes that include accommodation space and carbonate sediment supply. These factors are analyzed and integrated in the framework of sequence stratigraphy.

During the deposition of the Lower Cretaceous Ratawi Formation, the Wafra oilfield area was located between the Arabian Shelf and the Gotnia Basin along the Khurais-Wafra-Burgan-Zubair arch (Kuwait Arch). The sedimentological approach to sequence stratigraphy is used to interpret and predict local, regional and global processes that control Ratawi platform initiation, development and termination within idealized genetic packages identified on the basis of sedimentological and diagenetic data from the core study, in addition to the stacking pattern of the Ratawi parasequences.

Analyzing the different facies and surfaces in cores wells R-50 and R-48 identified eighty-four parasequences (5<sup>th</sup> order cycles). Fischer plots are used to identify systems tracts (4<sup>th</sup> order cycles) and greenhouse sequences (3<sup>rd</sup> order cycles) numbered 0, 1 and 2, and sequence boundary zones numbered 1, 2, 3 and 4. The integration of Ratawi stacking pattern data from this study with previous studies, resulted in construction of a Ratawi chronostratigraphic hierarchy framework that includes composite sequences (2<sup>nd</sup> order cycle) numbered 1 and 2 and composite sequence boundary zones numbered 1, 2 and 3 within the Lower Cretaceous Thamama Group, in addition to 1<sup>st</sup> order sub-sequence North Sea and North Atlantic cycles. Within this framework the local, regional and global controlling processes are examined.

The initiation, development and termination of the Ratawi platform and the development of reservoir and seal rocks seem to be controlled by interplay of changes in the rate of 2<sup>nd</sup> order eustatic sea-level, tectonics (local and regional) and carbonate sediment supply. <sup>oceanographic changes</sup> The composite sequence boundary zone between the Ratawi Oolite and Ratawi Limestone is inferred to be bounded by two major unconformity surfaces. The lower boundary surface is a type 1 sequence boundary in the study area on the Kuwait Arch and its correlative conformable surface is in the Gotnia Basin succession. The upper boundary surface is a type 3 sequence boundary in the Gotnia Basin and its correlative deepening-upward succession in the study area on the Kuwait Arch.

The reservoir and non-reservoir units have been considered within the sequence stratigraphy of the Ratawi Formation deduced from cycle thickness and facies patterns. Fischer plots in time domains have been used to relate the Ratawi cycle stacking pattern to reservoir units, wireline log signatures, lithology and petrophysical characteristics. The best reservoir zones are shown to occur within the highstand systems tract beneath a major subaerial exposure associated with a 2<sup>nd</sup> order sequence boundary (Unit E) and transgressive systems tract (Unit D), and within the highstand systems tract (Unit C) of the sequence below. The regional seal is shown to occur within the termination facies of the Ratawi platform, which is part of a deepening-upward succession.



## **Acknowledgements**

I would like to thank the Ministry of Petroleum and Mineral Resources in Saudi Arabia and the Joint Operations Unit for the Saudi Arabian Texaco Inc. and Kuwait Oil Co. for allowing me to use the data for this project. Special thanks to Hassan Al-Gaisi the petroleum geologist at Wafra Oilfield and all who helped me in the Department of Geological Sciences at the University of Durham. In particular I would like to thank my adviser Professor Maurice E. Tucker who help me in many ways to finish this thesis in the paradox subject of the Middle East sequence stratigraphy.

# Contents

<b>Chapter 1 Introduction.....</b>	<b>1</b>
1.1 Introduction .....	1
1.2 Aims of the study.....	3
1.3 Location of the Study Area .....	5
1.4 Material available in this study .....	6
 <b>Chapter 2 Regional Geology, the Ratawi Petroleum System and Previous Studies .....</b>	 <b>9</b>
2.1 Geotectonics .....	9
2.1.1 Geotectonic elements of the Arabian Plate .....	9
2.1.1.1 The Arabian-Nubian Shield .....	9
2.1.1.2 The Arabian Shelf .....	11
2.1.1.3 The Mobile-Belt .....	11
2.1.2 Basement lineaments and Arabian Folds .....	11
2.1.3 Hormuz Salt .....	16
2.1.4 Syndepositional structural growth of the Arabian Folds.....	17
2.2 Mesozoic Geological History .....	17
2.2.1 Development of the Arabian shelf during the late Jurassic and Cretaceous times.....	19
2.2.2 Lower Cretaceous Thamama Group.....	25
2.2.3 Boundaries of Thamama Group .....	26
2.2.4 Controlling processes on Thamama Group deposition and cyclicity .....	29
2.2.5 The Gotnia intrashelf basins.....	31
2.3 Previous studies of the Ratawi Formation in the Wafra oilfield area .....	33
2.3.1 Porosity and permeability .....	34
2.3.2 Ratawi Oolite marker zones and the three Wafra reservoir producing areas.....	35
2.3.3 Ratawi Oolite reservoir units .....	36
2.3.3.1 Unit A: Muddy peloidal wackestone-packstone.....	36
2.3.3.2 Unit B: Oolitic and skeletal grainstones. ....	36
2.3.3.3 Unit C: Coral and rudist wackestone-packstone. ....	36
2.3.3.4 Unit D: Peloidal and skeletal packstone. ....	36
2.3.3.5 Unit E: Skeletal / algal (Bacinella) grainstone-packstone. ....	37
2.3.3.6 Unit F: Transition of the Ratawi Oolite to Ratawi Limestone member. ....	38
2.3.4 Ratawi Oolite reservoir units .....	38
2.3.4.1 Depositional model for Unit A .....	41
2.3.4.2 Depositional model for Unit B.....	41
2.3.4.3 Depositional model for Unit C.....	41
2.3.4.4 Depositional model for Unit D.....	42
2.3.4.5 Depositional model for Unit E.....	42
2.3.4.6 Depositional model for Unit F.....	43
2.3.5 Diagenetic model for the Ratawi Oolite.....	43
2.4 Summary .....	43
 <b>Chapter 3 Facies and Microfacies of the Ratawi Formation.....</b>	 <b>44</b>
3.1 Introduction.....	44
3.1.1 The aims of this chapter .....	44
3.1.2 Geological reservoir characterisation .....	45
3.1.2.1 Reservoir and Non-Reservoir Units of the Ratawi zone.....	45
3.1.2.2 Porosity origin and geometry of the Ratawi reservoir unit.....	46
3.2 Microfacies of the Ratawi Formation.....	48
3.2.1 The basic microfacies concept.....	48
3.2.2 Taphonomy of the Ratawi Formation.....	49
3.2.3 Ratawi lithofacies associations.....	50



3.3 Sedimentological lithofacies associations.....	52
3.3.1 Back Ramp: wackestone-mudstone with restricted fauna.....	53
3.3.1.1 Microfacies BR1: bioclastic wackestone-mudstone with ostracods and black grains.....	53
3.3.1.2 Microfacies BR2: bioturbated bioclastic wackestone-mudstone with ostracods.....	56
3.3.1.3 Back ramp lithofacies association: discussion.....	59
3.3.2 Shallow Ramp: rudstone, grainstone-packstone with open-marine fauna.....	61
3.3.2.1 Microfacies SR1: peloidal bioclastic rudstone with coral and ooids.....	62
3.3.2.2 Microfacies SR2: cross-laminated peloidal bioclastic grainstone-packstone...	67
3.3.2.3 Microfacies SR3: peloidal bioclastic grainstone-packstone with ooids and aggregates.....	68
3.3.2.4 Microfacies SR4: peloidal bioclastic grainstone-packstone.....	73
3.3.2.5 Microfacies SR5: peloidal bioclastic packstone with black grains.....	74
3.3.3 Deep Ramp: mudstone-wackestone with open-marine fauna.....	75
3.3.3.1 Microfacies DR1: peloidal bioclastic floatstone.....	75
3.3.3.2 Microfacies DR2: bioturbated bioclastic mudstone.....	76
3.3.3.3 Microfacies DR3: bioturbated bioclastic wackestone.....	79
3.3.3.4 Microfacies DR4: biomorpha (whole-shell) wackestone.....	80
3.4 Diagenetic lithofacies associations.....	80
3.4.1 Microfacies DiagDol: crystalline dolomite .....	80
3.4.2 Microfacies DiagCal: pedogenic calcrete.....	82
3.4.3 Subaerial exposure features .....	83
3.4.3.1 Subaerial exposure recognition and application.....	83
3.4.3.2 Karst surfaces and facies.....	84
3.4.3.3 Subaerial exposure evidence from core description.....	85
3.4.3.3.1 Rootlets .....	86
3.4.3.3.2 Mudcracks and horizontal veins.....	86
3.4.3.3.3 Karst.....	86
3.4.3.4 Petrographic evidence for subaerial exposure.....	86
3.4.3.4.1 Leached and vuggy porosity.....	86
3.4.3.4.2 Rhizoliths.....	87
3.4.3.4.3 Alveolar septal structure.....	92
3.4.3.4.4 Calcified filaments.....	93
3.4.3.4.5 Micritization of particles and carbonate cement.....	93
3.4.3.4.6 Radial cracking (Circum-granular cracking).....	98
3.4.3.4.7 Complex cracks .....	98
3.4.3.4.8 Dense microfabric and floating sediment grains.....	98
3.4.3.4.9 Vadose compaction.....	98
3.5 Palaeoenvironmental Reconstruction.....	98
3.5.1 Facies and log-facies of the Ratawi Formation.....	99
3.5.2 Ramps sand-body geometry and carbonate Ramp Model.....	103
3.6 Ratawi Palaeoenvironmental Reconstruction and summary.....	106
 <b>Chapter 4: Diagenesis and Porosity of the Ratawi Formation.....</b>	<b>108</b>
4.1 Introduction.....	109
4.1.1 The aims of this chapter.....	109
4.2 Ratawi diagenetic environments.....	109
4.2.1 Introduction.....	109
4.2.1.1 Ratawi major diagenetic environments.....	111
4.2.2 Shallow marine diagenetic environment.....	111
4.2.2.1 Introduction.....	111
4.2.2.2 Micritization.....	112
4.2.2.2.1 Micritization by endolithic micro-organisms.....	113
4.2.2.2.2 Micritization by syndepositional recrystallization.....	114



4.3.2.3	Micrite envelopes.....	116
4.2.2.3.1	Destructive micrite envelopes.....	116
4.2.2.3.2	Constructive micrite envelopes.....	116
4.2.2.4	Grain reworking and boring.....	117
4.2.2.5	Marine cements.....	117
4.2.2.5.1	Introduction.....	117
4.2.2.5.2	Syntaxial rim cement.....	120
4.2.2.5.3	Hardground cement.....	120
4.2.2.6	Synsedimentary pyrite.....	122
4.2.2.7	Calcitization.....	123
4.2.2.7.1	Late calcitization in meteoric and burial environments.....	125
4.2.2.7.2	Early calcitization in the marine environment.....	125
4.2.3	Shallow-burial meteoric diagenetic environment.....	126
4.2.3.1	Introduction.....	126
4.2.3.2	Meteoric cements.....	127
4.2.3.2.1	Bladed / Granular cement.....	127
4.2.3.2.2	Columnar cement.....	130
4.2.3.2.3	Granular drusy cement.....	130
4.2.3.3	Meteoric dissolution.....	130
4.2.3.4	Calcite replacement of quartz.....	131
4.2.3.5	Ratawi soils.....	131
4.2.3.5.1	Heterogeneity of Reservoir unit-E and Palaeoclimate.....	132
4.2.3.5.1.1	Arid -type soil / arid palaeoclimate.....	133
4.2.3.5.1.2	'Well-developed' calcrete-type soil / moisture deficit wetter palaeoclimate.....	133
4.2.3.5.1.3	'Less-well developed' calcrete-type soil / wetter palaeoclimate.....	133
4.2.3.5.1.4	Organic-rich type soil / wettest palaeoclimate.....	134
4.2.3.5.1.5	Calcrete fabric model.....	134
4.2.3.5.1.5.1	Alpha fabric model.....	136
4.2.3.5.1.5.2	Beta fabric model.....	136
4.2.3.5.1.5.3	Rhizogenic fabric model.....	136
4.2.3.5.2	Calcrete profile development.....	137
4.2.3.5.2.1	Hard pan or petrocalcic layer development.....	138
4.2.3.5.2.2	Laminar unit development.....	138
4.2.3.5.2.3	Brecciated and pisoid unit development.....	138
4.2.4	Burial diagenetic environment.....	139
4.2.4.1	Introduction.....	139
4.2.4.2	Burial cement.....	139
4.2.4.2.1	Granular Drusy calcite .....	141
4.2.4.2.2	Poikilotopic calcite.....	141
4.2.4.3	Burial compaction .....	141
4.2.4.3.1	Physical compaction.....	142
4.2.4.3.2	Chemical compaction.....	142
4.2.4.4	Burial porosity.....	144
4.2.4.4.1	Burial dissolution.....	144
4.2.5	Dolomitization and dedolomitization.....	145
4.2.5.1	Introduction.....	145
4.2.5.2	Ratawi dolomitization models.....	145
4.2.5.2.1	Synsedimentary organic dolomite.....	149
4.2.5.2.2	Early diagenetic mixing-zone related dolomite.....	150
4.2.5.2.3	Late diagenetic (burial) dolomite.....	151
4.2.5.2.3.1	Dolomite associated with stylolites and dissolution seams.....	151
4.2.5.2.3.2	Saddle dolomite as a cement and replacement.....	151



4.2.5.3 Ratawi dedolomitization.....	156
4.2.5.3.1 Dedolomitization texture and porosity.....	156
4.2.5.3.2 Ratawi dedolomitization model.....	157
4.3 Ratawi porosity.....	157
4.3.1 Porosity in carbonate versus siliciclastic.....	157
4.3.2 Carbonate porosity classification.....	158
4.3.3 Ratawi basic porosity types.....	159
4.3.3.1 Interparticle pore type.....	160
4.3.3.2 Intraparticle pore type.....	162
4.3.3.3 Mouldic pore type.....	162
4.3.3.4 Vug pore type.....	162
4.3.3.5 Intercrystal pore type.....	163
4.3.3.6 Fracture pore type.....	163
4.3.3.7 Stylolitic pore type.....	168
4.3.3.8 Burrow pore type.....	168
4.3.3.9 Rootlet pore type.....	169
4.3.3.10 Dedolomite pore type.....	169
4.3.3.11 Microporosity pore type .....	170
4.3.4 Porosity preservation during burial.....	172
4.3.4.1 Introduction.....	172
4.3.4.2 Processes to reduce the effect of cementation.....	173
4.3.4.2.1 Absence of a source of carbonate cement.....	173
4.3.4.2.2 Isolation of the reservoir from the carbonate cement source.....	173
4.3.4.2.3 Reduced fluid mobility by early emplacement of hydrocarbons.....	174
4.3.4.2.4 High brine concentration in formation water.....	174
4.3.4.2.5 High carboxylic acids concentration in formation water.....	174
4.3.4.3 Processes to reduce the effect of chemical compaction.....	175
4.3.4.3.1 Early lithification.....	175
4.3.4.3.2 Early hydrocarbon emplacement.....	175
4.3.4.3.3 Structural growth, unconformity, and anhydrite buffer zone.....	175
4.3.4.4 Ratawi porosity preservation.....	176
4.3.4.4.1 Ratawi porosity preservation by reduction of compaction.....	176
4.3.4.4.2 Ratawi porosity preservation by reduction of cementation.....	177
4.4 Ratawi sequence stratigraphy and porosity development.....	179
4.4.1 Introduction.....	179
4.4.2 Methods to predict porosity with depth.....	179
4.4.2.1 Porosity-depth or maturity correlation model.....	179
4.4.2.2 Porosity-diagenesis and the chemical model.....	181
4.4.2.3 Porosity-diagenesis and sequence stratigraphy model.....	182
4.5 Summary.....	183

## **Chapter 5 Cycles and Sequences in the Ratawi Formation and Regional**

<b>Patterns.....</b>	<b>185</b>
5.1 Introduction.....	185
5.1.1 High-resolution sequence stratigraphy and reservoir characterization.....	187
5.1.2 Aims of this chapter.....	188
5.2 Ratawi cycles.....	188
5.2.1 Introduction.....	188
5.2.2 Ratawi parasequence style.....	190
5.2.3 Ratawi parasequence boundaries and types.....	190
5.3 Ratawi Formation cycles.....	191
5.3.1 Ratawi peritidal and subtidal parasequences.....	192
5.3.2 Ratawi parasequence symmetry.....	198
5.3.2.1 Regressive cycles.....	198
5.3.2.2 Transgressive-regressive cycles.....	199



5.3.2.3 Aggraded cycles.....	200
5.3.3 Ratawi Oolite and Ratawi Limestone cycles.....	200
5.3.3.1 Ratawi Oolite cycles.....	201
5.3.3.2 Ratawi Limestone cycles.....	202
5.4 Ratawi cycle stacking patterns.....	203
5.4.1 Introduction.....	203
5.4.2 Fischer Plots.....	203
5.4.2.1 Fischer plot for well R-50.....	208
5.4.2.2 Fischer plot for well R-48.....	208
5.4.2.3 Ratawi cycle hierarchy from Fischer plots.....	212
5.5 Ratawi log signature to cycles and surfaces.....	213
5.6 General correlation between well R-49 and R-50.....	215
5.7 Summary.....	217
<b>Chapter 6 The Ratawi Sequence Stratigraphic Model and Petroleum System.....</b>	<b>218</b>
6.1 Introduction.....	218
6.1.1 Ratawi Formation petroleum system.....	219
6.1.2 Thamama Group 2 <sup>nd</sup> order cycles.....	220
6.1.3 Aims of this chapter.....	223
6.2 Distribution of Ratawi Formation in the study area and adjacent countries.....	223
6.3 The cycle hierarchy of the Ratawi Formation.....	226
6.4 Ratawi Formation sequence stratigraphic model.....	227
6.4.1 Factors controlling Ratawi Formation cyclicity.....	228
6.4.1.1 Tectonic versus eustatic processes.....	234
6.4.1.1.1 Factors controlling composite sequence boundary zone CMS BZ-1..	234
6.4.1.1.2 Factors controlling composite sequence boundary zone CMS BZ-2..	235
6.4.1.1.2.1 Type 1 unconformity and its correlative conformable surface.....	235
6.4.1.1.2.2 Deepening succession and its correlative Type 3 unconformity.....	237
6.4.1.1.3 Factors controlling composite sequence boundary zone CMS BZ-3..	242
6.4.1.2 Eustatic versus sediment supply processes.....	242
6.4.1.2.1 Forced regression versus depositional regression.....	242
6.4.1.2.2 Valanginian-Hauterivian palaeoceanographic changes and carbonate sediment supply.....	243
6.4.1.3 Sediment supply versus tectonic processes.....	245
6.4.1.3.1 Tectonic events and the initiation of the Ratawi Oolite platform.....	248
6.4.1.3.2 Tectonic events and the development of the Ratawi Oolite platform.....	248
6.4.1.3.3 Tectonic events and the termination of the Ratawi Oolite platform..	249
6.4.2 Ratawi Formation and Thamama Group petroleum system.....	250
6.5 Summary.....	252
<b>Chapter 7 Synthesis and Conclusions.....</b>	<b>253</b>
<b>References.....</b>	<b>262</b>
<b>Appendix I: Location of samples and petrographic data.....</b>	<b>274</b>
<b>Appendix II: Ratawi parasequence data.....</b>	<b>300</b>
<b>Appendix III: Fischer Plots.....</b>	<b>307</b>

5.3.2.3 Aggraded cycles.....	200
5.3.3 Ratawi Oolite and Ratawi Limestone cycles.....	200
5.3.3.1 Ratawi Oolite cycles.....	201
5.3.3.2 Ratawi Limestone cycles.....	202
5.4 Ratawi cycle stacking patterns.....	203
5.4.1 Introduction.....	203
5.4.2 Fischer Plots.....	203
5.4.2.1 Fischer plot for well R-50.....	208
5.4.2.2 Fischer plot for well R-48.....	208
5.4.2.3 Ratawi cycle hierarchy from Fischer plots.....	212
5.5 Ratawi log signature to cycles and surfaces.....	213
5.6 General correlation between well R-49 and R-50.....	215
5.7 Summary.....	217
 <b>Chapter 6 The Ratawi Sequence Stratigraphic Model and Petroleum System.....</b>	 <b>218</b>
6.1 Introduction.....	218
6.1.1 Ratawi Formation petroleum system.....	219
6.1.2 Thamama Group 2 <sup>nd</sup> order cycles.....	220
6.1.3 Aims of this chapter.....	223
6.2 Distribution of Ratawi Formation in the study area and adjacent countries.....	223
6.3 The cycle hierarchy of the Ratawi Formation.....	226
6.4 Ratawi Formation sequence stratigraphic model.....	227
6.4.1 Factors controlling Ratawi Formation cyclicity.....	228
6.4.1.1 Tectonic versus eustatic processes.....	234
6.4.1.1.1 Factors controlling composite sequence boundary zone CMS BZ-1..	234
6.4.1.1.2 Factors controlling composite sequence boundary zone CMS BZ-2..	235
6.4.1.1.2.1 Type 1 unconformity and its correlative conformable surface.....	235
6.4.1.1.2.2 Deepening succession and its correlative Type 3 unconformity.....	237
6.4.1.1.3 Factors controlling composite sequence boundary zone CMS BZ-3..	242
6.4.1.2 Eustatic versus sediment supply processes.....	242
6.4.1.2.1 Forced regression versus depositional regression.....	242
6.4.1.2.2 Valanginian-Hauterivian palaeoceanographic changes and carbonate sediment supply.....	243
6.4.1.3 Sediment supply versus tectonic processes.....	245
6.4.1.3.1 Tectonic events and the initiation of the Ratawi Oolite platform....	248
6.4.1.3.2 Tectonic events and the development of the Ratawi Oolite platform.....	248
6.4.1.3.3 Tectonic events and the termination of the Ratawi Oolite platform..	249
6.4.2 Ratawi Formation and Thamama Group petroleum system.....	250
6.5 Summary.....	252
 <b>Chapter 7 Synthesis and Conclusions.....</b>	 <b>253</b>
 <b>References.....</b>	 <b>262</b>
 <b>Appendix I: Location of samples and petrographic data.....</b>	 <b>274</b>
<b>Appendix II: Ratawi parasequence data.....</b>	<b>300</b>
<b>Appendix III: Fischer Plots.....</b>	<b>307</b>



## LIST OF FIGURES

Figure 1-1 Structural trends over the major oil and gas fields in the Arabian Gulf Region.....	2
Figure 1-2 The location of the Partitioned Neutral Zone .....	6
Figure 1-3 Stratigraphic column at Wafra oilfield.....	7
Figure 1-4 The location of the study wells R-48, R-49 and R-50 as well as reference well R-43 in the main, southern and eastern Wafra areas.....	8
Figure 2-1 Structural elements of the Middle East.....	10
Figure 2-2 Plate movements and large-scale palaeogeography from late-Triassic to Present-day.....	14
Figure 2-3 Neoproterozoic salt basins of the Arabian-Persian Gulf Basin and major basement uplifts.....	16
Figure 2-4 Uppermost Jurassic to lowest Upper Cretaceous stratigraphic units of eastern Arabian platform (U.A.E. and Oman) .....	23
Figure 2-5 Lithostratigraphy correlation chart of the Mesozoic formations in Saudi Arabia Kuwait, Iraq and UAE .....	27
Figure 2-6 Palaeogeographic map of the Arabian Shelf during the Early to Middle Valanginian, showing the location of Wafra oilfield.....	33
Figure 2-7 Ratawi zone at reference well R-43 in Wafra oilfield.....	37
Figure 2-8 Type porosity logs for the lithofacies of the Ratawi Oolite reservoir at the crestal and flank locations.....	39
Figure 2-9 Stratigraphic cross-sections showing the spatial distribution of lithofacies in the Ratawi Oolite.....	39
Fig. 3-1 General facies model for a carbonate Ramp.....	49
Figure 3-2 Photomicrograph illustrating microfacies BR-1: bioclastic wackestone-mudstone with ostracods, bioclastic fragments and black grains and BR2: bioturbated bioclastic wackestone-mudstone with ostracods. ....	55
Figure 3-3 Photomicrograph of black grains in microfacies BR-1 and SR-5.....	56
Figure 3-4 Photomicrograph of oolitic grains characteristic of microfacies SR-1 in reservoir Unit D.....	65
Figure 3-5 Photomicrograph illustrating microfacies SR1: peloidal bioclastic grainstone-rudstone with coral debris and ooids and microfacies SR2: cross-laminated peloidal bioclastic grainstone-packstone.....	70

Figure 3-6 Photomicrograph of aggregates grains characteristic of microfacies SR-3 .....	71
Figure 3-7 Photomicrograph illustrating microfacies SR3: peloidal bioclastic grainstone-packstone with ooids and aggregates and microfacies SR4: peloidal bioclastic grainstone-packstone.....	72
Figure 3-8 Photomicrograph illustrating microfacies SR5: peloidal bioclastic packstone with black grains and microfacies DR1: peloidal bioclastic floatstone.....	77
Figure 3-9 Photomicrograph illustrating microfacies DR2: bioturbated bioclastic mudstone and DR3: bioturbated bioclastic wackestone.....	78
Figure 3-10 Photomicrograph illustrating microfacies DR4: biomorpha (whole shell) wackestone-mudstone and microfacies DiagDol: crystalline saddle dolomite.....	81
Figure 3-11 Diagram illustrates four styles of root zone calcification: root petrification, concentric micrite / microspar, dense peloidal micrite and alveolar septal fabric.....	87
Figure 3-12 Photomicrograph illustrating a rhizolith (root tubule) and <i>Bacinella irregularis</i> .....	88
Figure 3-13 Photomicrograph of calcified filaments.....	89
Figure 3-14 Photomicrograph of alveolar septal structure in tubular and in intergranular pore spaces types.....	89
Figure 3-15 Photomicrograph of micritization (neomorphic inversion) of carbonate particles.....	96
Figure 3-16 Photomicrograph of micritization (neomorphic inversion) of carbonate cement.....	97
Figure 3-17 Photomicrograph of vadose compaction in grainstone .....	98
Figure 3-18 Palaeogeographic map of the Zubair delta during the Barremian-Albian .....	94
Figure 3-19 Ratawi Formation depositional model during the deposition of Ratawi Oolite and Ratawi Limestone, and during the deposition of the Ratawi Limestone and Ratawi Shale ramp facies.....	95
Figure 4-1 Ratawi diagenetic processes and inferred diagenetic environments.....	110
Figure 4-2 Diagram showing two micritization models by microboring conventional micritic rim formation and concurrent filling.....	113
Figure 4-3 Photomicrograph of the two types of the micritic envelope: destructive micritic envelope and constructive micritic envelope.....	115
Figure 4-4 Photomicrograph of crinoid grain with syntaxial calcite cement under plane-polarized light and under cathodoluminescence .....	119



Figure 4-5 Diagram showing types of biogenic response to loose (soft), firm and hard (lithified) substrates.....	121
Figure 4-6 Photomicrograph of green algae and sponge spicules moulds filled by the coarse granular calcite cement.....	124
Figure 4-7 Photomicrograph illustrating the interparticle porosity in reservoir unit D and meteoric bladed and granular drusy cements in reservoir unit E.....	128
Figure 4-8 Photomicrograph illustrating meteoric columnar and poikilotopic.....	129
Figure 4-9 Photomicrograph of replacement of the quartz grains by calcite.....	131
Figure 4-10 Micromorphological classification of calcretes.....	135
Figure 4-11 Six stages in calcrete development in fine-grained sediment.....	137
Figure 4-12 Photomicrograph illustrating grainstone with burial granular drusy calcite cement under plane-polarized light and cathodoluminescence.....	140
Figure 4-13 Reduction of the primary interparticle porosity by the development of vadose and burial compaction.....	142
Figure 4-14 Photomicrograph illustrating fitted fabric developed by deep burial compaction and burial dissolution porosity in saddle dolomite cement.....	143
Figure 4-15 Dolomitization models interpreted in the framework of sequence stratigraphic model.....	146
Figure 4-16 Photomicrograph of selective dolomitization of a burrow fill by micro-euhedral dolomite crystals and two pseudomorphosed gypsum crystals in restricted back ramp, microfacies BR2.....	147
Figure 4-17 Photomicrograph of micro-euhedral dolomite crystals scattered through the sediment in mudstone and wackestone lithofacies and micro-euhedral dolomite crystals associated with a dissolution seam .....	148
Figure 4-18 Photomicrograph of saddle dolomite cement.....	152
Figure 4-19 Photomicrograph of scattered saddle dolomite cement under cathodoluminescence.....	153
Figure 4-20 Photomicrograph of dedolomite in reservoir Unit E.....	154
Figure 4-21 Photomicrograph of dedolomite and dedolomite porosity in reservoir unit D.....	155
Figure 4-22 Ratawi porosity measured from thin section related to texture and Ratawi facies belts.....	161
Figure 4-23 Photomicrograph of crinoid grain with fracture and syntaxial overgrowth calcite cement under plane-polarized light and under cathodoluminescence .....	164

Figure 4-24 Photomicrograph of vuggy, moldic and intraparticle porosities in wackestone (microfacies DR3) and interparticle porosity in reservoir unit E (microfacies DiagCal: pedogenic calcrete).....	165
Figure 4-25 Photomicrograph of vug porosity and fracture porosity.....	166
Figure 4-26 Photomicrograph of tectonic fractures and complex and irregular cracks associated with subaerial exposure, calcrete fabric.....	167
Figure 4-27 Photomicrograph of intraparticle porosity in skeletal grain of foraminifera.....	168
Figure 4-28 SEM micrographs of intercrystalline microporosity and microvugs.....	170
Figure 4-29 Porosity versus depth for carbonate rocks and porosity range of the Ratawi Formation in the Wafra oilfield.....	180
Figure 4-30 General diagenetic model during icehouse-greenhouse episodes in the framework of sequence stratigraphy .....	182
Figure 5-1 Sequence stratigraphic models for ramp systems.....	186
Figure 5-2 Composite idealized parasequence facies types recognized in the Ratawi Formation: regressive cycle, transgressive-regressive cycle and aggraded cycle.....	189
Figure 5-3 Processes controlling the hierarchy of relative sea-level changes.....	191
Figure 5-4 Allocyclic and autocyclic models for the genesis of parasequences .....	193
Figure 5-5 General stacking patterns for the parasequence during icehouse-greenhouse episodes .....	195
Figure 5-6 Greenhouse and icehouse periods have different climatic forcing effecting the nature of sea-level changes.....	196
Figure 5-7 Sea level and aridity-humidity cycles during the Mesozoic; showing the four 'little' ice ages during the greenhouse period of the Mesozoic.....	197
Figure 5-8 Fischer plot in depth domain for strata in well R-50 compared with log signatures and location of reservoir and non-reservoir units.....	204
Figure 5-9 Fischer plots in time domain for core well R-50.....	205
Figure 5-10 Fischer plots in depth domain for core well R-48 compared with 'total' gamma ray signatures in Ratawi Limestone.....	206
Figure 5-11 Fischer plots in time domain for core well R-48.....	207
Figure 5-12 Log signatures for strata in well R-49 and location of reservoir and non-reservoir units.....	216



Figure 6-1) 2 <sup>nd</sup> -order and 3 <sup>rd</sup> -order cycles recognized in this study compared to Tethyan stratigraphic cycles and 1 <sup>st</sup> sub cycle of Jacquin <i>et al.</i> (1998) .....	221
Figure 6-2 Lithostratigraphic-structural cross-section showing productive horizons in the major oil fields in southern Kuwait and the study area, the Partitioned Neutral Zone (PNZ) and Lithostratigraphic correlation of the Mesozoic formations in southern Iraq-Kuwait-PNZ and northeastern Saudi Arabia.....	224
Figure 6-3 Major transgressive / regressive cycles, source rocks and main phases of development of European basins.....	230
Figure 6-4 Transgressive / regressive cycles for the early Cretaceous of Western Europe....	231
Figure 6-5 Lower Cretaceous Eustatic Curve of Haq <i>et al.</i> (1987) compared to Hardenbol <i>et al.</i> (1998).....	232
Figure 6-6 Thamama Group 2 <sup>nd</sup> -order sequences and surfaces recognized in this study compared with equivalent surfaces in the Eustatic Curve of Haq <i>et al.</i> (1987) and Hardenbol <i>et al.</i> (1998) .....	239
Figure 6-7 Diagram showing Type 1, Type 2 and Type 3 sequence boundaries.....	240
Figure 6-8 Types and origin of drowning unconformities .....	241
Figure 6-9 The distribution of source, reservoir and seal rocks in Kuwait and the study area, the Partitioned Neutral Zone, during Mesozoic-Cenozoic.....	246

## LIST OF TABLES

Table 1-1 Oil reserves at end 2000.....	4
Table 3-1 Ratawi facies.....	51
Table 3-2 Summary of features in subaerial exposure facies.....	85
Table 5.1 Ratawi cycle types in cores of well R-50 and R-48 .....	200

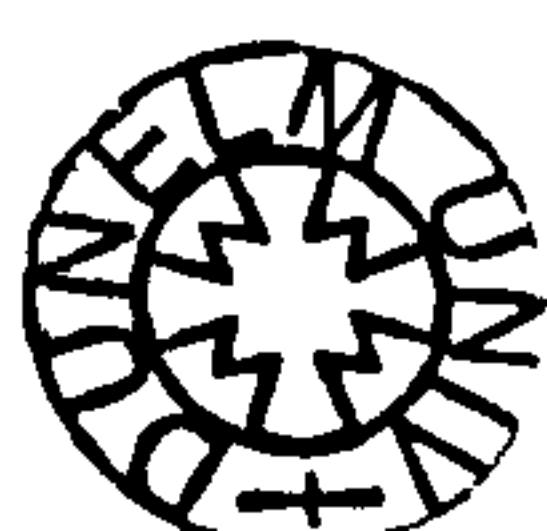
## Chapter 1 Introduction

### 1.1 Introduction

The Arabian-Iranian basin is the richest petroleum system in the world. The recoverable reservoirs of oil and gas here are about 66% and 34% of the world reservoir, respectively, and the implied ultimate recovery from the area would amount to about 980 billion barrels of oil (Table 1-1). The principal oil producing horizons in the region are within Mesozoic (middle and upper Jurassic, lower and middle Cretaceous) and Cenozoic (Oligocene and Miocene) strata, but in the southernmost part, in southern Oman, within Palaeozoic rocks too (basal Cambro-Ordovician to Devonian and Lower Permian). The enormous Arabian-Iranian hydrocarbon reserves occur in some 290 producing oilfields (Fig. 1-1) (Beydoun, 1998). Many geologists (Murris, 1980; Beydoun, 1988, 1991, 1998; Stoneley, 1990; Alsharhan and Nairn, 1997) have considered this basin to be an exceptional petroleum system in terms of oil and gas accumulation.

Different geological factors worked simultaneously to make the Arabian-Iranian basin the richest petroleum system in the world, including: (1) A long history of almost continuous sedimentation, (2) A very large volume of predominantly marine sediments, (3) Extensive and thick reservoir rocks, with many regional unconformities, (4) The close association of rich source rocks deposited in marine anoxic basins adjacent to excellent reservoir rocks deposited over extensive shelf areas, (5) Widely distributed and efficient seal rocks, (6) Large anticlinal structures that formed during hydrocarbon migration which helped to preserve large volumes of pore space from further diagenesis, (7) The absence of prolonged erosion (except after post-orogenic late Neogene uplift), strong tectonism and metamorphism, and (8) Easily fractured carbonate rocks predominant since the Permian, permitting vertical migration across the bedding to charge younger reservoirs (Beydoun, 1988).

Murris (1980) developed a model to explain the hydrocarbon systems of Qatar, within the central part of the Arabian-Iranian basin, for the Middle Jurassic to Middle Cretaceous interval. He suggested that the model could be extended to other parts of the basin. The model called for the association of source, reservoir and seal rock lithofacies in a cycle of transgression and regression. During the transgression the source rock lithofacies was deposited in a low-energy environment in starved basins





on the differentiated carbonate platform, and the reservoir rock lithofacies was deposited in high-energy environments on the carbonate platform, as marginal reefs, oolite sand bodies, rudistid banks and regressive sands. However, during the regressive part of the cycle, the seal rock lithofacies were deposited as supratidal evaporites and regressive shales.

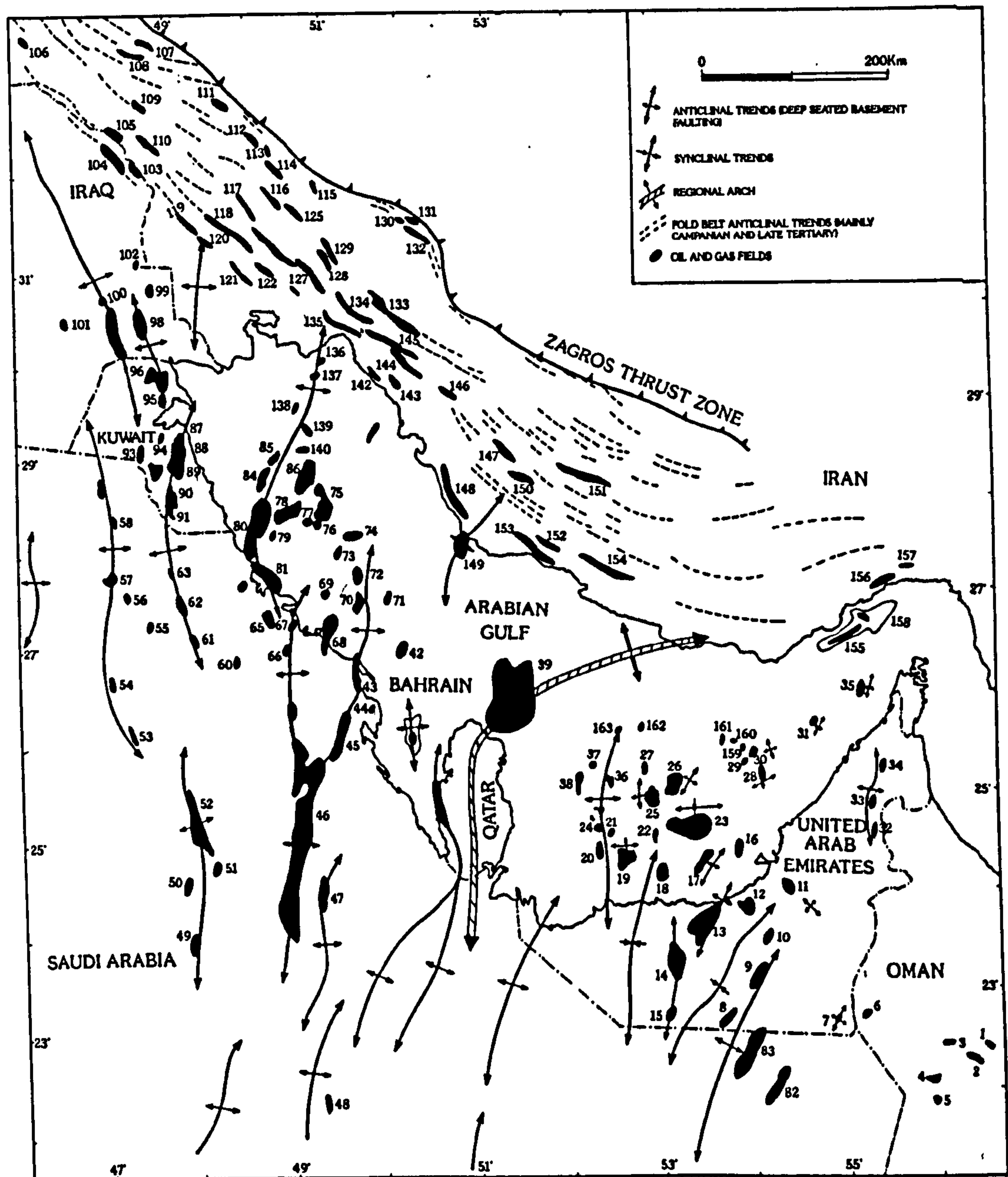


Figure 1-1 Structural trends over the major oil and gas fields in the Arabian Gulf region (after Alsharhan and Nairn, 1997). Main and southern Wafra areas are numbers 90 and 91 along the Kuwait arch. The first and second largest oilfields in the world are Ghawar and Burgan, numbers 46 and 89.

The modern concepts of carbonate sequence stratigraphy can be used as a tool to interpret the factors controlling the facies succession in the Arabian-Iranian basin at

different scales. These factors can be used to constrain the stratigraphic evolution of the basin and predict basin-filling stratal patterns that include the temporal and spatial distribution of source, reservoir and seal rocks, which are the principal elements for any petroleum system. In addition, high-resolution sequence stratigraphy can be applied in geological reservoir characterization modelling, which is the main element in interpretation and prediction of reservoir heterogeneity and flow units. Constraining the factors that control the petroleum system and reservoir flow units is important in hydrocarbon exploration and reservoir development and management.

## **1.2 Aims of the study**

The Wafra oilfield is a giant oilfield in the Arabian-Iranian basin, located in the Saudi Arabia-Kuwait Partitioned Neutral Zone. The main reservoir zone in this oilfield is the Ratawi zone (Ratawi Formation), which is also a major hydrocarbon zone in Kuwait and southern Iraq, but only in the northeastern area of Saudi Arabia. The aim of this project is to apply the concepts of sequence stratigraphy to determine the factors that control the temporal and spatial distribution of source, reservoir and seal rocks in the Ratawi Formation (Thamama Group) in the Wafra oilfield, in the Saudi Arabia-Kuwait Partitioned Neutral Zone. In addition, high-resolution sequence stratigraphy is used to outline some of the controls on Ratawi zone heterogeneity in the Wafra oilfield and the factors that lead to preservation of near-surface depositional and diagenetic porosity at depth.

The Ratawi Formation in the Wafra oilfield is studied through integrating sedimentary and diagenetic facies models, along with data from previous studies, within the framework of sequence stratigraphy at different cycle orders. On the global scale (2<sup>nd</sup> and 1<sup>st</sup> order sub-cycles), the aim is to interpret the long-term factors that were operating in the Tethys seaway during the lower Cretaceous, which controlled the initiation, development and termination of the Ratawi Oolite carbonate platform. On a more regional scale (3<sup>rd</sup> and 2<sup>nd</sup> order cycles), the aim is to interpret the source, reservoir and seal lithofacies in the Ratawi Formation. Finally, on a local scale (5<sup>th</sup> and 4<sup>th</sup> order cycles), the aim is to determine reservoir heterogeneity of the Ratawi zone in the Wafra oilfield.

The aims of this research include:

1. To present an account of the regional geology and tectonic control of the lower Cretaceous strata of the Saudi Arabia-Kuwait Partitioned Neutral Zone.



2. To describe and interpret the facies and succession of the Ratawi Formation in the Wafra oilfield from core samples, and produce a depositional model in the context of sequence stratigraphy.
3. To describe and interpret the diagenesis of the Ratawi Formation and produce a diagenetic model within the framework of sequence stratigraphy.
4. To determine the cyclostratigraphy of the Ratawi Formation from core and well-log data and consider the nature of reservoir and seal facies, and reservoir heterogeneity, within a sequence stratigraphic framework.
5. To use the concepts of sequence stratigraphy to interpret and predict seal, reservoir and source rocks of the Ratawi Formation in Wafra oilfield area.

Oil: Proved reserves		At end 2000
	Thousand million barrels	Share of total
Iran	89.7	8.6%
Iraq	112.5	10.8%
Kuwait	96.5	9.2%
Oman	5.5	0.5%
Qatar	13.2	1.3%
Saudi Arabia	261.7	25.0%
Syria	2.5	0.2%
United Arab Emirates	97.8	9.3%
Yemen	4.0	0.4%
Other Middle East	0.2	†
<b>Total Middle East</b>	<b>683.6</b>	<b>65.3%</b>
<b>Total North America</b>	<b>64.4</b>	<b>6.1%</b>
<b>Total S. &amp; Cent. America</b>	<b>95.2</b>	<b>9.0%</b>
<b>Total Europe</b>	<b>19.1</b>	<b>1.9%</b>
<b>Total Former Soviet Union</b>	<b>65.3</b>	<b>6.4%</b>
<b>Total Africa</b>	<b>74.8</b>	<b>7.1%</b>
<b>Total Asia Pacific</b>	<b>44.0</b>	<b>4.2%</b>
<b>TOTAL WORLD</b>	<b>1046.4</b>	<b>100.0%</b>
<b>Non-OPEC†</b>	<b>166.7</b>	<b>15.9%</b>
<b>OPEC</b>	<b>814.4</b>	<b>77.8%</b>

Table 1-1 Oil reserves at end 2000

In order to achieve these aims the microfacies and broad facies belts of the Ratawi Formation are analyzed and represented by a depositional facies model in Chapter 3. The diagenetic overprint and its effect on the reduction or enhancement of the Ratawi depositional porosity are analyzed and represented by a diagenetic model in Chapter 4. This chapter also discusses the different factors that lead to the preservation of primary and secondary near-surface porosity at the depths of the reservoir zones.

The cyclostratigraphic framework for the Ratawi Formation is constructed in Chapter 5 from data obtained from two wells, well R-50 and R-48. The different reservoir and non-reservoir units in the Ratawi zone in the Wafra oilfield are correlated from the type section in a well at the Wafra crest to these two wells on the flank of the main structure using different types of logs. This chapter integrates the Ratawi depositional and diagenetic models within the constructed cycle hierarchy to interpret and predict the depositional and diagenetic porosity for different reservoir units (reservoir heterogeneity). The global, regional and local factors that control the initiation development and termination of the Ratawi Oolite platform and influenced the development of the petroleum system of the Ratawi Formation are discussed in Chapter 6.

### **1.3 Location of the Study Area**

The Wafra oilfield is located in the Partitioned Neutral Zone, a region in the northeastern Arabian Peninsula, between Saudi Arabia and Kuwait (Fig. 1-2). Oil production in the area is jointly administered by the two governments represented by the Kuwait Oil Inc. and Saudi Arabian Texaco Inc. The oilfield is mapped as an anticline with a trend of the structural axis from north-northwest to south-southeast. Production comes from four horizons, which are the First and Second Eocene 'limestones', the Wara Formation (Middle Cretaceous) and the Lower Cretaceous Minagish Formation. The Minagish Formation is known in the Partitioned Neutral Zone as the Ratawi Oolite member, which is the most productive horizon in the oilfield. The estimated recoverable reserves in these horizons are about 2.3 billion barrels, and in 1988 this ranked the Wafra oilfield as the 101<sup>st</sup> largest oilfield in the world (Longacre and Ginger, 1988).

The Wafra oilfield has no surface expression; the ground consists of flat-lying terrain with a desert sand surface. The thickness of the stratigraphic column at the oilfield is more than 16 kilometres (Fig. 1-3). Thus, the interpretation of the field geology is based entirely on well and seismic data. The first wildcat in the field, Wafra no. 1, was put down in 1949, and was abandoned as a dry hole. In 1953, after a geophysical survey, Wafra no. 4 was found to be productive from the Middle Cretaceous Wara Limestone, the first productive horizon. Two other productive horizons, the Eocene Limestone<sup>(5)</sup> and Lower Cretaceous Ratawi Limestone (Fig. 1-4) were discovered in 1956 (Longacre, 1986).



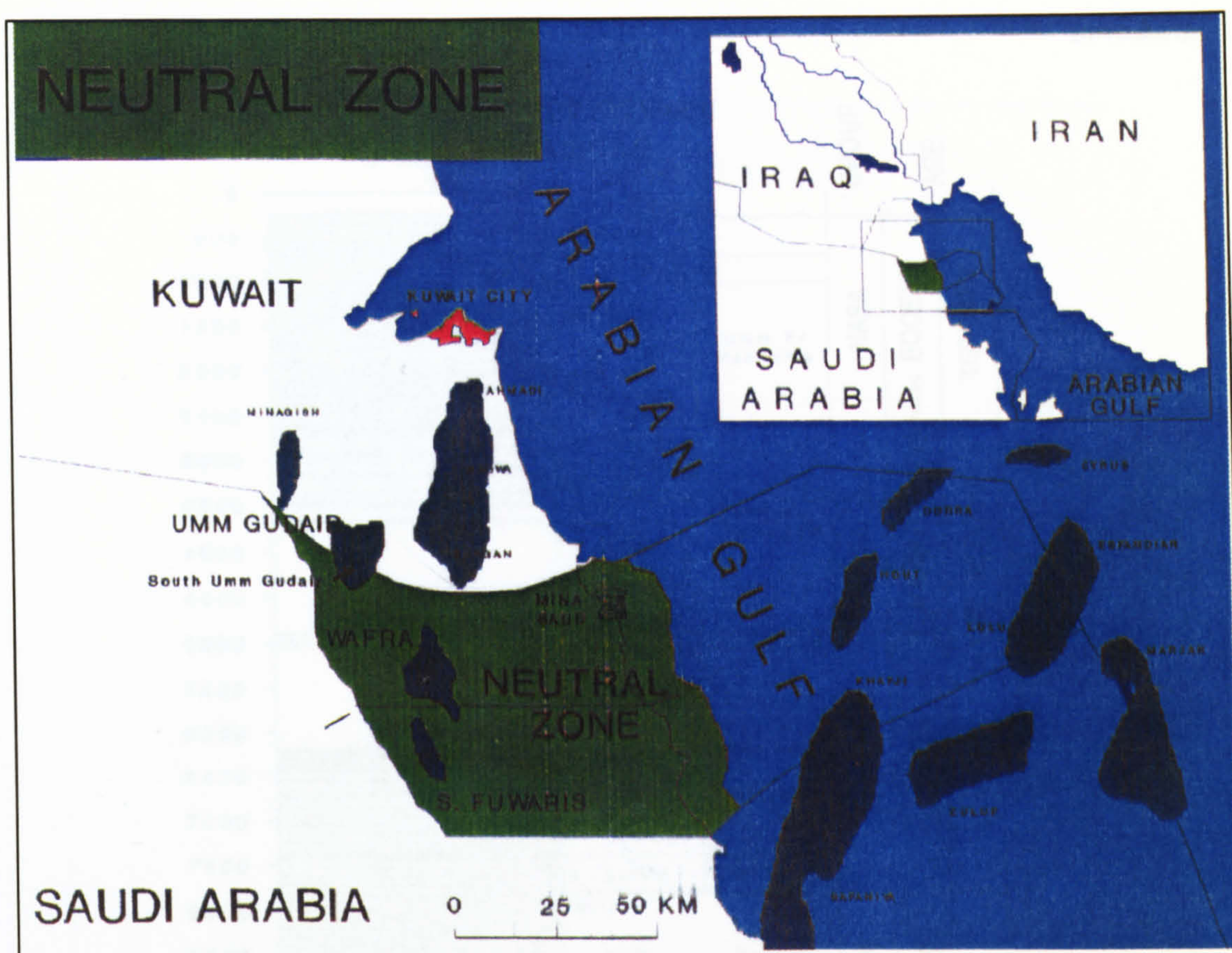


Figure 1-2 The location of the Partitioned Neutral Zone (after Al Harbi, 1994).

#### **1.4 Material available in this study**

The data available for this study include:

1. Two hundred and four core samples collected by the author from the Ratawi Oolite and Ratawi Limestone (the lower and middle members of the Ratawi Formation) from wells R-50 and R-48 in Wafra main area, and well R-49 in Wafra southern area drilled in 1996/7. No samples were available from the upper member, the Ratawi Shale.
2. General facies succession from core for wells R-50 and R-49, logged by the author, in addition to core description charts for these two cores prepared by Core Lab Company in the United Arab Emirates, at a scale of 1 to 50.
3. Different log types including gamma ray, spectral gamma ray, neutron and density logs from wells R-50, R-49 and R-48.
4. An unpublished Saudi Arabian Texaco Inc. report by Longacre (1986) describing the Ratawi Zone in the Wafra oilfield.
5. Published data on the Lower Cretaceous Thamama Group in the Arabian-Iranian basin and the development of the Tethyan Seaway during lower Cretaceous times.



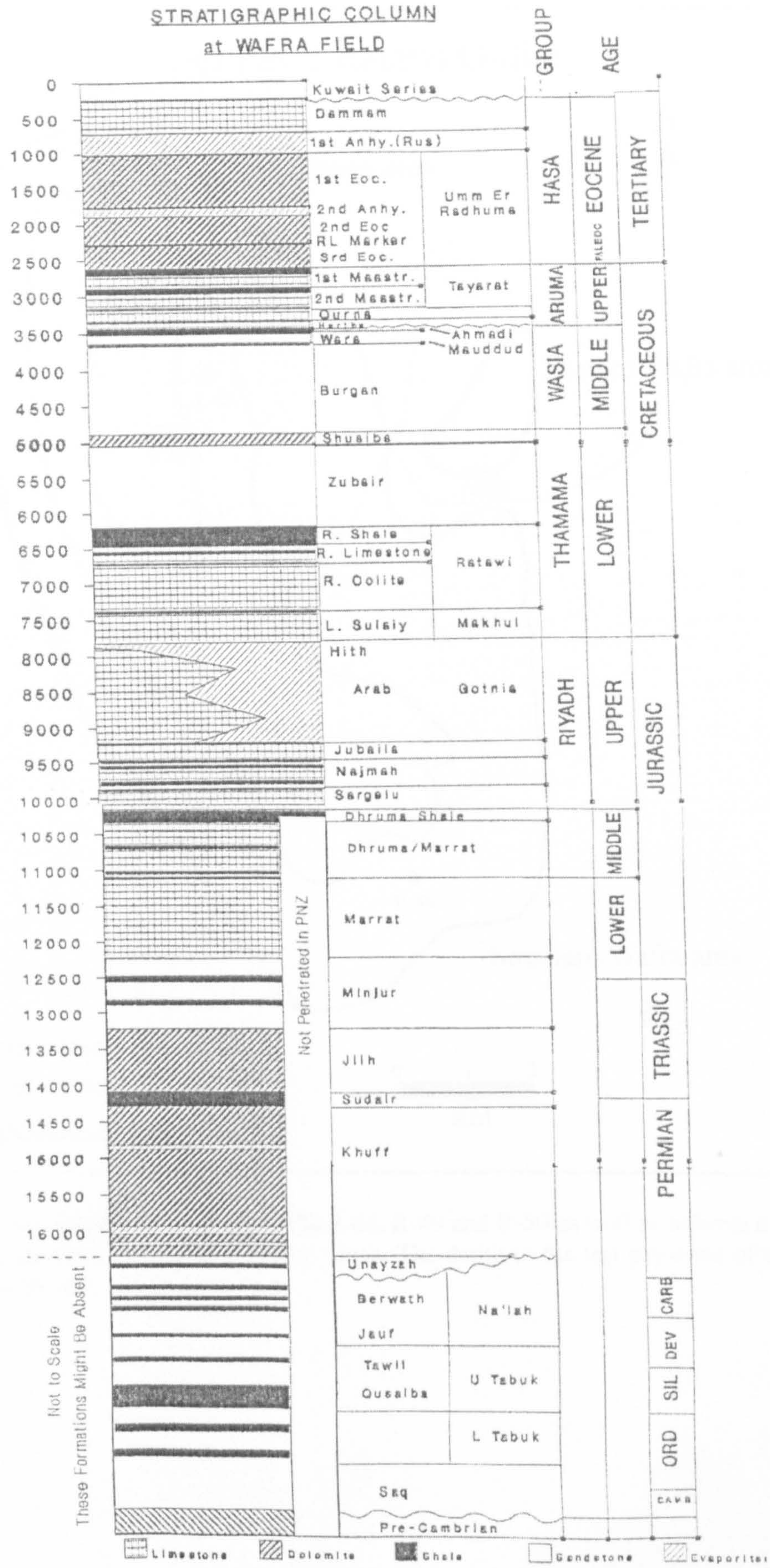


Figure 1-3 Stratigraphic column at Wafra oilfield. scale in feet .



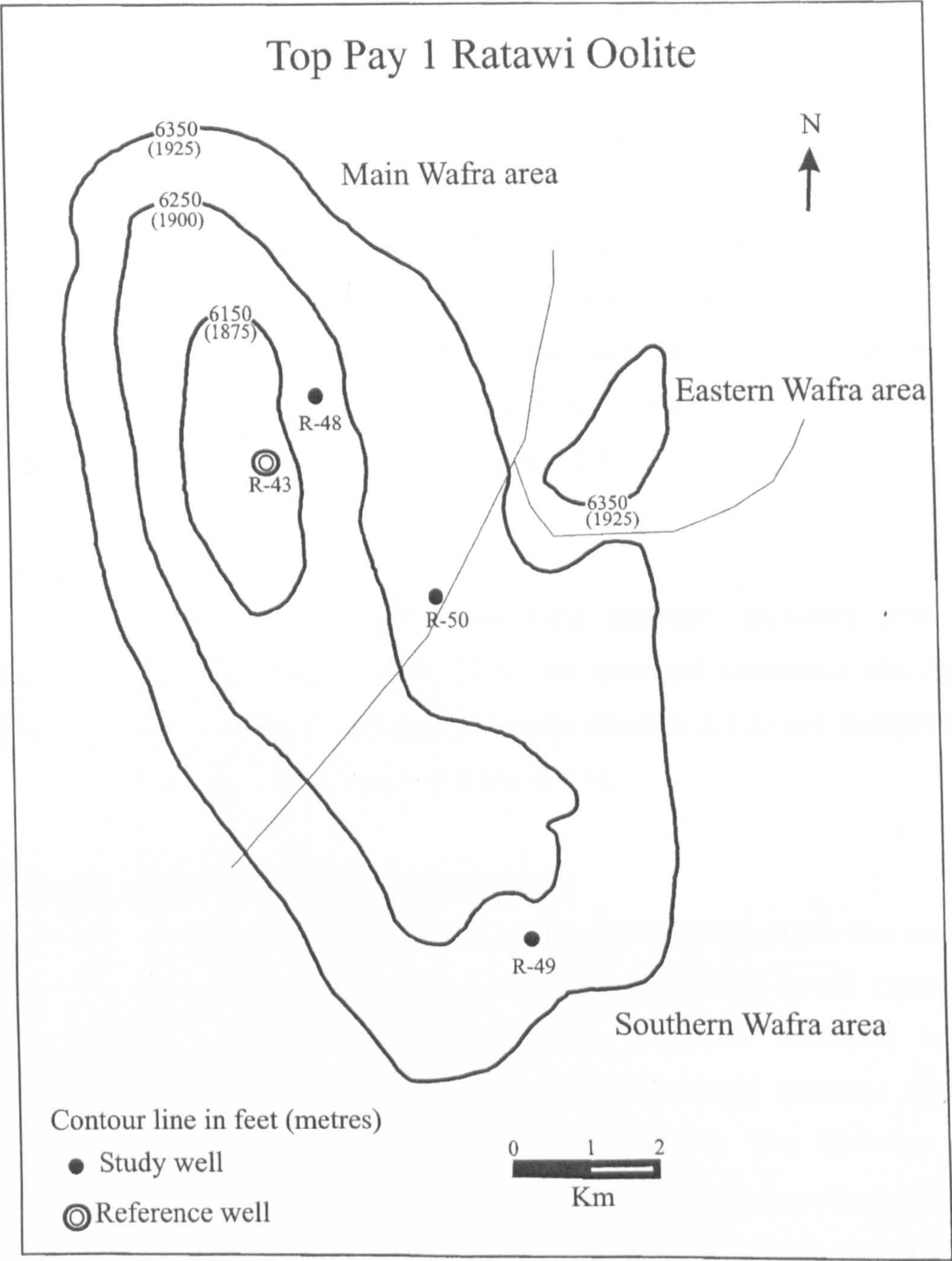


Figure 1-4 The location of the study wells R-48, R-49 and R-50 as well as reference well R-43 in the main, southern and eastern Wafra areas. The depth to the top pay-zone of the Ratawi Oolite is also shown.

## **Chapter 2 Regional Geology, the Ratawi Petroleum System and Previous Studies**

The main topics of this study are facies and microfacies of the Ratawi Formation (Chapter 3), porosity and diagenesis of the Ratawi Formation (Chapter 4), cycles and sequences in the Ratawi Formation and regional patterns (Chapter 5) and the Ratawi sequence stratigraphic model and petroleum system (Chapter 6). The necessary background to this study is reviewed in this chapter under three headings, geotectonics (Section 2.1), Mesozoic geological history (Section 2.2) and previous studies of the Ratawi Formation in the Thamama Group (Section 2.3).

### **2.1 Geotectonics**

This section will review the regional and local structure, including geotectonic elements of the Arabian Plate (Section 2.1.1), the basement lineaments and Arabian Folds trend (Section 2.1.2), the Hormuz salt basin (Section 2.1.3) and syndepositional structural growth of the Arabian Folds (Section 2.1.4).

#### **2.1.1 Geotectonic elements of the Arabian Plate**

The boundaries of the Arabian Plate were formed in the early Mesozoic (the northeast, southeast, north and older northwest margins) and in the middle to late Tertiary (the south, southwest, modified northeast and north, and new northwest margins) (Beydoun, 1991). The variation in lithofacies and sedimentary thickness across the Arabian-Iranian basin depends on the geotectonic setting. The thickness of the Phanerozoic cover in Kuwait and the Partitioned Neutral Zone is estimated to be 8-9 km; the sediments as a whole thicken towards the northeast and do not exhibit any intense deformation (Warsi, 1990). A number of authors have discussed and classified the tectonic framework of the region (Fig. 2-1) (e.g. Beydoun, 1991; Alsharhan and Nairn, 1997). There are three main geotectonic elements in the region, namely the Arabian-Nubian Shield (Section 2.1.1.1), the Arabian Shelf (Section 2.1.1.2) and the mobile-belt (Section 2.1.1.3).

##### **2.1.1.1 The Arabian-Nubian Shield**

The shield, mainly composed of igneous and metamorphic rocks, had a long and complicated history in the Precambrian; it became peneplaned and stabilized as a



craton by the onset of the Palaeozoic. Since the Precambrian the shield has been dry land or temporarily submerged by shallow-water, and has provided a source of terrigenous material for the Ratawi Formation and Zubair Formation. The Arabian Shield was separated from the Nubian Shield by the Red Sea in Neogene time.

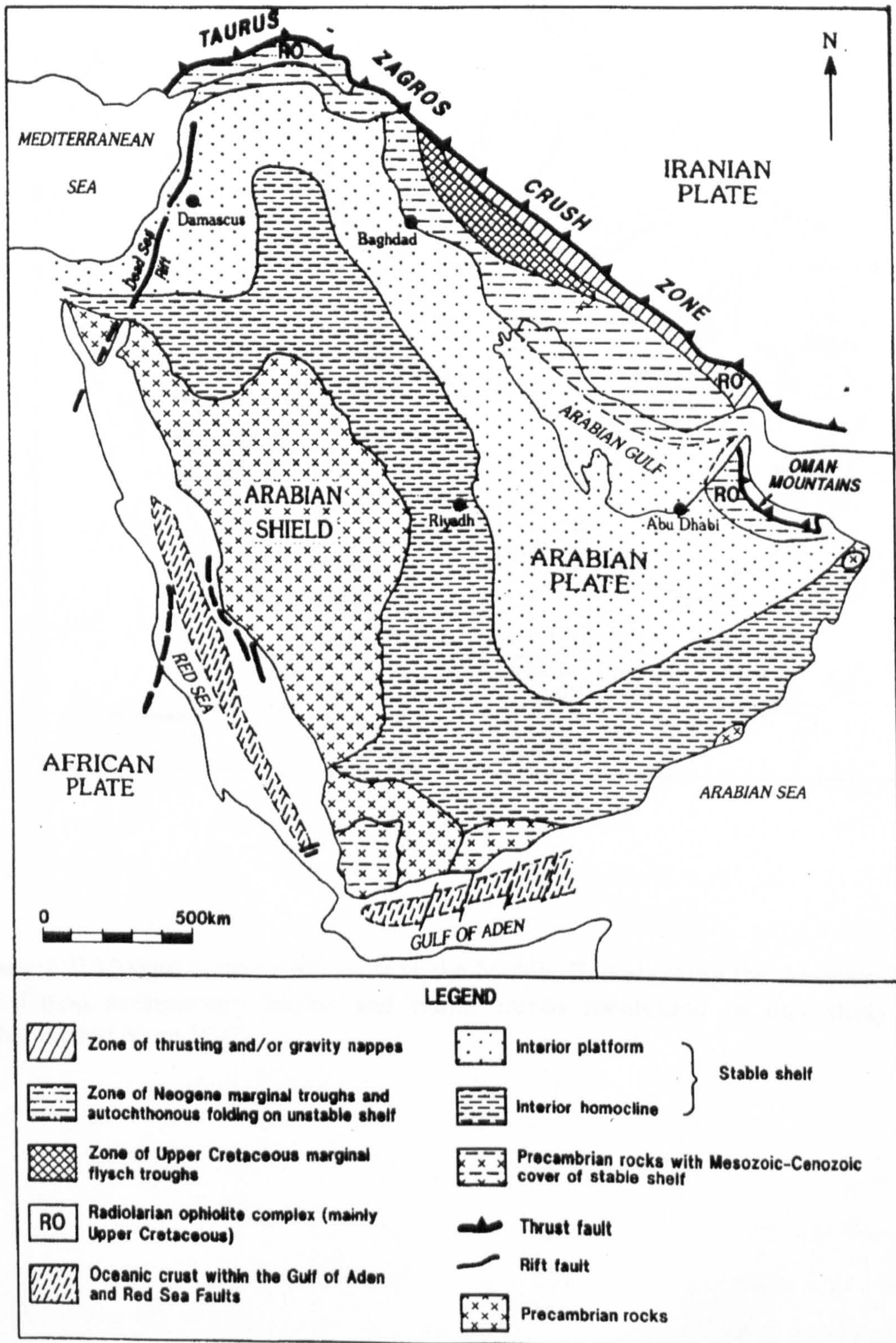


Figure 2-1 Structural elements of the Middle East (after Alsharhan and Nairn, 1997).



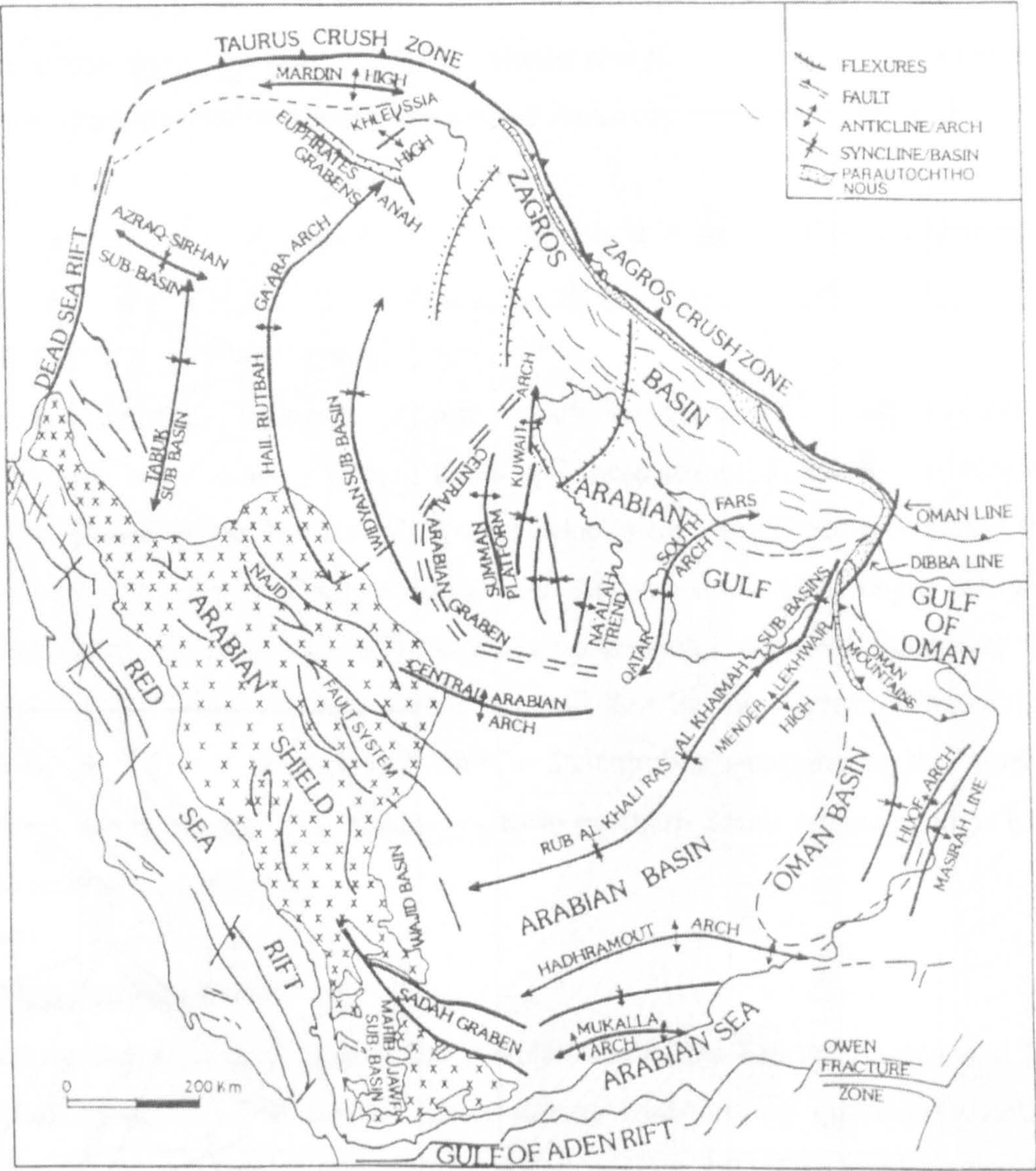


Figure 2.1b) Major tectonic elements in the Middle East showing the Arabian, Zagros and Oman sedimentary basins and major trends mentioned in this study (after Alsharhan and Nairn 1997).



### **2.1.1.2 The Arabian Shelf**

The area to the north and northeast of the shield was formed by slow subsidence and deposition of continental and shallow-marine Palaeozoic sediments. The Arabian Shelf can be divided into:

- (1) The stable shelf or interior homocline, which is a belt of thin continental and shallow-marine sediments surrounding the shield. It is characterized by relatively undisturbed and gently dipping beds.
- (2) The unstable shelf or interior platform, which is to the east of the stable shelf. It is marked by more steeply dipping strata and more irregular dip; this is where the Wafra oilfield in the Partitioned Neutral Zone is located. These are related to the existence of a number of major north-south Arabian folds. Most of the oilfields in the unstable shelf are controlled by this north-south basement lineament trend, including the Wafra oilfield, which is controlled by the Khurais-Wafra-Burgan-Zubair arch (the Kuwait Arch). This is an anticline plunging to the north and extends for more than 500 kilometres from northern Saudi Arabia through Kuwait into southern Iraq.

### **2.1.1.3 The Mobile-Belt**

The belt to the north and east of the Arabian shelf, the Taurus, Zagros and Oman Mountains, consists of sediments folded during mid-Tertiary continental collision, related to the Alpine system and closure of Tethys (Fig. 2-2). This orogeny led to the formation of the Zagros foreland basin and the imposition of the dominant northwest-southeast fold trend (the Zagros trend) on the Arabian Fold trend that developed in pre-Tertiary times. This effect is apparent in the outlines of the oilfields, with the transitional change from one trend to the other (Beydoun *et al.*, 1992).

## **2.1.2 Basement Lineament and Arabian Folds trend**

The basement of Precambrian igneous and metamorphic rocks forming the continental crust of the Arabian Plate, extends from the Arabian Shield across the Arabian Peninsula to the Zagros Mountains in Iran. The basement evolved into a craton during late Precambrian time by the accretion of island arcs and microplates (Stoesser and Camp, 1985). This evolution and consolidation of the basement were through several orogenies, the final Idsas Orogeny (640-620 Ma) created a prominent basement grain direction and shear fracture system. This orogeny uplifted the western part of the



Arabian plate, and folded and thrust-faulted the eastern part of the plate and Iranian platform along a north-south direction (Idsas, Arabian Trend), and was wrenched by conjugate northwest-southeast (Najd-Trend) and northeast-southwest fault systems (Hussein, 1989). The Precambrian basement trends of the Arabian Plate are evident in the overlying Phanerozoic cover rocks. These trends have been subject to later rejuvenation as a result of subsequent plate-margin evolution effecting the lithofacies type, thickness and distribution of the later stratigraphic record. This is evident in the region of the Khurais-Wafra-Burgan-Zubair arch (Kuwait Arch) in the study area (Beydoun, 1991).

The structural province of the Arabian shelf, with the Arabian Fold Trend (north-south), make a large angle with the structural province of the mobile belt, the Zagros Fold Trend (northwest-southeast). The younger Zagros Fold Trend, late Tertiary and younger, was superimposed on the older Arabian fold Trend in the region of the Zagros belt. The Arabian shelf with its Arabian Fold trend occupied the entire Arabian-Iranian basin through long periods of time, from Infracambrian to late Tertiary. This Arabian Fold trend indicates a relative independence of the Arabian shelf from tectonic pressure generated in the Zagros mobile belt (Kamen-Kage, 1970).

Edgell (1996) identified fourteen major Arabian fold lineaments, the significant ones to this study north of the Qatar-Kazerum Arch are: (1) the En Nala Uplift, that has the largest oilfield in the world, the Ghawar oilfield, (2) the Khurais-Wafra-Burgan-Zubair Arch (the Kuwait Arch), where the study area is located, (3) the Rumaila-Minagish Uplift, (4) the Jaham-Ma'aqala-Wariah Uplift, and (5) the Hail-Rutbah-Mosul Arch. Also, he inferred that the geotectonic influence of these uplifts and their intervening depressions extended from the Arabian shelf to the Mobile Belt (the Iranian coast). The Arabian fold trend of the Kuwait Arch provides a north-south alignment over the oilfields of Khurais, Wafra, Burgan, Magwa, Ahmadi, Bahra, Sabriya, Raudhatain and Zubair. These Precambrian basement alignment trends effect the subsequent sedimentary facies and thickness patterns of the Lower Cretaceous Ratawi Formation and its subsequent erosion or preservation.

The basement influenced both the sedimentary facies pattern and structural direction, which in turn controlled the major hydrocarbon occurrences in the Wafra oilfield. The basement trend also controlled the trend of syndepositional movements of the Hormuz salt, which in turn controlled the direction of the Ratawi carbonate ramp, depositional environments, and facies patterns. Also, the uplift of the basement along



the trend controlled the subsequent area of erosion and subaerial diagenesis of the Ratawi Formation. The lithofacies of the Ratawi Oolite and Ratawi Limestone members in the study area change to the Yamama Formation and Buwaib Formation at the outcrops in central Saudi Arabia. A disconformity has been reported from the outcrops between the Yamama and Buwaib formations; the disconformity appears to decrease in time-gap from the outcrops to the study area (Alsharhan and Nairn, 1997).

The inferred mechanism for the growth of the Kuwait Arch since the late Jurassic is the reactivation along the basement lineaments and faults, and mobilization of the Hormuz salt along linear pillows and swells since the Jurassic (Murriss, 1980; Warsi, 1990). Warsi (1990) studied the major geological structures in Kuwait using gravity measurements and interpreted the gravity high that extends north-south for 175 kilometres in eastern Kuwait (the Kuwait Arch) as basement relief. Also, he inferred that the arch was an anticlinal structure plunging northwards, extending up to the Zubair field in southern Iraq. In addition to geophysical data, well data support the northward-plunging structure of the Kuwait Arch; the top of the Zubair Formation in the Burgan oilfield is at 1.6 km depth whereas in the Zubair oilfield it is at 3.2 km. He interpreted the partial or full closure of the gravity field over the Wafra, Burgan and Bahra oilfields, and over Kuwait City, as indicating the presence of a significant subsurface domal structure.

Bou Rabee (1996) studied the tectonic and depositional history of Kuwait using subsidence curves and seismic reflection data. The subsidence curves showed that Kuwait and the study area underwent rapid subsidence from the Upper Carboniferous (300 Ma) to Middle Eocene (52 Ma). This rapid subsidence was interrupted by a decrease in rate of subsidence during the Middle Cretaceous, 97.5 Ma, due to the development of the unconformity between the Wasia and Aruma groups. Bou Rabee (1996) constructed a series of structure contour maps on the top seismic reflector of the Minjur Formation (Upper Triassic), Hith Formation (Upper Jurassic), Ahmadi Formation (Middle Cretaceous) and Rus Formation (Early Tertiary) and presented a series of isopach maps between these intervals. These maps show thinning of the formations over the Kuwait Arch (Burgan structure) and the other structures of the "Arabian Folds" in Kuwait and the Partitioned Neutral Zone. This supports the suggestion that the structures became active as early as the Jurassic.



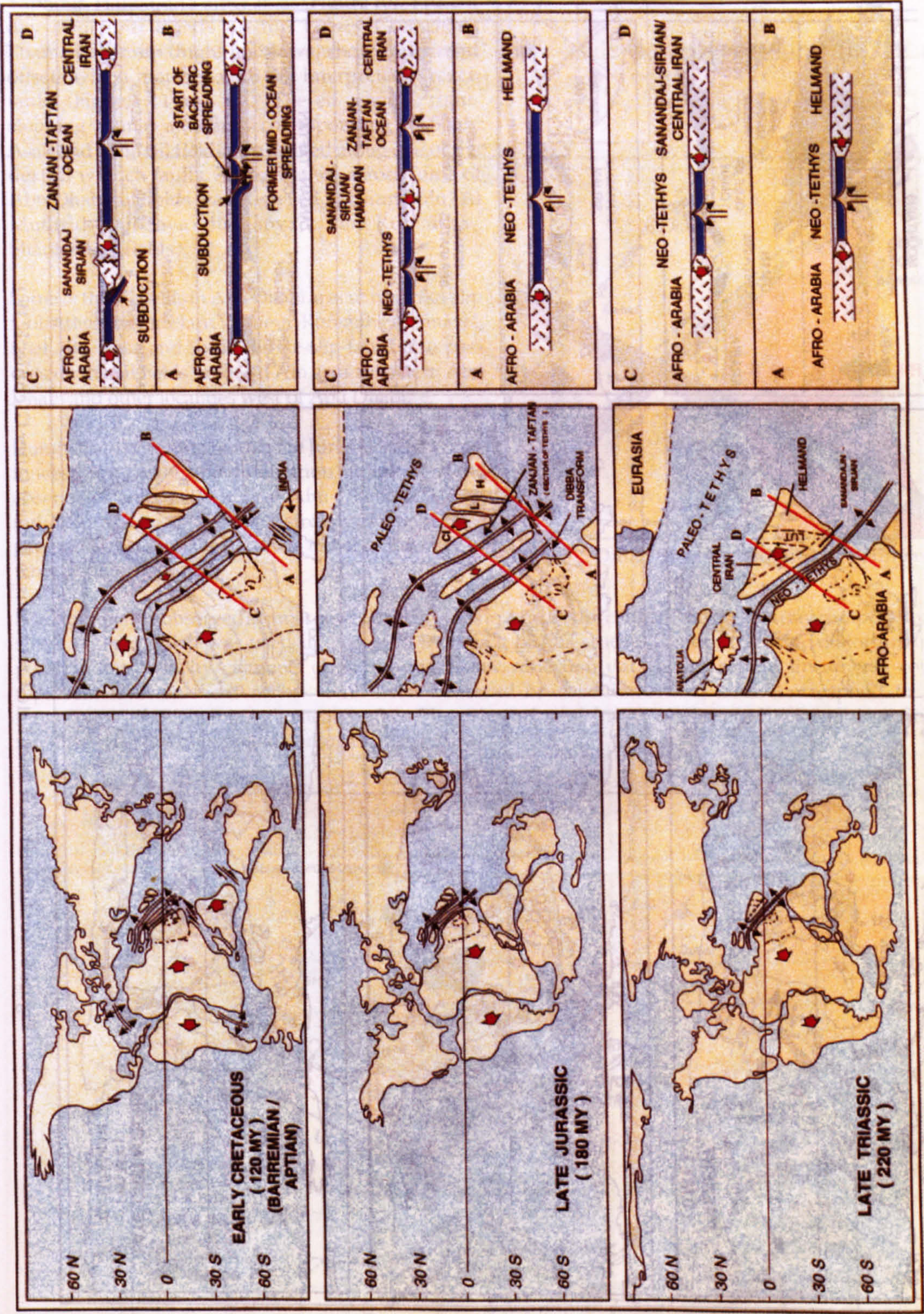
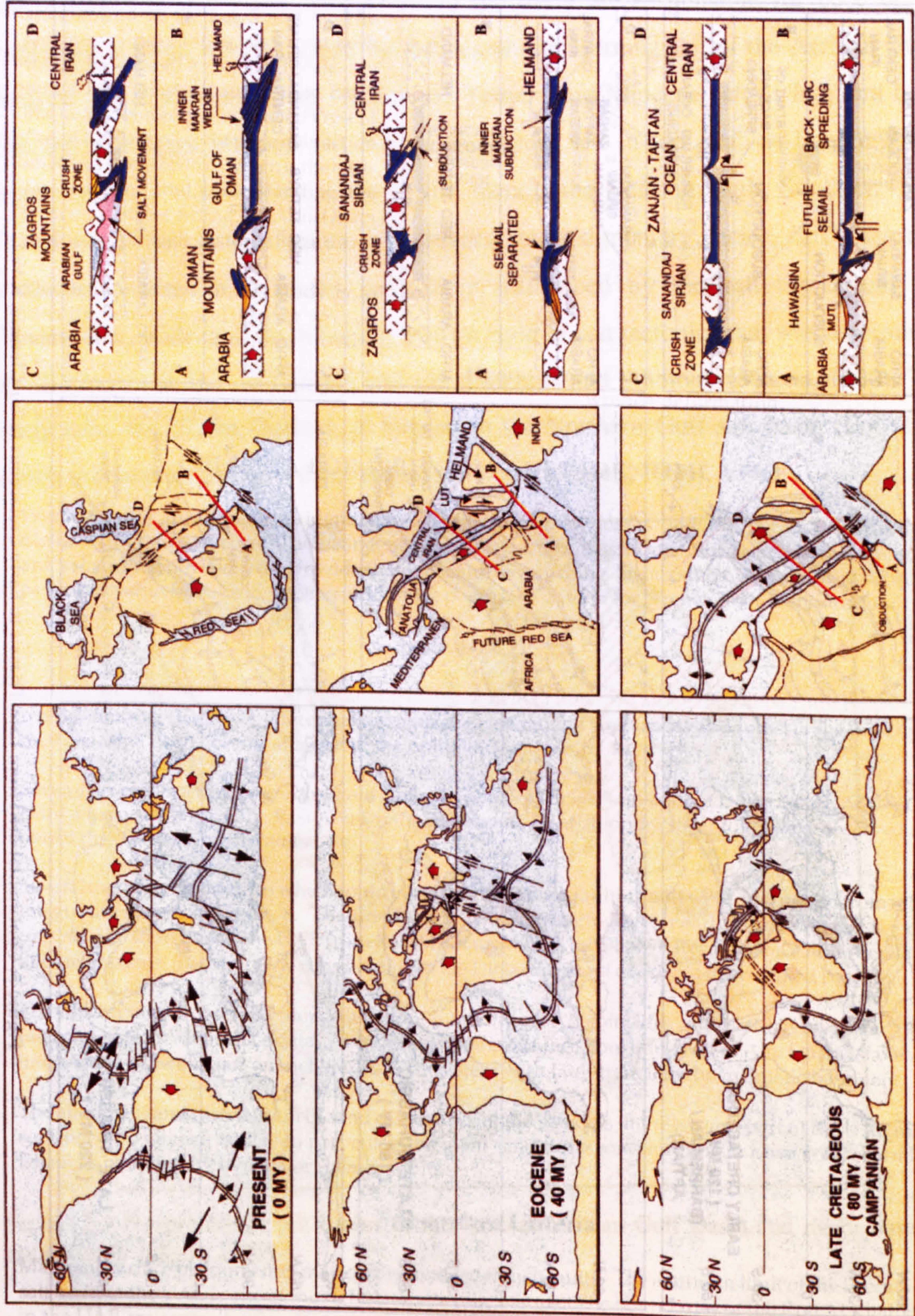


Figure 2-2 Plate movements and large-scale palaeogeography from late-Triassic to Early Cretaceous (after Marzouk and El Stattar, 1994)



Figure 2-2 continued plate movements and large-scale palaeogeography from Late Cretaceous to Present day (after Marzouk and El Stattar, 1994)





### 2.1.3 Hormuz Salt

According to Edgell (1996) the Arabian-Iranian Basin is the largest basin with active salt tectonics in the world. Evaporites in the basin are responsible for 60% of its hydrocarbon traps, which include the Infracambrian Hormuz salt of the Arabian Gulf, Jurassic salt of Kuwait, Saudi Arabia and Yemen, and Miocene salt of Iraq and Iran. The Infracambrian Hormuz salt and its equivalent salt in the Arabian-Iranian Basin were deposited in four distinct salt basins, namely the Northern Gulf, Southern Gulf, Fahud and Dhufar-Ghar basins. The subsequent sedimentary facies, thickness and structure in these four basins have been influenced by the salt throughout the Phanerozoic, with each basin having its own style of salt tectonics that was determined by differences in the overburden and salt thickness and lithology (Murriss, 1980). The study area, the Wafra Oilfield, is located in the Northern Gulf salt basin (Fig. 2-3), which is characterized by a deep-seated salt dome (Edgell, 1996).

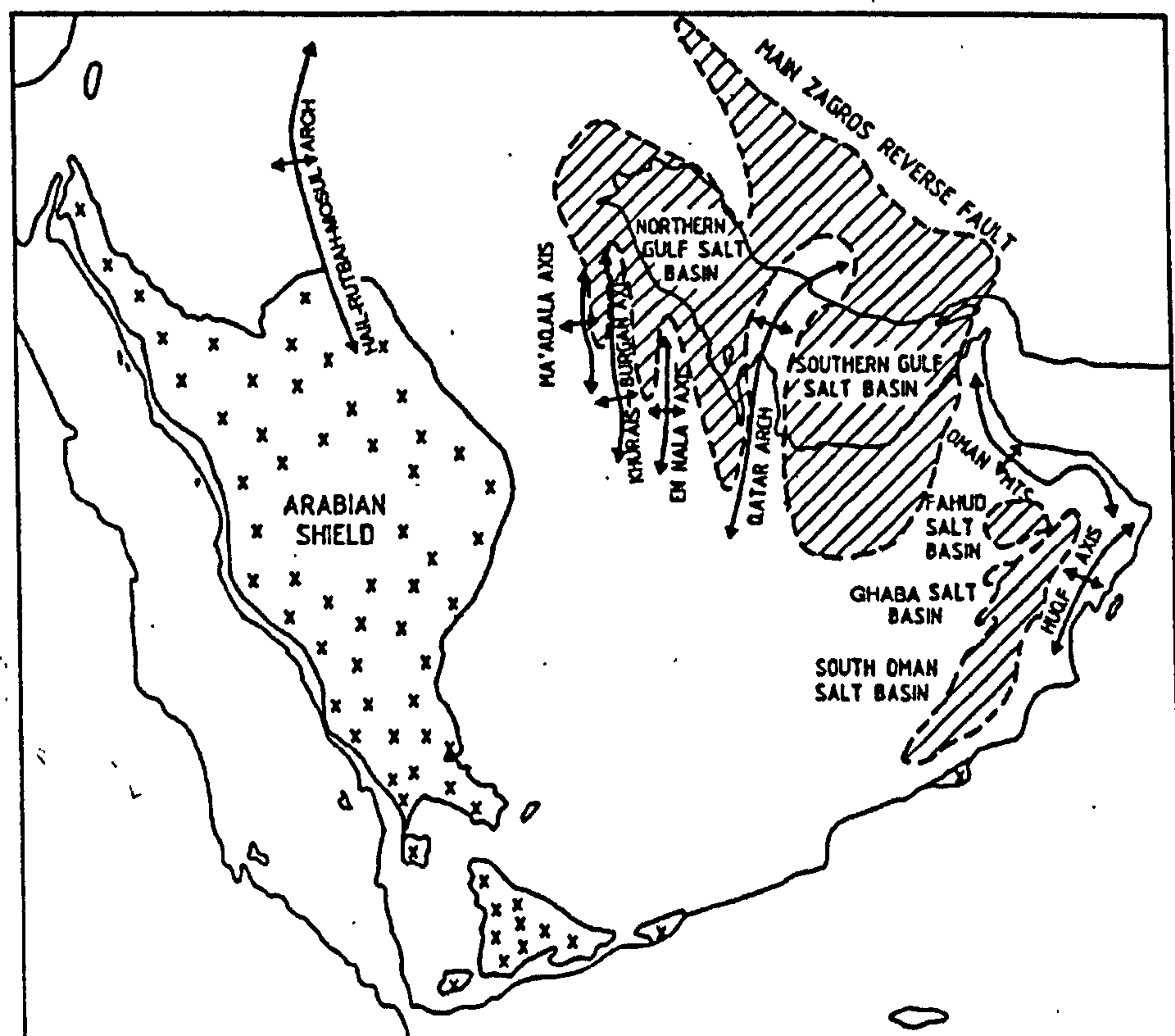


Figure 2-3 Neoproterozoic salt basins of the Arabian-Persian Gulf Basin and major basement uplifts (after Edgell, 1996).

The Infracambrian and Lower Cambrian Hormuz Formation of the Arabian Gulf and its equivalent the Ara Formation of south Oman, the Rava Formation of central Iran and the Salt Range Formation in Pakistan, were precipitated in rift basins



formed during the extensional part of a major tectonic cycle. According to Hussein (1988, 1989) this tectonic cycle on the Arabian Plate started with accretion and collision (about 720 to 620 Ma), followed by rifting and extension (about 620 to 450 Ma). By the end of the Cambrian and early Ordovician, the Arabian Plate was a peneplaned stable margin of Gondwanaland.

#### **2.1.4 Syndepositional structural growth of the Arabian Folds**

There are three different theories for the origin and structure of the north-south Arabian fold trend, which is distinctly different from the other major trends in the region, notably the northwest-southeast Najd or Zagros fold trend. These were reviewed by Warsi (1990) and are:

- (1) As compressional features, but it is difficult to explain the rapid growth of the arches (Arabian folds) during extension and subsidence of the northeastern Arabian continental margin during Late Jurassic through Middle Cretaceous.
- (2) As differential compaction structures, but the differential compaction within the sedimentary cover over a buried passive relief is insufficient to explain the growth of the arches.
- (3) As structural growth by a combination of movement of the Infracambrian and Lower Cambrian Hormuz salt along linear pillows and swells and basement reactivation along pre-existing faults.

Hormuz salt is inferred to have started to rise during the Jurassic or Early Cretaceous times causing thickness and depositional facies changes around the structures (Arabian folds) in the Arabian-Iranian Basin. Talbot and Alavi (1996) mentioned three different mechanisms, which may have triggered the Hormuz salt structures, which are:

- (1) Closing of the Palaeo-Tethys Sea during the Jurassic.
- (2) Opening and closure of the northeast-trending Oman basin with its foredeep parallel to the Oman line, and
- (3) Rift and drift of Neo-Tethys at some time between the Permian and earliest Cretaceous time.

#### **2.2 Mesozoic Geological History**

Throughout the Palaeozoic the Arabian Plate, which accommodated the Arabian-Iranian basin and the study area of the Partitioned Neutral Zone (PNZ), was attached to

Africa with the Turkish and Iranian continental blocks constituting the northern passive margin of Gondwana (Fig. 2-2). The study area (PNZ) was located in middle to high latitudes in the Southern Hemisphere and clastic sedimentation was dominant. The region during the Palaeozoic was characterized by epeirogenic tectonic movements (Murris 1980; Bou Rabee, 1996). During the middle Permian and Triassic to Jurassic, extension and rifting separated the Cimmerian, Turkish and Iranian continental blocks, from the northern and northeastern part of the Arabian Plate of Gondwana. These processes gave rise to the “Arabian Promontory” and a new ocean, the Southern Tethys (Neo-Tethys), along the line of the later Zagros suture (Beydoun, 1998).

This led to formation of the Arabian-Iranian basin as an extensive continental shelf, the Arabian shelf, at the passive margin of Neo-Tethys. The Arabian shelf during Triassic to late Cretaceous time was characterized by slow, steady subsidence that allowed deposition of shallow-marine sheet-like sediments on an extraordinarily wide epeiric sea more than 2000 km long (northwest to southeast) and almost 2000 km wide from the shelf break to the shield. A number of intrashelf basins that have different sizes and duration developed on the Arabian Plate by differential subsidence and sedimentation. The Gotnia / Garau basin is the largest of these intrashelf basins and formed at the edge of the Arabian Platform, as a result of extensional tectonics (Beydoun *et al.*, 1992). The study area is located at the margin of the intracratonic Gotnia basin adjacent to the Arabian Shelf.

During the Mesozoic the Arabian shelf was located in tropical latitudes and dominated by carbonate deposition with shorter intervals of marls, argillaceous carbonates and shales, and subordinate evaporites. During the early and middle Cretaceous, deltas carried continental clastics over the inner Arabian shelf, derived from the Arabian shield, and interfingered to the east with marine clastics and carbonates (Beydoun *et al.*, 1992).

With the closing of the Neo-Tethys sea towards the end of the Cretaceous (Turonian to end-Campanian early-Maastrichtian time) oceanic sedimentary prisms and ophiolite masses were overthrust onto the leading edge of the Arabian shelf from northwestern Syria to Oman. These tectonic movements gave rise to epeirogenic movements in the shelf interior including the study area (PNZ). Collision between the Arabian Plate and Eurasia along the Zagros line during mid-Tertiary time resulted in late Neogene suturing and overprinting of the Zagros foreland basin onto the outer



edge of the northeastern Arabian margin. This led to compressional structures in northwest Iraq and southwest Iran and further epeirogenesis in the study area (PNZ) with reactivation of fault blocks (Murris, 1980; Bou Rabee, 1996).

The geological history of the Mesozoic in the study area (PNZ) is discussed under five headings, namely the development of the Arabian shelf during the late Jurassic and Cretaceous times (Section 2.2.1), the Lower Cretaceous Thamama Group (Section 2.2.2), boundaries of Thamama Group (Section 2.2.3), controlling processes of the Thamama Group deposition and cyclicity (Section 2.2.4) and the Gotnia / Garau intrashelf basins (Section 2.2.5).

### **2.2.1 Development of the Arabian shelf during the late Jurassic and Cretaceous times**

The Cretaceous succession of the Arabian-Iranian basin is divided into three groups by three regional unconformities that record erosion or non-deposition, during middle Aptian, Turonian, and Tertiary times. A regional unconformity at the Jurassic-Cretaceous boundary has not been recognized. The three groups are lower Thamama (Berriasian through early Aptian) approximately 2000 ft (610 m) thick and a time span of nearly 30 m.y., middle Wasia (late Aptian through Turonian) approximately 2000 ft (610 m) thick and a time span of nearly 21 m.y. and upper Aruma (Coniacian through Maastrichtian) commonly 1500 to 3000 ft (457 to 914 m) thick and a time span of nearly 24 m.y. The three Cretaceous groups of the Arabian-Iranian basin and their confining unconformities seem to be correlative over the entire southern margin of Tethys from Syria, Turkey, Lebanon, Egypt, northern Libya and possibly Morocco (Harris *et al.*, 1984).

Harris *et al.* (1984) constructed palaeodepth curves for the Arabian Peninsula from lithostratigraphic and biostratigraphic data and interpreted the Cretaceous strata between the regional unconformities. Each of the three depositional cycles in the curve has its own characteristic features. The upper group represents the most extensive regression of the sea, whereas the middle group appears to have been a major transgression onto the craton. The lower group, that includes the Ratawi Formation, has an intermediate position.

The maximum extent of shallow-marine carbonate deposition on the Arabian Shelf was during the Lower and Middle Cretaceous, the Thamama and Wasia groups. <sup>Which?</sup> This phase of the stratigraphic evolution of the shelf succeeded the extensive Upper



Jurassic evaporative conditions of the Hith Formation across the Arabian platform and deep-water evaporative conditions of the Gotnia Formation in the Gotnia / Garau intrashelf basins. The latter phase followed the extensive peritidal conditions of the Arab Formation on the platform and the evaporative conditions of the Gotnia Formation in the intrashelf basins. The phase of maximum carbonate deposition was terminated in the Upper Cretaceous by the clastic Aruma Group in a foreland basin setting (Murris, 1980).

Pratt and Smewing (1993 a, b) suggested that the stratigraphic evolution of the Arabian platform in northeastern Oman during the deposition of Thamama and Wasia groups was controlled by three drowning events. These events marked the advance and retreat of Cretaceous shallow-water carbonate facies on the Arabian platform and intrashelf basin when the two major shallowing cycles (or sequences) of the Thamama and Wasia groups were deposited. Each drowning event led to a reduction of the shallow-water carbonate generating capacity of the Arabian platform and this was recorded as an abrupt change from shallow-water facies to deep-water facies. After diminishing the effect of the drowning process, shallow-water carbonate platform environments re-established themselves over the Arabian platform and deposited shallowing-upward cycles.

The three drowning events on the Arabian shelf were broadly synchronous with others around Neo-Tethys. The main control on these regional drowning events in northeastern Oman is not only the response to eustatic sea-level change (Alsharhan and Kendall, 1991), but also a response to sedimentological and tectonic processes, related to the configuration of the Arabian shelf-margin (Pratt and Smewing, 1993 a, b). In the concept of sequence stratigraphy, these drowning events are genetic surfaces (i.e. time surfaces), that define genetic units or time-rock units, which are the shallowing-upward depositional cycles. Each depositional cycle represents a transgressive and regressive stratigraphic sequence that records onlap and offlap of the lithological belts and depositional environments across the Arabian platform and intrashelf basins.

Each cycle of Thamama, Wasia and Aruma groups represents one genetic time rock-unit, and represents a shallowing-upward cycle of a major transgression and regression rhythm. Each of these three cycles formed under similar related processes of sediment supply, tectonics, eustasy and palaeogeography. Understanding the development of these processes in space and time provides insight for the



interpretation and prediction of the hydrocarbon system of the Ratawi Formation. Aigner *et al.* (1990) compared these cycles to the “sequences” of Sloss (1963), “supercycles” of Vail *et al.* (1977) and “second-order sequences” of Haq *et al.* (1988).

According to Yousif and Nouman (1997), new data and interpretations from a number of deep wells during the 1980s mark a revolution in the existing concepts for the Jurassic-Cretaceous succession in Kuwait and the study area (PNZ). These data showed that the Cretaceous strata underwent inversion with respect to the Jurassic succession. This was due to the reactivation of basement arches and the deposition of shallow-water facies during the Cretaceous, in sites of deep-water Jurassic sedimentation in the Gotnia Basin. The Cretaceous reactivation of basement arches is due to the changing convergence direction between the Arabian and Eurasian plates, which reactivated structures that first originated during the Infracambrian, Caledonian and Hercynian tectonic events.

The southern part of the Arabian shelf in northeastern Oman records rifting and development of a passive margin facing Neo-Tethys from the Middle Permian to the Middle Cretaceous. The Sahtan, Kahmah (Thamama) and Wasia Groups were deposited during the maximum extent of the broad epicontinental sea landward of the margin during the Upper Jurassic to Lower and Middle Cretaceous. These groups correlate with the groups in the study area and with the other principal hydrocarbon reservoirs in the Upper Jurassic and Lower and Middle Cretaceous strata of the Arabian Peninsula (Pratt and Smewing, 1993 a, b). The factors affecting the configuration and evolution of the edge of the Arabian passive margin in northeastern Oman during sedimentation of the Lower Cretaceous Kahmah (Thamama) Group would also have affected sedimentation of the Ratawi Formation in the platform interior (Murris, 1980; Beydoun, 1991).

Pratt and Smewing (1990, 1993 a, b) identified and interpreted three regional drowning events in the Upper Jurassic and Lower and Middle Cretaceous strata in the southern Arabian margin of northeastern Oman, which can be correlated with those recognized in the study area. They suggested that these drowning events (the beginning of each shallowing-upward cycle) were independent of eustatic sea-level change and are tectonically controlled. Shallow-water carbonate environments re-established themselves in the area each time after the drowning process diminished. The first regional drowning event occurred close to the Jurassic-Cretaceous boundary and was recorded in the central Oman Mountains and adjacent subsurface. The second

repeat from over



regional drowning event occurred in the late Aptian and is recorded in Jebel Akhdar. However, this event is not recorded in the east Saih Hatat area, which records a single regressive, shallowing-upward sequence, that changes to a prograding shallow-water carbonate platform during the Cenomanian to Turonian time. The third regional drowning event occurred in the Turonian and is also recorded at Jebel Akhdar.

Pratt and Smewing (1993 a, b) compared the Arabian shelf eustatic and relative sea-level changes of Haq *et al.* (1988), Harris *et al.* (1984), Scott (1988), and Alsharhan and Nairn (1988) with the Lower and Middle Cretaceous Kahmah (Thamama) and Wasia Groups of northeastern Oman. They showed that there was strong disagreement between these Lower and Middle Cretaceous eustatic and relative sea-level change curves on the Arabian platform. However, all curves show a world-wide, long-term rise in sea level through the Albian. Also the Arabian Shield was undergoing some tectonic movements during the Albian (Alsharhan and Nairn, 1988). Pratt and Smewing (1993 a, b) concluded that the large-scale evolution of the southern part of the Arabian shelf in northeastern Oman during the deposition of the Lower and Middle Cretaceous Kahmah (Thamama) and Wasia Groups was primarily driven by tectonic and sedimentological processes. They suggested that the three Cretaceous drowning events at the beginning of the Thamama, Wasia and Aruma Groups, could be explained as consequences of the tectonic behaviour of the Arabian platform and environmental change, and appeared to be independent of eustatic sea level.

The first regional drowning event could have been caused by compression along the southeastern side of the Arabian shelf margin by obduction of oceanic crust, the Masirah ophiolite, that lead to flexure and / or reactivation of rift blocks as part of a westward tilting of the Arabian shelf (Murriss, 1980). This lead to synsedimentary normal faulting during the Middle Jurassic in Oman followed by uplift of up to 300 metres and erosion during the Upper Jurassic. The hinge line of Arabian shelf tilting was the site of shoaling and deposition of the Upper Jurassic Asab Oolite in the UAE that may have led to restriction on the Arabian platform. The tectonic event induced a relative sea-level stillstand and reduced subsidence. Under the arid conditions of the Upper Jurassic these processes lead to widespread evaporative conditions on the Arabian platform interior and the deposition of the Hith Anhydrite and Gotnia Salt Formations, which are partly equivalent to the Lower Cretaceous Rayda Formation in Oman (Fig. 2-4). The Hith Formation is approximately coeval and could be related to the Tithonian regression across Europe (Pratt and Smewing, 1993 a, b) which is the



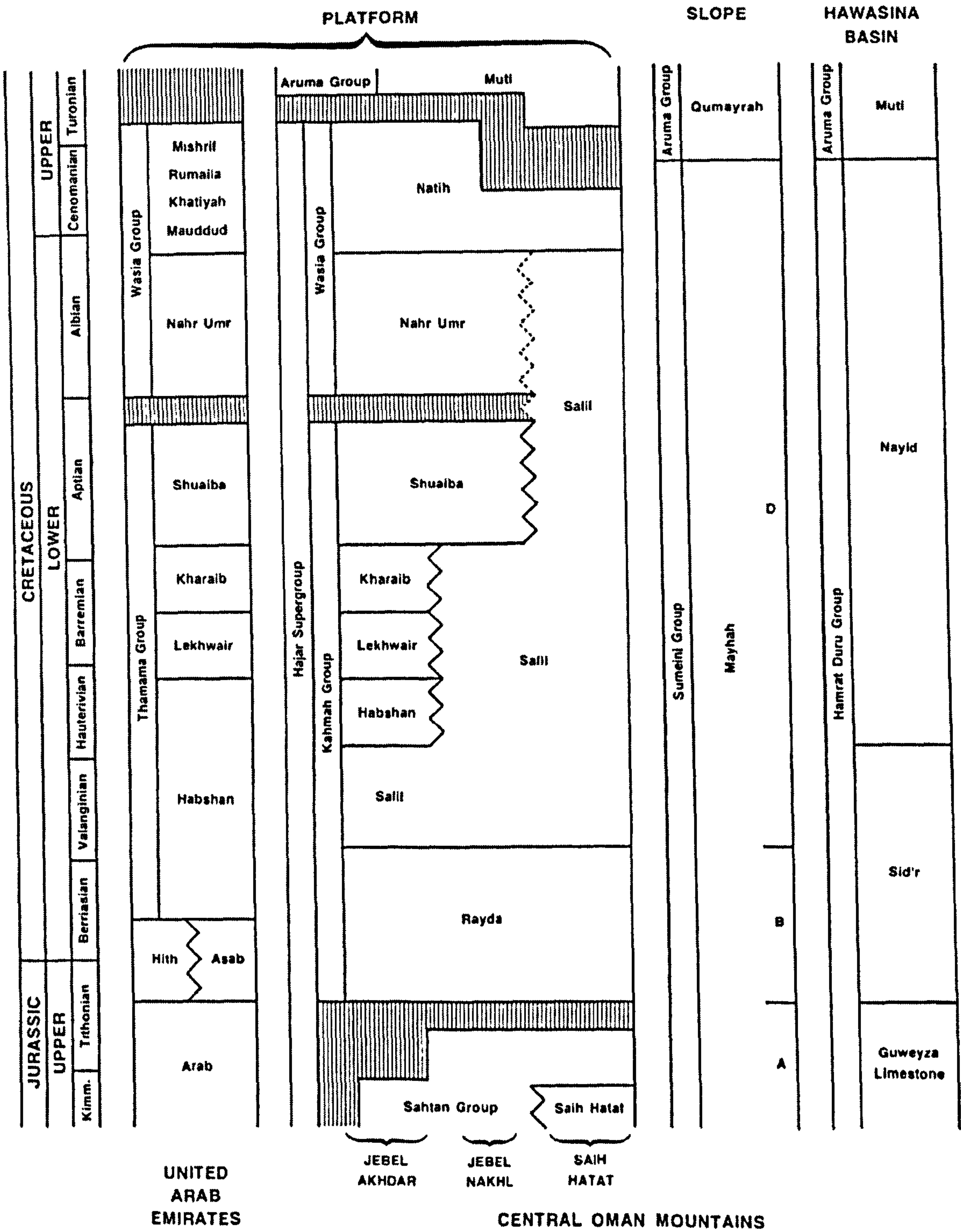


Figure 2-4 Uppermost Jurassic to lowest Upper Cretaceous stratigraphic units of eastern Arabian platform (U.A.E. and Oman) and adjacent slope and Hawasina basin preserved in obducted thrust slices, originally deposited to northeast of Oman Mountains (after Pratt and Smewing, 1993).



regressive phase of the 1<sup>st</sup> order sub-cycle, the “North Sea cycle”, in Europe (Jacquin and Graciansky, 1998).

The uplift was terminated around the Jurassic-Cretaceous boundary and followed by the first regional drowning event on the Arabian shelf that can be correlated with the start of the 1<sup>st</sup> order sub-cycle, the “North Atlantic cycle”, in Europe (Jacquin and Graciansky, 1998) and the deposition of the Lower Cretaceous Makhul (Sulaiy) Formation in the study area. Pratt and Smewing (1993 a, b) argued that the subsidence rate for the Arabian platform was slow during the deposition of the Hith Formation and Rayda (Makhul) Formation after the marginal rift blocks had downwarped to below storm wave base. In addition, the succession of Arab-Hith and Asab-Habshan records no major change in water depth. Therefore the first regional drowning event, at the onset of the Thamama Group, could be explained as a consequence of tectonic processes and not to the eustatic rise in sea level theory of Scott (1990).

The Rayda Formation in Oman represents “Maiolica facies”, which was generated when oceanic waters penetrated sediment starved Upper Jurassic and Lower Cretaceous Neo-Tethys platforms. The upper part of Rayda Formation in northeastern Oman can be correlated with the lower part of the Makhul (Sulaiy) Formation in the study area. After the drowning, the rate of carbonate sediment production exceeded the rate of accommodation space creation and the Arabian platform in northern Oman gradually <sup>accumulated</sup> filled up with sediment and prograded to the northeast. This can be seen in shoal-water oolitic and reefal facies of the Habshan Formation (Pratt and Smewing, 1993 a, b). The Habshan Formation can be correlated with the lower and middle member of the Ratawi Formation (the Ratawi Oolite and the Ratawi Limestone) in the study area (PNZ).

After a brief late Aptian episode of sea-level fall and the formation of a regional unconformity above the Thamama Group (Harris *et al.*, 1984), the second regional ‘drowning’ event occurred by detrital influx and environmental change, which lead to the deposition of the Middle Cretaceous Nahr Umr Formation (Wasia Group). This event could have been caused by eastward tilting of the Arabian shelf that exposed the western side to erosion. Pratt and Smewing (1993 a, b) suggested the model of Mountain and Prell (1990) of shifting oceanic plates off the northern or eastern margin of the Arabian Plate to explain the second regional drowning event. The movement of the oceanic plates lead to a tectonic change in the southern part of



the Arabian platform in northeastern Oman from passive continental margin to a transcurrent plate boundary during the Upper Cretaceous. The second regional drowning event does not occur in the east Saih Hatat area, Oman, due to subaerial exposure in that area. The third regional drowning event that terminated carbonate deposition of the Middle Cretaceous Wasia Group was caused by convergence of oceanic crust and the formation of a foreland basin.

The evolution of the palaeogeography during the Early Cretaceous was influenced by global tectonic movements around Neo-Tethys. Jadoul *et al.* (1998) reported that the Early Cretaceous stratigraphic evolution of South Tibet is similar to that of offshore northwest Australia. Both areas show a similar Early Cretaceous palaeogeographic evolution of the passive margin along the southern edge of Neo-Tethys. He related the magmatic episode which began during the Kimmeridgian / early Tithonian and lasted until Aptian times to global tectonics around Neo-Tethys and the detachment of India from Gondwanaland. This could support Pratt and Smewing (1993 a, b)'s suggestion that the first and second regional drowning events on the Arabian platform during Tithonian and Aptian times were related to shifting oceanic plates off the northern or eastern margin of the Arabian Plate.

### **2.2.2 Lower Cretaceous Thamama Group**

The Lower Cretaceous Thamama Group accumulated during a period of extensive flooding of the Arabian Peninsula. The group is a succession of shallowing-upward cycles produced by major transgressions and regressions across the Arabian shelf and intrashelf basins. The study area (PNZ) during deposition of the Ratawi Oolite member, in lower and middle Valanginian time, was a shallow carbonate shelf close to the boundary between the Arabian Shelf and the Gotnia / Garau intrashelf basin (Murris, 1980; Longacre and Ginger, 1988). Tectonics, sea-level fluctuations, sediment supply and palaeogeography influenced the stratigraphic succession of the Ratawi Formation. The regional facies variation of the Thamama Group, both vertically and laterally, can be understood in terms of the migration of predominantly shallow-water carbonate facies belts across the Arabian shelf (Alsharhan and Nairn, 1986) and in the filling of the deep-water Gotnia intrashelf basin.

There is a drastic environmental change from the Upper Jurassic into the Thamama group of the Lower Cretaceous. The arid environmental conditions that produced evaporites and carbonates during the Upper Jurassic were replaced by a



warm and more humid climate during which carbonates and siliciclastics of the Thamama group were deposited as the African-Arabian plate drifted northward to more equatorial latitudes (Bordenave ~~et al.~~, 1994). Alsharhan and Nairn (1986) correlated the Thamama Group across the Arabian Peninsula and they recognized two carbonate cycles, which are the two shallowing-upward cycles of Scott (1990) in south-eastern Arabia. During the second cycle there was increasing detrital influx in the northern part of the basin in the study area. Alsharhan and Nairn (1986) argued that the increase of siliciclastics and shallowing-upward trend in the second carbonate cycle in the northern part of the basin were due to the eastward tilting of the Arabian Plate and not due to eustatic sea-level change. Also, this tectonic tilting of the Arabian Plate may be the process that lead to transgression and infill of the deep-water intrashelf Gotnia basin in Kuwait, the Partitioned Neutral Zone, and the southern Iraq to northeastern Iran area (the Dezful Embayment of the Lurestan basin) towards the end of the lower Cretaceous Thamama Group.

### **2.2.3 Boundaries of Thamama Group**

The Lower Cretaceous Thamama Group in the study area (PNZ) is characterized by two cycles. The first cycle, during the early Lower Cretaceous (Berriasian and Valanginian age), includes the Makhul Formation (or Sulaiy Formation) and Ratawi Oolite member (or Minagish Formation in Kuwait and Yamama Formation in Saudi Arabia) (Fig. 2-5). The shallow-water facies of the Ratawi Oolite member were laid down on a shallow-marine ramp on the Arabian shelf, which dipped gently to the east. The Makhul Formation and its equivalents the Gadvan and Garau Formations to the northeast were deposited in the intrashelf Gotnia basin (Murriss, 1980; Alsharhan and Nairn, 1986).

The second cycle of the Thamama Group, deposited during the later Lower Cretaceous (Hauterivian, Barremian and Aptian), is distinguished from the first by the invasion of a clastic wedge from the northwest and the deposition of the sediments of the Ratawi Limestone, Ratawi Shale and Zubair Formation in the study area (or Buwaib and Biyadh Formations in Saudi Arabia). This lead to displacement of the shallow-water carbonate facies of the Lekhair and Kharaib Formations (equivalent to Ratawi Shale member and Zubair Formation) eastward and southward. During this time, the intrashelf Gotnia basin was infilled by detrital sediments (Ratawi Shale and Zubair Formation) from the west and the deeper-water Gadvan and Garau Formations



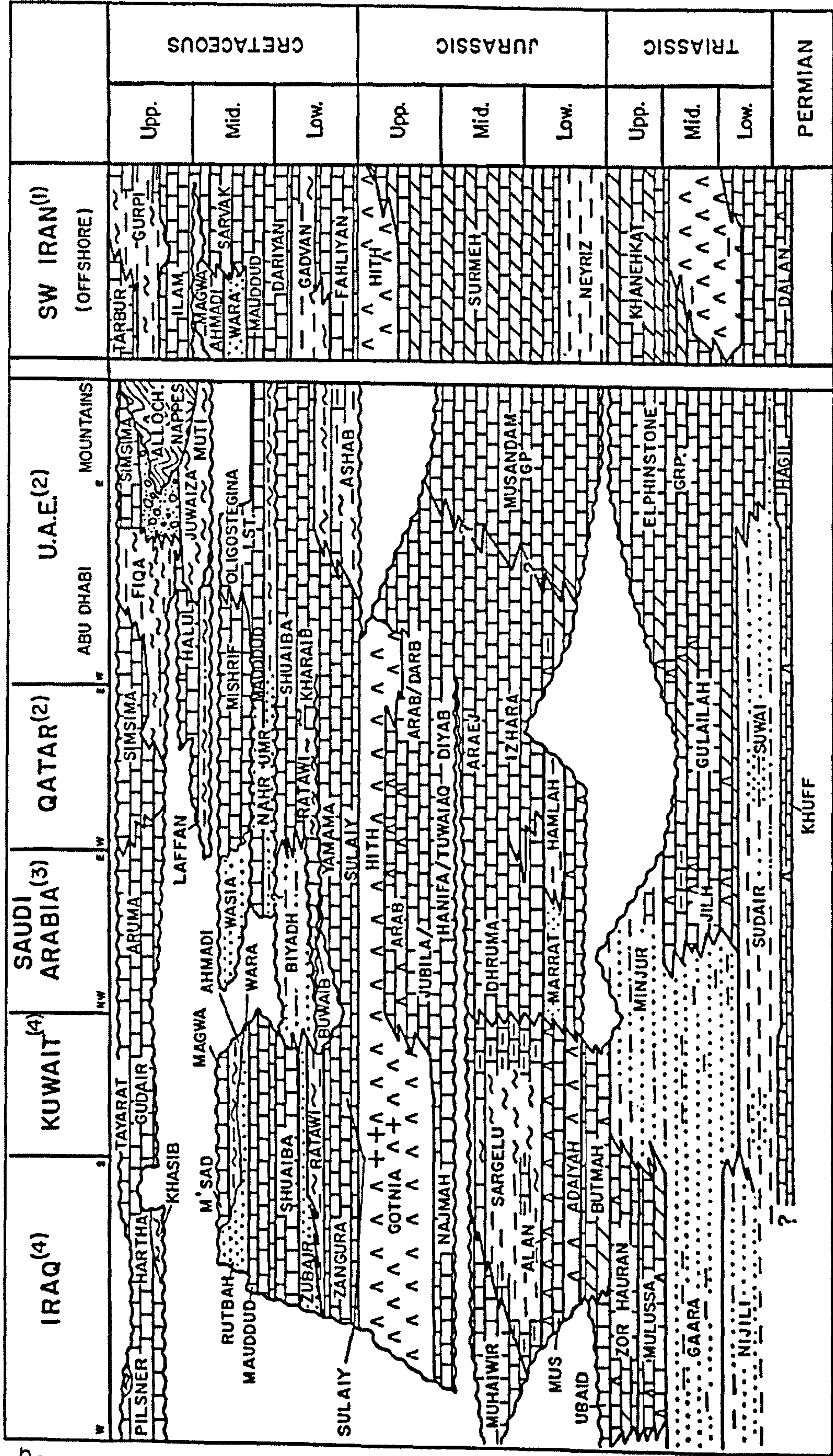
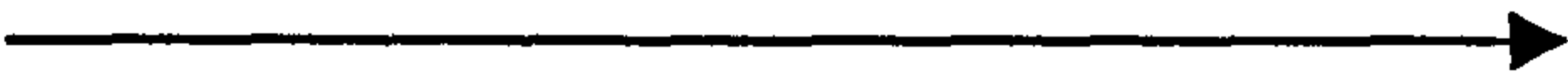


Figure 2-5 Lithostratigraphy correlation chart of the Mesozoic formations in Saudi Arabia, Kuwait, Iraq and UAE (after Beydoun, 1991).



Figure 2-5B) Lithostratigraphic correlation chart of the Cretaceous formations in the subsurface of Iraq, Kuwait, Saudi Arabia, Bahrain, Qatar and U.A.E. (after Alsharhan, A.S. & Nairn, A.E.M. 1997)





[illegible]



were displaced eastwards (Murriss, 1980; Alsharhan and Nairn, 1986)

At the maximum extent of the clastic wedge of the second cycle of the Thamama Group, clastics spread from the northwest into the central part of the Arabian platform, in the Qatar area, where they are represented by the basal Ratawi Shale. However, in the area to the south of Qatar in the United Arab Emirates, detrital, argillaceous material of the Zakum Member of the Lekhwair Formation does not appear to be directly related to the northwest detrital influx from Central Arabia. The presence of this detrital material is probably related to minor movements and erosion of uplifted areas along the Arabian Fold trend of the Qatar-Kazerum Arch. During the Aptian time, near the end of the second cycle, shallow-water carbonate settings of the Shuaiba Formation were re-established over most of the Arabian Shelf (Shebl and Alsharhan, 1994), terminating the deep-water environment of the intrashelf Gotnia basin in the study area.

The two cycles of the Thamama Group are separated by an unconformity formed during the Valanginian-Hauterivian, indicating a period of erosion and / or non-deposition. In the study area, this surface is between the Ratawi Oolite and Ratawi Limestone. The characteristics of the unconformity surface change from the northern to southern part of the Arabian Shelf. In the northern part the unconformity has been described from the outcrops in central Saudi Arabia as a disconformity with only a slight interruption in deposition between the Yamama Formation (Ratawi Oolite member) and the Buwaib Formation (Ratawi Limestone member) (Shebl and Alsharhan, 1994). In the southern part of the Arabian Shelf in Oman it has been described as a minor unconformity in the Habshan Formation (Ratawi Oolite member) where it onlaps the Jurassic of the Huqf arch and it does not appear in the Salil-Habshan succession of the central Oman Mountains (Pratt and Smewing, 1993 a, b).

Sadooni (1993) studied the Ratawi hydrocarbon system in southern Iraq. The Ratawi lithofacies there are controlled by tectonic processes on two scales, at the regional scale by the stable Arabian Platform and unstable zone of the Mesopotamian Gotnia basin, and at the local scale by growth of syndepositional structures. The Ratawi Formation was deposited in a setting that changed from an inner to outer ramp. The reservoir facies of the Ratawi Formation were deposited in a high-energy environment on the hinge-line separating the shallow-water Arabian Platform from the deep-water Gotnia basin and at the crestal area of the growing structures (Arabian folds). The seal facies were deposited in a low-energy, outer-ramp, deeper-water



environment.

The lower boundary of the Lower Cretaceous Thamama Group with the Upper Jurassic beds seems to be a conformity; no regional unconformity has been recognized. In the study area, the shallow-water carbonate ramp of the Sulaiy Formation overlies the Upper Jurassic Hith Anhydrite on the Arabian platform whereas the deep-water Makhul and Garau Formations overlie the Upper Jurassic Gotnia Formations in the intrashelf Gotnia basin (Murriss, 1980; Beydoun, 1991).

The upper boundary of the Lower Cretaceous Thamama Group with the Middle Cretaceous Wasia Group, which is the top of the Shuaiba Formation, is a regional unconformity according to Harris *et al.* (1984) and is a sequence boundary. According to Scott (1990) geochemical and petrographic data of the uppermost Shuaiba Formation from parts of Oman and UAE indicate that the top of the formation was not subaerially exposed there, but elsewhere it may well have been. The boundary surface in Oman and UAE is isochronous but it becomes older towards the Arabian platform margin; the basal Nahr Umr Formation (Wasia Group) onlaps the Shuaiba Formation from the east. These data support the concept of a peripheral bulge in Oman, which was first active during the early part of the Late Aptian and then moved westward. The Shuaiba-Nahr Umr disconformity drowning event (the second cycle drowning) is controlled by eustatic sea-level rise and not by tectonic or environmental change according to Scott (1990).

#### **2.2.4 Controlling processes on Thamama Group deposition and cyclicity**

The depositional patterns of the Thamama Group were controlled by the interplay of sea-level changes, sediment supply, epeirogenic movements, rejuvenation of the tectonic arches, and palaeogeography. The regional depositional patterns have a direct relation with the regional distribution of hydrocarbon source, reservoir and seal rocks. Understanding the relative importance of each of these factors and the reason why they interact in space and time provide insight data to interpret and predict the hydrocarbon system of the Ratawi Formation.

The literature listed two main possible factors controlling the Thamama Group, namely tectonic and environmental versus eustatic global sea-level factors. According to Pratt and Smewing (1990, 1993 a, b) the main control on the development of the



carbonate platform in the Lower Cretaceous Thamama Group was the tectonic and environmental factors that lead to a change in the rate of carbonate sediment-supply<sup>accumulation</sup> and production. These processes lead to the first and the second drowning events on the Arabian platform during the Cretaceous. However, according to Alsharhan and Kendall (1991), the main control on the Thamama Group was eustatic variations during gentle tectonic subsidence of the Arabian Shelf.

The main controlling factors seem to be global tectonics around Neo-Tethys and the “Arabian Promontory” that lead to changes in the size of the oceanic basin and global sea-level fluctuations (tectonic-eustatic cycle). These processes are used by this study in Chapter 6 to explain the drowning event on the Ratawi Oolite platform and the deposition of the drowning succession, the lower part of the Ratawi Limestone, in the study area. The following data could support this concept:

1. The three drowning events of the Arabian shelf are broadly synchronous with others around Neo-Tethys. The Rayda Formation is broadly contemporaneous with similar pelagic limestones (Maiolica facies) in the Mediterranean region. These data suggest that the tectonic activity on the southern Arabian shelf-margin in northeastern Oman was part of a widespread phase in the evolution of Neo-Tethys (Pratt and Smewing, 1993 a, b).
2. The three Cretaceous sequences of the Arabian-Iranian basin and their confining unconformities seem to be correlative over the entire southern margin of the Tethys from Syria, Turkey, Lebanon, Egypt, northern Libya and possibly Morocco (Harris *et al.*, 1984).
3. The Hith Formation could be related to the Tithonian regression across Europe (Pratt and Smewing, 1993 a, b), which is the regressive phase of the 1<sup>st</sup> order sub-cycle, the North Sea cycle of Jacquin and Graciansky (1998).
4. The clastic wedge spreading from the northwest into the middle of the Arabian platform (Ratawi Shale member and Zubair Formation of the Thamama Group and the Nahr Umr Formation and its equivalent in the Wasia Group) and detrital argillaceous material of the Zakum Member of the Lekhwair Formation, support the westward tilting of the Arabian platform (Murriss, 1980) and tectonic and environmental factors that lead to the change in rate of carbonate sediment supply at this time (Pratt and Smewing, 1990, 1993 a, b).
5. During the Jurassic, the regional primary dip in Kuwait was to the south and southwest. This regional dip was disrupted by regional tectonic events at the end of



the Jurassic and Early Cretaceous, and by the Tertiary it reversed to the present northeast (Yousif and Nouman, 1997).

### **2.2.5 The Gotnia intrashelf basins**

During the deposition of Lower Cretaceous Ratawi Formation, the study area was located between the Arabian Shelf and the Gotnia intrashelf basin (Fig. 2-6) (Longacre and Ginger, 1988). The stratigraphic evolution of the Ratawi Formation can be understood as a part of the geological development and infill of the Gotnia intrashelf basin. The vertical and lateral facies variation of the Ratawi Formation and its stratigraphic history can be modelled in terms of the eastward progradation of the Arabian Shelf and filling of the Gotnia intrashelf basin.

The basin has been referred to as the Gotnia / Garau basin (Beydoun *et al.*, 1992), Laurestan basin (Murris, 1980) and Gotnia basin (Ayres *et al.*, 1982). During the Jurassic, the Arabian Plate was the site of three intrashelf basins, the Dukan, Ghawar (Arabian), and Gotnia basins. The Gotnia basin is the largest of these intrashelf basins and formed as a result of extensional tectonics (Beydoun *et al.*, 1992). These processes can be related to the tectonic development of the Arabian platform that started rifting in the Triassic, followed by continental separation in early Jurassic times, and succeeded by relaxation and subsidence during the Middle Jurassic (Alsharhan and Nairn, 1997).

The geological development of the Gotnia intrashelf basin can be divided into three stages. The first stage is the initiation of the basin by tectonic differentiation of the northern Arabian Shelf, including the northern part of the study area (PNZ), that lead to intrashelf depression in the early Jurassic. The second stage is the expansion of the basin by inundation of the Arabian Shelf during late Callovian to Tithonian time. During the late Oxfordian to early Kimmeridgian time, the basin extended southwards. The centre of the basin during this time was several hundreds of metres deep, and laminated bituminous lime mudstone and marls were deposited in anoxic conditions. The Sargelu Formation in the Gotnia basin and Hanifa Formation in the Ghawar / Arabian basin (in Saudi Arabia) were deposited then. During the Tithonian the climate become arid, and salt, laminated anhydrite and shale of the Gotnia Formation were deposited in the basin, as a lowstand gypsum wedge and basin-fill halite. On the Arabian Shelf, anhydrite of the Hith Formation was deposited in a sabkha environment (Murris, 1980).



The final stage of the basin's geological history was progradation of the Arabian Shelf and the reduction of basin size. This stage started during the first cycle of the Thamama group (Berriasian-Valanginian) and ended in the study area (PNZ) by the second cycle of the Thamama group (Hauterivian-Aptian). During the Early Cretaceous there was a gradual return to a more humid climate and gradual replacement of the differentiated rimmed-type shelf by a carbonate ramp. Deep-water and anoxic conditions continued to be dominant in the Gotnia basin in the study area during the first cycle of the Thamama Group. Thin dark-grey argillaceous limestone of the Makhul / lower Sulaiy Formation, and its equivalent the Garau Formation to the east and northeast, was deposited in the basin. The lower member of the Ratawi Formation, the Ratawi Oolite (Minagish Formation), was deposited on the Arabian Shelf (Murris, 1980) and on the reactivated basement structure of the Kuwait arch in the study area (Alsharhan and Nairn, 1997).

During the second cycle of the Thamama Group (Hauterivian-Barremian) a trend of clastic influx began and continued to increase, leading to the deposition of the clay-rich Ratawi Limestone and Ratawi Shale members of the Ratawi Formation (Buwaib Formation) and the Zubair Formation (Biyadh Formation). The basin was much reduced in size through progradation of the Arabian Shelf. By middle-late Barremian time, the clastic regime of the Zubair (Biyadh) Formation occupied the western half of the basin, including the study area. This led to the migration of the shallow-water carbonate ramp facies of the Lekhair and Kharaib Formations towards the east and south, and deep-water facies of the Gotnia basin (the Garau Formation) towards the northeast (Murris, 1980; Yousif and Nouman, 1997).

The physiogeography of the study area during the deposition of the Ratawi carbonate platform, which was between the Arabian Shelf and the Gotnia intrashelf basin (Fig. 2-6), was one of the factors that controlled the development of the Ratawi Formation stratigraphic succession. In addition, the depositional site controlled the Ratawi petroleum system, which includes the distribution of source, reservoir and seal rocks. Other factors include sea-level changes, epeirogenic movements of the Arabian Plate, rejuvenation of the Kuwait arch (Arabian folds) and carbonate sediment supply.

Ayres *et al.* (1982) studied the hydrocarbon habitat in the main producing areas in Saudi Arabia and the study area (PNZ), and concluded that the Ratawi reservoir and other Cretaceous carbonate and clastic reservoirs are limited to northeastern Saudi



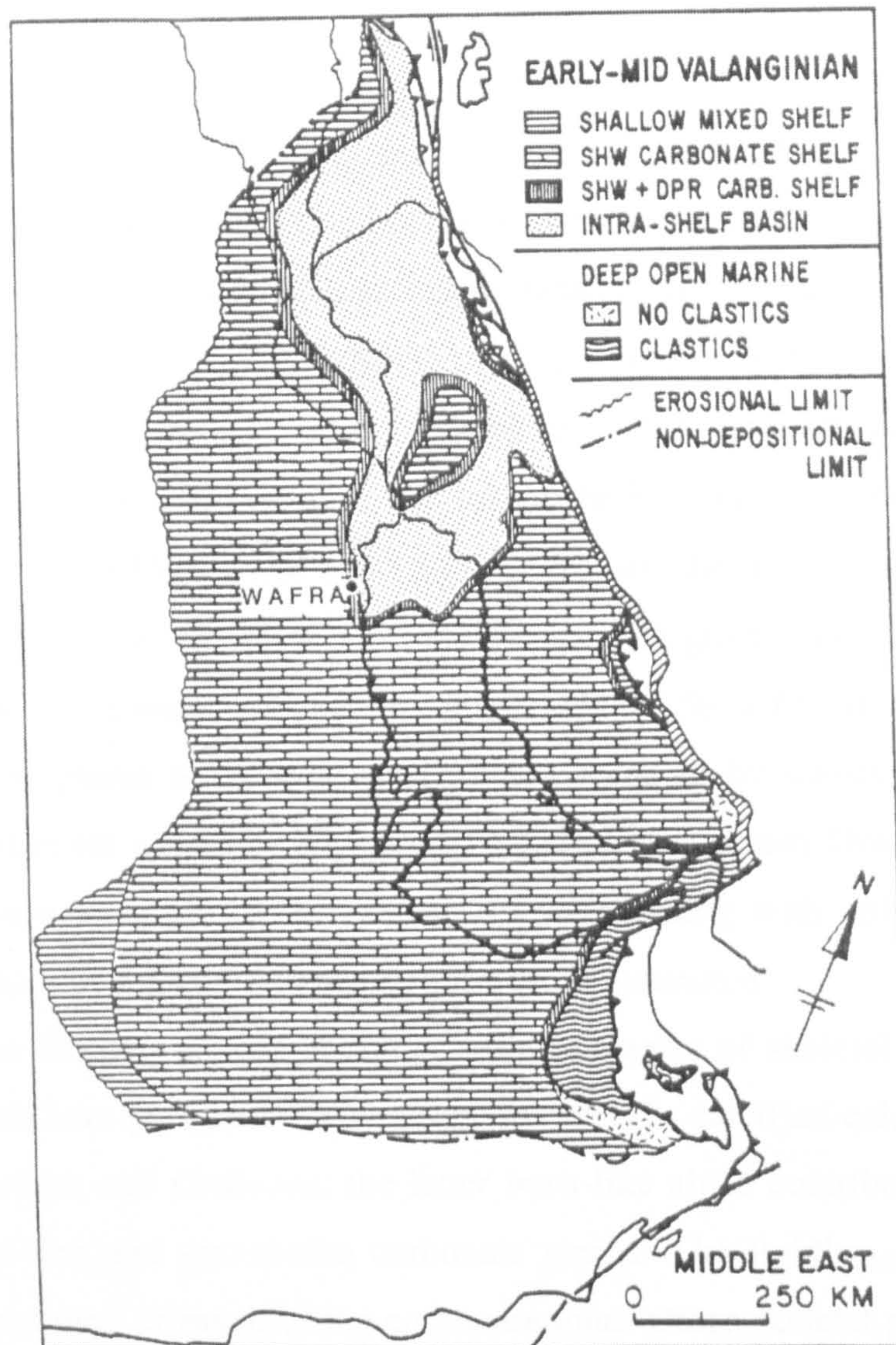


Figure 2-6 Palaeogeographic map of the Arabian Shelf during the Early to Middle Valanginian, the approximate time of accumulation of the Ratawi Oolite, showing the location of Wafra near the boundary between the Arabian shelf and the slope into the intra shelf Gotnia basin (after Murris, 1980 and Longacre and Elliott, 1988).

Ginger

Arabia and PNZ. They related this distribution to the thermally mature Cretaceous Valanginian source rocks in the Gotnia intrashelf basin or to the local lack of Jurassic seal facies separating these Cretaceous reservoirs from Jurassic source rock.

### 2.3 Previous studies of the Ratawi Formation in the Wafra oilfield area

The Ratawi Formation, with its three members the Ratawi oolite (Minagish Formation), Ratawi Limestone and Ratawi Shale, is the main producing hydrocarbon system in the Lower Cretaceous Thamama Group of the northern Arabian Gulf. The Ratawi Formation is the producing horizon in Saudi Arabia from the Manifa, Marjan,



Safaniya and Zuluf oilfields, in Kuwait from the Burgan, Bahra, Minagish, Umm-Gudair, Riqua and Mutriba oilfields, and in the Partitioned Neutral Zone from the Khafji, Hout, Dorra, Lulu, South Fawaris, South Umm-Gudair and Wafra oilfields.

Longacre and Ginger (1988) and Longacre (1986) studied the evolution of the Ratawi Oolite member (Lower and Middle Valanginian) in the Wafra oilfield, which is the deepest reservoir zone in the oilfield (Fig.1-3, 2-8 and 2-9). A few wells in the oilfield have drilled through the entire member and into the underlying Makhul (Sulayy) Formation. The average depth to the top of the Ratawi oolite member in the area is between 6100 ft (1859 m) and 6400 ft (1951 m), and the thickness is more than 600 ft (183 m). The general lithology is a porous carbonate grainstone with very little carbonate mud and / or cement between the grains, except for a few minor horizons. The majority of the grains have been rounded and polished by waves and currents giving them the external appearance of ooids. Most of the Ratawi Oolite is lacking obvious bedding structures and shows extremely poor sorting with only a few well sorted intervals which are commonly parallel and cross laminated.

The Ratawi Oolite member is composed dominantly of skeletal and peloidal grainstone and mud-lean packstone. Skeletal grains include calcified calcareous algae *Bacinella-Lithocodium* and *Codiacea*; the latter bush-like algae contributed abundant quantities of sand-size and gravel-size carbonate grains. The lightly calcified algae were the probable source of much of the carbonate mud. Other skeletal grains include a variety of bivalves (robust rudists, flat *Inoceramus*, and various others), numerous types of foraminifera, echinoderms, stromatoporoids, fragments of coral, and a few gastropods and brachiopods. The non-skeletal grains include peloids and ooids, although they are almost non-existent in the upper part of the Ratawi Oolite reservoir zone (Units C, D, E and F); they are present in the lower part of the reservoir zone (Unit B). The facies and microfacies of the Ratawi Formation are described in Chapter 3.

### **2.3.1 Porosity and permeability**

Porosity in the Ratawi Oolite ranges from less than 5% to more than 35% with average porosities ranging from 18 to 25%. It includes large amounts of depositional intergranular primary porosity, with abundant diagenetic dissolutional secondary porosity. Permeabilities in the Ratawi Oolite range from less than 0.01 mD to more than 5 Darcies, with average from 100 mD to more than 1 Darcy, in the productive



horizons. The cut-off porosity in the reservoir zone is 15% measured from core and porosity logs (Longacre and Ginger, 1988). Porosity is discussed at length in Chapter 4.

### **2.3.2 Ratawi Oolite marker zones and the three Wafra reservoir producing areas**

The studies of Longacre (1986) and Longacre and Ginger (1988) identified nine marker zones labelled “marker zone # 1” at the base to “marker zone # 9” at the top (Fig. 2-7). They represent interruption of Ratawi Oolite sedimentation and are recognized as tight intervals in cores and on gamma ray and porosity logs. The Saudi Arabian Texaco Inc. Co. used the nine marker zones to divide the Ratawi reservoir zone in the Wafra oilfield into six units, namely unit A, unit B, unit C, unit D, unit E and unit F, and correlated these units in the main, southern and eastern Wafra areas. At the crest of the main Wafra area (well R-43), units C, D and E are reservoirs with porosity more than the cut-off value of 15%. Porosity of units C and D decreases at the flank of the structure of the main Wafra area and these two units are non-reservoir in the southern and eastern Wafra areas. Unit E is the only unit in the Wafra oilfield that is a reservoir unit in the main, southern and eastern Wafra areas, whereas unit F is a non-reservoir unit across the whole oilfield.

The marker zones are recognized in well R-43 at the crest of the main Wafra oilfield area (Fig. 2-7) at the following depths:

- (1) Marker zone # 1: Top of unit A, at depth 7130 ft (2173 m)
- (2) Marker zone # 2: Top of unit B, at depth 6994 ft (2132 m)
- (3) Marker zone # 3: Within unit C, at depth 6891 ft (2100 m)
- (4) Marker zone # 4: Base of unit D, at depth 6858 ft (2090 m)
- (5) Marker zone # 5: Within unit D, at depth 6827 ft (2080 m)
- (6) Marker zone # 6: Top of unit D, at depth 6796 ft (2071 m)
- (7) Marker zone # 7: Within unit E, at depth 6775 ft (2065 m)
- (8) Marker zone # 8: Within unit E, at depth 6768 ft (2063 m)
- (9) Marker zone # 9: Unit F, from depth 6734 to 6718 ft (2052 to 2048 m)

These marker zones are used in this study (Chapters 3, 4, 5 and 6) to correlate the reservoir and non-reservoir units from the type locality well R-43 at the crest of the main Wafra area to the core description log at the flank of the main Wafra area (well



R-50) and the southern Wafra area (well R-49) and to relate these units to core samples, lithofacies, microfacies and cycle hierarchy.

### **2.3.3 Ratawi Oolite reservoir units**

The studies of Longacre (1986) and Longacre and Ginger (1988) identified fifteen sedimentary facies in the Ratawi Oolite reservoir zone in the Wafra area, which are assembled into six major sedimentary units. These can be correlated in the Wafra oilfield using the nine marker zones (Section 2.3.2). The units are ordered from “Unit A” at the base to “Unit F” at the top:

#### **2.3.3.1 Unit A**

Very muddy peloidal wackestone and packstone: the deposition took place on a carbonate mud-rich shelf or in a slightly restricted lagoon.

#### **2.3.3.2 Unit B**

Oolitic and skeletal grainstones: these appear to mostly represent deposition on a shallow sand shoal, a series of bars or sand flat. Some intervals are muddy tidal-flat sediments. Primary porosity in the grainstone was initially high, but an abundance of freshwater calcite cement has significantly reduced porosity in the crestal areas of the field. This cemented zone diminishes in thickness laterally to the flanks of the oilfield.

#### **2.3.3.3 Unit C**

Coral and rudist (packstone) and wackestone: the muddy sediments on the flanks of the structure become mud free and much more porous and permeable towards the centre of the structure.

#### **2.3.3.4 Unit D**

Peloidal and skeletal packstone: the presence of carbonate mud indicates slightly quieter-water conditions than in the overlying unit E. The rich fossil assemblage indicates that this muddy shelf environment supported an open-marine fauna. In the East Wafra area, stromatoporoids and a mixture of coarse coral and rudist debris and some boundstone suggest close proximity to a reefal area.



### 2.3.3.5 Unit E

Skeletal / algal (*Bacinella-Lithocodium*) grainstone and mud-poor packstone: the coarse-grained to gravel-sized-fragments dominated by green algae and other open-marine fossils indicate clear-water shelf conditions. The coarseness and abundance of the green algae suggest algal reefs or banks to the east of the main Wafra area. Rudist

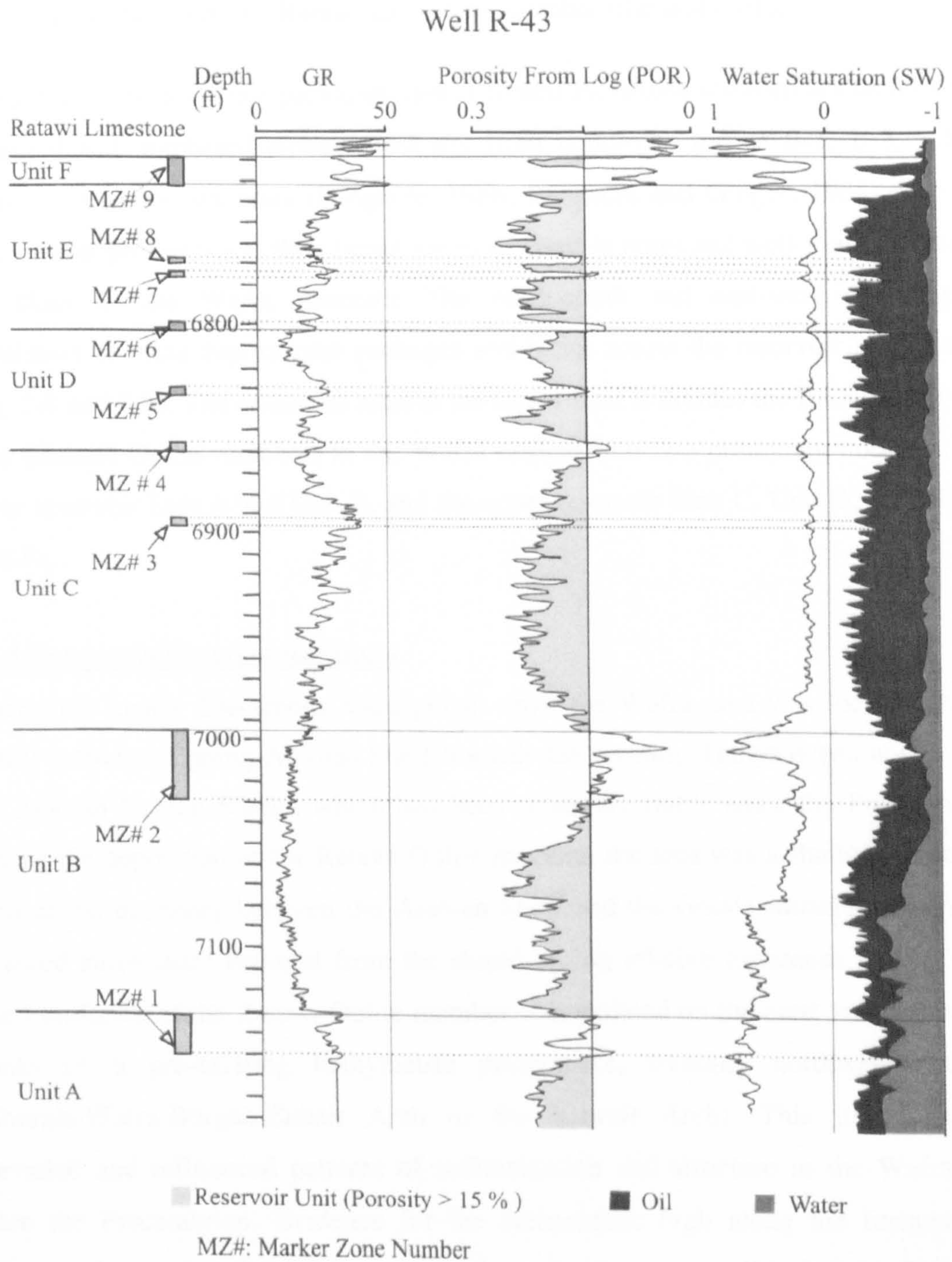


Figure 2-7 Ratawi zone at reference well R-43 in Wafra oilfield.



2.3.3.5 Unit E

Skeletal / algal (*Bacinella-Lithocodium*) grainstone and mud-poor packstone: the coarse-grained to gravel-sized-fragments dominated by green algae and other open-marine fossils indicate clear-water shelf conditions. The coarseness and abundance of the green algae suggest algal reefs or banks to the east of the main Wafra area. Rudist

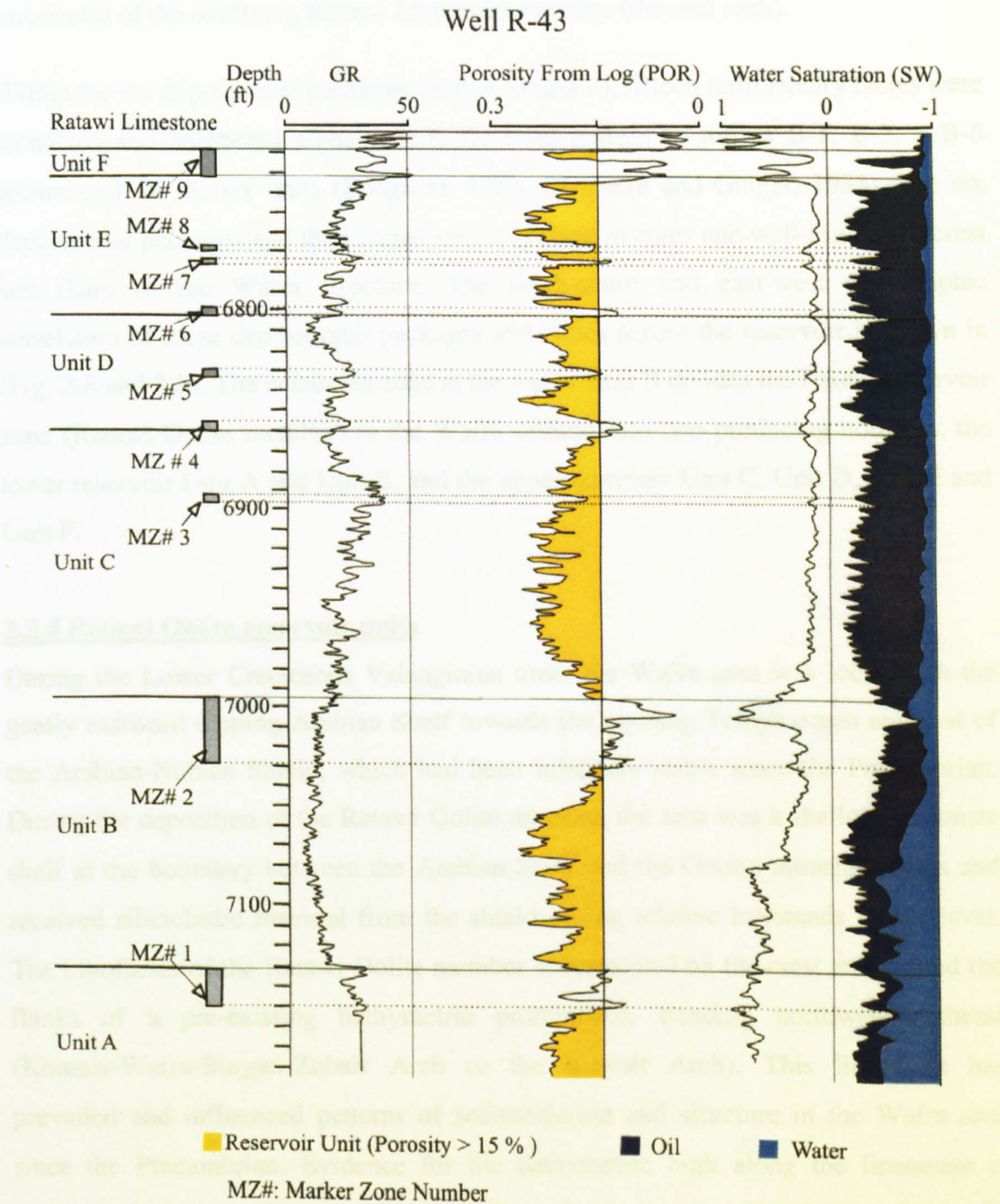


Figure 2-7 Ratawi zone at reference well R-43 in Wafra oilfield.



packstones are common and could represent mounds also to the east of the main Wafra area. All the grains in this unit are detrital in the main Wafra area.

#### **2.3.3.6 Unit F**

Interbedded transition of the Ratawi Oolite member (the reservoir zone) to the shaley carbonates of the overlying Ratawi Limestone member (the seal rock).

Within the six depositional packages (unit A to unit F), fifteen sedimentary facies were identified and numbered alphanumerically from bottom to top as B-1, B-2, ...B-6 within each of the six units (Longacre, 1986; Longacre and Ginger, 1988). The six depositional packages and their facies are recognized in cores and well-logs at the crest and flank of the Wafra structure. The north-south and east-west stratigraphic correlation of these depositional packages and facies across the reservoir is shown in (Fig. 2-8 and 2-9). The cemented zone at the top of Unit B divides the Ratawi reservoir zone (Ratawi Oolite member) in the Wafra oilfield into two producing horizons, the lower reservoir Unit A and Unit B, and the upper reservoir Unit C, Unit D, Unit E and Unit F.

#### **2.3.4 Ratawi Oolite reservoir units**

During the Lower Cretaceous Valanginian time, the Wafra area was located on the gently eastward dipping Arabian Shelf towards the opening Tethys ocean and east of the Arabian-Nubian Shield, which had been relatively stable since the Precambrian. During the deposition of the Ratawi Oolite member, the area was a shallow carbonate shelf at the boundary between the Arabian Shelf and the Gotnia intrashelf basin and received siliciclastic material from the shield during relative lowstands of sea level. The lithofacies of the Ratawi Oolite member accumulated on the crest and around the flanks of a pre-existing bathymetric prominence, trending northwest-southeast (Khurais-Wafra-Burgan-Zubair Arch or the Kuwait Arch). This lineament has prevailed and influenced patterns of sedimentation and structure in the Wafra area since the Precambrian. Evidence for the bathymetric high along the lineament is inferred from the distribution of high and low-energy lithofacies, from the development of tight zones and marker zones, and from lithofacies thicknesses (Longacre and Ginger, 1988).



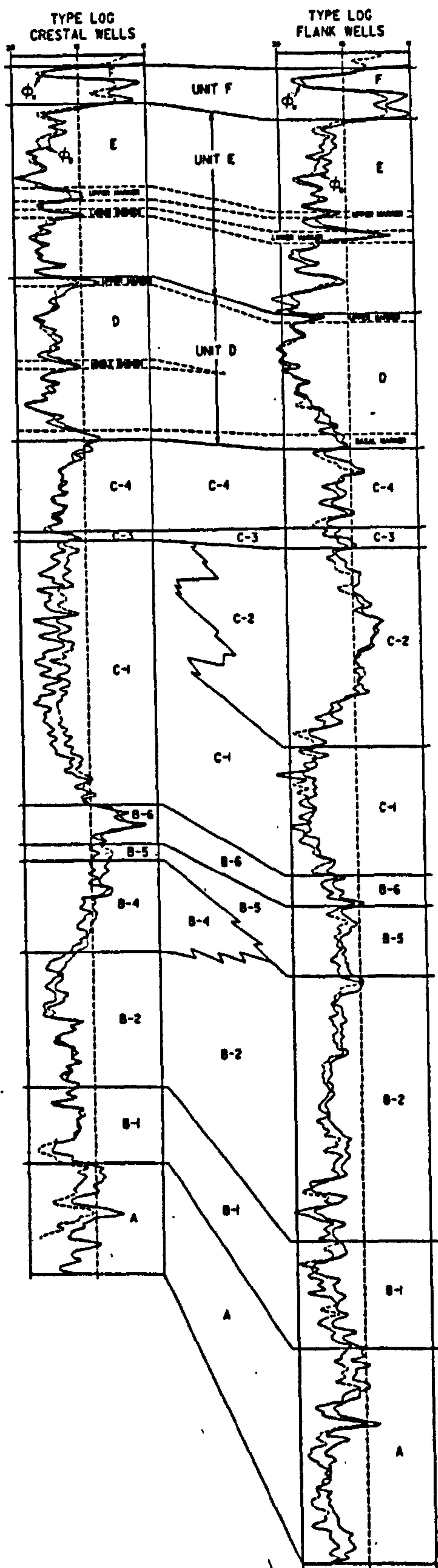
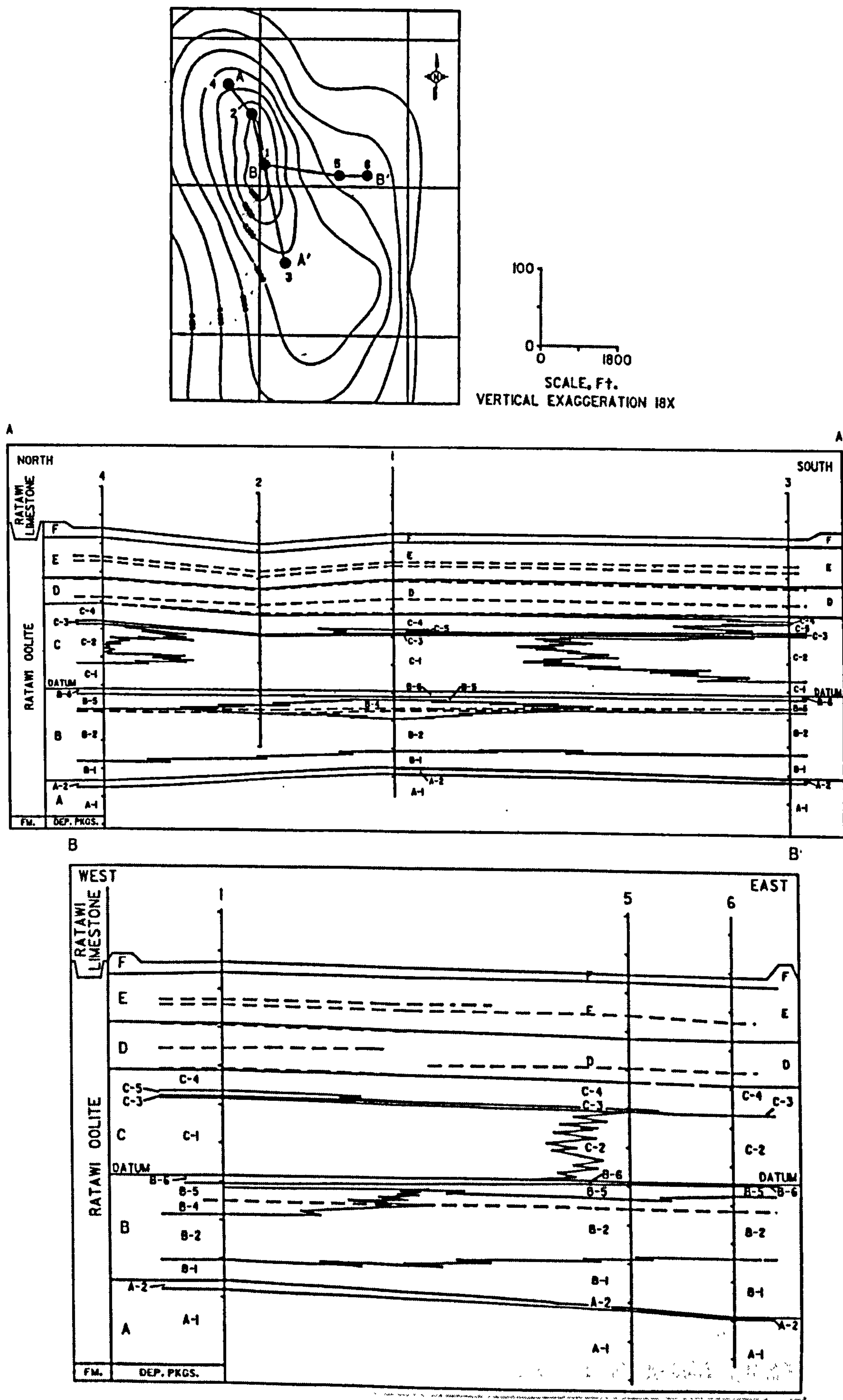


Figure 2-8 Type porosity logs for the lithofacies of the Ratawi Oolite reservoir. Examples are shown for both crestal and flank locations (after Longacre and ~~Elliott~~, 1988).  
Ginger

Figure 2-9 Stratigraphic cross-sections showing the spatial distribution of lithofacies in the Ratawi Oolite (after Longacre and ~~Elliott~~, 1988).  
Ginger







Longacre (1986) and Longacre and Ginger (1988) interpreted the origin of this basement lineament as the result of east-west compressional events in the Precambrian and later movements of the Infra-cambrian Hormuz salt. The depositional primary porosity in the Wafra reservoir was controlled by the bathymetric high during Ratawi Oolite sedimentation, which determined the distribution and geometry of the oolitic sand bodies which are now the reservoir units. They constructed a depositional facies model for each of the six units in the Ratawi Oolite member. These are:

#### **2.3.4.1 Depositional model for Unit A**

This unit is characterized by two facies, A-1 and A-2. The muddy peloidal wackestone and packstone, facies A-1, accumulated in a low-energy restricted environment, with influx of minor amounts of terrigenous clay to the Wafra area at the top of Unit A (facies A-2), which represents marker zone # 1.

#### **2.3.4.2 Depositional model for Unit B**

Five facies characterized this unit, B-1, B-2, B-4, B-5 and B-6 (B-3 was included in B-2). Five depositional environments developed in the Wafra area during deposition of the oolitic and skeletal grainstone, most of them reflecting shallow-water and high energy. These are: facies B-1 shallow-water lagoon, facies B-2 and B-4 mixed carbonate sand shoals, facies B-5 ooid sand shoals and facies B-6 tidal flats. After or during the deposition of facies B-6 a fresh-water phreatic lens was established that lead to pore-filling equant calcite cement in the upper part of unit B (upper B-2, B-4, B-5, B-6). This cement horizon (marker zone # 2) thins towards the Wafra flanks and inhibited the vertical migration of fluids.

#### **2.3.4.3 Depositional model for Unit C**

This unit is characterized by five facies, C-1, C-2, C-3, C-4 and C-5. Subtidal open-marine environments returned to the Wafra area and coral and rudist packstones and wackestones were deposited after a relative sea-level rise. The corals are always fragmented and abraded, not in-situ, and are more common in the eastern wells. The model suggests that reef growth was centred in deeper-water, more seaward positions to east of the Wafra area and debris was transported towards the Wafra area. The rudists, in contrast to the corals, are generally preserved whole and a local dense packing of rudists indicates that they grew in-situ.



Facies C-1, skeletal and peloidal grainstone-packstone, was deposited in subtidal open-marine environments with constant and moderate levels of water energy at the crest of the structure of the main Wafra area, that resulted in winnowing of some of the micrite. Facies C-2 is laterally equivalent to facies C-1, and is a mud-rich facies, which accumulated on the flanks of the structure of the main Wafra area. The environment was subtidal and open-marine with a slight increase in water depth compared to facies C-1. The cored sections of the thin facies C-3 are different in each well. The environment varied from a shallow subtidal lagoon to supratidal with subaerial exposure. This facies is marker zone # 3. Facies C-4 indicates the return of a high-energy, shallow-water, open-marine environment as in facies C-1. Facies C-5 is laterally equivalent to facies C-4 and restricted to the southern Wafra area. The environment of facies C-5 was similar to that of facies C-2.

#### **2.3.4.4 Depositional model for Unit D**

This unit is characterized by one facies (D-1). The facies was deposited in a low-energy, shallow-water, open-marine environment and has three marker zones # 4, # 5 and # 6. In the central part of the field, 20 to 30% of the micrite in unit D has been replaced by dolomite. The marker zones represent tight zones; porosity is less than 15% (the cut off porosity for the Ratawi Oolite) and was reduced by precipitation of equant calcite cement.

#### **2.3.4.5 Depositional model for Unit E**

This unit is characterized by one facies (E-1). The facies was deposited in a high-energy, shallow-water sand shoal environment and has two marker zones # 7 and # 8. In deep-water algal bioherms were deposited in the eastern Wafra area with rudist mounds, associated with *Bacinella-Lithocodium* bioherms. Sheets of skeletal material were washed from the bioherms by wave action to the Wafra area, and beds of coarse material derived from the buildups accumulated in the Wafra area by storm action. These conditions resulted in a lateral continuity of both lithology and good reservoir character. Marker zones # 7 and # 8 are characterized by low porosity mud-rich sediment and cemented horizons that formed during partial or complete exposure.



#### **2.3.4.6 Depositional model for Unit F**

This unit is also characterized by one facies (F-1). The unit is represented by an interbedded facies between the “clean carbonate facies” of the Ratawi Oolite and the “dirty carbonate facies” of the Ratawi Limestone. Beds of argillaceous carbonate and argillaceous peloidal wackestone are traceable across the area, interrupting the clean skeletal packstones to wackestones, which accumulated on a low-energy mud-flat or shallow shelf. There are two zones of argillaceous carbonate within unit F, and a third argillaceous zone at the base of the Ratawi Limestone member. This unit is marker zone # 9.

#### **2.3.5 Diagenetic model for Ratawi Oolite**

In addition to facies analysis for the Ratawi Oolite member (Ratawi reservoir zone) in the Wafra oilfield, Longacre and Ginger (1988) described three stages of diagenesis and porosity development in the Ratawi zone, syndepositional, early diagenetic and late diagenetic.

#### **2.4 Summary**

As explained in this chapter and the previous one, the regional geology and petroleum system of the Lower Cretaceous in the study area (PNZ), which is a good example for the numerous producing horizons in the Arabian-Iranian basin, are quite complicated, with the many factors that make this basin an exceptional petroleum system still requiring explanation. The previous studies of the Ratawi Formation and its petroleum system in the PNZ were mainly carried out by the oil industry in the 1980's.

Since then there have been many new developments in our understanding of stratigraphy, diagenesis and porosity development, and its preservation at reservoir depths. The aim of this thesis is to apply the new concepts of carbonate sequence stratigraphy, that made a revolutionary change in the science of stratigraphy and its application in studying petroleum systems during the 1990's, to give new insights to the Ratawi Formation petroleum system of the Saudi Arabia-Kuwait Partitioned Neutral Zone.



## **Chapter 3 Facies and Microfacies of the Ratawi Formation**

### **3.1 Introduction**

The Wafra oilfield is a giant oilfield producing from carbonates of the lower Cretaceous Ratawi Formation. Understanding the distribution of the carbonate reservoir facies in the oilfield and Ratawi oil system, which includes source, reservoir and seal rocks, in the regional framework, requires evaluating five main factors (Jordan and Wilson, 1994). These factors are (1) lithofacies, (2) carbonate platform type and palaeogeography, (3) pore types, (4) diagenetic overprint, and (5) sequence stratigraphy. Generally, the porosity in a sedimentary rock can be divided into depositional primary porosity, and diagenetic secondary porosity. Primary porosity is controlled by the depositional processes and texture, whereas secondary porosity is controlled by the diagenetic processes producing the diagenetic texture. The preservation of the porosity (primary and secondary) in a reservoir rock is controlled by the subsequent diagenetic processes, until oil emplacement (Moore, 1989; Tucker and Wright, 1990).

In this chapter, the Ratawi Formation lithofacies and microfacies are described and interpreted. In addition, the preserved primary porosity is related to depositional texture, depositional processes and depositional environment. In Chapter 4, the nature of the Ratawi pores (primary and secondary) is discussed. In addition the diagenetic processes in the Ratawi Formation that lead to the formation of the secondary porosity are described and interpreted, also those which lead to the preservation, reduction and elimination of the primary and secondary porosity. The sequence stratigraphy of the Ratawi Formation is described and interpreted in Chapter 5, and in Chapter 6, the sequence stratigraphic model for the Ratawi is compared with Cretaceous elsewhere in the world. The Ratawi sequence stratigraphic model is a tool to interpret and predict porosity and oil system within the regional and global framework

#### **3.1.1 The Aims of this Chapter**

Chapter 3 has two aims. The first aim is to describe and interpret the environment of deposition. In addition, the preserved primary depositional porosity is linked to the depositional textures and environments. The second aim is to construct the Ratawi



palaeogeography and interpret the type of carbonate platform. To reach these goals, the Ratawi facies are examined on two scales. First at the microfacies scale in Section 3.2, data from core samples, collected from the Ratawi Oolite and Ratawi Limestone, are described and interpreted. Second at the local and regional facies scale in Section 3.5. the palaeogeography is reconstructed. The broad Ratawi facies of the three members, Ratawi Oolite, Ratawi Limestone and Ratawi Shale, are examined in relation to each other and to the underlying Makhul Formation and overlying Zubair Formation.

The facies analysis of the Ratawi Formation at the two scales, microfacies and facies belt scales, is not only a useful tool in the identification of ancient Ratawi depositional environments, but also a powerful tool for evaluating Ratawi past climatic conditions, which is vital in interpreting the early overprinting diagenesis and the development of the Ratawi porosity (Chapter 4). In addition, facies analysis is used to distinguish different types and orders of surfaces that are significant in sequence stratigraphy (Chapter 5).

### **3.1.2 Geological reservoir characterization**

The geological reservoir characterization of the Ratawi zone in the Wafra oilfield involves four steps. The first step is dividing the Ratawi Formation into reservoir (flow-unit) and non-reservoir units. The second step is identifying the origin of porosity (primary and secondary) in each unit, which makes each unit a reservoir or non-reservoir. By understanding the porosity origin, the reservoir heterogeneity (reservoir or non-reservoir units) can be described and interpreted. The third step is identifying the geometry, the distribution in three-dimensions, of the reservoir units. This is done by understanding the depositional and diagenetic processes and environments that are controlling the porosity in the three- dimensions. The last step is determining the interaction between these units in the Wafra oilfield, but that is outside the scope of this study.

#### **3.1.2.1 Reservoir and non-reservoir units of the Ratawi zone**

The first step in Ratawi geological reservoir characterization is the subdivision of the Ratawi zone in the Wafra oilfield into reservoir and non-reservoir units. As mentioned in Chapter 2, Saudi Arabian Texaco Inc has divided the Ratawi zone at Wafra into 6 units. This study used core descriptions of wells R-48 and R-50 and log-facies to



identify these units. The Ratawi reservoir (flow unit) and non-reservoir units are identified by a 15% cut-off porosity, measured from neutron and density logs, and that is related to the economic permeability of the Ratawi zone in the oilfield (Longacre and Elliott, 1988). This study identified unit-D and unit-E as reservoir units in well R-50, at the flank of the main Wafra area, and unit-E as the reservoir unit in well R-49, at the southern Wafra area.

### 3.1.2.2 Porosity origin and geometry of the Ratawi reservoir unit

The second and third steps in Ratawi geological reservoir characterization are understanding the porosity origin, and then using this knowledge to interpret and predict the unit geometry. This study emphasizes the development of primary and secondary porosity and the processes that lead to the preservation of porosity. The main elements of the carbonate microfacies are grains (skeletal and non-skeletal), matrix, cements and porosity. The porosity of the rock is defined as the ratio of the total pore space to the total volume of the rock. The nature of the Ratawi pore system is one of the factors that effect the permeability and recovery efficiency of the reservoir. The nature of the pore system includes the pore size, pore-throat size, pore-surface roughness, and number of pore-connections, and these are related to the depositional and diagenetic environments (Chilingarian *et al.*, 1992).

The hierarchy of the geological controls on the porosity and permeability of the Ratawi zone in the Wafra oilfield, can be described and interpreted at three levels of reservoir heterogeneity by reservoir geologists and engineers (Chilingarian *et al.*, 1992). The three levels of the Ratawi reservoir heterogeneity are microscopic, megascopic and gigascopic. First, the controls on microscopic heterogeneity are microfacies, particle and pore properties. Second, the megascopic heterogeneity of non-reservoir and reservoir units is controlled by the depositional and diagenetic facies. Third, the gigascopic heterogeneity of the Wafra oilfield is controlled by the regional to global processes effecting the Ratawi depositional system that initiated, developed and terminated the Ratawi Oolite platform and determined the diagenesis of the reservoir and seal units at the oilfield scale. The Wafra oilfield is a porosity anomaly on a regional scale. Understanding the controlling factors at each scale allows "rules" to be deduced and prediction of the distribution of reservoir heterogeneity and oil system.



The porosity heterogeneity of the Ratawi zone in the Wafra oilfield at the gigascopic scale is controlled by the stratigraphic sequence and development of the basin fill that will be interpreted in Chapter 5. The porosity heterogeneity of the Ratawi zone at the microscopic and megascopic scales is controlled by the depositional and diagenetic environments. In this study, the Ratawi porosity at the microscopic scale is estimated as the percentage of the pore space in thin-section. Reservoir unit (flow unit) is identified by 15 % porosity cut off measured from the neutron and density logs.

The data from this study demonstrate that unit-D and unit-E with certain depositional and diagenetic overprint facies have a predictable and characteristic porosity and permeability. The study indicates that porosity in reservoir unit-D is mainly primary porosity, controlled by Ratawi depositional texture and environment, whereas in reservoir unit-E it is mainly secondary porosity, controlled by diagenetic processes and environment. The preservation of the porosity (primary and secondary) in unit-D and unit-E is controlled by subsequent diagenesis. The heterogeneity of the Ratawi zone at the flow-unit scale in reservoir unit-C and unit-E is interpreted and predicted from the depositional and the diagenetic environments. These are a depositional ramp sand-body for unit C, discussed in this chapter, and a 2<sup>nd</sup> order sequence boundary related diagenetic overprint of pedogenic calcretes for unit E, discussed in Chapter 4.

In this chapter, the depositional microfacies and the lithofacies of the Ratawi Formation are described and interpreted, and related to an 'epeiric' ramp model. In addition, the ramp sand-body that formed reservoir flow unit-D, at the microscopic and megascopic scale, is described and interpreted in the framework of the Ratawi depositional environment. In Chapter 4, the diagenetic overprint, which preserved, reduced, enhanced or blocked primary depositional porosity and created a new secondary porosity in the Ratawi Formation, is described and interpreted, and depicted as a diagenetic model. In addition, the diagenetic environment of pedogenic calcretes at the 2<sup>nd</sup> order sequence boundary that formed reservoir flow unit-E at the microscopic and megascopic scale, are described and interpreted in the framework of the Ratawi diagenetic environment.

The depositional epeiric ramp model of Chapter 3 and the diagenetic model of Chapter 4 for the Ratawi Formation are brought together in Chapter 5 by integration into the Ratawi sequence stratigraphic model. The integration of the data from both



models into the Ratawi sequence stratigraphic model allows a better understanding of the processes and prediction of the distribution of reservoir heterogeneity at the three scales in the Wafra oilfield.

### **3.2 Microfacies of the Ratawi Formation**

#### **3.2.1 The basic microfacies concept**

The data are based on Ratawi Oolite and Ratawi Limestone core samples from the main Wafra area, wells R-48 and R-50, and southern Wafra area well R-49. No samples are available from the Ratawi Shale or from the eastern Wafra area. The microfacies data from 204 Ratawi Oolite and Ratawi Limestone thin-sections given in Appendix 1, include types of non-skeletal and skeletal grains, cements, porosity types, sedimentary structures and diagenesis, with sample number and sample depth. In order to compile, compare and interpret the lithofacies data, this study uses the “lithofacies shorthand” of Jordan and Wilson (1994). This scheme is a semi-quantitative approach that normalizes the Ratawi Formation lithofacies data. The scheme follows Dunham’s (1962) classification of carbonate rocks and recognizes six lithofacies associations or textural families, namely mudstone, wackestone, packstone, grainstone, boundstone and crystalline dolomite. On the basis of the grain composition within the six textural families, the scheme reduced the number of common carbonate lithofacies observed at any geological time (including the Ratawi Formation) to 26 lithofacies types. This grouping indicates a limited number of combinations of rock compositions and textures occurring in nature (Wilson, 1975; Flügel, 1982; Tucker and Wright, 1990).

In order to interpret the Ratawi microfacies associations in terms of depositional facies belts (subenvironments) and to reconstruct the Ratawi palaeogeography, the Ratawi microfacies associations are compared with the standard microfacies models of Wilson (1975), Flügel (1982), and Tucker (1991) and Tucker *et al.* (1993). The lithofacies and microfacies of the Ratawi Formation are controlled by many factors, which include the rate of change of relative sea-level (eustasy and tectonics), sediment supply and platform type (Handford and Loucks, 1993). Tucker and Wright (1990) listed five main platform types or platform geometries, that include rimmed and ramp platform types. Wilson (1975) and Flügel (1982) used a typical shelf to basin profile for a rimmed-type platform, as a framework for compiling a list of 24 standard microfacies occurring in 9 standard facies belts (environments of deposition).



For a typical homoclinal carbonate ramp, Tucker (1991) and Tucker *et al.* (1993) recognized three broad facies belts for compiling general lithofacies associations. These are (1) back-ramp environments characterized by restricted fauna and wackestone-mudstone, (2) shallow-ramp environments characterized by open-marine fauna and grainstone, and (3) deep-ramp environments characterized by open-marine fauna and mudstone, wackestone and grainstone (Fig. 3-1). According to Spence and Tucker (1999), these standard microfacies models characterize palaeogeography using a series of discrete unrelated lithofacies associations that are based on common grain composition within the textural families. The carbonate subenvironments are identified by individual microfacies associations that are defined relative to fixed palaeogeographic positions within the platform and static palaeobathymetries. However, sequence stratigraphic concepts imply dynamic palaeobathymetries, which lead to gradual changes in lithofacies associations.

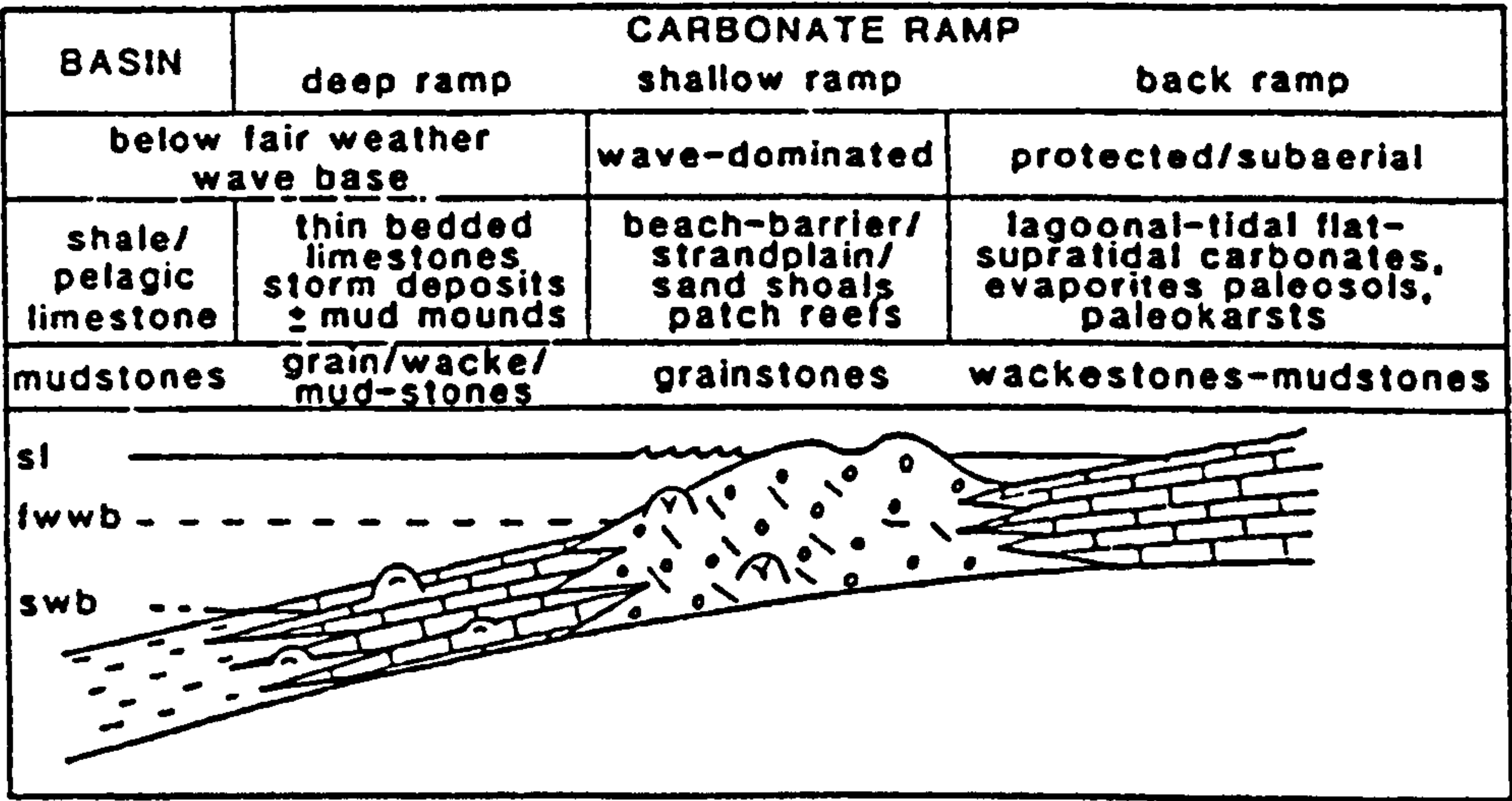


Fig. 3-1 General facies model for a carbonate Ramp (after Tucker, 1991)

3.2.2 Taphonomy of the Ratawi Formation

The concept of microfacies analysis assumes that the grain assemblages preserve sufficient evidence of initial sediment input to enable the environments of deposition to be deduced. Perry (1998) discussed the importance of taphonomy in the reconstruction of the depositional environments when using the approach of microfacies analysis. Taphonomy is the reconstruction of the history of an organism between the time of its death and the time when it is studied as a fossil. This study interprets Ratawi ecological information from the preserved Ratawi grain assemblages,



taking into consideration early marine and exposure related diagenetic processes that to some extent modified Ratawi texture, structure and composition. These diagenetic modifications are examined in Section 4.3.2 discussing the marine diagenetic environment, and in Section 4.3.3 discussing the exposure diagenetic environment. Early diagenetic modifications (marine and exposure) are used in this study to interpret these environments.

The preservation potential of Ratawi depositional texture is especially influenced by two early diagenetic processes, namely mineral stabilization (recrystallization) and micritization. In the first process, mineral stabilization of unstable original aragonite or siliceous grains, is observed in corals, gastropods, calpionellids, sponge spicules, green algae, and radiolarians. The process has three outcomes, the first two are complete (good) and partial (poor) preservation of the internal grain structure; the last is complete dissolution of the original unstable mineralogy and the space filled by granular drusy cement or preserved as a mould.

The second process, micritization of original grains, produces the most common particle in the Ratawi Formation, the peloid. These non-skeletal particles have polygenetic origins, which include the micritization of skeletal particles (Tucker and Wright, 1990). Peloids and micritization are discussed in Section 3.2.1.2.1 and in Chapter 4. The micritization process is interpreted in this study to have been formed by endolithic micro-organisms, algae and fungi, in the early marine environment, and through pedogenic processes during early exposure. These processes influence Ratawi grain preservation, and thus bias the composition of resultant Ratawi grain assemblages for the microfacies analysis.

### **3.2.3 Ratawi lithofacies associations**

The microfacies of the Ratawi Oolite and Ratawi Limestone are grouped into five main lithofacies associations when applying the “lithofacies shorthand” scheme of Jordan and Wilson (1994). 0.5% of the samples are crystalline dolomite; 26.7% of the samples are grainstone; 17% of the samples are packstone; 34.8% of the samples are wackestone, and 21% of the samples are mudstone. Selective thin sections have been stained in this study by Alizarin red S and potassium ferricyanide using the method of Miller in Tucker (1988). This method allows the differentiation between calcite and dolomite, in addition to ferroan phases in calcites and dolomites.



	Depositional or diagenetic texture	Characteristic fauna, sedimentary structures and grains	Depositional or diagenetic environment
BR-1	wackestone- mudstone	Reworked open-marine and restricted ostracod faunas, and black grains	<b>Back Ramp</b> Low-energy, low-salinity restricted lagoon near land with developed soil profiles
BR-2	wackestone- mudstone	Reworked open-marine and restricted ostracod faunas with pseudomorphosed gypsum	<b>Back Ramp</b> Low-energy, low-salinity restricted lagoon
SR-1	rudstone	Open-marine fauna, peloids with coral and ooids	<b>Shallow Ramp</b> Skeletal and non-skeletal sand shoals; coral reefs and ooid shoals were close to the area
SR-2	grainstone- packstone	Cross-laminated, flaser bedded, open-marine fauna and peloids	<b>Shallow Ramp</b> Intertidal and supratidal flat
SR-3	grainstone- packstone	Open-marine fauna, with ooids and aggregates	<b>Shallow Ramp</b> Behind peloidal bioclastic shoals near the restricted back-ramp lagoon
SR-4	grainstone- packstone	Open-marine fauna and peloids	<b>Shallow Ramp</b> In front of peloidal bioclastic shoals near the open sea
SR-5	packstone	Open-marine fauna, peloids and black grains	<b>Shallow Ramp</b> Peloidal bioclastic sand shoals affected by subaerial exposure
DR-1	floatstone	Open-marine fauna and peloids	<b>Deep Ramp</b> Below fairweather wave-base with occasional high-energy storm events
DR-2	mudstone	Open-marine fauna and bioturbation	<b>Deep Ramp</b> Below fairweather wave-base with few high-energy, storm events
DR-3	wackestone	Open-marine fauna and bioturbation	<b>Deep Ramp</b> Close to fairweather wave-base or somewhat below with few high- energy, storm events
DR-4	wackestone	Open-marine fauna biomorpha (whole shell)	<b>Deep Ramp</b> Below fairweather wave-base
DiagCal	pedogenic calcrete	Diagenetic facies	<b>Ramp Subaerial Exposure</b> Diagenetic facies superimposed on previous fabrics
DiagDol	crystalline dolomite	Diagenetic facies with peloid ghosts	<b>Burial Diagenetic</b> Replacing restricted shallow lagoon facies

Table 3-1 Ratawi facies



This study recognized 13 microfacies in the core samples of the Ratawi Oolite and Ratawi Limestone listed in Table 3-1. For interpretation and prediction of these five lithofacies associations, they are divided into (1) sedimentological lithofacies associations, Section 3.2.1, and (2) diagenetic lithofacies associations, Section 3.2.2. As mentioned in Section 3.1.2, the aim of this study is to interpret the origin of the Ratawi pore system. The sedimentological lithofacies associations include depositional facies that control depositional fabric and primary porosity. The diagenetic lithofacies associations include diagenetic facies that control diagenetic fabric and secondary porosity.

The microfacies of the Ratawi Formation are defined and interpreted on a purely qualitative basis, by selecting important features and giving less weight to unimportant ones (Tucker and Wright, 1990). As is explained in the Section 3.3, the broad lithofacies associations (Makhul Formation, Ratawi Formation and Zubair Formation) indicate deposition in a ramp type environment. This section uses the ramp model of Tucker (1991) and Tucker *et al.* (1993) as a framework for four broad facies belts. Each of these facies belts has distinctive microfacies associations for that particular environment, and is characterized by certain early diagenetic and porosity types. In the carbonate epeiric ramp model fair-weather-wave base and storm-wave base subdivide the ramp into three distinct energy zones or environments. These are back-ramp, shallow-ramp and deep-ramp environments.

Reservoir state, depositional environment and diagenetic environment are discussed for each microfacies identified in the Ratawi Formation. The reservoir state includes where this microfacies is a reservoir or non-reservoir unit in the Wafra oilfield, porosity % range, and common pore types. The depositional environment includes the sub-depositional facies belt as part of the epeiric ramp model of Tucker (1991) that controls primary depositional porosity. The diagenetic environment includes the main diagenetic environment controlling secondary diagenetic porosity. The percentage of each microfacies is given relative to the total 204 core samples, but this does not have stratigraphic statistical significance.

### **3.3 Sedimentological lithofacies associations**

The sedimentological lithofacies associations of the Ratawi Formation are grouped into four environments or broad facies belts, on the Ratawi ramp platform model of Tucker (1991). The first facies belt is the back ramp (BR), characterized by



wackestone-mudstone with restricted fauna (Section 3.2.1.1). The second facies belt is the shallow ramp (SR), characterized by rudstone, grainstone-packstone with an open marine-fauna (Section 3.2.1.2). The third facies belt is the deep ramp (DR), characterized by mudstone-wackestone with an open-marine fauna (Section 3.2.1.3). The last facies belt is the ramp with subaerial exposure, and pedogenic calcrete microfacies (DiagCal); this diagenetic microfacies is characterized by subaerial exposure facies superimposed on the three ramp facies. The microfacies DiagCal is discussed with the diagenetic lithofacies association. The microfacies analysis of the Ratawi Formation indicates that there are two microfacies in the Ratawi zone of the Wafra oilfield, with great economic potential. The first is the shallow ramp (SR) facies, and the second is the pedogenic calcrete facies (DiagCal).

### **3.3.1 Back Ramp: wackestone-mudstone with restricted fauna**

The back ramp (BR), wackestone-mudstone with restricted fauna lithofacies association is divided into two microfacies. The first is microfacies BR1, bioclastic wackestone-mudstone with ostracods and black grains (Section 3.3.1.1) and the second is microfacies BR2, bioturbated bioclastic wackestone-mudstone with ostracods (Section 3.3.1.2). The back ramp lithofacies association is discussed in Section 3.3.1.3.

#### **3.3.1.1 Microfacies BR1: bioclastic wackestone-mudstone with ostracods and black grains**

Bioclastic wackestone-mudstone with a restricted ostracod fauna and black grains characterize microfacies BR1 (Fig. 3-2 a). This facies is common in the Ratawi, about 24% of the core samples. The matrix is argillaceous micrite and this is often bioturbated, resulting in a homogeneous texture. Some discrete burrows are notable for the local development of micro-euhedral dolomite rhombs within them. This selective dolomitization process for the burrow fills is discussed in Chapter 4. Microfacies BR1 is characterized by wackestone and mudstone; the origin of the micrite is regarded as primary as discussed in Section 3.3.1.3. The non-skeletal particles are quartz and black grains (clast).

The terrigenous *quartz grains* are rare to common, mostly fine to medium sand in size (0.125-0.5 mm) and subangular in shape. Often the detrital quartz grains show evidence of partial to near complete replacement by calcite. This process of replacement is discussed in Chapter 4. The stratigraphic, vertical distribution of the



terrigenous quartz grains in the three members of the Ratawi Formation (Ratawi Oolite, Ratawi Limestone, and Ratawi Shale) has environmental significance.

The quartz grains are included within the clay percentage in the core-lab chart of the Ratawi Oolite (well R-50) and the Ratawi Limestone (well R-48). The clay content in the Ratawi Oolite, Ratawi Limestone and Ratawi Shale members and in the overlying Zubair Formation can also be inferred from the wireline logs. Analyzing these data indicate that there is a general increasing upward trend for the clay. The source for the detrital quartz and clay is interpreted to be the Zubair delta, which is discussed in Section 3.5.

The *black grains* (Fig. 3-3) are the second most common non-skeletal particle in microfacies BR1. This study, as other workers, considers black grains to be significant in microfacies analysis for two reasons, reconstruction of the palaeogeography, and their stratigraphic occurrence. Black grains in the BR1 microfacies are common to rare, up to coarse sand size (1 mm), and rounded in shape. They are composed of lime mud (micrite) mixed with other non-skeletal and skeletal particles in the argillaceous matrix. To use the black grains in reconstruction of the palaeogeography and stratigraphic development of the Ratawi Formation, the possible origin and the causes of the blackening of the grains is reviewed.

The black grains of the Cenomanian Breccia of Camporosello Epini Mountains Italy, were studied by Lang *et al.* (1997) using different methods including scanning electron microscope, X-ray diffraction, differential thermal analysis, and nuclear magnetic resonance. The study concluded that the blackening of the grains was mainly caused by organic matter, derived from rotting terrestrial plants, which may have been burned, and algae. In addition to the organic matter, there are small amounts of clay minerals and pyrite. The diagenetic environment of the blackening was anoxic and alkaline, when the partially altered carbonate sediment was impregnated by dissolved, colloidal or finely particulate organic matter, clay minerals and pyrite. This diagenetic environment was most probably within a soil profile, i.e. the black grains are pedogenic. The carbonate-crystal surfaces of the partially altered carbonate sediment, must go through a complex interplay of adsorption, neomorphism and microcrystalline cementation in the vadose or freshwater phreatic zones to fix the black coloration and make it relatively resistant to oxidation (Strasser, 1984; Lang *et al.*, 1997).

The black grains thus formed through erosion, reworking and transportation of the preferentially cemented and blackened sediment. The less-consolidated host



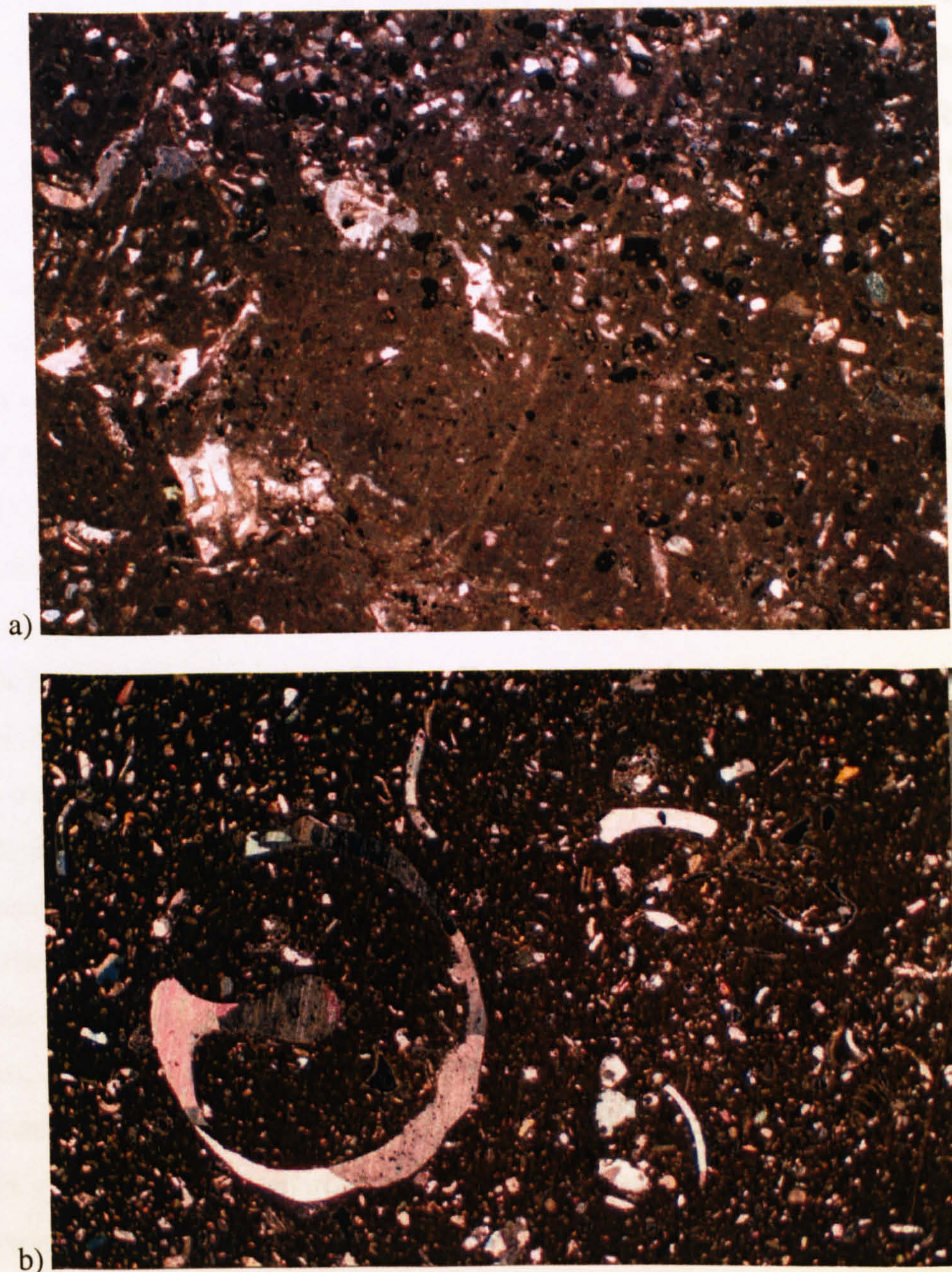


Figure 3-2 a) Photomicrograph of microfacies BR-1: bioclastic wackestone-mudstone with ostracods, bioclastic fragments and black grains. Note patchy distributions of the grains due to bioturbation and fine size of the black grains in the matrix. The sample is without porosity. Sample number is R-50 # 41, depth 6751 ft (2055 m), field of view 5 x 3 mm, under plane-polarized light. b) Photomicrograph of microfacies BR2: bioturbated bioclastic wackestone-mudstone with ostracods. Note bioturbation and patchy distribution of the molluscan bioclasts. Aragonite bioclasts have been dissolved out and molds filled with calcite cement. This microfacies has few moldic and vuggy pore spaces. Sample number is R-50 # 38, depth 6728 ft (2051 m), field of view 10 x 7 mm, under crossed polars.



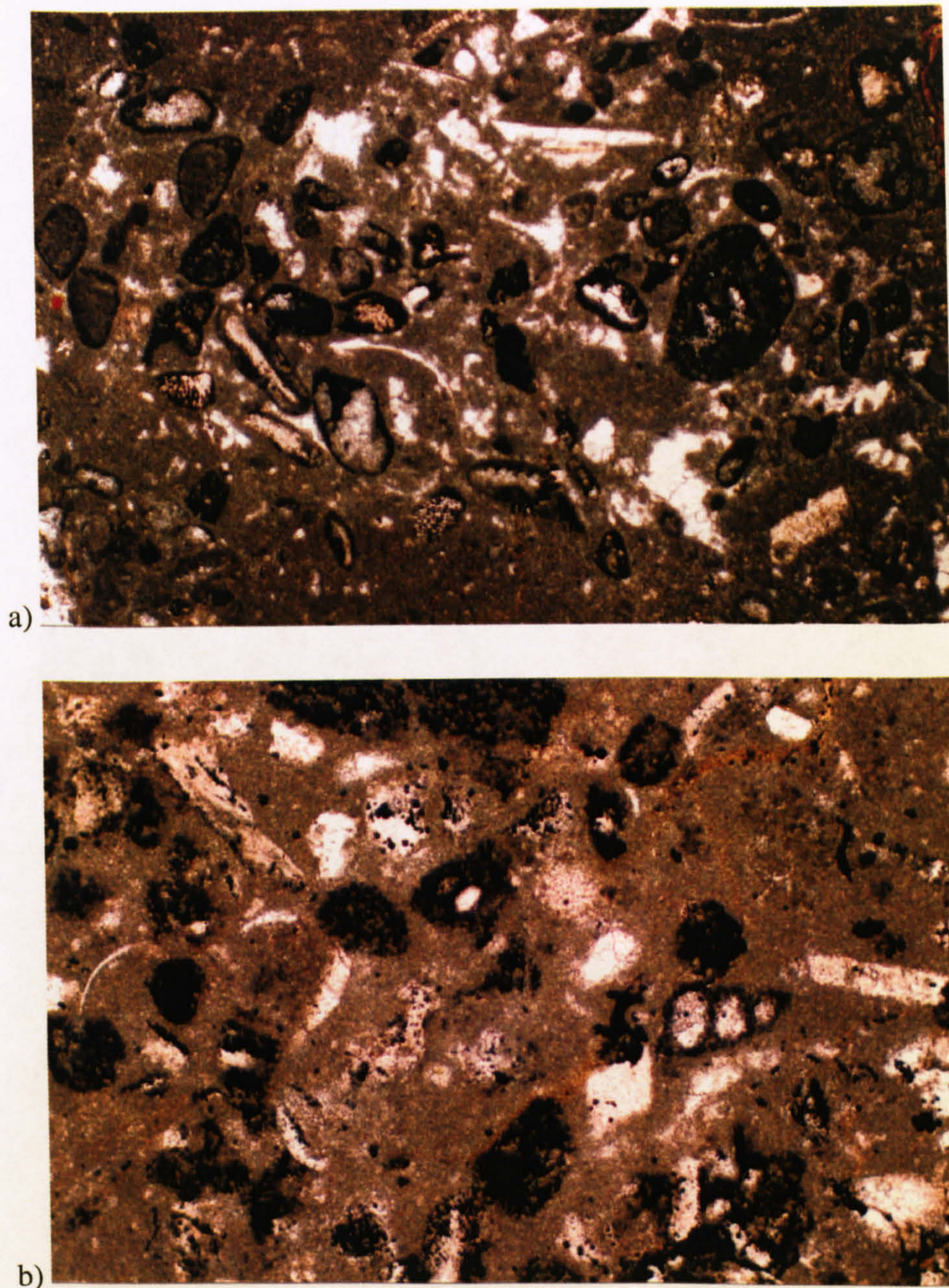


Figure 3-3 Photomicrograph of black grains a) in microfacies BR-1 and b) in microfacies SR-5. Note the different sizes of the grains and the skeletal, non-skeletal origin of the black grains and the presence of unblackened bioclasts. Sample numbers are a) R-50 # 49, depth 6783 ft (2067 m), field of view 3 x 2 mm, b) R-50 # 41, depth 6741 ft (2055 m), field of view 1 x 0.6 mm, under plane-polarized light.

sediment in the soil profile with the black grains would have been washed away, leaving the black grains as mostly relics. Black grains may be valuable indicators for the palaeogeographic reconstruction of ancient coastal and terrestrial environments (Strasser, 1984; Lang *et al.*, 1997). In addition, they may be valuable indicators for the stratigraphy.



a

Black grains were used with other exposure features by Strohmenger *et al.* (1991) to study the Upper Jurassic stratigraphy and the facies development of the Dinaric carbonate platform (northwest Yugoslavia) and the Jura carbonate platform (southeast France). Based on these exposure features, they recognized a sequence boundary and interpreted it as a type 1 sequence boundary, related to a global fall of sea level. The black grains are characteristic of a depositional environment with low sediment supply rate, which could have formed during a rapid marine transgression.

Tucker and Wright (1990) argued that the interpretative terms 'extra-clast', for reworked material from outside the area of deposition, and 'intra-clast' for reworked sediment from the immediate depositional area, are impossible to be distinguished from the limited data of core samples. They suggest in this case using the non-interpretative, descriptive term 'clast'. Black grains have been reported from various geological periods from the Ordovician to Holocene by Strasser (1984). This study interprets the black grains of the Ratawi Formation as clasts formed on land in the subaerial exposure environment, and eroded and transported into the low-energy shallow-water environment. Formation of the black grains in situ within organic-rich lagoonal muds is not preferred in this study because the grains are mixed with unblackened bioclasts (Fig. 3-3)

The *skeletal particles* of microfacies BR1 are grouped into two assemblages, which are restricted and open-marine assemblages. The first assemblage includes ostracods, which are the distinguishing feature for the restricted back-ramp lithofacies association (microfacies BR1 and BR2). The ostracods as a group are inhabiting nearly all types of depositional environment from fresh-water, restricted-water to normal marine-water. However, single species tend to be highly sensitive, ecologically, to the depositional environment (Scoffin, 1987). It has not been possible to determine the species of the ostracods.

The identification of the ecology of the ostracods as indicating a restricted environment depends on two lines of evidence. The first is that there are no ostracods in the shallow ramp (Section 3.3.1) or deep ramp (Section 3.3.3) facies. The second line of evidence is the association of the ostracods with the black grains and wackestone-mudstone texture, which indicates a low-energy, coastal environment. The ostracods in microfacies BR1 are common to rare. Most of the ostracod shells are disarticulated and well preserved; some shells are articulated, which indicate a low energy depositional environment, and little transportation or reworking.



The second assemblage includes open-marine skeletal organisms. The normal-marine salinity is inferred by the following groups: corals, bivalves, gastropods, brachiopods, crinoids, sponge spicules, green algae and foraminifera. The presence of the marine calcareous algae indicates water depths within the photic zone (Wilson and Jordan, 1983). These skeletal particles are rare to common, fine to medium sand in size (up to 0.5 mm), disarticulated and broken up, indicating some reworking and transportation.

*Reservoir state:* This facies BR1 is a non-reservoir unit. The range of the porosity is between 0 % to 7 %. The common pore types in this microfacies are vug, mouldic, fracture and stylolitic.

*Depositional environment:* The black grains and quartz sand and silt associated with the wackestone-mudstone depositional texture of microfacies BR1 indicate a low-energy marginal marine depositional environment. The exposed marginal lands were characterized by relatively high rain-fall and soil development (Alsharhan and Nairn, 1997). The articulated and good preservation of ostracods indicates little reworking and is evidence for low-salinity (hyposaline) restricted conditions. Mudstone-wackestone with reworked open-marine bioclasts indicates more reworking and occasional high-energy events, such as storms that transported the open-marine skeletal particles into the low-energy, low-salinity restricted lagoon.

### **3.3.1.2 Microfacies BR2: bioturbated bioclastic wackestone-mudstone with ostracods**

The bioturbated bioclastic wackestone-mudstone with ostracods, microfacies BR2 (Fig. 3-2 b), is a rare facies in the Ratawi, comprising about 5% of the core samples. Both microfacies BR1 and BR2 are distinguished by ostracods and a wackestone-mudstone depositional texture and similar skeletal particles and matrix. Microfacies BR2 is separated from microfacies BR1, on the absence of black grains. This indicates that microfacies BR2 was not deposited near exposed marginal lands.

*Reservoir state:* This facies BR2 is a non-reservoir unit. The measured porosity is 0% to 7%. The observed pore types in microfacies BR2 are vug, mouldic, fracture and stylolitic.



*Depositional environment:* The BR2 microfacies was deposited in a similar depositional environment to microfacies BR1, namely a low-energy, low-salinity, hyposaline, restricted lagoonal environment. However, microfacies BR2 differs from microfacies BR1 in that it was not deposited near marginal lands with soil profiles, which indicates deposition near the centre of the restricted lagoon environment.

### **3.3.1.3 Back ramp lithofacies association: discussion**

The back-ramp lithofacies association was deposited in a low-energy, shallow-water, restricted environment and was periodically affected by subaerial exposure. This lithofacies association is common in the Ratawi Oolite and Ratawi Limestone and accounts for about 29% of the core samples. The restricted conditions of the back-ramp environment could be formed by three processes: poor circulation, variations in salinity compared to normal seawater, and low-oxygen supply. The restricted conditions could be formed by poor circulation in the broad, sluggish lagoon behind oolitic, bioclastic and peloidal shoals on the shallow-ramp. Restricted conditions produced by salinity variation depend on the climate, and both hypersaline and hyposaline conditions may occur. The first type is usually associated with arid regions, where the seawater salinity is more than 35 ppm. The second type is usually associated with tropical areas with considerable freshwater runoff, and the seawater salinity is less than 35 ppm (Wilson and Jordan, 1983). Restricted conditions due to low oxygen could be formed through stratification of the water in the lagoon. This layering could be formed by the floating of lower density fresh water, on more dense, marine water. This condition could be associated with the poor circulation and the freshwater runoff. This process of water stratification and associated low oxygen-restricted condition has been suggested by Bordenave and Burwood (1995) to be the principal process~~es~~ for the creation of the anoxic environment in the Gotnia intracratonic basin during the Middle Cretaceous. An anoxic environment is the principal requirement for the preservation of organic matter in the stratigraphic record and formation of source rocks.

The restricted conditions of the Ratawi back-ramp environment could be formed by poor water circulation, low-salinity, and / or low-oxygen supply. The study area was located on an 'epeiric' ramp, south of the equator during the lower Cretaceous (Beydoun, 1991). The semi-tropical climatic could have brought considerable fresh-water runoff and low salinity, hyposaline conditions, in the



shallow-water lagoon, which could be associated with freshwater stratification and low-oxygen supply. In addition, the semi-tropical climate with the significant organic matter production could have produced the black grains (Section 3.2.1.1) through subaerial exposure.

The black grains were eroded and transported as clasts into the back-ramp shallow-water lagoon by the fresh-water runoff. This study suggests that the process of water stratification, which is associated with low oxygen-restricted conditions in the Gotnia intracratonic basin, could be the principal factor in the deposition of the source rocks of the Ratawi oil system. The low-energy environment is inferred from the depositional texture (wackestone-mudstone) which is the characteristic texture for the back-ramp facies in this section, and also in the deep-ramp (Section 3.2.3).

Many workers have reviewed the origin of micrite, including Flügel (1982), and Tucker and Wright (1990). All workers have considered micrite to be polygenetic in origin, and two main types are primary and secondary micrite. There are three main processes in the formation of micrite namely detrital supply, direct chemical precipitation, and diagenetic changes. The last mode is by diagenetic changes, and results in secondary micrite. This includes (1) grain degrading as a result of recrystallization, (2) cryptocrystalline cement, (3) recrystallized peloids, and (4) calcrete. The second mode is through change of water chemistry, and results in primary micrite. The second mode includes (1) temperature increase, salinity variation, and water energy, (2) bacterial action and decomposition of organic substances, and (3) assimilation by plants. The first mode is by supply of carbonate particles (detrital), and results in primary micrite. The first mode includes (1) submicroscopic calcareous algal fragments, (2) disintegrated parts of invertebrates, (3) borings of endolithic algae, fungi, and invertebrates, (4) fine detritus from bioerosion, (5) fine detritus from abrasion, (6) tests of micro-organisms, (7) nanno-organisms (Flügel, 1982).

The microfacies analyses of the Ratawi Formation support subaerial exposure diagenesis for the pedogenic calcretes (Section 3.4.2), but not for the back-ramp (Section 3.3.1), the shallow-ramp (Section 3.3.2), and the deep-ramp (Section 3.3.3) micrites. Some of the micrite in the pedogenic calcretes could be secondary micrite formed by diagenesis. The origin of secondary micrite through micritization is discussed in the subaerial exposure environment (Chapter 4).

Microfacies evidence supports a primary origin for the micrite and eliminates a secondary origin for the micrite in the lithofacies association of the back-ramp, the



shallow-ramp and the deep-ramp. The origin of the primary micrite of these lithofacies associations seems to be mainly by the second mode, direct chemical precipitation from seawater, and the first mode, supply of carbonate particles. A modern analogue, for the first and second mode, is the lime mud of the Trucial Coast of the Arabian Gulf, which may be a direct precipitate, and the Great Bahama bank, where mud is mainly formed from green algal disintegration (Tucker and Wright, 1990). The modern lime mud production rate was measured on the Little Bahama bank by Neumann and Land (1975). They concluded that the lagoon, the 'carbonate factory', is producing more lime mud than that accumulating in the lagoon. Therefore, the mud is being transported from the 'carbonate factory', the lagoon, into the deeper water periplatform area and on to adjacent tidal flats. To produce the grain-supported depositional texture of the ramp sand-body that characterizes the reservoir rock with the primary depositional porosity, most of the micrite must be winnowed away. The potential of the depositional lithofacies to be a reservoir rock would be reduced, if most of the lime mud had not been removed from the carbonate sand-body. A moderate to high-energy depositional environment is necessary for the removal of the micrite. This is discussed in the shallow ramp (Section 3.3.2), and Ratawi sand-body geometry and carbonate ramp model (Section 3.5.2).

### **3.3.2 Shallow Ramp: rudstone, grainstone-packstone with open-marine fauna**

The shallow ramp lithofacies has a great economic potential, during the exploration and the development of reservoir units A, B, C, and D. Under suitable diagenetic conditions, most of the shallow ramp primary depositional porosity is preserved, creating a reservoir unit with porosity more than 15%. The significance of the shallow ramp lithofacies becomes clear from microfacies analysis of core samples collected from reservoir unit-D, well R-50 on the flank of the main Wafra area. In addition, Longacre and Ginger (1988) reported that carbonate sand-bodies (shallow ramp lithofacies) with high primary depositional porosity were important in reservoir units A, B and C at the crest of the structure of the main Wafra area.

The microfacies analysis carried out in this study indicates two main causes of the loss of primary porosity, and so reservoir potential, in units C, D and F, well R-49 in the southern Wafra area, and unit-C and unit-F, well R-50 in the main Wafra area. The first cause is unsuitable early and late diagenetic conditions for the preservation of primary porosity in the carbonate sand-bodies of the shallow ramp (Chapter 4). The



second cause is the unsuitable environmental conditions for the development of the shallow-ramp carbonate sand-bodies. The development of the Ratawi sand-bodies was influenced by two factors. The first is the stratigraphic position of the ramp sand-body facies in the Ratawi sequence of initiation, development and termination of the Ratawi platform. The second is the palaeogeographic position within the Ratawi epeiric ramp, which controls the energy of the depositional environment. The different geometries of the shallow-ramp sand-bodies are reviewed in Section 3.5.2. Understanding the depositional environment that controls the occurrence and the geometry of the shallow-ramp sand-body lithofacies is important in Ratawi reservoir development and in the exploration for similar reservoir facies.

The shallow-ramp lithofacies association is common in the Ratawi Oolite and Ratawi Limestone and accounts for about 24% of the core samples. The lithofacies association of rudstone and grainstone-packstone with an open-marine fauna is divided into five microfacies. These microfacies are peloidal bioclastic rudstone with coral and ooids (SR1), cross-laminated peloidal bioclastic grainstone-packstone (SR2), peloidal bioclastic grainstone-packstone with ooids and aggregates (SR3), peloidal bioclastic grainstone-packstone (SR4), and peloidal bioclastic packstone with black grains (SR5).

### **3.3.2.1 Microfacies SR1: peloidal bioclastic rudstone with coral and ooids**

The most striking feature for this microfacies is the rudstone texture, which is a grain-supported depositional texture with more than 10% of the grains larger than 2 mm (Fig. 3-5 a). These grains consist of fragmented, reworked coral and bivalve (rudist) bioclasts. Microfacies SR1 is relatively rare, representing 3% of core samples. The dominant grains are non-skeletal with common skeletal particles.

Peloids are the most dominant particles composed of microcrystalline carbonate, without any internal structure. They are subrounded in shape, and medium to coarse sand size. Flügel (1982) and Tucker and Wright (1990) reviewed the origin of peloids, and concluded that peloids have polygenetic origins. The different origins of peloids include faecal pellets, calcareous algae, mud clasts and micritized non-skeletal and skeletal grains. This reflects the difficulty in applying the approach of microfacies analysis to interpret the palaeoecology from Ratawi grain assemblages. The occurrence of the Ratawi peloids is not in lenses; also the particles are not organic-rich nor have any internal structure, which eliminate an origin as faecal pellets and calcareous algae. This leaves two possible origins for Ratawi peloids, mud clasts



and micritized non-skeletal and skeletal grains. The micritization processes are produced by endolithic micro-organisms and by recrystallization, and these are discussed in Chapter 4. Modern-day peloids are an important constituent of shallow-marine carbonate sediments on the northern Belize Shelf and Trucial Coast. They are typically formed by micritization of grains, non-skeletal and skeletal, in shallow, low-energy, restricted marine environments (Tucker and Wright, 1990).

The skeletal particles include corals, bivalves, brachiopods, crinoids and forams, which constitute an open-marine fauna in addition to green algae *Bacinella* (Fig.3-12 b). Most of them have micritic envelopes, the origin of which is discussed in Chapter 4. This fossil assemblage indicates normal marine salinity (Wilson and Jordan, 1983). Coral bioclasts are common, usually more than 2 mm in diameter, bored and rounded. They indicate the presence of coral reefs near the study area. The coral bioclasts were eroded, reworked and transported to the site during high-energy, storm events. Mesozoic and Cenozoic corals are belonging to the scleractinian coral group. This group of corals has hard parts composed exclusively of aragonite (Adams and Mackenzie, 1998). The internal structure of the corals shows different degrees of preservation from well preserved to poorly preserved, discussed in Chapter 4.

Bivalve and brachiopod bioclasts are common, medium to coarse sand size, and disarticulated and not rounded. This shape indicates they were not transported any great distance. Some of the bivalve bioclasts have thick shells, derived from rudists. Crinoids are also common, medium sand in size and broken up. Forams are rare. The original mineralogy for most bivalves, brachiopods, crinoids and forams is calcite, therefore most of the internal structure of these particles is well preserved and not micritized. Rudist bivalves are typical and often very common in the Ratawi Formation. Rudist palaeoecology and stratigraphy are reviewed by Ross and Skelton (1993).

The rudist bivalves were sessile epifaunal suspension feeders, from the late Jurassic to the late Cretaceous. They flourished in shallow-marine carbonate settings at low latitudes. Rudists were largely bioclast contributors and not frame-builders. They could not themselves construct continuous branching reef frameworks, but occupied substrates typical for non-colonial benthic invertebrates. There was a close correlation between shell growth form, morphotypes, and the nature of the substrate. Rudist shells may be classified into three broad palaeoecological morphotypes. These are elevators, clingers and recumbents. The recumbent rudists evolved during the middle Cretaceous



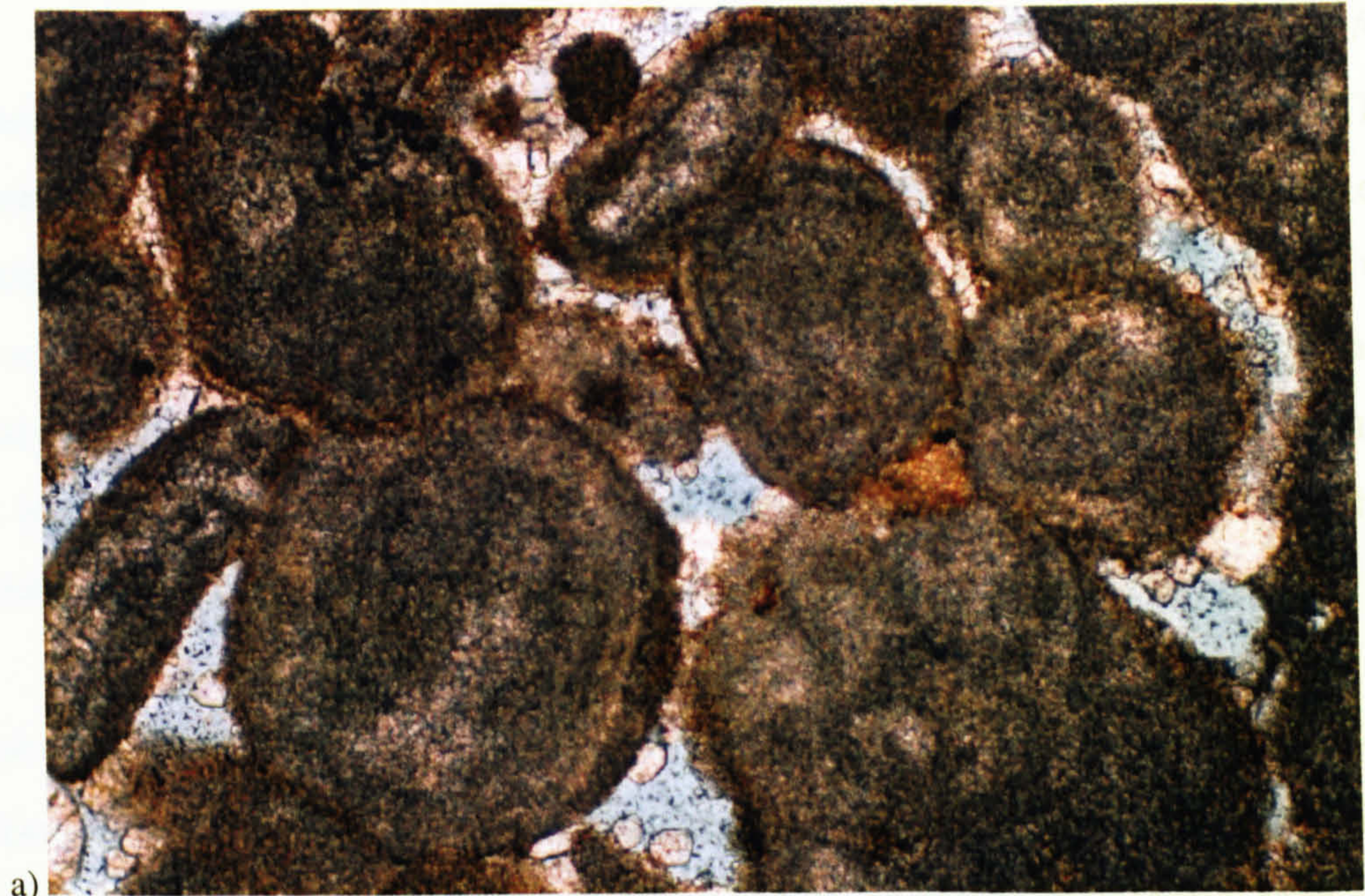
(early Aptian, Albian to Cenomanian and Campanian to Maastrichtian). The palaeoecology of this shell growth form is characteristic of a high-energy environment. During the lower Cretaceous Ratawi Formation, elevators and clingers evolved. The palaeoecology of this shell growth form is characteristic of a low energy environment.

The Arabian Gulf Cretaceous rudist-bearing carbonates were reviewed by Alsharhan (1995). The rudist-bearing carbonates in this region contain many giant oil fields, for their favourable depositional and diagenetic conditions. These rudist-bearing carbonate units include the Aptian Shuaiba Formation (Thamama Group), the Cenomanian Mishrif Formation (Wasia Group), and the Maastrichtian Simsima Formation (Aruma Group). A regional unconformity with subaerial diagenesis overprints the upper boundary of each of these formations. The Shuaiba Formation is dominated by rudists, mainly caprinids, with a smaller number of caprotinids, monopleurids and requienids. Associated with the rudists are calcareous algal crusts, foraminifera and echinoid plates.

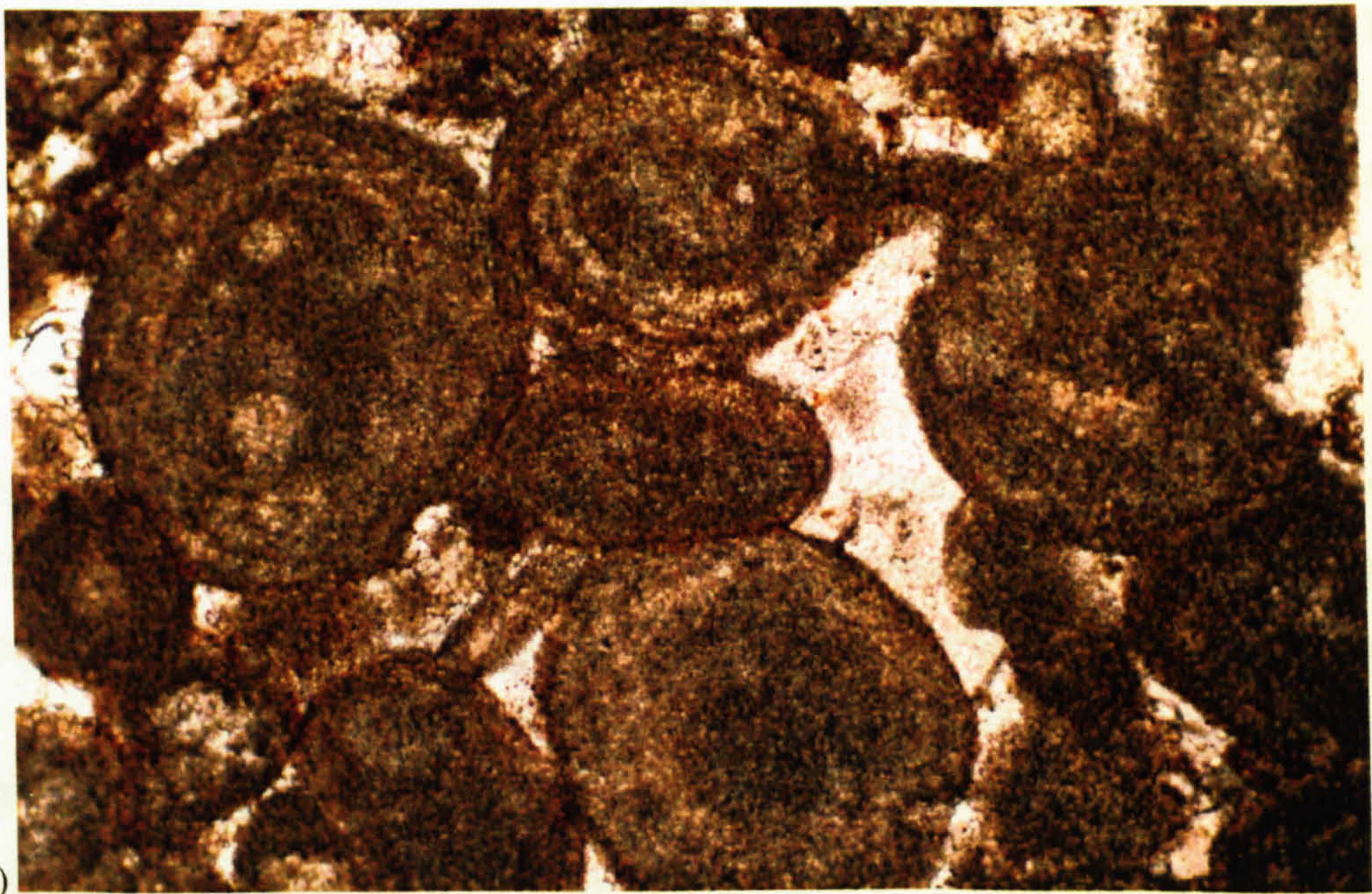
These accumulated in mudstones through packstones, and carbonate sands in a normal-marine shallow-shelf setting. The excellent reservoir porosity and permeability of rudist-bearing carbonates are the products of primary and secondary porosity. Freshwater leaching during post-Aptian, post-Cenomanian, and post-Maastrichtian erosion enhanced the secondary moldic porosity. Other porosity types that occur include interparticle, intraparticle, vuggy, growth framework, shelter, intercrystalline, and rootlet (karstic). Fracturing locally improved porosity and permeability. The Lower Cretaceous rudists are characterized by thick shells of calcite with some layers of aragonite. The thick rudist shells could supply a large quantity of bioclasts. Some of the peloids of the Ratawi Formation could be derived from the micritization of the rudist bioclasts.

Ooids are rare, but occur in units C, D, E and F in the Ratawi Oolite (Figure 3-4); they are medium sand in size (about 0.5 mm) and mixed with bioclasts and peloids. The ooids are normal in nature where there are more than three concentric laminae coating the small nucleus. All ooids have a similar microfabric, internal structure and size, which indicate they are the same generations of ooids. The origin of ooids is reviewed by Flügel (1982) and Tucker and Wright (1990). They described three types of ooids. These are superficial, micritic and normal ooids. The ooid microfabric is influenced by the energy level of the depositional environment and by mineralogy.





a)



b)

Figure 3-4) Photomicrograph of oolitic grains characteristic of microfacies SR-1 in reservoir Unit D. Note the large nucleus and the concentric laminae of the grains; most of the grains are severely micritized. In (a) depositional interparticle porosity is preserved to some extent from reduction by chemical and physical compaction by patchy early meteoric bladed cement, whereas in (b) most of the porosity is filled by post-compaction, granular cement. Sample numbers are a) R-50 # 73, depth 6925 ft (2111 m), field of view 1 x 0.6 mm, b) R-50 # 70, depth 6912 ft (2107 m), field of view 1 x 0.6 mm, under plane-polarized light.

The Ratawi normal ooids seem to have formed under a high-energy depositional environment and the 'calcite-sea' of the Lower Cretaceous period (Sandberg, 1983). The modern sites of active ooid formation are warm, shallow water generally less than 2 metres deep, saturated to supersaturated with respect to calcium



carbonate. The water must be agitated to form regular concentric coats. These environmental requirements for ooid formation are found in oolite shoal complexes in the Trucial Coast and the Bahamas (Tucker and Wright, 1990). Flügel (1982) used normal ooids and peloids with other non-skeletal grains in a scheme to infer the energy of the depositional environment, as is discussed in Section 3.2.1.2.3. Peloids in this scheme indicate a low-energy environment, whereas normal ooids indicate a high-energy environment.

*Reservoir state:* Microfacies SR1 is both a reservoir and a non-reservoir unit. When the primary depositional pores of this microfacies are not infilled by cement or reduced by burial compaction, or the porosity is enhanced by exposure diagenesis, then it is a reservoir rock with porosity more than 15%. This microfacies is seen in the upper part of reservoir unit D. The microfacies is a non-reservoir unit, with porosity between 5% to 10%, when most of the primary depositional pore space is lost by burial compaction and cementation. The common pore types in this microfacies are interpartic<sup>le</sup>al, fracture and vug.

*Depositional environment:* Microfacies SR1 contains faunas which are open-marine in nature. The rudstone depositional texture, with reworked coral bioclasts, suggests high-energy events, such as storms, during which coral was eroded and transported to the site. The rare ooids could also be transported to the site during these high-energy events. There is no evidence to support a faecal pellet or algal origin for the peloids, so that the peloids are interpreted as the result of micritization of skeletal and non-skeletal particles by endolithic micro-organisms, during periods of low-energy and low-sediment supply. This evidence suggests that microfacies SR1 was deposited in skeletal and non-skeletal sand shoals, which formed in agitated shallow water. Coral reefs and ooid shoals were close to the area. Shoal sediment was washed over to the back ramp, low-energy restricted lagoon and the skeletal and non-skeletal grains were micritized to peloids there.

Microfacies SR1, peloidal bioclastic rudstone with coral and ooids, compares most closely to standard microfacies SMF 11 of Wilson (1975), grainstone with coated bioclasts that may be micritized, in sparry cement. This suggests standard facies belt 6, environments of winnowed platform edge sands, an area with constant wave action close to and above wave base. This description could be similar to microfacies SR1,



when occasional high-energy events (storms) are added to form the rudstone texture.

### **3.3.2.2 Microfacies SR2: cross-laminated peloidal bioclastic grainstone-packstone**

The most conspicuous feature for microfacies SR2 is the flaser bedding and cross lamination of peloidal and bioclastic grainstone-packstone (Fig. 3-5 b). This microfacies is rare, representing around 1% of core samples. Sedimentary lamination, less than 1 cm in thickness, is produced by changes in sediment composition and/or grain size. The carbonate sand grains were transported as bedload, while micrite was transported in suspension. Carbonate sand was transported as ripples and dunes.

The proportions of the carbonate sand to micrite produce two types of ripple, flaser bedding and lenticular bedding. Flaser bedding is formed when mud is deposited intermittently with migrating carbonate sand ripples. This produces thin streaks of micrite between the sets of the cross lamination, and micrite is concentrated in ripple troughs. Lenticular bedding forms when isolated ripples of carbonate sand migrated over mud to produce cross-laminated lenses of carbonate sand within micrite. Flaser bedding and lenticular bedding are common in the carbonate tidal-flat environment, which are distinguished by fluctuations in sediment supply and flow strength of the flood and ebb tidal currents (Tucker, 1991).

The dominant particles are peloids with rare skeletal particles. Peloids are fine sand in size, subrounded in shape, without any internal structure, and composed of microcrystalline carbonate. As discussed in microfacies SR1 (Section 3.3.2.1), there is no evidence to support a faecal or algal origin for the peloids in microfacies SR2, which leaves two possible origins: mud clasts and micritized non-skeletal and skeletal grains. The micritization processes by endolithic micro-organisms and recrystallization are discussed in Chapter 4. The skeletal particles are crinoids and sponge spicules, which indicate normal-marine salinity (Wilson and Jordan, 1983). The crinoids are common to rare, broken up, medium to fine sand in size. The sponge spicules are rare; the original siliceous bioclasts were completely dissolved out and the moulds filled by granular drusy calcite. This process is discussed in Chapter 4.

*Reservoir state:* Microfacies SR2 is a non-reservoir unit. Most of the primary depositional pore space was lost by burial compaction and cementation. The common



pore types in this microfacies are interparticle and vug. The measured porosity is 4% to 5%.

*Depositional environment:* The fauna of microfacies SR2 is open-marine in nature. The most useful environmental indicator for microfacies SR2, is the sedimentary structure flaser bedding. This indicates fluctuations in sediment supply and flow strength of the flood and ebb tidal currents. This process is typical of shallow-subtidal to intertidal environments (Tucker, 1991).

### **3.3.2.3 Microfacies SR3: peloidal bioclastic grainstone-packstone with ooids and aggregates**

Microfacies SR3 is distinguished by the aggregate particles (Fig. 3-7 a). The percentage of this microfacies is about 6% of core samples. The dominant particles are non-skeletal with common bioclasts. The non-skeletal particles are peloids, ooids, aggregates and quartz grains. Peloids are the most dominant grains, medium to coarse sand in size and subrounded in shape. As in microfacies SR1 there is no evidence to support the origin of the peloids as faecal pellets and calcareous algae. This leaves two possible origins mud clasts and micritized non-skeletal and skeletal grains.

Ooids are common to rare, medium sand in size and mixed with the bioclasts and peloids. The ooids are of the normal type. The origin of ooids is discussed in Section 3.3.2.1. Quartz grains are rare, fine to medium sand in size, and subangular in shape. As discussed in Section 3.3.1.3, the source for the detrital quartz is interpreted to be the Zubair delta. The skeletal particles are coral, brachiopod, crinoid, foram and green algae. Corals are rare, up to 1 mm in size, bored and rounded. Brachiopods are rare to common, and usually disarticulated. Crinoids are rare to common, broken up and normally with syntaxial cement. Forams and green algae are rare. The original mineralogy for the green algae was aragonite, which was dissolved out and the mould infilled by drusy calcite cement.

Aggregate is the distinguishing grain for the microfacies SR3. Aggregates (Fig. 3-6) are common to rare, fine to coarse sand in size, irregular in shape, and with non-specific internal structures. Flügel (1982) and Tucker and Wright (1990) reviewed the origin of aggregates. Four types of aggregate grains have been recognized. These are



grapestone, algal lump, lump, and caliche lump. The fourth type formed in the vadose zone by exposure diagenesis. The first three types of aggregate grain form when several carbonate grains become bound and cemented together in the marine environment. Flügel (1982) argued that three types of the marine aggregate are overlapping, and it is more useful to group grapestone and lump together, since they are controlled by the energy of the environment (water agitation). Algal lumps are less controlled by energy of the environment. There is no evidence to support an algal origin, and most likely, the Ratawi aggregates are a form of grapestone.

Flügel (1982) discussed using grapestones and lumps (non-algal lumps) in a scheme to indicate the energy of the depositional environment. This is done by eliminating all particles, which are not controlled by energy of the environment, but are more controlled by diagenesis (like caliche lumps and vadose pisoids) and organisms (like fecal pellets, and algal lumps). This simplified scheme of environmental energy indication shows that there are correlations between increasing water energy and the formation of certain carbonate particles. With increasing water agitation, the following succession of carbonate particles are formed: (1) lime mud and silt, (2) peloids and cortoids (grains with micritic envelopes), (3) aggregates and oncoids (irregularly formed particles with non-concentric partially overlapping micritic laminae), (4) normal ooids. In this scheme (1) and (2) carbonate particles, occur in relatively low energy lagoonal environments, (3) form in areas of moving water, and (4) originate in strongly agitated water.

*Reservoir state:* Microfacies SR3 characterizes reservoir unit-D, with porosity more than 15%, when the primary depositional pores are not reduced by cement or burial compaction. The depositional porosity of reservoir unit-D is enhanced by vugs and dedolomitization. However, microfacies SR3 is also found in non-reservoir units, when the porosity is reduced by physical and chemical compaction, and cementation. The common pore types in this microfacies are interparticle, vug and fracture.

*Depositional environment:* The faunas of microfacies SR3 are open-marine in nature. The depositional texture, grainstone-packstone, is characteristic of a depositional environment with medium to high-energy. However, aggregates, the distinguishing particle for this microfacies, formed in areas of low to medium water circulation. Microfacies SR3 was deposited as peloidal bioclastic sand shoals in medium to high-



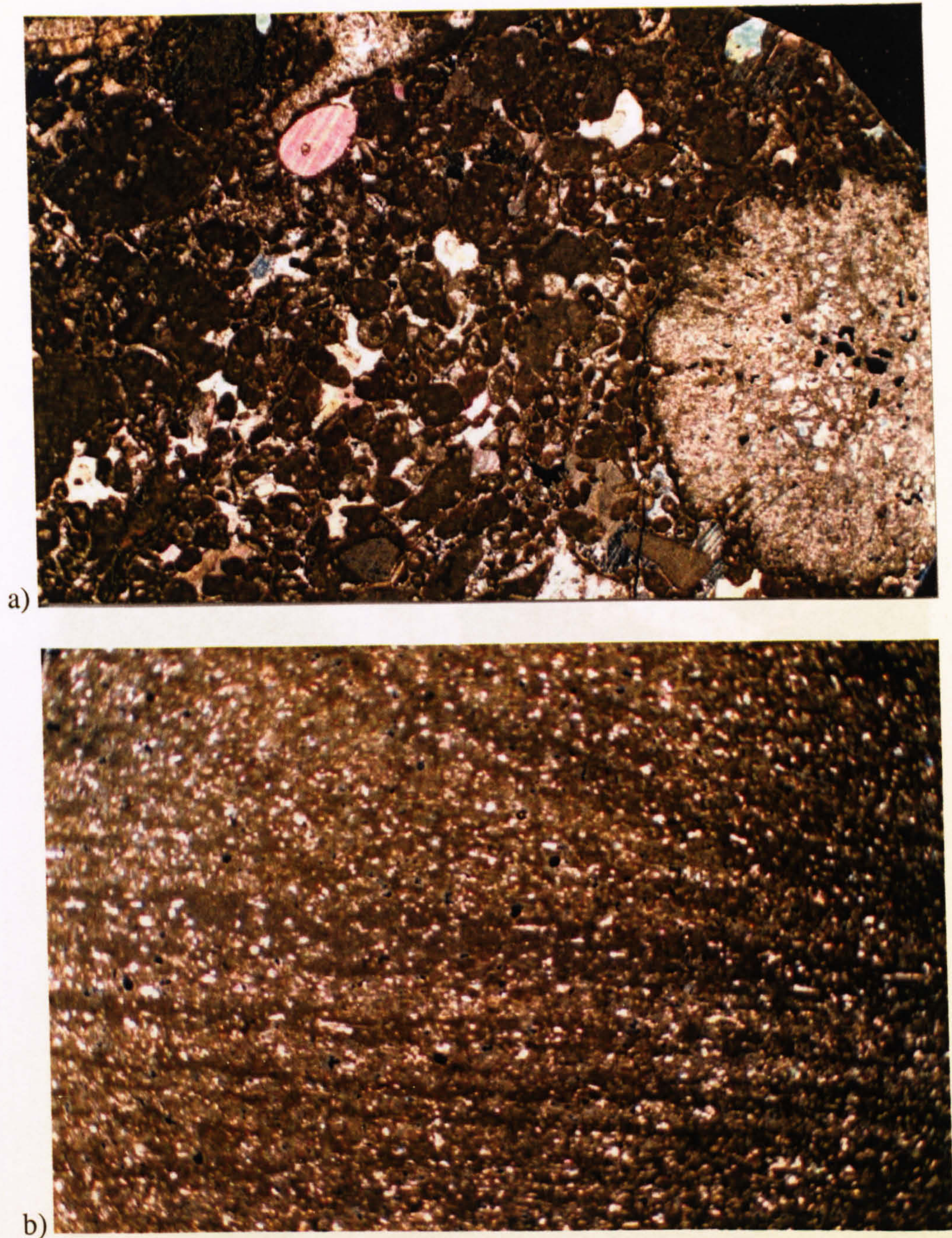


Figure 3-5 a) Photomicrograph of microfacies SR1: peloidal bioclastic grainstone-rudstone with coral debris and ooids. Note the eroded edges of the coral grain. Most of the interparticle porosity has been reduced by chemical compaction and later burial post-compaction cement. Sample number is R-50 # 87, depth 6994 ft (2132 m), field of view 10 x 7 mm, under crossed polars. b) Photomicrograph of microfacies SR2: cross-laminated peloidal bioclastic grainstone-packstone. The cross-lamination is marked by the compaction of micritic laminae. Sponge spicules are parallel to the lamina. This microfacies has little porosity. Sample number is R-49 # 56, depth 6832 ft (2082 m), field of view 10 x 7 mm, under crossed polars.



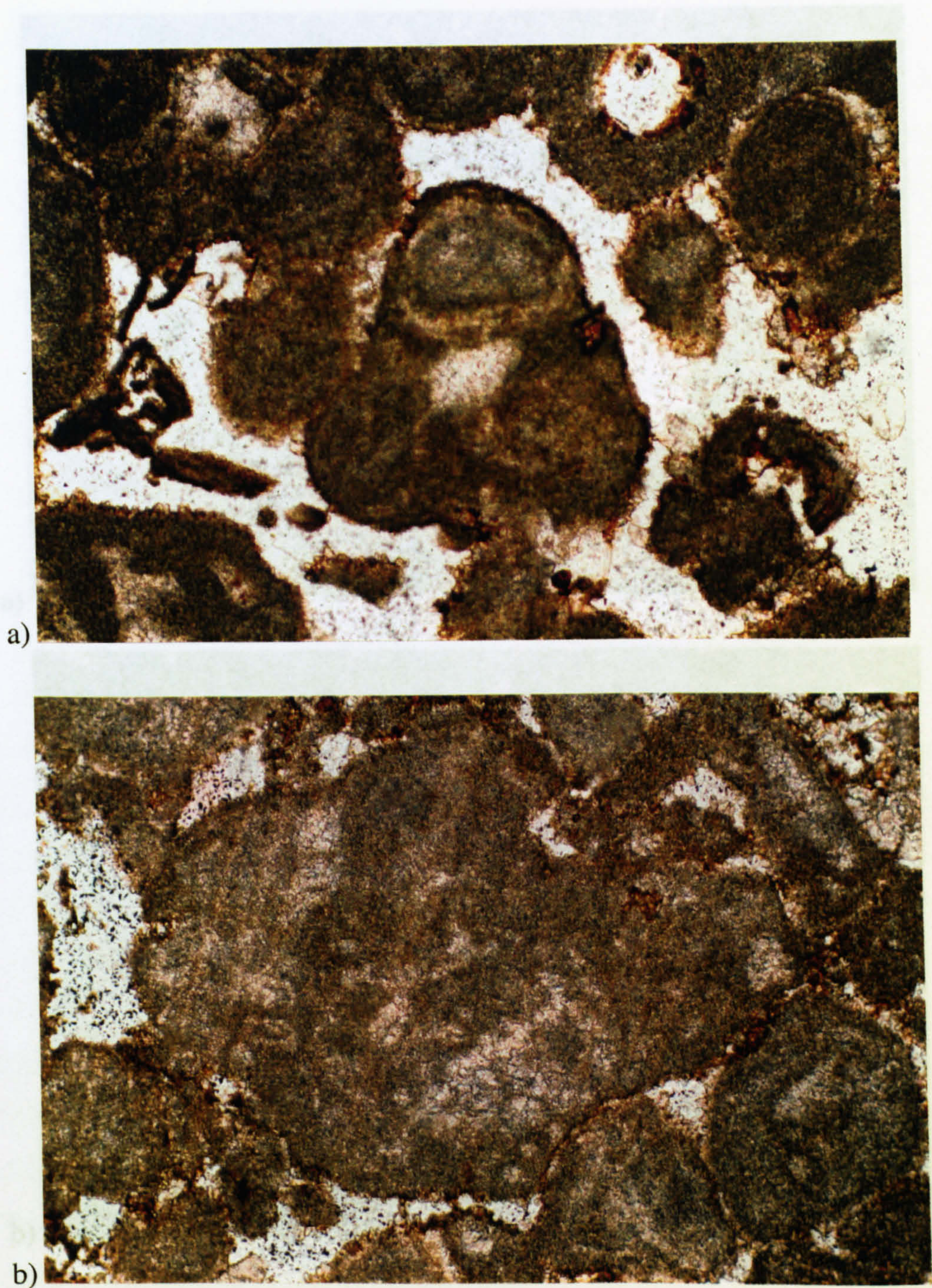


Figure 3-6) Photomicrograph of aggregate grains characteristic of microfacies SR-3. Most of the grains are severely micritized. Sample numbers are a) R-50 # 71, depth 6917 ft (2108 m), field of view 1 x 0.6 mm, b) R-50 # 70, depth 6912 ft (2107 m), field of view 1 x 0.6 mm, under plane-polarized light.



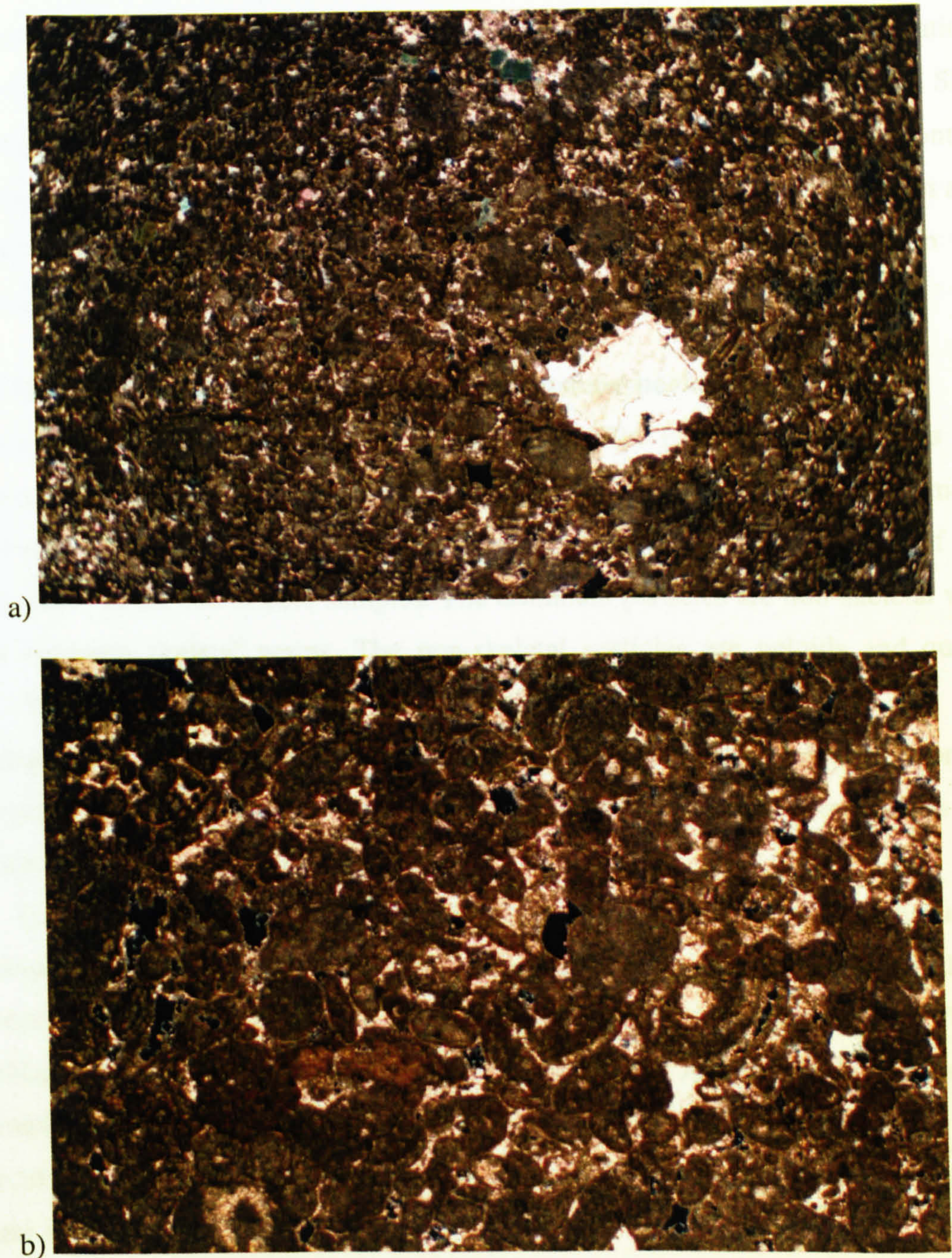


Figure 3-7 a) Photomicrograph of microfacies SR3: peloidal bioclastic grainstone-packstone with ooids and aggregates. Crinoid grain has a syntaxial cement. Some of the interparticle porosity is preserved from burial compaction by early meteoric cement; most of the depositional porosity is reduced by early vadose compaction and later burial compaction, in addition to burial calcite cement. Sample number is R-50 # 74, depth 6934 ft (2114 m), field of view 10 x 7 mm, under crossed polars. b) Photomicrograph of microfacies SR4: peloidal bioclastic grainstone-packstone. Some of the interparticle porosity is preserved from chemical compaction by meteoric cement; most of the porosity is reduced by early vadose compaction and late chemical compaction, as well as later burial calcite cement. Sample number is R-49 # 43, depth 7005 ft (2135 m), field of view 3 x 2 mm, under crossed polars.



energy environments with periods of low to medium water circulation to form the aggregates. These could be back shoal areas near a lagoon with restricted circulation. Oolitic sand shoals and coral reef could have been nearby. Microfacies SR3 and SR4 characterize the Ratawi carbonate sand-body. Understanding the factors that control the porosity and geometry of the Ratawi sand-body is important in the exploration and development of reservoir units A, B, C and D. These factors are analyzed in the framework of the Ratawi Oolite platform initiation, development and termination. | relevant.

#### 3.3.2.4 Microfacies SR4: peloidal bioclastic grainstone-packstone

The main difference between microfacies SR3 and SR4 is that the latter does not contain aggregate grains indicating a continuous medium to high energy environment, without periods of low to medium water circulation (Fig. 3-7 b). The percentage of this microfacies is about 7% of core samples. The dominant particles are non-skeletal with rare to common skeletal grains. The non-skeletal particles are peloids and quartz grains. Peloids are the most dominant particles, fine to coarse sand size and subrounded in shape. As in SR1 microfacies there is no evidence to support the origin for the peloids as faecal pellets or calcareous algae, and they are mostly mud clasts and micritized non-skeletal and skeletal grains.

Quartz grains are rare, fine sand in size, and subangular in shape. As discussed in Section 3.3.1, the source for the detrital quartz is interpreted to be the Zubair delta. The bioclasts are corals, bivalves, brachiopods, crinoids and forams. This fossil assemblage indicates normal-marine salinity (Wilson and Jordan, 1983). Corals are rare, rounded in shape and medium sand in size. Bivalves and brachiopods are rare, disarticulated, and of medium sand size. Crinoids are rare to common, broken up, and medium sand size. Forams are rare.

*Reservoir state:* microfacies SR4 like the previous microfacies SR3, characterizes reservoir unit-D, with porosity more than 15%. The diagenetic secondary porosity vugs and dedolomitization, enhance the depositional porosity of reservoir unit-D. Nevertheless, this additional secondary porosity is not the controlling porosity in this reservoir unit. The main dominant porosity in reservoir unit-D is the depositional primary porosity. In addition to interparticle pores, vugs and fractures are also common. This microfacies of the Ratawi sand-body is a non-reservoir unit when the primary depositional porosity has been reduced by cementation or burial compaction.



*Depositional environment:* The carbonate sand-body of the Ratawi is characterized by microfacies SR3 and SR4. Both microfacies were deposited in open-marine peloidal bioclastic shoals in medium to high-energy environments. Microfacies SR4 is characterized by a depositional environment without periods of low to medium water circulation that formed the aggregates in microfacies SR3. This difference between microfacies SR3 and SR4 could suggest that microfacies SR4 was deposited on the front of sand shoals near the open circulation of the sea, whereas microfacies SR3 was deposited in the back shoal area near the restricted circulation of the back-ramp lagoon.

### **3.3.2.5 Microfacies SR5: peloidal bioclastic packstone with black grains**

The main difference between this microfacies and microfacies SR4 and SR3 is that microfacies SR5 contains black grains (Fig. 3-3), which are evidence for subaerial exposure. In addition, the packstone depositional texture of microfacies SR5 indicates that this microfacies was deposited in the lowest energy environment in the sand-body microfacies of the Ratawi shallow ramp (Fig. 3-8 a). The percentage of this microfacies is about 6% of core samples. The dominant particles are non-skeletal with rare to common skeletal particles. The non-skeletal particles are peloids, grains and quartz grains.

The dominated particles are the peloids, fine to medium sand in size and subrounded in shape. As in microfacies SR1 there is no evidence to support an origin as faecal pellets and calcareous algae, leaving two possible origins: mud clasts and micritized non-skeletal and skeletal grains. Black grains are common to rare, fine to medium sand in size, and rounded in shape. The possible origin and the causes of the blackening of the grains is reviewed in Section 3.3.1.3. The occurrence of black grains in this study is taken to indicate deposition near coastal and terrestrial environments. Quartz grains are rare, fine sand in size, and subangular in shape. As discussed in Section 3.3.1, the source for the detrital quartz grains is interpreted to be the Zubair delta. The skeletal particles are bivalves, brachiopod, crinoid and foram, which indicate normal marine salinity (Wilson and Jordan, 1983). Bivalves and brachiopods are rare to common, disarticulated, and medium sand in size. Crinoids are rare to common, broken up, and medium sand in size. Forams are rare to common.



*Reservoir state:* Microfacies SR5 is a non-reservoir unit. The range of the porosity is between 0% to 10%. The common pore types in this microfacies are interparticle, vug, intraparticle and fracture. It seems that the packstone texture reduced the reservoir potential of this microfacies.

*Depositional environment:* Microfacies SR5 contains an open-marine fauna. The packstone texture and black grains indicate that it was part of the marine sand shoal, which <sup>was</sup> ~~were~~ affected by subaerial exposure and development of soil profiles. The black grains <sup>were</sup> ~~was~~ eroded, transported and redeposited in the moderate-energy environment of the inner part of the shallow ramp sand-body near the low-energy lagoon. There are two possible interpretations of the subaerial exposure of the Ratawi marine shoal. The first interpretation is the building up of the marine sand-body above sea level; the second is the lowering of sea level.

### **3.3.3 Deep Ramp: mudstone-wackestone with open-marine fauna**

The deep-ramp lithofacies association was deposited in a low-energy, deep-water, open-marine environment. This lithofacies association is common in the Ratawi Oolite and Ratawi Limestone, and accounts for about 11% of the core samples. The low-energy is inferred from the mud-support texture in the wackestone, mudstone and floatstone, which is a characteristic texture for a low-energy, deep-ramp. The origin of the micrite is discussed in Section 3.3.1, and the evidence from this study supports a primary origin for the lime mud.

A deep-water environment is inferred from an association of the open-marine fauna with the mud-support texture, which indicates deposition below fair-weather wave-base. The deep ramp (DR) wackestone-mudstone with open-marine fauna lithofacies association is divided into four microfacies: Microfacies DR1: peloidal bioclastic floatstone (Section 3.3.3.1); microfacies DR2: bioturbated bioclastic mudstone (Section 3.3.3.2), microfacies DR3: bioturbated bioclastic wackestone (Section 3.3.3.3), and microfacies DR4: biomorpha (whole-shell) wackestone (Section 3.3.3.4).

#### **3.3.3.1 Microfacies DR1: peloidal bioclastic floatstone**

The floatstone texture is the most striking feature for microfacies DR1, which has a mud-supported depositional texture with more than 10% of the grains larger than 2



mm (Fig. 3-8 b). These grains consist of fragmented, reworked corals and rudist bioclasts. The matrix is bioturbated. Microfacies SR1 is rare, representing 1% of core samples. The dominant particles are non-skeletal with common skeletal particles.

The non-skeletal particles are peloids and quartz grains. The dominant particles are peloids, fine to medium sand in size, and subangular in shape. As discussed in Section 3.3.2 there is no evidence to support a faecal pellet or calcareous algal origin, mud clasts and micritized non-skeletal and skeletal grains are likely. Quartz grains are rare, fine sand in size, and subangular in shape. The source for the detrital quartz grains is the Zubair delta, discussed in Section 3.3.1.

The skeletal particles are coral, bivalve, gastropod, brachiopod, crinoid and foram. This fossil assemblage indicates normal marine salinity (Wilson and Jordan, 1983). Corals are rare, mostly medium sand in size although some are much larger, up to 10 mm. They appear to have been transported from outside the area. Bivalves are rare to common, medium to coarse sand in size mostly and disarticulated. Rudist bivalve fragments reach 30 mm in size. Gastropods are common, fragmented, medium to coarse sand in size. The original mineralogy was aragonite, which dissolved out and the mould filled by drusy calcite. Brachiopods are rare, disarticulated and medium size. Crinoids are common, fragmented and fine to medium sand in size. Forams are rare.

*Reservoir state:* This facies is a non-reservoir unit. The range of the porosity is between 3% to 10%. The common pore types in this microfacies are mouldic, interparticle, vug and fracture

*Depositional environment:* Microfacies DR1 contains an open-marine fauna. The floatstone, mud-support texture, indicates deposition below fair-weather wave-base. The large grains, more than 2 mm, indicate high-energy storm events; a coral reef was probably located nearby. The depositional environment was a low-energy deep ramp, with occasional high-energy storm events.

### **3.3.3.2 Microfacies DR2: bioturbated bioclastic mudstone**

DR2 microfacies is characterized by a bioturbated argillaceous mudstone texture (Fig. 3-9 a). The percentage of this microfacies is about 3% of core samples. The evidence from this study supports a primary origin for the lime mud, which is discussed in





Figure 3-8 a) Photomicrograph of microfacies SR5: peloidal bioclastic packstone with black grains. The black grains have a variable size; residual clay occurs in dissolution seams. Sample number is R-50 # 49, depth 6783 ft (2067 m), field of view 5 x 3 mm, under plane-polarized light. b) Photomicrograph of microfacies DR1: peloidal bioclastic floatstone. Note large rudist shell fragments. There is little interparticle porosity. Sample number is R-49 # 27, depth 6889 ft (2100 m), field of view 5 x 3 mm, under plane-polarized light.



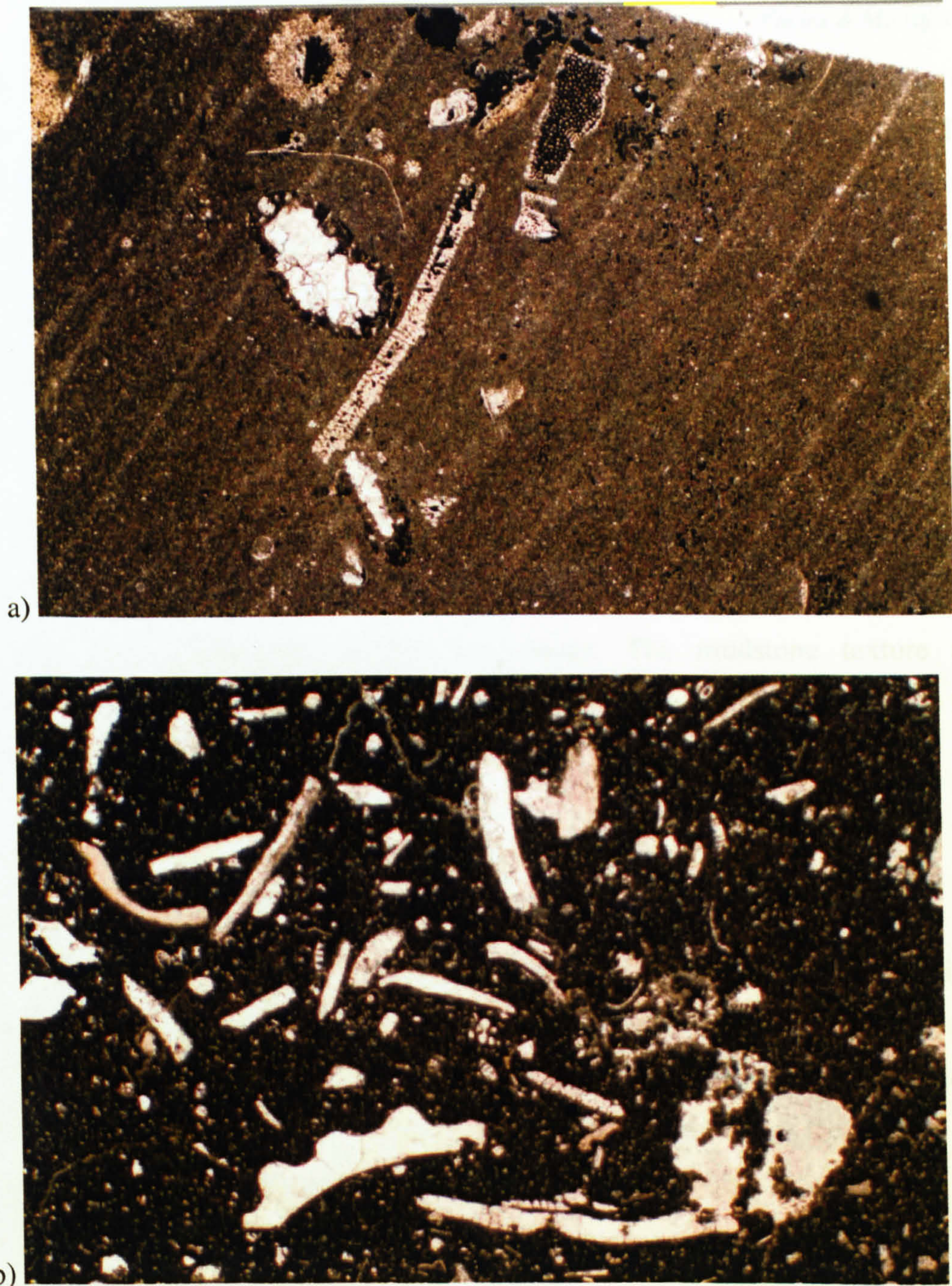


Figure 3-9 a) Photomicrograph of microfacies DR2: bioturbated bioclastic mudstone. Note the lack of syntaxial cement on the crinoid grain. Sample number is R-50 # 35, depth 6705 ft (2044 m), field of view 5 x 3 mm, under plane-polarized light. b) Photomicrograph of microfacies DR3: bioturbated bioclastic wackestone. Note the patchy distribution of the bioclasts as a result of bioturbation. Sample number is R-49 # 12, depth 6774 ft (2065 m), field of view 5 x 3 mm, under plane-polarized light.

Section 3.3.1. Quartz grains are rare to common, fine sand in size, and subangular in shape.

The skeletal particles are bivalves, brachiopods, crinoids, forams, radiolarians and calpionellids. This fossil assemblage indicates normal marine salinity (Wilson and Jordan, 1983), where radiolarians and calpionellids could indicate deep, open-marine



conditions (Scoffin, 1987). Bivalves, brachiopods and crinoids are disarticulated, rare to common, medium sand in size. Forams, radiolarians and calpionellids are rare. The original mineralogy for radiolarians was silica, which was dissolved out and the moulds were filled by drusy calcite cement. Burrows are marked by selective micro-euhedral dolomite. This process is discussed in Chapter 4.

*Reservoir state:* Microfacies DR2 is a non-reservoir unit. The range of the porosity is between 3% to 8%. The common pore types in this microfacies are vug, mouldic and fracture.

*Depositional environment:* Microfacies DR2 contains an open-marine fauna. Radiolarians and calpionellids indicate deep-water. The mudstone texture and bioturbation indicate low-energy, below fair-weather wave-base in a location with few high-energy, storm events.

### 3.3.3.3 Microfacies DR3: bioturbated bioclastic wackestone

Microfacies DR3 is very similar to the previous microfacies DR2. Both have a lime-mud support texture, and similar skeletal and non-skeletal particles. The only difference is that microfacies DR3 has more than 10% particles so that the depositional texture is a wackestone (Fig.3-9 b). Microfacies DR3 is interpreted as the deposit of a slightly higher energy environment than microfacies DR2. The percentage of this microfacies is about 6% of core samples.

*Reservoir state:* Microfacies SR3 is not found in reservoir unit D or E. The range of the porosity is between 0% to 16%. The common pore types in the microfacies are vug, mouldic, fracture and burrow.

*Depositional environment:* Microfacies DR3 is similar to DR2. Both microfacies contain an open-marine fauna. The bioturbated wackestone texture of DR3 indicates a slightly higher energy environment than DR2. Microfacies DR3 is interpreted to be deposited close to fair-weather wave-base or somewhat below it.



### 3.3.3.4 Microfacies DR4: biomorpha (whole-shell) wackestone

Microfacies DR4 has the same wackestone texture as the previous microfacies DR3, but the most noticeable feature is the presence of whole skeletal grains of thin-shelled bivalves (Fig. 3-10 a). The term biomorpha was coined by Flügel (1982) for whole skeletal grains. The preservation of the non-fragmented articulated shells requires a depositional environment of low-energy and / or rapid sedimentation. This microfacies is very rare, with only 0.5% of core samples.

*Reservoir state:* Microfacies DR2 is a non-reservoir unit. The porosity is about 3%. The common pore types in this microfacies are vug, mouldic and stylolitic.

*Depositional environment:* Microfacies DR4 is similar to microfacies DR3. Both microfacies have a wackestone texture, and open-marine faunas. The biomorpha and wackestone texture suggests deposition just below fair-weather wave-base. This microfacies is similar to the standard microfacies number 8 of Wilson (1975) and Flügel (1982).

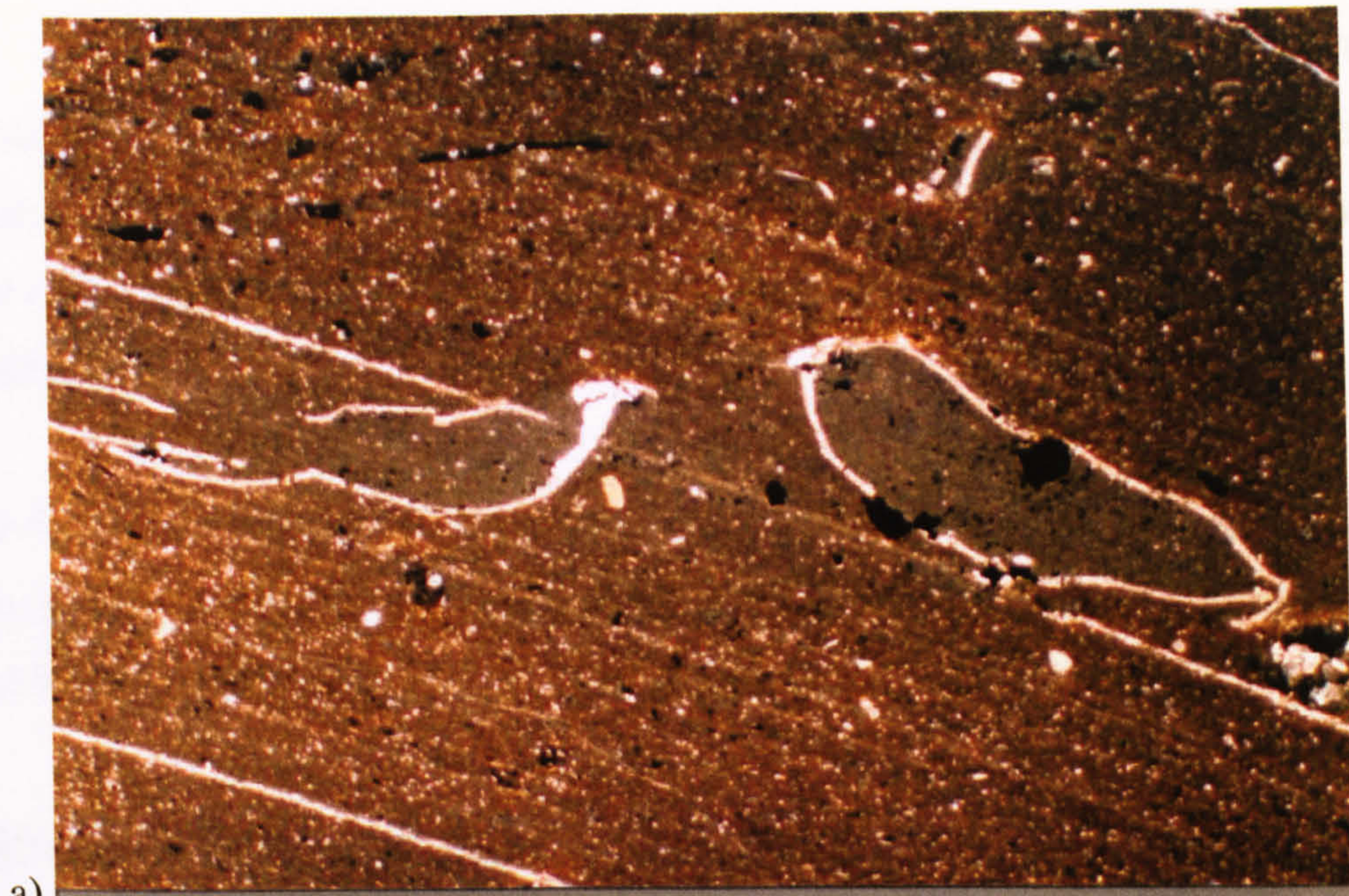
## 3.4 Diagenetic lithofacies associations

The diagenetic lithofacies association is the second lithofacies association observed in the Ratawi Oolite and Ratawi Limestone at Wafra oilfield. The diagenetic overprint modifies or obliterates the depositional texture and also affects the original depositional pore system resulting in an increase or decrease in the porosity of the Ratawi <sup>formation</sup>. The Ratawi <sup>formation</sup> diagenetic lithofacies association has two diagenetic facies: crystalline dolomite microfacies (DiagDol) and pedogenic calcrete microfacies (DiagCal).

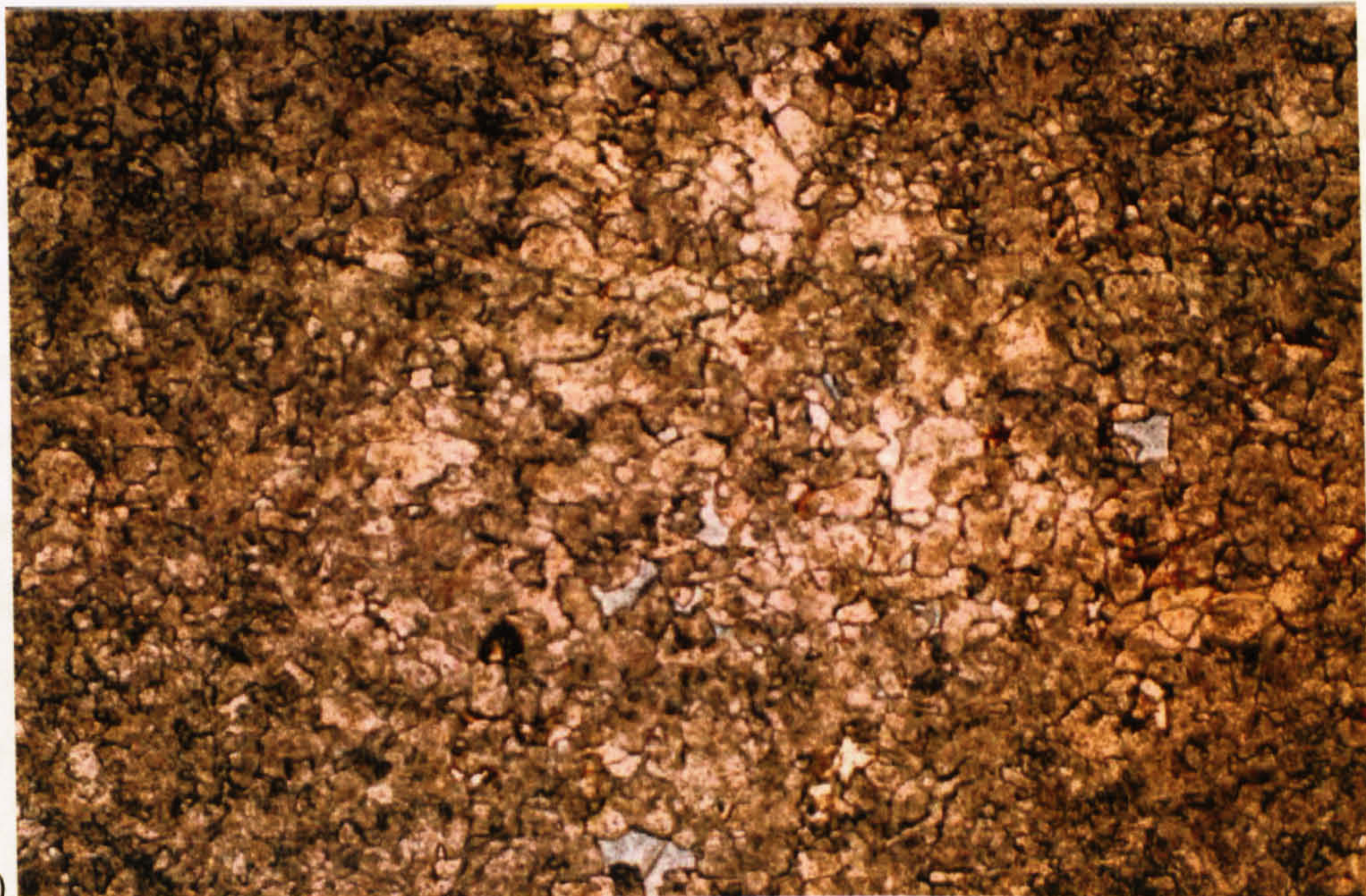
### 3.4.1 Microfacies DiagDol: crystalline dolomite

The crystalline dolomite microfacies (DiagDol) is characterized by 0.2-0.5 mm, curved dolomite crystals, with minor peloid ghosts (Fig.3-10 b). Under CL, the dolomite is mostly non-luminescent. This microfacies is very rare, only about 0.5% of the core samples. The microfacies is present in the Ratawi Oolite member in well R-49.





a)



b)

Figure 3-10 a) Photomicrograph of microfacies DR4: biomorpha (whole shell) wackestone-mudstone. The articulated thin bivalve shells have suffered mechanical compaction. This texture is termed biomorpha by Flügel (1982) (see Section 3.3.3.4 for additional explanation). Sample number is R-50 # 36, depth 6713 ft (2046 m), field of view 5 x 3 mm, under plane-polarized light. b) Photomicrograph of microfacies DiagDol: crystalline saddle dolomite. Crystal faces are non-planar surfaces and some intercrystalline porosity is present. Under CL, this facies is non-luminescent. Sample number is R-49 # 39, depth 6975 ft (2126 m), field of view 3 x 2 mm, under plane-polarized light.

*Reservoir state:* Microfacies DiagDol is a non-reservoir unit. The porosity is about 3%. The common pore types in this microfacies are intercrystalline, vug and fracture.



*Depositional environment:* Microfacies DiagDol is characterized by ghosts of peloids observed in the crystalline dolomite. This could indicate that this microfacies was originally deposited in a shallow subtidal carbonate environment, probably in a restricted lagoon.

*Diagenetic overprint:* This microfacies consists of saddle or baroque dolomite, and this typically forms as a deep burial cement filling pore space, or as a replacement. The origin of baroque dolomite is discussed in Chapter 4.

### **3.4.2 Microfacies DiagCal: pedogenic calcrete**

The pedogenic calcrete microfacies (DiagCal) is characterized by subaerial exposure features that formed through particular climatic conditions and duration of exposure (Fig. 3-13 and 3-14). Microfacies DiagCal is common, occurring in about 26% of the core samples. The microfacies analysis of the core samples collected from well R-50 indicates that microfacies DiagCal is the main controlling porosity in reservoir unit E, and upper-most part of unit D. The calcrete microfacies is the second lithofacies in the Wafra oilfield that has great economic potential, the first being the shallow ramp carbonate sand-body lithofacies (SR), discussed in Section 3.3.2.

In addition to the petrographic evidence (discussed in this section) that supports a pedogenic calcrete origin for reservoir unit-E, there is the stratigraphic evidence, that reservoir unit-E is located beneath a 2<sup>nd</sup>-order composite sequence boundary zone (Chapter 5). Reservoir unit E is the only one producing from the three areas of the Wafra oilfield, main Wafra, east Wafra, and southern Wafra (Longacre and Elliott, 1988).

The main controlling factors on the porosity development in reservoir unit E are the development of the subaerial exposure surfaces and calcrete microfacies (DiagCal), discussed under heterogeneity of reservoir unit E and palaeoclimate (Section 4.3.3.5.1). The preservation of the primary porosity, and the calcrete diagenetic porosity also depends on the subsequent diagenetic overprint until the oil emplacement in the pores, which is discussed in Chapter 4.

*Reservoir state:* Microfacies DiagCal characterizes reservoir unit-E, with porosity more than 15%, when the primary pores and diagenetic pores of the calcrete are not reduced by cementation or burial compaction. The range of the porosity is between 0%



to 16%. The common pore types in this microfacies are rootlet, vug, mouldic, interparticle, fracture and stylolitic,

*Diagenetic overprint:* Microfacies DiagCal is a subaerial exposure facies overprinted on lithofacies of the back ramp (BR) and shallow ramp (SR) lithofacies.

### **3.4.3 Subaerial exposure features**

Understanding subaerial exposure that leads to the formation of pedogenic and karst facies unconformities and porosity is important for the interpretation of Ratawi reservoir heterogeneity. Subaerial exposure is examined under two headings, recognition and application (Section 3.4.3 1) and karst surfaces and facies (Section 3.4.3 2).

#### **3.4.3.1 Subaerial exposure recognition and application**

Different methods and techniques can be used to detect subaerial exposure and unconformities. Budd *et al.* (1995) listed some of these techniques as (1) petrological features observed in cores and outcrops, (2) cycle stacking patterns (abrupt facies offsets), (3) interpretation of wireline logs, (4) eustatic sea-level curves, (5) seismic stratigraphy, (6) stable isotope geochemistry, (7) biostratigraphy and other methods of dating strata, and (8) computer modelling of tectonic, sea-level and basin evolution. The first four are applied in this study with different emphasis. The first method, petrological features observed in cores, is discussed in this section. The second method, cycle stacking patterns, is discussed in Chapter 5. The use of wireline logs, and eustatic sea-level curves is discussed in Chapters 5 and 6.

The Ratawi subaerial exposure surfaces and facies relate to three main topics in this study: (1) reservoir development and exploration of unit E, discussed in this Chapter, (2) palaeoenvironmental interpretation of the Ratawi, discussed in this Chapter, (3) Ratawi sequence stratigraphy modelling, discussed in Chapters 5 and 6. To achieve these aims, Ratawi subaerial exposure surfaces (unconformities) and associated subaerial exposure facies are analyzed in the framework of the Ratawi sequence stratigraphy. This is done by recognition of the cycle order of the Ratawi subaerial exposure surfaces, which are 5<sup>th</sup>, 4<sup>th</sup>, 3<sup>rd</sup> and 2<sup>nd</sup> orders and the factors that control the associated subaerial exposure facies with each exposure order.



Many of the Middle East Lower Cretaceous oilfields including the giant Wafra oilfield have secondary porosity generated through subaerial exposure (Harris *et al.*, 1984). Also Budd *et al.* (1995) associated subaerial exposure secondary porosity with many of the large oil and gas fields around the world including the Arun field of Indonesia, Yates field and Horseshoe atoll field of west Texas, and Golden Lane fields of Mexico. The importance of subaerially exposed carbonates in the development of reservoir zones and buried palaeokarst, is appreciated by many workers including Wright and Smart (1994) and Budd *et al.* (1995).

#### 3.4.3.2 Karst surface and facies

The term karst has been used in two ways, first to designate specific landforms that result mainly from the subaerial exposure and dissolution of carbonate rocks, and second to constitute a distinctive diagenetic facies (Esteban and Klappa, 1983). The term palaeokarst refers to karst features formed in the past, related to an earlier hydrological system or landsurface. There are three types of palaeokarst, relict, exhumed and buried (Wright and Smart, 1994). The Ratawi Formation reservoir unit E, in this study, is considered a buried palaeokarst with a calcrete diagenetic overprint, developed beneath a second-order sequence boundary, which is a subaerial exposure surface.

Depending on the climate, under which carbonate sediment and rock were subaerially exposed, different diagenetic overprints can be recognized. These diagenetic overprints modify the pore system of the exposed carbonate determining where the exposed carbonate would be a seal rock or reservoir rock and the heterogeneity of the reservoir. Pedogenic calcrete is one of these diagenetic overprints. The factors that control calcrete formation are discussed in Chapter 4.

This study used two data sets to identify exposure surfaces and facies. The first data set is core description of wells R-50 and R-48. The second data set is the petrographic analysis of the core samples collected from wells R-48, R-49 and R-50. The different exposure fabrics and environments have been reviewed by Esteban and Klappa (1983), James and Choquette (1988) and Wright (1994).

The processes operating on a subaerially exposed carbonate surface form palaeosols and two distinct components may be produced. The first component of the palaeosols at the surface is non-carbonate horizons, which are typically clay. The second component of the palaeosols usually beneath the clay horizons and is an



altered carbonate horizon formed by pedogenic processes. The calcrete features of the altered carbonate horizon are formed by redistribution and reorganization of the original calcium carbonate of the Ratawi. This is done by two main sets of processes, which are alteration-dissolution and carbonate precipitation (Wright, 1994).

Esteban and Klappa (1983) listed 32 features (Table 3-2) which could be used to identify the altered carbonate horizon as a calcrete. The evidence for subaerial exposure used in this study is examined under two headings, subaerial exposure evidence from core description (Section 3.4.3 3) and subaerial exposure evidence from petrography (Section 3.4.3 4).

<b>A. Diagnostic Features</b>	<b>B. Commonly Present But Non-diagnostic Features</b>	
(a) Diagnostic of Karst facies	(d) Commonly present in karst facies	25. Missing paleontological zones
1. Karst surface landforms	15. Phytokarst	26. In-place non-tectonic fracturing and brecciation
2. Karst collapse breccias	16. Kamenitzas	27. Microscopic features: clotted micrite, microspar, meniscus and gravitational cements, calcified filaments, calcified fecal pellets, microborings
3. Cavern porosity	17. Rillenkarren	28. Leached and vuggy porosity
4. Speleothems	(e) Commonly present in caliche facies	29. Lithoclasts in beds directly above sedimentary breaks
(b) Diagnostic of caliche facies	18. Black pebble limestone	30. Laminar micritic crusts
5. Rhizoliths	19. Floating texture and corroded grains	31. Chalky layers below a sedimentary break
6. Alveolar texture	20. Vesicles and vesicular texture	32. Crystal silt
7. <i>Microcodium</i>	21. Vermicular texture	
8. Tangential LMC needle fibers	22. Tepees	
9. Calcified cocoons	(f) Commonly present in karst and caliche facies	
10. Caliche glaebules	23. Irregular to planar sharp upper surfaces	
11. Clay cutans	24. Shallowing-upward sequences culminating in non-specified exposure surface	
12. Circum-granular cracking		
(c) Diagnostic of both karst and caliche facies		
13. Lichen structures		
14. Random LMC needle fibers		

Table 3-2 Summary of features in subaerial exposure facies (after Esteban and Klappa, 1983)

3.4.3.3 Subaerial exposure evidence from core description

From the examination of the core and the description charts elementary depositional cycles (parasequences) were identified and are discussed in Chapter 5. Evidence of subaerial exposure in wells R-48 and R-50 is provided by:



#### **3.4.3.3.1 Rootlets**

The origin of these features is discussed in the next section as 'Rhizoliths'. It is used to indicate minor subaerial exposure of only a short duration.

⇒ combine ro

#### **3.4.3.3.2 Mudcracks and Horizontal Veins**

The origin of these features is interpreted to be formed in two stages. The first stage is the formation of the mudcracks in lime mud through desiccation. The second stage is filling the mudcracks and horizontal cracks with sediment of different fabric, when deposition resumes. It is used to indicate minor subaerial exposure, with short duration of exposure.

#### **3.4.3.3.3 Karst**

The term is interpreted to be a group of features that indicate subaerial exposure under a humid climate. This includes irregular dissolution surfaces with associated breccia, and pore holes and cave systems. In this case, breccia with clast support fabric associated with sharp irregular discontinuity surfaces was observed in the cores.

#### **3.4.3.4 Petrographic evidence for subaerial exposure**

The second data set is the study of microfacies analysis of the Ratawi core samples. Petrographic evidence of subaerial exposure includes: (1) leached and vuggy porosity, (2) black grains, (3) rhizoliths, (4) alveolar septal structure, (5) calcified filaments, (6) micritization of carbonate particles and carbonate cement (microsapr), (7) radial cracking (circum-granular cracks), (8) complex cracks, (9) dense microfabric and floating sediment grains, and (10) vadose compaction. The origin of the black grains is discussed in Section 3.3.1.

##### **3.4.3.4.1 Leached and vuggy porosity**

Leached and vuggy porosity can form in different diagenetic environments, during shallow and deep diagenesis. The leached and vuggy porosity here is associated with subaerial exposure features and so is related to meteoric dissolution. The total Ratawi porosity is increased by the leached and vuggy porosity, but the permeability is only increased when this leached and vuggy porosity is connected to the other pore types.



### 3.4.3.4.2 Rhizoliths

The rhizolith is an organosedimentary structure produced by higher plant roots (Fig. 3-11 and 3-12 a). The structures are generally millimetres to centimetres in diameter and centimetres to metres in length. Rhizoliths are reliable indicators of subaerial exposure because evidence of marine plants is rarely if ever preserved (Esteban and Klappa, 1983). The different types of rhizolith depend on the degree and location of calcification. Three styles of root calcification are recognized (Wright and Tucker, 1991), which are (1) root zone, (2) root envelope or tubule, and (3) host substrate around the root. The calcification processes are by cementation around and/or within the roots, and by mineral replacement of the roots (Esteban and Klappa, 1983).

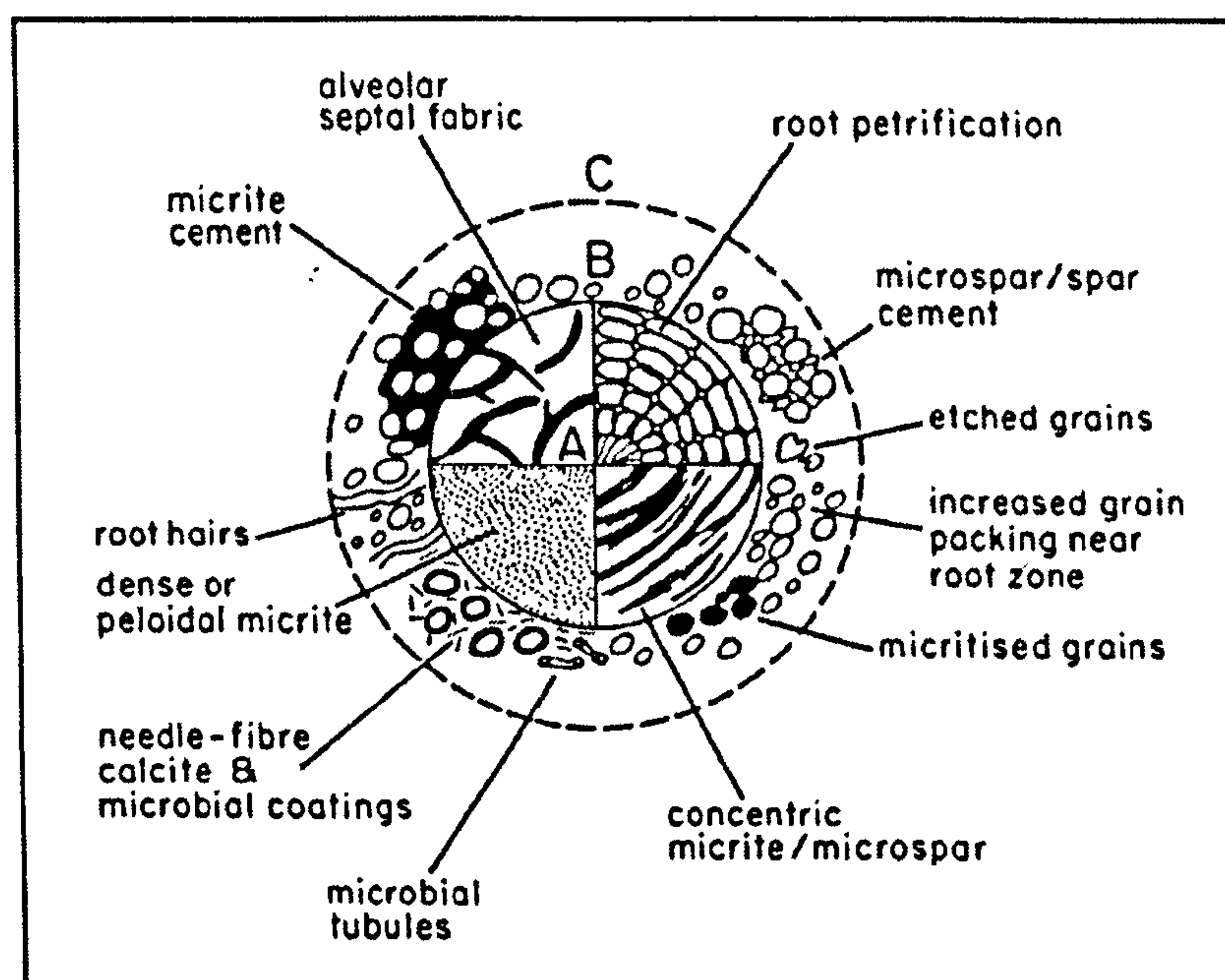


Figure 3-11 Styles of root calcification in rhizoliths. A = root zone; B = root envelope or tubule; C = host substrate. The diagram illustrates four styles of root zone calcification: root petrification, concentric micrite / microspar, dense peloidal micrite and alveolar septal fabric. The first style developed in living root, whereas the last three styles developed in a decaying root (after Wright and Tucker, 1991).

Also, Esteban and Klappa (1983) catalogued five basic types of rhizolith as: (1) root moulds and/or borings which are simply cylindrical pores left after root decay, (2) root casts which are sediment or cement-filled root moulds, (3) root tubules which are cemented cylinders around root moulds, (4) rhizocretions which are concretionary mineral accumulations around living or decaying roots, (5) root petrifications which are mineral encrustations, impregnations or replacements of organic materials whereby anatomical root features are partly or totally preserved.



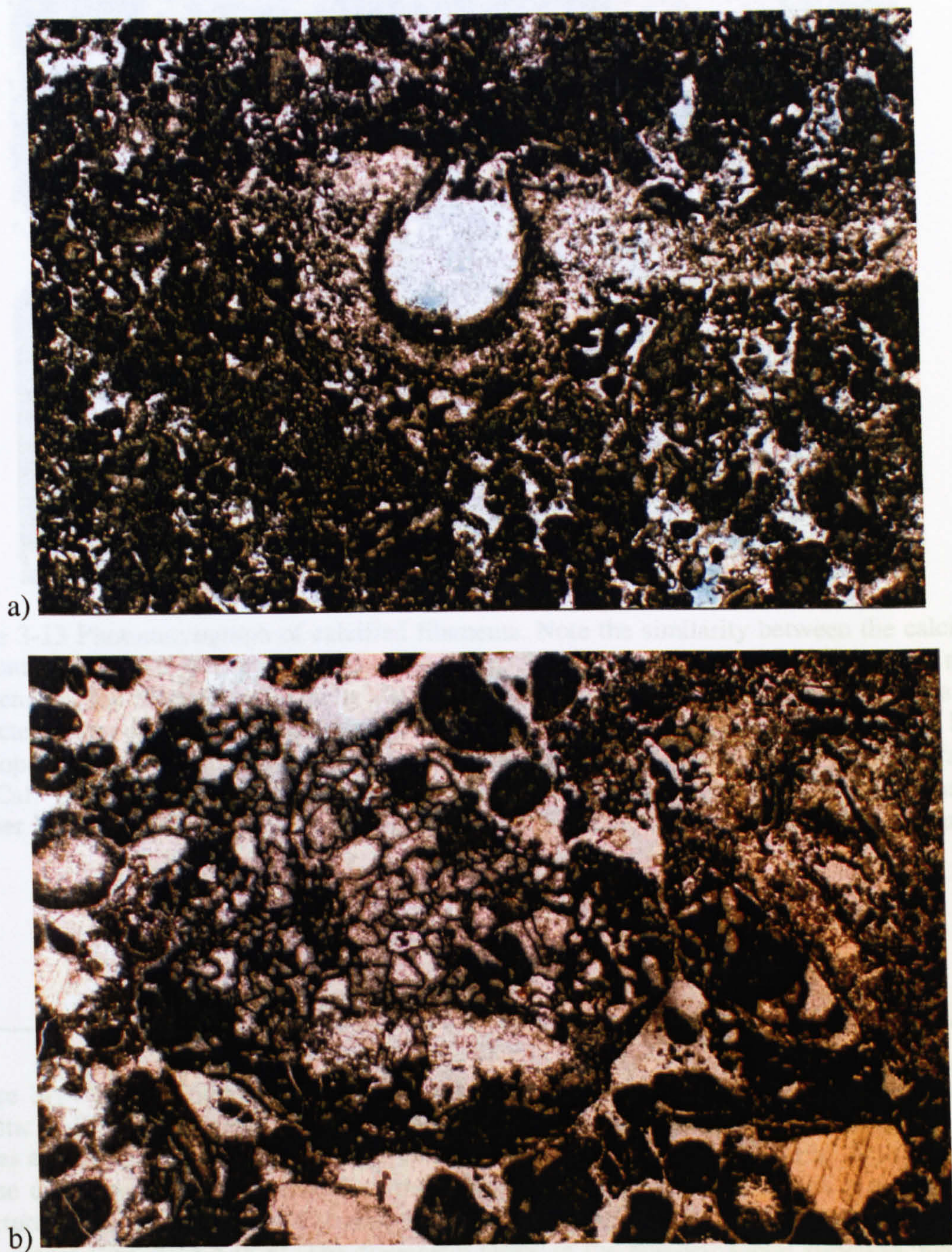


Figure 3-12 a) Photomicrograph of a rhizolith (root tubule). The calcification processes are cementation and mineral replacement around the open mold of the root. (microfacies DiagCal: pedogenic calcrete). Sample number is R-49 # 33, depth 6917 ft (2108 m), field of view 5 x 3 mm, under plane-polarized light. b) Photomicrograph of a clast of *Bacinella irregularis* (or algal oncolid). Note the sharp boundary between clast and the matrix, and evidence of erosion in broken chambers (at the upper boundary) of the clast. The green alga *Bacinella irregularis* constructs an organic fabric which is very similar to diagenetic alveolar septal structure (see Fig. 3-14 a to e for comparison). Sample number is R-50 # 66, depth 6864 ft (2092s m), field of view 5 x 3 mm, under plane-polarized light.



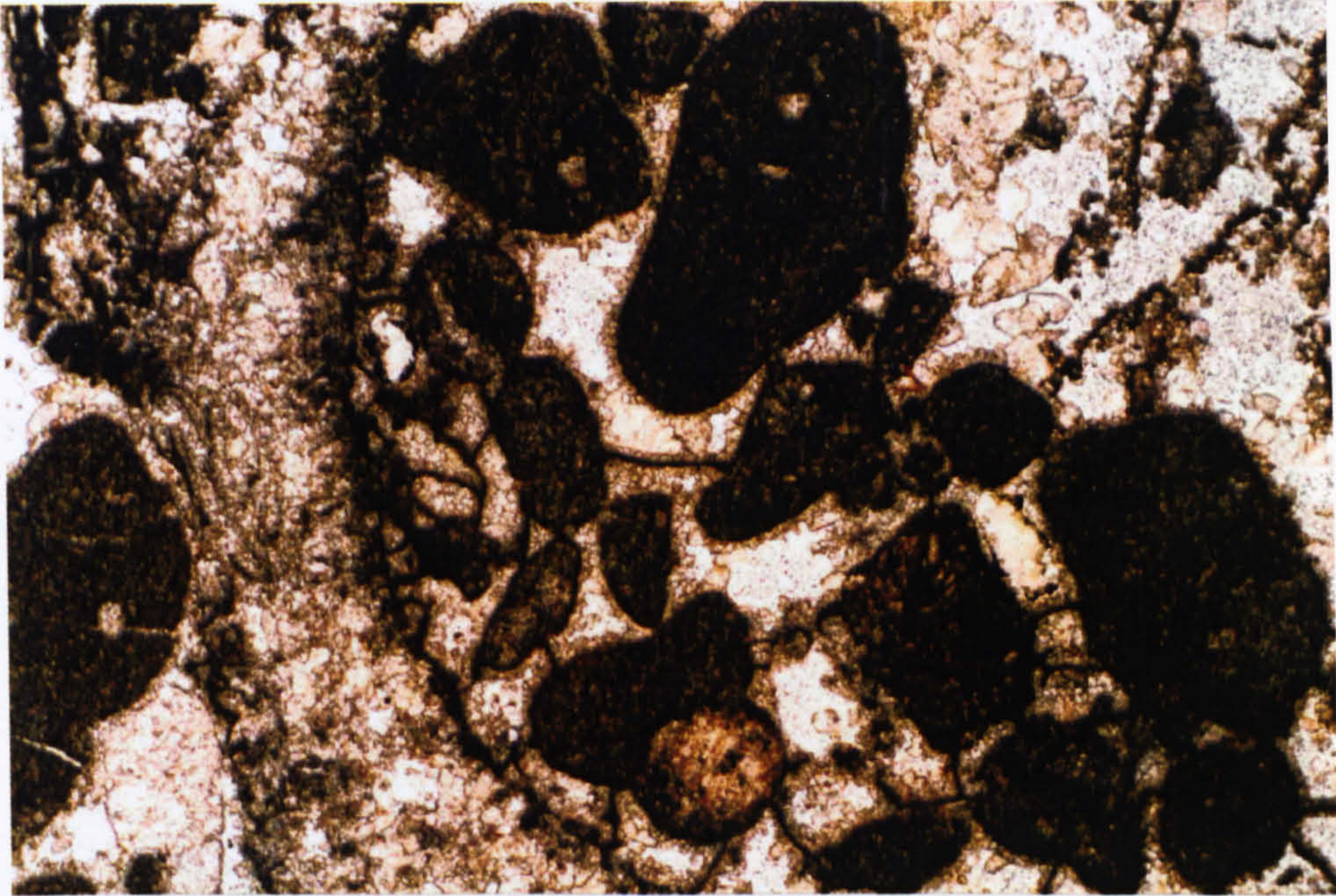


Figure 3-13 Photomicrograph of calcified filaments. Note the similarity between the calcified filaments and alveolar septal structure (see Fig. 3-14 a to e for comparison). The main difference is that the calcified filaments are without an organized fabric of pores and septa that characterize the alveolar structure. Crusts of meteoric bladed to rhombic cement crystals have developed on the calcified filaments and around the peloids. The porosity of microfacies DiagCal: pedogenic calcrete increases by the open fabric of calcified filaments. Sample number is R-50 # 60, depth 6835 ft (2083 m), field of view 3 x 2 mm, under plane-polarized light.

---

Figure 3-14 Photomicrograph of alveolar septal structure. Note a network of anastomosing micritic walls forming irregular to cylindrical pores; some of the pore walls as well as the pore spaces are encrusted or filled by meteoric microcrystalline calcite cement (Fig. 3-14 a to e) or coarse deep-burial saddle dolomite cement (Fig. 3-14 e). Both forms of the alveolar septal structure occur in the Ratawi Formation: (1) tubular type (Fig. 3-14 a) and in intergranular pore spaces (Fig. 3-14 b to e). The diagenetic fabric of the alveolar septal structure, which is characteristic of microfacies DiagCal: pedogenic calcrete is very similar to the organic fabric of the green alga *Bacinella irregularis* (see Fig. 3-12 b for comparison). The open fabric of the alveolar septal structure is an important rootlet pore type in reservoir Unit E. All the photomicrographs are under plane-polarized light. (Fig. 3-14 a) sample number is R-50 # 55, depth 6813 ft (2077 m), field of view 5 x 3 mm. (Fig. 3-14 b) sample number is R-48 # 52, depth 6530 ft (1990 m), field of view 3 x 2 mm. (Fig. 3-14 c) sample number is R-49 # 21, depth 6835 ft (2083 m), field of view 5 x 3 mm. (Fig. 3-14 d) sample number is R-49 # 20, depth 6822 ft (2079 m), field of view 5 x 3 mm. (Fig. 3-14 e) sample number is R-50 # 21, depth 6591 ft (2009 m), field of view 3 x 2 mm.



Figure 3-14

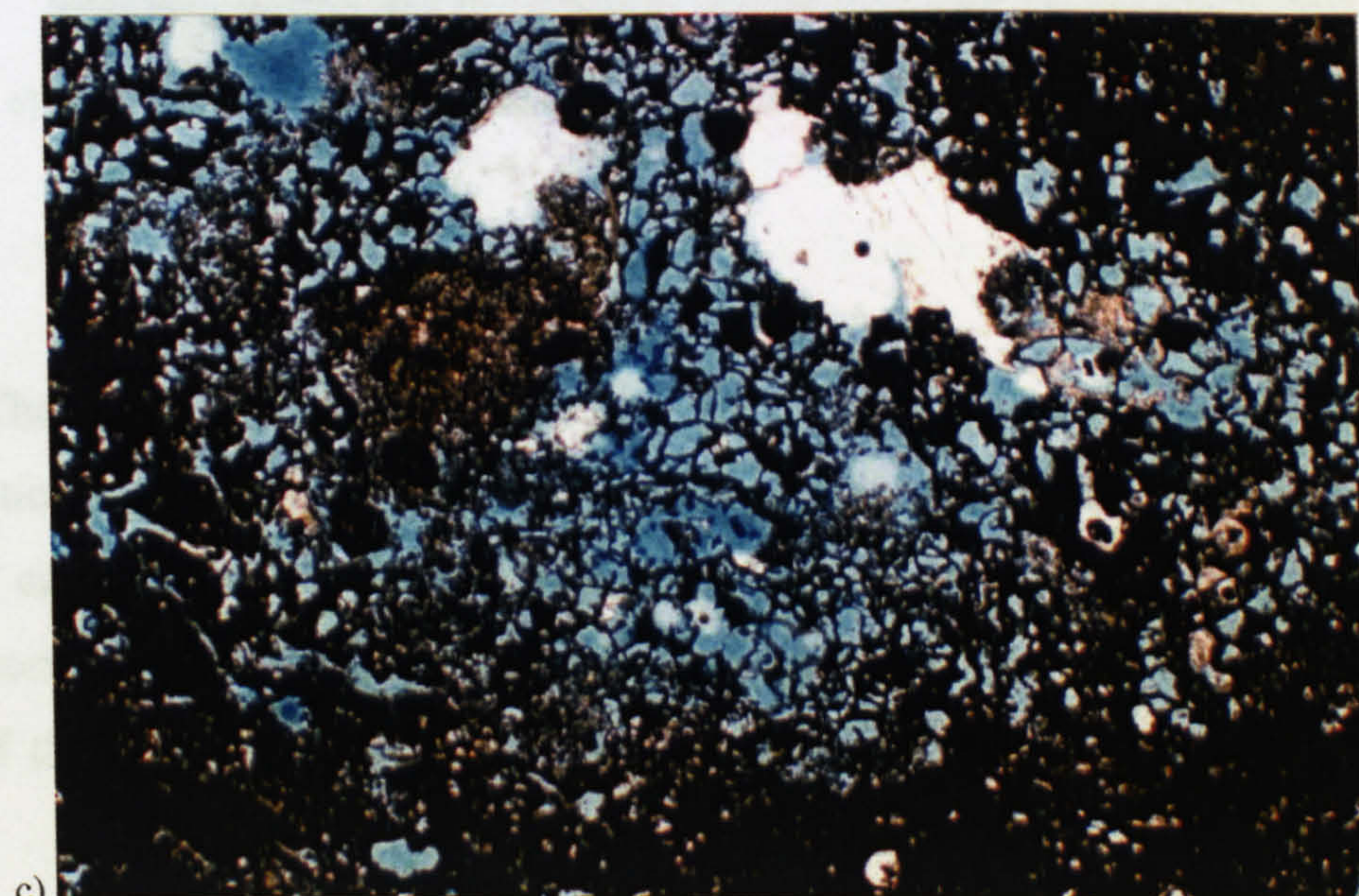
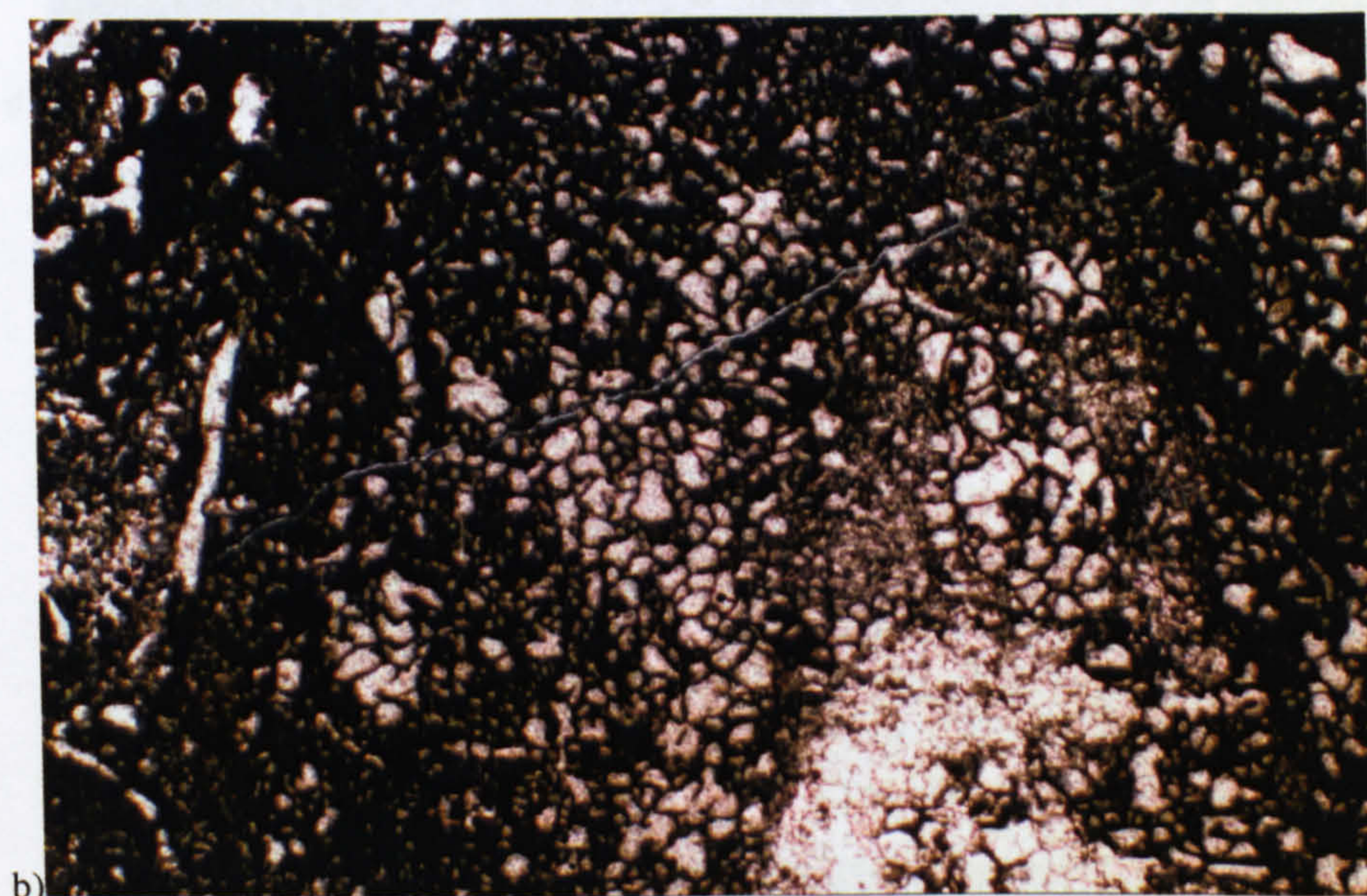
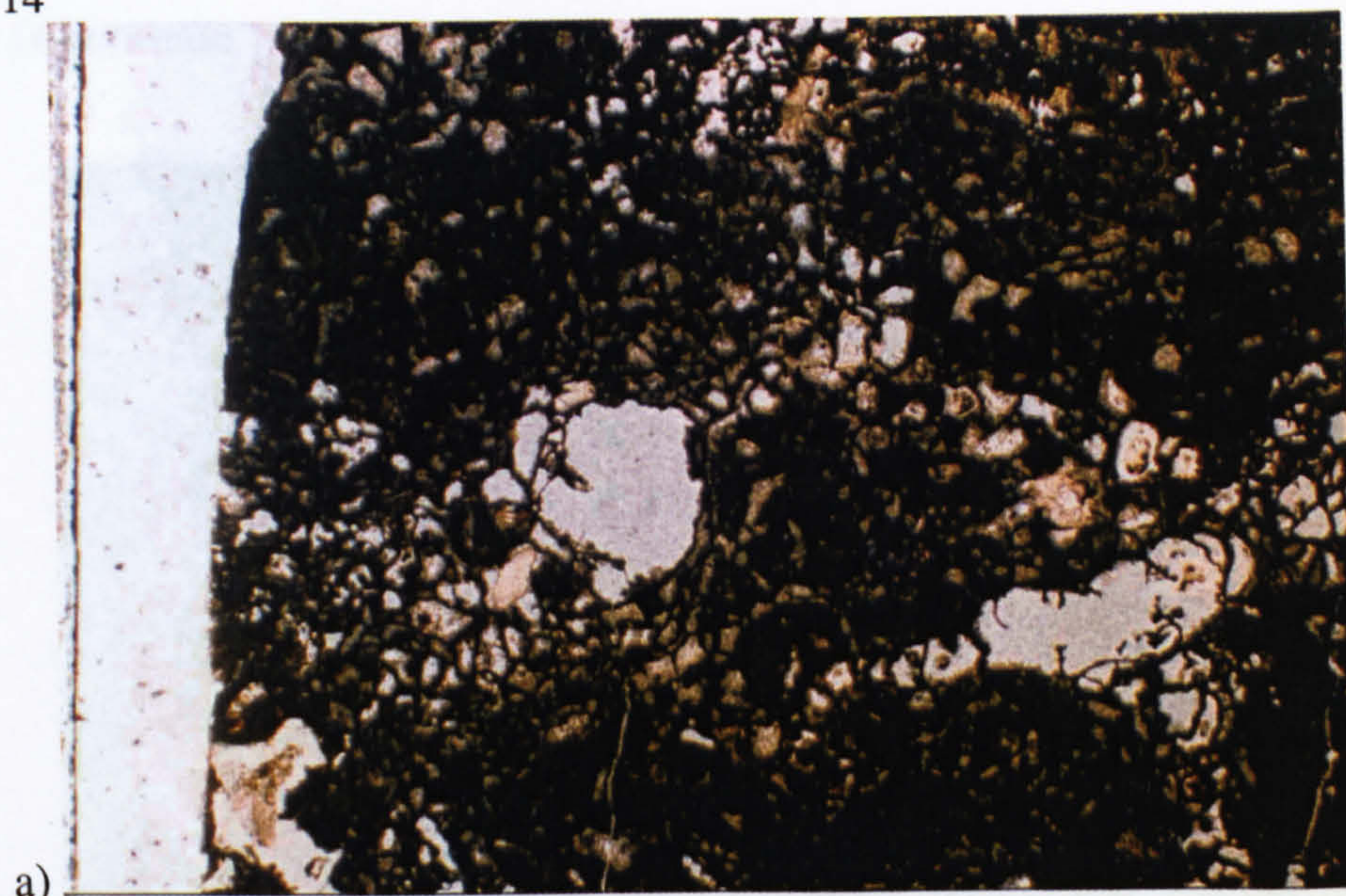
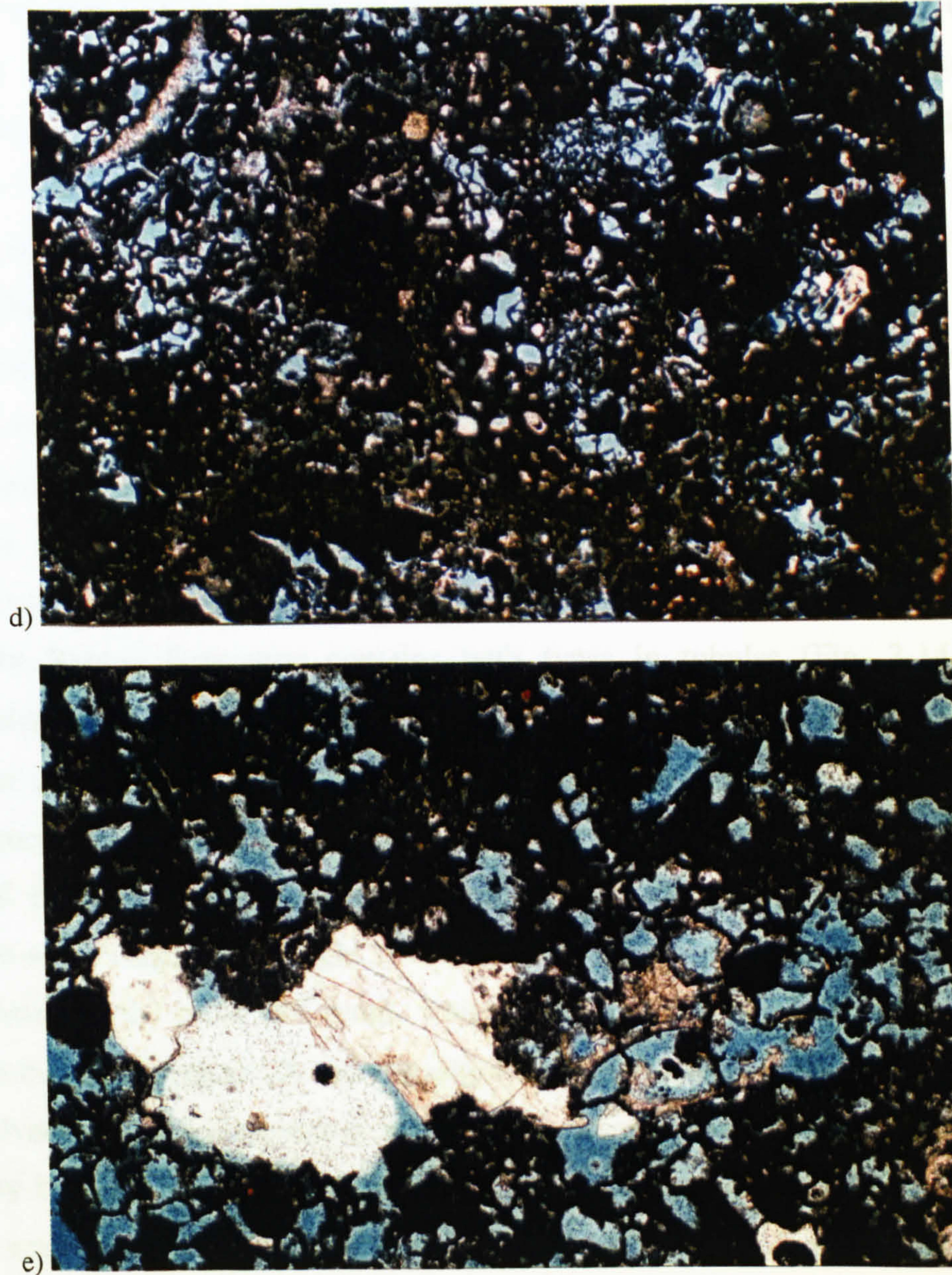




Figure 3-14 continue



The Ratawi rhizolith structures are a root mould type, preserved by cementation of the sediment around the root. This cemented envelope consists of micritic calcite. The envelope of the micritic cement may reflect the site of an ectomycorrhizae, a symbiotic fungal sheath-root association (Wright, 1986). The open fabric of the rhizolith tubules increases the porosity the Ratawi Formation, reservoir unit E.



### 3.4.3.4.3 Alveolar septal structure

The term 'alveoli texture' is used to describe cylindrical to irregular pores that are formed by a network of anastomosing micritic walls. These walls are commonly encrusted by microcrystalline or cryptocrystalline calcite. The alveolar pore diameter commonly ranges from 100 to 500 microns, but a few may reach 1.5 mm, and be preserved open, rather than filled with calcite cement. The alveolar texture is found mostly within the platy and hardpan horizon of the soil profile (Esteban and Klappa, 1983). Wright (1994) suggested the use of 'alveolar septal structure' in order to avoid confusion with the term 'alveoli structure' used to describe a fenestral-like fabric in soil micromorphology.

The alveolar septal structure occurs in two forms: (1) in tubules, within pore space of root moulds (Wright, 1986), and (2) in intergranular pore spaces (Adams, 1980). The Ratawi Formation contains both types in tubules (Fig. 3-14 a) and intergranular types (Fig. 3-14 b to e), the second type is the more common. According to Esteban and Klappa (1983) different workers interpret the origin of the alveolar septal structure as: (1) discrete channelways within sediment which had been penetrated by rootlets, (2) root moldic porosity, or (3) the product of coalesced millimetre-sized rhizoliths. Wright (1994) interpreted the origin as: (1) a symbiotic relation between the roots and fungi, which result in fungal precipitation of calcite needles in the walls (septa), (2) decomposition and calcification of the root.

Alveolar septal structure is important in reservoir unit E. The pore system, formed by both the pores of alveolar septal structure, in addition to the pores from leaching, seems to be the major contributor to the high porosity of unit E. The potential porosity of alveolar septal structure and leaching is reduced by cementation and compaction. The alveolar septal structure can give textures very similar to the lower Cretaceous green alga *Bacinella irregularis* (see Fig. 3-12 b). The former fabric indicates normal-marine conditions, whereas the second fabric is superimposed on the depositional fabric and indicates a period of subaerial exposure under specific palaeoclimatic conditions to produce the pedogenic calcrete zone. This study separates the two fabrics by evidence of erosion and transportation of the green algal clasts whereas the diagenetic fabric shows evidence of replacement of the original sediment without evidence of transportation.



#### **3.4.3.4.4 Calcified filaments**

The Ratawi calcified filaments are similar to walls (septa) of the alveolar septal structure but without the organized fabric of pores and septa that characterize the alveolar structure (Fig. 3-13). Wright (1994) argued that roots should be viewed as part of the 'rhizosphere', which is a 'micro-ecosystem' within the zone of rooting. A diverse range of organisms inhabits this micro-ecosystem, including bacteria, fungi and protozoa. The activities of these organisms could result in the calcified filaments. Calcified filaments could be formed by calcification of the root hairs of vascular plants (Goudie, 1996). The open fabric of calcified filaments contributes to the porosity of the Ratawi, when it is not reduced by cementation or compaction.

#### **3.4.3.4.5 Micritization of the carbonate particles and carbonate cement**

The origin of micrite is discussed in Section 3.3.1. Micrite is polygenetic in origin, and can be grouped into two main types, primary and secondary micrite. Secondary micrite is formed by diagenetic changes, which include grain and cement degrading as a result of recrystallization in the calcrete zone (Flügel, 1982). Esteban and Klappa (1983) in their description of the idealized calcrete profile indicate that micritization decreases downward from the hardpan and platy zones at the top, to the transition zone to unaltered host rock.

The process of micritization is degradation of large crystals to micrite crystal size. The calcrete profile develops in stages that are characterized by the progressive accumulation of carbonate within the host rock. This accumulation involves three processes, namely carbonate cementation, displacement and replacement of the original host rock. The replacement processes include two types: (1) mineralogical replacement, like the replacement of the Ratawi quartz silt by carbonate, (2) replacement of carbonate grains and cement by micrite. These processes produce textural inversion, diagenetic wackestone and mudstone fabric (Wright and Tucker, 1991).

Diagenetic secondary micrite is important in the calcrete, microfacies DiagCal. There are two types of micritization. The first type is the partial to total micritization of the granular sparry cement. Kahle (1977) termed this process 'sparmicritization', which is degrading recrystallization of sparry cement to micrite. This process takes place by dissolution of the calcite spar and simultaneous precipitation of micrite in the resulting void space. Kahle (1977) interpreted this process as a chemical reaction



between crystals, pore water and organic compounds released during bacterial decomposition of fungi, algae or both. Sparmicritization occurs in both marine and vadose diagenesis.

The second type of micritization is the partial to total micritization of skeletal particles. The micritization of the particles is a destructive process. The origin of this process could be related to the activity of macro- and micro- organisms, which include bacteria, fungi, algae and higher plants roots. The activity of the soil organisms ranges from a destructive to constructive process. The destructive processes of the roots in addition to micritization include dissolution of carbonate, which could be related to root respiration of carbon dioxide, and physical reorganization of the rock and sediment. The destructive micritization process of the fungi is by bioerosion processes of fine scale dissolution-precipitation (Wright, 1994).

In a case study, Jones and Kahle (1995) studied the origin of the modern micrite in the karst terrains of the Cayman Islands. They identified two types of micrite. The first type is primary depositional micrite, which is derived from sources external to the bedrock; they term it 'exogenetic micrite'. The second type is diagenetic micrite, which is derived from sources in the bedrock; they term it 'endogenetic micrite'. Endogenetic micrite can be produced by four processes that are operating in the confines of cavities in karst terrains. The first process is by etching, as constructive and destructive envelopes developed around spar calcite crystals. The second process is by calcification of microbes. The third process is by breakdown of calcified filamentous microbes. The last process is by precipitation of calcite from pore waters. They concluded that it is impossible to differentiate between the two types, exogenetic and endogenetic, after they are mixed.

The presence of calcrete, microfacies DiagCal, indicates the occurrence of the subaerial micritization of the granular cement and particles. The micrite is the end-product, and the study cannot differentiate between endogenetic micrite and exogenetic micrite. Marine micritization produces a micritic envelope and then later destroys all the internal structure of the particles, and the micritization of the micrite envelope started from the edge of the particles. The combination of sparmicritization and particle micritization, leads to textural inversion, diagenetic wackestone and mudstone fabric, reducing the Ratawi porosity.



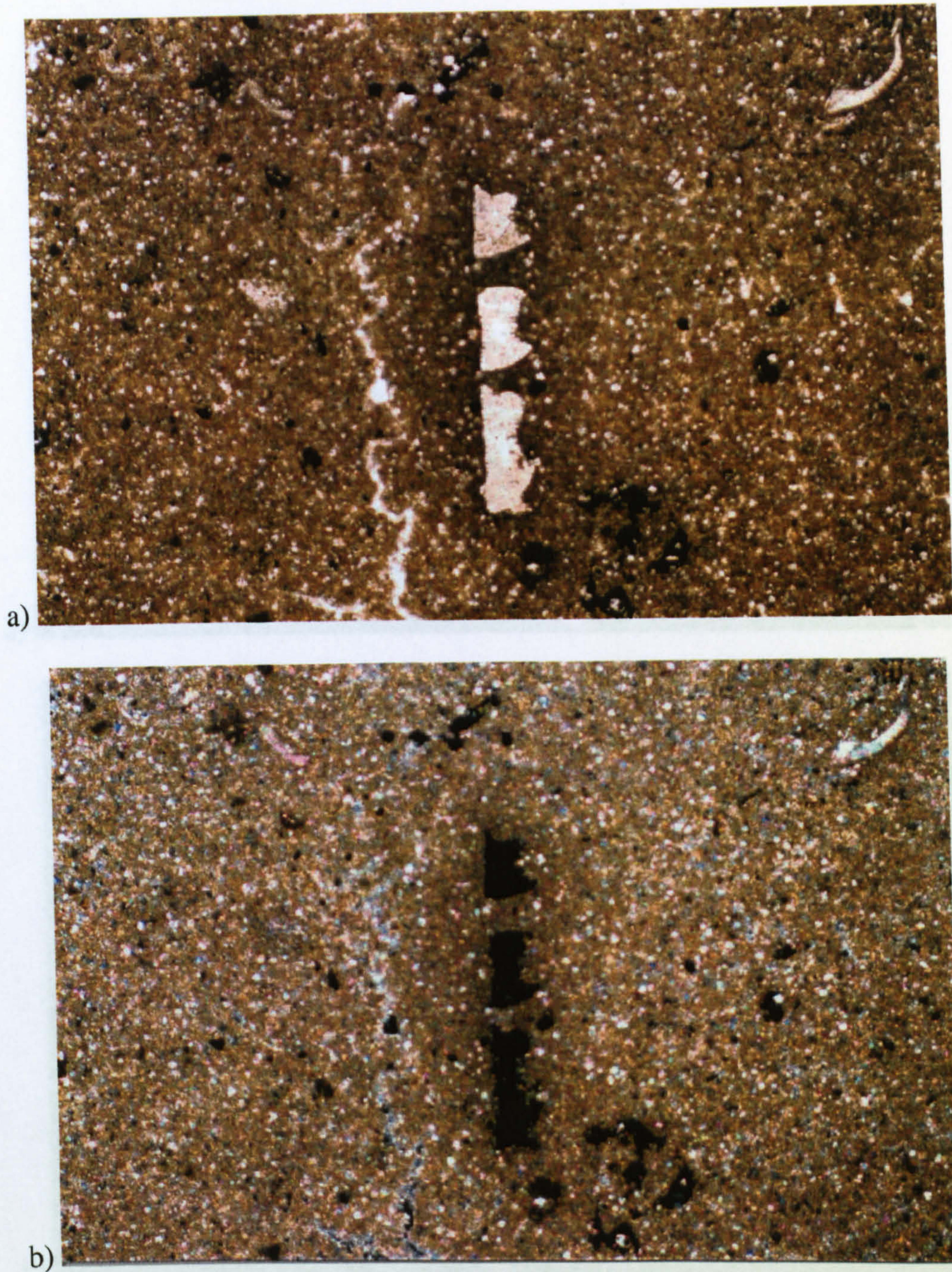


Figure 3-15 ) Photomicrograph of micritization (neomorphic inversion) of carbonate particles. Note three crinoid particles separated by micritic matrix under plane-polarized light (a) showing the same uniform extinction under crossed polars (b) indicating optical and crystal continuity of a single crystal grain (not broken grain). This evidence is used in this study to indicate that the micritic matrix within the grain was formed by micritization of different parts of a single crinoid particle. The micritization of carbonate grains results in the formation of a dense microfabric and floating sediment grains characteristic to microfacies DiagCal: pedogenic calcrete. Sample number is R-48 # 16, depth 6691 ft (2039 m), field of view 3 x 2 mm.



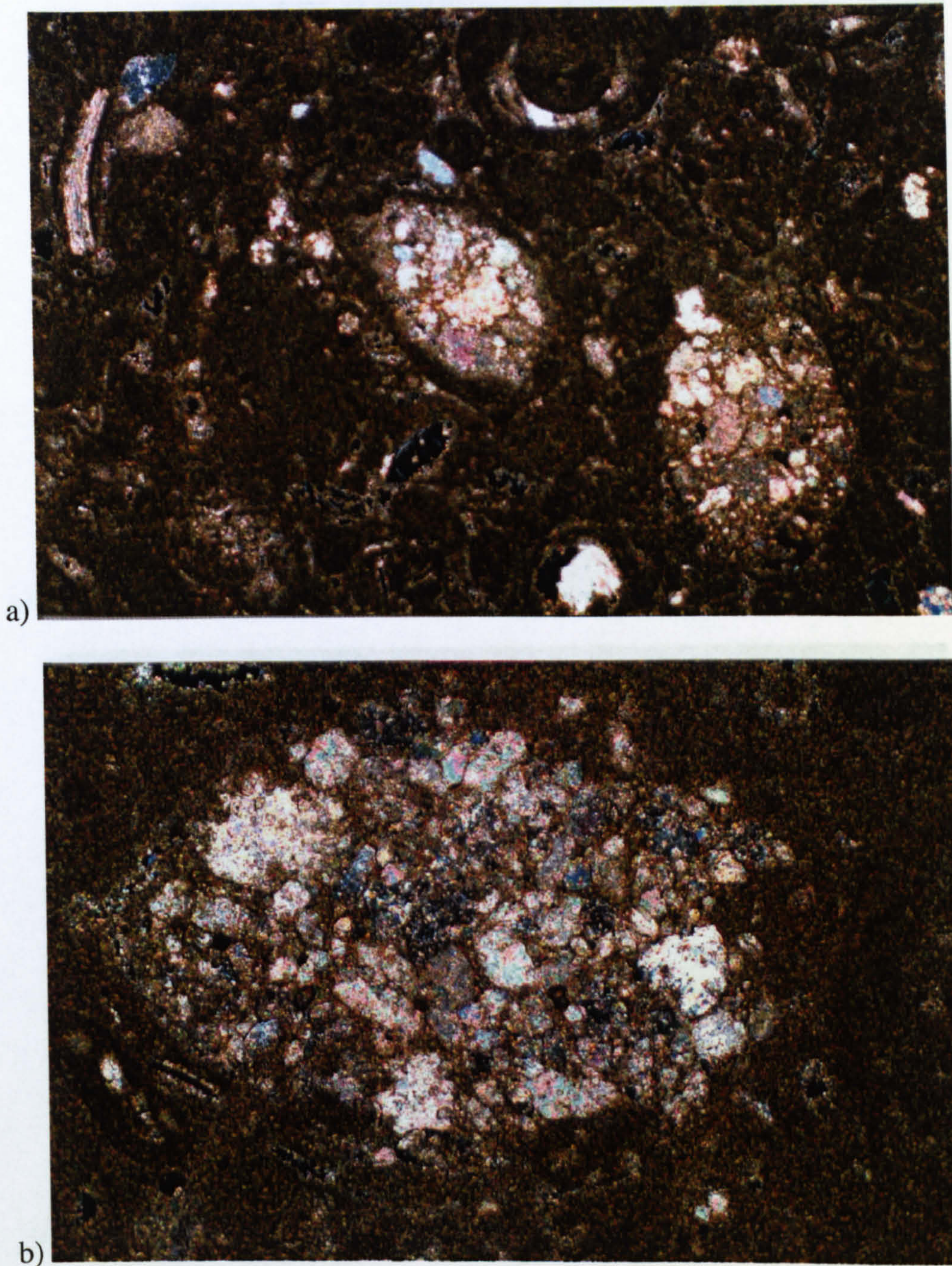


Figure 3-16 Photomicrograph of micritization (neomorphic inversion) of carbonate cement. Granular drusy cement fills two cavities (a) all interfaces between the cement crystals are rounded (not planar surfaces) and micritized (b). Sample number is R-50 # 51, depth 6790 ft (2070 m), field of view (a) 3 x 2 mm, (b) 1 x 0.6 mm.



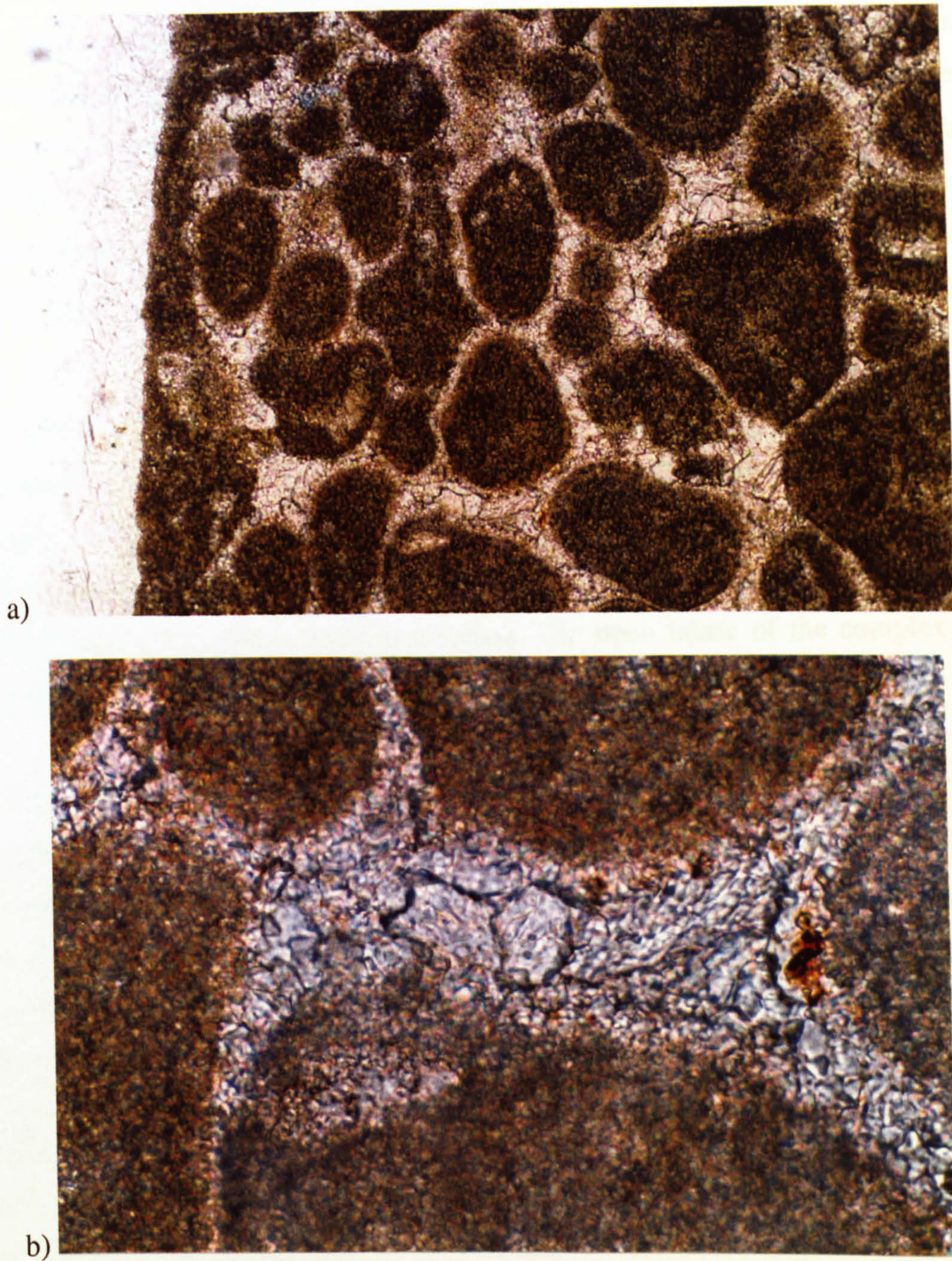


Figure 3-17 Photomicrograph of grainstone with some fitted fabric developed by vadose compaction. Some early meteoric cement occurs between the fitted grains. The early granular drusy cement reduced the effect of the deep burial compaction; the vadose compaction and the early meteoric cement eliminated all the interparticle porosity. Sample number is R-49 # 53, depth 7057 ft (2151 m), (a) field of view 1 x 0.6 mm, (b) field of view 0.25 x 0.15 mm, under plane-polarized light



#### **3.4.3.4.6 Radial cracking (Circum-granular cracking)**

Radial cracking is a non-tectonic fracturing radiating from the centre to the edge of the grains. The origin of this type of fracture could be similar to circum-granular cracks. The non-tectonic fractures formed when the Ratawi sediments were affected by alternation of shrinkage and expansion during wet and dry climatic periods, before significant burial and cementation. Circum-granular cracking is a common feature in calcrete (Esteban and Klappa, 1983). The porosity of the Ratawi is enhanced by the open fabric of these fractures, when it not reduced by cementation or compaction.

#### **3.4.3.4.7 Complex cracks**

The complex cracks (Fig. 4-7 b). are similar to radial cracks and are also non-tectonic fractures. The cracks cut more than one particle. Tectonic cracks are differentiated from complex cracks in calcrete by their preferred orientation. The origin of the complex cracks is similar to radial cracking. The open fabric of the complex cracks increases the porosity of the Ratawi

#### **3.4.3.4.8 Dense microfabric and floating sediment grains**

Floating sediment grains and dense microfabric are interpreted to be the result of the development of diagenetic micrite that originated by micritization of the carbonate particles (Fig. 3-15) and carbonate cement (Fig. 3-16). These processes produce diagenetic wackestone and mudstone fabric (textural inversion). The porosity of the Ratawi is decreased by the development of this fabric.

#### **3.4.3.4.9 Vadose compaction**

The vadose compaction texture is a fitted fabric formed when the Ratawi sediments were affected by freshwater in the vadose zone, before significant burial and cementation (Fig. 3-17). The texture is purely chemically controlled dissolution at grain contacts (Hird and Tucker, 1988) and is an indicator of near-surface diagenesis. Vadose compaction is discussed in Chapter 4. The fitted fabric of the vadose compaction reduces the porosity of the Ratawi.

### **3.5 Palaeoenvironment Reconstruction**

The depositional primary porosity of the shallow ramp sand-body is the main controlling porosity in reservoir unit A, B, C and D. Diagenetic secondary porosity



associated with calcretes developed below the 2<sup>nd</sup> order sequence boundary is the main controlling porosity in the reservoir unit E. The development the Ratawi shallow ramp sand-body in the Wafra oilfield depended on two factors. The first factor is the stratigraphic position of the initiation, development and termination of the Ratawi sand-body. The second factor is the palaeogeography within the Ratawi ramp that controlled the depositional energy, and so the microfacies.

Before the reconstruction of the Ratawi palaeoenvironment in Section 3.5.3, the shallow ramp sand-body is discussed under two topics. The first topic is the facies and log-facies of Ratawi Formation, Section 3.5.1. The initiation, development and termination of the Ratawi Oolite platform are analyzed in the framework of the regional stratigraphic development of the Makhul Formation, Ratawi Formation and Zubair Formation. The second topic is the sand-body geometry and carbonate ramp models, Section 3.5.2.

### **3.5.1 Facies and log-facies of the Ratawi Formation**

The aim of this section is to examine and interpret the broad vertical and lateral facies distribution of the three members of the Ratawi Formation and their relation to the underlying Makhul (Sulaiy) Formation and overlying Zubair Formation. The initiation, development and termination of the Ratawi ramp platform are the main controlling factors in the development of the lithofacies, and the reservoir and non-reservoir units in the Wafra oilfield. The data are based on different log types that include gamma ray, spectral gamma ray, neutron and density log. In addition, the data include detailed core description for the sampled intervals from well R-50, R-48, unpublished Saudi Arabian Texaco Inc. reports, and published data concerning the Thamama Group.

The palaeogeography of the Arabian Peninsula during the Early Cretaceous was characterized by the gradual establishment of ramp-type carbonate deposition related to a relative rise in sea level, with carbonates covering most of the Arabian Gulf area. The northern Arabian Gulf area was differentiated into the Gotnia intracratonic basin surrounded by shallow-water of the Arabian platform (see Section 2-2 and Murris, 1980; Alsharhan and Nairn, 1986). There are significant lithofacies changes from the outcrop of the Lower Cretaceous in the Arabian Peninsula to the study area, on the margin of the Gotnia intracratonic basin. The lithofacies that distinguish the Ratawi Formation occur only in the subsurface in the study area in the



Partitioned Neutral Zone, Kuwait and southern Iraq (Alsharhan and Nairn, 1997). Understanding the broad vertical and lateral Lower Cretaceous lithofacies change to the south of the Wafra oilfield area on the Arabian platform, in Saudi Arabia, and to the north of the Wafra oilfield area in the Gotnia intracratonic basin, Kuwait and southern Iraq, is the framework to interpret Ratawi Oolite platform initiation, development, and termination.

Ayres *et al.* (1982) studied the hydrocarbon habitat in the main producing areas in Saudi Arabia. The authors placed the Southern Wafra area on the Arabian platform and the Main Wafra area in the Gotnia basin, during the Upper Jurassic. This pattern continued during the lower Cretaceous and influenced the depositional and diagenetic environments of the Ratawi Formation. Alsharhan and Nairn (1997) in their review of the hydrocarbon habitat of the greater Arabian basin restricted the distribution of the lower member of the Ratawi Formation, the Ratawi Oolite (Minagish Formation) to the Kuwait arch. The Ratawi Oolite is a reservoir zone in the Burgan oilfield and the Wafra oilfield. Northward of the Kuwait arch, to the north of the Burgan oilfield, the lithofacies of the Ratawi Oolite changes from reservoir facies to a non-reservoir facies of the Makhul Formation.

The middle member the Ratawi Limestone in the Kuwait arch area overlies the Ratawi Oolite, but to the north of the arch the middle member is overlying the Makhul Formation (Fig. 6-2). The upper member of the Ratawi Formation, the Ratawi Shale, overlies the middle member and underlies the Zubair Formation. The vertical and lateral facies distribution of the sand-body of Ratawi Oolite platform (Ratawi Formation) seems to be controlled by location and development of the Kuwait arch, whereas the middle and upper members and the Zubair Formation are not.

The lithofacies of the Ratawi Oolite (Minagish Formation) change to the south to the lithofacies of the Yamama Formation, on the Arabian platform. The top of the Yamama Formation is separated from the overlying Buwaib Formation by an erosional surface. This unconformity decreases in down cutting from the outcrop on the Arabian platform to the study area in the Gotnia intracratonic basin (Alsharhan and Nairn, 1986). In the study area, the unconformity surface is correlated to a "major" exposure surface, a 2<sup>nd</sup> order sequence boundary, at the top of Unit-E. This unit is producing from calcrete facies, which is the only reservoir unit that produces from all areas of the Wafra oilfield (Longacre, 1986). In the Wafra oilfield, Unit-E underlies Unit-F, the upper unit of the Ratawi Oolite member, which is a transitional facies between the



“clean” carbonate of the Ratawi Oolite and the dirty Ratawi Limestone. The appearance of the dirty carbonate is the start of the termination of the developed Ratawi Oolite platform. The lithofacies of the Ratawi Limestone and Ratawi Shale at Wafra changes to the south to the lithofacies of the Buwaib Formation, on the Arabian platform.

The vertical and lateral lithofacies changes between the Ratawi Formation and underlying Makhul Formation and overlying Zubair Formation indicate that the three formations represent lateral depositional environments on the broad Arabian platform and in the Gotnia intracratonic basin. The log data indicate a gradual increase in clay percentage from the lithofacies of the Ratawi Oolite (skeletal and peloidal grainstones and packstones) to the Ratawi Limestone (peloidal and skeletal packstones and mudstones).

Longacre and Elliott (1988) assigned the upper unit of the Ratawi Oolite, Unit-E, as a transitional lithofacies between the Ratawi Oolite and Ratawi Limestone. The contacts between the Ratawi Limestone and Ratawi Shale members, and the Ratawi Shale and the Zubair Formation are not cored. However, the well logs from the Wafra oilfield also indicate a gradual increase in clay from the Ratawi Limestone to the Ratawi Shale. In addition, the log-facies indicate a gradual decrease in clay from the Ratawi Shale to the Zubair Formation. The log-facies indicate a transitional contact between the upper two members of the Ratawi Formation and between the Ratawi Formation and Zubair Formation. There are gradual vertical and lateral lithofacies changes between the Ratawi Oolite and the Makhul Formation (Alsharhan and Nairn, 1997).

Ali and Aziz (1993) studied the lithofacies of the Zubair Formation in central and southern Iraq and Kuwait and interpreted it as a deltaic succession. A number of depositional cycles have been defined, each cycle containing the following facies: marsh, chenier, interdistributary bay and delta-front. The contacts of the Zubair Formation with other formations are mostly gradational and conformable. Ali and Aziz (1993) interpreted previous studies that gave the Zubair Formation a variable age, Valanginian to Aptian, as a result of the time-transgressive nature of the Zubair Formation. The Zubair deltaic lobe migrated with time from northern into southern Iraq, and into the Kuwait-Wafra oilfield area by Barremian-Albian times (Fig. 3-18) (Ali and Aziz, 1993). This indicates that the lithofacies of the three members of the





Ratawi Formation (Ratawi Oolite, Ratawi Limestone and Ratawi Shale) in the study area are the lithofacies equivalent to the Zubair Formation to the north.

According to Sadooni (1993), the Ratawi Formation and equivalent Yamama Formation in southern Iraq is characterized by a complex carbonate lithofacies that was influenced by the two tectonic regimes of the stable Arabian platform and unstable Gotnia basin. The Ratawi Formation in southern Iraq was deposited over tectonic arches (Arabian folds, the equivalent to the Kuwait arch) and salt-cored structures. The Ratawi Formation was deposited in a setting that changed from an inner to an outer ramp. The high-energy shallow-water ramp sand-body facies (equivalent to the Ratawi Oolite facies in the study area) were deposited along the hinge-line separating the stable Arabian platform and unstable Gotnia basin and crestal areas of the growing structures. The low-energy deep-water carbonate facies (equivalent to Ratawi Limestone facies in the study area) were deposited in the structural, palaeotopographic lows.

In the study area, the contacts of the Ratawi Formation with the underlying Makhul Formation and overlying Zubair Formation are mostly gradational and conformable. Thus, the concepts of Walther's Law can be applied to the facies succession, suggesting that the facies sequence is produced by progradation or lateral migration of one environment over another (Tucker and Wright, 1990). The broad lithofacies and log-facies in the Wafra oilfield indicate a gradual change in facies from high energy to low energy without any significant barrier, reef or slope facies. This would rule out the rimmed platform model, and implies an "epeiric" ramp bordering the Arabian Platform to the south and the Gotnia intracratonic basin to the north.

The carbonate facies of the high- to moderate-energy ramp sand-body, the Ratawi Oolite, were deposited on a palaeotopographic high, the Kuwait arch, to the south of the terrigenous deltaic facies of the Zubair Formation. The shallow-water carbonate facies of the Ratawi Oolite change to deeper-water facies of the Makhul Formation away from the Kuwait arch. The lower member of the Ratawi Formation, the Ratawi Oolite, represents the initiation and the development of the Ratawi ramp sand-body on the Kuwait arch palaeotopographic high.

The middle and the upper members of the Ratawi Formation, the Ratawi Limestone and Ratawi shale, represent the termination and drowning of the Ratawi platform. The Ratawi Shale is interpreted in this study as the prodelta facies of the Zubair delta lobe developed to the north of the Wafra area. The Ratawi Limestone is a



transitional lithofacies between the shallow-water carbonate facies of the Ratawi Oolite and the deep-water delta-front facies of the Ratawi Shale.

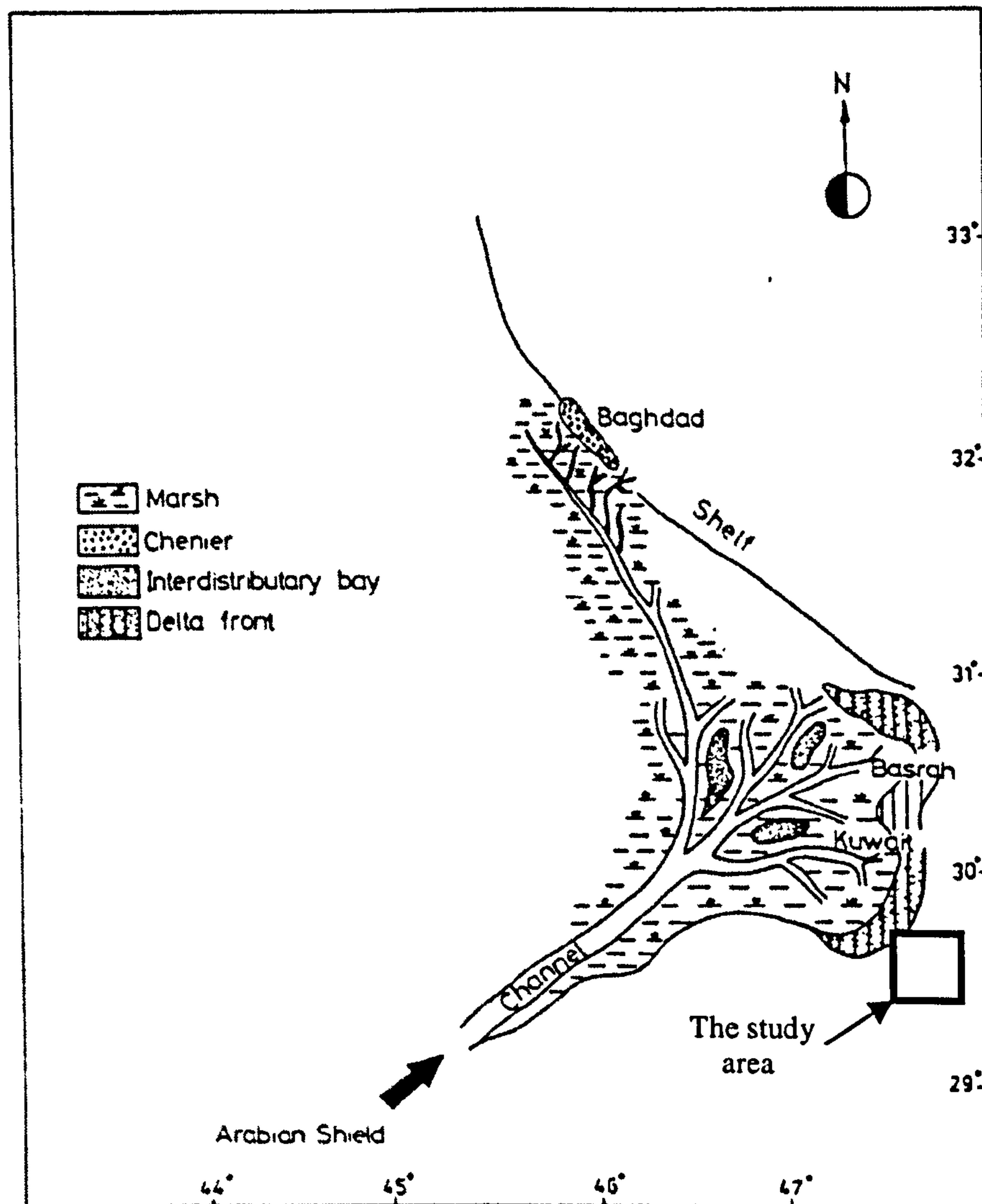


Figure 3-18 Palaeogeographic map of the Zubair delta during the Barremian-Albian (after Ali and Aziz, 1993).

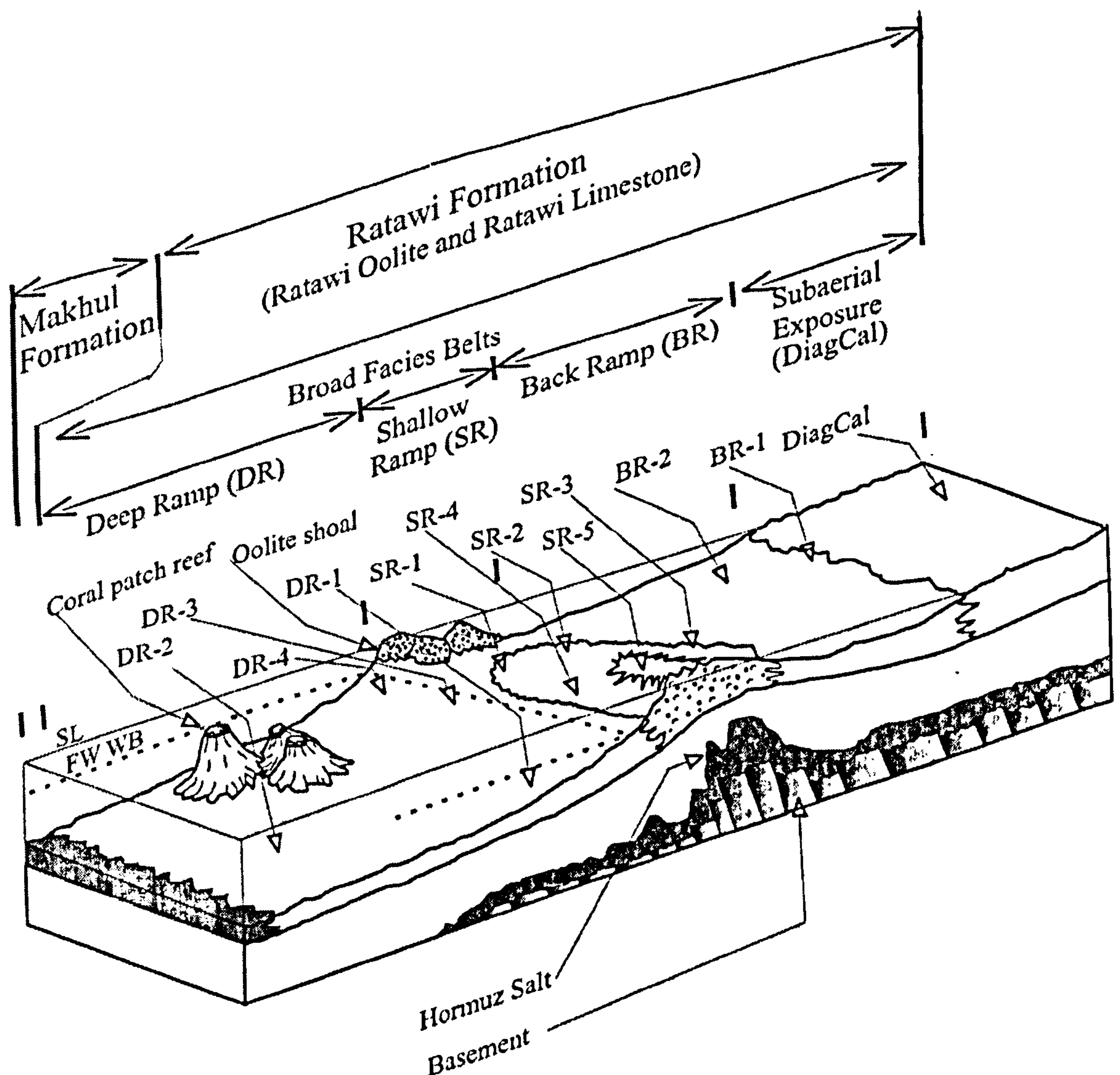
### **3.5.2 Ramp sand-body geometry and carbonate ramp model**

Ahr (1998) identified three factors that control the short-term characteristics of ramp carbonate facies, and long-term evolution of ramp architecture. The first factor is the location of sediment accumulation, which is controlled by the development of the accommodation space. This depends on the tectonic development of the Kuwait arch and global sea-level change at the time. The second factor is the rate of sediment production, which depends on the palaeoecology of the 'carbonate factory' of the Ratawi platform, and rate of sea-level change. The last factor is the mode and pattern



of sediment distribution, which depends on the facies belt of the ramp. There are two ramp models, and three end-member shallow ramp sand-body models.

Read (1985) defined two types of carbonate ramp: homoclinal ramps, where the slopes are relatively uniform, and distally-steepened ramps, where there is an increase in gradient in the outer, deep ramp region. The data from this study are not adequate to assign the Ratawi ramp to one of these categories, although a homoclinal ramp is more likely in the absence of any slope features.

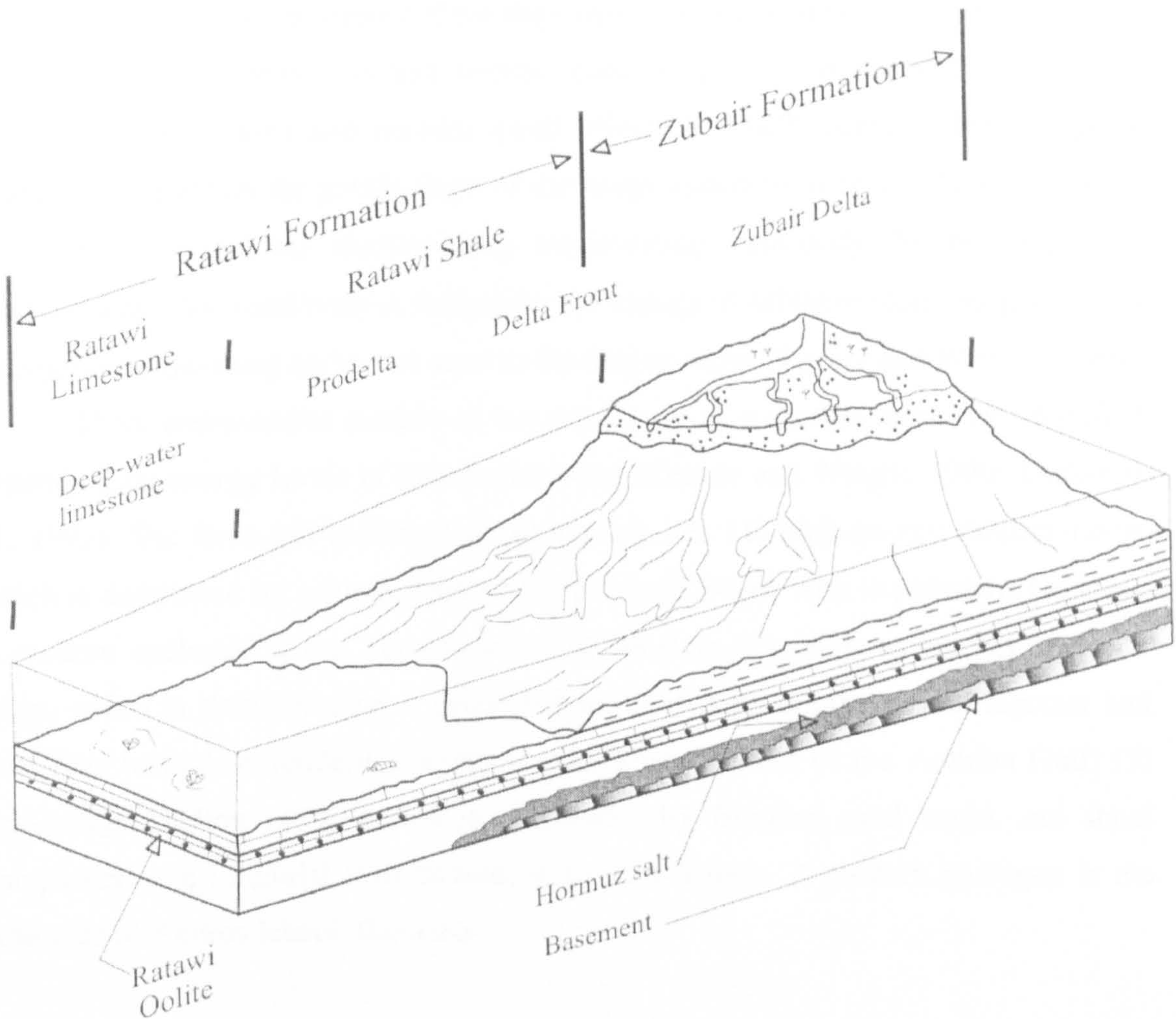


a)

Figure 3-19 Ratawi Formation depositional model showing the twelve Ratawi microfacies recognized in this study (see table 3-1), (a) during the deposition of Ratawi Oolite and Ratawi Limestone ramp facies and its equivalent basinal facies of the Makhul Formation, (b) during the deposition of the Ratawi Limestone and Ratawi Shale ramp facies and its equivalent delta facies of the Zubair Formation.



Figure 3-19 b) continue



The mode and pattern of shallow-water sediment distribution would be similar in distally-steepened and homoclinal ramp types. The deeper-water facies for distally-steepened ramps would be characterized by more gravity flow facies, slumps, debris flow deposits and turbidites than homoclinal ramps (Tucker and Wright, 1990). Carbonate ramps were subdivided by Tucker (1991) and Burchette and Wright (1992) into three bathymetric environments each characterized by depositional facies with different sand-body types and therefore reservoir potential. The three bathymetric environments define three energy zones on the carbonate ramp.

Above fairweather wave-base is the shallow-ramp and back-ramp of Tucker (1991) or the inner-ramp of Burchette and Wright (1992). Between fairweather wave-base and storm wave-base is the deep-ramp of Tucker (1991) or middle-ramp of Burchette and Wright (1992). Below storm wave-base is the third bathymetric



environment, the basin of Tucker (1991) or outer-ramp of Burchette and Wright (1992).

The facies patterns of the shallow-ramp (inner-ramp) carbonate sand-body depend on the level of the energy of the depositional environment. In the shallow-ramp (inner-ramp), wave energy is less intense than along the rimmed shelf, where the energy of storm waves and oceanic swell affect the shelf margin. This energy is gradually released on the gentle slope of the ramp, resulting in relatively strong wave action, which forms the shallow-ramp (inner-ramp) sand-body. In the deep-ramp (middle-ramp), the sand-body is formed by the energy of offshore storm surges, which transport shallow-ramp carbonate sand to the deeper-ramp (Tucker and Wright, 1990).

Three end-member models of the sand-body of a shallow-ramp are identified depending on energy levels of the environment (Tucker and Wright, 1990; Tucker *et al.*, 1993). The three-end members of the models are: (1) high-energy shallow-ramp, which is dominated by a strandplain of linear beach ridges with depressions (swales). A modern analogue is the Yucatan coast of Mexico; (2) moderate-energy shallow-ramp, which is dominated by a beach barrier-tidal delta complex with lagoons and tidal flats behind. A modern analogue is the Trucial Coast of the Arabian Gulf; (3) low-energy shallow-ramp, which is dominated by fringing sand banks and shoal complexes with intertidal flats behind, without a lagoon. A modern analogue is the west side of Andros Island, Bahamas.

### 3.6 Ratawi Palaeoenvironment Reconstruction and Summary

The microfacies analysis of the core samples of the Ratawi Oolite and Ratawi Limestone (Section 3.3) is the database used in this study for the reconstruction of the palaeoenvironment of the Ratawi Formation (Fig. 3-18). Tucker (1991) and Burchette and Wright (1992) subdivided the ramp into facies belts, each of them characterized by specific sedimentary processes and overprinted by specific early diagenesis. This model can be used to interpret and predict the Ratawi depositional fabric and early overprinted diagenetic fabric that influenced the pore system of the Ratawi Formation, and therefore the heterogeneity of the Ratawi zone in the Wafra oilfield. The ramp model is based on the interpretation of the palaeowater-depth and identifying the fairweather wave-base and storm wave-base.



The depositional textures and sedimentary structures provide the most important criteria for Ratawi ramp palaeowater-depth interpretation, in addition to bioturbation, skeletal and non-skeletal composition, and calcrete evidence. Grain-supported textures are interpreted to have been deposited above fairweather wave-base in a moderate to high-energy ramp setting. Mud-supported textures are interpreted to have been deposited below storm wave base or above fairweather wave-base in a low-energy ramp setting (Tucker, 1991; Burchette and Wright, 1992).

On this process-based model, this study identifies four sedimentological lithofacies associations that are interpreted as the products of four Ratawi facies belts. These are: (1) Wackestone-mudstone with restricted faunas and black grains, which is interpreted as a restricted ramp environment with two subenvironments (Section 3.3.1), (2) Rudstone, grainstone-packstone with open-marine fauna, which is interpreted as a shallow ramp environment with five subenvironments (Section 3.3.2), (3) Mudstone-wackestone with open-marine fauna, which is interpreted as a deep-ramp environment with four subenvironments (Section 3.3.3), and (4) Subaerial exposure facies (section 3.4.2).

The Ratawi ramp model is basically an inner ramp with restricted lagoon that formed behind a sand-body barrier. This lagoon and shallow-ramp sand-body model of the Ratawi ramp is similar to the second model, noted above, of Tucker and Wright (1990) and Tucker *et al.* (1993). The model indicates that the energy of the depositional environment for this ramp was mostly moderate.

The depth of the fairweather wave-base and storm wave-base of the Ratawi ramp depends on three factors (Burchette and Wright, 1992). The first factor is the physiogeography. The Kuwait arch controls the position and the development of the Ratawi platform, and deposition of the Ratawi Oolite. The Ratawi epeiric ramp was bordering the Arabian Platform to the south and the Gotnia intracratonic basin to the north. The development of the sand-body on the shallow ramp barrier was controlled by Hormuz salt antecedent structures. The second factor is the wind direction, which was from the northeast from the open sea of the Tethys. The last factor is the palaeoclimate of the lower Cretaceous, which was a greenhouse period.



## Chapter 4 Diagenesis and porosity of the Ratawi Formation

### 4.1 Introduction

The most important parameters for any hydrocarbon reservoir are porosity and permeability. Porosity of the rock is the capability of the rock to store fluids, whereas permeability of the rock is the ability of the rock to release the fluids under a pressure gradient. The permeability and recovery efficiency of the Ratawi reservoir depend on many factors that include the nature of the pore system. Ratawi diagenetic and depositional environments control the nature of the pore system that includes the pore size, pore-throat size, pore-surface roughness, and number of pore-connections (Chilingarian *et al.*, 1992). Diagenesis refers to all the processes that affect carbonate sediments after deposition until the realms of incipient metamorphism at elevated temperatures and pressures. The diagenesis of the carbonate involves many processes that can be grouped into three diagenetic environments, which are marine, meteoric, and burial. Understanding these diagenetic processes is vital to interpret and predict the evolution of the Ratawi porosity (Moore, 1989; Tucker and Wright, 1990).

Factors that determine the nature of the diagenetic end-product and porosity development can be grouped into three main categories: (1) the composition of the original sediment, its texture and mineralogy, (2) the nature of the interstitial fluids and their movements, and (3) the biological, physical and chemical processes involved and the time subjected to them (Scoffin, 1987). The first factor depends mostly on the nature of the depositional environment, whereas the second and the last factor depend mostly on the nature of the diagenetic environment.

Porosity development includes preservation of the primary depositional porosity, which could be enhancement by dissolution, reduced or occluded by cementation, and the formation of secondary porosity by such processes as dissolution, dolomitization, and fracturing. The rock fabric of the Ratawi reservoir is the end product of the depositional and diagenetic environments. The types of porosity can be related to the rock fabric as fabric-selective, non-fabric-selective, and fabric selective or not (Choquette and Pray, 1970). The high chemical reactivity of carbonates relative to siliciclastics leads to extensive early carbonate diagenesis in marine and meteoric environments. These early diagenetic processes strongly influence the fabric of the



carbonate rock that controls porosity development and type. In the burial diagenetic environment, carbonate rocks may be influenced by the near-surface diagenetic history and react to pressure dissolution more readily than a siliciclastic rock, leading to a greater loss of porosity with depth (Moore, 1989 and Chilingarian and Mazzullo, 1992).

Integrating the factors that controlled the Ratawi early diagenesis into a sequence stratigraphic framework may permit the porosity evolution of the Ratawi reservoir units to be predicted (Tucker, 1993 and Harris *et al.*, 1999). In addition to porosity evolution, diagenetic studies are also used in this study to interpret the depositional environments and distinguish the different types and order of surfaces that are significant to construct a sequence stratigraphic model for the Ratawi Formation.

#### **4.1.1 The aims of this chapter**

This chapter has three main aims. The first aim is to investigate the different diagenetic products and relate them to the three main diagenetic environments; the evolution of the porosity of the Ratawi is linked to these diagenetic processes. The diagenetic overprints used to interpret Ratawi depositional environments, and to identify different types and order of surfaces are discussed in Section 4.2. The second aim is to describe the Ratawi primary and secondary pore types, which characterize reservoir Unit D and Unit E, and non-reservoir units, at Wafra oilfield. In addition, the possible factors that preserve near-surface porosity are discussed in Section 4.3. The last aim is to interpret and predict Ratawi porosity, reservoir rock (reservoir Unit D and Unit E), and seal rock, which is done by integrating the Ratawi diagenetic model and Ratawi depositional model into the Ratawi sequence stratigraphic framework; this is discussed in Section 4.4.

### **4.2 Ratawi diagenetic environments**

#### **4.2.1 Introduction**

Diagenetic processes considerably modify the primary depositional porosity, and have an important role in porosity reduction, enhancement, creation of secondary diagenetic porosity, and preservation of the near-surface porosity (primary and secondary) with increasing burial depth. Carbonate sediments are composed of a small variety of minerals, which are aragonite, high Mg-calcite, low Mg-calcite and dolomite, that are



Diagenetic processes	Diagenetic environment	Shallow-marine	Subaerial exposure (meteoric)	Burial
1-Hardground		—		
2-Micritic envelope (constructive and destructive)		—		
3-Synsedimentary organic dolomitization for burrows and organic rich intervals (micro-euhedral dol.)		—		
4-Synsedimentary pyrite precipitation		—		
5-Micritization of carbonate grains		—		
6-Syntaxial rim cement		—	—	—
7-Calcitization of aragonite and high-Mg calcite		—	—	
8-Pseudomorphosed gypsum		—		
9-Mixing-zone related dolomite			—	
10-Dedolomitization and the formation of rhombohedral crystal-mould pores			—	
11-Micritization of carbonate grains and cements			—	
12-Formation of black grains			—	
13-Formations of alveolar septal structure, rhizolith and calcified filaments, in addition to related rootlet porosity			—	
14-Replacement of quartz grains by calcite			—	
15-Vadose compaction			—	
16-Bladed / granular cement			—	
17-Granular drusy cement			—	—
18-Columnar cement			—	
19-Vugs			—	—
20-Chemical and physical compaction				—
21-Micro-euhedral dolomite associated with dissolution seam				—
22-Saddle dolomite as cement and replacement				—
23-Poikilotopic cement				—
24-Fractures			—	—
25-Pulses of carboxylic acid and the formation of burial vugs				—
26-Emplacement of oil and the preservation of porosity from further reduction				—

Figure 4-1 Ratawi diagenetic processes and inferred diagenetic environments.

highly susceptible to chemical alteration, recrystallization and dissolution. The effects of carbonate diagenesis on porosity development are intensified by the tendency of shallow carbonate platforms to be subaerially exposed by building up to sea level and affected by falling sea level of different magnitudes and durations (Kupecz *et al.*, 1997).



Carbonate diagenesis includes six major processes: cementation, microbial micritization, neomorphism, dissolution, compaction, and dolomitization (Tucker and Bathurst, 1990). The development of porosity in the Ratawi zone in the Wafra oilfield is particularly influenced by cementation, compaction and dissolution. These processes can operate in several different diagenetic environments, early or late, shallow or deep. Ratawi diagenetic processes and inferred diagenetic environments are listed in Fig. 4-1

#### **4.2.1.1 Ratawi major diagenetic environments**

Carbonate diagenetic reactions are not solid-state reactions but take place in the presence of fluids (Bathurst, 1975). The fundamental difference in properties of these fluids can be used to identify three major diagenetic environments in the Ratawi, each characterized by a different set of diagenetic processes and porosity development. The Ratawi diagenetic environments are (1) marine (Section 4.2.1), with sea water ranging from supersaturated with the respect to  $\text{CaCO}_3$  in shallow, warm seas to undersaturated in deep cold seas, (2) meteoric (Section 4.2.2), with fresh water flowing through the subaerially exposed rock, and (3) deep burial (Section 4.2.3), where the interstitial fluids could be connate (marine) water, or they could be derived from different sources like clay diagenesis or fluids associated with organic matter diagenesis, and hydrocarbon generation (Scoffin, 1987). The different diagenetic products and environments for dolomitization and dedolomitization are discussed in Section 4.2.4.

### **4.2.2 Shallow-marine diagenetic environment**

#### **4.2.2.1 Introduction**

Marine diagenesis takes place on beaches and tidal flats, and on the shallow seafloor; the major factors in this environment are water depth, latitude and climate (Tucker and Wright, 1990). The Lower Cretaceous 'Ratawi Oolite platform' is characterized by a shallow-water depth located to the south of the equator with a warm semi-arid climate. The diagenetic processes of the shallow-marine diagenetic environment occur in three subenvironments. The first subenvironment is the active marine phreatic, in carbonate sand shoals and reef, and this is characterized by a high rate of seawater movement through the sediment that leads to widespread cementation (Tucker and Bathurst, 1990). This study has recognized this diagenetic environment in the shallow ramp microfacies SR (Section 3.3.2), characterized by a high-energy depositional



environment, but the amount of marine cement is minor. The possible reasons for the limited amount of marine cement in the Ratawi carbonate shoals are discussed in Section 4.2.2.5; this had a profound effect on the development of Ratawi porosity.

The second subenvironment is the stagnant marine phreatic, occurring in back-shoal lagoons and characterized by extensive microbial micritization of the skeletal and non-skeletal particles and minor cementation (Tucker and Bathurst, 1990). This study has recognized this diagenetic environment in the back ramp microfacies BR (Section 3.3.1), which is characterized by widespread microbial micritization and also very limited amounts of marine cement. The last subenvironment is marine vadose, occurring in the high intertidal and supratidal flats, along low energy shorelines and upper foreshore, and backshore of high-energy shorelines. This is characterized by evaporation of seawater that leads to cementation and possible microbial micritization (Tucker and Bathurst, 1990). This study has recognized this diagenetic environment in cross-laminated peloidal bioclastic grainstone-packstone microfacies SR2 (Section 3.3.2.2). This subenvironment is also characterized by a limited amount of marine cement but with extensive microbial micritization.

This study has recognized seven marine diagenetic processes: micritization (Section 4.2.2.2), micrite envelopes (Section 4.2.2.3), grain reworking and boring (Section 4.2.2.4), marine cementation (Section 4.2.2.5), syndimentary pyrite precipitation (Section 4.2.2.6), calcitization (Section 4.2.2.7), and syndimentary organic dolomitization (Section 4.2.5.2.1).

#### **4.2.2.2 Micritization**

The process of micritization is important in the Ratawi Formation; almost all the Ratawi particles are micritized or have micritic envelopes. The term micritization refers to all shallow-marine diagenetic processes that result in obliteration of the original microstructure of the carbonate grain by gradual alteration to a cryptocrystalline texture; the processes can cause wholesale destruction of all types of skeletal and non-skeletal grains (Reid and Macintyre, 2000). This process is inferred here to be the process that formed the most dominant grain type in the Ratawi Formation, namely the peloidal grain (Section 3.3.2.1). Micritization creates difficulties in identifying Ratawi grains (Section 3.2.2), and the reconstruction of Ratawi depositional environments.



There are two distinct mechanisms for early marine micritization, which seems to have had a different impact on the development of microporosity of the Ratawi zone (Section 4.3.3.11). These mechanisms are (1) endolithic micro-organisms (Section 4.2.2.2.1), and (2) syndepositional recrystallization (Section 4.2.2.2.2). This study did not differentiate between the two mechanisms; one approach to differentiate between the two processes is by identifying the microborings of the endolithic micro-organisms.

#### 4.2.2.2.1 Micritization by endolithic micro-organisms

Micritization by endolithic micro-organisms is a widespread feature of shallow-water carbonate environments of the Arabian Gulf, Florida Bay and the Bahamas; and can be interpreted by two models; Bathurst model (1975) and Reid and Macintyre model (2000) (Fig. 4-2). According to Bathurst (1975), the process has three ordered events, (1) boring and colonization by endolithic micro-organisms, (2) death of endolithic micro-organisms and vacation of bores, and (3) emplacement of micritic aragonite or high-Mg calcite in the tubes. In this model the endolithic micro-organisms play no direct part in the precipitation of the carbonate in the bores. The process of filling the bores is regarded as a form of marine carbonate cementation.

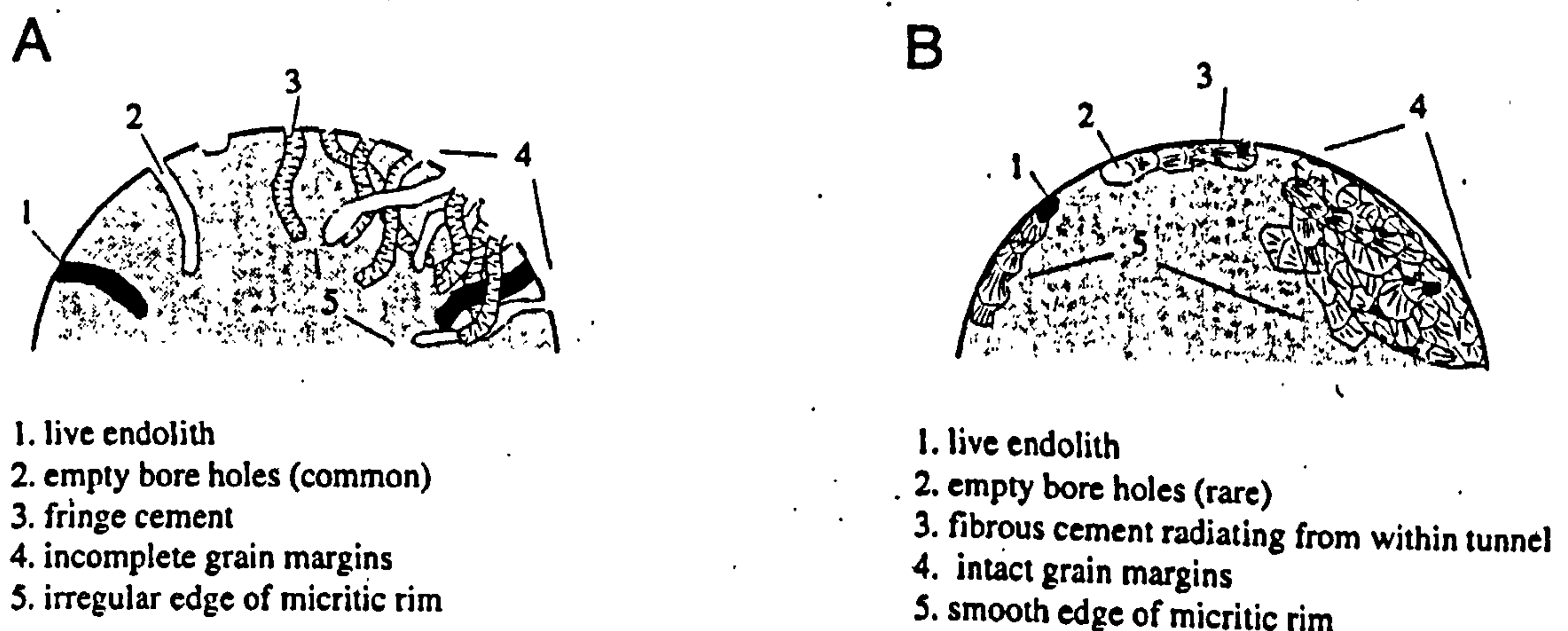


Figure 4-2 Diagram showing two micritization models by microboring (a) conventional micritic rim formation model of Bathurst, 1975, (b) concurrent filling model of Reid and Macintyre, 2000 (after Reid and Macintyre, 2000).

According to Reid and Macintyre (2000), endolithic micro-organisms take a direct part in the precipitation of the carbonate in the microbore; the microbores are filled by radial-fibrous aragonite that is precipitated as the endolithic micro-organism



advances. This model of micritization by boring and simultaneous filling of the boreholes could be difficult or impossible to distinguish from micritized grains formed by recrystallization (Section 4.2.2.2.2) (Reid and Macintyre, 2000). The endolithic micro-organisms include cyanobacteria (blue-green algae), chlorophytes (green algae), rhodophytes (red algae) and fungi. When the micritization process operates over a long period of time, all the internal structure of the grain is replaced by micrite by many cycles of boring and filling of boreholes. This is a centripetal, not a centrifugal oriented process (Bathurst, 1975).

The process of micritization by endolithic micro-organisms seems not to depend on the penetrated light, but on the depositional environment and carbonate grain types. Perry (1998) studied the boring activity of the endolithic micro-organisms within the reef environments of north Jamaica; the study recognized two distinct assemblages of endolithic micro-organisms: (1) an upper photic zone assemblage, water depth less than 18 m, dominated by cyanobacteria and chlorophytes, and (2) a lower photic zone assemblage, water depth more than 18 m, dominated by rhodophytes and fungi. The study concluded that the highest degree of grain micritization by endolithic micro-organisms occurs within shallow, low-energy lagoonal back-reef environments and the most susceptible grains are corals, molluscs and foraminifera in all environments.

The micritization of the Ratawi Formation by this process seems not to be controlled by the water depth but by the restricted circulation and low-energy environment of the 'Ratawi epeiric ramp'. The empty endolithic bores, unfilled by micrite, of the Bathurst model (1975) in the Lower Cretaceous calcite sea seem to enhance the microporosity of the Ratawi zone.

#### **4.2.2.2.2 Micritization by syndepositional recrystallization**

The alternative process for micritization by endolithic micro-organisms is by syndepositional recrystallization, which is a relatively new model for the micritization. According to Reid and Macintyre (1998, 2000), the syndepositional recrystallization micritization process is also a widespread feature of shallow-water, carbonate environments of Belize, Florida Bay and the Bahamas. The term recrystallization is used by Reid and Macintyre (1998, 2000) in a general sense, synonymous to neomorphism, for a reorganization of the size, shape or composition of carbonate minerals.



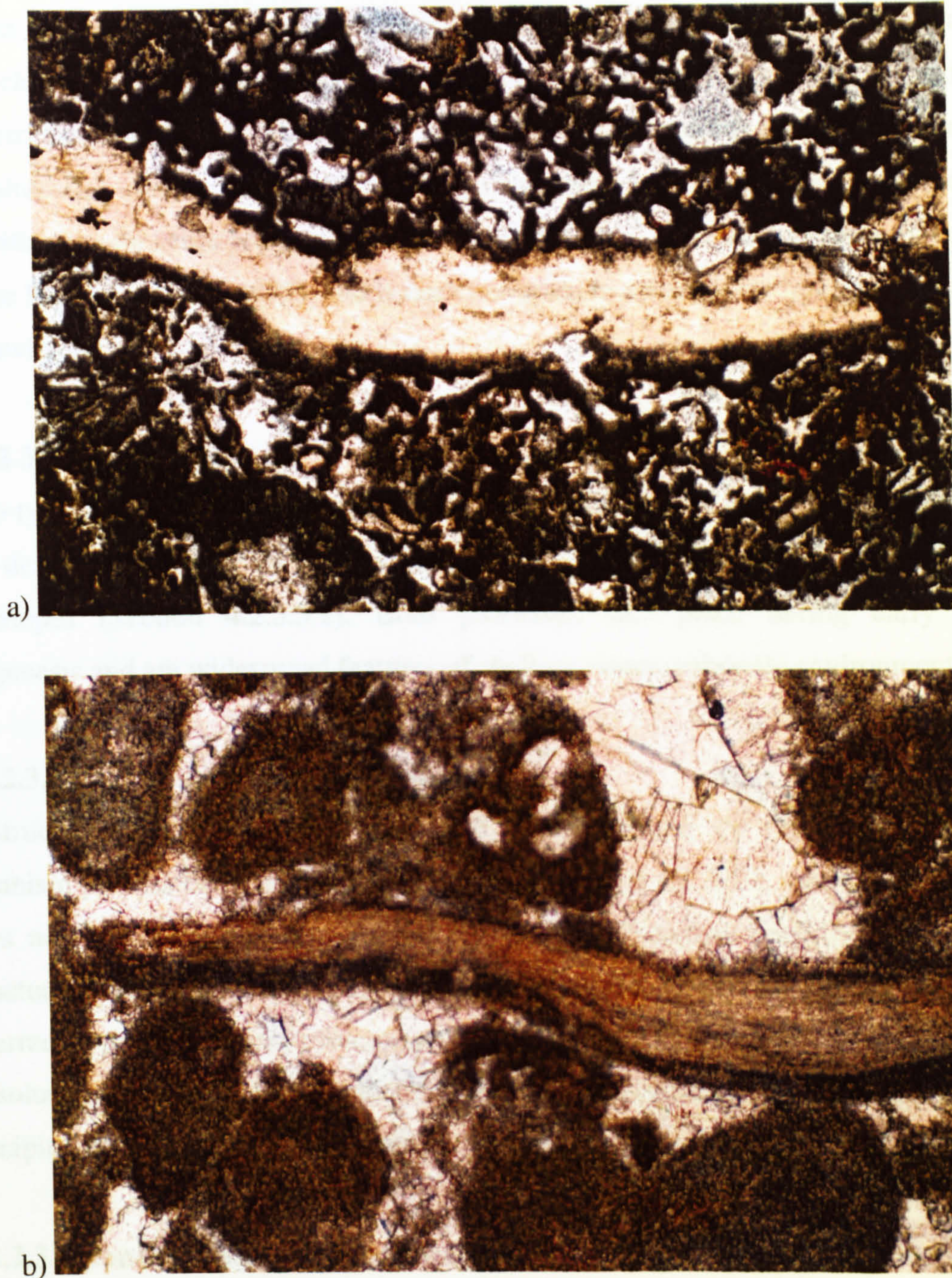


Figure 4-3 Photomicrograph of the two types of the micritic envelope, destructive micritic envelope (a) and constructive micritic envelope (b) both on brachiopod grains. Note the well-developed boundary between the grain and the envelope in the constructive type. Sample number (a) is R-49 # 22, depth 6837 ft (2084 m), field of view 3 x 2 mm, under plane-polarized light. Sample number (b) is R-50 # 89, depth 7002 ft (2134 m), field of view 1 x 0.6 mm, under plane-polarized light.

The micritization by syndepositional recrystallization is by crystal growth and transformation of metastable Mg-calcite and aragonite to calcite on the tropical shallow-marine sea floor. This process is influenced by organic reactions, surface free energy, and microboring activity (Reid and Macintyre, 1998, 2000). This process



seems not to be common in the Lower Cretaceous calcite-sea because the dominant particles would be composed of low Mg-calcite. As all ready mentioned, micritization by recrystallization is difficult to distinguish from micritization by boring and simultaneous cement filling of boreholes (Reid and Macintyre, 2000). The process of micritization by syndepositional recrystallization is not from the formation of bores as in the Bathurst model (1975), and it does not seem to enhance the microporosity of the Ratawi zone.

#### **4.2.2.3 Micrite Envelopes**

Two types of the micrite envelope are recognized by Flügel (1980) and Perry (1999): (1) destructive micrite envelopes (Section 4.2.3.3.1), and (2) constructive micrite envelopes (Section 4.2.3.3.2). Both processes take place during early marine diagenesis and are widespread features of shallow-water carbonate environments.

##### **4.2.2.3.1 Destructive micrite envelopes**

Destructive micrite envelopes (Fig. 4-3 a) are formed by the endolithic micro-organism process of micritization discussed in Section 4.2.2.2.1, in which the process does not take place over a long period of time. Therefore only the outer internal structure of the grain is replaced by micrite (Bathurst, 1975). This type is commonly referred to as a 'destructive micrite envelope' because it results from the biochemical dissolution of grain material by endolithic micro-organisms and subsequent internal precipitation of micrite (Perry, 1999).

##### **4.2.2.3.2 Constructive micrite envelopes**

This type is commonly referred to as a 'constructive micrite envelope' because it results from the accumulation of micrite around the external surface of the grains (Perry, 1999). The different processes for formation of the constructive micrite envelopes are reviewed by Perry (1999) who concluded that early micrite precipitation can occur as a result of external, extraskelatal or extracellular processes within a wide variety of environments. These include karst terrains, lacustrine and marine stromatolites, and marine microbial mats.

The constructive micrite envelopes (Fig. 4-3 b) are formed by biologically-mediated micrite precipitation, which occurs (1) within the biofilm mucilage, (2) around biofilm components, and (3) associated with trapping of carbonate mud and



fine-grained sediment (Perry, 1999). The boundaries between the grain and the micrite envelope could be used to distinguish between the destructive and constructive micrite envelopes (Flügel, 1980); the constructive micrite envelopes are characterized by well-defined boundaries, whereas the destructive micrite envelopes are not. According to the grain-envelope boundaries, the origin of the Ratawi micrite envelopes is mostly of the destructive micrite envelope type.

#### **4.2.2.4 Grain reworking and boring**

Most of the coarse sand-size coral grains show evidence of boring and reworking, which indicate significant transportation. Organisms play a crucial role in the sedimentation of the carbonate grains; this not only includes the supply of the skeletal grain but also an influence on the mode of disintegration, erosion, transport, deposition, burial and preservation of grains (Scoffin, 1987). The abundant evidence of reworking and boring could be a reflection of a low sediment supply.

#### **4.2.2.5 Marine cement**

##### **4.2.2.5.1 Introduction**

The process of cementation in the Ratawi Formation played a double role in controlling Ratawi reservoir heterogeneity, namely (1) reducing and eliminating primary and secondary porosity by filling the pore space, and (2) preserving primary depositional porosity in reservoir unit-D by forming a lithified framework that resisted deep burial compaction (Section 4.2.4). Cementation can occur in marine, meteoric and deep burial diagenetic environments; distinguishing the cement sequence is essential to interpret the heterogeneity of the Ratawi zone, which could be done by studying cement mineralogy, morphology and distribution (Moore, 1989).

Cementation processes take place when (1) pore-fluid is supersaturated with the cement phase and kinetic factors do not inhibit precipitation (Section 4.3.4), and (2) the fluid effectively transports the cement phase to the site of precipitation. Cement source and mineralogy depend on the diagenetic environment, which are (1) marine environment, sourced from seawater and mineralogy aragonite, high Mg-calcite or low Mg-calcite depending on the geological time-period, (2) meteoric environment, sourced from dissolution of grains with unstable carbonate mineralogy, aragonite and high Mg-calcite, and a mineralogy of low Mg-calcite, and (3) deep burial environment, sourced from dissolution of carbonate grains and matrix, in addition to basin fluids and



a mineralogy of low Mg-calcite, and saddle dolomite. Cement morphology and distribution depend on the original cement mineralogy and diagenetic environments (Scoffin, 1987; Tucker and Bathurst, 1990).

Modern marine environments are dominated by aragonite and high Mg-calcite cements and ooids, but in ancient seas, early Ordovician-middle Carboniferous and early Jurassic-late Cretaceous, low Mg-calcite was the dominant marine mineralogy. This oscillating trend between the 'aragonite sea' and 'calcite sea' is referred to as the Sandberg Curve, and this can be correlated to changes in global tectonic activity, atmospheric  $p\text{CO}_2$ , and seawater Mg/Ca ratio (Moore, 1989; Tucker and Bathurst, 1990; Tucker and Wright, 1990).

The Ratawi Formation was deposited in the Lower Cretaceous calcite sea, which is inferred to be correlated with first-order high stands of global sea level and high  $p\text{CO}_2$ , and low Mg/Ca ratio. The calcite sea not only influenced the mineralogy of the marine cements, but also influenced the taphonomy of the Ratawi Formation fossils (Section 3.2.2), in which Ratawi skeletal grains with an aragonite mineralogy (corals, gastropods, calpionellids, and green algae) were more soluble and some dissolved on the sea floor (Harper *et al.*, 1997).

The Ratawi shallow-ramp environment (Section 3.3.2) is characterized by rare marine cements even though the microfacies are rudstone and grainstone-packstone, which indicate high-energy environments. When these Ratawi facies are compared with their modern equivalents, as in the Arabian Gulf, one would expect Ratawi shoal facies to be cemented by marine cements of aragonite and high Mg-calcite mineralogy. This study has interpreted the rare marine cements in the Ratawi Formation as due to sluggish water circulation, and possible low precipitation rate of low Mg-calcite marine cements in the calcite sea compared to relatively rapid aragonite and high Mg-calcite cementation in modern aragonite seas.

To distinguish marine cement from meteoric or deep burial cement in the Ratawi, this study used criteria listed by Tucker and Bathurst (1990): (1) first cement generation, (2) commonly acicular or columnar fabric, and (3) isopachous fibrous fringes with polygonal compromise boundaries where fringes meet in pores of the grainstone. Ratawi marine cements identified in this study are syntaxial rim cement (Section 4.2.2.5.2), and hardground cement (Section 4.2.2.5.3).



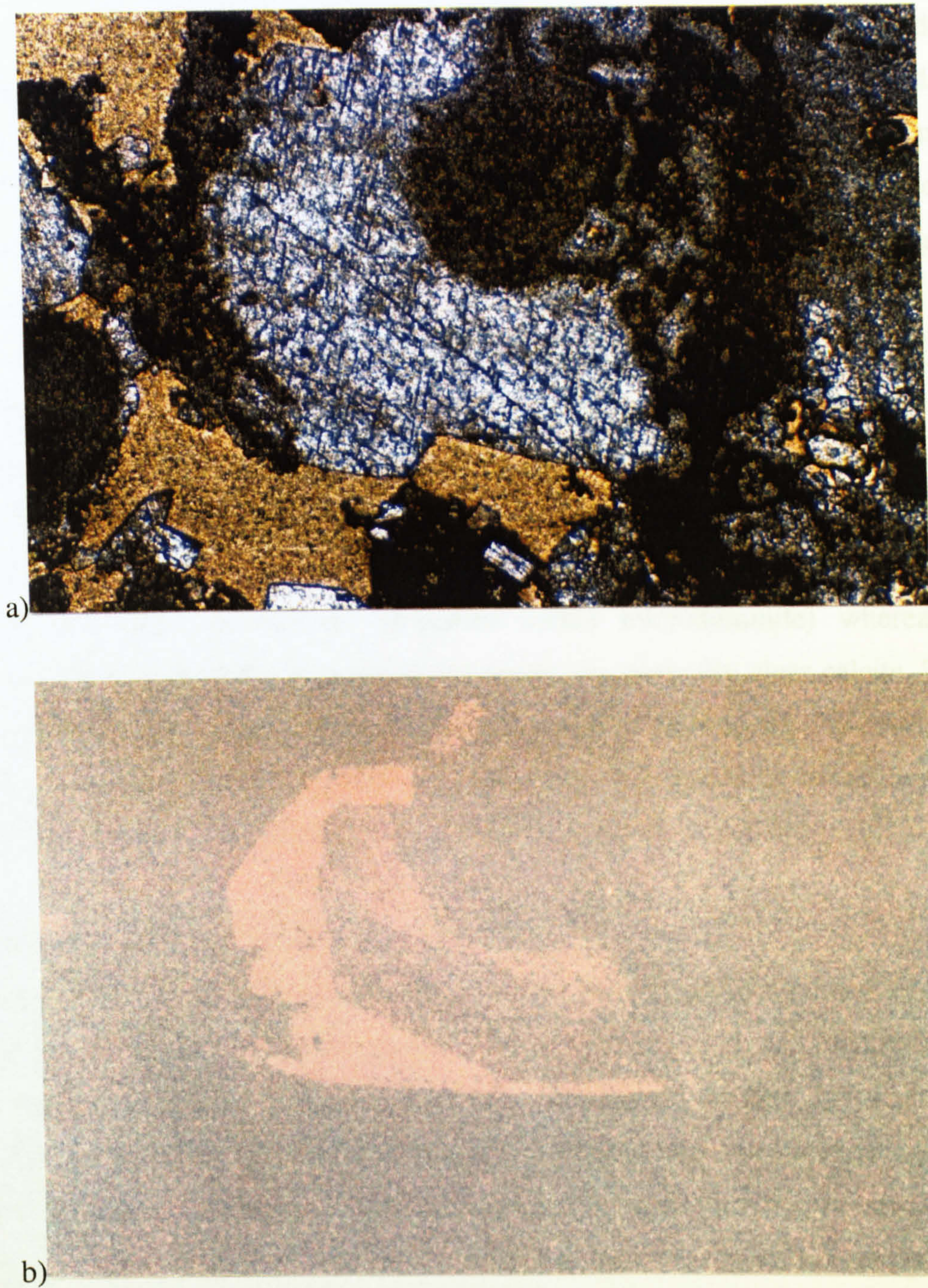


Figure 4-4 Photomicrograph of crinoid grain with syntaxial calcite cement (a) under plane-polarized light (b) under cathodoluminescence. Note the early part and outer part of the cement has a dull colour, whereas the middle zone is bright-orange. Sample number is R-48 # 7, depth 6760 ft (2060 m), field of view 3 x 2 mm



#### 4.2.2.5.2 Syntaxial rim cement

Most crinoids in the Ratawi have developed a syntaxial rim cement (Fig. 3-7 a), which is a large, optically continuous crystal on the crinoid plate. The overgrowths generally show a dull colour under CL, the crinoid early part, a bright-orange zone, and then a dull outer part (Fig. 4-4). The distribution of this type of cement is controlled by the depositional texture, and availability of the single crystal substrate of a crinoid plate. In a mud-supported texture, most crinoid plates are without a syntaxial rim cement; however, in a grain-supported texture all crinoid plates have syntaxial overgrowths that reduce the porosity. The syntaxial rim cement started to develop in the marine environment and continued to grow in the meteoric environment (Flügel, 1982). There are no modern analogues for the precipitation of the syntaxial rim cement in modern aragonite sea, but many examples of marine syntaxial rim cement have been reported from ancient carbonates deposited during periods of a calcite sea (Kim and Lee, 1996). Syntaxial overgrowth on crinoids precipitated in a marine environment are generally cloudy with fluid or mineral inclusions (often microdolomite) whereas those precipitated in a meteoric or burial environment are generally clear calcite. The dull nature of the early part of the crinoid overgrowth is most likely the result of low manganese content (and low iron too, since staining shows it to be non-ferroan calcite). It is quite likely that this early overgrowth calcite is a marine precipitate.

#### 4.2.2.5.3 Hardground cement

The recognition of breaks in deposition is important for grouping Ratawi lithofacies into a hierarchy of genetic units, as discussed in the Chapter 5, and identifying cycles and sequences. Two processes lead to stratigraphic breaks: (1) decreases in accommodation space recognized by subaerial exposure surfaces (Section 3.4.3.3), and (2) decreases in the sediment supply producing hardground surfaces. A hardground is a surface of synsedimentary lithification, having existed as hardened seafloor prior to the deposition of the overlying sediments (Bathurst, 1990); they are the result of marine cementation and lithification. Hardgrounds can be recognized by evidence of early lithification including (1) sharp lithological contacts with truncated grains, (2) mineralized surfaces, and (3) encrustation or boring by organisms (Kim and Lee, 1996).

Evidence for different degrees of early marine cementation in the Ratawi Formation comes from studying ichnofossil types in the cores from wells R-50 and R-



48, where the following were identified: (1) rootlets, (2) burrow mottling, (3) 1 mm diameter burrows, (4) 3 to 10 mm horizontal to vertical burrows, (5) larger than 10 mm diameter horizontal burrows, and (6) *Trypanites* ichnofossil. The larger than 10 mm diameter horizontal burrows are interpreted in this study to be *Thalassinoides* ichnofossils. The rootlet ichnofossils are used in Section 3.4.3.3 to infer subaerial exposure surfaces, whereas the other five ichnofossils are used in this Section to infer different degrees of early marine lithification.

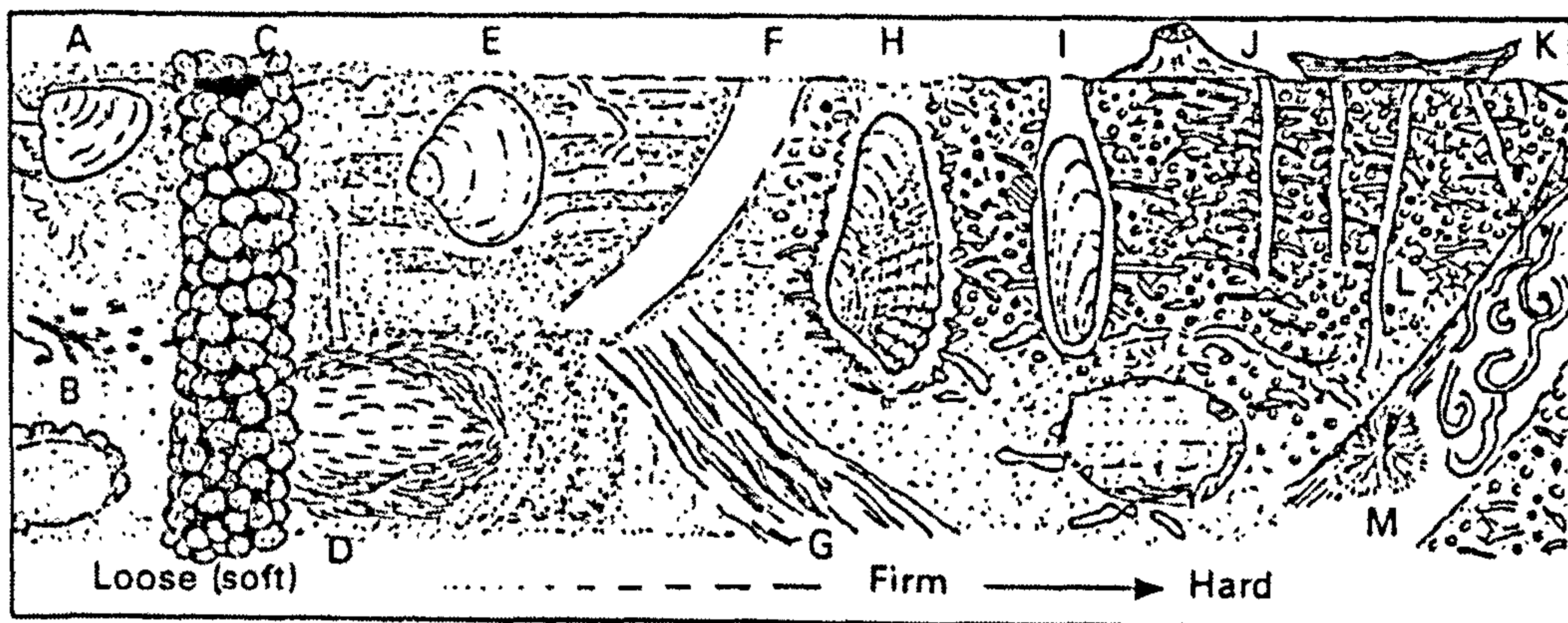


Figure 4-5 Diagram to show types of biogenic response to loose (soft), firm and hard (lithified) substrates. (A) *Nucula*, (B) *Chondrites*, (C) *Ophiomorpha*, (D) *Mercenaria* / *Arctica*, (E) *Thalassinoides*, (F) *Spongiomorpha*, (G) *Petricola*, (H) *Lithophaga*, (I) crinoid holdfast, (J) oyster, (K) *Trypanites*, (M) encrusting bryozoan and serpulids on burrow wall (after Goldring, 1995)

Sedimentological structures and fabrics produced by animals can be used in facies interpretation (Goldring, 1995) (Fig. 4-5). Organism activities, which include encrustation, feeding, burrowing and boring, can be evaluated and applied to environmental and facies interpretation that include the different degrees of early marine lithification. Goldring (1995) used burrowing and boring to identify four degrees of early marine lithification: (1) softground (mud that can be squeezed through the fingers) characterized by burrows exhibiting substantial compaction, with irregular outlines, and escape structures, (2) looseground (loose well-sorted to moderately well-sorted silt or sand grade sediment) characterized by burrows with a lining to stabilize the wall, made of pellet or mucus, (3) firmground (stiff substrate) characterized by burrows with minor burrow compaction and sharp outlines, and (4) hardground, rockground, and shellground characterized by an encrusting and boring biota and a mineralized crust.

Three different degrees of Ratawi early marine lithification are recognized in



this study: (1) softground and looseground characterized by the burrow mottling, 1 mm diameter burrows, and 3 to 10 mm horizontal to vertical burrows, (2) firmground characterized by *Thalassinoides*, and (3) hardground characterized by *Trypanites*. The identifications of Ratawi hardground by *Trypanites* is essential in distinguishing three types of Ratawi elementary depositional cycle (parasequence), namely (1) transgressive-regressive cycle, (2) regressive cycle, and (3) aggraded cycle. As discussed in the Chapter 5, each cycle has different depositional and diagenetic characteristics.

Ratawi hardgrounds are formed by three steps, (1) synsedimentary marine lithification by marine cement that formed the hardground just below the sea floor, (2) exhumation of the hardground by winnowing and erosion of the soft sediment above, and (3) erosion, mineralization, encrustation and boring of the hardground. The modern analogue to Ratawi hardground formation in a calcite-sea is the deep-sea environment, where seawater is undersaturated with respect to aragonite. The hardground features in this environment are driven by dissolution of biogenic aragonite and reprecipitation as low Mg-calcite at or near the sea floor (Kim and Lee, 1996).

#### 4.2.2.6 Synsedimentary pyrite

Synsedimentary pyrite is very important in the interpretation of the depositional environment of the Ratawi Formation. A restricted depositional environment can be inferred from a restricted fauna or a lithofacies that includes evaporites, organic matter, or pyrite (Paul, 1983). As discussed in Section 3.3 only the back-ramp environment of the Ratawi ramp is characterized by a restricted ostracod fauna, with the shallow-ramp and deep-ramp characterized by open-marine faunas. Pyrite, which is found in most of the Ratawi thin-sections (Appendix 1), together with the dark colour of the core samples, selective pyritization of fossils, and synsedimentary organic dolomitization of burrows (Section 4.4.2.1), indicate that a reducing environment existed just below the sea floor.

Synsedimentary pyrite selectively formed in fossils or precipitated in pore space requires anoxic conditions below the sediment-water interface. Anoxic environments can be subdivided into three types: (1) non-sulphidic methanic, (2) non-sulphidic post-oxic, and (3) sulphidic (Tucker, 1991). The non-sulphidic methanic environment is characterized by organic-rich sediments in which bacteria continue to



decompose organic matter, removing all  $O_2$ ,  $NO_3^-$ , and  $SO_4^{2-}$  and producing methane. The non-sulphidic post-oxic environment is characterized by less organic matter, which is only enough for the consumption of all dissolved oxygen by aerobic bacteria, but not enough to bring sulphate reduction. The sulphidic environment is characterized by enough organic matter for the consumption of all dissolved oxygen by aerobic bacteria, and which then permits bacterial sulphate reduction.

Synsedimentary pyrite  $FeS_2$  is formed by the reaction between the  $H_2S$  and  $Fe^{2+}$ , in which the source for  $H_2S$  is from bacterial reduction of sulphate to produce sulphide  $SO_4^{2-}$  that dissolves in the pore water; the source of the  $Fe^{2+}$  is the pore water, organic matter or clay minerals. Pyrite is not stable in the oxidizing meteoric diagenetic environment. Most of the pyrite in the Ratawi Oolite, beneath the karst surface of the 2<sup>nd</sup> order sequence boundary of reservoir unit-E, is inferred to have changed to goethite and limonite, giving the Ratawi core samples the yellow-brown colour.

#### 4.2.2.7 Calcitization

The unstable minerals aragonite and high Mg-calcite in the Ratawi sediments were altered to the stable mineralogy, low Mg-calcite, mostly by the process of neomorphism, which includes recrystallization and replacement, where there may have been a change in mineralogy (Tucker and Bathurst, 1990). The neomorphic replacement reaction is through dissolution-reprecipitation and this may have influenced the development of the Ratawi fabric in two ways: (1) porosity-permeability and (2) taphonomy - the preservation potential of corals, gastropods, calpionellids and green algae (Section 3.2.2).

The reaction is controlled by the rate of aragonite dissolution relative to calcite spontaneous nucleation, that is nucleation without the benefit of previous seed crystals or nuclei (Moore, 1989). James and Choquette (1984) recognized two styles of calcitization, namely (1) macroscale dissolution during the stabilization of aragonite, and (2) microscale dissolution during the stabilization of aragonite and high Mg-calcite. The first style is not included as a neomorphic replacement process.

The first style, macroscale dissolution, forms when there is large water flux, which is strongly undersaturated with respect to aragonite. The aragonite particles undergo wholesale dissolution and the dissolved  $CaCO_3$  would be carried a significant distance and precipitated as low Mg-calcite cement. This process could lead to the



development of a lithified rock and massive rearrangement of pore space in the meteoric phreatic system (James and Choquette, 1984; Moore, 1989). This stabilization process is inferred to have occurred in the Ratawi gastropods, calpionellids and green algae (Fig.4-24 a and 4-25 a) and is used to interpret the origin of some of the Ratawi mouldic pores (Section 4.2.3.3), which locally are filled by granular drusy cement (Fig. 4-6).

The second style, microscale dissolution, may alter both high Mg-calcite and aragonite. In the case of high Mg-calcite the process forms when there is not a very high water flux; the high Mg-calcite dissolves and  $\text{CaCO}_3$  is simultaneously precipitated as low Mg-calcite on the opposite side of the water film, which is nanometres to micrometres in thickness. The low Mg-calcite would precipitate on the readily available nucleation sites within the particle, preserving the ultrastructure of the original particle during the stabilization process (James and Choquette, 1984; Moore, 1989). This stabilization process is not inferred to have occurred in the Ratawi.

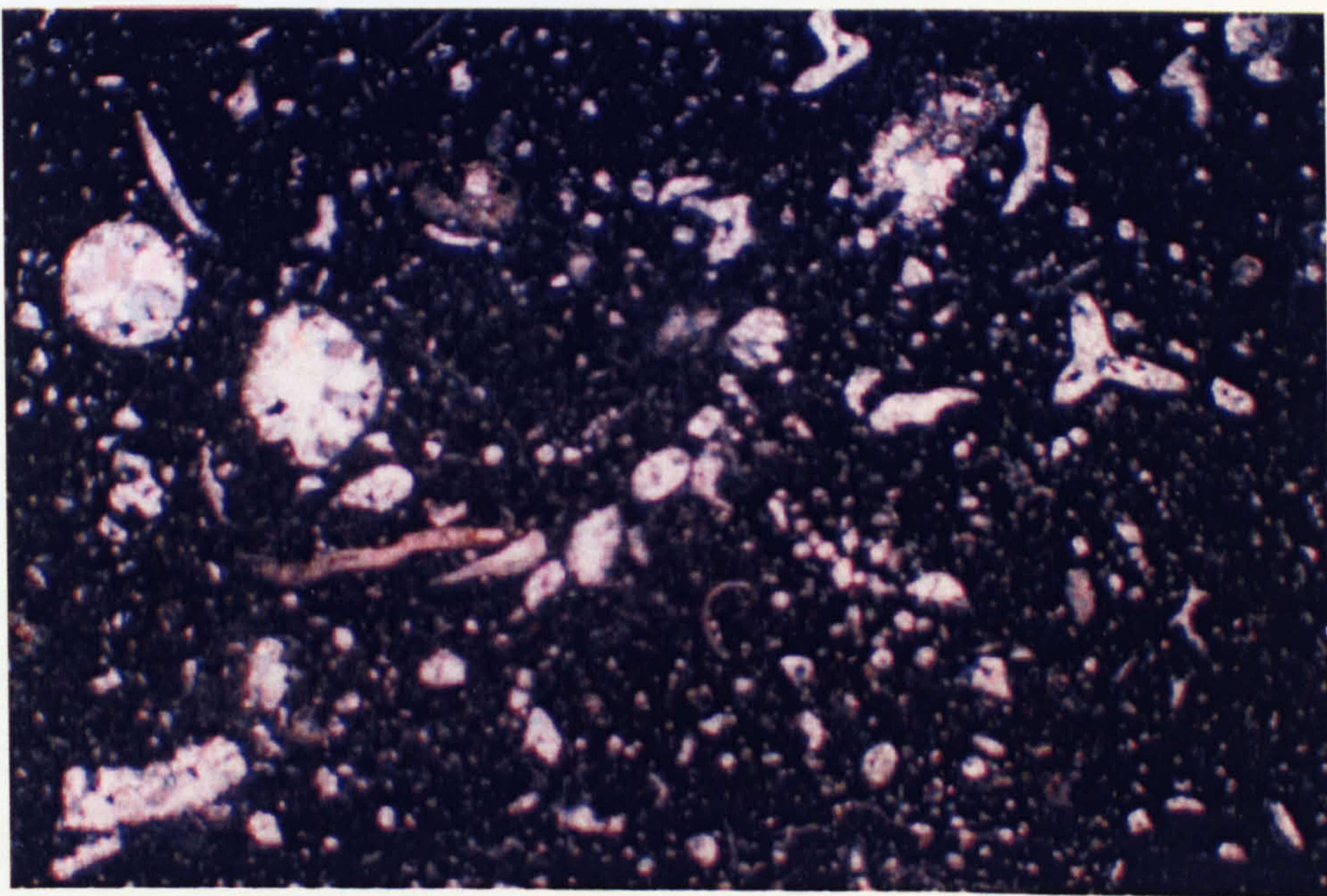


Figure 4-6 Photomicrograph of green algae and sponge spicules. Note the filling of the moulds by the coarse granular calcite cement. Sample number is R-50 # 25, depth 6609 ft (2014 m), field of view 5 x 3 mm, under crossed polars.

In the case of aragonite the process forms when there is slow water flux, which is slightly undersaturated with respect to aragonite. The aragonite dissolves and is simultaneously precipitated as low Mg-calcite on the opposite side of the water film, several millimetres in width, in a chalky zone. This process leads to a low Mg-calcite mosaic with relics of the original structure of the particle outlined by organic matter



and other insoluble material (James and Choquette, 1984; Moore, 1989). This stabilization process is inferred to have occurred in the Ratawi corals (Fig. 3-5 a).

The processes of calcitization by the microscale style unlike the macroscale style, does not lead to appreciable secondary porosity development or to significant calcite cementation outside the particle (James and Choquette, 1984; Moore, 1989). The calcitization process generally occurs under two different diagenetic conditions, (1) a late calcitization process, which could occur during meteoric or burial diagenesis (Section 4.2.3.7.1), and (2) an early calcitization process, which could occur under marine conditions (Section 4.2.3.7.2). Both models of calcitization produce a similar calcitized shell texture, but the two models would have different trace element and isotopic compositions (Hendry *et al.*, 1995).

#### **4.2.2.7.1 Late calcitization in meteoric and burial environments**

The calcitization process during meteoric and burial diagenesis involves a single generation of low Mg-calcite that may contain aragonite skeletal relics; this model requires subaerial exposure or deep burial. The reaction is driven by undersaturated, meteoric or deep burial pore water, with respect to aragonite and high Mg-calcite, and proceeds via inward migration of the neomorphic front (Maliva and Dickson, 1992).

#### **4.2.2.7.2 Early calcitization in the marine environment**

The calcitization process may begin at the sediment-water interface and continue into shallow burial. In contrast to meteoric and burial diagenesis, where the calcitization process, proceeded via inward migration of a neomorphic front, the calcitization process in the marine realm is initiated at numerous individual reaction centres through the shells. The early calcitization in the marine environment is influenced by two different factors: (1) oxidation of the organic matter that increases CO<sub>2</sub> and decreases pH of the pore-fluid, and (2) the calcite sea, which is undersaturated with respect to aragonite, but supersaturated with respect to calcite (Hendry *et al.*, 1995).

The Ratawi Formation is characterized by an anoxic environment below the sediment-water interface as explained in synsedimentary pyrite (Section 4.2.3.8) and synsedimentary organic dolomitization of burrow fills (Section 4.2.5.2.1); in addition the Lower Cretaceous Ratawi Formation was deposited in a calcite-sea. These data could support calcitization of the Ratawi particles by the second early calcitization model in a marine environment.



### **4.2.3. Shallow-burial meteoric diagenetic environment**

#### **4.2.3.1 Introduction**

Meteoric diagenesis takes place when carbonate sediment and rock is exposed to rainwater; this is an important diagenetic setting for the development and evolution of carbonate porosity because of the large volume of water available for dissolution and precipitation (Moore, 1989). This diagenetic environment can happen at two different times, (1) soon after deposition (eogenetic), when the sediment shallows up to sea level by shoreline progradation or by slight relative sea-level fall, also when sediment is thrown on to a supratidal flat, and (2) after many millions of years after deposition (telogenetic), when the rock is uplifted and exposed at the Earth's surface (Tucker and Wright, 1990).

The shallow meteoric diagenetic environment can be divided into three subenvironments each characterized by its diagenetic processes and porosity development. These subenvironments are (1) meteoric vadose zone, near the surface with water and air occupying the pore spaces, (2) meteoric phreatic zone, below the water table with higher water flux towards the top and more stagnant water near the base, and (3) the meteoric-mixing zone, at the contact between the fresh water and the denser saline marine water (Moore, 1989).

The Ratawi meteoric diagenetic environment has two important roles in the development of the Ratawi zone at Wafra oilfield, (1) preservation of the depositional porosity of reservoir unit-C by early meteoric lithification that reduced deep burial compaction (Section 4.3.4), and (2) formation of reservoir unit-E. James and Choquette (1984) identified two main factors that control the meteoric diagenetic environment, (1) intrinsic factors, including mineralogy, grain size, porosity and permeability, and (2) extrinsic factors, including climate, vegetation and time.

Ratawi facies are characterized by a range of textures from mudstone to rudstone (Section 3.3), and were exposed to the meteoric realm for different durations in the 5<sup>th</sup>, 4<sup>th</sup>, 3<sup>rd</sup>, and 2<sup>nd</sup> order sea-level cycles. Since the Ratawi Formation was deposited in a calcite-sea, all the marine cements and most of the particles are inferred to have been low Mg-calcite originally, such that few particles would enter the meteoric realm with aragonite or high Mg-calcite mineralogy. The palaeoclimate of the Ratawi in the study area is inferred to have been semi-arid; the significance of the palaeoclimate in terms of the diagenetic styles and porosity evolution, and development of reservoir or seal rock, and reservoir heterogeneity, is discussed in



detail in the Ratawi soil section (Section 4.2.3.4).

This study recognizes the product of meteoric vadose zones as Ratawi soils (Section 4.2.3.4), vadose compaction (Section 3.4.3.4.9), and meteoric dissolution (Section 4.2.3.3). The main product of the meteoric phreatic zone is meteoric cement (Section 4.2.3.2), and the main product of the meteoric mixing zone is early diagenetic mixing-zone related dolomite (Section 4.2.5.2.2).

#### **4.2.3.2 Meteoric cement**

Ratawi meteoric cements are distinguished from deep burial cements in this study by their formation before burial compaction, and from marine cements by the criteria given in Section 4.2.2.5. The morphology of the cements can be used to differentiate between meteoric vadose and phreatic subenvironments. The cement morphology depends on whether the pore space is alternately filled with water and air, in the vadose zone, or permanently filled with water, as in the phreatic zone (Moore, 1989; Tucker and Wright, 1990). The mineralogy of all meteoric cement is low Mg-calcite; the source is mostly the dissolution of unstable minerals, aragonite and high Mg-calcite, in meteoric water.

Meteoric cements are mostly precipitated in areas with high rates of water flow, and supersaturated with  $\text{CaCO}_3$ . In areas of sluggish water movement little or no cement would be precipitated; the greatest flow rate is usually in the upper part of the meteoric phreatic zone, whereas the deeper part could be stagnant (Tucker and Bathurst, 1990; Tucker and Wright, 1990). This study recognizes three types of meteoric phreatic cement, bladed/granular (Section 4.2.3.2.1), columnar (Section 4.2.3.2.2), and granular drusy (Section 4.2.3.2.3). The meniscus and dripstone cements that characterize the meteoric vadose zone have not been identified.

##### **4.2.3.2.1 Bladed and granular cements**

Meteoric bladed and granular cements have an important role in the preservation of depositional porosity in Ratawi reservoir Unit D at well R-50 (Fig. 4-7 a) (Section 4.2.4). The cement is characterized by circumgranular crusts of bladed to rhombic cement crystals (Fig. 4-7 b) developed around the grains; the crystal length to width ratio is about 4 to 1, with distinct rhombic ends that indicate an original mineralogy of low Mg-calcite, not aragonite. The cement is interpreted to be meteoric phreatic (Flügel, 1982; Moore, 1989).



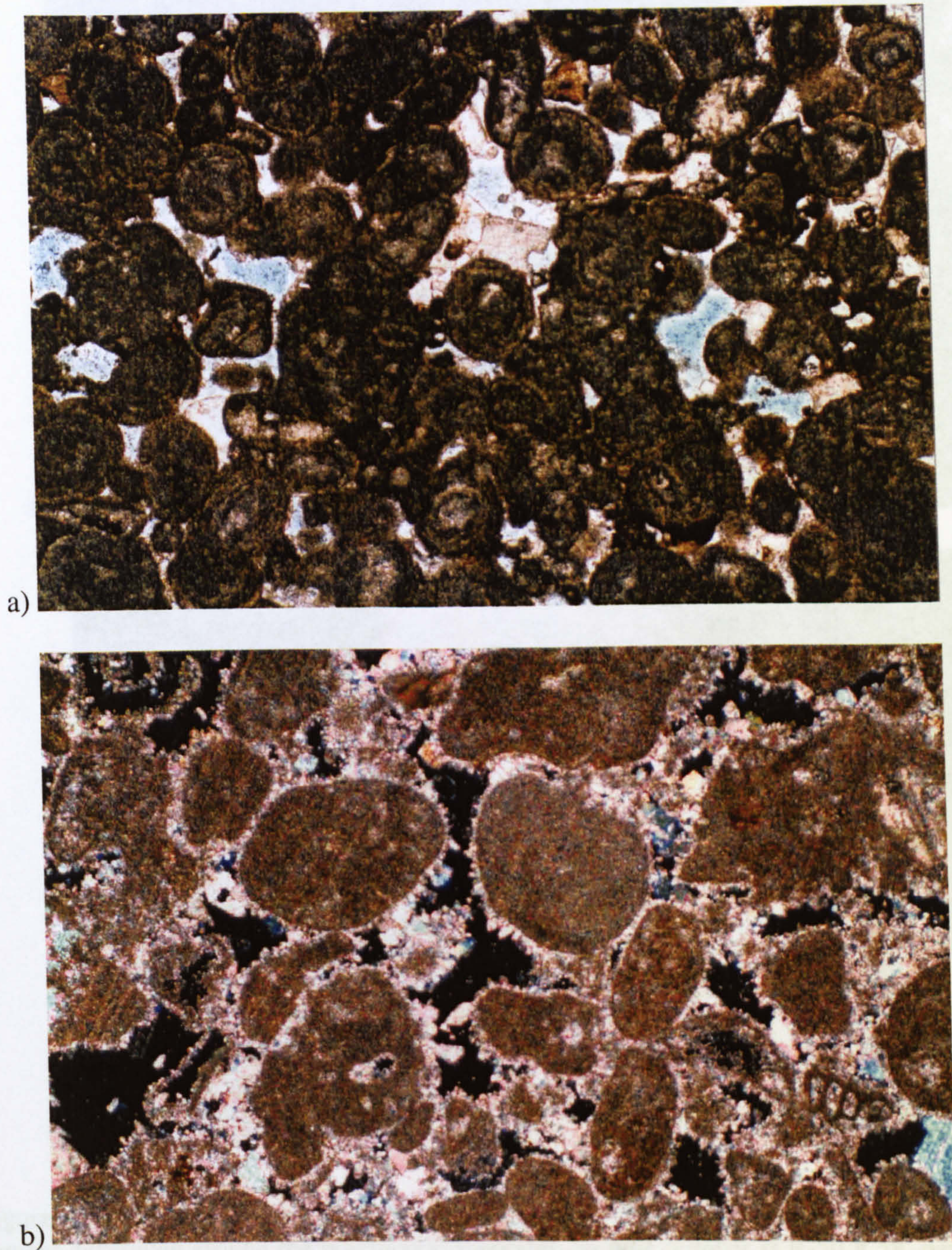


Figure 4-7 a) Photomicrograph of the interparticle porosity in reservoir unit D (microfacies SR: shallow-ramp). Note the presence of strongly micritized ooid grains; some interparticle porosity is preserved from burial compaction by early meteoric cement; interparticle pore spaces are filled by saddle dolomite that show effects of dissolution. Sample number is R-50 # 73, depth 6925 ft (2111 m), field of view 3 x 2 mm, under plane-polarized light. b) Photomicrograph of well developed meteoric bladed and granular drusy cements in reservoir unit E. Circumgranular crusts of meteoric bladed to rhombic cement crystals are developed around peloids. Interparticle porosity is still preserved. Sample number is R-50 # 66, depth 6864 ft (2092 m), field of view 3 x 2 mm, under crossed polars.



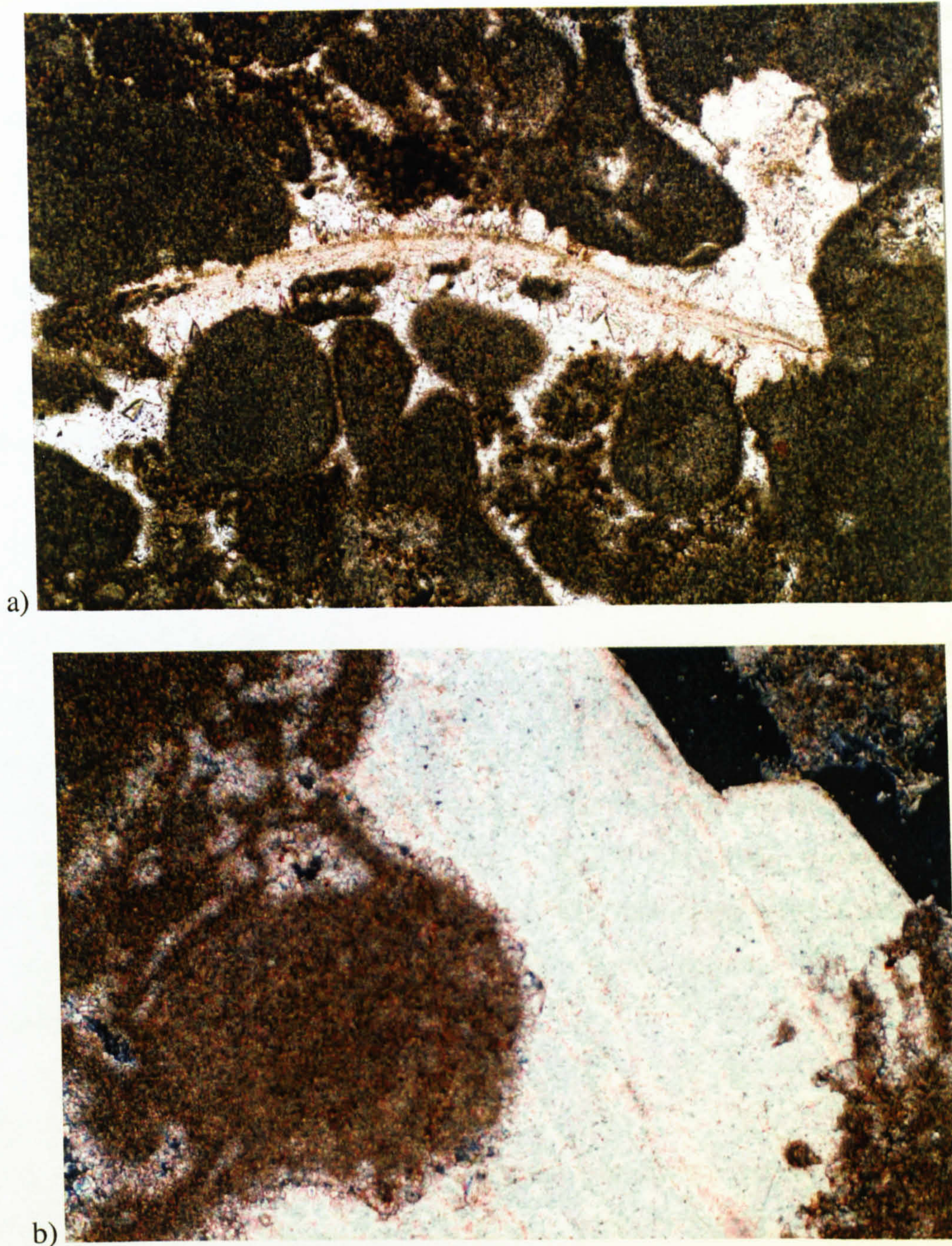


Figure 4-8 a) Photomicrograph of meteoric columnar cement. Crust of columnar meteoric cement developed around the brachiopod fragment. Sample number is R-50 # 58, depth 6827 ft (2081 m), field of view 1 x 0.6 mm, under plane-polarized light. b) Photomicrograph of poikilotopic cement in peloidal grainstone. This cement post-dates the first generation meteoric bladed cement. Sample number is R-50 # 66, depth 6864 ft (2092 m), field of view 1 x 0.6 mm, under crossed polars.

The reduction of the depositional porosity in reservoir unit-C, well R-50 in the main Wafra area, and reservoir unit-C and unit-D in the southern and eastern Wafra areas is interpreted in this study to be due to two factors, (1) presence of micrite, from the low-energy depositional environment, and (2) absence of meteoric bladed and granular cements, which could be the result of a low rate of meteoric flow at the edge



of the phreatic lens that formed within the antecedent structure of the main Wafra area, or to the absence of aragonite and high Mg-calcite in the sediment, the main source for the meteoric cement.

#### **4.2.3.2.2 Columnar cements**

The columnar cement (dog-tooth) is not a common cement in the Ratawi (Fig. 4-8 a). This cement is characterized by a circumgranular crust of elongate cement crystals, with length to width ratio about 5 to 2, and jagged dog-tooth terminations. The cement is interpreted to be meteoric phreatic (Flügel, 1982).

#### **4.2.3.2.3 Granular drusy cements**

Meteoric granular drusy cements are a common cement in the Ratawi (Fig. 4-6, 4-7 and Fig. 4-26 a), reducing the porosity of the reservoir zone. This cement is characterized by an equant crystal shape, which blocks the pore space; sometimes the crystals show an increase in size from the pore wall to pore centre. This cement fabric could be formed in a meteoric phreatic or deep burial environment; thermometry study by fluid inclusions or oxygen isotopes could be used to distinguish between these two diagenetic environments (Tucker and Wright, 1990). This study distinguished between the two cement environments by using petrographic criteria, which is cement precipitation relative to compaction.

#### **4.2.3.3 Meteoric dissolution**

Vug and mouldic porosity (Fig. 4-24 a) in addition to micro-vugs and micro-channels (Section 4.3) is a common secondary diagenetic porosity type in the Ratawi zone of the Wafra oilfield. Understanding the diagenetic conditions under which these porosity types developed is important for the reservoir development. These porosity types are formed by aggressive fluids, which selectively and non-selectively dissolve fabrics of the Ratawi rocks; the fluids could be generated under two different diagenetic conditions: (1) deep burial (Section 4.2.4.4), and (2) meteoric.

The aggressive fluids of the meteoric environment are produced by three processes: (1) dissolution of CO<sub>2</sub> from the atmosphere and soil, (2) the mixing zone, and (3) the oxidation of organic carbon and oxidation-reduction reactions involving sulphur (Mylroie and Carew, 1995). In this study most of the vug, mouldic, micro-vug, and micro-channel porosity types are inferred to be formed by aggressive dissolution



of CO<sub>2</sub> from the atmosphere and soil or mixing zone, when there is evidence for subaerial exposure.

#### 4.2.3.4 Carbonate replacement of quartz

The edges of most of the quartz particles in the Ratawi Formation are replaced by calcite (Fig. 4-9). This replacement process is interpreted in this study have taken place in the meteoric diagenetic environment with fluid supersaturated with carbonate.

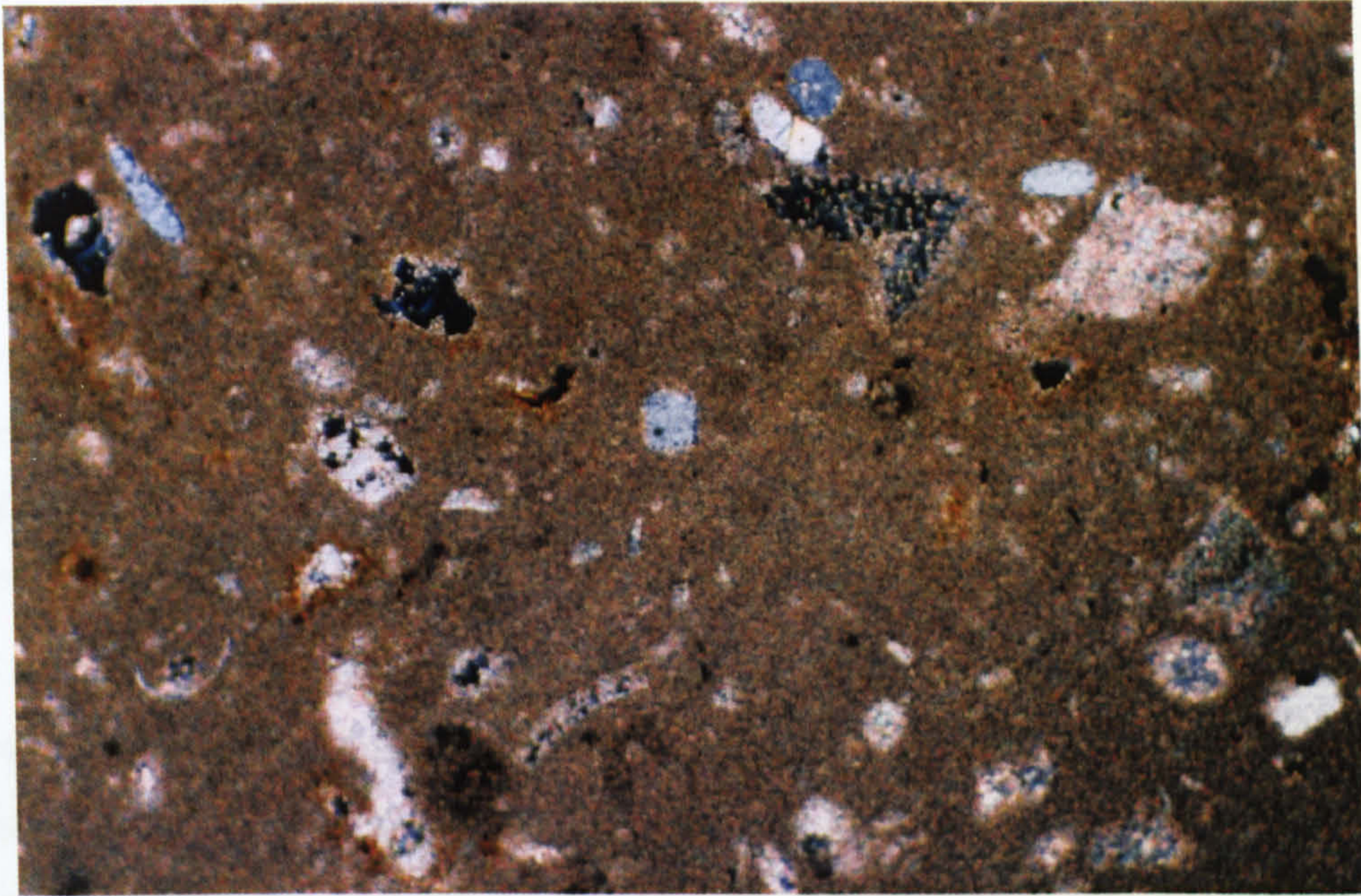


Figure 4-9 Photomicrograph of replacement of the quartz grains by calcite. This process is characteristic of the calcrete interval in the Ratawi Formation. The calcite replacement starts at the edges of the grains. Sample number is R-50 # 40, depth 6737 ft (2053 m), field of view 1 x 0.6 mm, under crossed polars.

#### 4.2.3.5 Ratawi soils

The microfacies analysis of Ratawi reservoir units in the Wafra oilfield indicates that unit-E was affected by pedogenic processes to form calcretes and buried palaeokarst associated with the 2<sup>nd</sup> order sequence boundary. Interpretation and prediction of the pore system, heterogeneity, and geometry of the reservoir unit associated with the calcretes and buried palaeokarst require an understanding of two factors: (1) the controls on the Ratawi subaerial exposure surfaces, and (2) the controls on the Ratawi subaerial exposure facies. The pore system associated with the subaerial exposure surfaces and subaerial exposure microfacies could increase or decrease the original porosity and permeability (Wright and Smart, 1994).



One of the main aims of this study is to interpret and predict the Ratawi reservoir heterogeneity at three levels, discussed in Section 3.1.1.2. This Section discusses the heterogeneity of unit-E at two levels: (1) thin-section scale, microscopic heterogeneity, the controls of the microfacies, particle and pore properties in the reservoir, and (2) the megascopic heterogeneity, the controls of the facies (depositional and diagenetic) on the porosity and permeability, which lead to the formation of reservoir unit-E, not just in the main Wafra area, but also in the southern and east Wafra areas. The heterogeneity of the Ratawi zone at the reservoir unit scale and microfacies scale is interpreted in this study by integrating different types of data in the framework of sequence stratigraphy. These data include depositional, diagenetic, stratigraphic, structural and tectonic data.

The types of subaerial exposure microfacies and surfaces, and the associated pore systems depend on many factors including: (1) duration of exposure, (2) accommodation space (base-level) changes, (3) depositional facies and stratigraphy, (4) mineralogy, (5) existing pore networks, (6) size and topography of the exposed area, (7) climate, (8) tectonic setting, and (9) reactive potential of ground water (Budd *et al.*, 1995). The factors that control Ratawi subaerial exposure surfaces and the calcrete facies of reservoir unit-E are examined under two headings: (1) heterogeneity of reservoir unit-E and palaeoclimate (Section 4.2.3.5.1), and (2) calcrete profile development (Section 4.2.3.5.2).

#### **4.2.3.5.1. Heterogeneity of reservoir Unit E and palaeoclimate**

The Ratawi porosity developments that control the distribution of seal rock and reservoir rock with different heterogeneity can be categorized under the climatic regime that effected the Ratawi palaeo-exposure surfaces. The palaeoclimate of the Ratawi controls the type of diagenesis at the exposure surfaces, which then influenced the subsequent diagenesis. This could allow interpretation and prediction of the subaerial diagenetic processes and level of porosity development in the carbonate sequences, when the subaerial diagenetic processes are integrated within the framework of sequence stratigraphy (Wright, 1994; Tucker, 1993).

Throughout the geological record, shallow-water carbonates exhibit numerous exposure surfaces, with different degrees of subaerial diagenetic overprints, reflecting the processes of progradation and sea-level oscillations, and processes active at the subaerial surface (Wright, 1994). When carbonate sediment and rock are exposed



under subaerial processes, the carbonate is altered by pedogenic processes to form soil. The preserved palaeosoils in the geological record are characterized by a range of macro- and micro-features reflecting these palaeo-pedogenic processes. The pedogenic diagenetic overprint modifies the pore system, which leads to an increase or decrease of the total porosity and permeability of the rock. Climate has a great control on the pedogenic process, physicochemical and biological, and its record at subaerial exposure facies (Goudie, 1996).

A range of carbonate rock textures is generated depending on the prevailing climate. Wright (1994) recognized four-component gradient soils, which develop on carbonate exposure surfaces under four different climatic regimes ranging from arid to humid. The main consideration with climate is the actual amount of rainfall, and in addition how it was distributed seasonally. The four regimes of climatic-carbonate exposure surfaces are:

#### **4.2.3.5.1.1 Arid-type soil / arid palaeoclimate**

Soils developed under semi-arid to arid climates are characterized by the precipitation of carbonates, sulphates and other salts from the groundwater. The lack of moisture and carbonate dissolution leads to limited development of calcrete profiles. This type of soil is often associated with sabkha and supratidal flats, and is characterized by replacive evaporites, tepees, brecciation and vadose pisoids (Wright, 1994).

#### **4.2.3.5.1.2 'Well-developed' calcrete-type soil / moisture-deficit wetter palaeoclimate**

The 'well developed' calcrete-type soil develops under wetter climatic conditions but still with a net moisture deficit. This climatic condition leads to carbonate dissolution in the wet phases and precipitation during drier periods, which leads to the formation of the calcrete features and calcrete profiles. There are three models for calcrete formation, discussed in the calcrete fabric model (Section 4.2.3.5.1.5).

#### **4.2.3.5.1.3 'Less-well developed' calcrete-type soil / wetter palaeoclimate**

The 'less-well developed' calcrete-type soil developed under wetter climatic conditions that allow more vegetation cover, which lead to more aerosol accumulation. The exposure surfaces are characterized by thin clay-rich horizons with their mineralogy depending on three factors: (1) the original mineralogy of the clay in the



aerosols, (2) the length of the exposure which depends on the cycle order; duration of the exposure increases from the 5<sup>th</sup>, 4<sup>th</sup>, 3<sup>rd</sup> to 2<sup>nd</sup> order cycle of sea-level change, (3) prevailing climate. When the rate of aerosol accumulation is high, the zone of carbonate accumulation may shift from the lower altered carbonate horizon to the upper clay-rich horizon, and this then leads to the formation of massive calcretes (Wright, 1994).

#### **4.2.3.5.1.4 Organic-rich type soil / the wettest palaeoclimate**

Organic-rich soils develop under the wettest climatic conditions, which lead to the dissolution of the carbonate in the soil zone and the development of karstic surfaces. The karst is characterized by small-scale karren, with small dissolution hollows or root pipe features. The dissolved carbonate precipitates as cement in the lower vadose zone or in the phreatic zone.

The non-carbonate aerosols, under these wetter climatic conditions, break down to release iron. Under a seasonal climate aluminous lateritic soils are developed with boehmite, hematite and Al-goethite; the formation of gibbsite is inhibited by the buffering action of the carbonate. Distinctive thin, iron-rich layers, termed terra rossa, accumulate at the clay-limestone contact. Most of the non-carbonate clay zone is eroded from the fossil soil during the next marine transgression. In the geological record, calcretes are the most common type (Esteban and Klappa, 1983; Wright, 1994).

During the Upper Jurassic the study area was located south of the equator and characterized by a very arid climate, which lead to the precipitation of the thick evaporitic Gotnia Formation. During the Lower Cretaceous, the Arabian plate moved northwards towards the equator, and the climate became less arid (Murriss, 1980). These climatic conditions could have lead to the development of the second type of exposure surface described by Wright (1994), in the Ratawi Formation at the 2<sup>nd</sup> order cycle sequence boundary, that is characterized by a 'well-developed' calcrete.

#### **4.2.3.5.1.5 Calcrete fabric model**

The term calcrete is defined as a near-surface, terrestrial accumulation of predominantly calcium carbonate in a variety of forms from powdery to nodular to highly indurated. It results from cementation and displacive and replacive introduction



of calcium carbonate into soil profiles, bedrock and sediments, in areas where vadose and shallow phreatic ground-water becomes saturated with respect to calcium carbonate (Wright and Tucker, 1991).

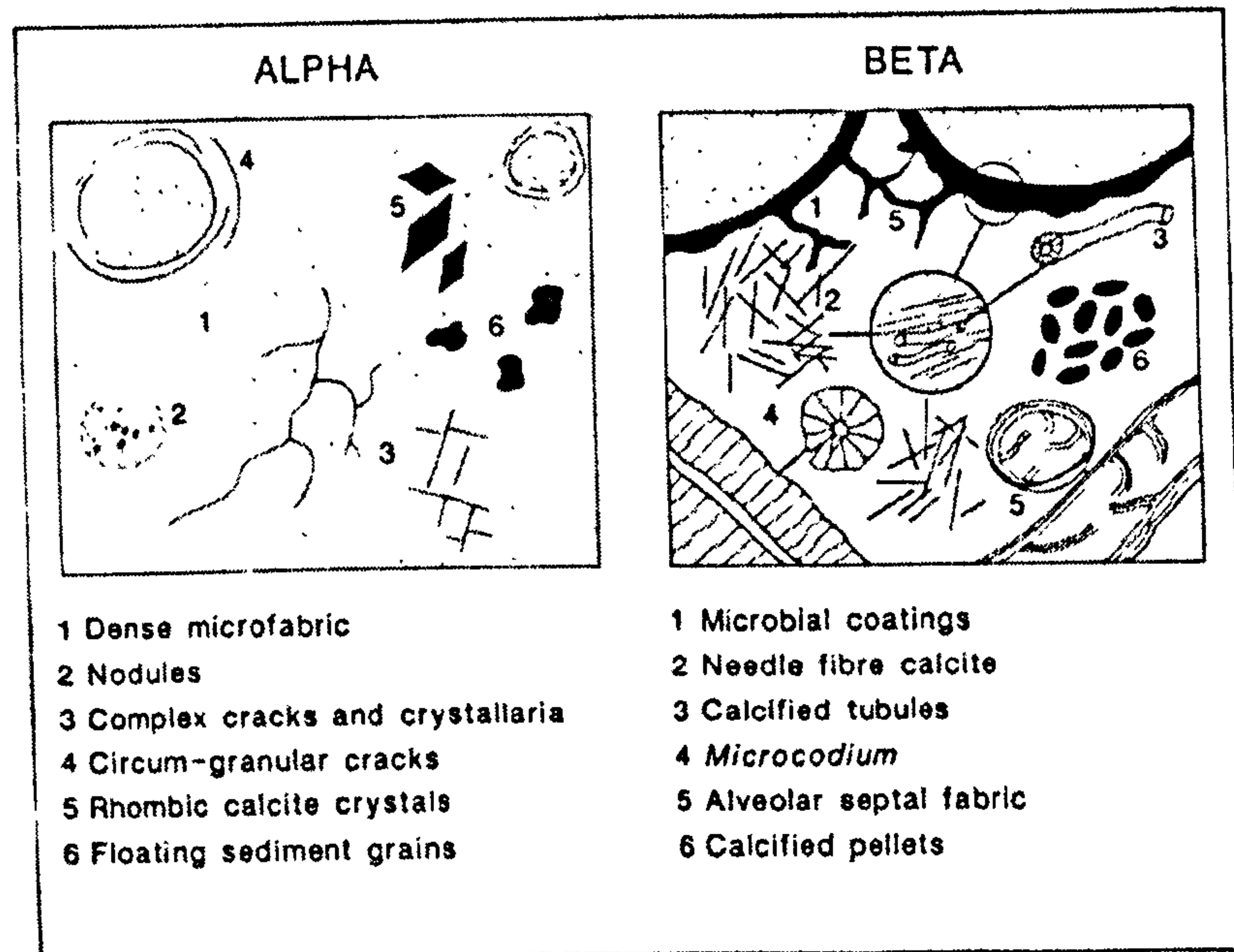


Figure 4-10 Micromorphological classification of calcretes (after Wright and Tucker, 1991). Note Ratawi pedogenic calcrete formed under strong physicochemical processes (alpha and beta fabric model) and weak biological processes (rhizogenic fabric model).

There are two different diagenetic processes to form the calcrete fabric: pedogenic calcrete and groundwater calcrete. Pedogenic calcrete forms at subaerial exposure surfaces in the soil formation zone by pedogenic processes. Groundwater calcretes form below the soil formation zone, within the vadose zone or at the capillary fringe, and below the water table (Wright and Tucker, 1991). The microfacies of the Ratawi Formation, discussed in Section 3.2.1.4.1, support the regional stratigraphic evidence that the exposure surfaces of the Ratawi would alter to pedogenic calcrete. The origin of the fabrics in pedogenic calcrete is interpreted by three models. These models can be arranged with increasing biological activity and fixing of calcium carbonate in soil by biological processes, in addition to fixing of calcium carbonate in soil by physicochemical processes, namely alpha fabric, beta fabric and rhizogenic fabric models. Pedogenic calcretes can exhibit a mixture of fabrics between each of these two-end member models (Wright and Tucker, 1991; Wright, 1995). The diagenetic fabric of Ratawi reservoir unit-E is interpreted in the framework of these end-members models. The three pedogenic calcrete models are: alpha fabric model,



beta fabric model and rhizogenic fabric model.

#### 4.2.3.5.1.5.1 Alpha fabric model

This model is characterized by the products of mainly physicochemical processes, which include evaporation, degassing, desiccation and replacive growth (Fig. 4-10). The features that characterize this model are dense microfabric, nodules, complex cracks, circum-granular cracks, rhombic calcite crystals, and floating sediment grains. This end member model develops in areas with a more arid climate and less biological activity (Wright and Tucker, 1991).

#### 4.2.3.5.1.5.2 Beta fabric model

This model exhibits a variety of microscale features attributable to the existence of macro- and micro- organisms, which include bacteria, fungi, algae and higher plant roots (Fig. 4-10). Microbial coatings, needle-fibre calcite, calcified tubes, *Microcodium*, calcified pellets and alveolar septal fabrics are the features that characterize this model. This end-member model develops in sub-humid to semi-arid areas with extensive vegetation cover. The pedogenic process reflects a relatively high degree of biological activity (Wright and Tucker, 1991).

#### 4.2.3.5.1.5.3 Rhizogenic fabric model

This model is dominated by biological activity, largely through calcification in, on, or around, plant roots. The decreasing degree of root (rhizogenic) calcification is grouped into three types. The first type is intracellular calcification. This type results from the actual cells calcifying during the life of the plant or after death but before the cell shape is lost by decay processes. The features that characterize this type are *Microcodium* calcrete. The *Microcodium* structure consists of sheets, tubules and connected or unconnected spheroids consisting of cell-like crystals of calcite.

The second type is extracellular calcification. This type is the result of calcification around roots and is a widespread feature in carbonate-rich dunes. Rhizcretions and calcareous cementation around root mats are the characteristic features. The third type is the peloid-pisoid association. This type is the result of calcification related to root mats. The features that characterize this type are peloidal and coated grain fabrics (Wright *et al.*, 1995).



Microfacies DiagCal, discussed in Section 3.3.1.4.1, that characterizes reservoir Unit E of the Wafra oilfield, exhibits fabrics characteristic of pedogenic calcretes. The features of microfacies DiagCal display a fabric mixture between the two end-members of the alpha and beta fabric models. This is interpreted in this study that the Ratawi pedogenic processes reflect an environment of subaerial exposure fluctuating between semi-arid to more arid palaeoclimate. This petrographic interpretation of the Ratawi palaeoclimate is in agreement with that proposed by Murris (1980) for the Arabian plate under the Lower Cretaceous palaeoclimate.

#### 4.2.3.5.2 Calcrete profile development

The different stages in the development of calcrete profiles influence Ratawi fabrics, which influence the Ratawi pore system. These stages are reviewed by Wright and Tucker (1991), Wright (1994) and Wright *et al.* (1995). The development of these stages depends on many factors, which include time of exposure, mineralogy of the host sediment, and the degree of biological activity and biological precipitation (fixing) of calcium carbonate, and rate of aerosol accumulation.

The length of time of exposure depends on the cycle order of relative sea-level changes, 5<sup>th</sup>, 4<sup>th</sup>, 3<sup>rd</sup>, 2<sup>nd</sup> cycle order. When the mineralogy of the host sediment is carbonate, carbonate from the saturated fluids is precipitated as a cement, but if the mineralogy is non-carbonate, carbonate is precipitated as displacement nodules. Different pedogenic calcrete models have a different degree of biological activity and biological precipitation (fixing) of calcium carbonate. If the rate of aerosol accumulation is high on the top of the altered carbonate zone, the zone of carbonate accumulation moves upward forming a new calcrete zone.

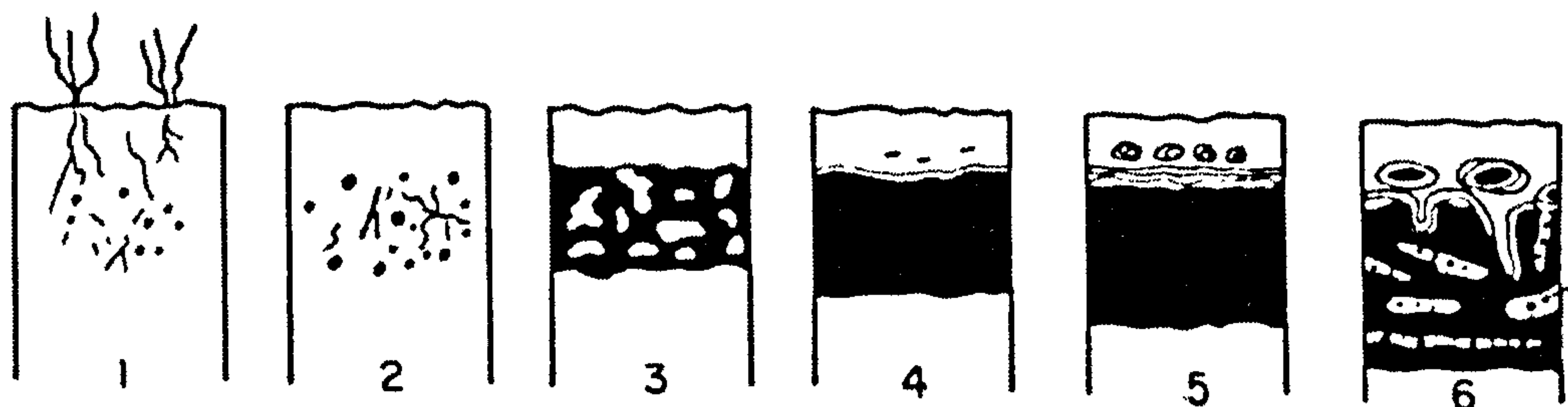


Figure 4-11 Stages in calcrete development in fine-grained sediment (after Wright and Tucker, 1991). These six stages could be grouped into three main stages of fabric development: stage 4 hard pan or petrocalcic layer, stage 5 laminar unit and stage 6 brecciated and pisoid unit. The abundance of alveolar septal structure in the Ratawi puts the development of Ratawi calcrete in stage 4.



According to the reviews by Wright and Tucker (1991), all calcrete profiles are developed by progressive increase in the diagenetic carbonate within exposed soil, sediment or rock. This is done through a combination of three diagenetic processes, replacement, displacement and cementation. The development of the fabric of pedogenic calcrete is grouped into six stages (Fig. 4-11), which represent the development (maturity) of the pedogenic calcrete profile with time. These six stages developed through three main stages of fabric development:

#### **4.2.3.5.2.1 Hard pan or petrocalcic layer development**

The unaltered and exposed host sediment or rock with time becomes substituted through the three diagenetic processes to form a diagenetic <sup>Microtic</sup> calcic-rich horizon. This horizon is the hard pan or petrocalcic layer, which is characterized by continuation, hardening, and very low permeability. This calcrete fabric developed at stage 4.

#### **4.2.3.5.2.2 Laminar unit development**

The low permeability hard pan acts as a downward barrier for fluids saturated with calcium carbonate, which leads to the formation of the laminar unit on the hard pan.

#### **4.2.3.5.2.3 Brecciated and pisoid unit development**

The hard pan and laminar unit with time are fractured, which leads to the formation of the brecciated and pisoid unit. This calcrete fabric developed at stage 6.

The microfacies analysis of the Ratawi samples puts the development of the Ratawi pedogenic calcrete profile in stage 4. The alveolar septal structure is most abundant in the main hard pan stage (Esteban and Klappa, 1983), which is stage 4. However, according to the profile development model, the hard pan stage should be characterized by low porosity, but in the Ratawi reservoir there is good porosity in this facies.



## **4.2.3 Burial diagenetic environment**

### **4.2.4.1 Introduction**

The burial environment controls the final pathways of carbonate porosity evolution that produce the reservoir or seal rock. The major porosity trend in this diagenetic environment is porosity loss by physical and chemical compaction, and cementation. This general porosity-depth relationship can be reversed by processes which create new secondary porosity, or by preservation of near-surface porosity (Section 4.3) (Scholle and Halley, 1985). Burial diagenesis takes place when <sup>the</sup> carbonate rock is buried below the zone affected by surface processes to the zone of metamorphic dehydration. Carbonate sequences could spend most of their geological history in the burial diagenetic environment, which is quite different from the marine and meteoric environments encountered by newly formed sediments during the early stages of lithification and burial (Moore, 1989; Tucker & Wright, 1990).

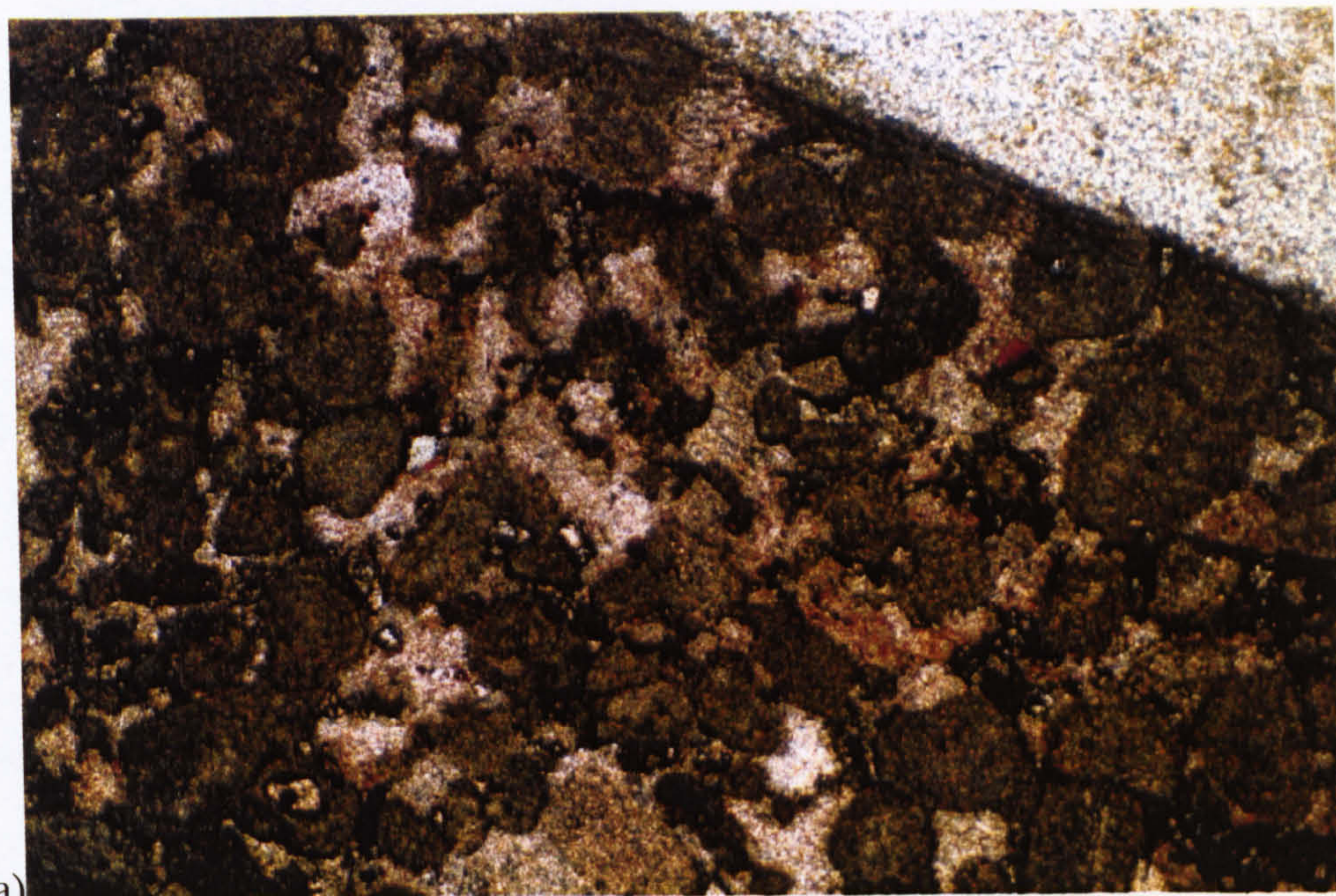
Burial diagenesis is the consequence of the accumulation of overburden in a subsiding sedimentary basin and related changes in temperature, pressure, basin hydrology and pore-fluid chemistry. In addition to compaction and cementation, burial diagenesis includes replacement, neomorphism, dissolution and fracturing (Scholle and Halley, 1985). Different workers have used different terms to describe the burial diagenetic environment, including mesogenetic, subsurface, post-compaction, and deep burial; there is no unified diagenetic model that incorporates all the aspects of the carbonate deep burial diagenesis (Heydari, 1997).

In the deep burial diagenetic environment of the Ratawi Formation porosity is decreased by burial cementation (Section 4.2.4), physical compaction (Section 4.2.4.3.1), and chemical compaction (Section 4.2.4.3.2), where the Ratawi reservoir zones have not been effected by processes that preserve near-surface porosity (Section 4.2.4.). Also the deep burial diagenetic environment creates new porosity that increases the total porosity of the Ratawi reservoir zone by deep burial dissolution (Section 4.3.4.4.1), fracturing (Section 4.3.4.4.2), and stylolitization (Section 4.3.4.4.3).

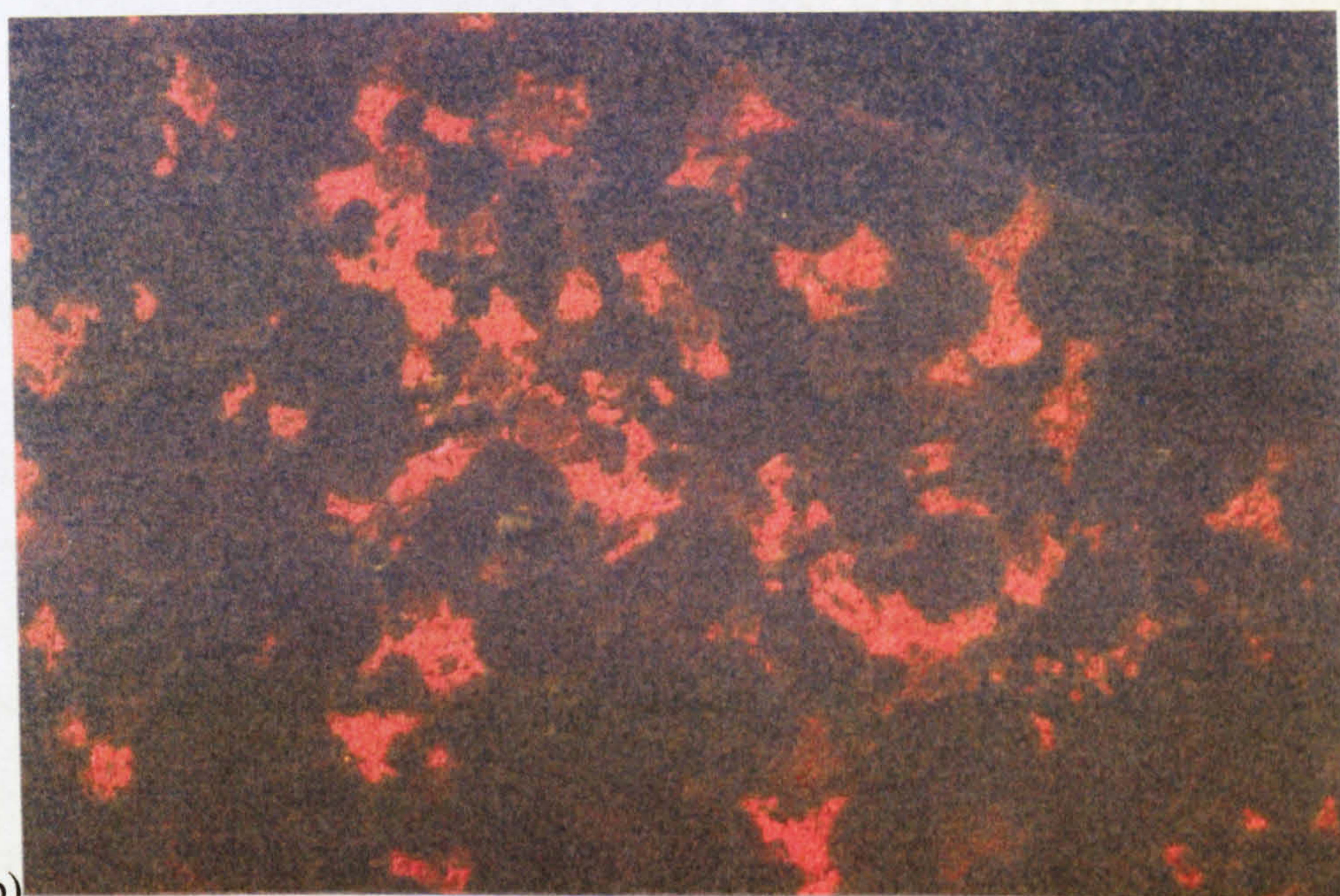
### **4.2.4.2 Burial cement**

The source of  $\text{CaCO}_3$  for burial cements could be from chemical compaction, or deep burial dissolution by corrosive fluids associated with shale-water expulsion and the beginning of hydrocarbon maturation of the source rocks in the Makhul and Ratawi





a)



b)

Figure 4-12 Photomicrograph of grainstone with burial granular drusy calcite cement (a) under plane-polarized light (b) under cathodoluminescence. Most of the interparticle porosity is reduced by granular drusy cement precipitated after the burial compaction. The cement under the CL is a red colour. Sample number is R-50 # 92, depth 7013 ft (2138 m), field of view 3 x 2 mm.



Formations (Moore, 1985). This study has identified three different types of deep burial cement: (1) saddle dolomite (Section 4.2.5), (2) granular drusy calcite (Section 4.2.4.2.1), and (3) poikilotopic calcite (Section 4.2.4.2.2).

#### 4.2.4.2.1 Granular drusy calcite

Late deep burial granular drusy calcite cement is distinguished from early meteoric granular drusy cement (Section 4.2.3.2.3) in this study by two petrographic lines of evidence, (1) cement is found between particles that are effected by grain-grain chemical compaction, which indicates that the cement was precipitated after the compaction (Fig. 4-12 a), and (2) cement is found in fractures that are interpreted in Section 4.2.3.6 to be formed through deep burial tectonic processes (Fig. 4-26 a) (Moore, 1989; Tucker and Wright, 1990). Under CL, the bright calcite is commonly a red colour (Fig. 4-12 b).

#### 4.2.4.2.2 Poikilotopic calcite

Poikilotopic cement is characterized by a single large crystal (Fig. 4-8 b) that surrounds several grains. This fabric indicates slow crystal growth from fluids with a low level of calcite supersaturation (Moore, 1989; Scholle and Halley, 1985).

#### 4.2.4.3 Burial compaction

The compaction process is driven by the stresses acting on the rock, which is the pressure difference between the hydrostatic and lithostatic pressure; the first pressure is transmitted through water, whereas the latter is transmitted through the rock framework (Moore, 1989). The nature and extent of burial compaction and the loss of near-surface porosity depends on many factors including (1) sediment grain-size and packing, (2) early diagenetic fabric, and (3) amount and rate of overburden stresses (Scholle and Halley, 1985).

The near-surface porosity in the Ratawi zone is reduced by the development of fitted fabric formed by two different diagenetic processes namely vadose and burial compaction (Fig. 4-13). The preservation of near-surface porosity in the Ratawi zone could have been achieved by reducing the effect of burial compaction and the development of a fitted fabric, which is inferred in this study to be formed by near-surface cementation and mineral stabilization in the marine and meteoric environments (Section 4.2.2 and 4.2.3). Burial compaction is divided into physical compaction



(Section 4.2.4.3.1) and chemical compaction (Section 4.2.4.3.2).

#### 4.2.4.3.1 Physical compaction

Physical (and mechanical) compaction is common in the Ratawi Formation; two types of physical compaction are recognized (1) plastic grain deformation illustrated by concavo-convex contacts between peloid particles (Fig. 3-7 a), and (2) brittle grain deformation illustrated by fractured bivalve shells (Fig. 4-24 b). This type of compaction is the consequence of overburden or tectonic stresses at a rate that effectively exceeds the ability of the sediment to respond through chemical dissolution (Scholle and Halley, 1985; Moore, 1989).

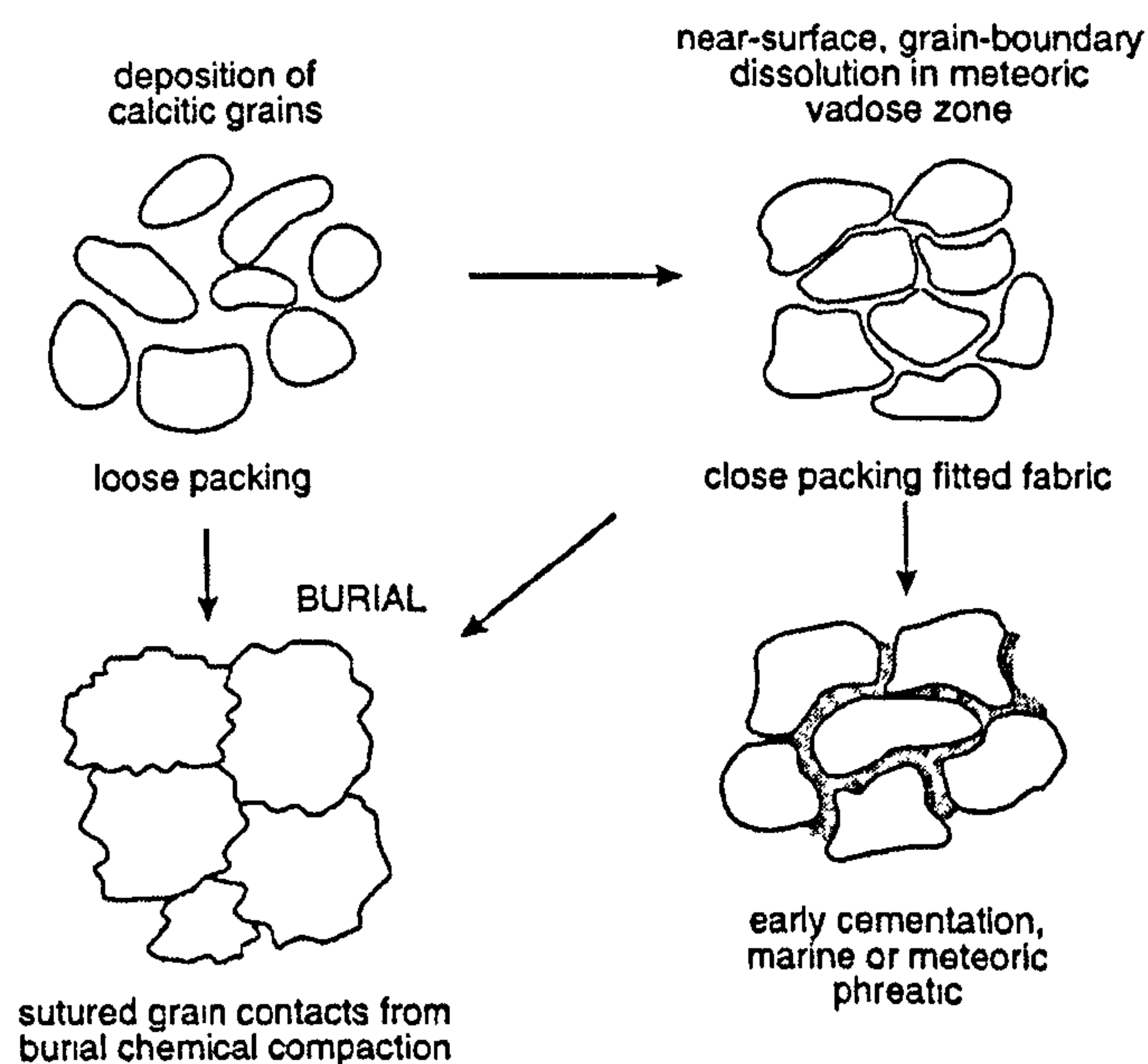


Figure 4-13 Reduction of the primary interparticle porosity by the development of vadose and burial compaction (personal communication Tucker, 2002).

#### 4.2.4.3.2 Chemical compaction

Chemical compaction is also common in the Ratawi Formation; the features of the chemical compaction can be grouped into three types, (1) intergranular fitted fabric, (Fig. 3-4) (2) stylolites (Fig. 4-14 a), and (3) dissolution seams (Fig. 4-17 b) (Scholle and Halley, 1985; Tucker and Wright, 1990). The first type, intergranular or microstylolite fitted fabric, is developed between peloids and ooids, reducing the depositional porosity of reservoir unit-C. Microstylolites are the first stage in the development of stylolites, which are usually found in grain-supported facies of the Ratawi.



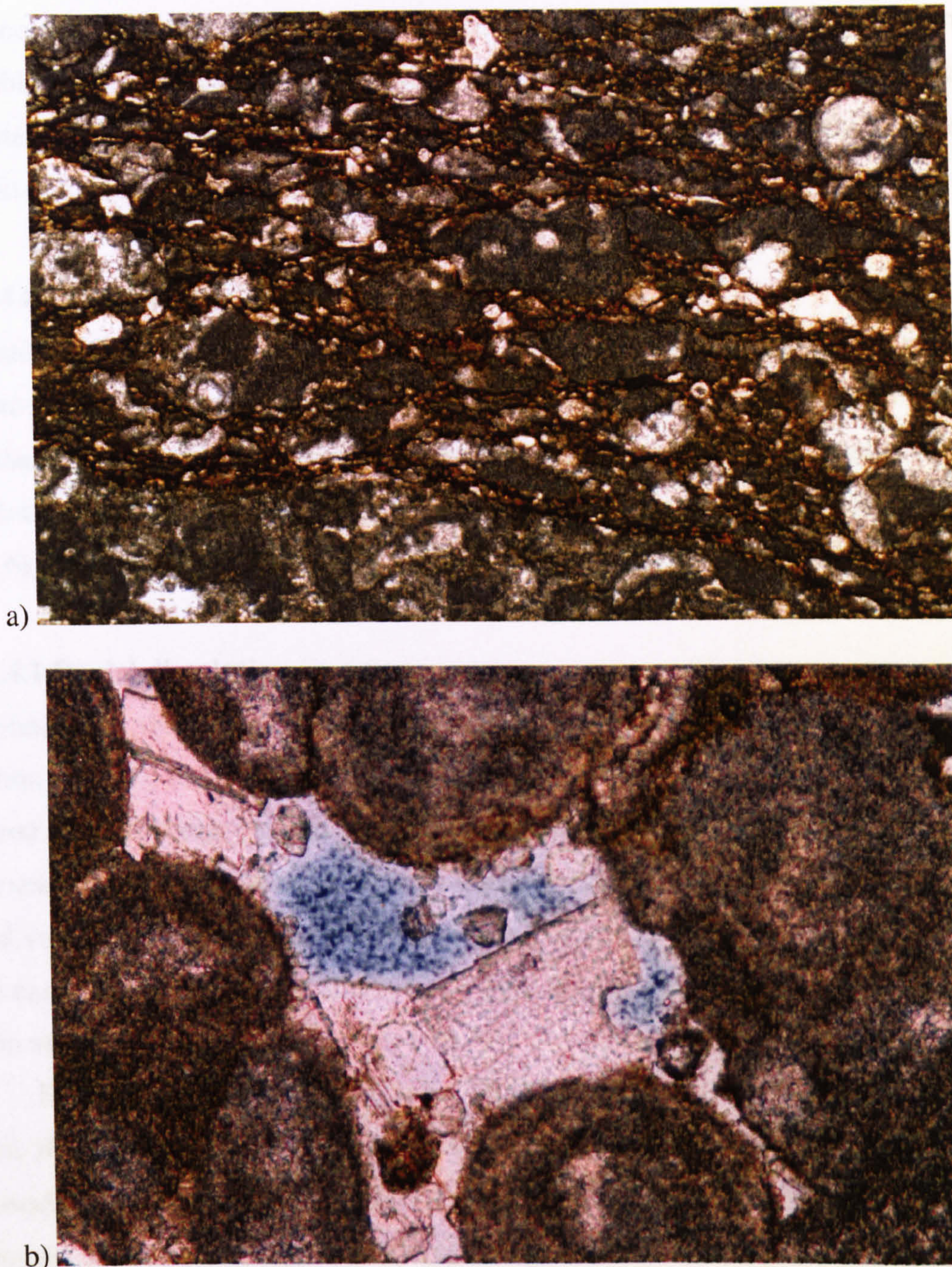


Figure 4-14 a) Photomicrograph of fitted fabric developed by deep burial compaction. Note the development of microstylolitic contacts between the peloids and the dissolution seams with residual iron-rich clay. The burial compaction eliminated all the original interparticle porosity. Sample number is R-49 # 52, depth 7051 ft (2149 m), field of view 3 x 2 mm, under plane-polarized light. b) Photomicrograph of interparticle porosity and burial dissolution porosity in saddle dolomite cement. Sample number is R-50 # 73, depth 6925 ft (2111 m), field of view 0.5 x 0.3 mm, under plane-polarized light.

The second type, stylolites (Fig. 4-14 a), transect the Ratawi fabric, cutting across the particles, matrix and cement, with amplitudes from a few millimetres in thin-section to about 10 mm or more in core samples. Stylolites in the Ratawi zone



locally are open and act as pores (Section 4.3.4.4). The last type, dissolution seams also known as residual or clay seams, are characterized by smooth undulose seams of insoluble residue, which are usually found in mud-supported facies. This type, like the stylolites, occur on different scales, from thin-section to core; in contrast to stylolites they do not act as pores in the Ratawi.

#### **4.2.4.4 Burial porosity**

As mentioned before, the general trend in the deep burial environment is the reduction of near-surface porosity by compaction and cementation, but the existing porosity can be enhanced and new porosity created during burial diagenesis. The total porosity of the Ratawi zone is increased by three deep burial processes, fracturing (Section 4.2.3.6), stylolitization (Section 4.2.3.7), and dissolution (Section 4.2.4.4.1).

##### **4.2.4.4.1 Burial dissolution**

Dissolution in the Ratawi zone could have formed in the meteoric environment (Section 4.2.3.3), and / or the burial diagenetic environment; in this study, vugs are inferred to have been formed by aggressive deep burial fluids, where there is no evidence for subaerial exposure or they occur within deep burial cement. Also, deep burial vugs seem to be random in three dimensions, like 'spongework' (Hill, 1995). A good example of deep burial dissolution in the Ratawi zone is the occurrence of vugs within saddle dolomite cement (Fig. 4-14 b).

Hill (1995) interpreted the deep burial porosity as 'H<sub>2</sub>S-related porosity' in which the aggressive fluids of the deep burial environment are produced by two processes: (1) mixing of waters of different H<sub>2</sub>S concentration in equilibrium with carbonate, producing an aggressive fluid undersaturated with respect to carbonate, and (2) H<sub>2</sub>S dissolution in pore water to produce sulphuric acid H<sub>2</sub>SO<sub>4</sub>. These two processes can dissolve carbonate rock creating micro-pore to cave-size dissolution features; the source of the H<sub>2</sub>S is the maturation of the source rock that produces H<sub>2</sub>S before expulsion and migration of the hydrocarbons to the trap (Hill, 1995). The maturation of the Lower Cretaceous source rocks (Makhul Formation, Section 4.2.4.4.1) is inferred in this study to be the source of H<sub>2</sub>S.



### **4.2.5 Dolomitization and dedolomitization**

#### **4.2.5.1 Introduction**

The Ratawi dolomite facies (Fig. 3-10 b) is not a reservoir facies at Wafra oilfield, although it is an important reservoir facies in other giant oilfields. Warren (2000) cited Zenger (1980) that 50 % of the world's carbonate reservoirs occur in dolomites. The different dolomitization models for the Ratawi Formation are discussed in Section 4.2.5.2; these different models can be interpreted in the framework of sequence stratigraphy (Fig. 4-15). The porosity and permeability of the Ratawi dolomite depend on the dolomite texture, which varies between near mimetic to complete obliteration of the original texture.

The crystalline textures of the dolomite are classified into two types: (1) planar dolomite, characterized by many crystal face junctions, developed during early diagenesis, usually below 50°C, and (2) non-planar dolomite, characterized by few crystal face junctions, developed during late diagenesis, usually greater than 50°C. The permeability of the dolomite textures depend on the pore geometry, which depends on crystal size and shape. With increasing crystal size, three types of dolomite pore systems are developed: (1) polyhedral pores, (2) tetrahedral pores, and (3) intercrystalline pores (Warren, 2000). Ratawi microfacies DiagDol, discussed in Section 3.4.1, mostly has an intercrystalline porosity, which generally has the lowest porosity and permeability.

Dedolomite is the replacement of dolomite by calcite (Purser, 1986). Some workers including Purser (1986) have argued that dedolomitization is important in the development of porosity, and all leached reservoirs of the Mesozoic of the Middle East should be examined for dedolomite porosity. The dedolomitization models for the Ratawi Formation are discussed in Section 4.2.5.3. Dedolomite porosity depends on the degree of dissolution during the replacement of dolomite by calcite.

#### **4.2.5.2 Ratawi dolomitization models**

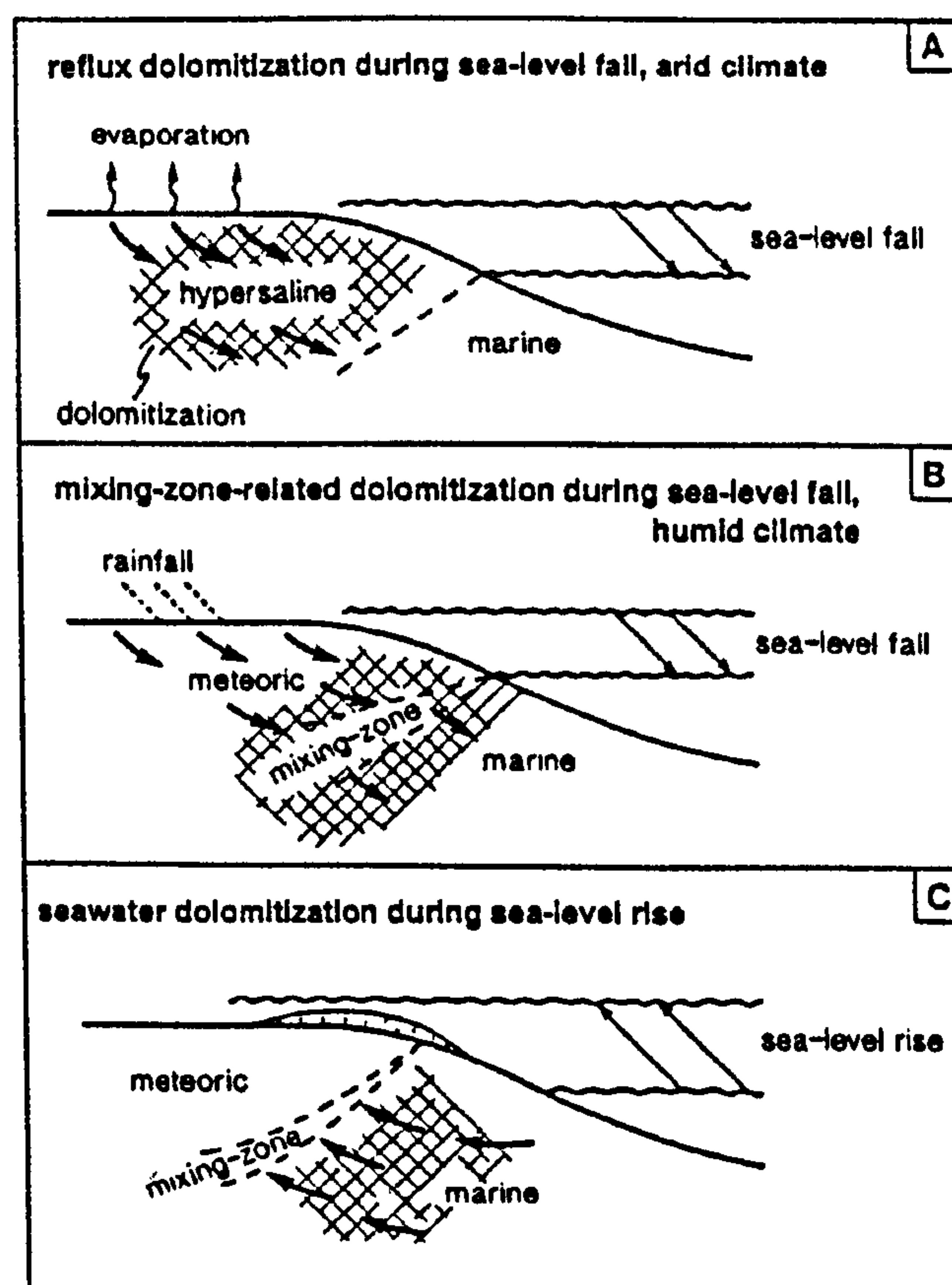
Dolomite can be formed under different diagenetic conditions, and the various models for dolomitization are reviewed by Tucker and Wright (1990), and Warren (2000). These models can be grouped into three categories: (1) synsedimentary dolomitization models, which include normal marine, lacustrine (Coorong-style), arid peritidal (sabkha-style) and organic models, (2) early diagenetic, active phreatic (shallow burial) dolomitization models, which include brine reflux and mixing-zone related



## DOLOMITIZATION AND RELATIVE SEA-LEVEL CHANGE

Some dolomitization models relate to unconformities (sequence boundaries), climate and major changes in relative sea-level, notably:

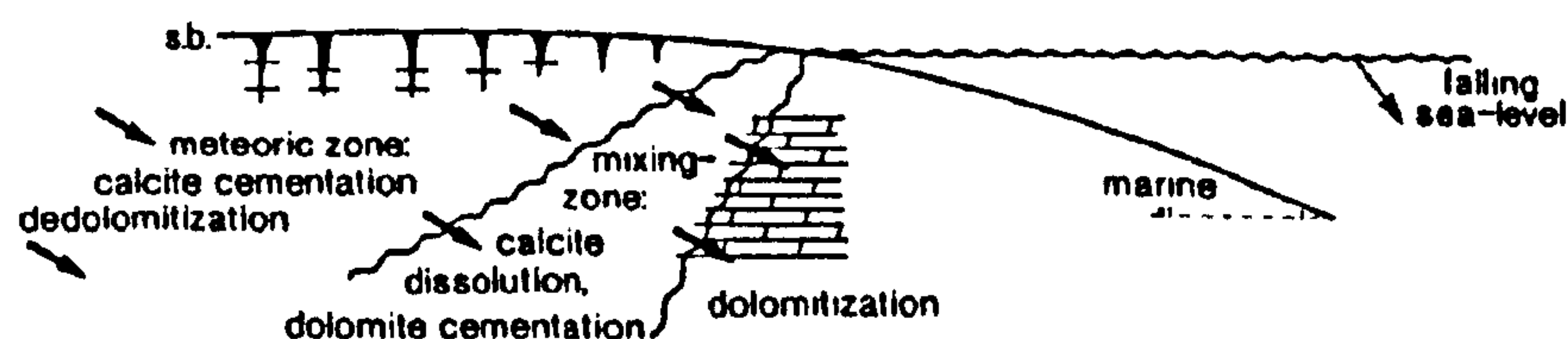
1. mixing-zone-related dolomitization during sea-level falls (lowstands) and humid climate,
2. circulating seawater dolomitization during sea-level rises (transgressive times),
3. evaporative/reflux dolomitization during sea-level falls (lowstands) and arid climate.



Models for dolomitization induced by relative changes in sea-level.

Mixing-zone-related dolomitization refers to dolomitization taking place within the mixing-zone (which probably does not happen) and to dolomitization taking place within the circulating marine groundwaters ahead of the mixing zone.

humid climate, late HST to LST



during late HST to LST groundwater zones move seaward  
dolomitization followed by meteoric diagenesis

Figure 4-15 Dolomitization models interpreted in the framework of sequence stratigraphic model (after Tucker, 1993). Note the mixing-zone related dolomitization model, used in this study to interpret dolomitization in reservoir Unit D, is formed during sea-level rise.



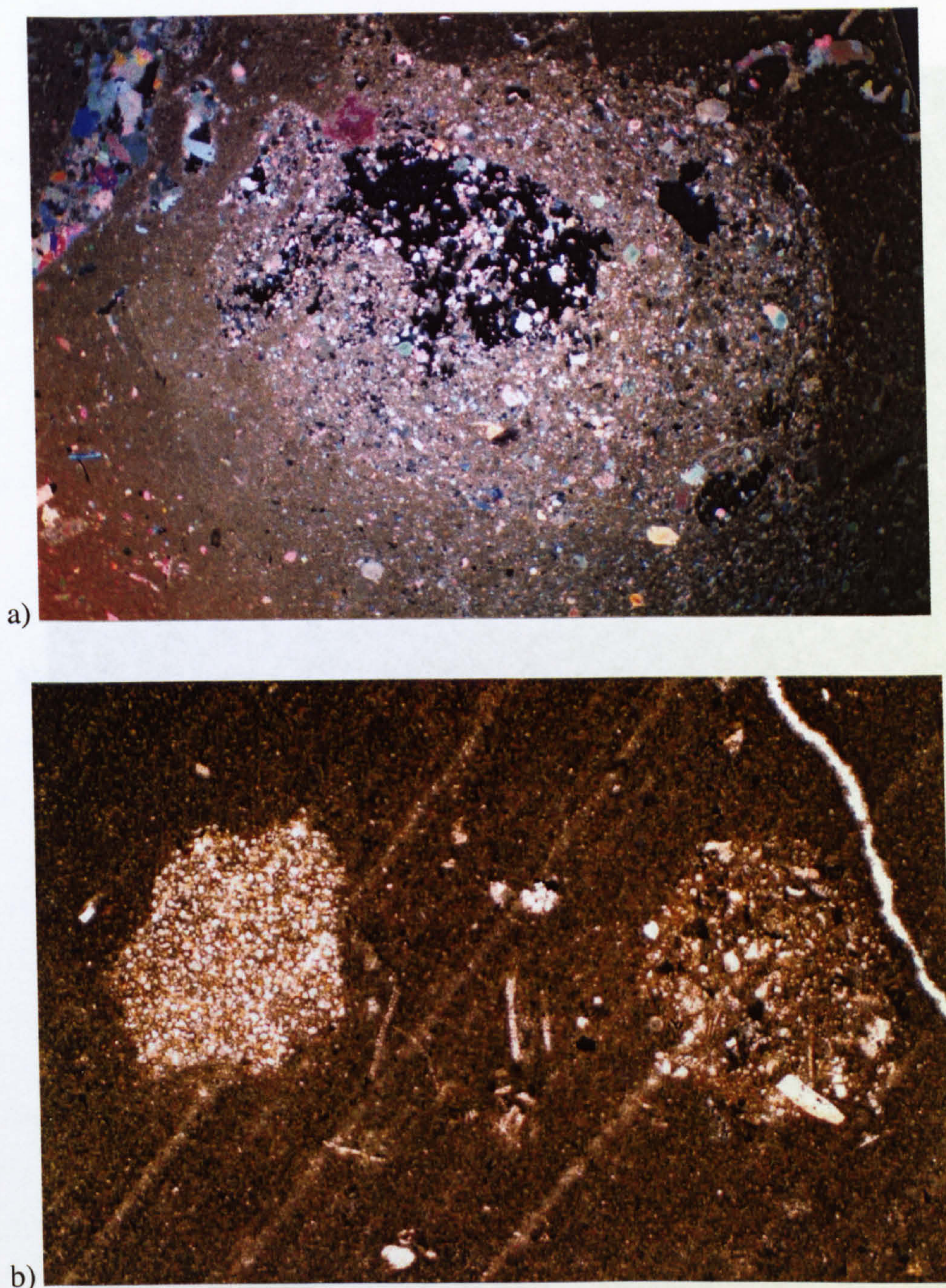


Figure 4-16 a) Photomicrograph of selective dolomitization of a burrow fill by micro-euhedral dolomite crystals. Some porosity is evident (black). Sample number is R-49 # 12, depth 6774 ft (2065 m), field of view 10 x 7 mm, under plane-polarized light. all the original interparticle porosity. Sample number is R-49 # 52, depth 7051 ft (2149 m), field of view 3 x 2 mm, under plane-polarized light. b) Photomicrograph of two pseudomorphosed gypsum crystals in restricted back ramp, microfacies BR2: bioturbated bioclastic wackestone-mudstone with ostracods. Note the well preserved straight-edges of the twin-crystal growth of the gypsum (on the left), which has been replaced by micro-euhedral dolomite crystals; whereas the original crystal on the right-hand was dissolved soon after formation and the mold filled with sediment. Sample number is R-50 # 1, depth 6475 ft (1974 m), field of view 3 x 2 mm, under plane-polarized light.



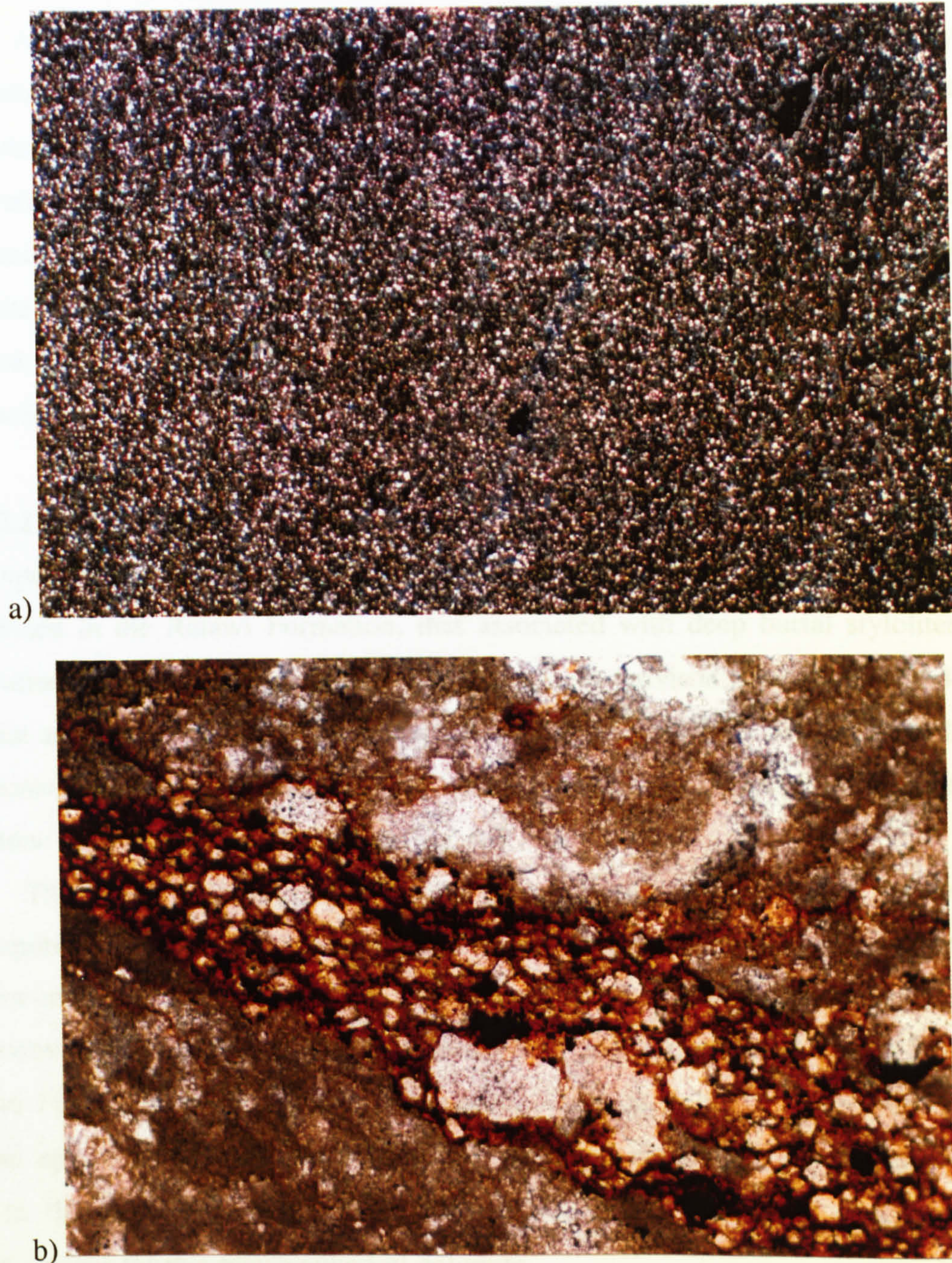


Figure 4-17 a) Photomicrograph of micro-euhedral dolomite crystals scattered through the sediment in mudstone and wackestone lithofacies. Note the uniform distribution of the dolomite crystals. Sample number is R-50 # 4, depth 6499 ft (1981 m), field of view 5 x 3 mm, under crossed polars. b) Photomicrograph of micro-euhedral dolomite crystals associated with a dissolution seam. Note the uniform crystal size in the residual clay of the dissolution seam. Sample number is R-50 # 8, depth 6525 ft (1989 m), field of view 1 x 0.6 mm, under plane-polarized light.



models, and (3) late diagenetic (deep burial) dolomitization models, which include regional and focused models.

All dolomitization models need to consider the source of Mg necessary for dolomitization, in addition to the mechanism of delivery. Ideally, stable isotopes, trace elements, fluid inclusions, in addition to petrographic and stratigraphic data are used to interpret the depositional and diagenetic history of the dolomite (Warren, 2000). This study depends only on the petrographic and stratigraphic data to interpret Ratawi dolomite, and three models are applicable (1) synsedimentary organic dolomite (Section 4.4.1.1), and (2) mixing-zone related dolomite (Section 4.4.1.2), and (3) late diagenetic (deep burial) dolomite (Section 4.4.1.3).

#### **4.2.5.2.1 Synsedimentary organic dolomite**

Two types of micro-euhedral dolomite crystals, with crystal size 10 to 20 microns, are recognized in the Ratawi Formation, that associated with deep burial stylolites and dissolution seams, discussed in the burial diagenetic environment Section (4.4.1.3), and that associated with selective dolomitization of burrows (Fig. 4-15 a) or replacing pseudomorphosed gypsum crystals (Fig. 4-16 b) or scattered through the sediment in mudstone and wackestone lithofacies (Fig. 4-17 a).

The petrographic data, the selective dolomitization of burrows and the absence of evaporites, indicate that this type of dolomite is syndepositional having formed in shallow-marine normal-salinity seawater. The stratigraphic data and palaeoenvironmental reconstruction (Section 3.5) indicate a facies change from the Ratawi Formation to the Makhul Formation, which is rich in organic matter. The Ratawi epicontinental ramp was characterized by restricted circulation, which would have lead to the preservation of organic matter. These data support a synsedimentary organic origin for this micro-euhedral dolomite.

Synsedimentary organic, shallow-marine dolomite is formed in normal-salinity seawater by anaerobic sulphate-reducing bacteria that live in the near surface and shallow-subsurface. The bacteria use organic compounds as energy sources by reducing  $\text{SO}_4^{2-}$  ions; this process produces ammonia that raises the pH and carbonate alkalinity of the pore water, which may result in a reaction between  $\text{HCO}_3^{2-}$  and alkali earth metals,  $\text{Ca}^{2+}$  and  $\text{Mg}^{2+}$ , to form biogenic-syndepositional (epigenetic) calcite, aragonite, magnesite and dolomite (Aref, 1998).



This dolomitization took place during the deposition of the Ratawi Formation. Magnesium could be supplied from seawater or from the breakdown of organic compounds (Wright, 1997). A modern example could be Kau Bay, Indonesia, where organic dolomite is forming in a deep-water lagoon, 400 m depth, in the organic-rich sediments (Middelburg *et al.*, 1990).

#### 4.2.5.2.2 Early diagenetic mixing-zone related dolomite

The most important dolomite type in the Ratawi Formation is ferroan dolomite in reservoir unit-D with medium-size crystals 0.16 to 0.33 mm. These were later dedolomitized under meteoric conditions. This process produced dedolomite moulds that enhance the porosity of reservoir unit-D (Section 4.2.3.1); the process of dedolomitization is discussed in Section 4.2.5.3. During the dissolution of the ferroan dolomite, the ferrous iron of the ferroan dolomite oxidizes to form dark, brown, amorphous limonite-goethite around the dissolved dolomite moulds.

Several lines of evidence suggest an early diagenetic reduced mixing-zone related dolomite model for the formation of the ferroan dolomite. This type of dolomite is restricted to grainstone-packstone facies of the shallow ramp. The palaeoenvironment reconstruction of the study area (Section 3.5) indicates that the climate during the Upper Jurassic was very arid. This climatic condition changes to a more humid climate during the Lower Cretaceous, as indicated by the near-absence of evaporite minerals and the presence of meteoric cement, as well as the calcrete fabric of the Ratawi reservoir unit-E of both alpha and beta fabric (Section 4.2.3.5). The Ratawi facies are generally rich in organic matter (Sections 4.2.2.6 and 4.2.5.2.1) which could have produced a more reducing mixing-zone related diagenetic environment.

These data support the formation of ferroan dolomite under reducing conditions in association with a mixing-zone around the antecedent structures of the main Wafra area. The source of Mg would have been the seawater. The physical driving mechanism for the mixing-zone related model depends on the circulation of seawater induced by the mixing of meteoric and marine water (Tucker, 1993). The chemical driving mechanism of the mixing-zone model itself is that when two waters that are saturated with a particular phase are mixed, the resulting solution may be undersaturated with respect to one phase (calcite) while at the same time may remain saturated with the other phase (dolomite) (Warren, 2000). However, it is generally



believed that mixing-zone dolomite *sensu stricto* does not form because of calcite dissolution taking place much faster than dolomite precipitation. In the mixing-zone related model, dolomitization takes place in seawater with its circulation through the carbonates driven by the fluid movement in the mixing-zone. A modern analogue for mixing-zone related dolomitization could be the middle Eocene Avon Formation, Florida, where dolomite cement is forming in the present aquifer system (Cander, 1994).

#### **4.2.5.2.3 Late diagenetic (burial) dolomite**

Two types of deep burial dolomite are recognised in this study: (1) dolomite associated with stylolites and dissolution seams (Section 4.2.5.2.3.1), and (2) saddle dolomite as a cement and replacement (Section 4.2.5.2.3.2). The Ratawi burial diagenetic environment is discussed in Section 4.2.4.

##### **4.2.5.2.3.1 Dolomite associated with stylolites and dissolution seams**

Micro-euhedral dolomite, crystal size 10 to 20 microns, associated with stylolites and dissolution seams is a second type of micro-euhedral dolomite (Fig. 4-17 b). It is considered to be formed during burial diagenesis because it formed <sup>following</sup> ~~in association with~~ chemical compaction. The source of Mg could be from fluids associated with chemical compaction, moving along the stylolites and dissolution seams. Tobin *et al.* (1997) reported this type of dolomite from middle Ordovician carbonate buildups in Alabama, USA.

##### **4.2.5.2.3.2 Saddle dolomite as a cement and replacement**

Saddle (or baroque) dolomite is a variety of dolomite with undulose extinction characterized by curved crystal faces and cleavages due to the high iron content (Fig. 4-18). The evidence for a deep burial origin is the occurrence of saddle dolomite in tectonic fractures and association with high temperature (60 to 150° C) sulphide mineralization, and hydrocarbon migration and accumulation (Radke and Mathis, 1980). Saddle dolomite in the Ratawi occurs as cement filling pore space, and a replacement in microfacies DiagDol crystalline dolomite (Section 3.4.1). Scattered saddle dolomite crystals are mostly non-luminescent or dull but with a bright overgrowth- red zone. In addition, from the CL, there is evidence for some dissolution of the bright overgrowth zone and infill by non-luminescent dolomite (Fig. 4-19).



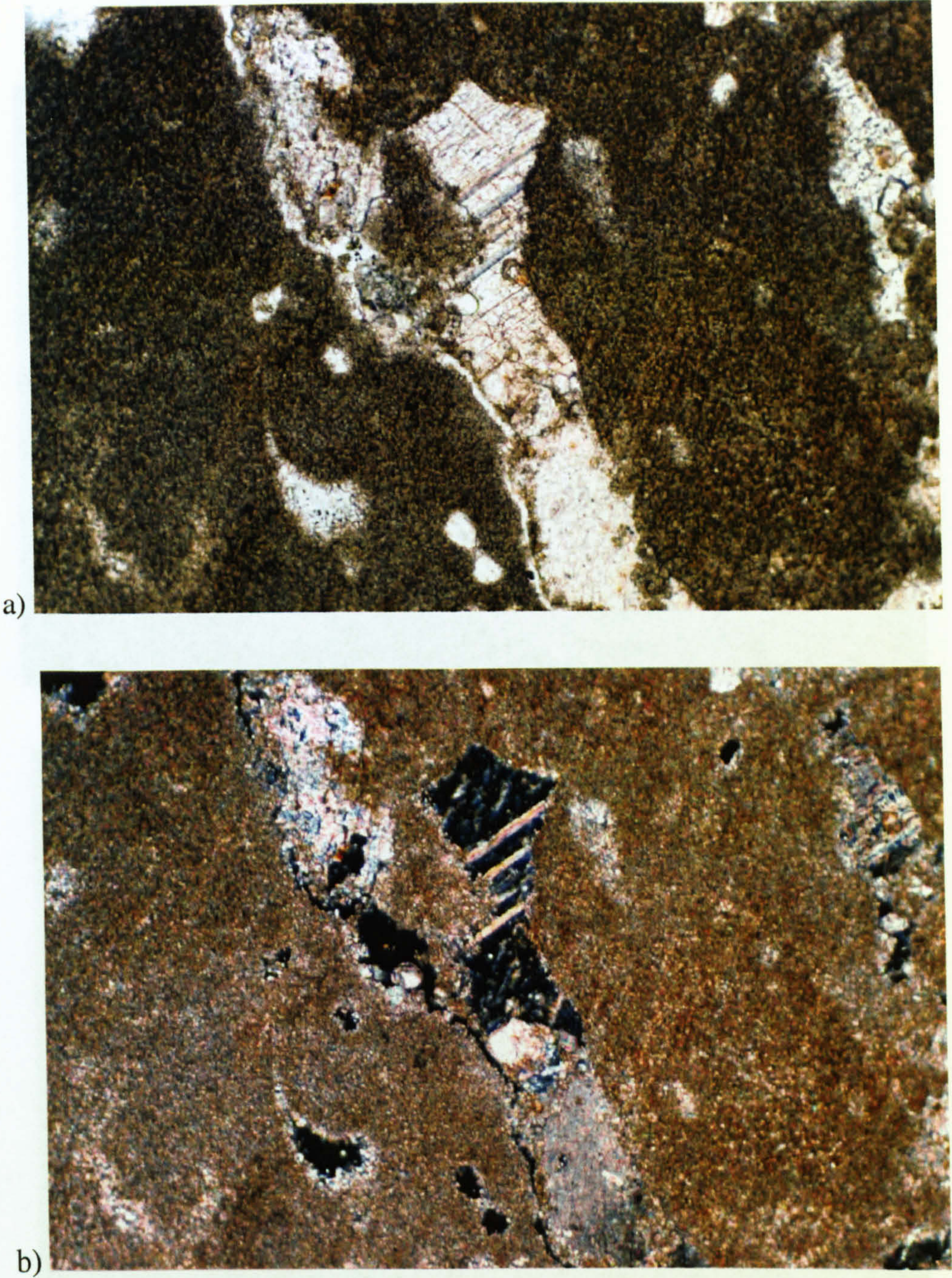


Figure 4-18 Photomicrograph of saddle dolomite cement. Note the rhombic cleavage and wavy extinction; burial dissolution has created some porosity in the cement. Sample number is R-50 # 94, depth 7028 ft (2142 m), field of view 1 x 0.6 mm, a) under plane-polarized light, b) under crossed polars.



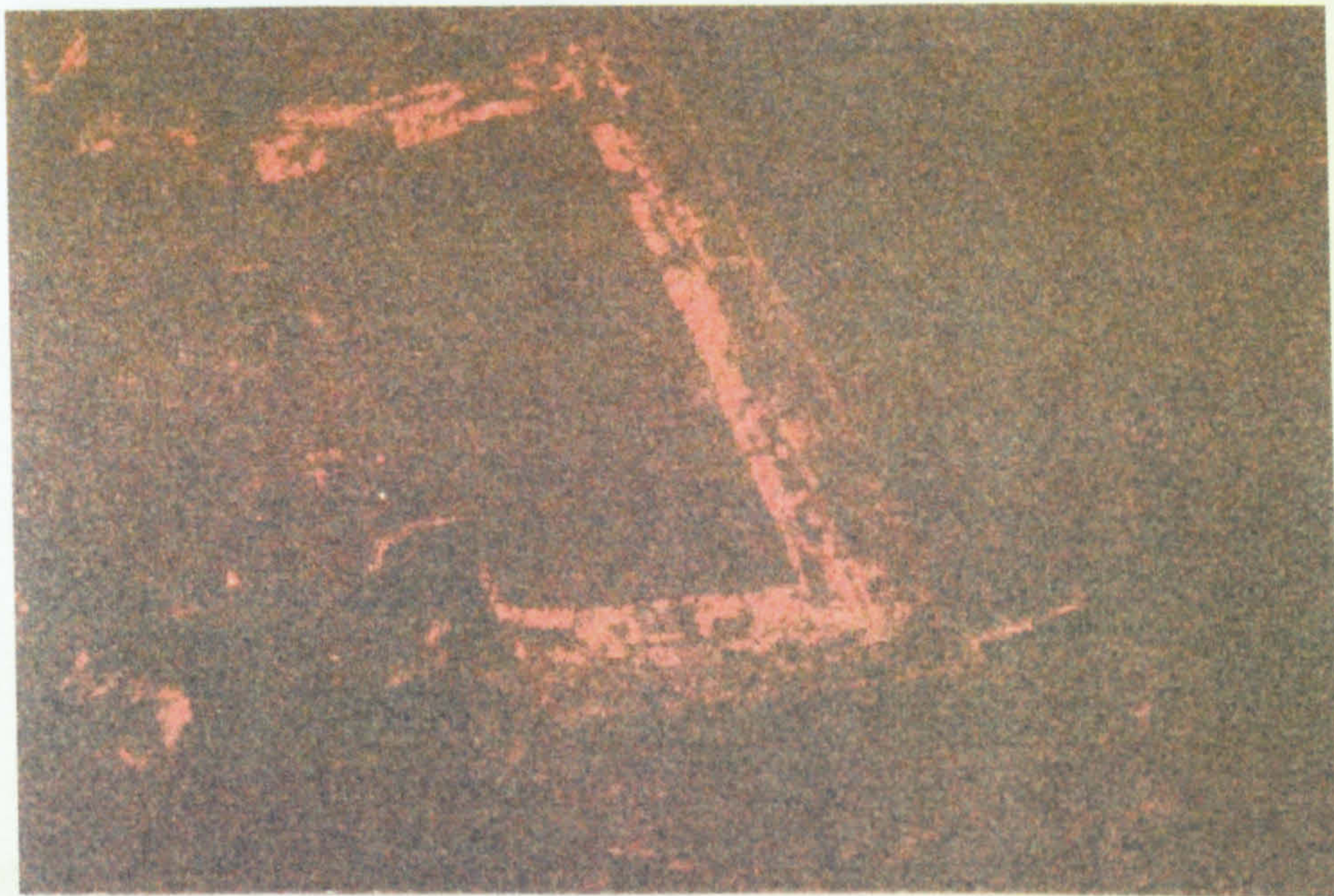
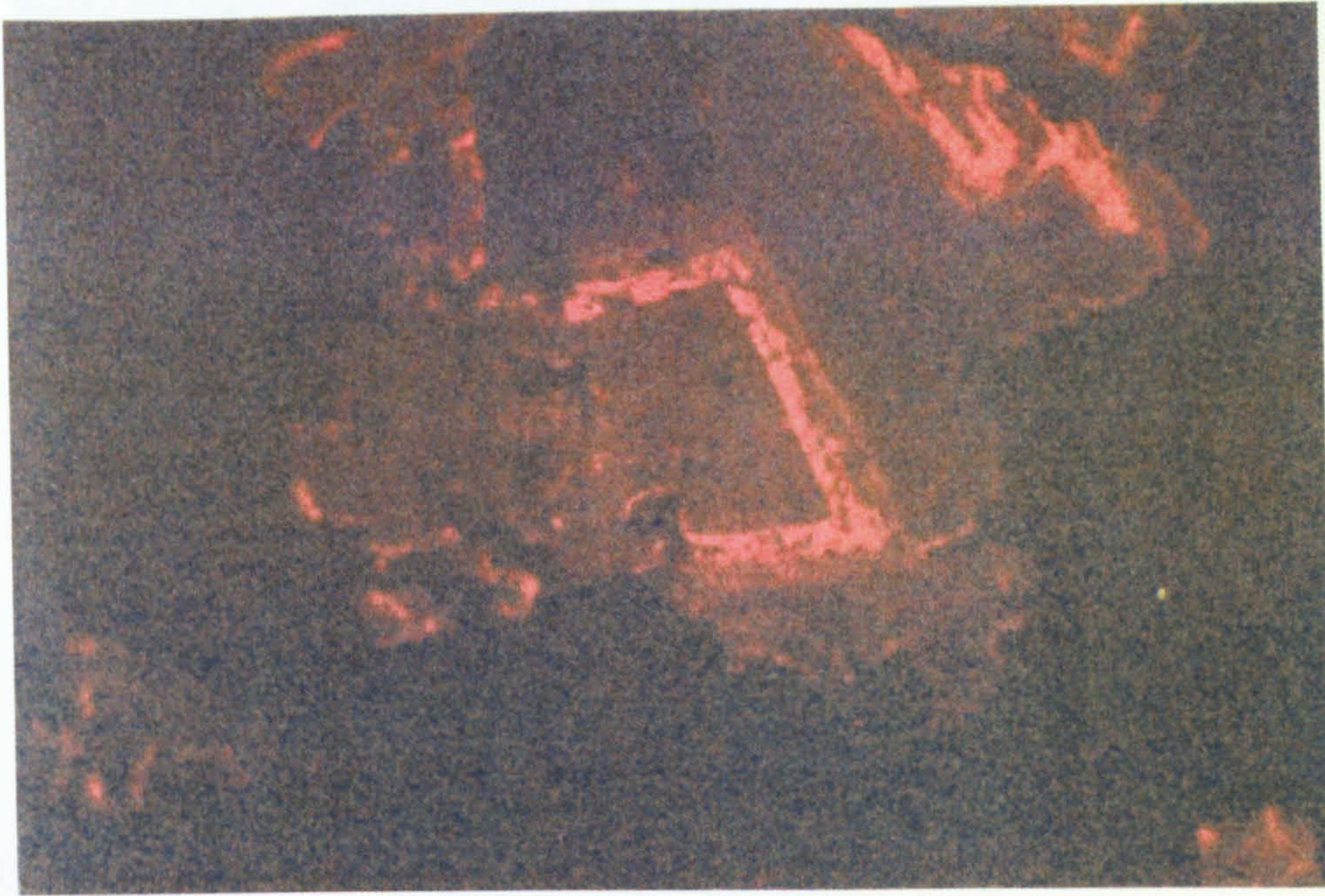


Figure 4-19 Photomicrograph of scattered saddle dolomite cement under cathodoluminescence. The core of the cement is non-luminescent or dull followed by a luminescent orange-red zone and then a dull outer zone. (a) field of view 3 x 2 mm (b) field of view 1 x 0.6 mm. Note irregular non-luminescent areas within in the luminescent zone indicating some dissolution (cement unconformity) between the early luminescent and later non-luminescent zone. Sample number is R-50 # 75, depth 6936 ft (2114 m).



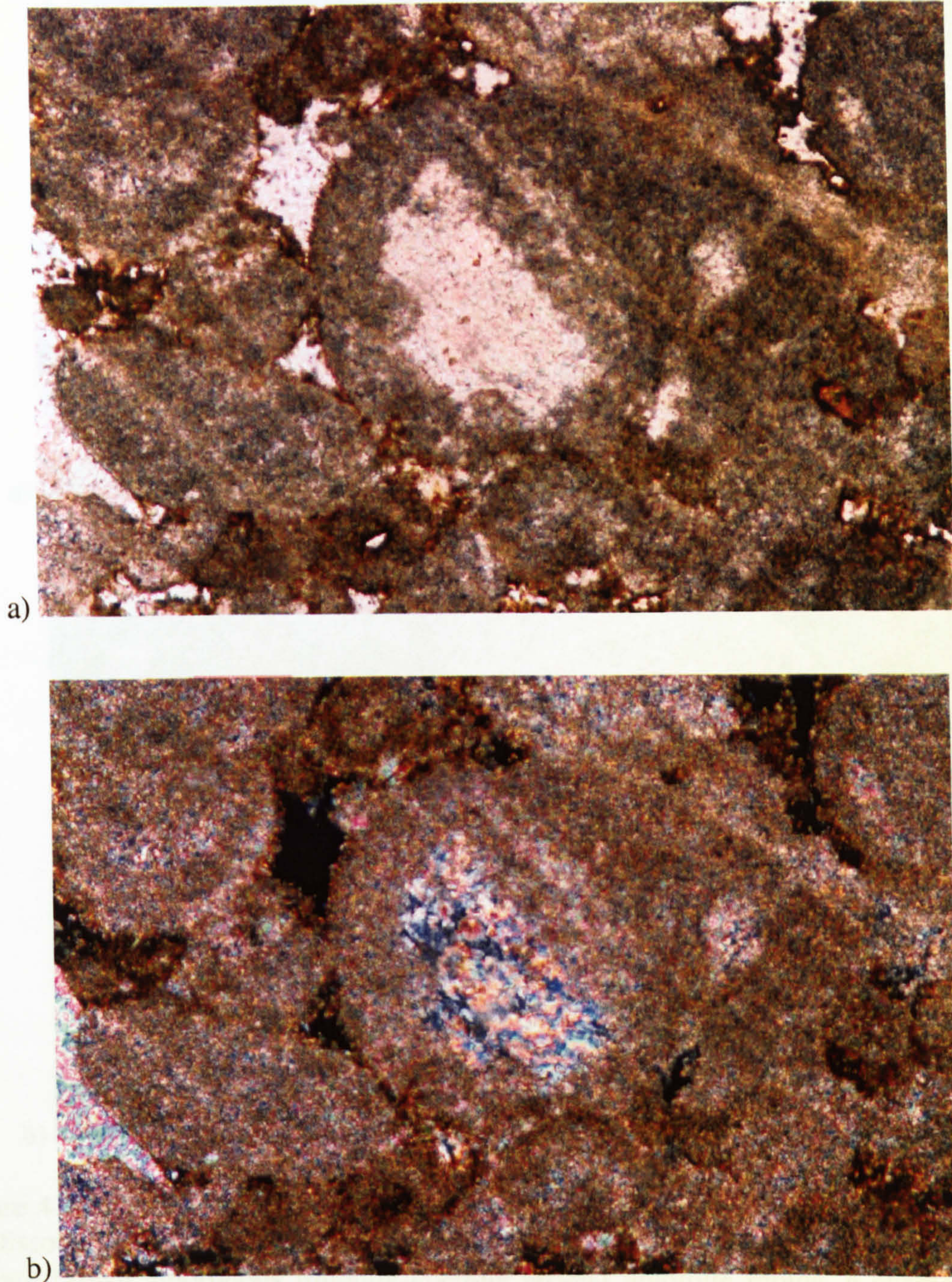


Figure 4-20 Photomicrograph of dedolomite in reservoir Unit E. The dedolomitization processes resulted in open dolomite rhomb moulds (dedolomite porosity) and filling the moulds by low-Mg calcite. Note the straight and 'V' shape of the moulds, in addition to fine calcite crystals filling the moulds in the centre. Sample number is R-50 # 68, depth 6891 ft (2100 m), field of view 0.5 x 0.3 mm, a) under plane-polarized light, b) under crossed polars.



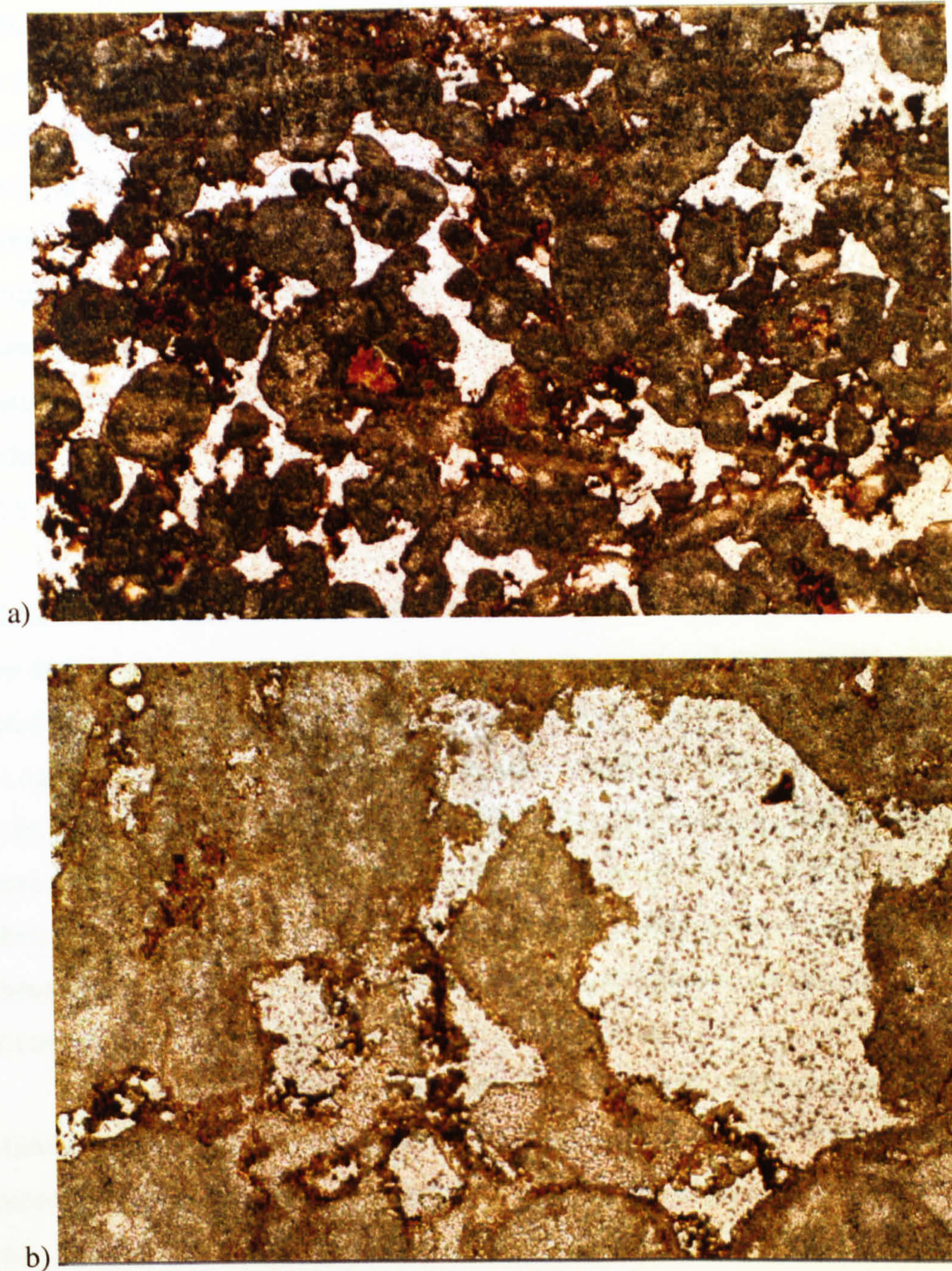


Figure 4-21 Photomicrograph of dedolomite and dedolomite porosity in reservoir unit D. Dissolution of ferroan dolomite has produced dedolomite porosity and precipitation of dark brown amorphous limonite-goethite around dolomite molds, a characteristic feature for the dedolomitization process in the Ratawi, in addition to the 'v' shapes and straight edges modeling the positions of rhombohedral crystal molds. Some dolomite molds are filled with calcite cement. All the particles are heavily micritized. Sample number is R-50 # 68, depth 6891 ft (2100 m), (a) field of view 3 x 2 mm, under plane-polarized light, (b) field of view 1 x 0.6 mm, under plane-polarized light.



#### 4.2.5.3 Ratawi dedolomitization

The dedolomitization (calcitization) of dolomite is important in the development of the Ratawi zone in the Wafra oilfield. The primary depositional porosity of the reservoir unit-D is enhanced by dedolomite porosity as discussed in Section 4.3.3.10. The dolomitization of the reservoir unit-D and the formation of ferroan dolomite is interpreted in Section 4.2.5.2.2 to be mixing-zone related, formed through the abundance of organic matter. The upper-most part of reservoir unit-D at well R-50 is characterized by subaerial exposure and rootlet porosity. Dedolomitization is discussed further here under two headings: dedolomitization texture and porosity (Section 4.2.5.3.1), and Ratawi dedolomitization model (Section 4.2.5.3.2).

##### 4.2.5.3.1 Dedolomitization texture and porosity

The dedolomite textures of reservoir Unit D are associated with marine, meteoric and burial diagenetic features. Two types of dedolomite calcite textures in the Ratawi are (1) calcite pseudomorphs of dolomite rhombs (rare); the calcite is identified by a lack of rhombic cleavage, a drusy texture (Fig. 4-20) and staining, and (2) rhombohedral pores (Fig. 4-21), with limonite and goethite iron oxide around the rhomb mould; this fabric is more common and is important in the development of the Ratawi porosity. These fabrics formed by the dissolution of ferroan dolomite rhombs and the oxidation of ferrous to ferric iron.

Dedolomite porosity is important in the Mesozoic carbonate reservoirs of the Middle East (Purser, 1986); so that understanding the genesis of dedolomite porosity is important in the development of the Ratawi zone and exploration. Textures, processes and timing of dedolomitization are reviewed by Taberner *et al.* (1998). Dedolomitization is a process in which dolomite dissolves and then in some cases calcite is precipitated; the process liberates magnesium into solution and consumes calcium. This can be (1) a one-step dedolomitization process, in which the dolomite rhombs are dissolved and calcite simultaneously precipitated in such a manner that the original dolomite rhomb fabrics are inherited by the calcite; Ratawi dedolomite calcite rhomb fabrics are inferred to have been formed by this process, (2) a two-step dedolomitization process, in which dolomite is dissolved to form cavities that may be filled by calcite either during the same overall process or from a different solution at a later time. The Ratawi dedolomite rhombohedral pores are inferred to have formed in this way.



The total porosity of the dedolomite rock is controlled by the type of dedolomite fabric, which may be (1) the same as before the dedolomitization when the dedolomitization process preserves exactly the shape of the dolomite rhombs replaced, (2) a decrease when the dedolomitization process seals the open pores by precipitation of calcite, or (3) an increase when the dedolomitization process is dominated by dissolution of the dolomite (Taberner *et al.*, 1998). The total porosity of reservoir unit-D has been increased through large-scale dissolution of the ferroan dolomite during the dedolomitization process, without much subsequent precipitation of calcite.

#### **4.2.5.3.2 Ratawi dedolomitization model**

Dedolomitization processes and the development of dedolomite porosity could be developed at two different times: (1) early (near-surface) dedolomitization during subaerial exposure, reflecting either an erosional unconformity at a sequence boundary or late, post-burial uplift and weathering; this process would lead to the development of karst, with the dedolomitization process driven by oxidizing meteoric ground waters (Canaveras *et al.*, 1996), and (2) late diagenetic dedolomitization during deep diagenesis. This dedolomitization process is driven by Ca-rich brines moving up into the dolomites (Budaj *et al.*, 1984). The meteoric cement and calcrete features in Ratawi reservoir Unit D support the early exposure-related dedolomitization and the development of the dedolomite porosity before the deposition of unit-F.

### **4.3 Ratawi porosity**

#### **4.3.1 Porosity in carbonates versus siliciclastics**

The pore types and distribution are basically different in carbonates compared to siliciclastics (Choquette and Pray, 1970). The dominant pore type in siliciclastic sandstone is the primary depositional interparticle pore; the pore diameter and pore-throat size, that influence permeability, are a function of grain size and sorting. The processes working in the depositional environment of a siliciclastic sandstone control the rock fabric, grain size and sorting. The pore nature in a siliciclastic sandstone remains unchanged to a certain extent when the porosity is reduced by cementation and physical compaction. Only after the number of the pore connections are reduced would there be a major change in the porosity-permeability relation (Evans *et al.*, 1997; Kupecz *et al.*, 1997).



However, in carbonate rocks, there <sup>may be</sup> is little relationship between depositional environment, energy, sorting and grain size, with primary pore types, which are highly variable in size and shape; the pore types in a carbonate are more varied than in a siliciclastic rock because of diagenetic modification. The size of the carbonate pores can range from less than one micron to caverns more than 100 meters across, and these could juxtaposed within the same rock unit. The complexity of porosity in a carbonate is the result of a combination of biological, chemical and physical depositional processes, and the diagenetic overprint of chemically reactive carbonates throughout their <sup>diagenetic</sup> burial history (Kupecz *et al.*, 1997).

#### **4.3.2 Carbonate porosity classification**

Flügel (1982) reviewed carbonate porosity classifications, which are mostly founded upon three bases: (1) geometry of pores, (2) interconnection of pores, and (3) relationship between rock-types and porosity types. The most widely used classification is that of Choquette and Pray (1970) (Tucker and Wright, 1990), which is based on pore geometry, the relations between pore types and origin of pores. The classification has two elements, which are (1) the basic carbonate porosity types, and (2) three sets of modifying terms for the basic porosity types, which are time of porosity formation, pore size and shape, and porosity abundance.

Choquette and Pray (1970) recognized 15 basic porosity types, which can be placed in three groups in relation to the rock fabric, namely (1) fabric-selective; the pores are defined by fabric elements of the rock, (2) non-fabric-selective; the pores are not defined by fabric elements of the rock, the pores cross-cut the actual fabric, and (3) fabric-selective or not, the pores may or may not exhibit fabric control. It is important to assess fabric selectivity in order to describe, interpret and classify carbonate porosity better, which is determined by (1) the configuration of the pore boundary, and (2) the position of the pore relative to rock fabric (Choquette and Pray, 1970; Moore, 1989; Tucker and Wright, 1990).

The classification divides porosity into primary and secondary porosity. Primary porosity is any porosity present in a sediment or rock at the termination of depositional processes, and two basic types are (1) pre-depositional stage, which includes intraparticle porosity, within individual particles, such as foraminifers and gastropods or in non-skeletal particles (pellets and ooids), and (2) depositional stage, which includes interparticle and framework porosity, formed at the site of deposition



or in a growing organic framework.

Secondary porosity is any porosity developed at any time after final deposition. Choquette and Pray (1970) divided this time of secondary porosity formation into three stages, eogenetic, telogenetic and mesogenetic. The eogenetic stage is the time interval between the deposition and before deep burial, when the sediment is still under the influence of surficial diagenetic processes. The mineralogy is generally unstable or in the process of stabilization at this time (Choquette and Pray, 1970; Moore, 1989). Diagenetic processes of this zone include cementation, dolomitization, and dissolution, which are active in the meteoric (Section 4.2.3) and marine (Section 4.2.2) diagenetic environments. This zone is very important for Ratawi porosity formation.

The mesogenetic stage starts when the sediment is buried below the influence of surficial diagenetic processes. The diagenetic processes of this zone include burial cementation and compaction, which are active in the deep burial diagenetic environment (Section 4.2.3), and are responsible for the reduction of the near-surface porosity of the Ratawi. The rock could spend a long geological time in this zone, which is characterized by slow diagenetic modification; the porosity development is generally destruction, and may end by complete elimination of the porosity (Choquette and Pray, 1970; Moore, 1989). This zone is very important for Ratawi porosity reduction.

The telogenetic stage is the stage after the mesogenetic stage when the carbonate succession is exhumed to the influence of surficial diagenetic processes associated with unconformities. This stage is inferred in this study to be responsible for the development of reservoir unit-E below a 2<sup>nd</sup> order sequence boundary, and is characterized by a stable calcite mineralogy that is less susceptible to surficial meteoric diagenetic processes (Choquette and Pray, 1970; Moore, 1989). This zone is very important for Ratawi porosity formation.

Ratawi reservoir unit-D is dominated by primary porosity enhanced by minor secondary porosity from the eogenetic and mesogenetic stages, in addition to some telogenetic alternation. Reservoir unit-E is dominated by secondary porosity of the telogenetic stage enhanced by minor mesogenetic porosity.

#### **4.3.3 Ratawi basic porosity types**

Microfacies analysis of the Ratawi oolite and Ratawi Limestone recognizes eleven basic porosity types (Appendix 1). Dedolomite pore type is listed with



dedolomitization, and the microporosity pore type is inferred to be in all Ratawi core samples. This study estimates the percentage of the Ratawi porosity from the thin sections and relates it to rock textures and position on the ramp facies belts (Fig. 4-22). Ratawi basic porosity types are:

#### 4.3.3.1 Interparticle pore type

Interparticle pores, which are fabric-selective primary depositional type, are the main controlling pore type in reservoir unit-D (Fig. 4-7 and 4-14 b). at the flank of the main Wafra area. Also this type is the main controlling pore type in reservoir unit A, B and C at the crest of the main Wafra area (Longacre and Elliott, 1988). The interparticle pores occur between non-skeletal and skeletal grains within grainstones and packstones, which are controlled by the energy of the depositional environment. Moderate to high energy is necessary to winnow out most of the lime mud, which is characteristic of the shoal sand-bodies of the Ratawi shallow ramp facies belt (Section 3.3.2).

This porosity type varies with sorting, and grain shape: better sorting, and irregular or angular grain shape effect the grain packing and increase porosity; the packing of the rock fabric is also influenced by unidirectional currents and bioturbation. Unidirectional currents impose an alignment of grains, which imposes a degree of anisotropy to the flow of the fluids through the interparticle porosity. Bioturbation mixes the fabric, and imposes a degree of isotropy to the flow (Scoffin, 1987; Moore, 1989). Interparticle porosity may also form by selective dissolution of the matrix (lime mud) from between larger grains (Flügel, 1982).

The interparticle pores, which characterize reservoir unit-D with more than 15% porosity cut off, are reduced by cementation and chemical compaction. Only a small amount of early meteoric cement is required to reduce the effect of the burial compaction in reducing the reservoir interparticle porosity and preservation of near surface porosity. Consequently, the preservation of the primary interparticle porosity of reservoir unit-D is favoured in the shallow-water, moderate to high energy facies of the Ratawi shallow ramp, where sand-bodies built-up to sea level. Then there was a sea level drop to expose the sand-body for a short period of time to meteoric diagenesis, so that small amounts of meteoric cement were precipitated to reduce the effect of burial compaction on the reservoir quality.



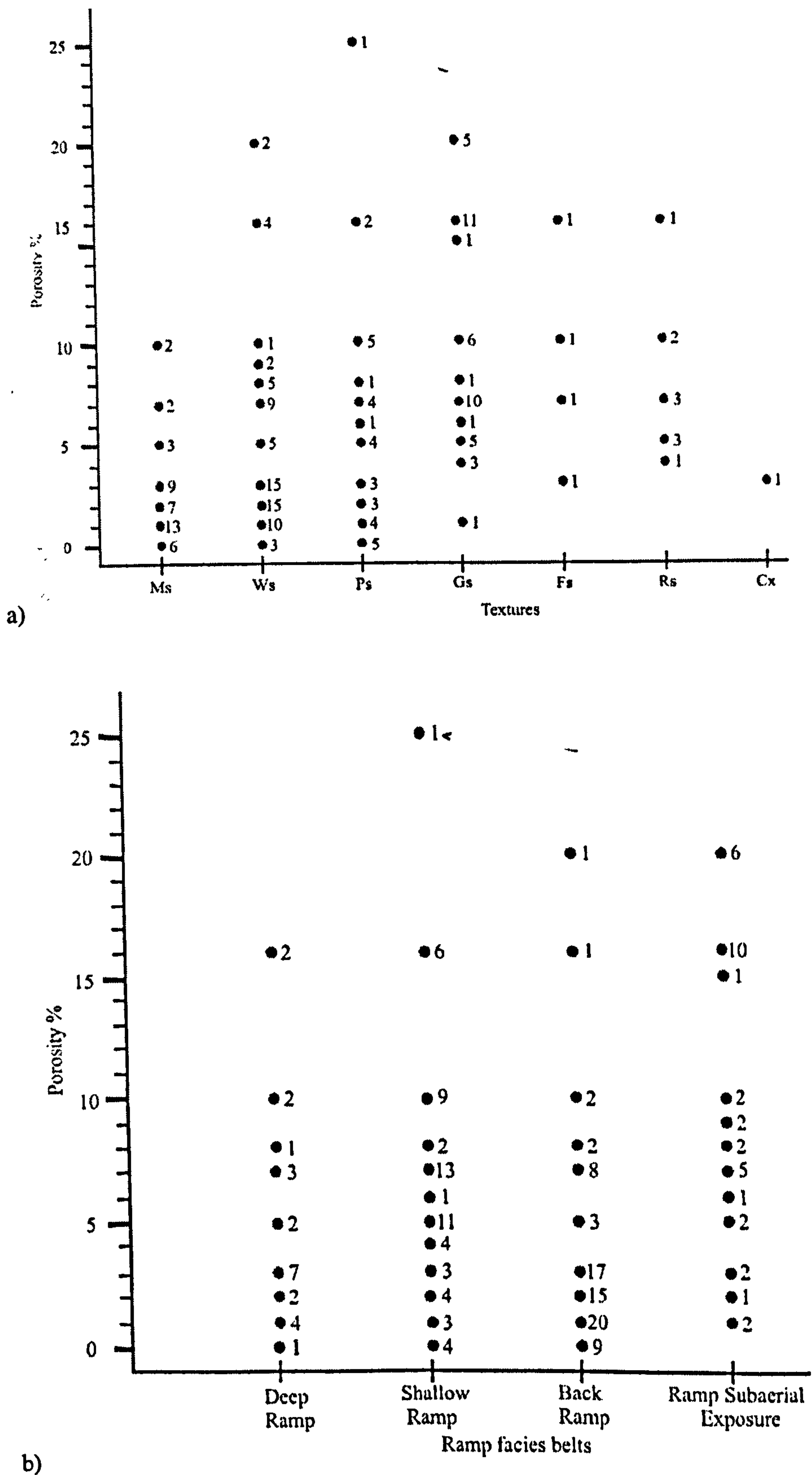


Figure 4-22 Ratawi porosity measured from thin section related to (a) texture and (b) Ratawi facies belts. Numbers are numbers of samples with that porosity. Note most of the reservoir zone (porosity equal or more than 15%) is in the grainstone texture (a) that occur in the shallow-ramp and ramp subaerial exposure belts (b). (Ms = mudstone, WS = wackestone, Ps = packstone, Gs = grainstone, Fs = floatstone, Rs = rudstone and Cx = crystalline carbonate).



#### 4.3.3.2 Intraparticle pore type

Intraparticle pores are a fabric-selective primary type, which is formed within the grains, and is not necessarily interconnected between grains (Fig. 4-27). Its effect on permeability will depend on the micropermeability of the grain, and on overall fabric of the rock (Scoffin, 1987; Tucker and Wright, 1990). This type is a minor pore type in the Ratawi; this study recognizes it only in foraminifers and gastropod skeletal chambers.

#### 4.3.3.3 Mouldic pore type

Mouldic pores are a fabric-selective secondary type, which is formed by selective removal of grains by dissolution during early diagenesis (Fig. 4-24 a and 4-25 a). This selective dissolution is due to a difference in solubility between the grain and the framework that can be related to (1) a difference in mineralogy, like aragonite and calcite, and (2) a difference in crystal size, crystallinity, and organic inclusions. The permeability of the rock increases when mouldic pores are connected to another pore system as in a grain-supported texture. However, when they are not connected, as in a mud-supported texture, then the permeability of the rock dose not change (Flügel, 1982; Scoffin, 1987; Tucker and Wright, 1990).

This study recognizes mouldic pores of sponge spicules and crinoids in the Ratawi. The original mineralogy of sponge spicules is siliceous or calcareous, whereas crinoids were calcareous. The non-reservoir microfacies with a porosity of more than 15% are characterized by mouldic pores in a mud-supported texture with no connection, giving the rock a low permeability.

#### 4.3.3.4 Vug pore type

Vug pores are a non-fabric-selective secondary type, formed by non-selective dissolution that cuts across the rock fabric, grains and cement boundaries (Fig. 4-24 a and 4-14 b). These could represent dissolution enlargement of fabric-selective mouldic pores. The diameter of the vugs is greater than 0.05 mm, and they are visible to the naked eye. Smaller vugs are a form of microporosity (Section 4.3.3.11); larger vugs are termed caves or cavernous porosity, which may be linked by channels. The total porosity and permeability of the rock are determined by the size and the number of the vugs.

The vuggy porosity is formed during meteoric diagenesis (eogenetic and



telogenetic stages) and also during deep diagenesis, mesogenetic stages (Scoffin, 1987; Tucker and Wright, 1990). Vuggy porosity is common in the Ratawi and is the result of early meteoric dissolution (Section 4.2.3.3), when there is evidence of subaerial exposure, as in reservoir unit-E. Where there is no evidence of subaerial exposure, the origin of the vuggy porosity is inferred to be late deep dissolution (Section 4.2.4.4).

Some of the Ratawi vuggy porosity is within saddle dolomite cements. This indicates deep burial dissolution of dolomite.

#### **4.3.3.5 Intercrystal pore type**

Intercrystal pores are a fabric-selective secondary type (Fig. 3-10 b), occurring between crystals that could be replacive dolomite, evaporite or recrystallized calcite. The permeability is influenced by many factors including the size of the crystals, and the abundance of compromise boundaries. The smaller crystal size would cause a higher surface tension, which would lower permeability. Where there are fewer compromise boundaries giving large pore-throats, a higher permeability is generated (Scoffin, 1987; Tucker and Wright, 1990). This type of porosity is rare in the Ratawi, but it does occur in the deep burial saddle dolomite microfacies (DiagDol) that formed as a replacement (Section 4.2.5).

#### **4.3.3.6 Fracture pore type**

Fracture pores are a non-fabric selective secondary type (Fig. 4-25 b and 4-26 a), which is formed in brittle rock, usually with a homogeneous fabric. Fracture porosity is characterized by little relative displacement of adjacent blocks and grades into breccia porosity where blocks are jumbled and chaotic. To have an open fracture porosity, fracturing has to be post-burial, and this is usually associated with folding, faulting, salt doming, salt dissolution or fluid overpressure. Fractures can increase permeability by many times, especially when occurring in interconnected conjugate sets, even with low total porosity, and allow an increase in recovery efficiency. However, the permeability of the rock fabric becomes strongly anisotropic and with low recovery efficiency, when fractures follow the trend of the local tectonics that produce parallel fractures. Fractures allow the passage of post-burial fluids, which could create a vuggy porosity (Scoffin, 1987; Tucker and Wright, 1990). This type of porosity is not very common in the Ratawi; some of the fracture porosity is occluded by coarse granular deep burial cements. Under CL (Fig. 4-23) the fracture-filling



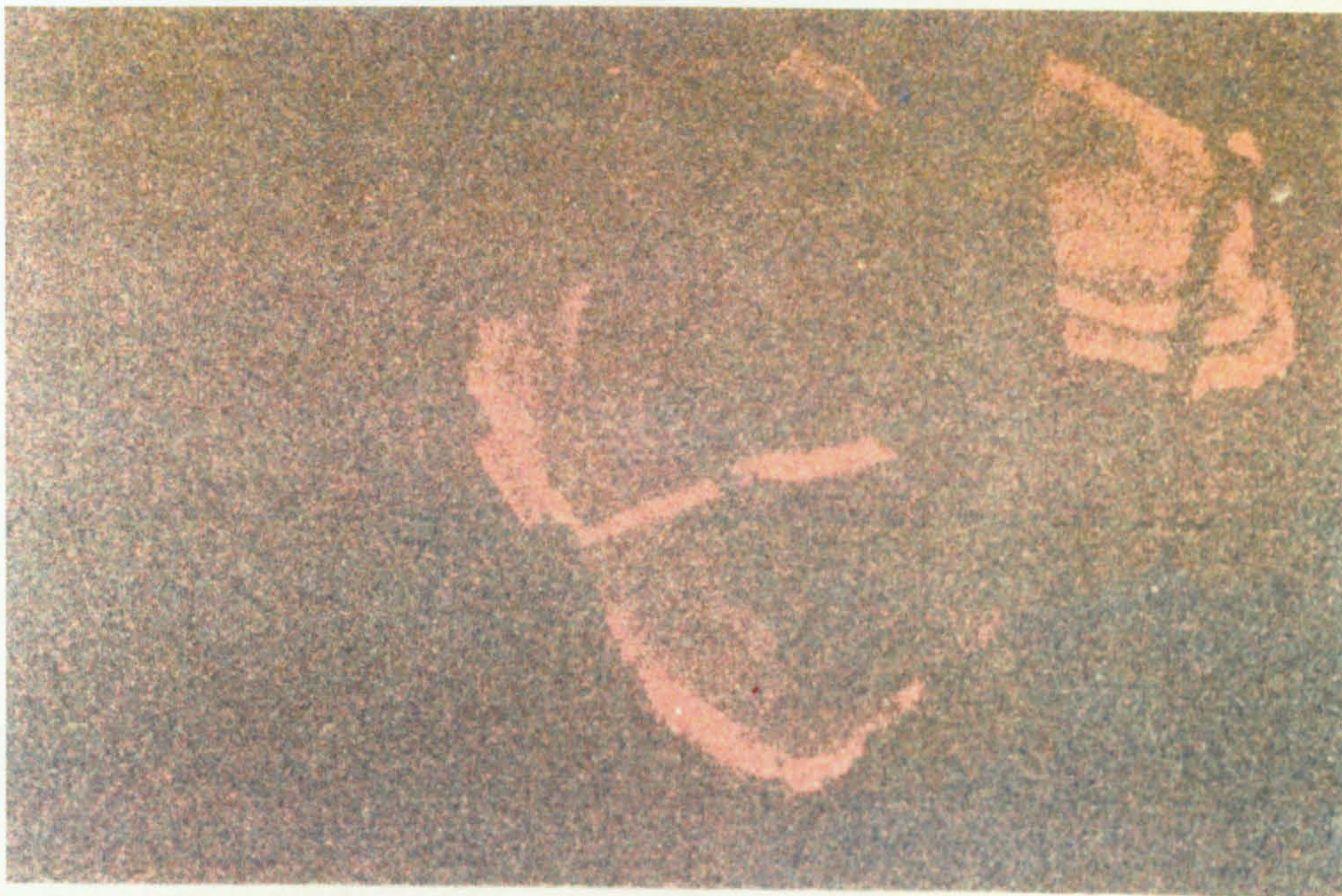
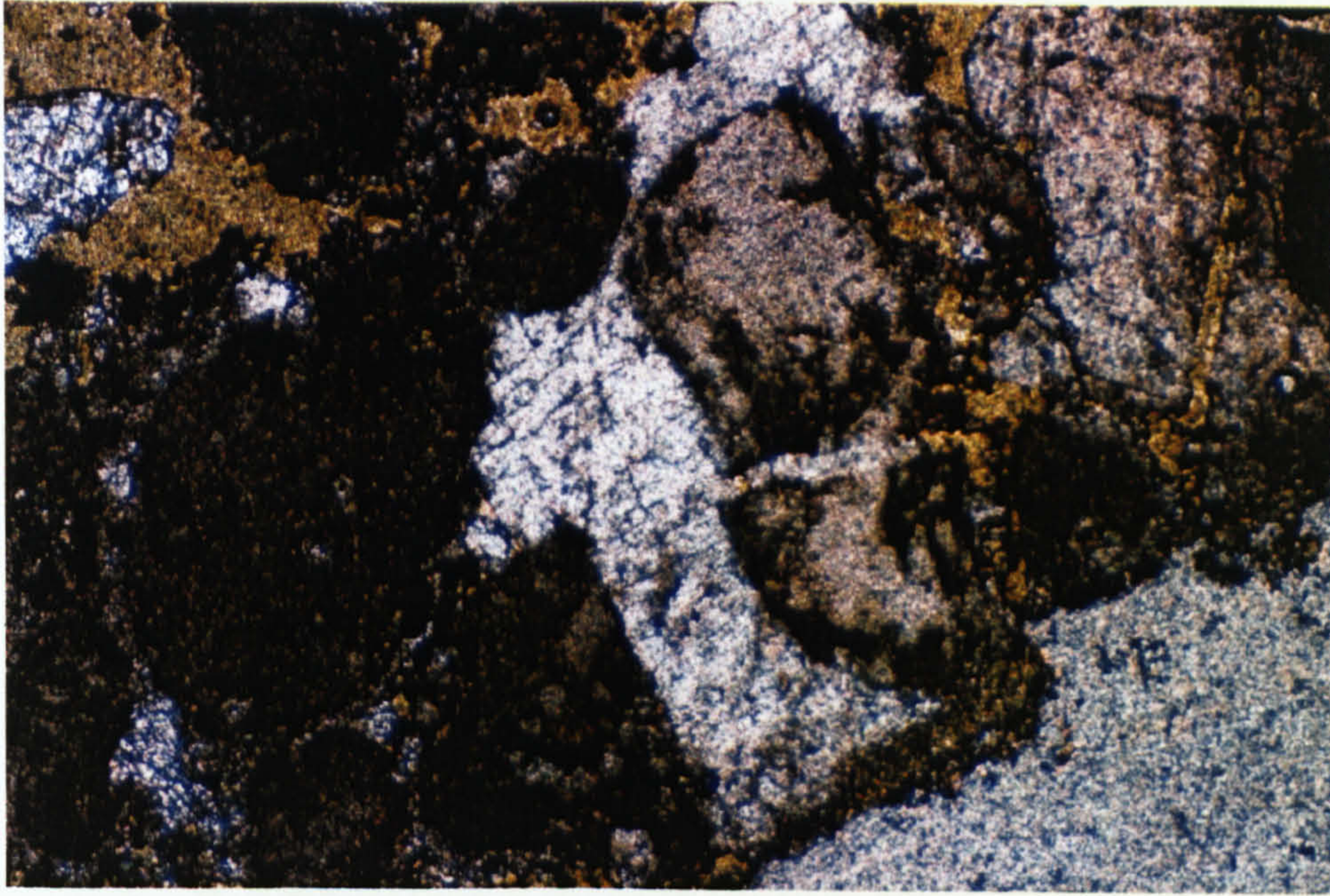


Figure 4-23 Photomicrograph of crinoid grain with fracture and syntaxial overgrowth calcite cement (a) under plane-polarized light (b) under cathodoluminescence field of view 3 x 2 mm. Note the luminescence of the granular drusy calcite cement in the fracture. Sample number is R-50 # 73, depth 6925 ft (2114 m).



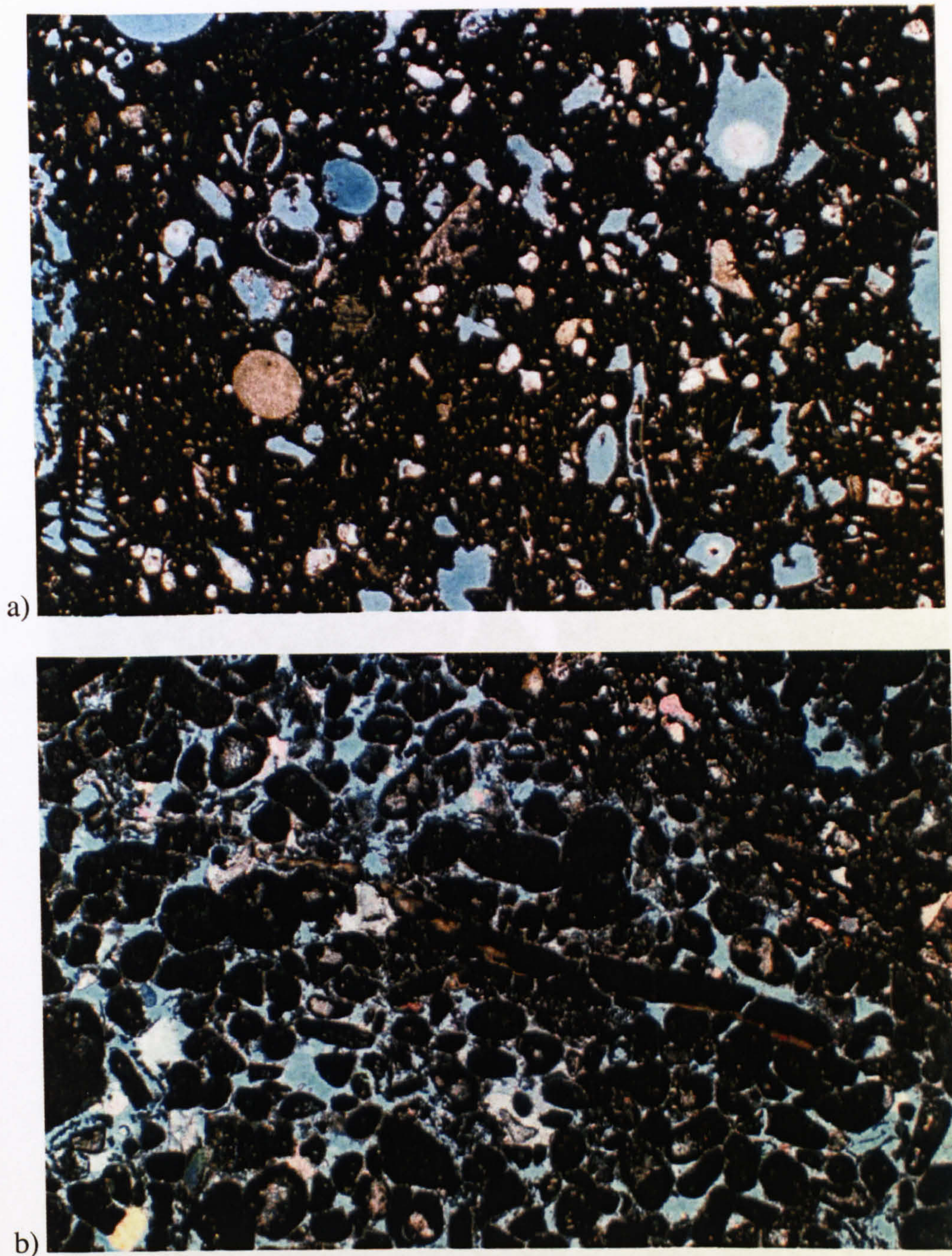


Figure 4-24 a) Photomicrograph of vuggy, moldic and intraparticle porosities in wackestone (microfacies DR3). Note the presence of moldic porosity from dissolution of gastropods, crinoids and sponge spicules. Some of the moldic pores were enlarged by dissolution. Sample number is R-49 # 13, depth 6789 ft (2069 m), field of view 5 x 3 mm, under plane-polarized light. b) Photomicrograph of the interparticle porosity in reservoir unit E (microfacies DiagCal: pedogenic calcrete). Interparticle porosity was preserved from subsequent burial compaction by meteoric cement formed in the calcrete zone. The interparticle porosity is reduced by chemical and physical compaction as evidenced by the development of dissolution seams and the fracture of brachiopod shell. Early crinoid overgrowth also preserved (white). Sample number is R-49 # 18, depth 6814 ft (2077 m), field of view 5 x 3 mm, under plane-polarized light.



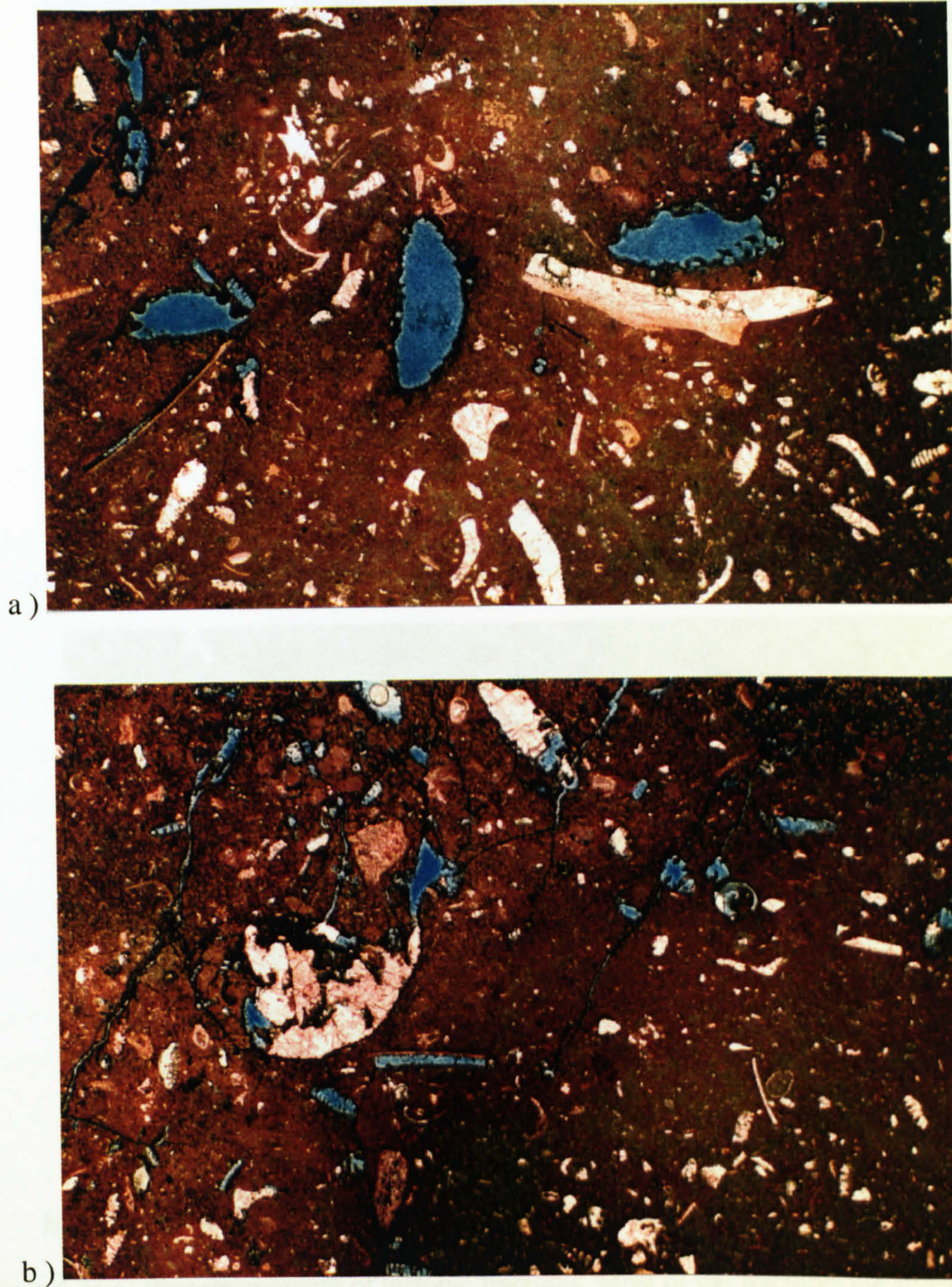


Figure 4-25 Photomicrograph of vug porosity and fracture porosity. Note selective dissolution of skeletal grains in (a) and similar orientation of the fractures in (b) Sample number is R-48 # 7, depth 6760 ft (2060 m), field of view 5 x 3 mm, under plane-polarized light.



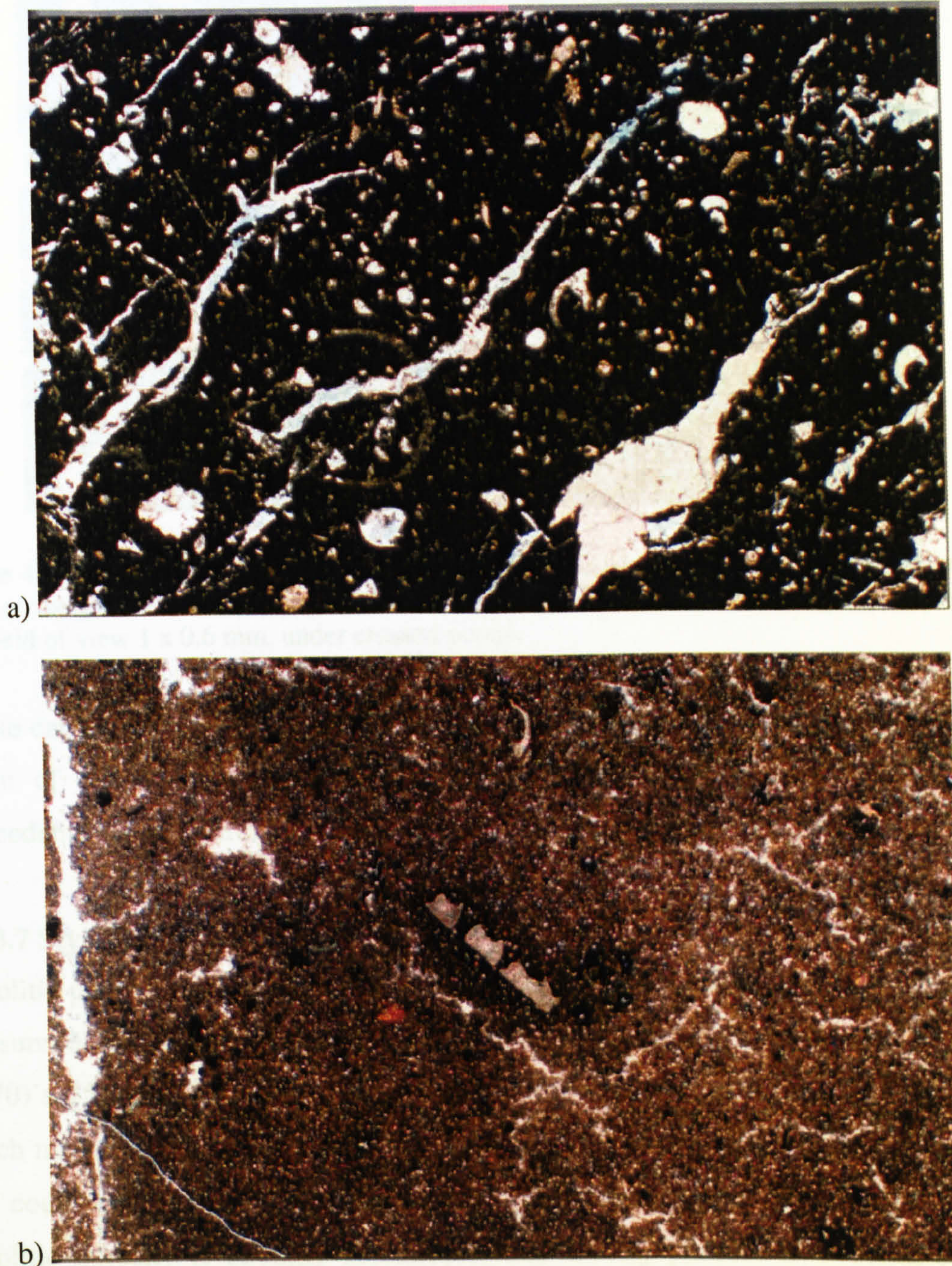


Figure 4-26 a) Photomicrograph of tectonic fractures. Most of the fractures are filled by drusy cement. Sample number is R-50 # 30, depth 6675 ft (2034 m), field of view 5 x 3 mm, under plane-polarized light. b) Photomicrograph of complex and irregular cracks associated with subaerial exposure, calcrite fabric. The calcrite fabric consists of micritized grains, dense microfabric and floating bioclasts. Sample number is R-48 # 16, depth 6691 ft (2039 m), field of view 5 x 3 mm, under plane-polarized light.

#### 4.3.3.8 Burrow pore type

Burrow pores may be fabric selective or non-fabric selective. They are a primary type of pore created by burrowing organisms in relatively soft sediment (Ginsburg, 1987).





Figure 4-27 Photomicrograph of intraparticle porosity in skeletal grain of foraminifera. Note most of the grains are severely micritized. Sample number is R-50 # 70, depth 6912 ft (2107 m), field of view 1 x 0.6 mm, under crossed polars.

calcite can be a bright orange colour. Some fractures are still open (Fig. 4-23 b). The origin of the fracture porosity is probably related to the growth of the Wafra antecedent fold structure.

#### 4.3.3.7 Stylolitic pore type

Stylolitic pores are a non-fabric selective secondary type, which is developed through pressure dissolution; this type of porosity is not included in Choquette and Pray (1970)'s 15 basic pore types. The stylolitic porosity is similar to fracture porosity, which may serve as a pathway for migrating fluid, hydrocarbons and formation water that could create a vuggy porosity along these pathways. The permeability of the stylolitic porosity is strongly anisotropic, and usually parallel to bedding (Scoffin, 1987). The stylolitic porosity is not very common in the Ratawi; the origin of the porosity is by deep burial chemical compaction (Section 4.2.4.2) in the mesogenetic stage. Open stylolites indicate a release of the pressure that generated the chemical compaction.

#### 4.3.3.8 Burrow pore type

Burrow pores may be fabric selective or not (Fig. 4-16 a); they are a primary type, created by burrowing organisms in relatively unconsolidated sediment (Scoffin, 1987;



Tucker and Wright, 1990). This type of porosity is rare in the Ratawi and is recognized in this study by micro-euhedral dolomite rhombs, which have formed as a selective dolomitization of burrows (discussed in Section 4.3.5.2.1). There is a minor amount of porous saddle dolomite cement around the open burrow porosity, which could indicate a diagenetic sequence of deep burial cement first filling the pore space, followed by selective dissolution of the saddle dolomite cement. The burrow porosity is isolated in a mud-supported texture, and so does not increase the permeability.

#### **4.3.3.9 Rootlet pore type**

The term rootlet porosity is used in this study to describe all open fabric features that formed during subaerial exposure, which have not been blocked by cement or micrite; thus rootlet pores are a non-fabric selective secondary type. This type of pore is the main controlling pore type in reservoir unit-E, which is the only reservoir unit that is producing from the three areas of the oilfield, main, southern and east Wafra areas. The rootlet porosity includes rhizoliths (Fig. 3-12 a) (Section 3.4.3.4.2), alveolar septal structure (Fig. 3-14) (Section 3.4.3.4.3), calcified filaments (Fig. 3-13) (Section 3.4.3.4.4), radial cracking (Section 3.4.3.4.6), and complex cracks (Fig. 4-26 b) (Section 3.4.3.4.7). Choquette and Pray (1970) used the term shrinkage porosity for pore space formed by shrinkage of the sediment soon after deposition through desiccation. The radial cracks and complex cracks are interpreted in this study as the result of diagenesis during subaerial exposure.

#### **4.3.3.10 Dedolomite pore type**

The term dedolomite porosity was used by Purser (1986) to describe secondary porosity associated with dedolomitization of middle Jurassic carbonate reservoirs in the Paris basin. The dedolomite pores (Fig. 4-21) are a fabric selective secondary type that is recognised by distinctive rhombohedral crystal-mould pores. Dedolomite porosity is formed by dolomite dissolution and in this study is associated with subaerial exposure (Section 4.4.3). Purser (1986) argued that although the dedolomitization process has been known since the 19th Century, dedolomite porosity is more widespread in hydrocarbon reservoirs than is generally believed; recognition of dolomite rhomb moulds, which is the direct evidence for dedolomitization in reservoir rocks, may be exceptional. However, reservoir rocks with leached-fossil porosity is common, as in much of the Cretaceous Ratawi zone and Jurassic of the



Middle East. These reservoir rocks should be re-examined in the light of possible dedolomitization processes that form dedolomite porosity and control reservoir heterogeneity. Dedolomite pores are only found in reservoir unit-D, enhancing the porosity of the unit, which is dominated by interparticle pore types.

#### 4.3.3.11 Microporosity pore type

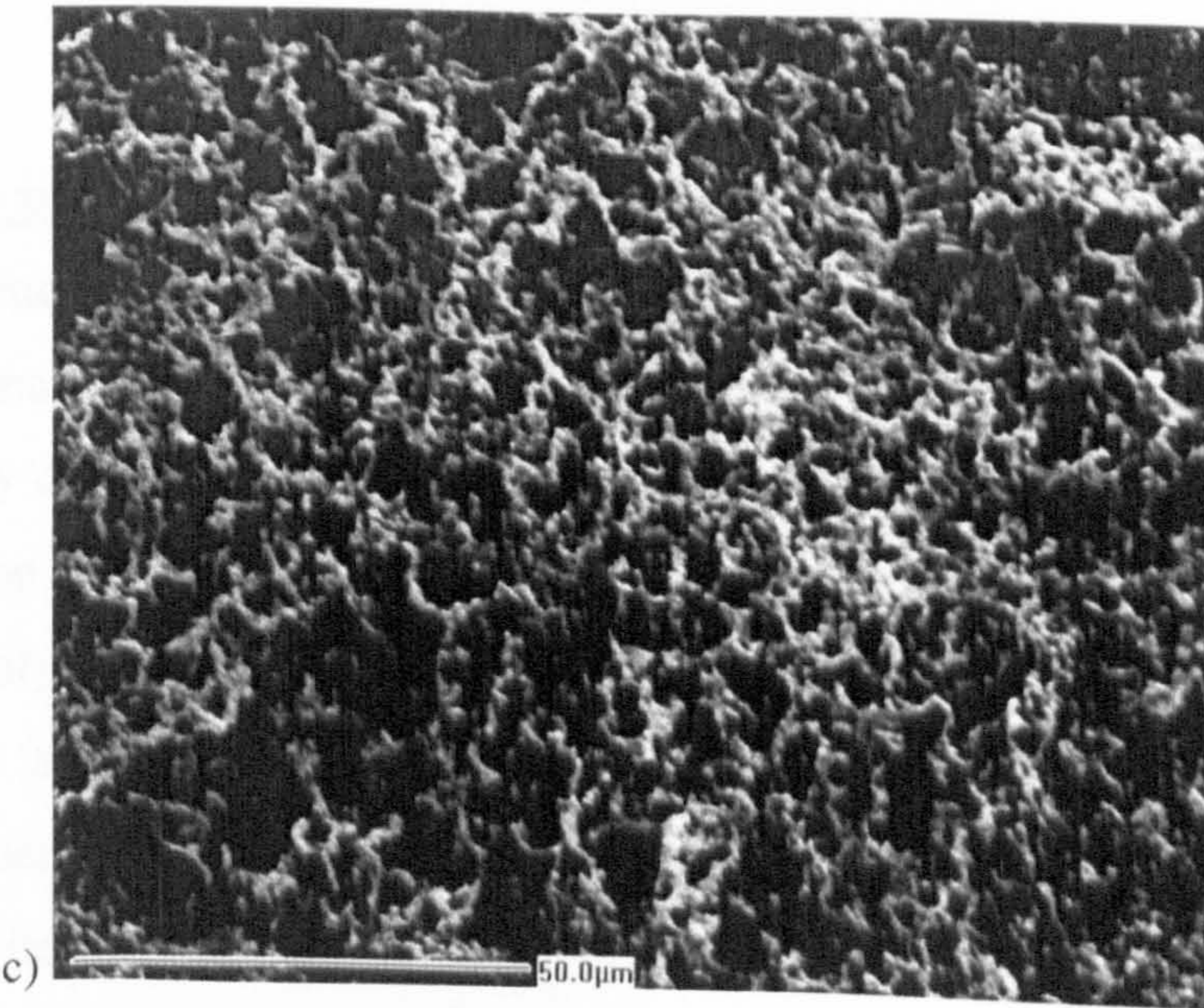
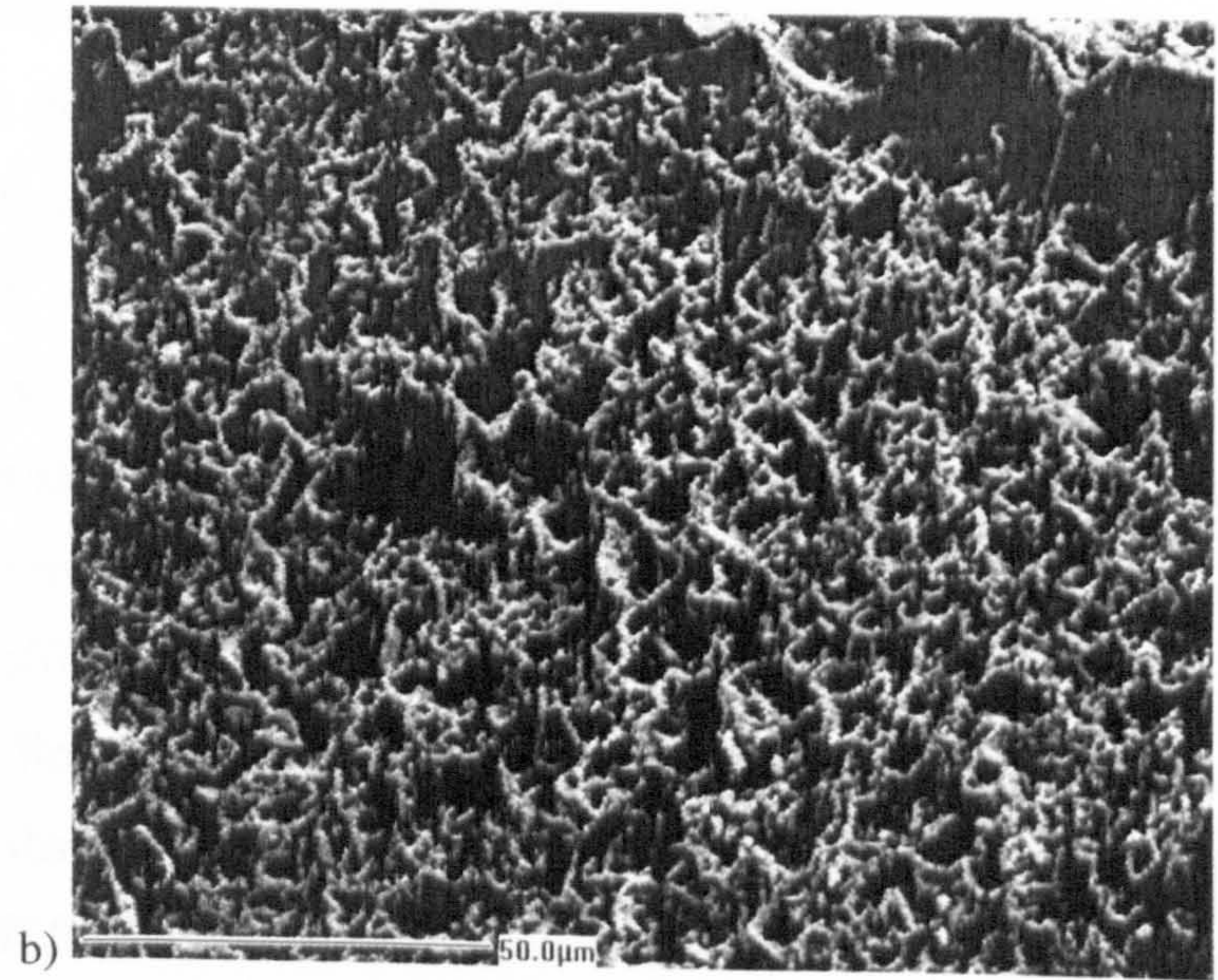
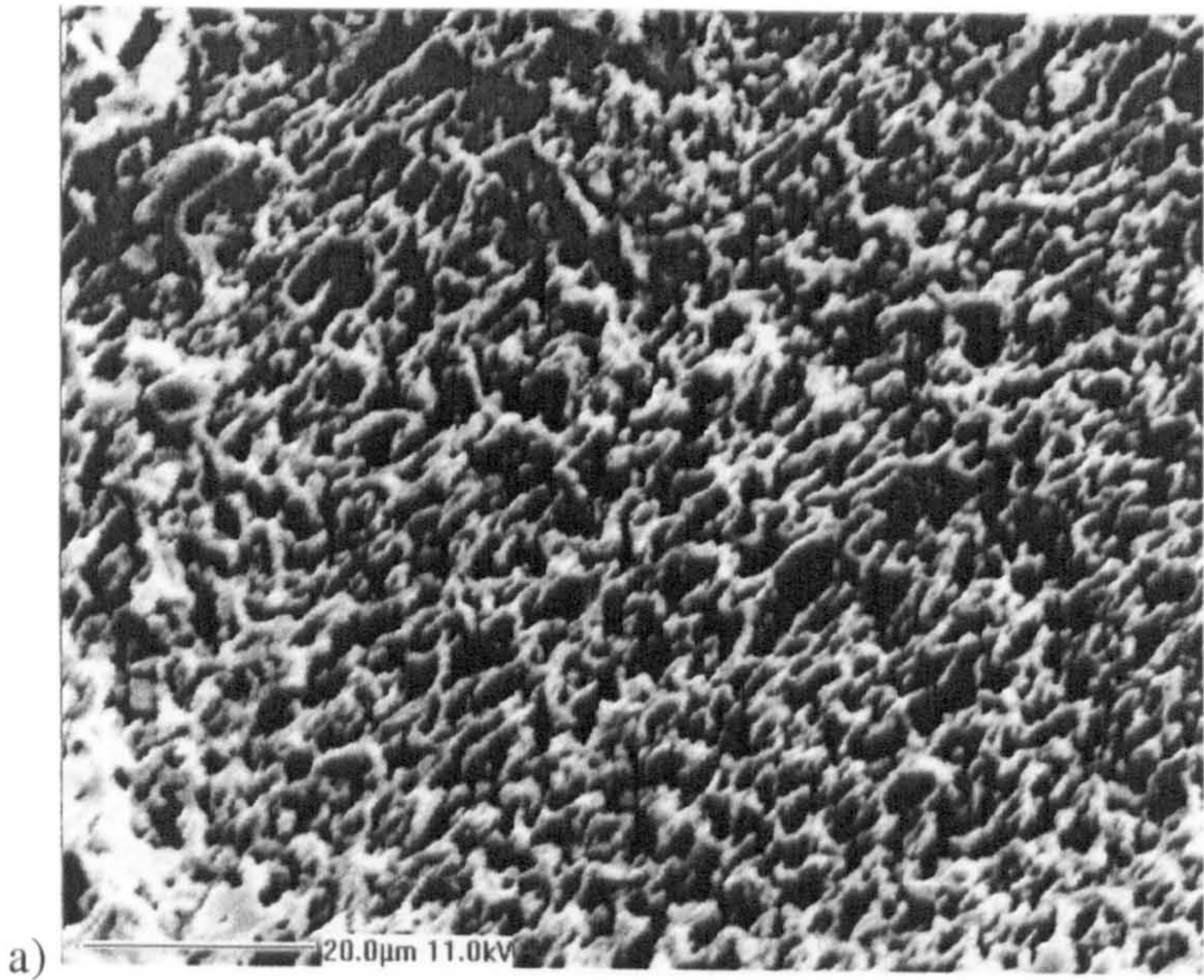
Microporosity is very important in the Ratawi zone at Wafra oilfield, and so understanding this type of porosity is significant for reservoir development and exploration. Chalky texture is common in the Mesozoic and Tertiary carbonate reservoirs of the Middle East (Wilson, 1975) and forms major reservoirs for oil, gas and condensate in the Thamama Group throughout the Arabian basin (Moshier, 1989a). The chalky texture of the Middle East reservoirs is formed by the development of microporosity within the matrix component of the shallow-water carbonates, which is different from that in the true chalks that formed through deep-sea accumulation of calcareous nannofossil tests with abundant interparticle and intraparticle microporosity (Al-Aasm and Azmy, 1996).

Choquette and Pray (1970) defined the micropores as voids of less than 62 microns in average diameter; the term microporosity is equivalent to matrix microporosity, intramicrite porosity, chalky-porosity, matrical porosity, and pin-point porosity (Moshier, 1989b). Micropores with values larger than 5 microns could be significant with respect to reservoir performance and evaluation (Moshier, 1989b). However, Al-Aasm and Azmy (1996) studied the diagenesis and evolution of microporosity of Middle-Upper Devonian Kee Scarp reefs, Norman Wells, Northwest Territories, Canada and concluded that the best reservoir microporosity type is microvugs 4 to 10 microns.



Figure 4-28 SEM micrograph intercrystalline microporosity and microvugs. Polished and etched resin-impregnated samples (a) and (b) sample number is R-50 # 70, depth 6912 ft (2107), (b) sample number is R-48 # 8, depth 6755 ft (2059 m). Note the high percentage of the microporosity, inferred in this study to be ineffective porosity, making the cut off porosity for the Ratawi zone equal or more than 15%.







Three Ratawi core samples were examined by scanning electron microscope to study the diagenetic texture and microporosity types. The samples were impregnated with blue resin, polished and etched with 50% acetic acid for two minutes. Three types of microporosity are found: micro-vugs, micro-channels, and micro-intercrystalline; the average microporosity is 10 % ranging up to 20%. There are three possible origins for the Lower Cretaceous Thamama Group microporosity (Moshier, 1989 a, b) namely: (1) shallow meteoric diagenesis during exposure and unconformity formation (Harris *et al.*, 1985), (2) lack of cementation during mineral recrystallisation and stabilisation, which could be related to the calcite-sea of the Cretaceous (Wilson, 1980), and (3) deep burial diagenesis. This study inferred that most of the microporosity of the Ratawi zone formed by the first process, meteoric diagenesis during formation of a sequence boundary above reservoir unit-E, and by the second process, a lack of early cementation

The cut-off porosity for the Ratawi zone at Wafra oilfield is 15% (Longacre and Ginger, 1987), which could indicate that there is a high percentage of ineffective porosity in the Lower Cretaceous Ratawi Formation. This ineffective porosity is inferred in this study to be caused by the presence of the microporosity. As mentioned before, the nature of the pore system, among other factors, controls the permeability and recovery efficiency of the Ratawi reservoir (Chilingarian *et al.*, 1992). This study infers that the limited amount of fracture porosity and the small pore size, pore-throat size, and number of pore-connections of the microporosity contribute to the high porosity cut-off for the Ratawi zone.

#### **4.3.4 Porosity preservation during burial**

##### **4.3.4.1 Introduction**

Ancient carbonates with porosity greater than a few percent are relatively uncommon, whereas newly deposited carbonate sediments typically have porosities of 40 to 70%. The destruction of the near-surface carbonate porosity with burial is the dominant trend of porosity evolution (Choquette and Pray, 1970). Schmoker and Halley (1982) recommended a change in geological emphasis, from the establishment of the correlations between early history (depositional environments and near-surface diagenetic environments) and porosity 'evolution', to the establishment of correlations between early history and porosity 'preservation' in the subsurface.



According to Alsharhan and Magara (1995) the main concerns of workers is not the creation of new porosity with burial, but the preservation of near-surface porosity at the burial depths of the reservoir. To preserve the high near-surface porosity to the reservoir burial depth, the effects of cementation and compaction processes must be reduced (Scholle and Halley, 1985). The possible geological, physical and chemical factors that reduce these deep diagenetic processes is reviewed under two headings, processes to reduce the effect of cementation (Section 4.3.4.2) and processes to reduce the effect of chemical compaction (Section 4.3.4.3); this information, plus regional data are used in this study to interpret the preservation of the near-surface porosity in the Ratawi zone at Wafra oilfield (Section 4.3.4.4).

#### **4.3.4.2 Processes to reduce the effect of cementation**

To cause significant cementation, formation water must be characterized by two main features: (1) the formation fluid must contain certain minimum amounts of ions in solution, and (2) the formation fluid must be flowing to supply the ions to the cement site (Harris *et al.*, 1985). The absence of early cement could be due to processes that reduce ion concentration in the fluid or slow the fluid movement. These processes include:

##### **4.3.4.2.1 Absence of a source of carbonate cement**

There are three potential sources for carbonate cement, when they are reduced the preservation potential for the near-surface porosity increases. These are (1) a near-surface source during mineral stabilization; cement from this source rarely destroys all the porosity. (2) A deep phreatic source that is generated by an effective hydrodynamic flow system. This system precipitates cement near the carbonate source because carbonate solutions rapidly attain equilibrium; therefore this process also rarely destroys all the porosity. (3) A local source of  $\text{CaCO}_3$  liberated during pressure dissolution (Alsharhan and Magara, 1995).

##### **4.3.4.2.2 Isolation of the reservoir from the carbonate cement source**

Alsharhan and Magara (1995) cited Wilson (1981) that the deposition of an extensive seal rock above a reservoir rock would protect the porosity of the reservoir from late cementation by fresh water. This process was suggested for the preservation of the porosity in the Arab Formation by the deposition of the Hith Anhydrite seal.



#### 4.3.4.2.3 Reduced fluid mobility by early emplacement of hydrocarbons

Diagenetic processes take place in the presence of water. Early hydrocarbon emplacement in a reservoir would increase the pressure to the level of excess pressure and this reduces the flow of the formation water, and reduces cementation in the oil-saturated interval, so preserving porosity (Magara *et al.*, 1993). This process requires early migration of the hydrocarbons from the source rock to the reservoir rock.

#### 4.3.4.2.4 High brine concentration in formation water

Formation fluid must contain a certain minimum amount of  $\text{CaCO}_3$  in solution to cause significant cementation. High brine concentrations up to 250,000 ppm may interfere with cement mineral solubility, which could slow the precipitation of cement (Magara *et al.*, 1993; Alsharhan and Magara, 1995).

#### 4.3.4.2.5 High carboxylic acid concentration in formation water

The stability of carbonate minerals during progressive burial depends on two factors: (1) the aqueous species calcite ( $\text{Ca}^{2+}$ ), carbon dioxide ( $\text{CO}_2$ ), carbonic acid ( $\text{H}_2\text{CO}_3$ ), bicarbonate ( $\text{HCO}_3^-$ ), and carbonate ( $\text{CO}_3^{2-}$ ) and (2) the alkalinity (pH) that depends on pressure of the carbon dioxide ( $\text{pCO}_2$ ) and organic acids, including carboxylic acid anions. Surdam *et al.* (1989) suggested that oxygen-bearing functional groups and water-soluble carboxylic acid are generated before or simultaneous with hydrocarbons and that pulses of organic compounds could control inorganic diagenesis, which include cement precipitation and enhancement of porosity by dissolution.

Over the temperature range 80 to 120°C, the pH of formation waters is typically controlled by carboxylic acid, not by  $\text{pCO}_2$ . Below 80°C bacteria consume short-chained organic groups of the acid and keep the acid at a relatively low concentration, but at elevated temperature, over 80°C, the bacterial activity is reduced and the acid concentration increases. However at elevated temperature, more than 120°C, the acid is destroyed by thermal decarboxylation. When the pH is low, low alkalinity, and temperature between 80 to 120°C, the carbonate solubility may be high, which results in carbonate dissolution or lack of carbonate cement precipitation (Surdam *et al.*, 1989).



#### 4.3.4.3 Processes to reduce the effect of chemical compaction

Chemical compaction is a very important factor in reducing near-surface porosity (Scholle and Halley, 1985). Therefore the processes that reduce chemical compaction would increase the preservation of near-surface porosity. These processes include:

##### 4.3.4.3.1 Early lithification

Early lithification processes include early near-surface cementation that produces a lithified framework which resists deep burial pressure dissolution. This process has been suggested to preserve the porosity in the Arab Formation and Smackover Formation (Alsharhan and Magara, 1995).

##### 4.3.4.3.2 Early hydrocarbon emplacement

The early hydrocarbon emplacement in the reservoir would build up the pressure to the level of excess pressure in the oil-saturated zone by the oil buoyancy effect. This excess pressure would reduce the effect of the overburden stress, and so reduce the process of chemical and physical compaction (Magara *et al.*, 1993).

##### 4.3.4.3.3 Structural growth, unconformity and anhydrite buffer zone

Magara *et al.* (1993) suggested three possible processes which could reduce the effect of burial compaction and therefore increase the preservation of near-surface porosity of the Arab Formation. The first is continuous or repeated growth of the structure (hydrocarbon trap) which could reduce the effect of the overburden stress at the crestal location of the structure and so reduce compaction at the crest where the reservoir would occur. This process might explain the porosity difference between a crest of the structure and a down-dip position, which is often reduced.

The second is regional unconformity which might provide periods of elastic rebound of the rock, that would tend to reduce the effect of the overburden stress and compaction. The last is the presence of thick anhydrite beds, Hith and Arab B, C, and D anhydrite, which might have provided protection from the overburden pressure. These anhydrite zones might absorb part of the overpressure by yielding vertically and laterally through ductile and plastic deformation, and so reduce the effective stress on the reservoir rock.



#### 4.3.4.4 Ratawi porosity preservation

The porosity of the Ratawi zone at the Wafra oilfield, like all hydrocarbon reservoirs, represents a single point of porosity evolution along the continuum of porosity diagenesis (Schmoker and Halley, 1982). The Ratawi zone at Wafra oilfield is more than 152 m (500 ft) thick, at an average depth of 2133 m (7000 ft), with average porosity ranging from 18 to 25% and average permeability ranging from 100 md to more than one Darcy (Longacre and Ginger, 1987). The microfacies analysis of the Ratawi zone recognized two reservoir units, each with different reservoir lithofacies and controlling porosity types, but the porosity of both reservoir units originated by near-surface processes.

Reservoir unit D is controlled by primary intergranular porosity of the shallow ramp sand-body, whereas reservoir unit E is controlled by secondary diagenetic porosity formed during subaerial exposure at the 2<sup>nd</sup> order sequence boundary. The geometries of reservoir unit D, and unit E depend on the nature of their porosities, which are mainly controlled by depositional and diagenetic subaerial exposure environments.

There are two factors which account for the existence of the high porosity of the Ratawi zone at the Wafra oilfield: (1) preservation of the near-surface porosity, and (2) deep burial diagenetic enhancement of the near-surface porosity and creation of new porosity by acidic fluids, and fracturing. The possible processes for the first factor are examined under two headings, Ratawi porosity preservation by reduction of compaction (Section 4.3.4.4.1), and Ratawi porosity preservation by reduction of cementation (Section 4.3.4.4.2). The second factor is examined in the burial diagenetic environment (Section 4.3.4).

##### 4.3.4.4.1 Ratawi porosity preservation by reduction of compaction

This study has inferred three possible processes which could reduce the effect of compaction in the Ratawi zone. The first process is early lithification and mineral stabilization (Section 4.3.4.2.1). The preservation of the depositional intergranular porosity of reservoir unit-D from burial compaction is by early lithification through precipitation of meteoric cement during a brief period of subaerial exposure. This also stabilized the mineralogy, and aragonite and high Mg-calcite changed to low Mg-calcite. With reservoir unit-E, secondary diagenetic rootlet porosity and stable minerals formed during a long period of subaerial exposure that is interpreted in this



study to be a 2<sup>nd</sup> order sequence boundary.

The second process is early hydrocarbon emplacement (Section 4.3.4.2.2). The development of the Wafra anticlinal structure may have been critical in permitting early oil migration into a growing structure and so preserved the reservoir quality by halting diagenesis. The Wafra structure, as other 'Arabian Folds' in Kuwait and Saudi Arabia, became active as early as the Jurassic and continued to developed until the early Tertiary, as evidence from structure contour maps (Bou Rabee, 1996). The evidence for the development of 'Arabian Folds' from the Ratawi zone at Wafra oilfield is the thinning of the reservoir and non-reservoir units over the Wafra main area antecedent structure and facies changes on the crest and flank of the structure (Longacre and Ginger, 1987) (see Fig. 2-8 and 2-9).

The Lower Cretaceous source rocks in the study area, Makhul (Sulaiy), Minagish (Ratawi Oolite Member) and Zubair formations, subsided without major anomalies in burial rate or heatflow. They then entered the oil window during the Late Cretaceous and Early Tertiary, whereas oil expulsion occurred throughout Tertiary time. Quantification of expelled oil volumes suggests that the Makhul Formation was the most productive source rock in Kuwait (Abdullah *et al.*, 1997). These data indicate hydrocarbon generation and migration from the Makhul source rock juxtaposed to the Ratawi zone and accumulation in the growing anticlinal structure started during the Late Cretaceous.

The last process is structure growth and unconformity formation (Section 4.3.4.2.3). The Wafra structure was continuously developing from the early Jurassic up to the recent time (Bou-Rabee, 1996). In addition, the regional unconformity during the end of the Lower, Middle and Upper Cretaceous in the study area (Alsharhan and Nairn, 1997) could have reduced the effect of the overburden stress by providing periods of possible elastic rebound of the rock.

#### **4.3.4.4.2 Ratawi porosity preservation by reduction of cementation**

This study has inferred five possible processes, which could have reduced the effect of cementation in the Ratawi zone. The first process is the absence of a source of carbonate cement (Section 4.3.4.1.1). The Ratawi Formation was deposited in a restricted depositional environment at a time of calcite sea in the Lower Cretaceous (Tucker and Wright, 1990). This could have led to a lower rate of marine cementation compared to the relatively fast rates of modern aragonite cementation under conditions



of strong marine water circulation. The low percentage of aragonite particles, skeletal and non-skeletal within the Ratawi, could have lead to limited cement sources during subaerial meteoric mineral stabilization.

The second process is the isolation of the reservoir from the carbonate cement source (Section 4.3.4.<sup>2</sup>1.2). The Ratawi Formation consists of three members; the Ratawi Oolite, the lower member, is shallow-water carbonate, whereas the second and the third members, Ratawi Limestone and Ratawi Shale, are interpreted in this study to be part of a drowning sequence. According to Murris (1980) the last two represent a regional seal. This extensive seal at the top of the Ratawi zone could have protected the porosity of the reservoir from late cementation by fresh water.

The third process is reduced fluid mobility by early emplacement of hydrocarbons (Section 4.3.4.2.3). As explained in the previous section, oil generation and migration from source rock to Ratawi reservoir started during the Late Cretaceous. Early oil emplacement in the trap could have reduced the flow of formation water and reduced cementation in the Ratawi oil-saturated zone.

The fourth process is high brine concentration in formation water (Section 4.3.4.<sup>2</sup>1.4). The Upper Jurassic in the study area is characterized by a thick sequence of evaporites rock of the Gotnia Formation. This could have lead to high brine concentrations in the formation waters of the Lower Cretaceous Ratawi Formation, which could have interfered with cement mineral solubility and slowed the precipitation of cement.

The last process is carboxylic acids in formation water (Section 4.3.4.<sup>2</sup>1.5). This process could be the most significant process for the preservation of the near-surface Ratawi porosity (depositional and early diagenetic) during burial and deep burial enhancement of the porosity by dissolution. As mentioned before, the source rocks for the Ratawi oil system entered the oil window during Late Cretaceous and Early Tertiary (Abdullah *et al.*, 1997). This could indicate that the Ratawi source rock started to generate carboxylic acids, which migrated into Ratawi formation water from the Middle Cretaceous. This process could have lead to lower alkalinity of formation water; between 80 to 120°C, carbonate dissolution or lack of carbonate cement precipitation would result (Surdam *et al.*, 1989).



## **4.4 Ratawi sequence stratigraphy and porosity development**

### **4.4.1 Introduction**

Porosity and permeability are largely controlled by two factors: (1) the original fabric and composition of the sediments, and (2) the subsequent diagenetic processes. The prediction of porosity in a reservoir is important for exploration as well as development; there are different approaches to construct models to predict carbonate porosity with depth. The models can be used in two main ways: (1) to provide standards, which are used as a tool to estimate porosity prior to drilling, and (2) to identify anomalies with higher porosity than the average, which allow the focusing of attention on specific factors that act to preserve near-surface porosity (Section 4.3.4), and create new secondary porosity at depth (Section 4.2.4.4) (Scholle and Halley, 1985).

### **4.4.2 Methods to predict porosity with depth**

According to Horbury and Robinson (1993) there are three main methods for predicting carbonate porosity with depth: (1) correlation between porosity and depth or maturity (Section 4.4.2.1), (2) predicting porosity by chemical modelling (Section 4.4.2.2), and (3) predicting porosity in the framework of sequence stratigraphy (Section 4.4.2.3). The last approach, which is one of the major aims of this study, is considered by Horbury and Robinson (1993) to be intermediate between the first approach of straightforward porosity-depth plots, and the second more theoretical chemical approach.

#### **4.4.2.1 Porosity-depth or maturity correlation model**

The destruction of porosity is the dominant trend of porosity evolution in carbonates with increasing burial depth. The influence of burial diagenetic history on carbonate porosity evolution commonly is illustrated by porosity-loss curves (Fig. 4-29), in which porosity is plotted versus depth (Halley and Schmoker, 1983; Schmoker, 1984). According to Amthor *et al.* (1994) the variable thermal maturity and increase in temperature, could be a better variable to use than burial depth to correlate with porosity evolution. Generally, carbonate porosity decreases with increasing maturity and increasing temperature; in general the bulk of porosity losses are more rapid in lower porosity rock. Dolomites appear to retain their porosity and permeability much better than limestone during burial, which indicates that dolomites are more resistant to



porosity and permeability reducing processes. The better porosity and permeability of dolomites relative to limestones at greater depths could have economic significance during exploration (Amthor *et al.*, 1994).

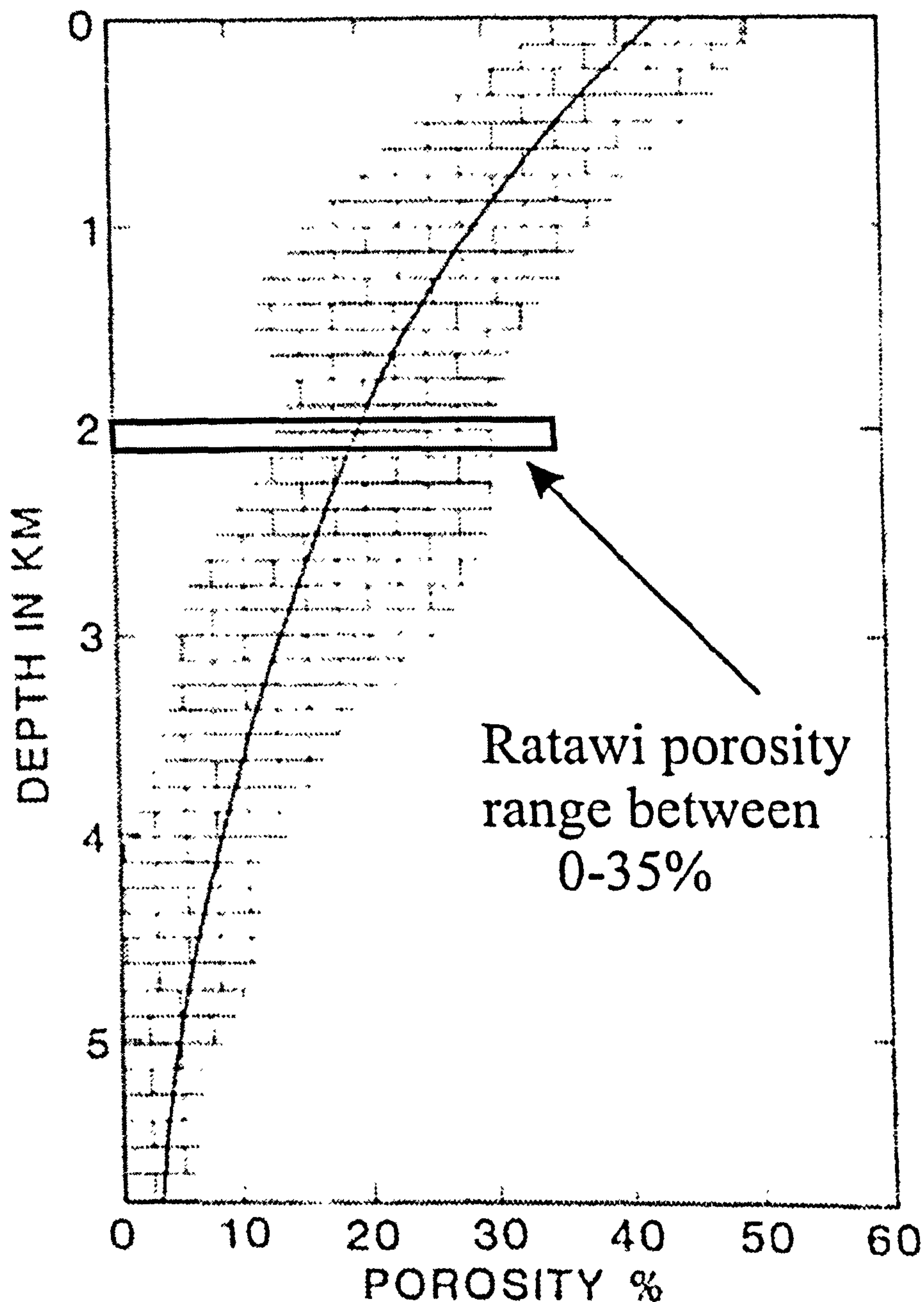


Figure 4-29 Porosity versus depth for carbonate rocks. The curved line is the average and the ornament shows the range (after Tucker and Wright, 1990). Also shown is the depth and porosity range of the Ratawi Formation in the Wafra oilfield.



The relation of carbonate porosity to depth for the Cenozoic and Mesozoic South Florida basin was studied by Schmoker and Halley (1982) who showed that the average porosity for a shallow-water carbonate composite <sup>s</sup>ection for South Florida was reduced by a factor of two at a depth interval of about 1740 m (5700 ft). Deep-water carbonate shows a greater rate of porosity loss with depth. The study concluded that the regional porosity relations in South Florida are not primarily dependent upon the imprint of the highly variable depositional environments and near-surface diagenetic environments, but relate instead to more predictable parameters of burial depth. This regional porosity-depth relation could represent a general basic property of carbonate rocks. Schmoker and Halley (1982) suggested a change in the study of carbonate porosity from an emphasis on examining the pattern between early history and porosity 'evolution' to examining the pattern between early history and porosity 'preservation' in the subsurface.

The regional porosity trend of the Ratawi Formation at the Ratawi reservoir burial depth can be inferred by correlating the Ratawi depth to the porosity-depth curves for the Mesozoic carbonates of South Florida (Schmoker and Halley, 1982). The average depth of the Ratawi zone at Wafra oilfield is 2074 m (6800 ft) and porosity ranges from 18 % to 25 %, whereas the regional porosity at a similar depth from the porosity-depth curves is less than 18 %. This indicates that the Ratawi reservoir is an anomaly, with a higher porosity than the standard regional porosity trend; thus this study should focus on factors that act to preserve the Ratawi near-surface porosity and create new secondary porosity at depth.

#### 4.4.2.2 Porosity-diagenesis and the chemical model

As mentioned in the introduction, porosity depends on depositional and <sup>abric / texture</sup> subsequent diagenesis. The second approach, porosity-diagenesis and the chemical model, predicts porosity by predicting the processes of diagenesis. The chemical models interpret and predict the processes responsible for diagenesis by assuming theoretically the cause of the dissolution-precipitation processes, and calculating water flow through the burial history of the sediment and subsequent dissolution-precipitation processes. However, these models assume a closed chemical system, which is not usually the case (Horbury and Robinson, 1993). Ratawi diagenetic processes did not take place in a closed chemical system, but were a response to the evolution of the Arabian basin, which included basin tectonics, heat flow, palaeoclimate and eustatic sea-level changes.



These processes can be evaluated within the framework of sequence stratigraphy, as discussed in the next section.

#### 4.4.2.3 Porosity-diagenesis and sequence stratigraphy

Early near-surface diagenesis is important in the evolution of carbonate porosity. Near-surface diagenesis, which includes marine and subaerial exposure, generally has a greater impact on porosity development, and therefore reservoir heterogeneity, than deep diagenetic processes, because the water / rock ratio during subaerial exposure with meteoric flushing and repeated seawater inundation is much larger than that experienced during deep burial conditions. Near-surface diagenesis influences the subsequent diagenetic pathways and porosity evolution (Kupecz *et al.*, 1997). Carbonate porosity can be predicted by studying the near-surface diagenesis in the framework of sequence stratigraphy (Fig 4-15 and 4-30) (Read and Horbury, 1993; Tucker, 1993; Sun and Wright, 1998).

### DIAGENESIS AND ICEHOUSE-GREENHOUSE EPISODES

#### During icehouse times (Permo-Carboniferous, Quaternary):

greater amplitude of sea-level changes (up to 100m), more rapid sea-level changes, higher rate of porefluid movements through platforms.

Consequences: deeper karsts at sequence boundaries and unconformities, deeper meteoric leaching from unconformities, more mixing-zone-related/reflux dolomitization during late highstand and lowstand of sea-level, more marine cementation and dolomitization during transgressive times.

#### During greenhouse times (Cambrian-Carboniferous, Triassic-Cretaceous):

smaller amplitude of sea-level changes (<5m), slower sea-level changes, sluggish pore-fluid movements through platforms.

Consequences: minor karsts at parasequence boundaries, most diagenetic processes near-surface, e.g. supratidal dolomitization, shallow meteoric leaching.

Figure 4-30 General diagenetic model during icehouse-greenhouse episodes in the framework of sequence stratigraphy (Tucker, 1998).

The petrographic study in Sections 3.3 and 3.4 indicates that in the Ratawi zone at well R-50, the main controlling porosity type in reservoir unit-D is depositional interparticle porosity, whereas in unit-E it is calcrete porosity formed during subaerial exposure (Section 4.3.3.5). The preservation of the depositional porosity is also



controlled by short periods of subaerial exposure that precipitate the meteoric bladed cement (Section 4.3.3.2.1) and stabilizes the mineralogy before deep burial. The duration of the subaerial exposure is one of the factors that controls Ratawi stratigraphy, as well as the nature and intensity of subaerial exposure. The Ratawi sequence stratigraphic model presented in Chapter 5 can be used to predict the duration, the diagenetic pattern, and porosity development during the subaerial exposure, when integrated with palaeoclimate and carbonate sediment mineralogy (Section 4.3.3.5) (Read and Horbury, 1993; Tucker, 1993). However, the model does not predict near-surface porosity preservation during burial (Section 4.3.4) which must be integrated and analyzed within the framework of the Ratawi sequence stratigraphic model.

This study interprets and predicts the Ratawi reservoir and seal geometry and stratigraphic succession at Wafra oilfield by integrating two models: the Ratawi epeiric ramp model with sand-bodies, and the Ratawi diagenetic processes-products model, within the framework of the Ratawi sequence stratigraphic model. The stratigraphic position and geometry, and distribution of porosity in three dimensions in reservoir unit-E is controlled by the development of the calcrete fabrics (Section <sup>3.4.3</sup>~~4.3.3.5~~) at the 2<sup>nd</sup> order sequence boundary. this could explain the development of this unit in the main, southern and eastern Wafra areas.

The stratigraphic position of reservoir unit-D is controlled by the initiation, development and termination of the 'Ratawi Oolite platform' (Section 3.5), and the geometry and distribution of porosity in three dimensions, is controlled by the ramp sand-body model (Section 3.5.2). The stratigraphic position of the regional seal unit, Ratawi Limestone and Ratawi Shale, for the Ratawi zone at Wafra oilfield is controlled by the termination of the 'Ratawi Oolite platform' by a deepening succession, resulting from a rapid sea-level rise at the start of a new 2<sup>nd</sup> order sequence and decrease in carbonate sediment supply, discussed in Chapter 5 and 6.

#### **4.5 Summary**

This chapter has been concerned with the diagenesis and porosity of the Ratawi Formation and shown that diagenesis took place in three diagenetic environments, the marine, meteoric-pedogenic and burial realm. High porosity zones occur within shallow-ramp grainstone (controlled mainly by interparticle depositional primary porosity) and back-ramp packstone-wackestone with porosities enhanced by exposure-



related diagenesis. The near-surface porosity (depositional and diagenetic) preserved at the reservoir depth by early hydrocarbon migration to the antecedent Wafra structure, and was enhanced by the formation of burial porosity, burial vugs and fractures.

Dolomitization was not a major process in the Ratawi, but early dissolution of dolomite during the dedolomitization process and the formation of dolomite rhomb moulds (dedolomite porosity) has enhanced the porosity within the Ratawi zone. The different flow-units in the Ratawi zone at the Wafra oilfield (Units C, D, E and F) can be interpreted by integration of the Ratawi depositional model (Chapter 3), controlling the depositional porosity, and diagenetic model (this Chapter), controlling the diagenetic porosity, in the framework of sequence stratigraphy (discussed in Chapters 5 and 6). The flow-units (with primary and secondary porosity) are associated with the development of carbonate sand-bodies and with a major unconformity (type 1 unconformity associated with a 2<sup>nd</sup> order sequence boundary) during the initiation and development of the Ratawi platform. The regional seal, the Ratawi Limestone, is associated with the deposition of a deepening-upward drowning succession (type 3 unconformity) associated with the termination of the platform.



## **Chapter 5 Cycles and sequences in the Ratawi Formation and regional patterns**

### **5.1 Introduction**

The twelve microfacies of the Ratawi Formation, defined from core samples of Ratawi Oolite and Ratawi Limestone, were grouped into four broad facies belts, deep ramp, shallow ramp, back ramp, and ramp subaerial exposure (see Chapter 3). Each of these facies belts can be interpreted and predicted through the depositional facies model. The association of these facies belts creates the Ratawi facies tract and depositional system, which is the assemblage of lithofacies in three dimensions. The composition and architecture of the Ratawi facies tracts and depositional system exhibit systematic variations that can be related to variations in two factors: (1) stratigraphic processes that include accommodation space and sediment supply and (2) sedimentological processes that include Ratawi platform type and geological age, in the lower Cretaceous greenhouse period (Fitchen, 1997).

The initiation, development and termination of the 'Ratawi Oolite platform' that control the primary depositional porosity of the carbonate sand-body of reservoir unit-A, unit-B, unit-C and unit-D and the second-order sequence boundary that controls the subaerial exposure diagenesis and secondary diagenetic porosity of reservoir unit-E, in addition to regional source and seal rocks, can be modelled, interpreted and predicted within chronostratigraphic units. The significance of the construction of a Ratawi chronostratigraphic hierarchy framework is not so much the origin or exact duration but rather the recognition that a hierarchy with different scales of stratal units exists and can be used to predict Ratawi stratigraphic correlation and facies distributions beyond well-control points at Wafra oilfield (Kerans and Tinker, 1997; Fitchen, 1997).

Ratawi lithofacies and facies tracts migrate across the chronostratigraphic units, resulting in changes in stratal geometries and termination pattern of the Ratawi platform, in addition to facies shifts or offsets across bounding surfaces of the parasequence, parasequence set (systems tract), and sequence (Fig. 5-1) (Fitchen, 1997). The Ratawi oil system and reservoir heterogeneity can be studied by analyzing the distribution of Ratawi lithofacies and petrophysical characteristics within a cyclic



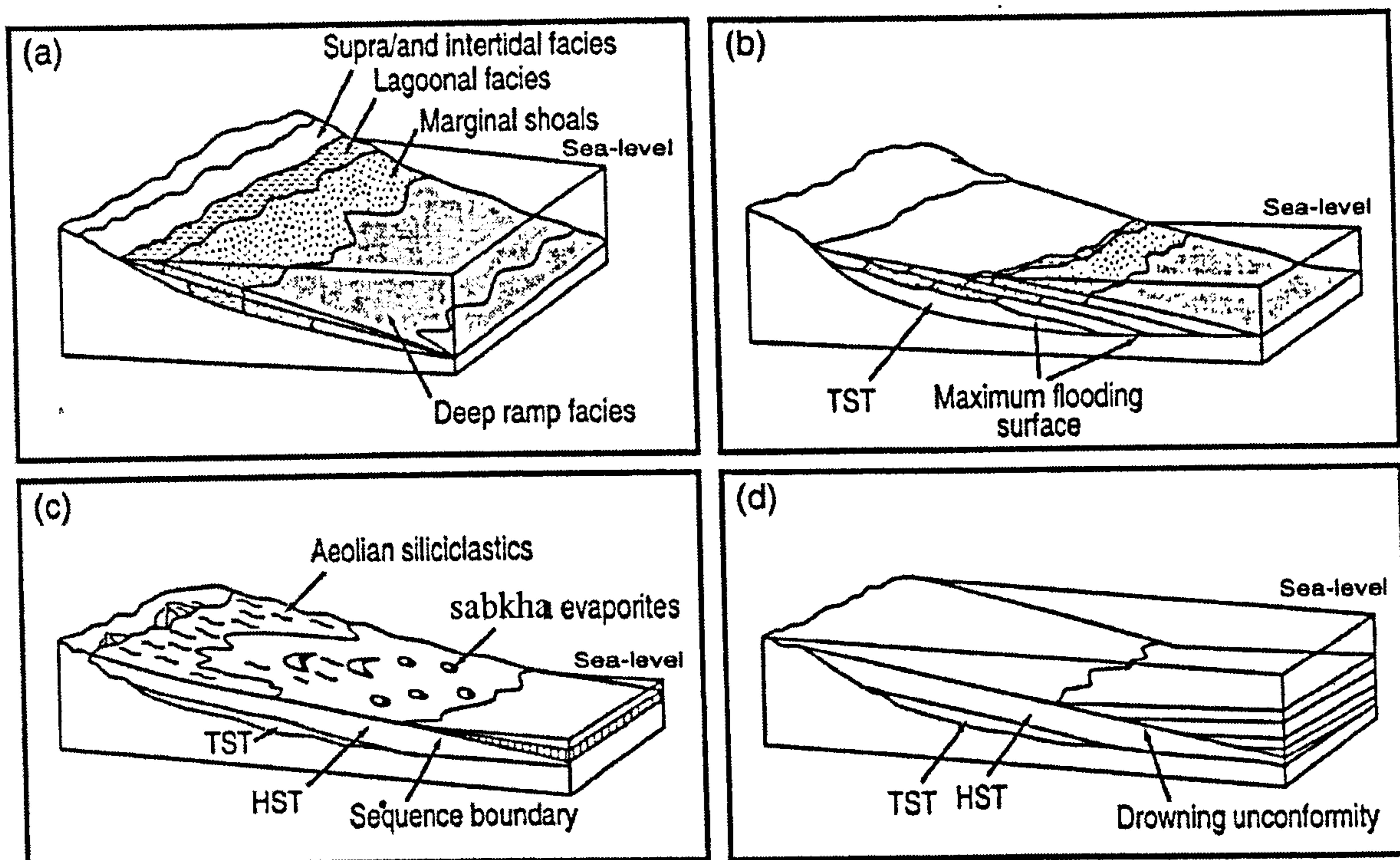


Figure 5-1 Sequence stratigraphic models for ramp systems. (a) transgressive systems tract, (b) highstand systems tract, (c) lowstand systems tract, and (d) drowning unconformity (after Emery and Myers, 1996).

framework of chronostratigraphic units (Kerans and Tinker, 1997).

Sequence stratigraphy is a powerful tool for constructing a chronostratigraphic framework for the Ratawi in which source, reservoir and seal lithofacies can be interpreted and predicted within the idealized genetic packages at different scales. Sequence stratigraphy is the study of genetically related lithofacies within a framework of chronostratigraphic significant surfaces (Van Wagoner *et al.*, 1990). This provides a theoretical basis and methodology for placing Ratawi lithofacies into a chronostratigraphic framework by integrating the available data for this study.

Depending on the type of data available, the level of stratigraphic resolution desired, types of problem to be solved, carbonate sequence stratigraphic analysis can be performed using two main approaches that can be integrated during reservoir development and hydrocarbon exploration (Fitchen, 1997, Harris *et al.*, 1999). The first approach is from seismic lines in which genetic units and seismic sequences are defined on the basis of the large-scale stratal patterns and geometry. This approach can also be applied to large outcrops by the identification of the large-scale stratal patterns and geometry from field work (Hunt and Tucker, 1993). The second approach is from the sedimentology in which the genetic units, parasequence and sequence, are defined



on the basis of their sedimentological and diagenetic data from outcrop, core and well logs that define different chronostratigraphic surfaces (Everts *et al.*, 1995). The second approach is also known as high-resolution stratigraphy, which is in contrast to 'coarse-resolution' of the first approach.

The seismic stratigraphic concept emphasizes single surfaces for sequence boundaries and maximum flooding surfaces, whereas the sedimentological stratigraphic approach suggests that these surfaces could be represented by several cycles (Montanez and Osleger, 1993). The high-resolution framework is fundamental to defining flow units, to interpolating well data, and thereby to modelling fluid flow (Kerans and Tinker 1997). In analyzing the Ratawi Formation, this study used the sedimentological approach to sequence stratigraphy and follows the sequence stratigraphic terminology defined by Lehrmann and Goldhammer (1999).

### **5.1.1 High-resolution sequence stratigraphy and reservoir characterization**

The significance of high-resolution sequence stratigraphy in the Ratawi reservoir study is the analysis of Ratawi facies and petrophysical characteristics in a time-significant context as opposed to a lithostratigraphic context. This allows the construction of a tight chronostratigraphic framework, which is essential for the generation of a porosity-permeability model and prediction of fluid-flow performance (Kerans and Tinker 1997).

The characterization of a carbonate reservoir by applying high-resolution sequence stratigraphy can be accomplished through three main steps (Kerans and Tinker 1997). The first step is one-dimension core and well log analysis; this step has three goals, which are (1) core description and interpretation of cycles and parasequences, (2) identification and interpretation of parasequence-sequence hierarchy by Fischer plot and regional data, and (3) calibration of core data with well-log data to be correlated with uncored wells.

The second step is to produce a two-dimensional cross-section and map analysis, which includes drawing a cross-section for the reservoir zone using key chronostratigraphic surfaces and vertical and lateral stacking of lithofacies systems tracts. The last step is three-dimensional reservoir interwell heterogeneity modelling, which includes inter-well porosity, permeability and saturation distribution in three-dimensions.



The accuracy of the reservoir heterogeneity model depends on the accuracy of the first step, and the construction of a high-resolution stratigraphic framework. Depending on the scope and data available for this study from the Ratawi zone at Wafra oilfield, this chapter discusses in detail the first step; the last step is outside the scope of this study, whereas the second step is discussed in this chapter as a general correlation between well R-49 and R-50.

### **5.1.2 Aims of this chapter**

This chapter has five main aims. The first aim is to define and describe parasequences that occur within the Ratawi Oolite and Ratawi Limestone cored interval in wells R-50 and R-48 (Section 5.2). The second aim is to examine the pattern of Ratawi Formation cycles and interpret its origin (Section 5.3). The third aim is to examine the stacking pattern for the cored interval in wells R-50 and R-48 by constructing and interpreting Fischer plots, and relating Ratawi lithofacies and petrophysical characteristics to the stacking pattern (Section 5.4). The fourth aim is to correlate between log signature and Ratawi core cycles, and surfaces (Section 5.5). The last aim is to correlate between well R-49 and R-50 (Section 5.6).

## **5.2 Ratawi cycles**

### **5.2.1 Introduction**

The twelve Ratawi microfacies, which are recognized in the Ratawi Oolite and Ratawi Limestone core from Wells R-48, R-49 and R-50 (Chapter 3) are arranged into distinct units, and repeated many times in the core succession. These distinct units can be referred to as cycles, cyclothems, rhythms or parasequences (Tucker, 1982). Parasequence is the smallest genetic unit that can be recognized from outcrop and core and is defined by Lehrmann and Goldhammer (1999) as a relatively conformable succession of genetically related beds or bedsets bounded by marine flooding surfaces.

The term parasequence is synonymous to the metre-scale shallowing-upward cycle of James (1979) and Goldhammer *et al.* (1987) and punctuated aggradational cycle of Goodwin and Anderson (1985). The parasequence is the basic building block of a depositional sequence. The developments of the world's largest oil and gas fields are strongly influenced by the textures and arrangement of the parasequences in the reservoir formation (Read and Horbury, 1993).



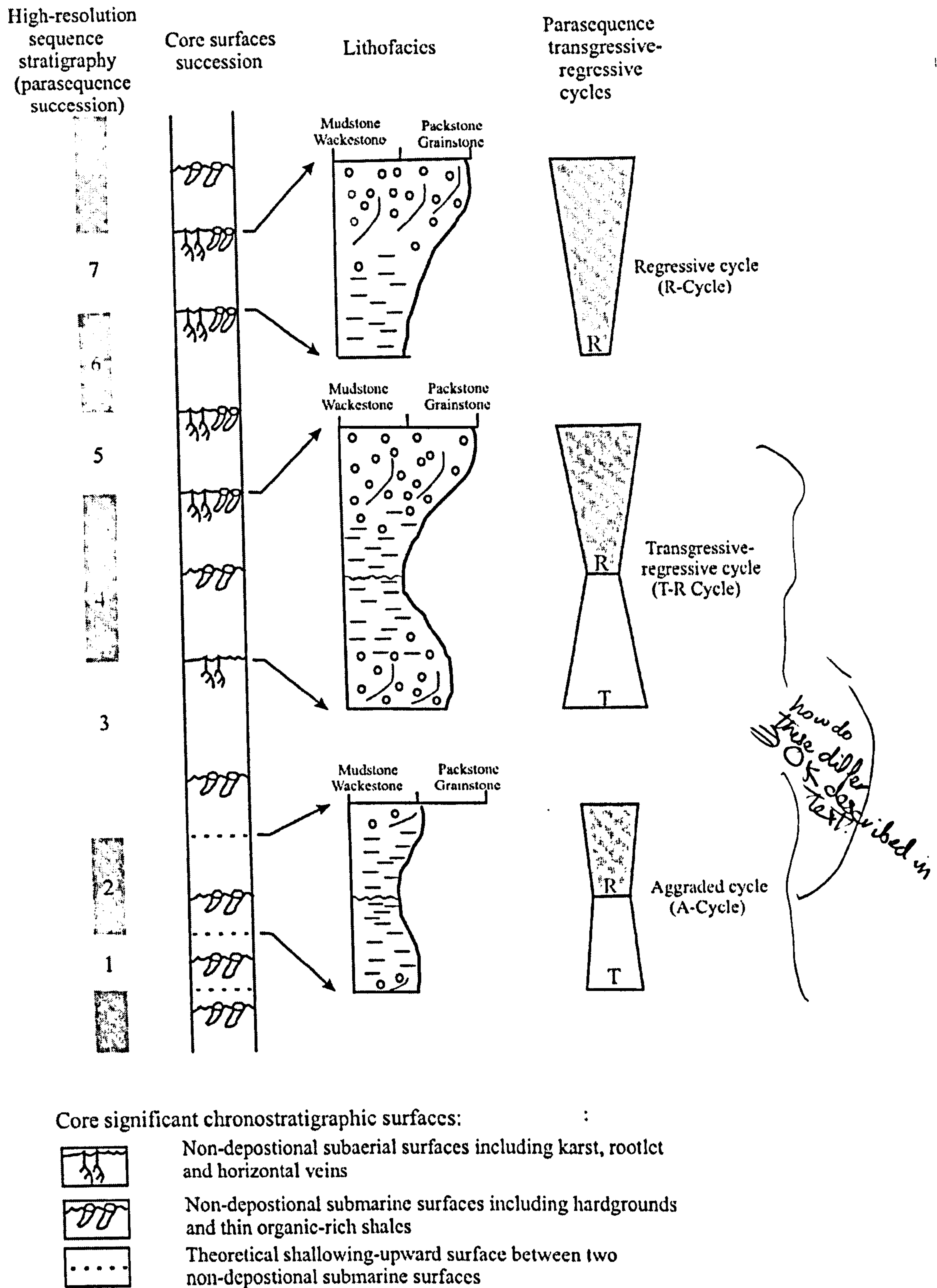


Figure 5-2 Composite idealized parasequence facies types recognized in the Ratawi Formation: regressive cycle (R- Cycle), transgressive-regressive cycle (T-R Cycle) and aggraded cycle (A- Cycle).



The data available for this study are 204 core samples from wells R-48, R-49 and R-50, the core description charts for core wells R-49 and R-50 at a scale of 1 : 50, and different types of well logs for wells R-48, R-49, and R-50, in addition to the author's own observations of the cores in Kuwait.

The core description chart for well R-50 is for 258 ft (79 m) from 6775 ft (2065m) to 7032.42 ft (2143 m) depth; the lower part from 6797.90 ft (2072 m) to 7032.42 ft (2143 m) is in the Ratawi Oolite, whereas the upper part from 6775 ft (2065 m) to 6797.90 ft (2072 m) is in the Ratawi Limestone. The core description chart for well R-48 is for 274 ft (84 m) from 6520 ft (1987 m) to 6794 ft (2071 m) depth in the Ratawi Limestone.

### **5.2.2 Ratawi parasequence style**

Facies and composition of carbonate parasequences vary considerably depending on depositional and early diagenetic environments. Generally, carbonate parasequences can be grouped under two groups (Tucker and Wright, 1990), namely (1) those dominated by carbonate mineralogy, calcite and dolomite; this group includes carbonate shallowing-upward and carbonate-diagenetic cycles, and (2) those with alternating mineralogy, including carbonate-evaporite and carbonate-clastic cycles. All the cycles of the Ratawi Oolite and Ratawi Limestone are carbonate shallowing-upward cycles. The amount of siliciclastic material increases in the Ratawi Limestone, so that the Ratawi Oolite consists of 'clean' carbonate shallowing-upward cycles, whereas the Ratawi Limestone has more 'dirty' carbonate shallowing-upward cycles.

### **5.2.3 Ratawi parasequence boundaries and types**

This section examines the depositional and early diagenetic criteria used to define breaks in the Ratawi succession that probably represent significant chronostratigraphic surfaces, as seen in the cores (Fig.5-2). Two types of surface are recognized:

- (1) non-depositional subaerial surfaces, including karst, rootlets and horizontal veins; the origin of these surfaces is discussed in Section 3.4.3.3.
- (2) non-depositional submarine surfaces, including hardgrounds and firmgrounds; the origin of these surfaces is discussed in Section 4.2.2.5.

Thin organic-rich shales in the cores are taken to indicate non-depositional surfaces formed in restricted relatively deep water. When there is no depositional and



early diagenetic evidence to indicate a break in sedimentation in a thick interval, an abrupt grain-size change is used to infer a break in sedimentation in the subtidal environment. The different types of surface and their depth distinguished in this study in wells R-48 and R-50 are listed in Appendix 2.

From the core study, 84 carbonate shallowing-upward parasequence cycles were identified, each beginning with a marine flooding surface and ending with the marine flooding surface of the next cycle. Marine flooding surface is defined by Van Wagoner *et al.* (1990) as a surface that separates younger from older strata, across which there is evidence of an abrupt increase in water depth. The cored interval at well R-50 contains 20 cycles, whereas the core interval in well R-48 contains 64 cycles (Appendix 2).

### **5.3 Ratawi Formation cycles**

Defining a hierarchy of cycles is considered by Kerans and Tinker (1997) and others to be the basic step for constructing a stratigraphic framework, in which parasequence is the fundamental chronostratigraphic building block. Sequence stratigraphic units used in this study are parasequence, systems tract, greenhouse sequence and composite sequence, as defined by Lehrmann and Goldhammer (1999). These units are genetically related packages, of fifth (0.01 – 0.1 my), fourth (0.1 – 1 my), third (1 – 10 my), second (10 – 100 my) and first (> 100 my) order eustatic / tectonic-eustatic cycles (Fig. 5-3). The first two orders of cycle can be produced by Milankovitch rhythms and glacio-eustasy (Tucker and Wright, 1990).

## **HIERARCHY OF RELATIVE SEA-LEVEL CHANGE**

**1<sup>st</sup>-order** tectonoeustasy / sea-floor spreading rates, supercontinent breakup / formation

**2<sup>nd</sup>-order** basin-forming processes, rifting, subsidence, tectonoeustasy

**3<sup>rd</sup>-order** tectonoeustasy, intraplate stress changes, glacioeustasy

**4<sup>th</sup>-order** glacioeustasy, tectonics, sedimentary processes / autocyclicity

**5<sup>th</sup>-order** glacioeustasy, tectonics, sedimentary processes / autocyclicity

Figure 5-3 Processes controlling the hierarchy of relative sea-level changes (after Tucker, 1991).



Carbonate cycles are controlled by many factors including relative change in sea level, sedimentation rate, climate, water quality, tectonic setting, antecedent topography, and evolution of carbonate-secreting organisms. The most important factor is relative change in sea level, and accommodation space, which is recorded in the form of a hierarchy of genetic units (Read *et al.*, 1995; Lehrmann and Goldhammer, 1999).

Parasequences (5<sup>th</sup> order cycles) in the Ratawi Formation are interpreted in this section, whereas the origin of the systems tracts (4<sup>th</sup> order cycles), greenhouse sequences (3<sup>rd</sup> order cycles) and composite sequences (2<sup>nd</sup> order cycles) are interpreted in Section 5.4 on the Ratawi stacking pattern, and in Chapter 6 Ratawi sequence stratigraphic model. The origin of the Ratawi parasequences is investigated under three headings: the Ratawi peritidal and subtidal parasequences (Section 5.3.1), Ratawi parasequence symmetry (Section 5.3.2) and Ratawi Oolite and Ratawi Limestone cycles (Section 5.3.3).

### **5.3.1 Ratawi peritidal and subtidal parasequences**

There are two types of parasequence in the Ratawi Formation. The first type is a peritidal parasequence, defined by the upper surface of the cycle with evidence of subaerial exposure, indicating that all the available accommodation space is filled by sediment. The second type is a subtidal parasequence, defined by the upper surface of the cycle without any evidence of subaerial exposure, indicating subtidal deposition and not all the available accommodation space being filled by sediment. Autocyclic and allocyclic models (Fig. 5-4) could be used to interpret the origin of these two Ratawi parasequence types.

The autocyclic model is driven by internal mechanisms of depositional processes and fluctuations in sediment supply or production. This includes the tidal flat progradation model (Ginsburg, 1971), tidal island model (Pratt and James, 1986), and lateral migration of tidal channels (Kozar *et al.* 1990). Detailed core and petrographic analysis for each cycle in the core succession is required to identify which model forms the Ratawi parasequences. Peritidal parasequences formed by the allocyclic model are characterized by early diagenetic subaerial features superimposed on subtidal facies. The available data for this study are not enough to make this distinction.



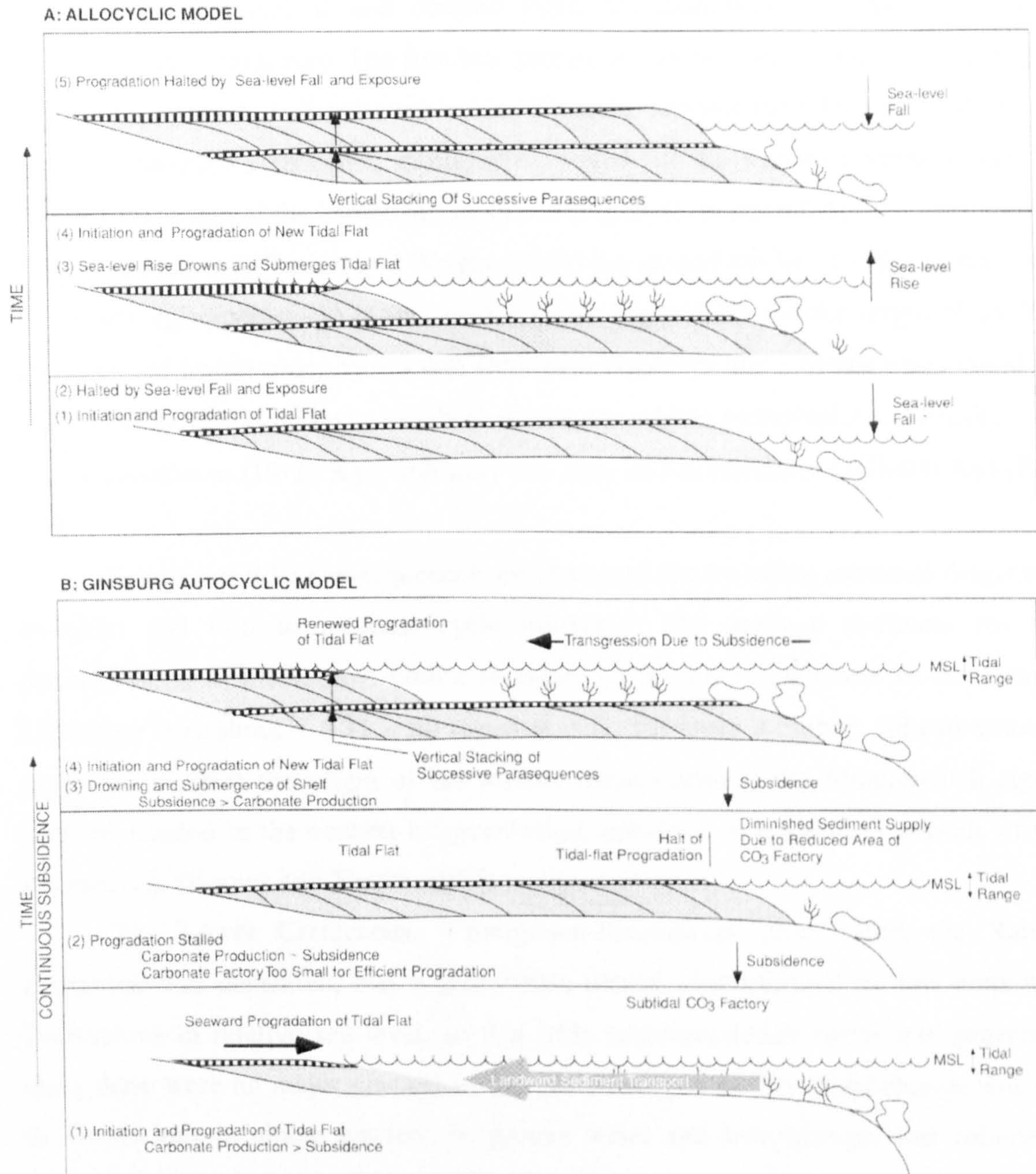


Figure 5-4 Allocyclic (A) and autocyclic (B) models for the genesis of parasequences (after Lehrmann and Goldhammer, 1999).

The distinction between autocyclic and allocyclic models could have an impact on reservoir characterization and development. Parasequences formed by allocyclic processes generally have a greater lateral continuity than parasequences formed by the autocyclic model. However, at the scale of the Wafra oilfield, a parasequence formed by tidal flat progradation would have a higher lateral continuity than a parasequence formed by the tidal island model (Lehrmann and Goldhammer, 1999).

Subsidence through tectonic processes include thermal subsidence of the crust after rifting, changes in rates of sea-floor spreading (tectono-eustasy), in-plate stress



changes after continental and oceanic plate rearrangement, and synsedimentary faulting (jerky subsidence). The first two processes can be used to interpret the origin of 2<sup>nd</sup> order cycles and 1<sup>st</sup> order sub-cycles. Episodic tectonic subsidence is used in this study to construct a sequence stratigraphic model for the Ratawi Formation and to interpret the origin of the composite sequence (Fig. 5-3) (Section 6.4).

According to Tucker and Wright (1990) the second model, changes in sea level by climate (glacio-eustasy) is the most popular explanation for the origin of cycles. The fifth and fourth-order cycles that form parasequences and systems tracts could be controlled by glacio-eustasy, which is driven by orbital perturbations, Milankovitch cycles, precession (19-23 Ky), obliquity (41 Ky), and eccentricity (100-400 Ky) (Fig. 5-5).

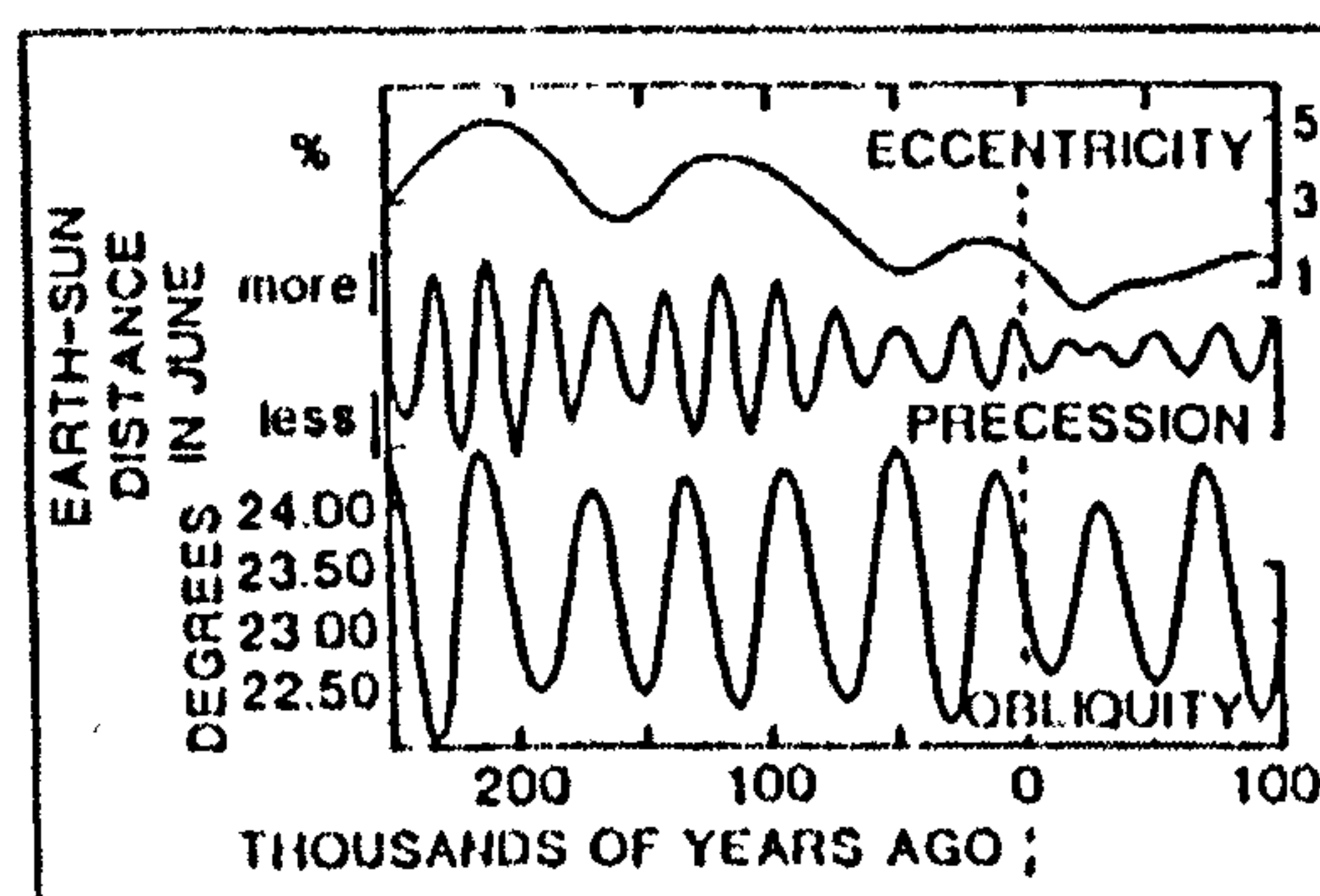
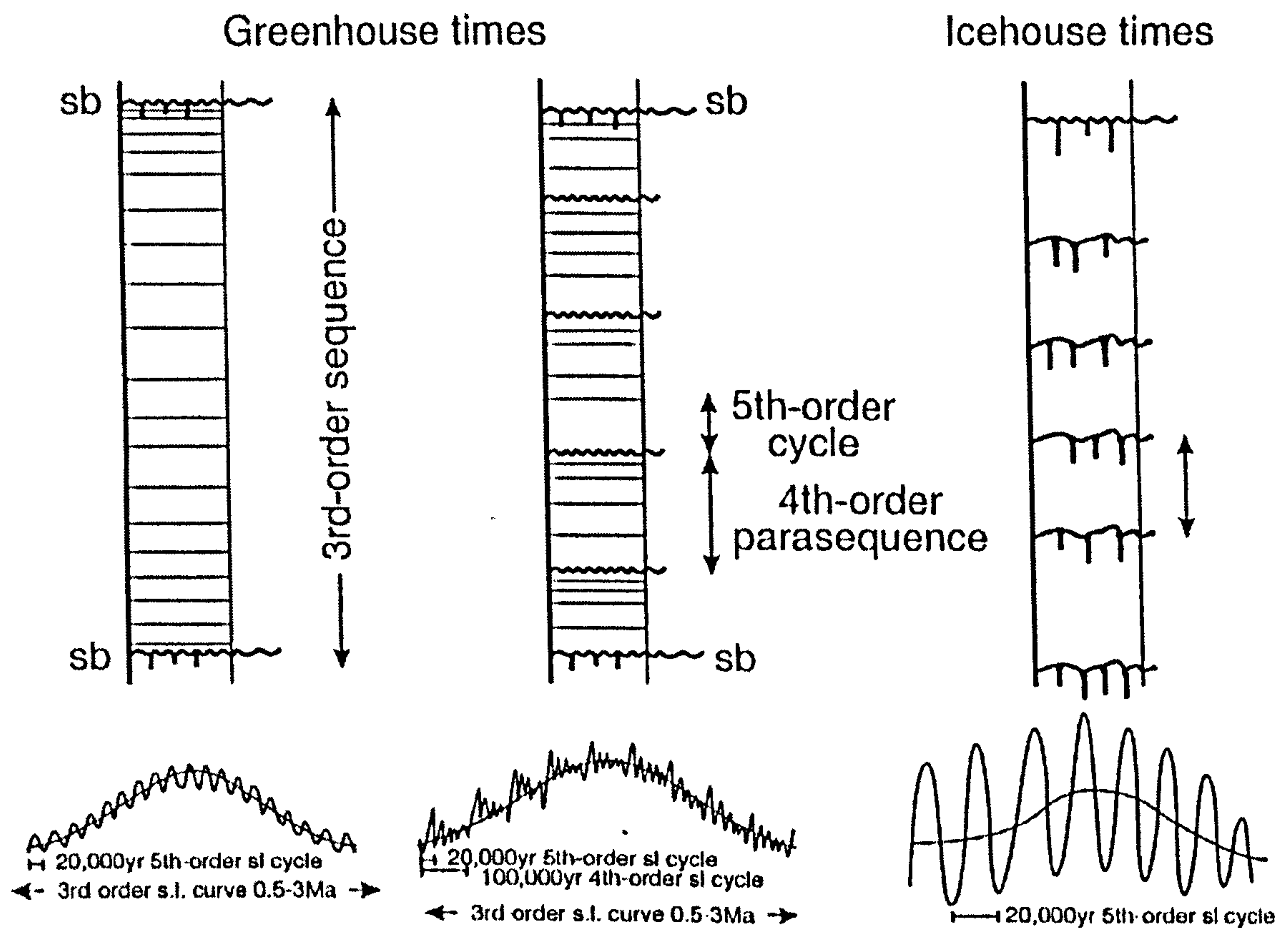
Ratawi peritidal parasequences are characterized by minor subaerial diagenetic overprint and thin to medium cycle thickness. The average thickness for the parasequences in the Ratawi Oolite is about 15 ft (4.6 m) whereas in the Ratawi Limestone it is about 4 ft (1.2 m) (Section 5.3). To apply a climate (glacio-eustasy) model to interpret the origin of the Ratawi parasequences, the Milankovitch signal must be studied in the context of greenhouse, transition and icehouse periods of the Phanerozoic (Kerans and Tinker, 1997).

The Lower Cretaceous, Valanginian-Hauterivian time, when the Ratawi Formation was deposited, was a greenhouse period, characterized by low amplitude fluctuations in relative sea level, so that little accommodation space was generated, since there were no major glaciers in this period (Fig. 5-6). Sea-level change was due to fluctuations in alpine glaciers, in ground water and lake storage, and volume of ocean water (Tucker and Wright, 1990).

This period was characterized by small volumes of water removed from and released to the oceans by 4<sup>th</sup> / 5<sup>th</sup> order astronomic insolation cycles, so that the low-frequency (third-order) sea-level cycle has a higher amplitude than the fourth- and fifth- order sea-level cycles. Due to weak stratigraphic forcing, the formation of parasequences by autocyclic processes during a greenhouse period may be more common than during an icehouse period (Lehrmann and Goldhammer, 1999).

Price (1999) reviewed evidence for polar ice during the Mesozoic period (Fig. 5-7), which represents the longest period of warm climate during the Phanerozoic. He suggested four episodes of cold or sub-freezing polar climates, which are, Bajocian-Bathonian, Tithonian, Valanginian and Aptian. These four periods were characterized





*Milankovitch rhythms of the last 250 000 years*

Figure 5-5 General stacking patterns for the parasequence during icehouse-greenhouse episodes (Tucker and Wright, 1990).



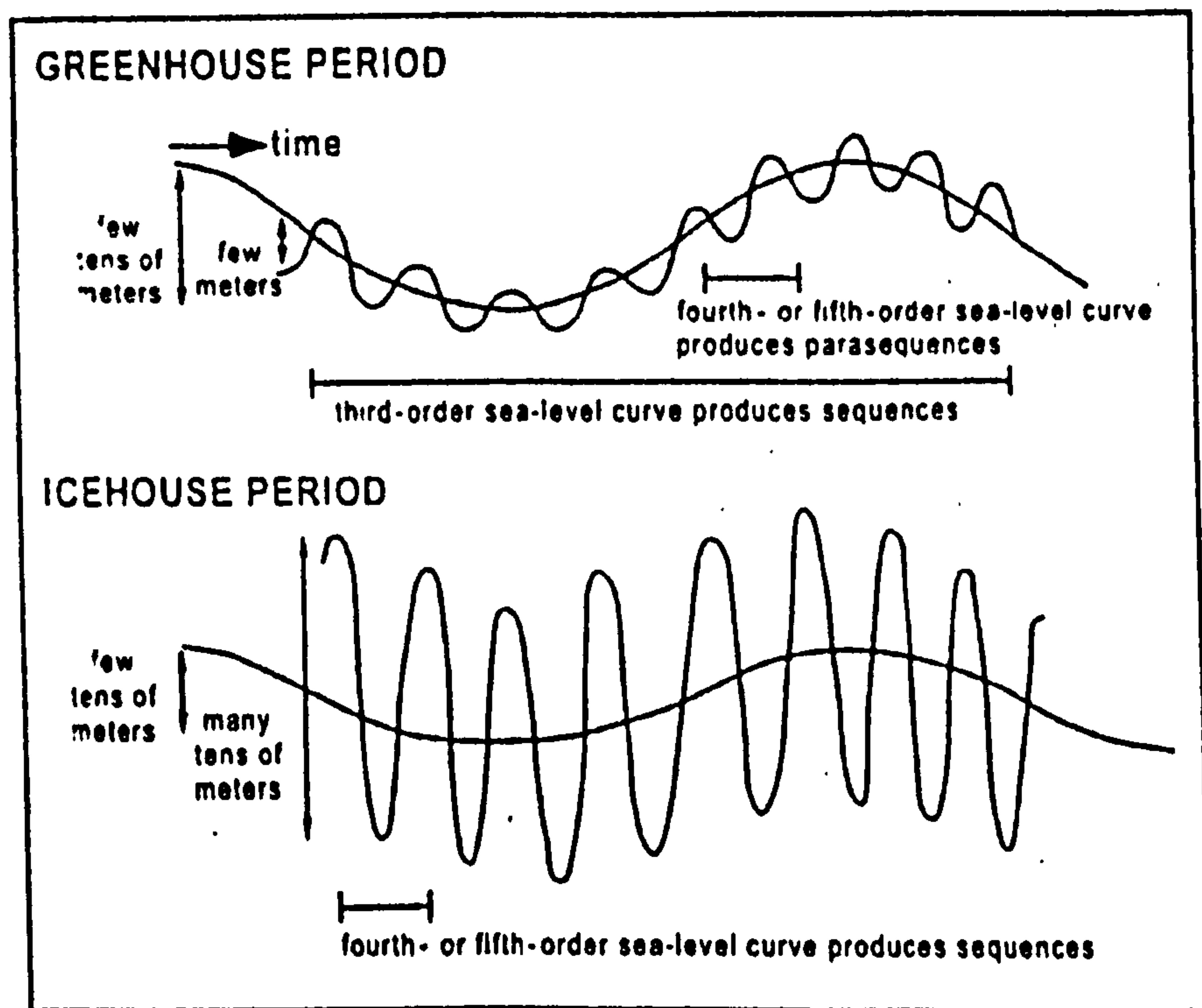
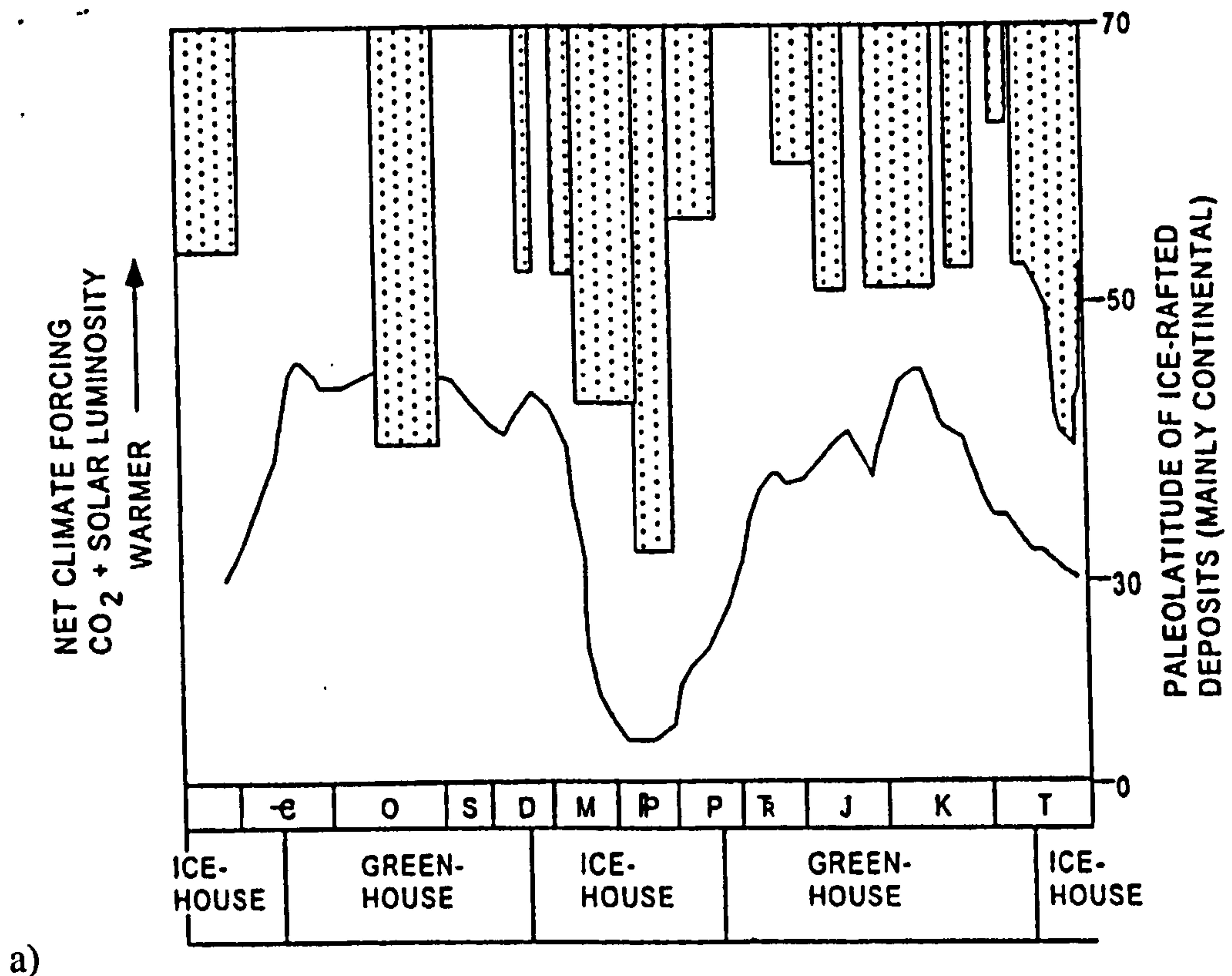


Figure 5-6 Greenhouse and icehouse periods have different climatic forcing effecting the nature of sea-level changes. (a) Secular changes in climate from climate models and palaeolatitude of ice-rafted deposits. (b) Schematic illustration of differences in signature of sea-level fluctuations; greenhouse periods are shown with low-amplitude, high-frequency sea-level fluctuations, whereas icehouse periods are shown with high-amplitude, high-frequency fluctuations (after Lehrmann and Goldhammer, 1999). Note the lower Cretaceous Ratawi Formation was deposited in a greenhouse period characterized by low-amplitude, high-frequency sea-level fluctuations.



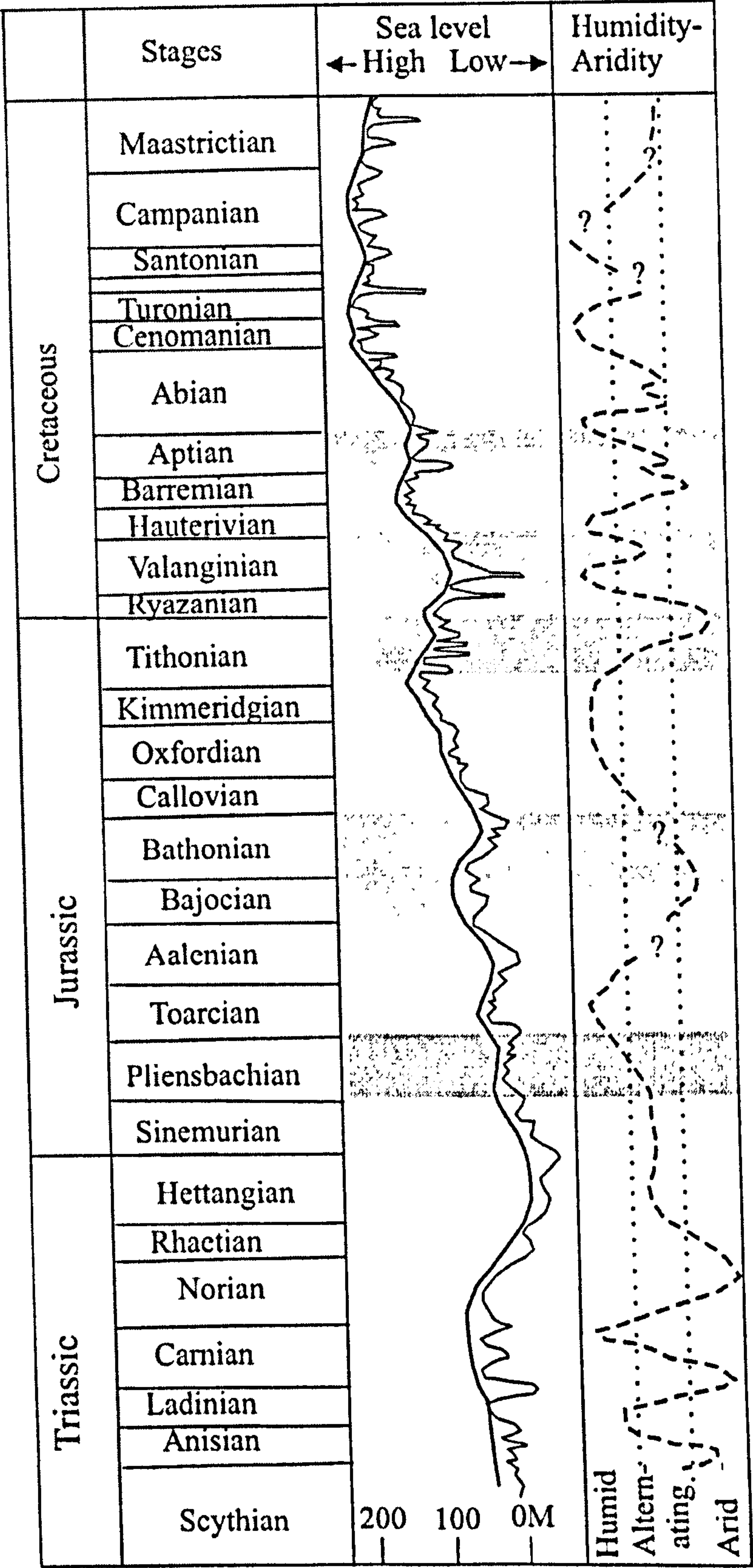


Figure 5-7 Sea level and aridity-humidity cycles during the Mesozoic; showing the four 'little' ice ages during the greenhouse period of the Mesozoic (after Price, 1999). Note the Valanginian stage during the deposition of the Ratawi Oolite was characterized by 'little' ice ages, whereas the Hauterivian stage during the deposition of the Ratawi Limestone and Ratawi Shale were without.



by 'little icehouse' with 'small' ice caps, about one-third the size of the present ice caps, largely restricted to continental interiors. Waxing and waning of the ice caps during the 'little icehouse' periods could have produced larger sea-level fluctuations than the periods without.

The lower member of the Ratawi Formation, the Ratawi Oolite, is inferred in this study to have been deposited in the Valanginian, whereas the middle member the Ratawi Limestone was deposited in the Hauterivian. Price's (1999) suggestion of a 'little icehouse' during the Valanginian period is used in this study to explain the thicker parasequences and higher percentage of peritidal parasequences in the Ratawi Oolite compared to the Ratawi Limestone.

### **5.3.2 Ratawi parasequence symmetry**

Changes in the Ratawi environment are expressed in the different types of non-depositional surface. These surfaces are inferred in this study to reflect the vertical development of the Ratawi depositional fabric and petrophysical properties in each parasequence. A shallowing-upward sequence is generally inferred to be a coarsening upward facies trend, increasing the depositional porosity, whereas a deepening-up then shallowing-upward sequence is inferred to start with a fining upward facies, decreasing the depositional porosity before it increases in the shallowing-upward part. Three types of vertical lithofacies evolution can be inferred in the Ratawi parasequences, reflecting the dynamics of the Ratawi depositional environment, (1) regressive cycle (Section 5.3.2.1), (2) transgressive-regressive cycle (Section 5.3.2.2), and (3) aggraded cycle (Section 5.3.2.3).

#### **5.3.2.1 Regressive cycles**

A regressive cycle (R-cycle) (Fig. 5-2) is defined as a simple shallowing-upward succession. The non-depositional submarine surface (interpreted in this study to be formed in the deepest depositional environment) when it is present in the parasequence, is superimposed on the subaerial exposure surface at the bottom of the cycle (e.g. hardground superimposed on a subaerial exposure surface). The R-cycles are found in wells R-48 and R-50 (Table 5.1).

According to Holland *et al.* (1997) this cycle type can be interpreted by the parasequence model of cyclicity of Van Wagoner *et al.* (1990) of a simple shallowing



upward cycle bounded by marine flooding surfaces. The shallowing of the cycle is attributed to either progradation or aggradation under relatively constant sea level, follow the rapid transgression which initiated the cycle. This model is inferred in this study to produce an asymmetric parasequence, of an upward-shallowing lithofacies succession.

### 5.3.2.2 Transgressive-regressive cycles

Transgressive-regressive cycles (T/R-cycle) (Fig. 5-2), which are composed of two parts, a deepening-upward followed by a shallowing-upward succession, are defined in this study by the non-depositional submarine surface which is in the middle of the cycle. This indicates that the lower part of the cycle is transgressive, with deepening-upward facies, whereas the upper part of the cycle is regressive, with shallowing-upward facies. The top surface of the T/R-cycle has evidence of subaerial exposure whereas in an aggraded cycle (A-cycles) there is a shallowing-upward surface without evidence of subaerial exposure (Section 5.3.2.3). T/R-cycles are found in wells R-48 and R-50 (Table 5.1).

According to Holland *et al.* (1997) the deepening-upward transgressive part of these cycles cannot be interpreted by the parasequence model. This model assumes the main control on cycle formation is the change in the rate of accommodation space, relative sea level, and constant carbonate sediment supply that increase after a lag time after the rapid transgression which initiated the cycle. This model can interpret only the simple shallowing cycle of R-cycle type.

Holland *et al.* (1997) recommend the interpretation of T/R-cycles by sequence stratigraphy (Chapter 6) and consider the T/R-cycle as a type of 'high frequency sequence'. They assume the main control on the cycle formation is a change in the rate of accommodation space and carbonate sediment supply. The deepening-upward transgressive part of the T/R-cycle can be interpreted by changing rate of carbonate sediment supply in addition to relative sea level.

This model is inferred in this study to produce symmetric parasequences with an upward-deepening to upward-shallowing lithofacies succession. The symmetry of the parasequence increases basin-ward, with increasing water depth, and accommodation space (Fitchen, 1997); in other words the T/R-cycle is interpreted to have formed in a deeper depositional environment than the R-cycle.



### 5.3.2.3 Aggraded cycles

Aggraded cycles (A-cycle) (Fig. 5-2) are a subtype of the T/R-cycle. The A-cycles are observed in succession of R- and T/R-cycles in cores of wells R-50 and R-48 (Table 1 and Appendix 2). The aggraded cycles are composed of two parts, a deepening-upward followed by a shallowing-upward succession without evidence of subaerial exposure. The lower and upper surfaces of the cycle are theoretically shallowing-upward surfaces, positioned in the middle of two non-depositional submarine surfaces described from the core.

Cycle Type	Number of cycle in core	% of cycles in core	Cycle total thickness in core	Total % in core	Average cycle thickness
Core well R-50 <b>R-Cycle</b>	6	30%	34(ft) (10.4 m)	14%	5.7 ft (1.7 m)
Core well R-48	13	20%	83(ft) (25.3 m)	30%	6.4 ft (1.9 m)
Core well R-50 <b>T/R-Cycle</b>	10	50%	153.5(ft) (46.8 m)	62%	15.4 ft (4.7 m)
Core well R-48	32	50%	133.5(ft) (40.7 m)	49%	4 ft (1.3 m)
Core well R-50 <b>A-Cycle</b>	4	20%	59.5(ft) (18 m)	24%	14.9 m (4.5)
Core well R-48	19	30%	54.5(ft) (16.6 m)	20%	2.9 ft (0.9 m)

Table 5.1 Ratawi cycle types in cores of well R-50 and R-48. Number of each cycle type and percentage to total cycles in the core. Total thickness of each cycle type and percentage to the core interval in feet.

### 5.3.3 Ratawi Oolite and Ratawi Limestone cycles

This study identifies 84 parasequences (Section 5.2.3) listed in Appendix 2, the occurrence of the different parasequence types in wells R-50 and R-48 are given in Table 5.1. The origins of these parasequences can be interpreted using the autocyclic and allocyclic models discussed in the previous section. This section discusses the general characteristic of the Ratawi Oolite (Section 5.3.3.1), and the Ratawi Limestone parasequences (Section 5.3.3.2). The Ratawi Oolite is the reservoir zone, whereas the Ratawi Limestone is the seal zone at Wafra oilfield.



### 5.3.3.1 Ratawi Oolite cycles

Arabian Texaco Incorporated divide the Ratawi zone at Wafra oilfield into six units, which are unit-A, unit-B, unit-C, unit-D, unit-E and unit-F, using nine marker beds defined by gamma ray and porosity logs (Fig. 2-6). The marker beds are used to correlate these units in the main, southern and eastern Wafra areas (Section 2.3.2). This study has analyzed spectral gamma ray, computed gamma ray, bulk density and neutron porosity logs for well R-50 to define these marker horizons and correlate the Ratawi reservoir units to well R-50 in order to compare the reservoir units with the parasequence succession defined in this study from the cored interval.

The company define unit-F, marker horizon number 9, as the upper unit in the lower member of the Ratawi Oolite. The unit is a transitional lithofacies from 'clean' carbonate of the lower member to 'dirty' carbonate of the middle member of the Ratawi Limestone. The depth of the lower boundary of this unit is defined by the company in logs at the deepest 'big' positive spike on the gamma ray log, with the upper boundary of the unit at the third positive spike. This study defines the lower boundary of unit-F at a depth of 6805 feet (2074 m) and the upper boundary of the unit at a depth of 6791 feet (2070 m), which is the lower boundary for the Ratawi Limestone. The thickness of unit-F is about 14 feet (4.3 m).

The rest of the marker horizons (numbers 8, 7, 6, 5, 4 and 3) are defined by high density, low porosity and high gamma ray peaks. Marker number 6 is between reservoir unit-E and unit-D, defined by this study at a depth of 6872 feet (2096 m); the thickness of unit-E is about 67 feet (20 m). This reservoir unit has two marker beds, marker number 8, defined at a depth of 6847 feet (2087 m), and marker number 7, defined at a depth of 6858 feet (2090 m). Marker number 4 is between reservoir unit-D and unit-C, defined in this study at a depth of 6932 feet (2113 m); the thickness of unit-D is about 60 feet (18 m). This reservoir unit has one marker bed, marker number 5, defined at a depth of 6908 feet (2105 m). The thickness of the upper part of unit-C, in the cored interval, is about 98 feet (30 m); marker number 3 occurs at a depth of 6974 feet (2126 m).

Twenty parasequences are recognized in this study in the 254 feet (77 m) of cored interval in well R-50; the lower seventeen parasequences are in the Ratawi Oolite, whereas the upper three parasequences are in the lower part of the Ratawi Limestone (parasequences number 18 to 20) (Appendix 2). The subtidal cycles are defined in this study by their upper surface boundary with subaerial exposure diagenetic overprint



evidence but the peritidal cycles without. The two cycle types with its third subtype (R-cycle, T/R-cycle and A-cycle) describe two types of cycle symmetry (symmetric and asymmetric). Most of the R- and T/R-cycles are subtidal type whereas all the A-cycles are peritidal, listed in Appendix 2.

unclear  
rewrite

The seventeen parasequences of the Ratawi Oolite have an average thickness of about 14 feet (4 m). The number of subtidal cycles is 4 (23 %) and the number of peritidal cycles is 13 (77%). Hydrocarbon production from well R-50 is from unit-D and unit-E, whereas unit-C and unit-F are non-reservoir units. The production in reservoir unit-D comes from parasequence number 9, which is a peritidal T/R-cycle, about 60 feet (18 m) thick. The main controlling porosity in unit-D is primary interparticle porosity (Chapter 4). The production of reservoir unit-E comes from parasequence number 15, which is a subtidal R-cycle, about 27 feet (8 m) thick. Secondary exposure-related (rootlet porosity) is the main controlling porosity in unit-E (Chapter 3), which is inferred in this study to be controlled by a 2<sup>nd</sup> order sequence boundary (Chapter 4 and Chapter 6).

#### 5.3.3.2 Ratawi Limestone cycles

The cored interval in well R-48 is in the Ratawi Limestone, which is a seal rock at Wafra Oilfield. Sixty-four parasequences are recognized in the 271 feet (83 m) interval (Appendix 2). The Ratawi Limestone parasequences are characterized by an average thickness of about 4 feet (1.2 m), with the number of subtidal parasequences 35 (55 %) and the number of peritidal parasequences 29 (45 %).

The Ratawi Limestone is characterized by a higher percentage of subtidal cycles (55%) than the Ratawi Oolite (24%). This is interpreted in this study to show that the middle member was deposited in deeper-water environments, whereas the lower member was deposited in shallower environments on the 'Ratawi epeiric ramp'. The three members of the Ratawi Formation (Ratawi Oolite, Ratawi Limestone, and Ratawi Shale) are inferred in this study to represent an overall deepening-upward succession (Chapter 6).



## **5.4 Ratawi cycle stacking patterns**

### **5.4.1 Introduction**

The depositional facies and early diagenetic fabrics of the Ratawi Formation, in addition to the petrophysical characteristics of the Ratawi reservoir and seal zones can be analyzed in the framework of the stacking pattern of the Ratawi cycles. Stacking pattern analysis is considered by Lehrmann and Goldhammer (1999) to be a subset of sequence stratigraphy that can be used to evaluate the vertical parasequence thickness, facies types, and unconformities into cyclic stratal packages of various scales and character.

This study has distinguished 20 cycles in well R-50, and 64 cycles in well R-48. These cycles are the result of cyclic variation in either or both of the factors that control Ratawi sedimentation: (1) accommodation space and (2) sediment supply. Due to the limited data available to this study, the Ratawi cycles have been mainly defined on the basis of identifying non-depositional key surfaces (Section 5.2.3) from the Core Lab charts and visual examination of the core.

These data, from a one-dimensional core succession, permit the analysis of each cycle thickness, cycle type, peritidal versus subtidal, and cycle symmetry, to evaluate the long-term patterns and trends. Ideally, stacking pattern analysis requires analyzing a stacking pattern for thickness trends in addition to facies proportions and early diagenetic features in each cycle (Fitchen, 1997), which is not available to this study.

### **5.4.2 Fischer Plots**

A Fischer plot is a tool for graphically analyzing one-dimensional data for cycle thickening and thinning patterns, as normalized to a constant subsidence amount (Kerans and Tinker, 1997). The basic assumption behind the plot is that parasequence thickness provides an indication of the long-term variations in accommodation space. In addition the hierarchy of the fine-scale units (parasequence) nested within coarser scale units (systems tracts and sequences) is driven primarily by hierarchical fluctuations in which lower-frequency sea-level cycles force the higher-frequency sea-level cycles through composite interaction (Fig.5-5 and 5-6).

The composite interaction results in organizing the vertical and lateral distributions of parasequence thickness, lithofacies, lateral geometry, and early diagenesis relative to sequence (Fitchen, 1997; Lehrmann and Goldhammer, 1999).



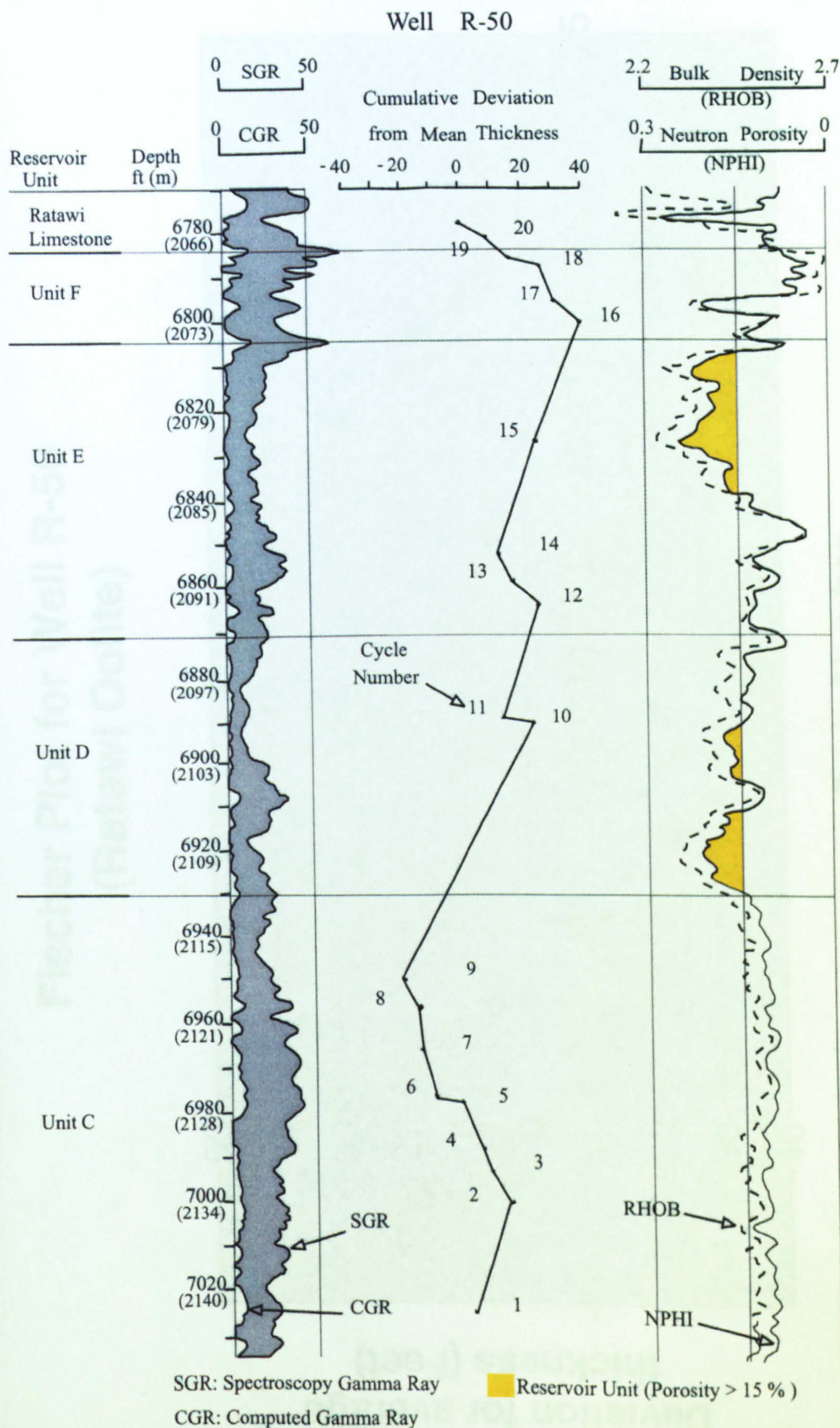


Figure 5-8 Fischer plot in depth domain for strata in well R-50 compared with log signatures and location of reservoir and non-reservoir units.



**Fischer Plot for Well R-50  
(Ratawi Oolite)**

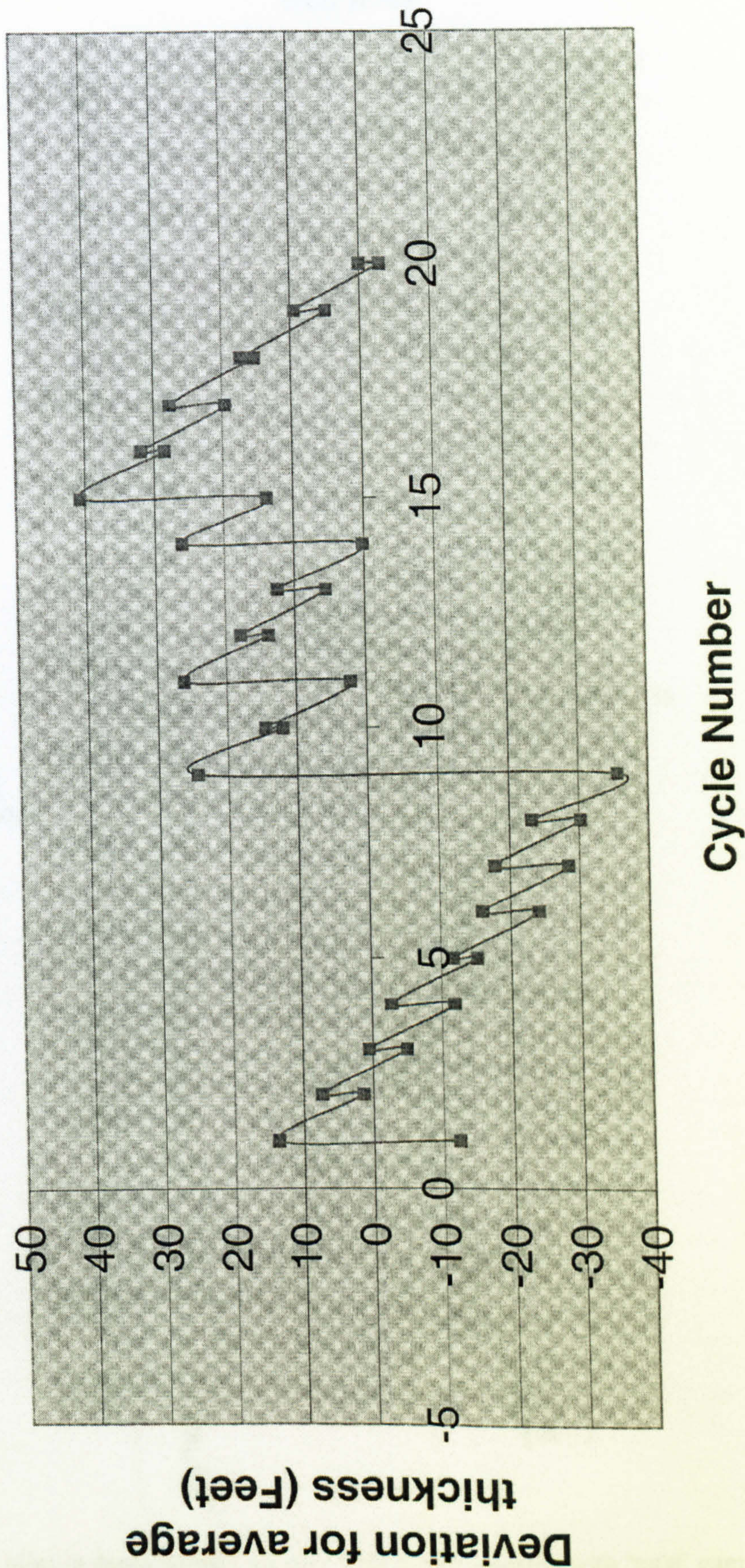


Figure 5-9 Fischer plots in time domain for core well R-50.



## Well R-48

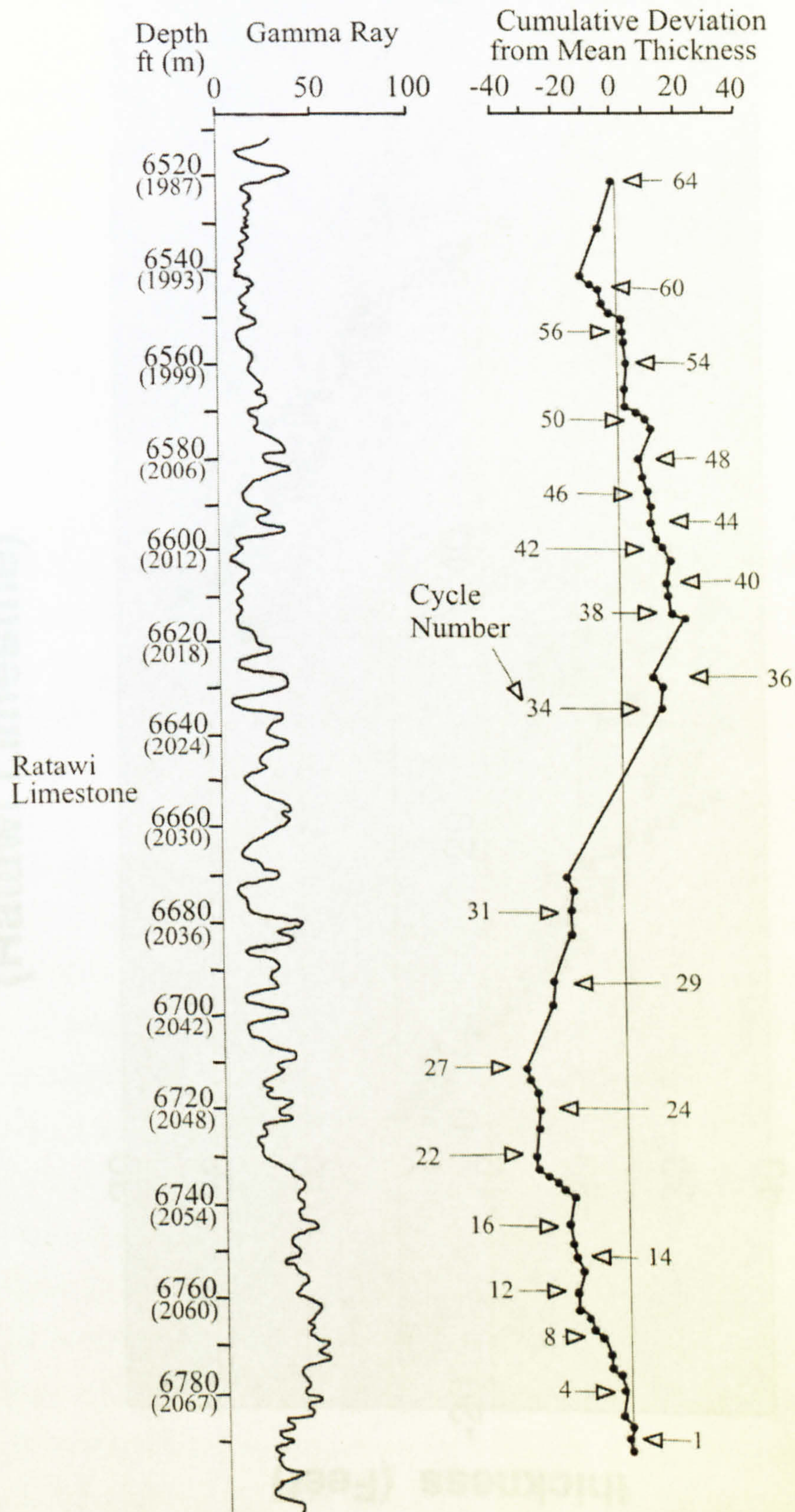


Figure 5-10 Fischer plots in depth domain for core well R-48 compared with 'total' gamma ray signatures in Ratawi Limestone.



# **Fischer Plot for Well R-48 (Ratawi Limestone)**

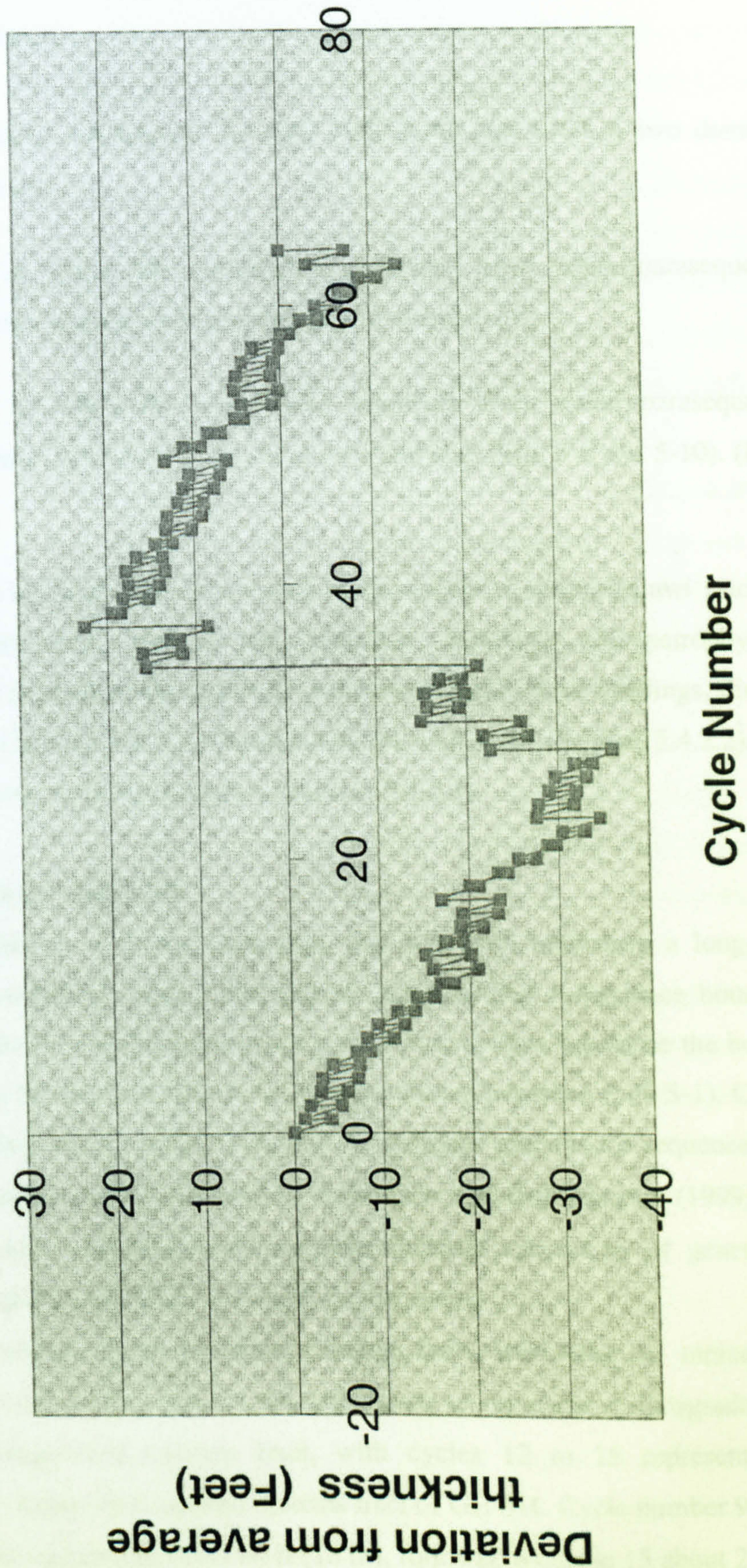


Figure 5-11 Fischer plots in time domain for core well R-48.



These vertical and lateral patterns are used in this study to interpret and predict Ratawi reservoir characterization.

Fischer plots have been constructed for core wells R-48 and R-50 in two domains (Appendix 3), which are:

- (1) Time domain in which the cumulative departure from mean parasequence thickness is plotted against cycle number (Fig. 5-9 and 5-11).
- (2) Depth domain in which the cumulative departure from mean parasequence thickness is plotted against cycle depth in core and logs (Fig. 5-8 and 5-10). (Day, 1997).

Fischer plot in depth domain is used in this study to relate Ratawi stacking pattern to reservoir units, wireline log signatures, lithology, and petrophysical characteristics. The analysis of Fischer plots is discussed under three headings, Fischer plot for well R-50 (Section 5.4.2.1), Fischer plot for well R-48 (Section 5.4.2.2), and Ratawi cycle hierarchy from Fischer plots (Section 5.4.2.3).

#### 5.4.2.1 Fischer plot for well R-50

Cycles <sup>2?</sup>1 to 8 represent a falling limb (Fig. 5-8 and 5-9), indicating a long-term decrease in accommodation space. This pattern suggests that a sequence boundary zone number 1 (SBZ-1) should occur near cycles 7 and 8. This would be the bottom sequence boundary for the first Ratawi Oolite greenhouse sequence (GH S-1). Cycles 1 to 6 represent a highstand system tracts for the previous greenhouse sequence (GH S-0). A greenhouse sequence is defined by Lehrmann and Goldhammer (1999) as a relatively conformable retrogradational to progradational succession of genetically related strata bounded by minimum-accommodation zones.

Cycles numbered 9 to 15 form a rising limb, indicating an increase in accommodation space. Cycles 9 to 11 are interpreted to represent a retrogradational succession or transgressive systems tract, with cycles 12 to 15 representing a progradational succession or highstand systems tract of GH S-1. Cycle number 9 is the thickest cycle in the succession about 60 ft (18 m), followed by cycle 15 about 27 ft (8 m), cycle 14 about 26 ft (7.9 m), and cycle 11 about 24 ft (7 m). These thick parasequences are interpreted in this study to be formed by subtidal amalgamation and



indicate missing beats in the cycle succession. Subtidal amalgamation could be formed during a long-term flooding phase, when sea-level oscillation occurred too far above the sediment surface to cause a distinct change in lithofacies (Montanez and Osleger, 1993).

Cycle numbers 16 to 20 create a falling limb, and indicate a decrease in accommodation space. A sequence boundary zone, number 2 (SBZ-2), probably occurs somewhere between cycles numbered 16 and 20. This sequence boundary is the upper boundary for GH S-1, inferred in this study to represent a second-order boundary of composite sequence (2<sup>nd</sup> order sequence) between the Ratawi Oolite and Ratawi Limestone (Chapter 6).

In this study, the wireline logs of well R-50 were analyzed and the depth of marker bed numbers 3 to 9. The available data for this study of wireline logs and core description do not show an 'ideal' correlation between the cycle surfaces identified in this study and the log response (Section 5.5). However, this study infers that the lower part of the middle member of the Ratawi Limestone is cycle numbers 18 to 20; non-reservoir unit-F, the transition unit between the lower and middle member, corresponds to the upper part of cycle number 15 to cycle number 17. These cycles, upper cycle 15 to cycle 20, generally represent the sequence boundary zone. This study interprets the low porosity of unit-F as a result of the low-energy muddy depositional environment associated with the sequence boundary zone.

Reservoir unit-E is the upper part of cycle number 11 to the lower part of cycle number 15, roughly representing the highstand systems tract. The main controlling porosity in reservoir unit-E is secondary diagenetic soil-related and rootlet porosity. This study interprets the origin of the porosity of this unit as a result of its location beneath a surface with a long period of subaerial exposure (a 2<sup>nd</sup> order sequence boundary) under a semi-arid climate (Chapter 4).

Reservoir unit-D is the upper part of cycle number 9 to the lower part of cycle number 11, roughly representing the transgressive systems tract. The main controlling porosity in reservoir unit-D is primary interparticle porosity. This study interprets the origin of the porosity of this unit as a result of the high-energy depositional environment associated with the transgressive systems tract, and the removal of carbonate mud from between grains and deposition of a packstone-grainstone sand-body on the shallow Ratawi ramp (Chapter 4).



The cored upper part of non-reservoir unit-C is cycle number 1 to the lower part of cycle number 9, roughly representing the sequence boundary zone and upper part of the highstand systems tract of the previous sequence. This study interprets the low porosity of unit-C on the flank of the main Wafra area as due to the low-energy depositional environment associated with the highstand systems tract and relatively short period of subaerial exposure associated with a 3<sup>rd</sup> order sequence boundary zone.

The Ratawi zone of the Wafra oilfield is divided into three separate structural areas, which are main, southern and eastern Wafra areas. Unit-E, unit-D and unit-C are reservoir units at the top of the structure in the main Wafra area. Unit-E is the only unit that is a reservoir in the three Wafra areas, whereas unit-D and unit-C progressively lose their porosity from the top of the structure to the flank of the structure of the main Wafra area (Chapter 2).

The core under investigation, R-50, is at the flank of the main area, where unit-D becomes less porous and where unit-C is a non-reservoir unit. This study interprets the increase of the porosity of unit-D and unit-C from well R-50 at the flank of the structure to the top of the main Wafra structure as due to the development of an 'antecedent Wafra structure' (Chapter 1 and Chapter 6).

The syndepositional development of the structure is interpreted in this study to be a result of movements of the Infra-Cambrian Hormuz salt (Chapter 1) and is inferred to have had two major effects on the development of the porosity of unit-D and unit-C, namely:

1. Depositional effects: increased energy of the depositional environment on this topographic high that lead to higher concentration of packstone-grainstone at the top of the structure with its associated increase in porosity than at well R-50 to the side.
2. Early diagenetic effects: subaerial exposure of the top of the structure longer than the flank, which lead to intensive subaerial diagenesis at the top of the structure, more than at well R-50, leading to the increase in porosity.

#### **5.4.2.2 Fischer plot for well R-48**

The distance between well R-48 and R-50 is about 3.6 kilometres. All the cored interval in the first well is in the Ratawi Limestone seal zone at Wafra oilfield, whereas only the upper 11 ft (3 m), cycle numbers 18 to 20 in the second well, is in the Ratawi Limestone. The available data for this study are not enough to infer the depth



of marker bed number 9 in well R-48, which is the boundary between the Ratawi Oolite and the Ratawi Limestone, nor to correlate SBZ-2 between the two wells.

From the Fischer plot core of R-48 (Fig. 5-10 and 5-11), cycle numbers 1 to 28 occur on a falling limb, suggesting deposition at a time of decreasing accommodation space. A sequence boundary zone (number 3, SBZ-3) could occur in the region of cycles 21 and 22. This study interprets SBZ-2 between the lower and the middle member of Ratawi Formation at well R-50 to be equivalent to SBZ-3 at the bottom of the Ratawi Limestone in the cored interval of well R-48. Cycle numbers 28 to 57 generally occur on a rising limb suggesting deposition at time of increasing accommodation space. Cycle numbers 28 to 37 are thought to represent a broadly retrogradational succession or transgressive systems tract, whereas cycle numbers 38 to 57 represent a broadly progradational succession or highstand systems tract of GH S-2.

The thickest cycles are cycle number 34, about 37 ft (11 m), followed by cycle number 37, about 14 ft (4.2 m), cycle number 28, about 13.5 ft (4 m), and cycle number 30, about 11 ft (3.3 m). These cycles could contain several smaller cycles which were not recorded (missed beats), as a result of a subtidal amalgamation (Montanez and Osleger, 1993). Cycles numbered 58 to 64 occur upon a falling limb of the Fischer plot and indicate deposition during a decrease in accommodation space. A sequence boundary zone, number 4 (SBZ-4), is suggested to occur in the region of cycles 62 and 63.

This study interprets the low porosity of the middle member of the Ratawi Limestone, which is the seal rock for the Ratawi zone at Wafra oilfield, as the result of two factors:

- (1) Deposition effects: the middle member was deposited in a lower-energy, deeper-water environment on the Ratawi epeiric ramp than the lower member. This lead to deposition of a mudstone / wackestone facies with low primary porosity.
- (2) Early diagenesis effects: a relatively short period of subaerial exposure associated with a 3<sup>rd</sup> order sequence boundary zone (SBZ-4) compared with the 2<sup>nd</sup> order sequence boundary zone at SBZ-2, and also the end of the development of the antecedent Wafra structure (Chapter 6). This lead to a shorter period of subaerial exposure, which would have lead to less secondary diagenetic porosity development in the middle member.



### 5.4.2.3 Ratawi cycle hierarchy from Fischer plots

The hierarchy of cycles recognized in the Ratawi Oolite (Section 5.4.2.1) and Ratawi Limestone (Section 5.4.2.2) can be used to interpret and correlate the Ratawi chronostratigraphic units in order to construct a high-resolution chronostratigraphic framework for the Wafra oilfield. The vertical stacking patterns of the Ratawi Oolite and Ratawi Limestone are generally characterized by relatively thin parasequences at sequence boundary zones SBZ-1, SBZ-2 and its equivalent SBZ-3 (interpreted in this study to be the boundary between the lower and middle member of the Ratawi Formation recognized in two different cores) and SBZ-4.

Ratawi sequences GH S-1 and GH S-2 are generally characterized by poorly developed parasequence grouping (e.g. bundling of 5 precessional cycles into one set of an eccentricity cycle); the average thickness for the Ratawi Oolite parasequences is about 15 ft (4.5 m) whereas in the Ratawi Limestone it is about 4 ft (1.2 m). Both sequences in the Ratawi Oolite and Ratawi Limestone include thick cycles interpreted in this study as the result of missing beats (Section 5.4). Ratawi greenhouse sequences are inferred in this study to be generally characterized by gross transgressive-regressive facies shifts without a well-defined maximum flooding surface.

To correlate Ratawi cycle hierarchy with confidence between wells at Wafra oilfield, the different levels of resolution that are recognized in the stratigraphic record need to be appreciated. The level of resolution for the Ratawi Formation depends on the geological period, Lower Cretaceous, and the depositional system, an epeiric ramp, and the tectonic setting, a passive continental margin (Lehrmann and Goldhammer, 1999).

The spectrum of order and randomness of carbonate cycles in the geological record is recognized by Lehrmann and Goldhammer (1999). They identified six secular classes of order in shallow-marine carbonates on the basis of age: (1) Proterozoic-Early Ordovician, (2) Silurian-Devonian, (3) Pennsylvanian, Early Permian, Late Triassic, and Neogene, (4) middle to Late Permian, (5) Early to Middle Triassic, and (6) Jurassic to Cretaceous.

The studied interval, Ratawi Formation in the Thamama Group, is in the Jurassic to Cretaceous secular class, which, according to Lehrmann and Goldhammer (1999) is characterized by:

- (1) Vertical stacking patterns; parasequence grouping is characterized by a range of development from poorly developed to some extent developed at sequence



boundaries; depositional sequences are characterized by gross transgressive-regressive facies shifts.

- (2) Lateral stacking patterns; parasequences are characterized by being partly or highly discontinuous; parasequence sets (systems tract) could be continuous; depositional sequences are characterized by regional extent.

The general vertical stacking patterns for the Ratawi Formation seem to be in agreement with Lehrmann and Goldhammer's (1999) model.

The general lateral stacking patterns of the Ratawi Formation are examined by correlating the Ratawi Oolite at wells R-50 with R-49 by using spectral gamma ray, and computed gamma ray logs (Section 5.6). The available data for this study used in lateral correlation seem to indicate:

- (1) No lateral correlation for parasequences (no 'ideal' correlation between surfaces of parasequences in core R-50 and log signatures, also no 'ideal' correlation between signatures of logs R-50 with R-49).
- (2) A 'good' lateral correlation of reservoir units to systems tracts (generally, unit-E matches highstand systems track and unit-C matches the transgressive systems track; upper unit-C correlates to a highstand systems track) and these reservoir units can be correlated using marker zones.
- (3) Regional lateral correlation for 3<sup>rd</sup> order sequence boundary zones (Ratawi Formation and its equivalent in the Thamama Group of the Arabian basin).
- (4) Regional to global lateral correlation for the 2<sup>nd</sup> order sequence boundary zone (between different basins and different passive margins of the Lower Cretaceous Tethyan seaway, Chapter 6).

The general lateral stacking patterns for the Ratawi Formation seem to be in agreement with the Lehrmann and Goldhammer (1999) model.

### **5.5 Ratawi log signature to cycles and surfaces**

Wells at Wafra oilfield with a cored interval in the Ratawi Formation are very limited. Construction of a chronostratigraphic framework for the Ratawi zone requires calibration of core data with well logs (Section 5.1.1), and ideally these should result in a correlation of the Ratawi chronostratigraphic surfaces recognized in the core description between the wells.

This study depends on data from three wells at Wafra oilfield: (1) well R-50, with core samples, detailed core chart description, spectral gamma ray, computed



gamma ray, bulk density and neutron porosity logs, (2) well R-48, with core samples, detailed core chart description, and gamma ray log, and (3) well R-49, with core samples, spectral gamma ray, computed gamma ray, bulk density and neutron porosity logs, the well does not have detailed core chart description.

Carbonates in their pure state are not radioactive; three elements in carbonate rocks produce natural gamma radiation, potassium (K), thorium (Th) and uranium (U). The first element is found in clay as well as mica, feldspar and evaporite minerals; the second element is found in clay and heavy minerals, and the last element is found in organic matter and phosphate (Rider, 1991). The petrographic study of the Ratawi core samples (Chapter 3), core observations and the core description chart indicates a virtual absence of evaporite minerals, but there are clay, phosphate and organic-rich shale layers.

The variations in these elements are measured by spectral gamma ray, and computed gamma ray; they can be used to distinguish stratigraphic surfaces, sedimentary environments and processes (Ehrenberg and Svana, 2001; North and Boering, 1999). The aim of this section is to calibrate Ratawi core data with log data by testing the correlation of total gamma ray and relative amounts of K, Th and U elements measured by logs with the different Ratawi surfaces and stacking patterns identified in this study.

This study uses computed gamma ray logs and measures the presence of K and Th as a shale indicator. The space difference between the spectral gamma ray log, which measures K, Th and U, and the computed gamma ray log (measures only K and Th) is used to measure U and in this study, also to indicate phosphate, and organic shale laminae (Rider, 1991).

The analysis of the core (observation and chart description), Fischer plot, spectral gamma ray and computed gamma ray logs for the Ratawi Oolite in well R-50 show that:

- (1) Marker bed number 9, the boundary between the Ratawi Oolite and the Ratawi Limestone, is marked by a 'big' spike on the spectral gamma ray log, and a relatively small peak on the computed gamma ray log. This is interpreted as showing the presence of organic-rich shale laminae and clay minerals.
- (2) Marker beds number 3, 4, 5, 6, 7 and 8 are marked by 'big' peaks on the spectral gamma ray log and smaller peaks on the computed gamma ray log. These are interpreted in this study as the result of phosphate in hardgrounds and clay



minerals.

- (3) The stacking patterns for sequence boundary zone number 1 (SBZ-1) and sequence boundary zone number 2 (SBZ-2) are generally marked by higher values on the spectral gamma ray log, whereas the stacking pattern for the transgressive-regressive sequence GH S-1 is generally marked by a relatively low response on spectral gamma ray log. This is interpreted in this study as due to the high concentration of clay minerals in the sequence boundary zones.
- (4) There is no perfect correlation between the different parasequence surfaces identified from the core description for R-50 in this study and the log signatures. This is interpreted in this study as due to the low concentration of clay minerals and phosphate generally, which host the K, Th and U elements, on these surfaces.

The analysis of the cores, the core chart description, Fischer plots, and 'total' gamma ray logs for the Ratawi Limestone for well R-48 in this study show that:

- (1) The stacking pattern for sequence boundary zone number 3 (SBZ-3) is generally marked by a high 'total' gamma ray log response, whereas the stacking pattern for sequence boundary zone number 4 (SBZ-4), and the transgressive-regressive sequence GH S-2 are generally marked by a relatively low response on the 'total' gamma ray log. This is interpreted in this study as the result of the high concentration of clay minerals in SBZ-3, but not in SBZ-4 and GH S-2.
- (2) There is no perfect correlation between the different surfaces identified from core chart R-48 in this study and log signature. This is interpreted in this study as the result of the low concentration of clay minerals and phosphate on these surfaces.

### **5.6 General correlation between well R-49 and R-50**

To examine the Ratawi Oolite lateral stacking patterns in the Wafra oilfield, a correlation is attempted for the reservoir zones between wells R-50 (Fig. 5-8) and R-48 (Fig. 5-12). The distance between the two wells is about 4.8 kilometres. Spectral gamma ray, computed gamma ray, bulk density and neutron porosity logs were used for the correlation.

As explained in the previous section, the available data for this study do not show perfect correlation between core description data and wireline logs for well R-50. This difficulty in correlation could be caused by low sensitivity of the logging tools,



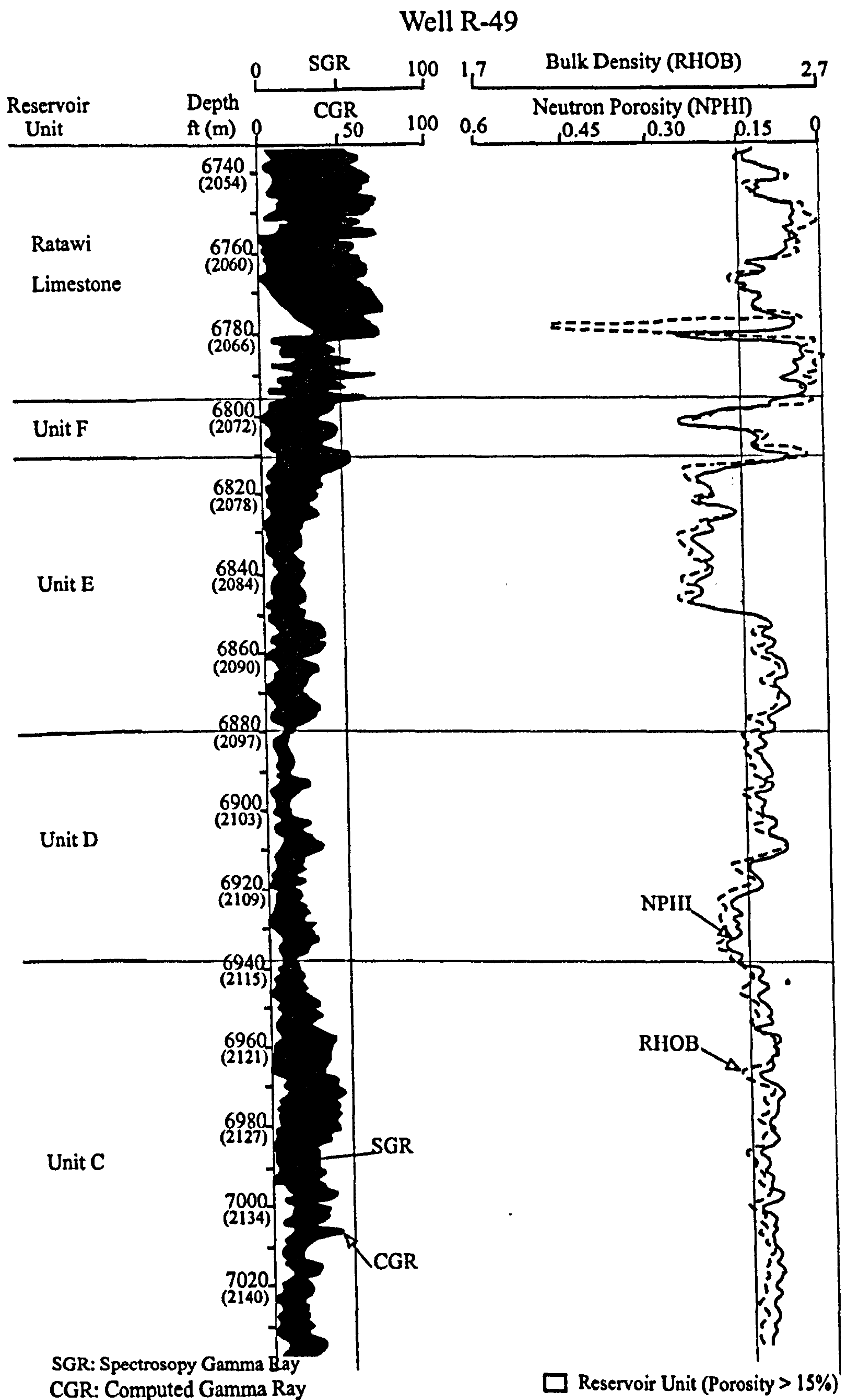


Figure 5-12 Log signatures for strata in well R-49 and location of reservoir and non-reservoir units.



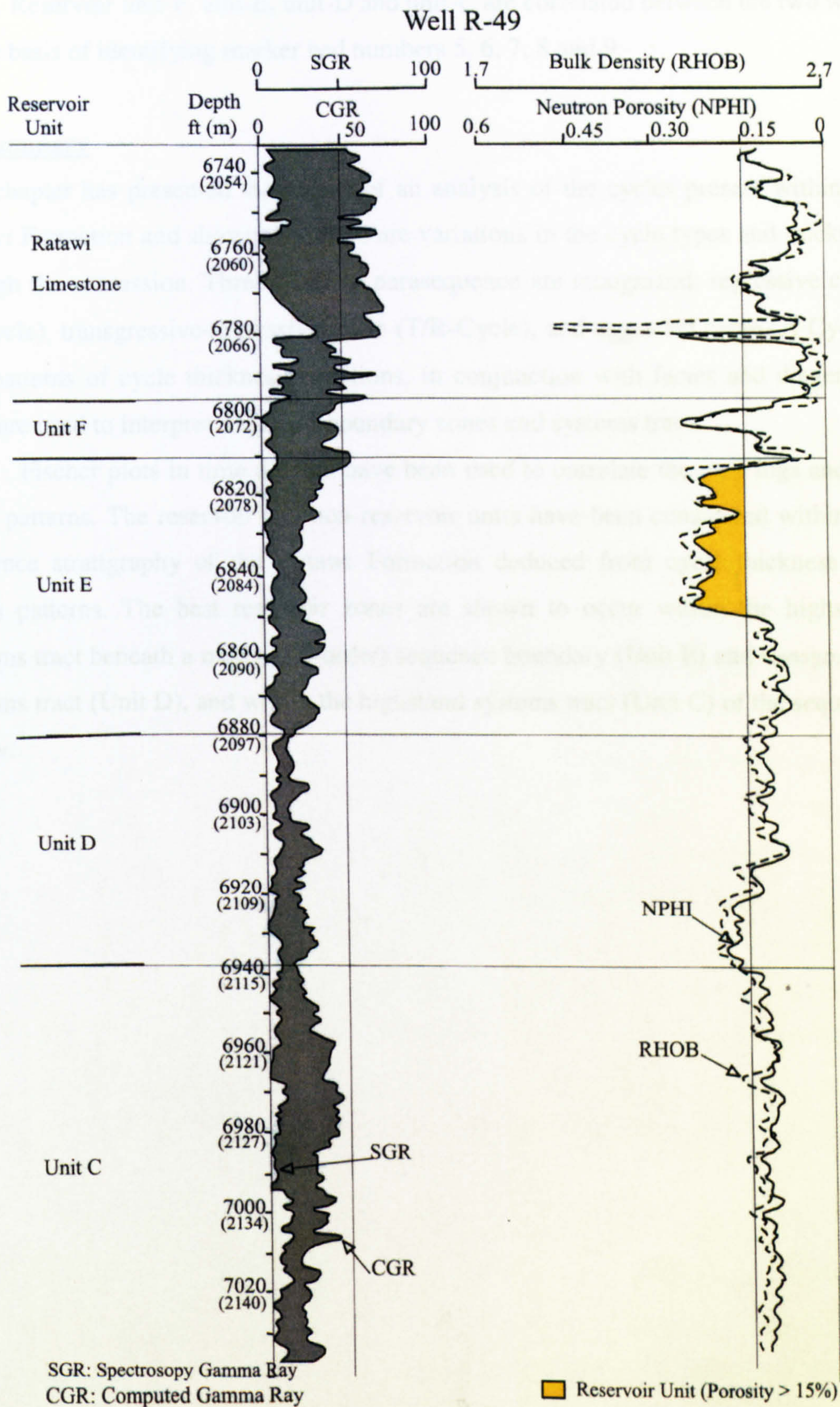


Figure 5-12 Log signatures for strata in well R-49 and location of reservoir and non-reservoir units.



variation of carbonate mineralogy, changes in rock fabric and grain types (Fitchen, 1997). Reservoir unit-F, unit-E, unit-D and unit-C are correlated between the two wells on the basis of identifying marker bed numbers 5, 6, 7, 8 and 9.

### **5.7 Summary**

This chapter has presented the results of an analysis of the cycles present within the Ratawi Formation and shown that there are variations in the cycle types and thickness through the succession. Three types of parasequence are recognized: regressive cycle (R-Cycle), transgressive-regressive cycle (T/R-Cycle), and aggraded cycle (A-Cycle). The patterns of cycle thickness variations, in conjunction with facies and diagenetic data, are used to interpret sequence boundary zones and systems tracts.

Fischer plots in time domain have been used to correlate the well logs and the cycle patterns. The reservoir and non-reservoir units have been considered within the sequence stratigraphy of the Ratawi Formation deduced from cycle thickness and facies patterns. The best reservoir zones are shown to occur within the highstand systems tract beneath a major (2<sup>nd</sup>-order) sequence boundary (Unit E) and transgressive systems tract (Unit D), and within the highstand systems tract (Unit C) of the sequence below.



## Chapter 6 The Ratawi Sequence Stratigraphic Model and Petroleum System

### 6.1 Introduction

Ratawi reservoir heterogeneity at Wafra oilfield, and regional source, reservoir and seal rocks of the Ratawi Formation petroleum system are analyzed as part of the dynamic evolution of the Arabian-Iranian basin. The Ratawi sequence stratigraphic model provides a set of concepts and methodologies in which to integrate available data from this study. A sequence stratigraphic model can be used to evaluate local, regional and global factors controlling heterogeneity in the Ratawi reservoir zone, in addition to distribution and chronostratigraphic relationships of source, reservoir and seal facies of the Ratawi Formation petroleum system. The model interprets platform stratal geometry, and depositional and early diagenetic facies, by three basic parameters, accommodation history, depositional system (including sediment supply), and platform-margin profile (Tucker and Wright, 1990; Posamentier and Allen, 1993; Fitchen, 1997).

A sequence stratigraphic model can be used to interpret sequence stratigraphic cycles at different scales: 2<sup>nd</sup> order cycle composite sequence, 3<sup>rd</sup> order cycle greenhouse sequence (Section 6.4), and 5<sup>th</sup> order cycle transgression-regression parasequence (Section <sup>5.3</sup>~~5.2.4.2.2~~). Generally, the timing of sequence bounding surfaces is determined by accommodation space, which is controlled by eustasy, subsidence and uplift, where the stratal architecture between those bounding surfaces is determined by carbonate platform type and sediment supply. Only the eustasy factor of the three basic parameters of the sequence stratigraphic model is globally significant; the other three factors could be locally to regionally significant (Posamentier and Allen, 1993).

In the previous chapters of this study, the depositional system of the Ratawi Formation is interpreted as an epeiric ramp characterized by four broad facies belts (Chapter 3). Each of these facies belts is characterized by particular early diagenetic facies superimposed on depositional facies, and petrophysical properties (Chapter 4). Diagenetic secondary porosity of reservoir unit-E, and depositional primary porosity of reservoir unit-D, in addition to non-reservoir unit-C, unit-F, and Ratawi Limestone



seal rock at wells R-49 and R-50, are interpreted within a cyclic framework of three sequences GH S-0, GH S-1 and GH S-2 (Chapter 5).

To use the inferred Ratawi sequence stratigraphic framework to interpret and predict heterogeneity of the Ratawi zone at Wafra oilfield, and regional source, reservoir and seal rocks of the Ratawi Formation petroleum system, the controlling factors on Ratawi cyclicity hierarchy must be interpreted and predicted. Local, regional and global parameters that control the cyclicity of the Ratawi Formation are interpreted in a framework of the sequence stratigraphic model.

There are no single sequence stratigraphic models or templates that can be used to characterize carbonate platforms of all ages (Fitchen, 1997). Factors that control the Ratawi Formation sequence stratigraphic model should be inferred from the processes that control the dynamic evolution of the lower Cretaceous Arabian-Iranian basin, which includes the shallow-water Arabian Shelf and deep-water Gotnia Basin. The development of the Arabian-Iranian basin is part of the dynamic evolution of the Tethyan seaway, which is associated with the geological history of Gondwana fragmentation and the opening, widening and closing of the Neo-Tethys.

#### **6.1.1 Ratawi Formation petroleum system**

The lithofacies of the petroleum system of the Ratawi Formation can be interpreted within the framework of the long-term accommodation change and basin fill of the Arabian-Iranian basin. Greenlee and Lehrmann (1993) proposed using the 2<sup>nd</sup> order cycle to evaluate basin tectonism and basin-filling stratal patterns and to recognize the temporal and spatial distribution of source, reservoir and seal rocks in the basin.

The 2<sup>nd</sup> order cycle is a large-scale, long-term transgressive-regressive cycle developed over periods of 5 to 20 m.y. and is represented in this study by a composite sequence (CM S). A composite sequence, like a parasequence, may be symmetric or asymmetric (Chapter 5); their stratigraphic signature results from the interplay among different factors including depositional system, basin geometry, subsidence, sea level, climate and palaeoceanographic conditions (Greenlee and Lehrmann, 1993; Fitchen, 1997).

The cycle of basin filling is represented by transgressive to regressive lithofacies packages forming the 2<sup>nd</sup> order composite sequence, which is similar to a transgressive-regressive 5<sup>th</sup> order cycle parasequence and 3<sup>rd</sup> order cycle greenhouse sequence. This similarity is due to the fact that they are developed during similar



accommodation history, increasing accommodation during transgressive phase and decreasing accommodation during regressive phase, but on different time-scales (Greenlee and Lehrmann, 1993; Fitchen, 1997).

Composite sequences are bounded by composite sequence boundary zones (CMS BZ) that document major relative falls in sea level, and large-scale reorganization of the basin's depositional system. They represent distinctive stratigraphic architectures in the basin that appear to be driven by global tectonic processes related to changing rates of sea-floor spreading (Greenlee and Lehmann, 1993).

Douban and Al Medhadi (1999) applied the concepts of sequence stratigraphy to the Cretaceous succession in the Saudi Arabia-Kuwait Partitioned Neutral Zone and in Kuwait to analyze the petroleum system of this period. They identified five 2<sup>nd</sup> order composite sequences (megasequences) and four major breaks of sedimentation. This model can be used to interpret and predict source, reservoir and seal lithofacies. The five composite sequences are Berriasian to Valanginian, Late Hauterivian / Barremian to Aptian, Albian to Early Cenomanian, Cenomanian to Early Turonian, and Late Coniacian / Santonian to Maastrichtian. The four major breaks in sedimentation are Valanginian to Hauterivian, Early Albian, Turonian to Coniacian, and Late Maastrichtian.

The sequence stratigraphic model of Douban and Al Medhadi (1999) divides the Lower Cretaceous Thamama Group in the study area into two 2<sup>nd</sup> order composite sequences, which are Berriasian to Valanginian and Late Hauterivian / Barremian to Aptian. Both composite sequences of the Thamama Group contain a well-developed petroleum system.

### **6.1.2 Thamama Group 2<sup>nd</sup> order cycles**

The stratigraphic succession of the Cretaceous period in the Arabian-Iranian basin is divided into Thamama, Wasia and Aruma groups (Chapter 2). According to Douban and Al Medhadi (1999), the Cretaceous petroleum system of the Thamama Group (Berriasian through early Aptian) and Wasia Group (late Aptian through Turonian) each consists of two 2<sup>nd</sup> order sequences, whereas the Aruma Group (Coniacian through Maastrichtian) has one 2<sup>nd</sup> order sequence. Alsharhan and Nairn (1986) divided the Thamama Group into two predominately carbonate cycles, with the maximum development of the marginal clastic facies occurring within the upper cycle.



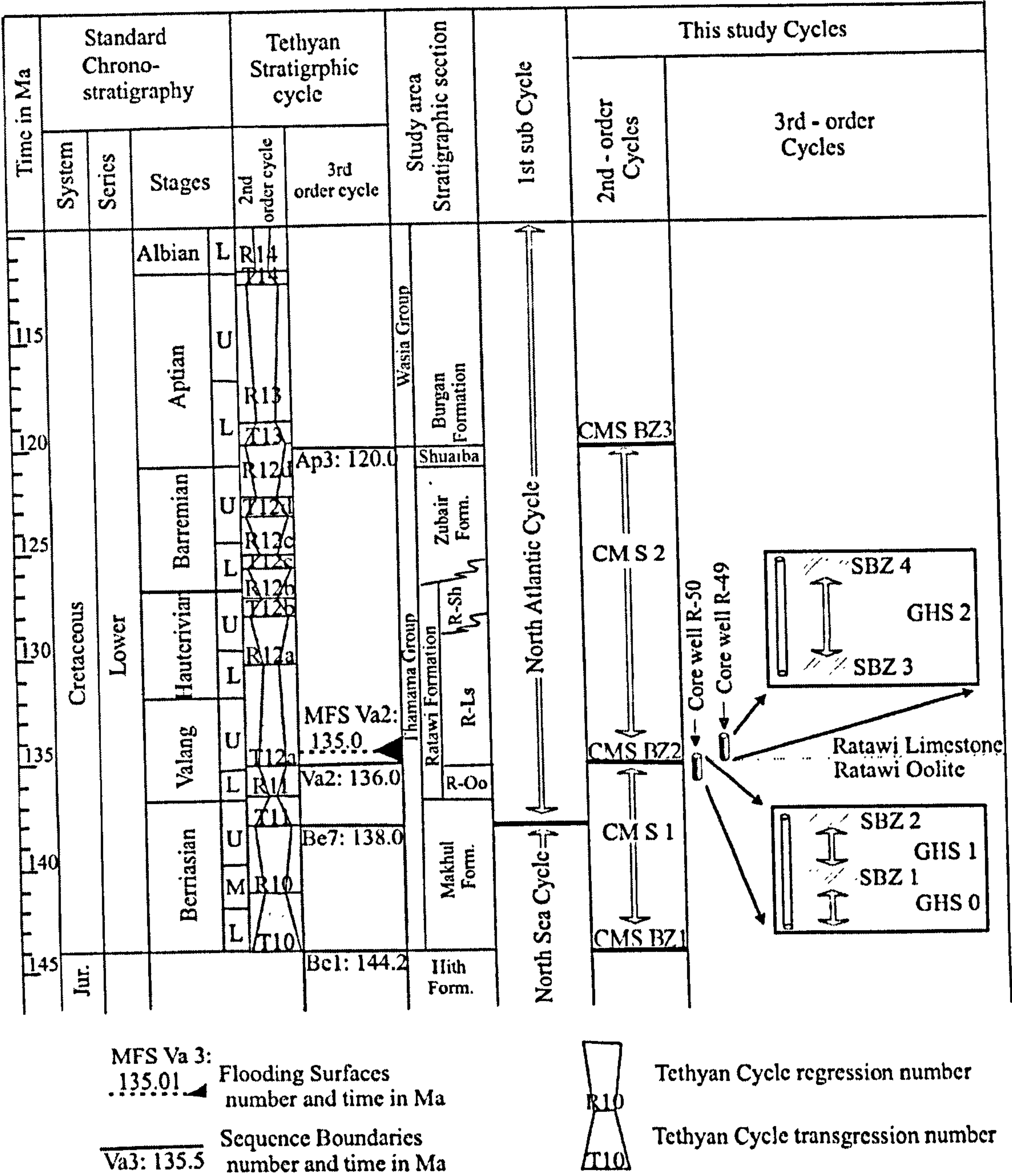


Figure 6-1 2<sup>nd</sup>-order and 3<sup>rd</sup>-order cycles recognized in this study compared to Tethyan stratigraphic cycles and 1<sup>st</sup> sub cycle of Jacquin *et al.* (1998). The 3<sup>rd</sup> order sequence boundary SBZ 1 (in core from well R-50) is equivalent to SBZ 2 (in core from well R-49) and is equivalent to 2<sup>nd</sup> order sequence boundary CMS BZ2. The latter surface is bounded by two major unconformity surfaces. The lower surface is a type 1 unconformity and its correlative conformable surface compares to Tethyan cycle surface Va2; the upper surface marks the beginning of a deepening upward succession and its correlative type 3 unconformity correlates to Tethyan cycle flooding surface number MFS Va2. (R-Oo = Ratawi Oolite, R-Ls = Ratawi Limestone, R-Sh = Ratawi Shale, GH S-1 = greenhouse sequence number 1, SB Z-1 = sequence boundary zone number 1, CM S 1 = composite sequence number 1 and CMS BZ 1 = composite sequence boundary zone number 1).



This study infers that each of these two Thamama Group cycles is equivalent to a 2<sup>nd</sup> order, composite sequence (CM S) (Fig.6-1), separated by a second-order composite sequence boundary zone (CMS BZ). The lower cycle is labelled in this study as CM S-1 and the upper cycle as CM S-2. The lower boundary zone of the first composite sequence is labelled in this study as CMS BZ-1 at the bottom of the Group; the middle boundary zone between the two composite sequences is CMS BZ-2, and the upper boundary zone of the second composite sequence is CMS BZ-3 at the top of the Group.

The development of two 2<sup>nd</sup> order cycles of long-term accommodation changes in the Thamama Group is associated with cycles of Arabian-Iranian basin fill, which represent different stages in the development of the shallow-water Arabian shelf and deep-water Gotnia Basin. These long-term 2<sup>nd</sup> order cycles could be related to different stages of tectonic development of the Arabian plate, which is associated with the development of the Tethyan seaway.

This study has no available chronostratigraphic data to determine the duration of the two composite sequences of the Thamama Group. The duration of CM S-1 and CM S-2 could be calculated by estimating the date of the CMS BZ-1, CMS BZ-2, and CMS BZ-3. Lehrmann *et al.* (2000) correlated the upper boundary zone of the Thamama Group CMS BZ-3 to a carbonate platform surface Ap 3 in Mexico and Texas, about 120 ma. on the Hardenbol *et al.* (1998) chart.

The petrographic and stratigraphic data in this study indicate that the development of the Ratawi Oolite platform was terminated by deposition of the deep-water Ratawi Limestone and Ratawi Shale, after a long period of subaerial exposure (Chapter 5). This study interprets the lithofacies succession of the middle and upper members as a deepening (drowning) succession.

This deepening succession is inferred in this study to be correlated with the 'global' drowning event associated with the start of the second 2<sup>nd</sup> order cycle of the Thamama Group (Section 6.4). This study used the Hardenbol *et al.* (1998) composite "global" sequences and "eustatic" curves from the Mesozoic and Cenozoic chronostratigraphic chart to correlate CMS BZ-2 to sequence boundary surface number Va 2, dated at about 136 million years, which is positioned under a 'major' maximum flooding surface (global drowning event). This event is inferred in this study to be correlated with the Ratawi deepening succession (Section 6.4).



This study inferred from the Hardenbol *et al.* (1998) chart that CMS BZ-1 may be the first sequence boundary in the Cretaceous, which is surface number Be 1, about 144 ma. These data are used to calculate the duration of the two 2<sup>nd</sup>-order sequences of the Thamama Group; CM S-1 was about 8 million years, whereas CM S-2 was about 16 m.y.

This study interprets and predicts the vertical succession (temporal) and areal distribution (spatial) of lithofacies of the Ratawi reservoir zone at Wafra oilfield and components of the petroleum system (source, reservoir and seal rocks) in the framework of different stages of development of the two 2<sup>nd</sup>-order composite sequences.

### **6.1.3 Aims of this chapter**

The end goal for this chapter and this study is to construct a sequence stratigraphic model for the Ratawi Formation in the Thamama Group in which location, cycle succession, depositional and early diagenetic facies, and petrophysical properties of the Ratawi Formation at Wafra oilfield as well as regional source, reservoir and seal rocks in the study area can be interpreted and predicted. This chapter has four aims, namely:

1. Analyzing factors controlling the distribution of the Ratawi Formation in the study area, discussed in Section 6.2.
2. Documenting the hierarchy of cyclicity of the Ratawi sequence stratigraphic framework that constituted the Ratawi zone, Ratawi Oolite platform, from the cored interval at Wafra oilfield, discussed in Section 6.3.
3. Interpreting the local and regional versus global controls on initiation, development, and termination of the Ratawi Oolite platform that can act as a predictive tool for reservoir heterogeneity for the Ratawi zone at Wafra oilfield, discussed in Section 6.4.1.
4. Interpreting the local, regional and global control on the development of the Ratawi Formation petroleum system, discussed in Section 6.4. 2.

### **6.2 Distribution of Ratawi Formation in the study area and adjacent countries**

Understanding the factors that control the areal (spatial) and vertical (temporal) distribution of the three members of the Ratawi Formation (Ratawi Oolite, Ratawi Limestone and Ratawi Shale) in the study area and adjacent countries is important for



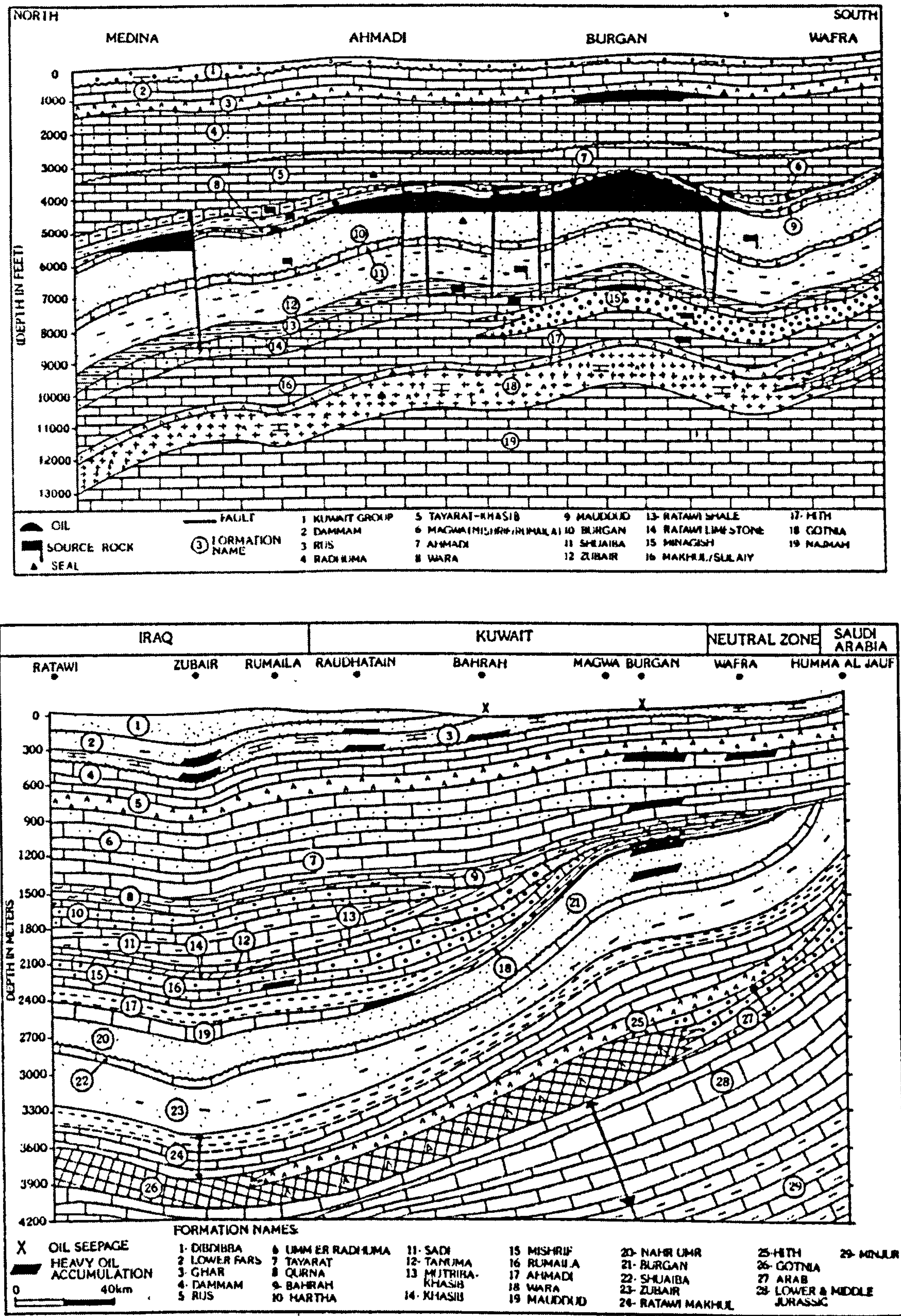


Figure 6-2 Lithostratigraphic-structural cross-section showing productive horizons in the major oil fields in southern Kuwait and the study area, the Partitioned Neutral Zone (PNZ) (upper). Lithostratigraphic correlation of the Mesozoic formations in southern Iraq-Kuwait-PNZ and northeastern Saudi Arabia (lower) (after Alsharhan and Nairn, 1997). The regional temporal and spatial distribution of the lower Cretaceous Thamama Group in the Arabian-Iranian basin is used in this study to interpret the regional processes controlling the deposition of the Ratawi Formation.



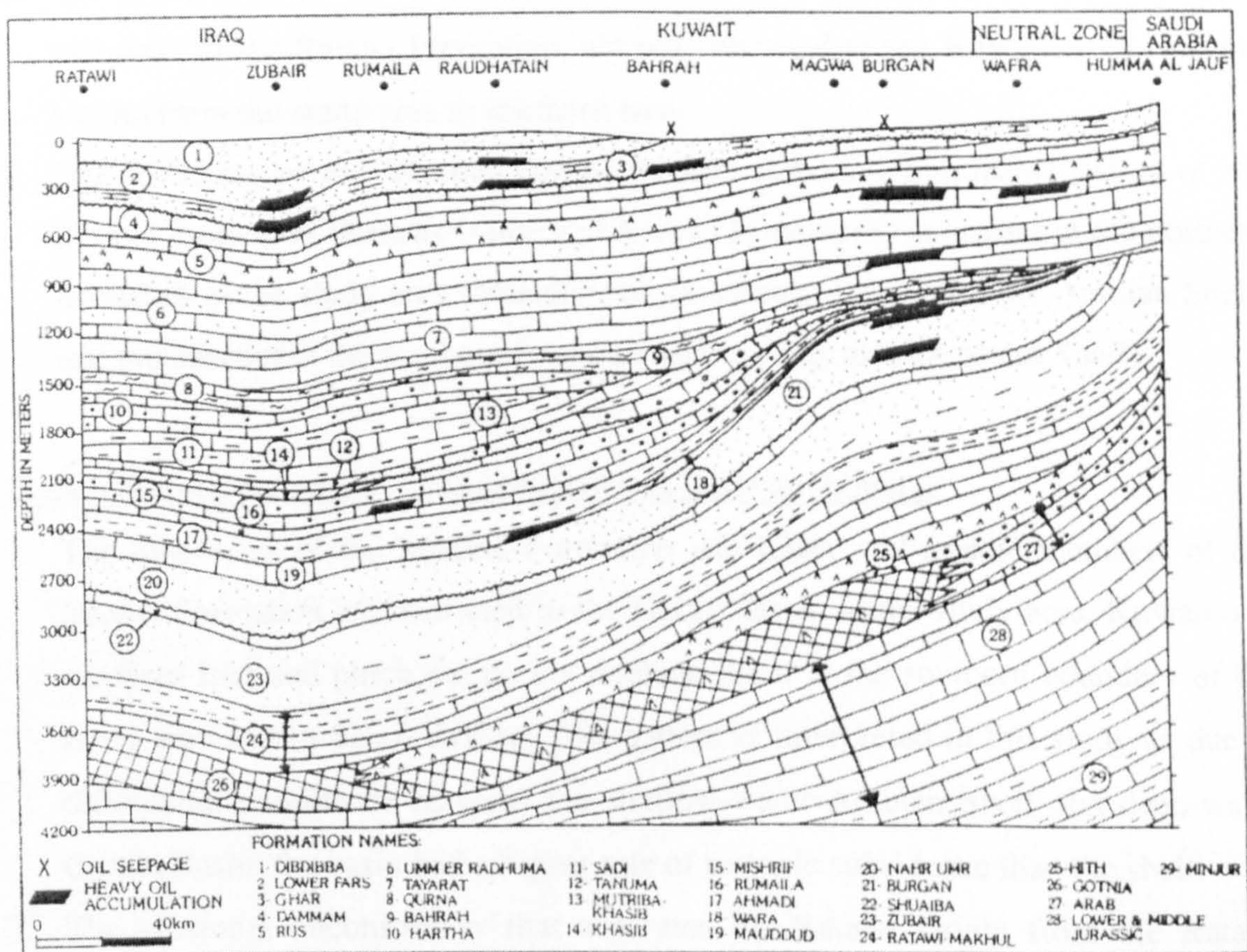
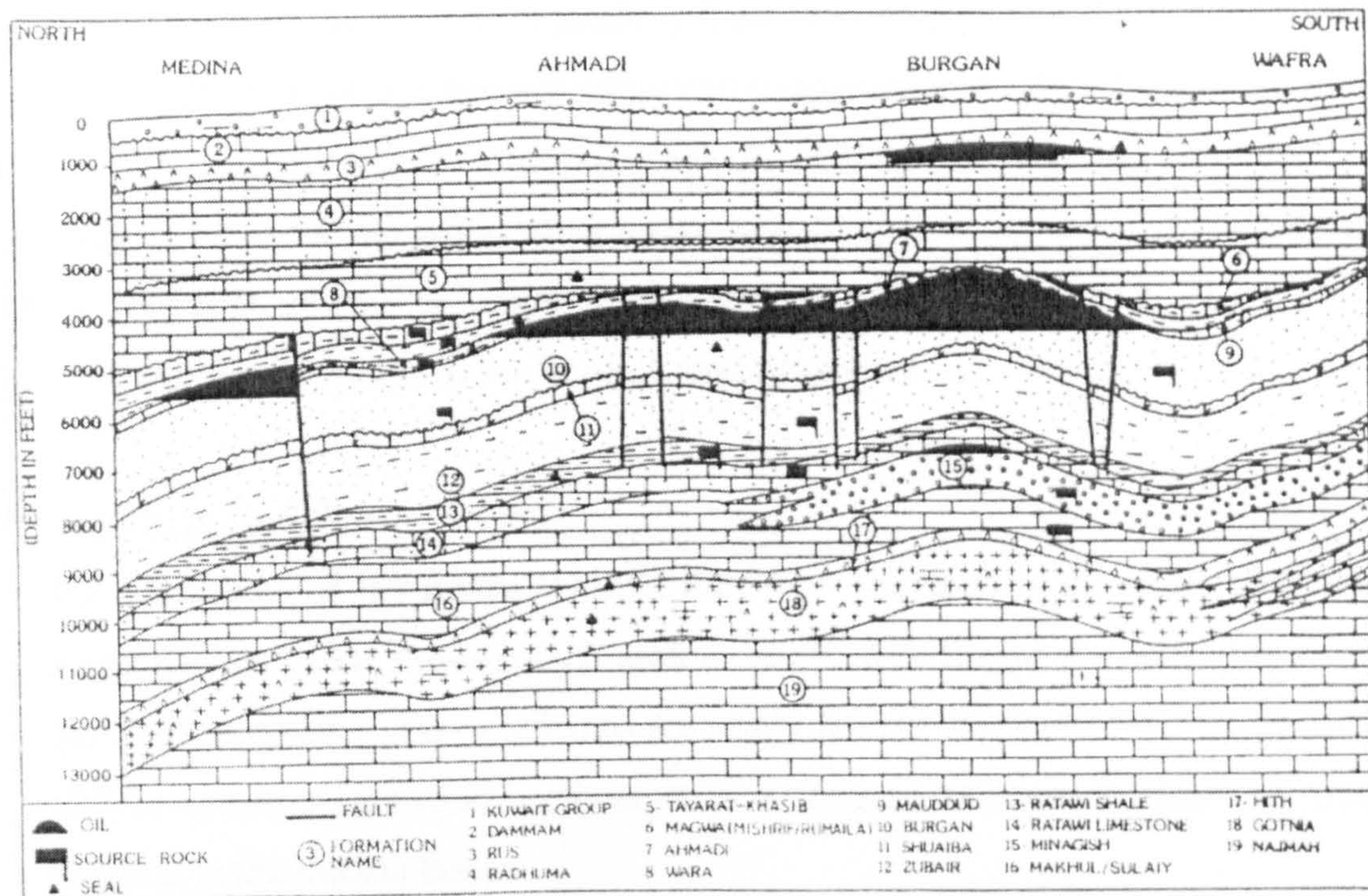


Figure 6-2 Lithostratigraphic-structural cross-section showing productive horizons in the major oil fields in southern Kuwait and the study area, the Partitioned Neutral Zone (PNZ) (upper). Lithostratigraphic correlation of the Mesozoic formations in southern Iraq-Kuwait-PNZ and northeastern Saudi Arabia (lower) (after Alsharhan and Nairn, 1997). The regional temporal and spatial distribution of the lower Cretaceous Thamama Group in the Arabian-Iranian basin is used in this study to interpret the regional processes controlling the deposition of the Ratawi Formation.



the interpretation of the factors controlling Ratawi architecture, and these are essential for the construction of the Ratawi sequence stratigraphic model. This study reveals several important factors by analyzing the published data and the lithofacies and thickness patterns in the regional cross-section published by Alsharhan and Nairn (1997) (Fig.6-2) which are north-south cross-sections through the Saudi Arabia-Kuwait Partitioned Neutral Zone, Kuwait, and southern Iraq.

These patterns include:

1. The lithofacies of the Ratawi Oolite, the lower member of the Ratawi formation, are restricted to the Kuwait Arch area in the Gotnia Basin; the arch extends from the Arabian Shelf in the south into the study area at Wafra oilfield to the Burgan oilfield and ends (plunges) in the north at a distance between Burgan and Ahmadi oilfields in the Gotnia Basin.
2. The lithofacies of the Ratawi Limestone and Ratawi Shale, the middle and upper members of the Ratawi Formation, are not restricted to the Kuwait Arch area but extend from the study area to southern Iraq.
3. The thickness of the Makhul Formation and carbonate-dominated facies of the Ratawi Formation (Ratawi Oolite and Ratawi Limestone) is greater at the northern boundary of the study area (boundary of the Gotnia Basin with the Arabian Shelf) and pinches out at the southern boundary of the study area (Arabian Shelf).

These observed patterns are interpreted in this study as showing:

1. The lithofacies of the Makhul Formation and lower and middle members of the Ratawi Formation are restricted to the Gotnia Basin in the study area, Kuwait and southern Iraq and pinch out on the Arabian Shelf at the southern boundary of the study area and in Saudi Arabia. This pattern is interpreted in this study as due to differential subsidence between the shallow-water Arabian Shelf and deep-water Gotnia Basin; the basin had a higher rate of tectonic subsidence than the shelf.
2. The erosional unconformity that separates the Ratawi Oolite from the Ratawi Limestone (CMS BZ-2) decreases in intensity from the south (on the shelf) to the north (in the basin) due to an increase in differential subsidence. This unconformity and the overlying deepening succession (Ratawi Limestone and Ratawi Shale) in the study area may be correlated to a conformable surface and drowning



unconformity in the basin to the north of the study area, discussed in Section 6.4.

3. The lithofacies of the lower member of the Ratawi Oolite (the reservoir zone) is considered in this study to be a 'local' vertical and lateral lithofacies change of the Makhul Formation. This study infers tectonic activation of the Kuwait arch in the study area by differential subsidence between the arch and the deep-water Gotnia Basin, which created the shallow-water depositional environment of the Ratawi Oolite platform.
4. The shallow-water depositional environment of the reservoir facies ended through differential subsidence between the arch and the basin in the study area after a long period of subaerial exposure (CMS BZ-2), and the deposition of the deepening succession of the Ratawi Limestone and Ratawi Shale. The differential subsidence between the Arabian Shelf and the Gotnia Basin continued during the deposition of the deepening succession.
5. The differential subsidence between the shelf and the basin ended in the study area by deposition of shallow-water carbonate facies of the Shuaiba Formation, the upper lithofacies of the second composite sequence of the Thamama Group (CMS S-2).

### **6.3 The cycle hierarchy of the Ratawi Formation**

Eighty-four parasequences are recognized in this study from the cored interval of the Ratawi Oolite and Ratawi Limestone in wells R-50 and R-48 by applying a high-resolution sequence stratigraphic approach. Since well data provide one-dimensional data that do not resolve stratal geometry and the termination of the Ratawi Oolite platform, this study used stacking pattern analysis to identify the cycle hierarchy of the Ratawi Formation (Chapter 5). Integrating these data with petrographic and stratigraphic data from this study and published data resulted in an integration of the hierarchy units of the Ratawi Formation into the Thamama Group hierarchy units.

The cycle hierarchy recognized in this study is 5<sup>th</sup> order parasequence, 4<sup>th</sup> order systems tract, 3<sup>rd</sup> order greenhouse sequence (GH S-0, GH S-1 and GH S-2 in the Ratawi Formation), in addition to 2<sup>nd</sup> order composite sequence (CM S-1 and CM S-2) in the Thamama Group (Appendix II and Fig. 6-1). These genetic units are characterized by systematic vertical and lateral distributions of Ratawi microfacies, lithofacies, ramp depositional system, early diagenetic facies and petrophysical properties.



The recognition of a cycle hierarchy in the Ratawi Formation within the Thamama Group cycle hierarchy provides a predictive sequence stratigraphic framework for the Ratawi reservoir zone in which the petrophysical properties of the reservoir and non-reservoir units, in addition to the Ratawi Formation petroleum system, are interpreted and predicted (Chapter 5).

Petrographic and stratigraphic data indicate a sequence boundary zone (SBZ-2) between the lower and middle member of the Ratawi Formation that is equivalent to the 2<sup>nd</sup> order sequence boundary zone CMS BZ-2, which divides the Thamama Group into two 2<sup>nd</sup> order composite sequences (CM S-1 and CM S-2) (Fig. 6-1). The GH S-0 and GH S-1 of the lower member (Ratawi Oolite) is at the top of CM S-1, whereas the GH S-3 of the middle member (Ratawi Limestone) is at the bottom of the CM S-2.

These petrographic and stratigraphic data include:

1. The petrographic data in this study indicate that the main controlling porosity in Unit E is diagenetic secondary <sup>or alveolar</sup> rootlet porosity formed by a long period of subaerial exposure (Chapter 4). Reservoir Unit E is the only reservoir unit in the Ratawi zone at Wafra oilfield that is producing in the main, southern and eastern Wafra areas.
2. The regional stratigraphic data indicate that the lithofacies of the lower member of the Ratawi Oolite in the study area are correlated to the Yamama Formation and erosional unconformity to the south (Saudi Arabia) and Minagish Formation to the north (Kuwait) (Chapter 2). The lithofacies of the middle member (Ratawi Limestone) and upper member (Ratawi Shale) in the study area are correlated to the Buwaib Formation to the south (Saudi Arabia) and Ratawi Formation to the north (Kuwait). There is a subaerial erosional unconformity on the Arabian Shelf between the Yamama Formation and the overlying Buwaib Formation. The intensity of the erosional unconformity decreases from the outcrop on the Arabian Shelf to the south of the study area, into the subsurface in the study area and the Gotnia Basin, to the north (Alsharhan and Nairn, 1997).

#### 6.4 Ratawi Formation sequence stratigraphic model

To use the constructed Ratawi Formation Thamama Group sequence stratigraphic framework as a predictive tool for Ratawi reservoir heterogeneity and petroleum system, the local, regional and global factors controlling the Ratawi Formation in the



Thamama Group cycle hierarchy must be interpreted and predicted. Many workers including Handford and Loucks (1993), Greenlee and Lehrmann (1993), and Fitchen (1997) proposed generalized sequence stratigraphic models for carbonate successions.

These models interpret platform stratal geometry, depositional and early diagenetic facies by three basic parameters, namely accommodation history, depositional system (sediment supply), and platform margin-profile (platform type) (Fitchen, 1997). The model is used in this study to interpret and predict sequence stratigraphic cycles at different scales (Sections 6.5 and <sup>5.3</sup>~~5.2.4.2.2~~).

However, to construct a specific sequence stratigraphic model for the Ratawi, this study must consider the specific factors and rate of change of processes that control the Ratawi Oolite platform initiation, development and termination (Fitchen, 1997; Harris *et al.*, 1999). The specific factors that are considered in this study include:

1. The carbonate organisms which were living during the Lower Cretaceous Valanginian-Hauterivian time, and the Cretaceous 'calcite-sea'.
2. The configuration of the Ratawi epeiric ramp platform, which was at the boundary between the shallow-water Arabian Shelf and the deep-water Gotnia Basin (Chapter 2).
3. The rate of subsidence, inferred in this study to be linear subsidence associated with the passive continental margin of the Arabian plate, and differential subsidence between the Kuwait Arch, Gotnia Basin and Arabian Shelf, in addition to the development of a local antecedent topographic high by movement of Hormuz salt (Chapter 2).
4. The eustatic sea-level fluctuations during the Lower Cretaceous Valanginian-Hauterivian, which was a greenhouse time with 'little icehouse' periods (Chapter 5).
5. The climatic conditions during the Lower Cretaceous, which was a semi-arid climate after the very arid climate during the Upper Jurassic (Chapter 3).
6. The detrital siliciclastic influx to the study area, inferred to be associated with the migration of the Zubair delta from southern Iraq into the study area (Chapter 2).

#### **6.4.1 Factors controlling Ratawi Formation cyclicity**

The stratigraphic evolution of the 'Ratawi Oolite platform', and its initiation, development and termination, and the four broad facies belts, deep-ramp, shallow-ramp, back-ramp, and subaerial exposure, are controlled by the interplay between



eustasy, tectonics and sediment supply at the second and third-order cycle scale. These three parameters control the architecture of the Ratawi Oolite platform by controlling the platform keep-up, catch-up and give-up phases.

The petrographic and stratigraphic data in this study indicate that the lower member (Ratawi Oolite) represents a keep-up phase, whereas the lower part of the middle member (Ratawi Limestone) represents a catch-up phase, and the upper part represents a give-up phase. The amount of carbonate sediment decreases whereas detrital siliciclastic material increases upward from the lower member to the middle and upper members of the Ratawi Formation. The upper member (Ratawi Shale) represents complete drowning and burial of the Ratawi Oolite platform by the deep-water prodelta shale of the Zubair delta.

The keep-up phase of the Ratawi Oolite member was formed when the rate of carbonate sediment supply was matched by the rate of accommodation space increase. The 'Ratawi Oolite platform' aggraded to form a shoaling-upward cycle. This phase of platform development is characterized by peritidal parasequences. The accommodation space was created by differential subsidence between the Gotnia Basin and Kuwait Arch, and eustatic sea-level change during the Lower Cretaceous greenhouse and 'small icehouse' (Chapter 5).

The catch-up phase of the lower part of the Ratawi Limestone member was formed when the rate of carbonate sediment supply was unable to keep pace with the rate of accommodation space increase, but it then later aggraded to sea level. The give-up phase of the upper part of the Ratawi Limestone member formed when the rate of carbonate sediment supply was unable to match the rate of accommodation space increase, and the Ratawi Oolite platform was then buried under the prodelta shale of the Zubair delta (Ratawi Shale member) (Kendall *et al.*, 1991). These two phases of platform development are characterized by subtidal parasequences (Chapter 5).

Goldhammer and Wilson (1991) divided the Upper Jurassic and Lower Cretaceous in north-eastern Mexico and the northern Gulf Coast of Mexico into four 2<sup>nd</sup> order sequences. Sequences number 1 and 2 are in the Upper Jurassic, and sequences number 3 and 4 are in the Lower Cretaceous. Sequence number 3 is correlated in this study to the Thamama Group, which is divided by Douban and Al Medhadi (1999) into two 2<sup>nd</sup>-order sequences.

Jacquin *et al.* (1998) divided the Berriasian to Albian Lower Cretaceous of Western Europe, which includes the northern North Sea, southern England, western



Netherlands and north west Germany, Paris Basin, northern sub-Alpine Chains and Vocontian Basin, into six 2<sup>nd</sup> order cycles. They correlated these six 2<sup>nd</sup> order cycles to six Tethyan 2<sup>nd</sup> order cycles, which are Tethyan cycle numbers 10 to 15. Cycle number 10 is the upper part of the 1<sup>st</sup> order sub-cycle 'North-Sea cycle', and cycles 11 to 15 are in the lower part of the 1<sup>st</sup> order sub-cycle 'North Atlantic cycle' (Fig. 6-3 and Fig 6-4).

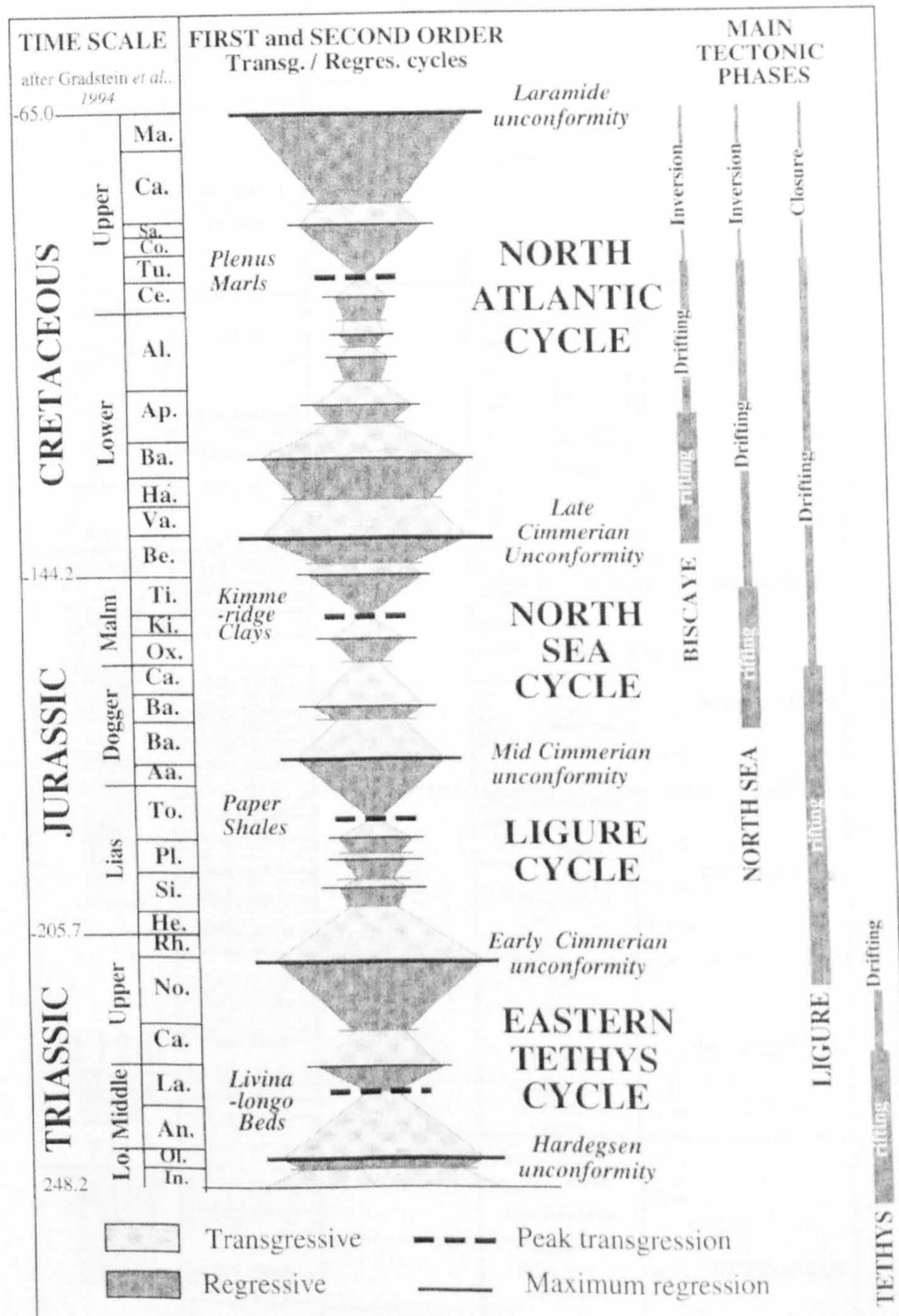


Figure 6-3 Major transgressive / regressive cycles, source rocks and main phases of development of European basins. The different tectonic phases are simplified and split into several pulses, each area recording the effects of other basin's development ( after Jacquin and de Graciansky, 1998).



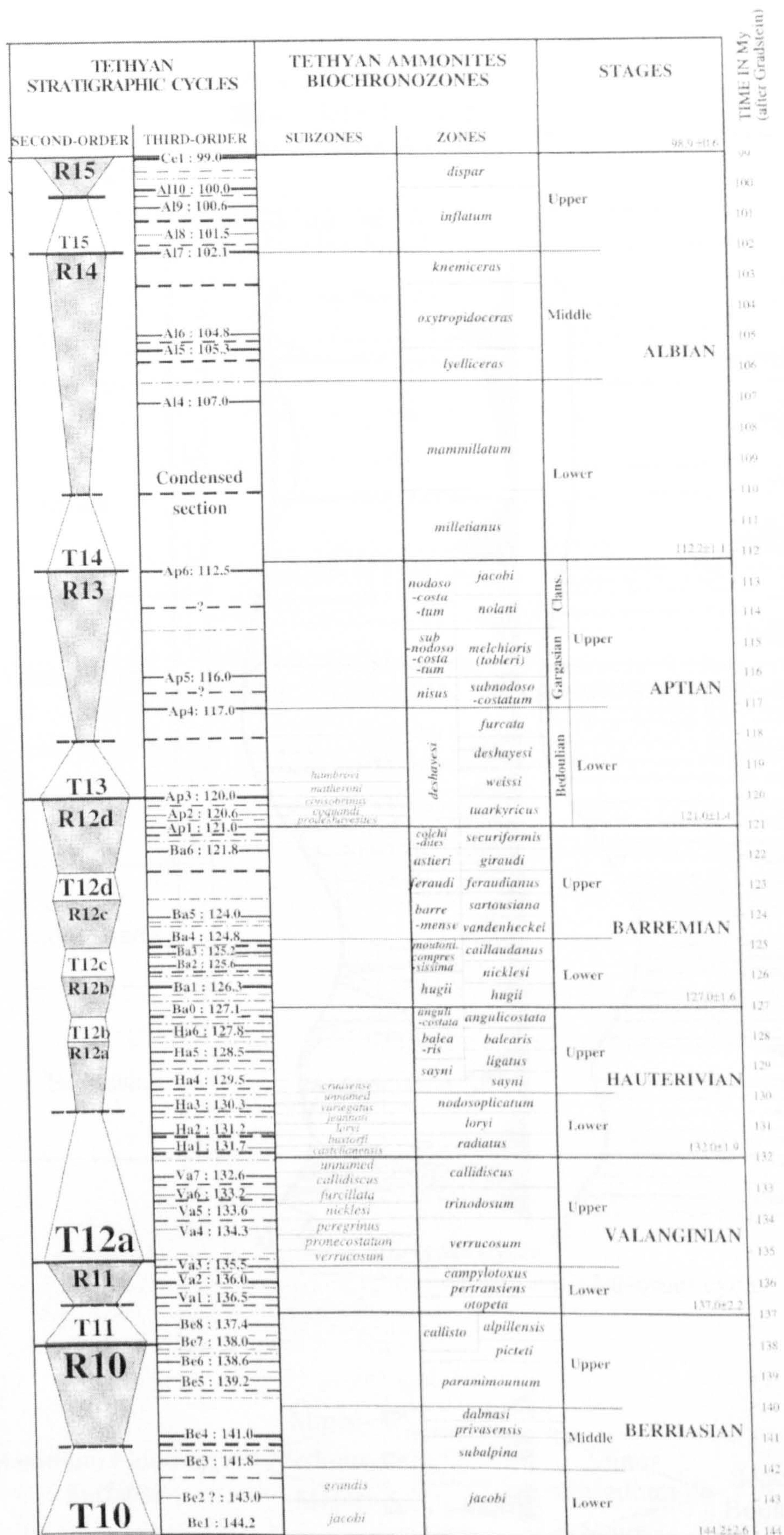


Figure 6-4 Transgressive / regressive cycles for the early Cretaceous of Western Europe (after Jacquin *et al.*, 1998).



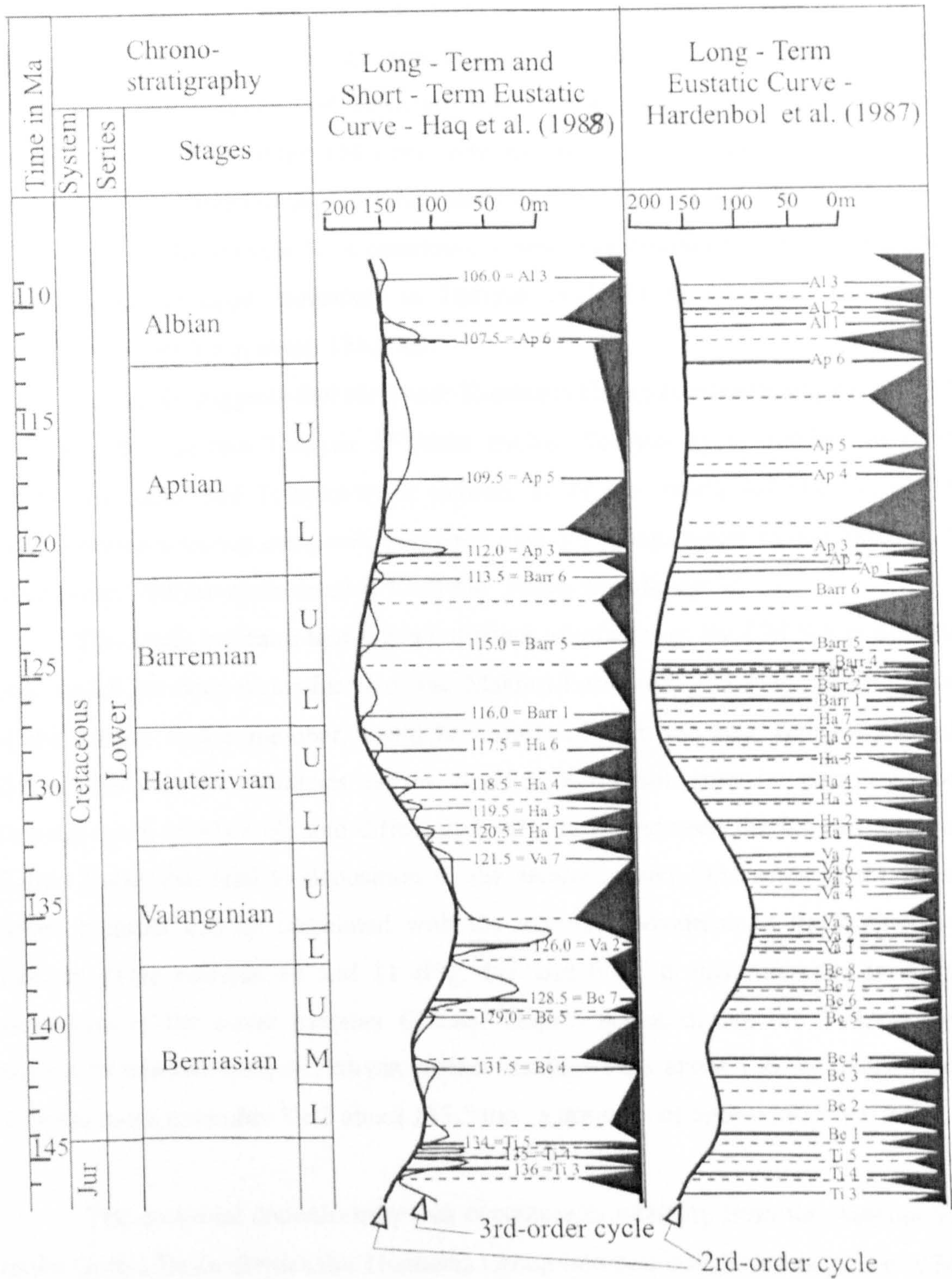


Figure 6-5) Lower Cretaceous Eustatic Curve of Haq *et al.* (1988) compared to Hardenbol *et al.* (1998) (after Hardenbol *et al.*, 1998).



This study has inferred that Tethyan cycles number 10, 11 and 12 are equivalent to the Thamama Group. Similar to the sequence boundary of the Thamama Group, the lower boundary of Tethyan cycle number 10 is correlated to sequence boundary number Be 1, about 144.2 ma., whereas the upper boundary of Tethyan cycle number 12 is correlated to sequence boundary number Ap 3, about 120 ma. The upper boundary for Tethyan cycle 10 is correlated to sequence boundary number Be 7, about 138 ma, and the upper boundary to Tethyan cycle 11 is correlated to sequence boundary number Va 3, about 135.5 ma.

This study suggests that the lower Thamama Group composite sequence CM S-1 is equivalent to two Tethyan 2<sup>nd</sup> order cycles, Tethyan cycle number 10 of the 'North-Sea cycle' and Tethyan cycle number 11 of the 'North Atlantic cycle'. The upper Thamama Group composite sequence CM S-2 is equivalent to one Tethyan 2<sup>nd</sup> order cycle, Tethyan cycle number 12 of the 'North Atlantic cycle'.

This study indicates that the two distinct lithofacies of the CM S-1 in the study area, which are deep-water facies of the Makhul Formation and shallow-water facies of the Ratawi Oolite member, could be correlated with the two Tethyan 2<sup>nd</sup> order cycles. Deep-water lithofacies of the Makhul Formation may be correlated with Tethyan cycle number 10, and differential subsidence between the Kuwait Arch and Gotnia Basin that lead to deposition of the shallow-water lithofacies of the Ratawi Oolite member can be correlated with the tectonic movement at the boundary of Tethyan cycle number 10 and 11 (Fig. 6-1 and 6-4). If this inference is correct, deposition of the lower member (Ratawi Oolite) began during the Tethyan cycle regression number R10, at Tethyan surface number Va 1 about 136 ma, and ended at Tethyan surface number Va 2 about 135.5 ma, a duration of approximately 0.5 my.

The erosional unconformity that decreases in intensity from the Arabian Shelf to the Gotnia Basin divides the Thamama Group into two composite sequences CM S-1, and CM S-2 (Section 6.1.2). Reservoir heterogeneity of the Ratawi zone at Wafra oilfield and the petroleum system of the Ratawi Formation are controlled by the development of two Thamama Group 2<sup>nd</sup> order cycles. The factors controlling the development of the two composite sequences, CM S-1 and CM S-2, and the three composite sequence boundary zones, CMS BZ-1, CMS BZ-2, CMS BZ-3, are discussed in the following sections.



To construct a Ratawi sequence stratigraphic model, the relative importance of eustasy, tectonics and sediment supply at global, regional and local scales on the development of composite sequences CM S-1 and CM S-2 must be distinguished. One method to constrain the relative significance of each of these three main variables is to compare the pattern for two of the variables. This study analyzes tectonic versus eustatic processes (Section 6.4.1.1), eustatic versus sedimentary processes (Section 6.4.1.2), and sediment supply versus tectonic processes (Section 6.4.1.3) on the initiation, development and termination of the 'Ratawi Oolite platform', and the development of the Ratawi Formation petroleum system.

#### **6.4.1.1 Tectonic versus eustatic processes**

In order to separate the relative significance of regional and local tectonics from eustatic global sea-level change, this study correlates the Ratawi Formation in cycle hierarchy at the 2<sup>nd</sup> order cycle scale to the published eustatic cycle chart of Hardenbol *et al.* (1998) and Haq *et al.* (1988) (Fig 6-5). Only those sequence boundaries that can be correlated over large areas of the globe could have been formed by some kind of eustatic control (Bosellini *et al.*, 1999).

##### **6.4.1.1.1 Factors controlling composite sequence boundary zone CMS BZ-1**

According to Douban and Al Mēdhadi (1999), sequence boundary zone CMS BZ-1 is associated with the onset of the first 2<sup>nd</sup> order relative sea-level rise during the lower Cretaceous that deposited the first composite sequence CM S-1 of the Thamama Group. This relative sea-level rise was after a relative sea-level low, which produced an Upper Jurassic thick evaporite succession in the study area (Section 6.1.2).

There are no available data for this study to locate the position of this surface on the eustatic cycle chart of Hardenbol *et al.* (1998) and Haq *et al.* (1988). This study assumes that the CMS BZ-1 is the first sequence boundary at the start of the Cretaceous period, which is surface number Be 1, about 144 ma (Fig. 6-6) This surface separates the shallow-water evaporites of the Upper Jurassic Hith Formation from the deeper-water lower Cretaceous Makhul Formation in the study area.

The regressive phase during the late Jurassic in the Arabian-Iranian basin could be correlated to a similar phase in Europe during the end of the North Sea cycle (Jacquin and De Graciansky, 1998). Sequence boundary surface Be 1 is controlled by global sea-level rise, a eustatic process.



#### 6.4.1.1.2 Factors controlling composite sequence boundary zone CMS BZ-2

Composite sequence boundary zone CMS BZ-2 is associated with the onset of the Thamama Group second 2<sup>nd</sup> order cycle, which started during the Hauterivian (Lower Cretaceous) and deposited the second composite sequence CM S-2 (Section 6.1.2). This sequence boundary zone separates the lower member (Ratawi Oolite) from the middle member (Ratawi Limestone) in the study area.

In a review of sequence boundary types, Schlager (1999) listed three types of sequence boundary, type 1, type 2 and type 3 (Fig. 6-7). The first two types are restricted to surfaces with evidence of subaerial exposure, whereas the last type is without a long period of subaerial exposure. Sequence boundary type 1 is formed when the maximum rate of eustatic fall exceeds the rate of subsidence. Sequence boundary type 2 is formed when maximum rate of eustatic fall approximately equals the rate of subsidence. Sequence boundary type 3 is formed when maximum rate of eustatic fall is distinctly less than the rate of subsidence.

The petrographic and stratigraphic data from this study indicate that the upper boundary of the Ratawi Oolite, CMS BZ-2, marks the termination of the Ratawi Oolite platform by the deposition of the deepening-upward succession of the overlying Ratawi Limestone on the subaerially exposed surface of the platform (Section 6.3). This composite sequence boundary zone is inferred in this study to be bounded by two major unconformity surfaces.

The lower boundary surface is a type 1 sequence boundary in the study area on the Kuwait Arch and its correlative conformable surface is in the Gotnia Basin succession (Section 6.4.1.1.2.1). The upper boundary surface is a sequence boundary type 3 in the Gotnia Basin and its correlative deepening-upward succession in the study area on the Kuwait Arch (Section 6.4.1.1.2.2).

##### 6.4.1.1.2.1 Type 1 unconformity and its correlative conformable surface

The stratigraphic and petrographic data in this study infer subaerial exposure of the Ratawi Oolite in the study area on the Kuwait Arch but continuous deposition in the Gotnia Basin. This was due to one or two processes. The first is a change in rate of differential subsidence between the arch and the basin, which would have lead to tectonic uplift of the arch at the start of Tethyan cycle number 11 (Section 6.4.1); the second is an increase in the rate of eustatic sea-level fall. During the relative sea-level low, the four facies belts of the Ratawi epeiric ramp (deep-ramp, shallow-ramp, back-



ramp, and subaerial exposure facies) were shifted in the direction of the deep-water Gotnia Basin, with the expansion of the subaerial facies belt of the Arabian Shelf onto the Kuwait Arch in the study area.

This study used the Hardenbol *et al.* (1998) and Haq *et al.* (1988) composite "global" sequences and "eustatic" curves from the Mesozoic and Cenozoic chronostratigraphic chart to correlate the lower boundary unconformity surfaces of composite sequence boundary zone CMS BZ-2 to sequence boundary surface number Va 2, dated at about 136 ma (Fig. 6-5 and 6-6). As explained in the previous section the Thamama Group first composite sequence CM S-1 can be correlated to Tethyan cycles number 10 and 11. The Reservoir zone, which is the lower member of the Ratawi Oolite, is inferred in this study to be equivalent to Tethyan cycle number 11.

According to Jacquin *et al.* (1998) the 1<sup>st</sup> order sub-cycle of the 'North Atlantic cycle' is defined by the onset of the Upper Ryazanian transgression onto the European craton, and this is equivalent to the onset of Tethyan cycle number 11. In Europe this is a major turning point between the overall progradation of the underlying late Jurassic - lowermost Cretaceous regressive phase and the overall Cretaceous transgressive episode.

The most erosional surface in the 'North Atlantic cycle' interval in Europe is not at the base of the succession, the lower sequence boundary of Tethyan cycle number 11, but at the upper sequence boundary of this cycle. The unconformity at the end of Tethyan cycle number 11, which is equivalent to the unconformity at the end of the Ratawi Oolite member in this study, is the last of four Late Cimmerian unconformities, which are dated respectively as Lower Volgian (Tithonian), Upper Volgian, Late Ryazanian (upper Berriasian), and Lower Valanginian.

This Lower Cretaceous major unconformity in Europe is inferred in this study to be correlated to the lower boundary surface of CMS BZ-2 between the Ratawi Oolite and the Ratawi Limestone. This unconformity is identified in the study area as a type 1 sequence boundary on the Kuwait Arch and Arabian Shelf, and its correlative conformable surface in the Gotnia Basin succession. This unconformity is inferred in this study to have had a major impact on the development of heterogeneity in the Ratawi reservoir zone at Wafra oilfield.

During the long unconformity period of subaerial exposure under semi-arid conditions in the study area, a mature calcrete zone developed in the main, southern, and eastern Wafra areas (Chapter 4). This diagenetic overprint on the Ratawi Oolite



platform and its diagenetic secondary rootlet porosity is inferred in this study to be the main control on reservoir unit-E, which is the only reservoir unit producing from the three Wafra areas.

This study infers that the onset of tectonic movements associated with the 1<sup>st</sup> order sub-cycle of the 'North Atlantic cycle' that started at the base of Tethyan cycle number 11, surface number Va 7, at about 138 ma might have lead to the tilting of the Arabian Shelf (eastern part of the Arabian plate) to the east and uplift of the western side (Pratt and Smewing, 1993). This tectonic movement would have lead to differential subsidence between the Kuwait Arch and the Gotnia Basin in the study area, and a subaerial erosional unconformity on the Arabian Shelf. The movement of the arch induced the differential depositional environments of the Ratawi epeiric ramp, with subaerial exposure over the Arabian Shelf, a shallow-ramp (Ratawi Oolite platform facies) over the Kuwait Arch and a deep-ramp in the Gotnia Basin.

This model indicates that the reservoir zone in the Ratawi Oolite member was only deposited in the shallow-water over the arch within the Gotnia Basin. The lower member of the Ratawi Formation is time equivalent to the subaerial unconformity on the Arabian Shelf and is considered in this study as a 'local' facies change of the deep-water Makhul Formation.

#### **6.4.1.1.2.2 Deepening succession and its correlative Type 3 unconformity**

The stratigraphic and petrographic data in this study interpret the termination of the shallow-water deposition of the Ratawi Oolite platform by the deposition of a deepening-upward succession of the Ratawi Limestone on the subaerial unconformity surface over the Kuwait Arch (Chapter 3). This unconformity surface is inferred in this study to be correlated to a conformable surface in the Gotnia Basin, where the deepening-upward succession of the Ratawi Limestone on the arch may be correlated to the drowning event on the conformable surface in the Gotnia Basin.

The drowning event, a type 3 unconformity and its correlative deepening-upward succession, is the upper boundary surface for CMS BZ-2, where the subaerial exposure type 1 unconformity and its correlative conformable surface is the lower boundary surface. This deepening-upward succession and drowning event is the stratigraphic record of the interplay between two processes, the change in the rate of sediment supply and accommodation space (Fig. 6-8). Factors controlling sediment supply are discussed in eustatic versus sedimentary processes (Section 6.4.1.2); factors



controlling relative sea-level rate change are discussed in this section.

The upper boundary surface, which represents a deepening-upward succession of catch-up and give-up phases, was formed when the rate of accommodation space exceeded carbonate sediment supply and accumulation. The rate of change of accommodation space in the study area, during the formation of the upper boundary ~~surface~~<sup>zone</sup>, was controlled by the interplay of two processes. The first is the differential subsidence between the arch and the basin, which is inferred in this study to have ended at this time so that the Kuwait Arch subsided at the same rate as the Gotnia Basin; this is from the regional stratigraphic relations that indicate termination of the shallow-water facies of the Ratawi Oolite. The second is a rapid increase in the rate of relative sea-level rise.

During the fast relative sea-level rise, the four facies belts of the Ratawi epeiric ramp, deep-ramp, shallow-ramp, back-ramp and subaerial exposure, were shifted in the direction of the shallow-water Arabian Shelf, with the expansion of the deep-ramp facies of the Ratawi Limestone over the Kuwait Arch.

To evaluate the significance of global sea-level processes in the formation of the upper boundary surface of CMS BZ-2, this study correlates this change in the accommodation space with other parts of the world. This study used the Hardenbol *et al.* (1998) and Haq *et al.* (1988) composite "global" sequences and "eustatic" curves from the Mesozoic and Cenozoic chronostratigraphic chart to correlate the upper boundary unconformity surface to major flooding surface number MFS Va 2, dated at about 135 ma. This drowning event is associated with the onset of Tethyan 2<sup>nd</sup> order cycle number 12.

According to Bosellini *et al.* (1999) the lower Valanginian drowning unconformity event is well known in a large part of the world, from the Caribbean to eastern Arabia. This event is documented in (1) the western continental margin of the Atlantic Ocean (Scotian Shelf, Baltimore Canyon, Caribbean); (2) the eastern continental margin of the Atlantic Ocean (Iberia, Morocco); (3) the western peri-Alpine domain, the northern and western continental margin of the Ligurian Ocean (western Tethyan) (southern France, Helvetic Alps, Estremadura, eastern Prebetic and Betic areas); and (4) the margins of the Adria Plate (Apulia Platform).

The synchronized termination of widespread carbonate platforms during lower Valanginian time could be the result of several processes, including (1) rapid eustatic sea-level rise; (2) globally increased tectonic movements; (3) pulses in ocean-crust



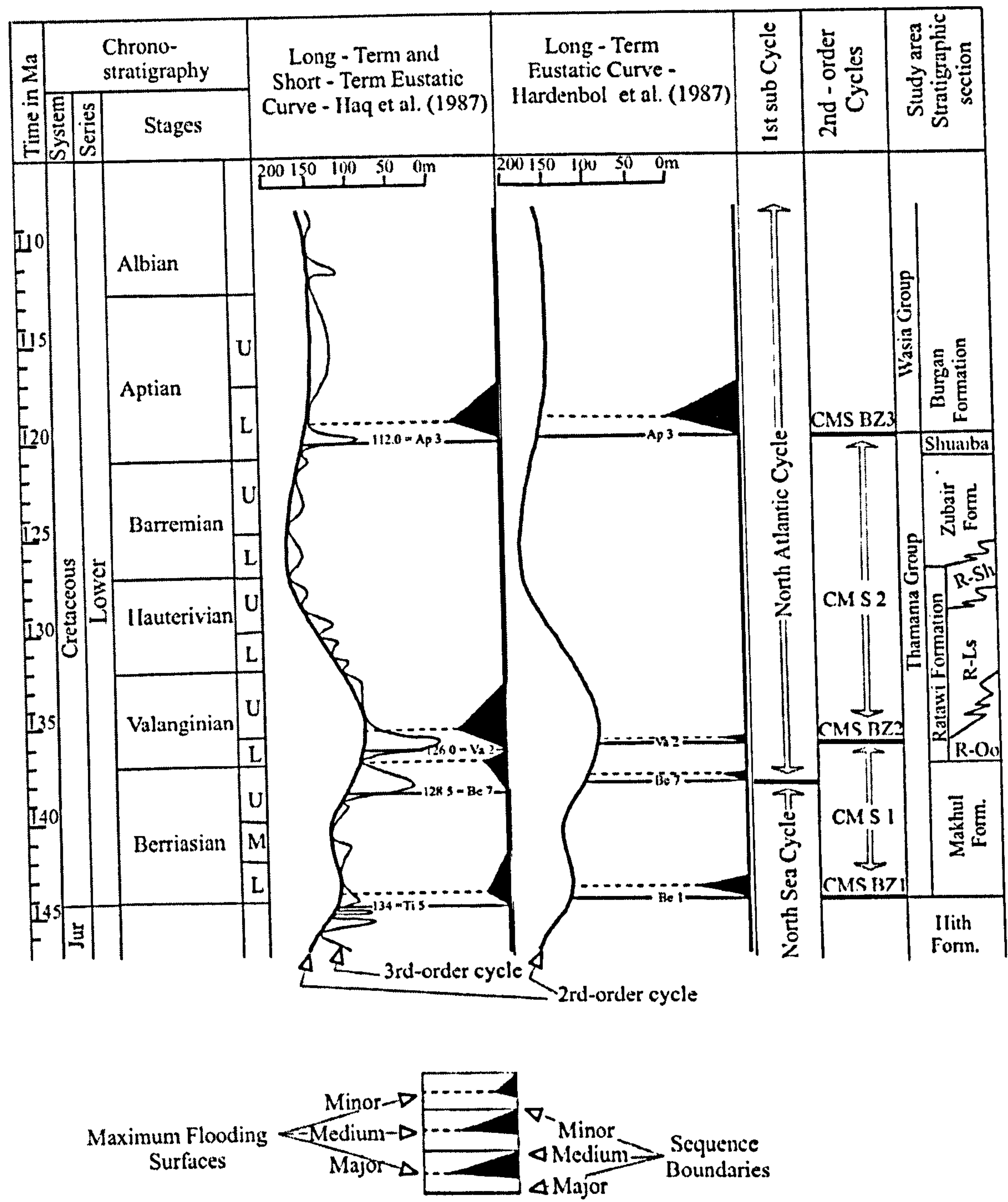


Figure 6-6) Thamama Group 2<sup>nd</sup>-order sequences and surfaces recognized in this study compared with equivalent surfaces in the Eustatic Curve of Haq *et al.* (1987) and Hardenbol *et al.* (1998). Note minor to medium flooding surface for MFS Va2 in Hardenbol *et al.* (1998) curve, whereas it is a major surface in Haq *et al.* (1987) curve. (R-Oo = Ratawi Oolite, R-Ls = Ratawi Limestone, R-Sh = Ratawi Shale, GH S-1 = greenhouse sequence number 1, SB Z-1 = sequence boundary zone number 1, CM S 1 = composite sequence number 1 and CMS BZ 1 = composite sequence boundary zone number 1). The lower boundary of the Ratawi Limestone showing evidence of subaerial exposure, probably varies locally from middle Valanginian to lower Hauterivian. There may be a condensed section between the Ratawi Oolite and Ratawi Limestone in the Gotnia Basin.



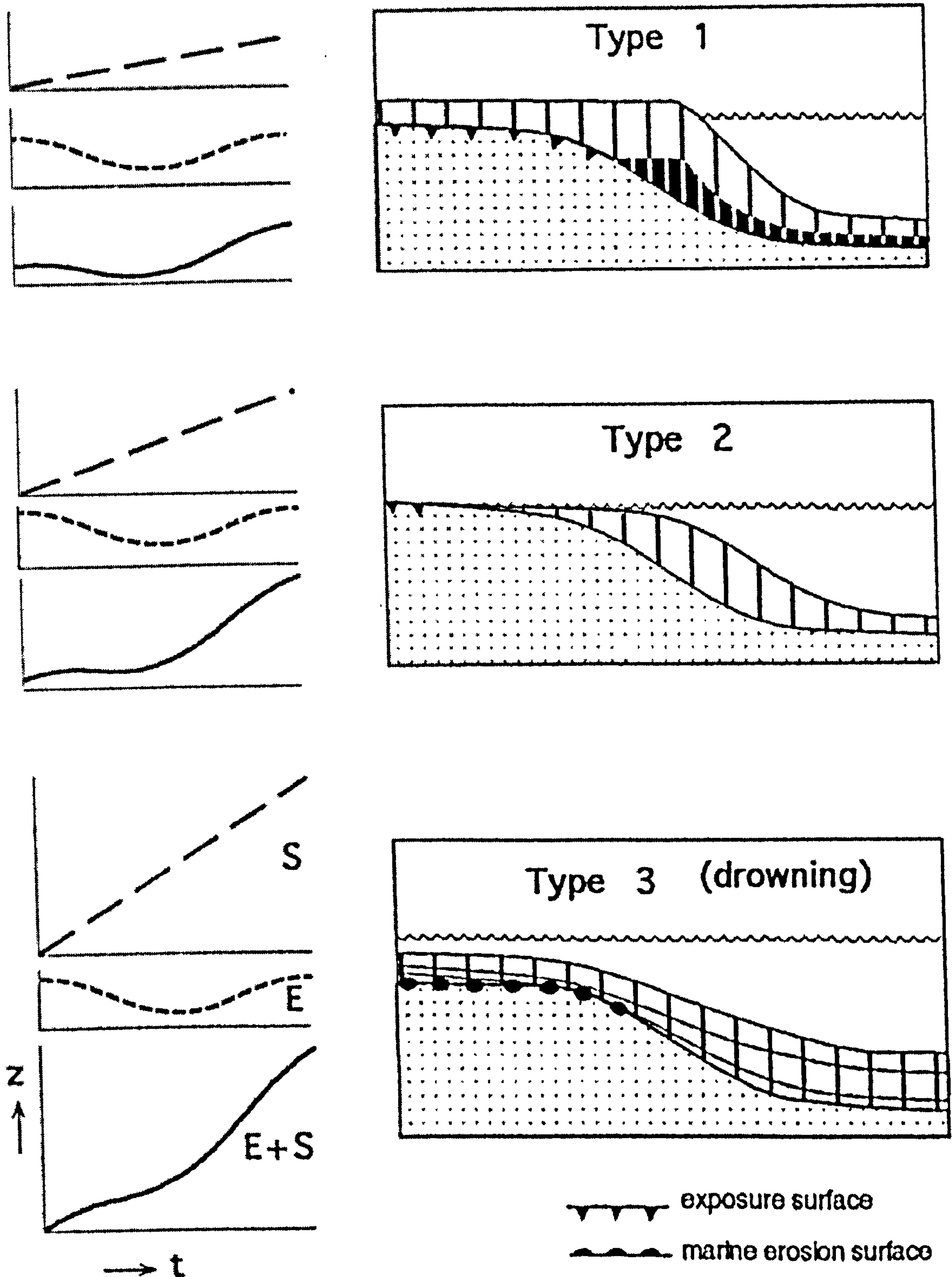


Figure 6-7 Diagram showing the three types of sequence boundaries recorded as an imaginary eustatic cycle in three areas with different rates of subsidence ( $t$  = time,  $Z$  = relative sea-level). Type 1 sequence boundary formed when maximum rate of eustatic fall ( $E$ ) comfortably exceeds the rate of subsidence ( $S$ ) (top). Type 2 sequence boundary formed when maximum rate of eustatic fall is approximately equal to the rate of subsidence (middle). Type 3 sequence boundary formed when maximum rate of eustatic fall is distinctly less than the rate of subsidence (top) (after Schlager, 1999).



**Origin of drowning unconformities:**

1. very rapid relative sea-level rise; e.g., a glacio-eustatic rise in an icehouse time.
2. environmental change or deterioration:
  - a. siliciclastic contamination, e.g., many Tertiary platforms in SE Asia.
  - b. change in oceanic circulation and upwelling, e.g., Urgonian (Cretaceous) French Alps.
  - c. basin salinity changes in intracratonic basins, e.g., Carboniferous, central England.
  - d. oceanic anoxic events, e.g., mid-upper Cretaceous.
  - e. long-term migration of platforms out of subtropical zones, e.g., Jurassic-Cretaceous, eastern U.S.
  - f. other contributing factors: change in pCO<sub>2</sub> of ocean/atmosphere, temperature (too high, too low), energy (too high, too low), light/turbidity, nutrient supply.

**Types of drowning unconformity**

## 1. Carbonate - Siliciclastic

Abrupt: due to catastrophic drowning. Progradation of siliciclastic shoreline on land-attached platforms or axial source of siliciclastics.

Gradual: due to siliciclastic encroachment and interfingering of carbonates with fine-grained basin-filling siliciclastic deposits.

## 2. Carbonate - Carbonate

abrupt and gradual; grain-size and textural unconformities; facies change to deeper-water carbonates.

Figure 6-8 Types and origin of drowning unconformities (Tucker and Wright, 1990).

formation; (4) large-scale oceanic anoxia and (5) widespread eutrophism (Bosellini *et al.*, 1999). This study suggests that the interplay among all these factors could have led to the deepening succession of the Ratawi Limestone and its correlative drowning event type 3 unconformity. The first three processes are discussed in this section. The last two processes could be associated with an increase in nutrient supply, discussed in Section 6.4.1.2.

The widespread termination of shallow-water depositional environments of carbonate platforms during the lower Valanginian, including the 'Ratawi Oolite platform' is interpreted in this study to be associated with three processes: (1) increase in sea-floor spreading and formation of oceanic crust associated with onset of the 'North Atlantic cycle', (2) intracratonic stress and subsidence of depositional basins, which were associated with a decrease in ocean basin volume, and (3) a 2<sup>nd</sup> order global sea-level rise cycle, of tectono-eustatic origin.



#### 6.4.1.1.3 Factors controlling composite sequence boundary zone CMS BZ-3

The upper composite boundary zone for the Shuaiba Formation CMS BZ-3, which is the upper boundary for CM S-2 and the Thamama Group, is correlated to surface number Apt 3 positioned beneath the 'major' maximum flooding surface MFS Apt 3, dated at about 119 ma (Section 6.1.2). Bosellini *et al.* (1999) correlated this global drowning event to oceanic anoxic event 1 (OAE 1) that occurred during the late Barremian and continued through the Albian; this is interpreted to be a world-wide oceanographic and climatic event.

This study interprets the origin of sequence boundary zone CMS BZ-3, the upper boundary for the second composite sequence CM S-2 and ending of the Thamama Group, in a similar way to CMS BZ-2 (Section 6.4.1.1.2) (Fig. 6-6). The decrease in ocean basin volume accompanied with the formation of new oceanic crust could have lead to a 2<sup>nd</sup> order global sea-level rise (tectono-eustasy) along with the reorganization of continental plates, intracratonic stress and depositional basins at this time. The drowning event MFS Apt 3 is associated with the onset of the first 2<sup>nd</sup> order eustatic sea-level rise in the Middle Cretaceous Wasia Group.

#### 6.4.1.2 Eustatic versus sediment supply processes

The termination of shallow-water deposition on the 'Ratawi Oolite platform' by deposition of a deepening-upward succession (the Ratawi Limestone) is interpreted in this study as the result of the interplay between a change in the rate of accommodation space and sediment supply. The role of carbonate sediment supply in the initiation, development and termination of the shallow-water Ratawi Oolite platform is discussed under two headings: Forced regression versus depositional regression (Section 6.4.1.2.1) and Valanginian-Hauterivian palaeoceanographic changes and carbonate sediment supply (Section 6.4.1.2.2).

##### 6.4.1.2.1 Forced regression versus depositional regression

The architecture of the Ratawi Oolite platform was created by the interplay of several factors including rate of change of accommodation space and sediment supply. Regression can occur through two different processes, depositional regression and forced regression. Depositional regression results when the rate of sedimentation is higher than the rate of accommodation space creation at the time; the forced regression results when the rate of sedimentation is lower than the rate of accommodation space



creation and there is a fall in relative sea-level (Hunt and Tucker, 1993).

The lower surface of sequence boundary zone CMS BZ-2 that separates the Ratawi Oolite from the Ratawi Limestone is a type-1 unconformity, with subaerial exposure, on the Arabian Shelf and Kuwait Arch and its correlative conformable surface in the Gotnia Basin (Section 6.4.1.1.2). The stratigraphic and petrographic data in this study indicate development of calcrete and karst facies superimposed on the shallow-water Ratawi Oolite facies (Chapter 4).

These data are interpreted in this study to indicate that the lower boundary surface of CMS BZ-2 was formed by forced regression, the decrease in the rate of accommodation space creation was much higher than rate of sediment supply. The change in accommodation space was mainly controlled by a drop of eustatic sea level associated with the late highstand systems tract of composite sequence CM S-1 that ended at the lower boundary surface of the composite sequence boundary zone CMS BZ-2, surface number Va 2, dated at about 136 ma.

#### **6.4.1.2.2 Valanginian-Hauterivian palaeoceanographic changes and carbonate sediment supply**

The upper boundary surface of sequence boundary zone CMS BZ-2 records a deepening-upward succession in the Ratawi Limestone on the Kuwait Arch and inferred correlative drowning event in the Gotnia Basin. The deposition of this facies at this surface marks the start of the termination of the shallow-water environment of the reservoir facies on the Ratawi Oolite platform and the deposition of the local regional muddy seal facies. The Mesozoic period is characterized by a widespread platform drowning in the Toarcian, Valanginian, Aptian and Albian, and near the Cenomanian-Turonian boundary (Follmi *et al.*, 1994).

The rhythm of initiation, development and termination in the life span of these platforms was influenced by regional environmental and tectonic processes in addition to global processes. The widespread but episodic synchronicity of the termination of these platforms has been interpreted as the result of widespread eutrophism, large-scale oceanic anoxia, and globally increased tectonic movements. The development of carbonate platforms is influenced by two types of relative sea-level rise, constructive and destructive sea-level rise (Follmi *et al.*, 1994). A constructive sea-level rise enables a platform to recover from widespread exposure, usually through a slow-modulated rise coupled with the development of oligotrophic water. A destructive sea-



level rise forces a platform to retrograde and there is usually limited platform growth in proximal areas, whereas the remainder of the platform is subjected to biological and physical erosion and condensation, usually associated with eutrophic water.

The terms oligotrophic and eutrophic are qualitative terms used to refer to regimes of low and high dissolved nutrient availability, respectively, and their associated levels of primary productivity. An increase in nutrient supply in the depositional environment generally decreases the rate of carbonate production and increases the rate of bioerosion. Both processes decrease the rate of carbonate sediment production and carbonate accumulation (Brasier, 1995). The activities of bacteria and microbes tend to increase at a time of eutrophic conditions and high nutrient supply.

The stratigraphic and petrographic data in this study indicate that all sea-level changes in the Ratawi Oolite are associated with a constructive-type sea-level rise, whereas the destructive-type sea-level rise is associated with CMS BZ-2 at the base of the Ratawi Limestone. The increase in terrigenous material, starting from the upper Ratawi Oolite into the Ratawi Limestone and ending in the Ratawi Shale and Zubair Formation, is interpreted in this study to be associated with the migration of the 'Zubair delta' from southern Iraq towards the study area (Chapter 3).

An increase in nutrient supply into the marine environment is inferred in this study to be associated with the migration of the 'Zubair delta' and associated increase in terrestrial runoff, which would have led to an increase in eutrophic water from the upper Ratawi Oolite time through into the Ratawi Limestone and ending in the Ratawi Shale and Zubair Formation. The decrease in carbonate sediment supply and accumulation, and increase in bioerosion associated with an increase in nutrient supply, in addition to a rapid 2<sup>nd</sup> order eustatic sea-level rise (Section 6.4.1.1) are proposed here as the reasons for the termination of shallow-water deposition on the Ratawi Oolite platform.

Global palaeoceanographic changes during the lower Cretaceous are used to interpret the widespread carbonate platform drowning events during this period that include the termination of the shallow-water Ratawi Oolite platform and the deepening succession of the Ratawi Limestone over the Kuwait Arch and inferred correlative drowning event in the Gotnia Basin. A palaeoceanographic model for the Valanginian-Hauterivian was constructed by Follmi *et al.* (1994), Weissert *et al.* (1998), and de Schootbrugge *et al.* (2000). The models used carbon isotope data to suggest a relation between the global carbon cycle and platform drowning. The model interprets the



positive increase in carbon isotope values during the drowning events as reflecting partition of carbon between the organic and carbonate (inorganic) carbon sinks. The models suggest episodes of intensified greenhouse climatic conditions as a result of an increase in CO<sub>2</sub> from volcanic activity that then led to an increase in weathering, erosion and runoff rates and to elevated nutrient transfer rates from continents to oceans.

The resulting increase in oceanic nutrient levels favoured marine phytoplankton production and black shale deposition (organic carbon sink) while conditions for the carbonate-producing biota (inorganic carbon sink) became unfavourable. This would have reduced carbonate sediment supply and accumulation along river-influenced coasts and resulted in widespread carbonate platform drowning and the deposition of a drowning succession during rapid sea-level rise. Contemporaneous with these processes was the deposition of widespread black shale.

The stratigraphic and petrographic data from this study seem to agree with this model. The volcanic activity associated with the start of the 'North Atlantic cycle' could have lead to the intensification of greenhouse climatic conditions towards the end of the Valanginian. This was associated with an increase in tectonic activity in Jordan and Lebanon that resulted in block faulting and emergence of Jurassic rocks in the region associated with movement along the Dead Sea rift during the Berriasian-Valanginian (Amireh, 1997). This would have lead to an increase in weathering, erosion and runoff rates and to have elevated nutrient transfer rates from continents into the Gotnia Basin and the study area in association with the 'Zubair delta'.

The increase in nutrient supply in the study area could have lead to an increase in organic carbon sinks in the Ratawi Limestone and equivalent facies in the Gotnia Basin, which is considered to be a good source rock (Alsharhan and Nairn, 1997). At the same time, the decrease in the inorganic carbon sink is represented by termination of the shallow-water carbonates on the Ratawi Oolite platform.

#### **6.4.1.3 Sediment supply versus tectonic processes**

Tectonic processes seem to have played important roles in the initiation, development and termination of the Ratawi Oolite platform within which occurs the Ratawi reservoir zone in the Wafra oilfield. Changes in lithofacies and thickness of the Ratawi Formation are used in this study to evaluate the role of tectonic processes on different scales. The Arabian plate was a passive margin, relatively stable tectonically



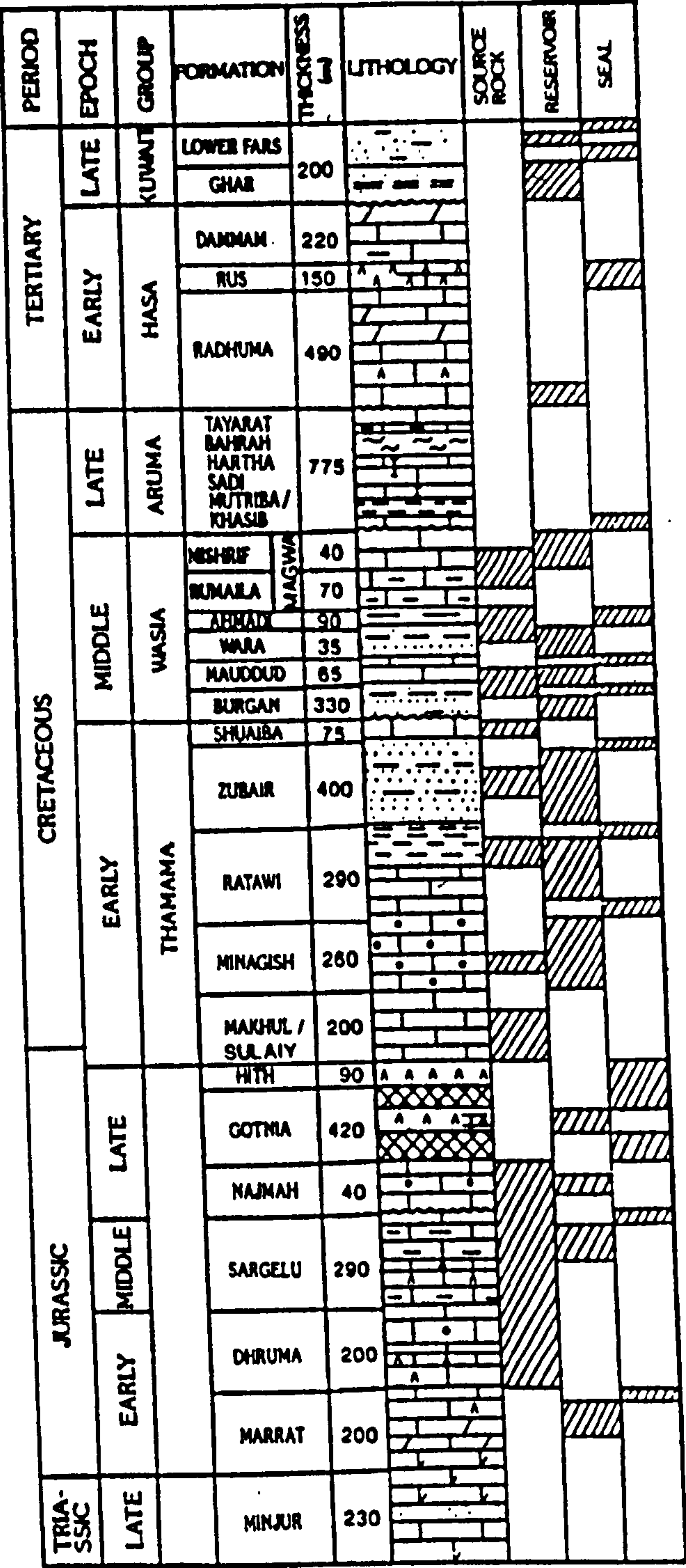


Figure 6-9 The distribution of source, reservoir and seal rocks in Kuwait and the study area, the Partitioned Neutral Zone, during Mesozoic-Cenozoic (after Alsharhan and Nairn, 1997).

throughout the Triassic to the middle Cretaceous (Chapter 2). During this period the plate experienced different faulting and tilting events that controlled the evolution of the lithofacies and thickness of the Upper Jurassic and Lower Cretaceous strata (Murriss, 1980; Pratt and Smewing, 1993).



These tectonic events had major effects on the nature and distribution of source, reservoir and seal rocks in the Arabian-Iranian basin (Fig.6-9). The factors affecting the configuration and evolution of the leading edge of the Arabian plate also affected sedimentation in the platform interior in the study area (Murriss, 1980; Alsharhan and Nairn, 1997). The events can be interpreted in the framework of the tectonic evolution of the 'North Sea cycle' and 'North Atlantic cycle', which are parts of the tectonic evolution of the Tethyan seaway. According to Pratt and Smewing (1993) the two flooding events of the Arabian Shelf at the start of the lower Cretaceous Thamama Group and middle Cretaceous Wasia Group could be interpreted as the result of tectonic rather than eustatic events. Tectonic events reduced the carbonate sediment supply on the Arabian platform, causing shallow-water facies to be abruptly overlain by deeper-water facies.

The first tectonic event occurred during the late Jurassic, resulting in the uplift of the eastern side of the plate and tilting of the plate to the west. The origin of this tectonic event was due to the thrusting of the Masirah ophiolite against the southeastern side of the Huqf Arch (east of Oman), before obduction. This tectonic event induced a relative sea-level stillstand and restricted circulation on the Arabian Shelf and Gotnia Basin. Under arid conditions, during the late Jurassic, this event was recorded as evaporitic lithofacies of the Hith and Gotnia Formations in the interior of the plate (in the study area), and high-energy oolitic facies at the edge of the plate (in United Arab Emirates). The rapid subsidence of the eastern side of the plate (after the end of the thrusting) resulted in the first flooding event on the Arabian Shelf, recorded in the study area as composite boundary zone CMS BZ-1, the lower boundary of composite sequence CM S-1.

The second tectonic event occurred during the Aptian, and resulted in the uplift of the western side of the plate. The origin of this tectonic event may be due to compressional effects of shifting oceanic plates off the northern or eastern margin of the Arabian plate. This tectonic event resulted in strong detrital influx from the west over the entire Arabian platform, recorded in the study area as composite boundary zone CMS BZ-3 and the deposition of the Burgan Formation.

This study suggests that tectonic stress associated with the rearrangement of tectonic plates and rapid sea-floor spreading could cause 2<sup>nd</sup> order eustatic sea-level rises (tectono-eustatic). The effect of the tectonic events is discussed under three headings: tectonic events and the initiation of the Ratawi Oolite platform (Section



6.4.1.3.1), tectonic events and the development of the Ratawi Oolite platform (Section 6.4.1.3.2), and tectonic events and the termination of Ratawi Oolite platform (Section 6.4.1.3.3).

#### **6.4.1.3.1 Tectonic events and the initiation of the Ratawi Oolite platform**

The study area is located at the edge of the Arabian Shelf and Gotnia Basin. The basin is interpreted to be an intracratonic basin, originated by differential subsidence between the shelf and basin (Chapter 1). The western uplift and eastern subsidence of the Arabian plate that led to the first flooding event during the early Cretaceous (Pratt and Smewing, 1993), which is recorded as the lower boundary of the Thamama Group CMS BZ-1, is inferred in this study to have continued during deposition of the lower Cretaceous Thamama Group. This regional tectonic event on the Arabian plate was associated with a 2<sup>nd</sup> order eustatic sea-level rise during the onset of the 'North Atlantic cycle'.

As explained in Section 6.4.1, the lower composite sequence of the Thamama Group CM S-1 is correlated in this study to Tethyan cycle numbers 10 and 11. This study suggests increasing the tilt of the Arabian plate led to reactivation of the basement faults and differential subsidence between the Kuwait Arch and Gotnia Basin, which could be correlated with the lower boundary of Tethyan cycle number 11, surface number Be 7, dated at about 138 ma. This surface is correlated with the start of the 1<sup>st</sup> order sub-cycle of the 'North Atlantic cycle'.

This event caused shallow-water deposition over the arch and the initiation of the Ratawi Oolite platform, which is considered in this study to be a 'local' facies change of the deep-water Makhul facies in the Gotnia Basin. The increase in the tilt caused a subaerial erosional unconformity on the Arabian Shelf during the deposition of the Ratawi Oolite platform.

#### **6.4.1.3.2 Tectonic events and the development of the Ratawi Oolite platform**

The reservoir zone at Wafra oilfield is the Ratawi Oolite, the lower member of the Ratawi Formation. There are two main types of controlling porosity in the reservoir zone, primary depositional porosity in units A, B, C and D, and diagenetic secondary porosity in unit-E (Chapters 3 and 4). The best primary porosity is associated with grainstone-packstone textures, and decreases with increasing lime mud in wackestone, and mudstone.



The high-energy depositional environment that controls the distribution of the grainstone-packstone texture is best developed on the crest of the Wafra antecedent structure and decreases towards the flanks of the structure. The Wafra main area is inferred in this study to be a syndepositional structural growth formed by movement of the Hormuz salt diapir (Chapter 1). The Infracambrian salt was mobilized through the increasing tectonic tilt of the Arabian plate.

The stratigraphic and petrographic data in this study indicate a lithofacies change and increase of lime mud in units A, B, C and D between well R-43 at the crest and well R-50 on the flank of the structure of the main Wafra area, a distance about 3.5 km. Unit-E is the only unit in the reservoir zone that is producing from in the main, southern and eastern Wafra areas; the main controlling processes in the development of the porosity of this unit is subaerial diagenesis associated with the composite boundary zone CMS BZ-2 (Chapter 4). The depth of fairweather wave base necessary to produce this change in the lithofacies and increase in lime mud, decreasing the depositional porosity in each unit between the crest and the flank, is about 25 ft (7.5 m). This depth is used in this study to indicate the height of the Wafra main area antecedent structure at the end of deposition of unit-D. This study used these data to infer that the Valanginian relative sea-level fall at the end of deposition of unit-E, that produced the 2<sup>nd</sup> order composite sequence boundary zone CMS BZ-2 of unit-F (Chapter 5), was about 25 to 30 ft (7.5 to 9 m).

#### **6.4.1.3.3 Tectonic events and the termination of the Ratawi Oolite platform**

The stratigraphic and petrographic data in this study indicate termination of shallow-water depositional environments on the Ratawi Oolite platform by the deposition of the deeper-water facies of the Ratawi Limestone. The Ratawi Oolite facies is restricted to the Kuwait Arch area in the Gotnia Basin, whereas the Ratawi Limestone facies is restricted to the basin and is not present on the Arabian Shelf. Also, the data indicate an increase in terrigenous detritus from the upper Ratawi Oolite, through the Ratawi Limestone, to the Ratawi Shale and Zubair Formation.

These data are interpreted in this study to be a reflection of continued increase in the tilt of the Arabian plate, uplifting the western side, associated with increased movement along the Dead Sea rift, during early Cretaceous time (Amireh, 1997). The plate movement may have ended the differential subsidence between the Gotnia Basin and Kuwait Arch, which started to subside at a higher subsidence rate similar to the



basin, after the deposition of the lower member. Continued tectonic events on the western side of the plate could have increased the amount of terrigenous material supplied to the study area by the 'Zubair delta'.

The Thamama Group in the study area was ended by the deposition of shallow-water carbonates of the Shuaiba Formation in the upper CM S-2. These data indicate that differential subsidence between the Gotnia Basin and Arabian Shelf decreased and the basin in the study area was then filled with the Ratawi Limestone, Ratawi Shale and Zubair Formation.

#### **6.4.2 Ratawi Formation and Thamama Group petroleum system**

One of the factors that make the Arabian-Iranian basin the richest petroleum region in the world is the presence of many petroleum systems, which are defined as 2<sup>nd</sup> order composite sequences. Each composite sequence repeats extensive source rocks, excellent reservoir rocks, and regional seal rocks (Beydoun, 1998).

The petroleum system of the Lower Cretaceous Thamama Group can be studied in the framework of sequence stratigraphy. These lithofacies of the petroleum system are interpreted and predicted within each depositional system at a scale of the 3<sup>rd</sup> order depositional sequence and 2<sup>nd</sup> order composite sequence.

Any cycle, which is characterized by a repetition of extensive source, reservoir and seal rocks, could have the potential to be a rich petroleum system (a lucky cycle). According to Douban and Al Medhadi (1999) the Cretaceous petroleum system model in Kuwait, in the Thamama Group, is divided into two 2<sup>nd</sup> order cycles. This study divides the Thamama Group into two 2<sup>nd</sup> order composite sequences CM S-1 and CM S-2, with each sequence characterized by its distribution of source, reservoir and seal rocks. The sequence stratigraphic model can be used to interpret the porosity of the carbonate rocks that create the seal and reservoir rocks, as discussed in Chapter 4 (Read and Horbury, 1993; Tucker, 1993), as well as the type and amount of organic matter that creates the source rock (Pasley *et al.*, 1993).

The hydrocarbon trap type of the Ratawi zone at Wafra oilfield is interpreted in this study to be a stratigraphic trap, a depositional trap for units A, B, C and D and diagenetic trap for unit-E. The Ratawi reservoir zone occurs in the upper part of the composite sequence CM S-1 beneath the 2<sup>nd</sup> order sequence boundary zone CMS BZ-2. The interpretation and prediction of reservoir depositional and diagenetic porosity in the framework of sequence stratigraphy are discussed in Chapters 3 and 4. The Ratawi



Limestone is the local seal in the Arabian-Iranian basin (Murriss, 1980). The source rock in composite sequence CM S-1 in Kuwait and the study area is the Makhul Formation, as well as Ratawi Limestone and Ratawi Shale members (Abdullah and Kinghorn, 1996).

The Makhul Formation, the deep-water Gotnia Basin facies equivalent to the shallow-water Ratawi Oolite platform, contains kerogen types 1 and 2, and its maturity has reached the oil generation zone. The Ratawi Limestone contains type 3 kerogen and it is either mature or just entering the oil-generation zone. The Ratawi Shale contains terrestrial material (spores, cuticle and wood tissue, indicating a prodelta environment) and is mature in northern Kuwait. The Makhul Formation is characterized by an average of 10% organic matter, and is up to 300 ft (100 m) thick; it is considered the most productive source rock in Kuwait according to the model of its thermal history by Abdullah *et al.* (1997).

All lithofacies in the Thamama Group, including the Makhul Formation, change to Garau Formation lithofacies to the northeast of the study area, which is a deeper-water lithofacies in the Gotnia Basin and is considered also to be a good source rock (Bordenave and Burwood, 1994). The maximum total organic carbon is interpreted in the framework of sequence stratigraphy to be generally associated with the maximum flooding surface (Creaney and Passet, 1993). This study infers the richest source rock interval in the Makhul Formation in the study area to be associated with maximum flooding surface CM S-1 and to increase in the direction of the deep-water Gotnia Basin.

The occurrence of extensive source, good reservoir and regional seal rocks, that make composite sequence CM S-1 a rich petroleum system, 'a lucky cycle', is in agreement with the model of Murriss (1980) that explains the hydrocarbon system in the central part of the Arabian-Iranian basin. The model called for the association of source, reservoir and seal rock lithofacies in a cycle of transgression and regression. During the transgression, the source rock lithofacies was deposited in a low-energy environment in starved basins on the differentiated carbonate platform; in the study area this is the Gotnia basin. The reservoir rock lithofacies were deposited in high-energy environments on the carbonate platform as marginal mounds, oolite bars and sheets, rudistid banks and regressive sands. In the study area these were the high-energy environments of reservoir units A, B, C and D and the subaerial diagenetic environments of reservoir unit-E that developed on the Ratawi Oolite platform.



However, during the regressive part of the cycle, the seal lithofacies were deposited as regressive supratidal evaporites or transgressive shales. In the study area this is the prodelta deepening-upward transgressive succession of the Zubair delta that terminates the Ratawi Oolite platform.

### **6.5 Summary**

This chapter has been concerned with the regional sequence stratigraphy of the Lower Cretaceous in the Saudi Arabia-Kuwait Partitioned Neutral Zone area, and has shown how correlation can be made on regional and global scales. In the study area, apart from eustasy, it is clear that local tectonics, movement of the antecedent Wafra structure, in addition to regional tectonics, notably differential subsidence between the Kuwait Arch, the Gotnia intrashelf basin and the Arabian Platform, played a major role in the development of reservoir facies in the Ratawi Oolite. The reduction in carbonate sediment supply seems to have played a role in the development of the local regional seal facies (Ratawi Limestone).

The initiation, development and termination of the Ratawi Platform system have been placed within a sequence stratigraphic framework. Source rocks formed during times of transgression, reservoir rocks were mostly deposited in high-energy environments and were affected by exposure, and seal rocks were deposited during the late drowning event that followed by transgression of the Zubair delta.



## **Chapter 7 Synthesis and Conclusions**

The Arabian-Iranian basin is the richest petroleum system in the world; the recoverable reservoirs of oil and gas here are about 65% and 34% of the world reservoir, respectively. This huge hydrocarbon reservoir is the end result of many geological factors working simultaneously towards the generation, migration, accumulation and preservation of the hydrocarbons. The factors that control the formation and disruption of the lithofacies of the source, reservoir and seal rocks in time and space of the petroleum system can be analyzed in the framework of sequence stratigraphy. Some of these factors are analyzed in this study for the Lower Cretaceous Ratawi Formation (Ratawi Oolite, Ratawi Limestone and Ratawi Shale members), of the Thamama Group in the giant Wafra oilfield, as an example for the many producing zones in the basin.

The Ratawi sedimentary and diagenetic facies models (Chapters 3 and 4) are constructed in this study and integrated along with data from previous studies within the framework of sequence stratigraphy at different cycle orders. The constructed Ratawi sequence stratigraphic model (Chapters 5 and 6) is used as a tool to interpret and predict Ratawi lithofacies and oil system within the Lower Cretaceous regional and global framework.

The nine marker zones defined by Saudi Arabian Texaco Inc. in logs from well R-43 (type locality well) are used in this study to correlate the different reservoir units that are defined at the crest of the main Wafra area to cores from wells R-50 and R-48 on the flank of the main Wafra area and well R-48 in the southern Wafra area (Chapter 2). This study identified reservoir units C, D, E and F in the Ratawi Oolite in the cored intervals and logs of wells R-50 and R-49, and the Ratawi Limestone in the cored interval and logs of well R-48 and in the upper part of the cored interval of wells R-49 and R-50. The cutoff porosity that defines reservoir and non-reservoir units is 15% porosity. The permeability and recovery efficiency of the different Ratawi reservoir units depend on many factors that include the nature of the pore system, in particular the pore size, pore-throat size, pore-surface roughness, and number of pore-connections. The depositional and subsequent diagenetic environments of the Ratawi Formation control the nature of the pore system.



Microfacies analysis performed in this study on 204 core samples from wells R-48, R-49 and R-50 can be grouped into two lithofacies associations, namely sedimentological and diagenetic lithofacies associations. The carbonate ramp model is used as a framework to organize the Ratawi facies and microfacies into four broad facies belts. These are (1) back-ramp environments characterized by a restricted fauna and wackestone-mudstone, (2) shallow-ramp environments characterized by an open-marine fauna and grainstone, (3) deep-ramp environments characterized by an open-marine fauna and mudstone, wackestone and packstone, and (4) ramp subaerial exposure facies, with pedogenic textures.

The four broad facies belts of the Ratawi epeiric ramp migrated with time as a result of changing rate of accommodation space and sediment supply. Each of these facies belts has distinctive microfacies associations for that particular environment, and is characterized by certain early diagenetic fabric and porosity types. Thirteen microfacies are recognized in this study and listed in Table 3-1. Eleven basic porosity types are recognized in the Ratawi microfacies, namely interparticle, intraparticle, mouldic, vug, intercrystal, fracture, stylolitic, burrow, rootlet, dedolomite and microporosity.

According to Horbury and Robinson (1993) predicting Ratawi near-surface porosity in the framework of sequence stratigraphy is an intermediate approach between using the correlation between porosity and depth or the maturity method, and predicting porosity by chemical modelling (Chapter 4). Read and Horbury (1993) and Tucker (1993) used sequence stratigraphic models to interpret the porosity of the carbonates that create the seal and reservoir rocks. Also sequence stratigraphy was used by Pasley *et al.* (1993) to interpret the type and amount of organic matter that creates the source rock.

The primary and secondary near-surface porosity is preserved at the Ratawi reservoir depth by the reduction of the effects of cementation and chemical compaction by different processes reviewed in Chapter 4. This study infers early emplacement of hydrocarbons, that started to be generated from the Makhul Formation during the Upper Cretaceous, and high carboxylic acid concentration in formation waters associated with pre-expulsion of the hydrocarbons to have had an important role in the preservation of Ratawi near-surface porosity.



The reservoir (flow) units in well R-50 are units D and E, whereas in well R-49 it is unit E; the latter unit is the only reservoir unit producing from the main, southern and east Wafra areas. At the crest of the main area, units C and D are reservoir units and their porosity decreases in the direction of the flanks. The data from this study demonstrate that units D and E with their depositional and diagenetic overprint facies have a predictable and characteristic porosity and permeability.

This study indicates that porosity in reservoir unit D is mainly primary depositional porosity, controlled by the depositional texture and environment of the sand-body on the shallow ramp, and enhanced by dedolomitization. In reservoir unit-E, by way of contrast, it is mainly secondary porosity, controlled by diagenetic processes of subaerial exposure developed beneath a 2<sup>nd</sup> order sequence boundary. The high cut-off porosity for the reservoir unit, which is 15%, is inferred in this study to be mainly due to the high percentage of ineffective microporosity in the Ratawi Formation.

Different diagenetic processes played important roles in preserving, reducing, enhancing or eliminating the primary depositional porosity and creating secondary diagenetic porosity in the Ratawi zone at Wafra oilfield. These diagenetic processes are organized in this study into a diagenetic model with three diagenetic environments, namely (1) shallow-marine, (2) shallow-burial meteoric and (3) burial diagenetic. The first diagenetic environment is characterized by micritization and rare marine cements; the second environment is characterized by meteoric cements and development of exposure zones; the last environment is characterized by physical and chemical compaction, and burial cementation.

The development of pedogenic fabrics is very important in the formation of reservoir zone E in the main, southern and eastern Wafra areas. The fabric is inferred in this study to be developed as pedogenic calcrete under conditions characterized by strong physicochemical processes (alpha and beta fabric model) and weak biological processes (rhizogenic fabric model).

The systematic variations in Ratawi lithofacies in three dimensions (Ratawi facies tract and depositional system) and its reservoir characteristics are analyzed in this study as the product of variations in two factors (1) sedimentological processes that include the Ratawi platform type and geological age: the Lower Cretaceous greenhouse period, and (2) stratigraphic processes that include accommodation space and sediment supply.



The Wafra oilfield is located on the interior platform (unstable shelf) of the Arabian Shelf along the Khurais-Wafra-Burgan-Zubair arch (Kuwait Arch). The arch, part of the Arabian folds, is an anticline plunging to the north and extends for more than 500 kilometres from northern Saudi Arabia through Kuwait into southern Iraq; it is controlled by north-south basement lineament trend. During the deposition of the Lower Cretaceous Ratawi Formation, the study area was located between the Arabian Shelf and the Gotnia Basin that started to develop as a deep-water basin during the middle Jurassic. The inferred mechanism for the growth of the Kuwait Arch since the late Jurassic and the antecedent Wafra structure during the deposition of the Ratawi Oolite are the reactivation along the basement lineaments and faults, and mobilization of the infracambrian Hormuz salt along linear pillows and swells.

The lithofacies of the Ratawi zone, including source, reservoir and seal rocks, are interpreted and predicted in this study within the idealized genetic packages identified by a sedimentological approach to sequence stratigraphy. The approach defined 5<sup>th</sup> order cycles (parasequence), 4<sup>th</sup> order cycles (systems tracts), 3<sup>rd</sup> order cycles (greenhouse sequences), a 2<sup>nd</sup> order cycle (composite sequence) and a 1<sup>st</sup> order sub-cycle (1<sup>st</sup> order sub-sequence) on the basis of sedimentological and diagenetic data from the core study, in addition to the stacking pattern of the Ratawi parasequences. The integration of the Ratawi facies and stacking pattern data from this study with previous studies, including the Hardenbol *et al.* (1998) chart of Cretaceous sequence chronostratigraphy, resulted in construction of a Ratawi chronostratigraphic hierarchy framework.

From the study of the cores, 84 shallowing-upward parasequences are identified, each beginning with a marine flooding surface and ending with the marine flooding surface of the next cycle; 20 cycles were noted in the cored interval of well R-50 and 64 cycles in the cored interval of well R-48. These parasequences are grouped into two types, namely peritidal and subtidal parasequences (Appendix 2). The vertical lithofacies evolution of these cycles can be a shallowing-upward succession, a regressive cycle (R-cycle, asymmetric) or deepening then shallowing-upward succession a transgressive-regressive cycle (T/R-cycle, symmetric). Evidence of subaerial exposure is present in the peritidal cycles but not in the subtidal cycles.

The origin of the Ratawi parasequences can be interpreted using two models. The first is the autocyclic model, driven by internal mechanisms of depositional processes and fluctuations in sediment supply or production. The second is the



allocyclic model, driven by external mechanisms, which include tectonic and eustatic models. To apply a glacio-eustatic model to interpret the origin of the Ratawi parasequences, the Milankovitch signal must be studied in the context of greenhouse, transition and icehouse periods of the Phanerozoic.

The Cretaceous time was a greenhouse period, characterized by low amplitude fluctuations in relative sea level, since there were no major glaciers in this period, and little accommodation space was generated. The Ratawi Oolite is inferred to have been deposited in the Valanginian, whereas the middle member, the Ratawi Limestone, was deposited in the Hauterivian. A 'little icehouse' during the Valanginian period is suggested by Price (1999) and is used in this study to explain the thicker parasequences and higher percentage of peritidal parasequences in the Ratawi Oolite compared to the Ratawi Limestone. The formation of parasequences by autocyclic processes in the Ratawi Formation during the Cretaceous greenhouse period may be more common than during an icehouse period, due to weak stratigraphic forcing.

The stacking patterns of these parasequences are analyzed in this study by constructing Fischer plots in time and depth domains. The depth domain plots are used to relate the Ratawi cycle stacking pattern to reservoir units, wireline log signatures, lithology and petrophysical characteristics. The Fischer plot analysis for core from well R-50, the cored interval of the Ratawi Oolite, identified the upper part of greenhouse sequence number 0 (GH S-0), sequence boundary zone number 1 (SB Z-1), GH S-1 and SB Z-2.

Unit D, the reservoir unit with interparticle depositional primary porosity, is interpreted in this study as retrogradational (a transgressive systems tract), the lower part of GH S-1, characterized by high-energy facies developed over the antecedent Wafra structure. Unit E, the reservoir unit with calcrete-rootlet diagenetic secondary porosity, is interpreted as progradational (a highstand systems tract), the upper part of GH S-1, characterized by low-energy facies and located beneath the 2<sup>nd</sup> order sequence boundary (SB Z-2), with long periods of subaerial exposure under a semi-arid climate. Unit C and unit F are not reservoir units, since porosity is less than 15%. Unit C unit is interpreted as the highstand systems tract of GH S-0 and the transition zone SB Z-1, characterized by low-energy facies and located under a 3<sup>rd</sup> order sequence boundary, whereas Unit F is interpreted as SB Z-2 that occurs within the transition zone characterized by low-energy facies.



The Fischer plot analysis for core from well R-48, the cored interval of the Ratawi Limestone, identifies SB Z-3, GH S-2 and SB Z-4. This interval in the Ratawi Limestone does not contain reservoir units, and porosity is less than 15%, due to lower-energy, deeper-water facies on the Ratawi epeiric ramp. This mark the end of the development of the antecedent Wafra structure and a relatively short period of subaerial exposure associated with a 3<sup>rd</sup> order sequence boundary zone. The thickest parasequences in the cored interval of wells R-49 and R-50 could contain several smaller cycles which were not recorded (missed beats), as a result of subtidal amalgamation.

The Ratawi facies and stacking pattern data from this study identifying parasequences (5<sup>th</sup> order cycle), systems tracts (4<sup>th</sup> order cycle), and greenhouse sequences (3<sup>rd</sup> order cycle), are integrated with the previous studies. This results in the identification of a Ratawi composite sequence (2<sup>nd</sup> order cycle) and 1<sup>st</sup> order sub-sequence (1<sup>st</sup> order sub-cycle) and the construction of the Ratawi chronostratigraphic hierarchy framework. In this framework, this study evaluates the regional and global processes in the initiation, evolution and termination of the Ratawi platform and the distribution of the source, reservoir and seal rocks of the Ratawi petroleum system.

The Ratawi chronostratigraphic hierarchy framework divides the Lower Cretaceous Thamama Group into two 2<sup>nd</sup> order cycles, composite sequence (CM S), the lower one is labeled CM S1 and the upper CM S2. These sequences are separated by composite sequence boundary zone (CMS BZ); the bottom boundary in the Thamama Group is labeled as CMS BZ1, the second CMS BZ2 separating the two composite sequences, and CMS BZ3 at the top of the Thamama Group. The Ratawi Oolite is at the top of CM S1, whereas the Ratawi Limestone and Ratawi Shale are at the bottom of CM S2. The Ratawi 3<sup>rd</sup> order boundary zone, SB Z-2, that separates the Ratawi Oolite and Ratawi Limestone, is equivalent to 2<sup>nd</sup> order boundary zone CMS BZ2.

This study has correlated the Thamama Group to Tethyan cycles number 10, 11 and 12 of Jacquin *et al.* (1998); Tethyan cycles number 10 and 11 are correlated to the lower Thamama Group composite sequence (CM S-1) and Tethyan cycle number 12 is correlated to the upper composite sequence (CM S-2). The Thamama Group CMS BZ1 is correlated to sequence boundary number Be 1, about 144.2 ma; CMS BZ2 is correlated to sequence boundary number Va <sup>2</sup><sub>2</sub>, about <sup>136</sup><sub>135.5</sub> ma. and CMS BZ3 is correlated to sequence boundary number Ap 3, about 120 ma. The Tethyan cycle



number 10 is correlated to the upper part of the 1<sup>st</sup> order sub-cycle of the 'North Sea', whereas Tethyan cycles number 11 and 12 are correlated to the bottom part of 1<sup>st</sup> order sub-cycle of the 'North Atlantic'.

This study suggests a tectonic event tilted the Arabian plate, which led to reactivation of the basement faults and differential subsidence between the Kuwait Arch and Gotnia Basin. This led to the deposition of the shallow-water Ratawi Oolite over the arch as 'local' facies changes of the deep-water Makhul Formation. The tilt caused a subaerial erosional unconformity on the Arabian Shelf during the deposition of the Ratawi Oolite platform. This tectonic event could be correlated with the lower boundary of Tethyan cycle number 11, surface number Be 7, dated at about 138 ma. This surface is correlated with the start of the 1<sup>st</sup> order sub-cycle of the 'North Atlantic cycle'.

The initiation and development of the Ratawi Oolite platform were controlled by the differential subsidence between the Kuwait Arch and Gotnia Basin and by the low amplitude fluctuations in relative sea level during the general greenhouse period of the Cretaceous and the little icehouse of the Valanginian. These conditions, in addition to the development of the antecedent Wafra structure during the deposition of the Ratawi Oolite, influenced the deposition of the high-energy sand-body of the Ratawi ramp and the depositional porosity of reservoir units A, B, C and D at the main Wafra area. The Ratawi Oolite platform during the initiation and development was characterized by keep-up phases.

The shallow-water depositional environment of the Ratawi Oolite platform was terminated by the deposition of the deepening-upward succession of the overlying Ratawi Limestone on the subaerially exposed surface of the platform. The CMS BZ-2 that separates the lower and the middle member of the Ratawi Formation is inferred in this study to contain two major unconformity surfaces. The lower boundary surface is a type 1 sequence boundary in the study area on the Kuwait Arch and its correlative conformable surface is in the Gotnia Basin succession. The upper boundary surface is a type 3 sequence boundary in the Gotnia Basin and its correlative deepening-upward succession in the study area on the Kuwait Arch.

The lower boundary surface, a type 1 unconformity, formed under semi-arid conditions under a long period of subaerial exposure associated with a 2<sup>nd</sup> order sequence boundary. This surface influenced the development of the calcrete zone and the secondary diagenetic porosity of reservoir unit E, which is the only reservoir unit



that is producing from the main, southern and eastern Wafra areas. This unconformity surface is correlated to the Hardenbol *et al.* (1998) chart and surface number Va 2, dated at about 136 ma. The unconformity at the top of the Ratawi Oolite platform is correlated to the unconformity at top of Tethyan cycle number 11; in Europe this unconformity is the most erosional surface in the North Atlantic cycle. This unconformity is the last of four Late Cimmerian unconformities, which are dated respectively as Lower Volgian (Tithonian), Upper Volgian, Late Ryazanian (upper Berriasian), and Lower Valanginian.

The subaerial exposure of the Ratawi Oolite platform, in the study area on the Kuwait Arch, and the continuous deposition in the Gotnia Basin, are inferred in this study to be due to one or two processes. The first is a change in the rate of differential subsidence between the arch and the basin, which would have lead to tectonic uplift of the arch at the end of Tethyan cycle number 11. The second is an increase in the rate of eustatic sea-level fall at the end of the 2<sup>nd</sup> order cycle. During the relative sea-level low, the four facies belts of the Ratawi epeiric ramp (deep-ramp, shallow-ramp, back-ramp, and subaerial exposure facies) were shifted in the direction of the deep-water Gotnia Basin, with the expansion of the subaerial facies belt of the Arabian Shelf onto the Kuwait Arch in the study area.

The upper boundary surface, deepening-upward succession and its correlative drowning event, a type 3 unconformity, is the stratigraphic record of the interplay between two processes, the change in the rate of sediment supply and accommodation space. The surface was formed when the rate of <sup>creation of</sup> accommodation space exceeded carbonate sediment supply and accumulation. The deposition of the deepening-upward succession in the study area lead to termination of the shallow-water environment of the Ratawi Oolite platform. In this study, the unconformity surface is correlated to the Hardenbol *et al.* (1998) chart minor to medium flooding surface number MFS Va 2, dated at about 135 ma., which is a major surface in Haq *et al.* (1988) chart. According to Bosellini *et al.* (1999) the lower Valanginian drowning unconformity event is well known in a large part of the world, from the Caribbean to eastern Arabia.

This study suggests that the upper boundary surface was formed by the interplay of several processes, including (1) rapid eustatic sea-level rise, associated with the onset of Tethyan 2<sup>nd</sup> order cycle number 12; (2) globally increased tectonic movements that lead to ending the differential subsidence between the Kuwait Arch and Gotnia Basin and rapid subsidence of the arch; (3) pulses in ocean-crust formation



that lead to sea-level rise (tectono-eustatic); (4) large-scale oceanic anoxia and (5) widespread eutrophism associated with the migration of the 'Zubair delta' from southern Iraq to the study area and increase in terrestrial runoff, leading to increase in eutrophic water.

The first three processes lead to an increase in accommodation space, whereas the last two processes lead to a decrease in carbonate sediment supply and accumulation, and increase in bioerosion. The Ratawi Oolite platform, during the termination of the shallow-water environment by the deposition of the deepening-upward succession of the Ratawi Limestone and Ratawi Shale, was characterized by catch-up and give-up phases. This last phase in platform development lead to deposition of a regional seal rock in the study area.

The application of the modern concepts of carbonate sequence stratigraphy in this study to the Ratawi zone at Wafra oilfield seems to support Murriss's (1980) model that explains the hydrocarbon system in the central part of Arabian-Iranian basin. The model interprets the association of the lithofacies of the petroleum system, source, reservoir and seal rocks, in a 2<sup>nd</sup> order cycle of transgression and regression. The source rock lithofacies was deposited in a low-energy environment in starved basins on the differentiated carbonate platform; the reservoir rock lithofacies was deposited in high-energy environments on the carbonate platform, during the transgressive part of the cycle. The seal lithofacies were deposited as supratidal evaporites or deltaic shales, during the regressive part of the cycle.



## References

- Abdullah, F.H.A. & Kinghorn, R.R.F. 1996. A preliminary evaluation of Lower and Middle Cretaceous source rocks in Kuwait. *Journal of Petroleum Geology*, 19, 461-480
- Abdullah, F.H.A., Nederlof, P.J.R. & Ormerod, M.P. 1997. Thermal history of the Lower and Middle Cretaceous source rocks in Kuwait. *GeoArabia*, 2, 151-164
- Adams, A.E. 1980. Calcrete profiles in Eyam Limestone (Carboniferous) of Derbyshire: petrology and regional significance. *Sedimentology*, 27, 651-660
- Adams, A.E. & Mackenzie, W.S. 1998. *A Colour Atlas of Carbonate Sediments and Rocks Under the Microscope*. Manson publishing, pp.180
- Ahr, W.M. 1998. Carbonate ramps, 1973 – 1996: A historical review. In: *Carbonate Ramps* (V.P. Wright & T.P. Burchette, eds.). *Geological Society of London Special Publication*, 149, 7-14
- Aigner, T., Brandenburg, A., Vanvliet, A., Doyle, M., Lawrence, D. & Westrich, J. 1990. Stratigraphic modeling of epicontinental basins - 2 applications. *Sedimentary Geology*, 69, 167-190
- Al Harbi, M. 1994. Geological study of the Ratawi Reservoir South Umm Gudair field, Partition Neutral Zone. *Texaco Houston Research Centre Unpublished report*, pp.14
- Al-Aasm, I.S. & Azmy, K.K. 1996. Diagenesis and evolution of microporosity of Middle-Upper Devonian Kee Scarp reefs, Norman Wells, Northwest Territories, Canada: petrographic and chemical evidence. *American Association of Petroleum Geologists Bulletin*, 80, 82-100
- Ali, A.J. & Aziz, Z.R. 1993. The Zubair Formation, east Baghdad oilfield, central Iraq. *Journal of Petroleum Geology*, 16, 353-364
- Alsharhan, A.S. 1995. Facies variation, and exploration potential of the Cretaceous rudist-bearing carbonates of the Arabian Gulf. *American Association of Petroleum Geologists Bulletin*, 79, 531-550
- Alsharhan, A.S. & Kendall, C.G.St. 1991. Cretaceous chronostratigraphy, unconformities and eustatic sea-level changes in the sediments of Abu Dhabi, U.A.E. *Cretaceous Res.*, 12, 379-401
- Alsharhan, A.S. & Magara, K. 1995. Nature and distribution of porosity and permeability in Jurassic carbonate reservoirs of the Arabian Gulf Basin. *Facies*, 32, 237-253
- Alsharhan, A.S. & Nairn, A.E.M. 1986. A review of the Cretaceous formations in the Arabian Peninsula and Gulf: Part I, Lower Cretaceous (Thamama Group), stratigraphy and paleogeography. *Journal of Petroleum Geology*, 9, 365-392
- Alsharhan, A.S. & Nairn, A.E.M. 1997. *Sedimentary Basins and Petroleum Geology of the Middle East*. Elsevier, pp.843
- Alsharhan, A.S. & Nairn, A.E.M. 1988. A review of the Cretaceous formations in the Arabian Peninsula and Gulf: Part II, Mid-Cretaceous (Wasia Group), stratigraphy and paleogeography. *Journal of Petroleum Geology*, 11, 89-112



- Amireh, B.S. 1997. Sedimentology and palaeogeography of the regressive-transgressive Kurnub Group (Early Cretaceous) of Jordan. *Sedimentary Geology*, 112, 69-88
- Amthor, J.E., Mountjoy, E.W. & Machel, H.G. 1994. Regional-scale porosity and permeability variations in Upper Devonian Leduc buildups - implications for reservoir development and prediction in carbonates. *American Association of Petroleum Geologists Bulletin*, 78, 1541-1559
- Aref, M.A.M. 1998. Biogenic carbonates: Are they a criterion for underlying hydrocarbon accumulations? An example from the Gulf of Suez region, Egypt. *American Association of Petroleum Geologists Bulletin*, 82, 336-352
- Ayres, M.G., Bilal, M., Jones, R.W., Slentz, L.W., Tartir, M. & Wilson, A.O. 1982. Hydrocarbon habitat in main producing areas, Saudi Arabia. *American Association of Petroleum Geologists Bulletin*, 66, 1-9
- Bathurst, R.G.C. 1975. *Carbonate Sediments and Their Diagenesis*. Elsevier, pp.658
- Beydoun, Z.R. 1988. *The Middle East: Regional Geology and Petroleum Resources*. Scientific Press Ltd., pp.292
- Beydoun, Z.R. 1991. Arabian plate hydrocarbon geology and potential – a plate tectonic approach: *American Association of Petroleum Geologists, Studies in Geology*, 33, PP.77
- Beydoun, Z.R. 1998. Arabian plate oil and gas: Why so rich and so prolific?. *Episodes*, 21, 74-81
- Beydoun, Z.R., Hughes-Clarke, M.W. & Stoneley, R. 1992. Petroleum in the Zagros Basin: A Late Tertiary foreland basin overprinted onto the outer edge of a vast hydrocarbon-rich Palaeozoic-Mesozoic passive margin. In: *Foreland Basin and Foldbelts* (R. Macqueen & D. Leckie, eds.). *American Association of Petroleum Geologists Memoir*, 55, 309-339
- Bordenave, M.L. & Burwood, R. 1994. The Albian Kazhdumi Formation of the Dezful Embayment, Iran: one of the most efficient petroleum generating systems. In: *Petroleum Source Rocks* (B. Katz, ed.). Springer-Verlag, 183-207
- Bosellini, A., Morsilli, M. & Neri, C. 1999. Long-term event stratigraphy of the Apulia Platform margin (Upper Jurassic to Eocene, Gargano, southern Italy). *Journal of Sedimentary Research*, 69, 1241-1252
- Bou-Rabee, F. 1996 a. The tectonic and depositional history of Kuwait from seismic reflection data. *Journal of Petroleum Geology*, 19, 193-198
- Bou-Rabee, F. 1996 b. Geologic and tectonic history of Kuwait as inferred from seismic data. *Journal of Petroleum Science and Engineering*, 16, 151-167
- Brasier, M.D. 1995. Fossil indicators of nutrient levels 2: evolution and extinction in relation to oligotrophy. In: *Marine Palaeoenvironmental Analysis from Fossils* (D.W. J. Bosence & P.A. Allison, eds.) *Geological Society of London Special Publication*, 83, 133-150
- Budaj, J.M., Lohmann, K.C. & Owen, R.M. 1984. Burial dedolomite in the Mississippian Madison limestone, Wyoming and Utah thrust belt. *Journal of Sedimentary Petrology*, 54, pp. 276-288
- Budd, D.A., Saller, A.H. & Harris P.M. 1995. Foreword. In: *Unconformities and Porosity in*



- Carbonate Strata* (D.A. Budd, A.H. Saller & P.M. Harris, eds.). *American Association of Petroleum Geologists Memoir*, 63, viii-xii
- Burchette, T.P. & Wright, V.P. 1992. Carbonate ramp depositional systems. *Sedimentary Geology*, 79, 3-57
- Canaveras, J.C., Sanchez, M.S., Calvo, J.P., Hoyos, M. & Ordonez, S. 1996. Dedolomites associated with karstification. An example of early dedolomitization in lacustrine sequences from the Tertiary Madrid basin, central Spain. *Carbonates and Evaporites*, 11, 85-103
- Cander, H.S. 1994. An example of mixing-zone dolomite, Middle Eocene Avon Park Formation, Floridan aquifer system. *Journal of Sedimentary Research*, 64, 615-629
- Chilingarian, G.V. & Mazzullo, S.J. 1992. Diagenesis and origin of porosity. In: *Carbonate Reservoir Characterization: a Geologic-Engineering Analysis, part 1* (G.V. Chilingarian, S.J. Mazzullo & H.H. Rieke, eds.) *Developments in Petroleum Science*, 30, Elsevier, 199-270
- Chilingarian, G.V., Mazzullo, S.J. & Rieke, H.H. 1992. Introduction. In: *Carbonate Reservoir Characterization: a Geologic-Engineering Analysis, part 1* (G.V. Chilingarian, S.J. Mazzullo & H.H. Rieke, eds.) *Developments in Petroleum Science*, 30, Elsevier, 1-35
- Choquette, P.W. & Pray, L.C. 1970. Geologic nomenclature and classification of porosity in sedimentary carbonates. *American Association of Petroleum Geologists Bulletin*, 54, 207-250
- Creaney, S. & Passey, Q.R. 1993. Recurring patterns of total organic carbon and source rock quality within a sequence stratigraphic framework. *American Association of Petroleum Geologists Bulletin*, 77, 386-401
- Day, P.I. 1997. The Fischer diagram in the depth domain: A tool for sequence stratigraphy. *Journal of Sedimentary Research*, 67, 982-984
- de Schootbrugge, B., Follmi, K. B., Bulot, L. G. & Burns, S.J. 2000. Pale oceanographic changes during the early Cretaceous (Valanginian-Hauterivian): evidence from oxygen and carbon stable isotopes. *Earth and Planetary Letters*, 181, 15-31
- De Schootbrugge, B.V., Follmi, K.B., Bulot, L.G. & Burns, S.J. 2000. Palaeoceanographic changes during the early Cretaceous (Valanginian-Hauterivian): Evidence from oxygen and carbon stable isotopes. *Earth and Planetary Science Letters*, 181, 15-31
- Douban, A.F. & AL Medhadi, F. 1999. Sequence chronostratigraphy and petroleum system of the Cretaceous Megasequence, Kuwait. *American Association of Petroleum Geologists Bulletin*, 83, 1297
- Dunham, R.J. 1962. Classification of carbonate rocks according to depositional texture. In: *Classification of Carbonate Rocks* (W.E. Ham, ed.). *American Association of Petroleum Geologists Memoir*, 1, 108-121
- Edgell, H.S. 1996. Salt tectonism in the Persian Gulf basin. In: *Salt Tectonics* (G.I. Alsop, D.J. Blundell & I. Davison, eds.). *Geological Society of London Special Publication*, 100, 129-151
- Ehrenberg, S. N. & Svana, T. A. 2001. Carbonate strata, an example from the Finnmark carbonate platform (Carboniferous-Permian), Barents Sea. *American Association of Petroleum Geologists Bulletin*, 85, 295-308
- Emery, D. & Myers, K. 1996. *Sequence Stratigraphy techniques*. Blackwells, pp297



- Esteban, M. & Klappa, C.F. 1983. Subaerial Exposure Environment. In: *Carbonate Depositional Environments* (P.A. Scholle, D.G. Bebout, C.H. Moore, eds.) *American Association of Petroleum Geologists Memoir*, 33, 1-96
- Everts, A.J.W., Stafleu, J., Schlager, W., Fouke, B.W. & Zwart, E.W. 1995. Stratal patterns, sediment composition and sequence stratigraphy at the margin of the Vercors carbonate platform (Lower Cretaceous, SE France). *Journal of Sedimentary Research Section B*, 65, 119-131
- Evans, J., Cade, C.A. & Bryant, S. 1997. A geological approach to permeability prediction in clastic reservoirs. In: *Reservoir Quality Prediction in Sandstone and Carbonates* (J.A. Kupecz, J.G. Gluyas & S. Bloch, eds.) *American Association of Petroleum Geologists Memoir*, 69, 91-101
- Fitchen, W.M. 1997. Carbonate sequence stratigraphy and its application to hydrocarbon exploration and reservoir development. In *Carbonate Seismology* (P. Ibrahim & K.J. Marfurt, eds.) *Society of Exploration Geophysicists, Geophysical Developments Series*, 6, 121-178
- Flügel, E. 1982. *Microfacies Analysis of Limestones*. Springer Verlag, pp.632
- Follmi, K.B., Weissert, H. & Bisping, M. 1994. Phosphogenesis, carbon-isotope stratigraphy, and carbonate-platform evolution along the Lower Cretaceous northern Tethyan margin. *Geological Society of America Bulletin*, 106, 729-746
- Ginsburg, R.N. 1971. Landward movement of carbonate mud: new model for regressive cycles in carbonates (abst.). *American Association of Petroleum Geologists Bulletin*, 55, 340
- Goldhammer, R.K. & Wilson, J.L. 1991. Part 3 – Tectonic development. In: *Sequence Stratigraphy and Cyclostratigraphy of the Mesozoic of the Sierra Madre Oriental, northeast Mexico, a Field Guidebook* (R.K. Goldhammer, P.J. Lehmann, R.G. Todd, J.L. Wilson, W.C. Ward & C.R. Johnson, eds.) *Society of Economic Paleontologists and Mineralogists Foundation, Gulf Coast Section*, 7-14
- Goldhammer, R.K., Dunn, P. A. & Hardie, L.A. 1987. High-frequency glacio-eustatic sea-level oscillations with Milankovitch characteristics recorded in Middle Triassic platform carbonates in northern Italy. *American Journal of Science*, 287, 853-892
- Goldring, R. 1995. Organisms and the substrate: response and effect. In: *Marine Palaeoenvironmental Analysis from Fossils* (D.W.J. Bosence & P.A. Allison, eds.) *Geological Society of London Special Publication*, 83, 151-180
- Goodwin, P.W. & Anderson, E.J. 1985. Punctuated aggradational cycles: A general hypothesis of episodic stratigraphic accumulation. *Journal of Geology*, 93, 515-533
- Goudie, A.S. 1996. Organic agency in calcrete development. *Journal of Arid Environments*, 32, 103-110
- Greenlee, S.M. & Lehmann, P.J. 1993. Stratigraphic framework of productive carbonate buildups. In: *Carbonate Sequence Stratigraphy: Recent Developments and Applications* (C.R. Handford & J.F. Sarg, eds.) *American Association of Petroleum Geologists Memoir*, 57, 43-63
- Handford, C.R. & Loucks, R.G. 1993. Carbonate depositional sequences and systems tracts-responses of carbonate platforms to relative sea-level change. In: *Carbonate Sequence Stratigraphy: Recent Developments and Applications* (C.R. Handford & J.F. Sarg, eds.) *American Association of Petroleum Geologists Memoir*, 57, 3-42



- Haq, B.U., Hardenbol, J. & Vail, P.R. 1988. Mesozoic and Cenozoic chronostratigraphy and cycles of sea-level change. In: *Sea-level changes: An Integrated Approach* (Wilgus, C.K.; Hastings, B.S.; Kendall, C.G.St.C.; Posamentier, H.W., Ross, C.A. & Wagoner, J.C. Economic Paleontologists V., eds.) *Society of Economic Paleontologists and Mineralogists Special Publication*, 42, 71-108
- Hardenbol, J., Jacquin, T., Farley, M.B., Jacquin, T., de Graciansky, P.C. & Vail, P.R. 1998. Mesozoic and Cenozoic sequence chronostratigraphic framework of European basins In: *Mesozoic and Cenozoic Sequence Stratigraphy of European Basins* (P.C. de Graciansky, J. Hardenbol, T. Jacquin & Vail, P.R., eds). *SEPM (Society for Sedimentary Geology) Special Publication*. 60, Charts
- Harper, E.M., Palmer, T.J. & Alpey, J.R. 1997. Evolutionary response by bivalves to changing Phanerozoic sea-water chemistry. *Geological Magazine*, 134, 403-407
- Harris, P.M., Frost, S.H., Seiglie, G.A. & Schneiderman, N. 1984. Regional unconformities and depositional cycles, Cretaceous of the Arabian Peninsula. In: *Interregional Unconformities and Hydrocarbon Accumulation* (J.S. Schlee, ed.). *American Association of Petroleum Geologists Memoir*, 36, 67-79
- Harris, P.M., Kendall, C.G.S.C. & Lerche, I. 1985. Carbonate cementation - a brief review. *Society of Economic Paleontologists and Mineralogists Special Publication*, 36, 79-95
- Harris, P.M., Saller, A.H. & Simo, J.A. 1999. Introduction. In: *Advances in Carbonate Sequence Stratigraphy: Application to Reservoirs, Outcrops and Models* (P.M Harris, A.H Saller, J.A Simo, eds.) *SEPM (Society for Sedimentary Geology) Special Publication*., 63, 1-10
- Hendry, J.P., Ditchfield, P.W. & Marshall, J.D. 1995. Two-stage neomorphism of Jurassic aragonitic bivalves - implications for early diagenesis. *Journal of Sedimentary Research*, 65, 214-224
- Heydari, E. 1997. The role of burial diagenesis in hydrocarbon destruction and H<sub>2</sub>S accumulation, Upper Jurassic Smackover Formation, Black Creek Field, Mississippi. *American Association of Petroleum Geologists Bulletin*, 81, 26-45
- Hill, C.A, 1995. H<sub>2</sub>S-related porosity and sulfuric acid oil-field karst. In: *Unconformities and porosity in carbonate strata* (D.A. Budd, A.H. Saller & P.M. Harris, eds.) *American Association of Petroleum Geologists Memoir*, 63, 301-306
- Hird, K. & Tucker, M.K. 1988. Contrasting diagenesis of two Carboniferous oolites from South Wales: a tale of climatic influence. *Sedimentology*, 35, 587-602
- Holland, S.M., Miller, A.I., Dattilo, B.F , Meyer, L.D. & Diekmeyer, S.L. 1997. Cycle anatomy and variability in the storm-dominated type Cincinnati (Upper Ordovician: coming to grips with cycle delineation and genesis. *Journal of Geology*, 105, 135-152
- Horbury, A. & Robinson, A.1993. Diagenesis, basin development, and porosity prediction in exploration - an introduction. In: *Diagenesis and basin development* (A. Horbury & A Robinson, eds.) *American Association of Petroleum Geology Studies in Geology*, 36, 1-4
- Hunt, D.& Tucker, M.E. 1993. Sequence stratigraphy of carbonate shelves with an example from the mid-Cretaceous (Urgonian) of southeast France. In: *Sequence stratigraphy and facies associations* (H.W. Posamentier, ed.) *IAS Special Publication*, 18, 307-341
- Hussein, M.I. 1988. The Arabian Infracambrian extensional system. *Tectonophysics*, 143, 93-103



- Hussein, M.I. 1989. Tectonic and depositional model of Late Precambrian-Cambrian Arabian and adjoining plates. *American Association of Petroleum Geologists Bulletin*, 73, 1117-1131
- Jacquin, T. & de Graciansky, P. 1998. Major transgressive cycles: The stratigraphic signature of European basin development. In: *Mesozoic and Cenozoic sequence stratigraphy of European basins* (P.C. de Graciansky, J. Hardenbol, T. Jacquin & Vail, P.R., eds.) *SEPM (Society for Sedimentary Geology) Special Publication*, 60, 17-29
- Jacquin, T., Rusciadelli, G., Amedro, F. & de Graciansky, P. 1998. The North Atlantic cycle: An overview of 2<sup>nd</sup>-order transgressive / regressive facies cycles in the Lower Cretaceous of Western Europe. In: *Mesozoic and Cenozoic sequence stratigraphy of European basins* (P.C. de Graciansky; J. Hardenbol; T. Jacquin & Vail, P.R., eds.) *SEPM (Society for Sedimentary Geology) special publication*, 60, 397-409
- Jadoul, F., Berra, F. & Garzanti, E. 1998. The Tethys Himalayan passive margin from Late Triassic to Early Cretaceous (South Tibet). *Journal of Asian Earth Sciences*, 16, 173-194
- James, N.P. and Ginsburge, R.N., 1979. The seaward margin of Belize barrier and atoll reefs. *Spec. Publ. int. Assoc. Sedimentol.* 3, 191.
- James, N.P. & Choquette, P.W. 1984. Diagenesis 9. Limestone – the meteoric diagenetic environment. *Geoscience Canada*, 11, 161-194
- James, N.P. & Choquette, P.W. (eds.) 1988. *Paleokarst*. Springer-Verlag, pp416
- Jones, B. & Kahle, C.F. 1995. Origin of endogenetic micrite in karst terrains - a case-study from the Cayman Islands. *Journal of Sedimentary Research*, 65, 283-293
- Jordan, J.R. & Wilson, J.L. 1994. Carbonate reservoir rocks. In: *The petroleum system - from source to trap* (L.B. Magoon & W.G. Dow, eds.) *American Association of Petroleum Geologists Memoir*, 60, 141-158
- Kahle, C.F. 1977. Origin of Holocene calcareous crusts: role of algae, fungi and sparmicritisation. *Sedimentology*, 24, 413-435
- Kamen-Kage, M. 1970. Geology and productivity of Persian Gulf synclinorium. *American Association of Petroleum Geologists Bulletin*, 54, 2372-2394
- Kendall, C.G.St.C., Bowen, B., Alsharhan, A., Cheong, D.k. & Stoudt, D. 1991. Eustatic controls on carbonate facies in reservoirs, and seals associated with Mesozoic hydrocarbon fields of the Arabian Gulf and the Gulf of Mexico, *Marine Geology*, 102 (1-4), 215-238
- Kerans, C. & Tinker, S.W. 1997. Sequence stratigraphy of carbonate reservoirs. *SEPM (Society for Sedimentary Geology) short course*, 40, pp130
- Kim, J.C. & Lee, Y.I. 1996. Marine diagenesis of lower Ordovician carbonate sediments (Dumugol Formation), Korea: Cementation in a calcite sea. *Sedimentary Geology*, 105, 41-257
- Kozar, M.G., Weber, L.J. & Walker, K.R. 1990. Field and modelling studies of Cambrian carbonate cycles, Virginia Appalachians-Discussion. *Journal of Sedimentary Petrology*, 60, 790-794
- Kupecz, A.J., Gluyas, J. & Bloch, S. 1997. Reservoir quality prediction in sandstone and carbonates: An overview. In: *Reservoir quality prediction in sandstone and carbonates* (J.A. Kupecz, J.G. Gluyas & S. Bloch, eds.). *American Association of Petroleum Geologists Memoir*, 69, vii-xxiv



- Lang, R.A. & Tucci, P. 1997. A preliminary study of the causes of the blackening of pebbles in the Cenomanian 'Breccia with black pebbles' of Camporosello (Lepini Mountains-Italy). *Geologica Romana*, 33, 89-97
- Lehmann, C., Osleger, D.A. & Montanez, I. 2000. Sequence stratigraphy of Lower Cretaceous (Barremian-Albian) carbonate platforms of northeastern Mexico: regional and global correlations. *Journal of Sedimentary Research*, 70, 373-391
- Lehrmann, D.J. & Goldhammer, R.K. 1999. Secular variation in parasequence and facies stacking patterns of platform carbonates: a guide to application of Stacking-patterns analysis in strata of diverse ages and settings. In: *Advances in Carbonate Sequence Stratigraphy: Application to Reservoirs, Outcrops and Models* (P.M Harris, A.H Saller, J.A Simo, eds.) *SEPM (Society for Sedimentary Geology) Special Publication*, 63, 187-225
- Longacre, S.A. & Ginger, E.P. 1988. Evolution of the Lower Cretaceous Ratawi Oolite reservoir, Wafra Field, Kuwait-Saudi Arabia partitioned neutral zone. In: *Giant oil and gas fields: a core workshop* (A.J. Lomando, ed.). *SEPM Core Workshop*, 12, 273-331
- Longacre, S.A. 1986. Geology of the Ratawi Oolite reservoir, Wafra field, Partitioned Neutral Zone. *Texaco Houston Research Centre, Unpublished report*, pp61
- Magara, K., Khan, M.S., Sharief, F.A. & Alkhatib, H.N. 1993. Log-derived reservoir properties and porosity preservation of Upper Jurassic Arab Formation in Saudi-Arabia. *Marine And Petroleum Geology*, 10, 352-363
- Maliva, R.G. & Dickson, J.A.D. 1992. The mechanism of skeletal aragonite neomorphism - evidence from neomorphosed mollusks from the Upper Purbeck Formation (Late Jurassic-Early Cretaceous), Southern England. *Journal of Sedimentary Research*, 76, 221-232
- Marzouk, I. & Abd El Satter, M.. 1994. Wrench Tectonics in Abu Dhabi, United Arab Emirates. In: *GEO'94 The Middle East petroleum Geosciences* (M.I. Al-Husseini ed.). *Gulf PetroLink*, 655-668
- Middelburg, J.J., Delange, G.J. & Kreulen, R. 1990. Dolomite formation in anoxic sediments of Kau Bay, Indonesia Middelburg. *Geology*, 18, 399-402
- Montanez, I.P. & Osleger, D.A. 1993. Parasequence stacking patterns, third-order accommodation events, and sequence stratigraphy of the Middle-Upper Cambrian platform carbonates, Bonanza King Formation, Southern Great Basin. In: *Carbonate Sequence Stratigraphy: Recent Developments and Applications* (R.G. Loucks and J.F. Sarg, eds.) *American Association of Petroleum Geologists Memoir*, 57, Chapter 12, 305-326
- Moore, C.H. 1989. *Carbonate diagenesis and porosity*. Developments in Sedimentology, Elsevier 46, pp120
- Moshier, S.O. 1989a. Development of microporosity in a micritic limestone reservoir, Lower Cretaceous, Middle-East. *Sedimentary Geology*, 63, 217-240
- Moshier, S.O. 1989b. Microporosity in micritic limestones - a review. *Sedimentary Geology*, 63, 191-213
- Mountain, G.S. & Prell, W.L., 1990. A multiphase plate tectonic history of the southeast continental margin of Oman. In: *The Geology and Tectonics of the Oman Region* (A.H.F. Robertson, M.P. Searle & A.S. Ries, eds.). *Geological Society of London Special Publication*, 49, 725-743



- Murris, R.J. 1980. Middle East: Stratigraphic evolution and oil habitat. *American Association of Petroleum Geologists Bulletin*, 64, 597-618
- Mylroie, J.E. & Carew J.L. 1995. Karst development on carbonate islands. In: *Unconformities and porosity in carbonate strata* (D.A. Budd, A.H. Saller & P.M. Harris, eds.). *American Association of Petroleum Geologists Memoir*, 63, 55-76
- Neumann, A.C. & Land, L.S. 1975. Lime mud deposition and calcareous algae in the Bight of Abaco, Bahamas: a budget. *Journal of Sedimentary Petrology*, 45, 763-786
- North, C.P. & Boering, M. 1999. Spectral gamma-ray logging for facies discrimination in mixed fluvial-eolian successions: A cautionary tale. *American Association of Petroleum Geologists Bulletin*, 83, 155-169
- Pasley, M.A.; Riley, G.W. & Nummedal, D., 1993. Sequence stratigraphic significance of organic matter variations: example from the Upper Cretaceous Mancos Shale of the San Juan Basin, New Mexico. In: *Source Rocks in a Sequence Stratigraphic framework* (Katz, B.J. & Pratt, L.M., eds.). *AAPG studies in geology*, 37, 221-241
- Paul, E. 1983. Shelf Environment. In: *Carbonate Depositional Environments* (P.A. Scholle, D.G. Bebout, C.H. Moore, eds.) *American Association of Petroleum Geologists Memoir*, 33, 267-296
- Perry, C.T. 1998. Grain susceptibility to the effects of microboring: implications for the preservation of skeletal carbonates. *Sedimentology*, 45, 39-51
- Perry, C.T. 1999. Biofilm-related calcification, sediment trapping and constructive micrite envelopes: a criterion for the recognition of ancient grass-bed environments? *Sedimentology*, 46, 33-45
- Posamentier, H.W. & Allen, G.P. 1993. Variability of the sequence stratigraphic model: effects of local basin factors. *Sedimentary Geology*, 86, 91-109
- Pratt, B.R. & James, N.P. 1986. The St. George Group (Lower Ordovician) of western Newfoundland: tidal island model for carbonate sedimentation in shallow epeiric seas. *Sedimentology*, 33, 313-343
- Pratt, B.R., & Smewing, J.D. 1990. Jurassic and Early Cretaceous platform margin configuration and evolution, central Oman Mountains. In: *The geology and tectonics of the Oman region* (A.H.F. Robertson, M.P. Searle & A.S. Ries, eds.). *Geological Society of London Special Publication*, 49, 69-88
- Pratt, B.R., & Smewing, J.D. 1993 a. Early Cretaceous platform margin configuration and evolution in the central Oman Mountains, Arabian Peninsula. *American Association of Petroleum Geologists Bulletin*, 77, 225-244
- Pratt, B.R., & Smewing, J.D. 1993 b. Early Cretaceous platform margin, Oman, Eastern Arabian Peninsula. In: *Cretaceous Carbonate Platforms* (J.A.T. Simo, R.W. Scott & J. Masse). *American Association of Petroleum Geologists Memoir*, 56, 201-212
- Price, G.D. 1999. The evidence and implications of polar ice during the Mesozoic. *Earth-Science Reviews*, 48, 183-210
- Purser, B.H. 1986. Dedolomite porosity and reservoir properties of Middle Jurassic carbonates in the Paris basin, France. In: *Carbonate Petroleum Reservoirs* (P.O. Roehl & P.W.



Choquette, eds.). Springer-Verlag, 341-355

Radke, R.L. & Mathis, R.L. 1980. On the formation and occurrence of saddle dolomite. *Journal of Sedimentary Petrology*, 50, 1149-1168.

Read, J.F. & Horbury, A.D. 1993. Eustatic and tectonic controls on porosity evolution beneath sequence-bounding unconformities and parasequence disconformities on carbonate platforms. In: *Diagenesis and basin development* (A.D. Horbury & A.G. Robinson, eds.). *American Association of Petroleum Geologists, Studies in Geology*, 36, 155-197

Read, J.F. 1985. Carbonate platform facies models. *American Association of Petroleum Geologists Bulletin*, 66, 860-878

Read, J.F. & Horbury, A.D. 1993. Eustatic and tectonic controls on porosity evolution beneath sequence-bounding unconformities and parasequence disconformities on carbonate platforms. In: *Diagenesis and basin development* (A.D. Horbury & A.G. Robinson, eds.). *American Association of Petroleum Geologists, Studies in Geology*, 36, 155-197

Read, J.F., Kerans, C., Wright, L.J., Sarg, J.F. & Wright, F.M. 1995. Milankovitch sea-level changes, cycles, and reservoirs on carbonate platforms in greenhouse and ice-house worlds. *SEPM (Society for Sedimentary Geology) Short Course*, 35, pp81

Reid, R.P. & Macintyre, I.G. 1998. Carbonate recrystallization in shallow marine environments: A widespread diagenetic process forming micritized grains. *Journal of Sedimentary Research*, 68, 928-946

Reid, R.P. & Macintyre, I.G. 2000. Microboring versus recrystallization: Further insight into the micritization process. *Journal of Sedimentary Research*, 70, 24-28

Rider, M.H. 1991. *The Geological Interpretation of Well Logs*. Whittles Publishing, pp174

Ross, D.J. & Skelton, P.W. 1993. Rudist formations of the Cretaceous: a palaeoecological, sedimentological and stratigraphical review. In: *Sedimentology Review* (V.P. Wright, ed.), 1, 73-91

Sadooni, F.N. 1993. Stratigraphic sequence, microfacies and petroleum prospects of the Yamama Formation, Lower Cretaceous, Southern Iraq. *American Association of Petroleum Geologists Bulletin*, 77, 1971-1988

Sandberg, P.A. 1983. An oscillating trend in Phanerozoic non-skeletal carbonate mineralogy. *Nature*, 305, 19-22

Schlager, W. 1999. Type 3 sequence boundaries. In: *Advances in Carbonate Sequence stratigraphy: Application to Reservoirs, Outcrops and Models* (P.M. Harris, A.H. Saller, J.A. Simo, eds.) *SEPM (Society for Sedimentary Geology) Special Publication*., 63, 35-45

Schmoker, J.W. & Halley, R.B. 1982. Carbonate porosity versus depth: a predictable relation for south Florida. *American Association of Petroleum Geologists Bulletin*, 66, 2561-2570

Schmoker, J.W. 1984. Empirical relation between carbonate porosity and thermal maturity: an approach to regional porosity prediction. *American Association of Petroleum Geologists Bulletin*, 68, 1697-1703

Scholle, P.A. & Halley, R.B. 1985. Burial diagenesis: out of sight, out of mind (porosity-depth relationships). In: *Carbonate Cements* (N. Schneidermann & P.H. Harris, eds.). *Spec.*



*Publ. Soc. Econ. Paleont.*, 36, 309-334

Scoffin, T.S. 1987. *An Introduction to Carbonate Sediments and Rocks*. Blackie, pp274

Scott, R.W. 1988. Models and stratigraphy of mid-Cretaceous reef communities, Gulf of Mexico. *SEPM Concepts Sedimentology Paleontology*, 2, pp102

Scott, R.W. 1990. Chronostratigraphy of Cretaceous carbonate shelf, southeastern Arabia. *The Geology and Tectonics of the Oman Region* (A.H.F. Robertson, M.P. Searle & A.S. Ries, eds.). *Geological Society of London Special Publication*, 49, 89-108

Shebl, H.T. & Alsharhan, A.S. 1994. Sedimentary facies and hydrocarbon potential of Berriasian-Hauterivian carbonates in central Arabia. In: *Micropalaeontology and hydrocarbon exploration in the Middle East* (M.D. Simmons, ed.). *Chapman and Hall*, 159-174

Sloss, L.L. 1963. Sequences in the cratonic interior of North America. *Geological Society of America Bulletin*, 74, 93-114

Spence, G.H. & Tucker, M.E. 1999. Modeling carbonate microfacies in the context of high-frequency dynamic relative sea-level and environmental changes. *Journal of Sedimentary Research*, 69, 947-961

Stoesser, D.B. & Camp, V.E. 1985. Pan-African microplate accretion of the Arabian Shield. *Geological Society of America Bulletin*, 96, 817-826

Strasser, A. 1984. Black-pebble occurrence and genesis in Holocene carbonate sediments (Florida Keys, Bahamas and Tunisia). *Journal of Sedimentary Petrology*, 54, 1097-1109

Strohmenger, C. 1991. Kimmeridgian / Tithonian eustacy and its imprints on carbonate rocks from the Dinaric and the Jura carbonate platforms. *Societe Geologique de France Bulletin*, 162, 4, 661-671

Sun, S.Q. & Wright, V.P. 1998. Controls on reservoir quality of an Upper Jurassic reef mound in the Palmers Wood Field area, Weald basin, southern England. *American Association of Petroleum Geologists Bulletin*, 82, 497-515

Surdam, R.C., Crossey, L.J., Hagen, E.S. & Heasler, H.P. 1989. Organic-inorganic interactions and sandstone diagenesis. *American Association of Petroleum Geologists Bulletin*, 73, 1-23

Taberner, C., Saaltink, M.W. & Carrera, J. 1998. The genesis of dedolomites: a discussion based on reactive transport modeling. *Journal of Hydrology*, 209, 346-365

Talbot, C.J., & Alavi, N. 1996. The past of a future syntaxis across the Zagros. In: *Salt tectonic* (G.I. Alsop, D.J. Blundell & I. Davison, eds.). *Geological Society of London Special Publication*, 100, 89-109

Tobin, K.J., Walker, K.R. & Goldberg S.G. 1997. Burial diagenesis of middle Ordovician carbonate buildups (Alabama, USA): documentation of the dominance of shallow burial conditions. *Sedimentary Geology*, 114, 223-236

Tucker, M.E. 1982. *Field Deposition of Sedimentary Rocks*. Enterprise, Milton Keynes, pp128

Tucker, M.E. (ed.). 1988. *Techniques in Sedimentology*. Blackwells, pp394



- Tucker, M.E. 1991.** *Sedimentary Petrology*. Blackwell Scientific Publications, pp260
- Tucker, M.E., 1993.** Carbonate diagenesis and sequence stratigraphy. In: *Sedimentology Review*, 1, (V.P. Wright, ed.). Blackwell Scientific, 51-72
- Tucker, M.E. & Bathurst, R.G.C. 1990.** *Carbonate Diagenesis*. Int. Ass. Sediment. Reprint Series, 1, pp312
- Tucker, M.E. & Wright, V.P. 1990.** *Carbonate Sedimentology*. Blackwell, pp482
- Tucker, M.E., Calvet, F. & Hunt D. 1993.** Sequence stratigraphy of carbonate ramps: systems tracts, models and application to the Muschelkalk carbonate platforms of eastern Spain. In: *Sequence stratigraphy and facies associations* (H.W. Posamentier, ed.). *International Association Sedimentologists Special Publication*, 18, 397-415
- Vail, P.R., Mitchum, R.M. & Thompson, J.R. 1977.** Seismic stratigraphy and global changes of sea level, Part 4: Global cycles of relative changes of sea level. In: *Seismic stratigraphy application to hydrocarbon exploration* (C.E. Payton, ed.). *American Association of Petroleum Geologists Memoir*, 26, 83-97
- Van Wagoner, J.C., Mitchum, R.M., Campion, K.M. & Rahmanian, V.D. 1990.** Siliciclastic sequence stratigraphy in well logs, core, and outcrops. *American Association of Petroleum Geologists; Methods in Exploration Series*, 7, pp55
- Warren, J. 2000.** Dolomite: occurrence, evolution and economically important associations. *Earth Science Reviews*, 52, 1-81
- Warsi, W.E.K. 1990.** Gravity field of Kuwait and its relevance to major geological structures. *American Association of Petroleum Geologists Bulletin*, 74, 1610-1622
- Weissert, H., Lini, A., Follmi, K.B. & Kuhn, O. 1998.** Cretaceous carbon isotope stratigraphy and platform drowning events: a possible link?. *Palaeogeography Palaeoclimatology palaeoecology*, 137, 189-203
- Wilson, A.O. 1981.** Jurassic Arab-C and D carbonate petroleum reservoir Qatif Field, Saudi Arabia. 2<sup>nd</sup> Middle East Oil Show, Bahrain. *Soc. Petrol. Engrs. (SPE)*, 9594, 171-177
- Wilson, J.L. & Jordan, C. 1983.** Middle shelf environment. In: *Carbonate Depositional Environments* (P.A. Scholle, D.G. Bebout, C.H. Moore, eds.) *American Association of Petroleum Geologists Memoir*, 33, 345-462
- Wilson, J.L. 1975.** *Carbonate Facies in Geological History*. Springer Verlag, pp471
- Wright, D.T. 1997.** Organogenic origin for widespread dolomite in the Cambrian Eilean Dubh Formation, northwestern Scotland. *Journal of Sedimentary Research*, 67, 54-64
- Wright, P.V. and Tucker, M.E. 1991.** Calcretes: An introduction. In *Calcretes* (V. P. Wright & M.E. Tucker, eds.). *Int. Ass. Sediment. Reprint Series*, 2, 1-22
- Wright, V.P. & Smart, P.L. 1994.** Paleokarst (dissolution diagenesis): its occurrence and hydrocarbon exploration significance. In: *Developments in Sedimentology*, 51, *Diagenesis*, 4 (K.H. Wolf & G.V. Chilingarian, eds.). Elsevier, 477-517
- Wright, V.P. 1986.** The role of fungal biomineralization in the formation of Early Carboniferous soil fabrics. *Sedimentology*, 33, 831-838



- Wright, V.P. 1994.** Paleosols in shallow marine carbonate sequences. *Earth-Science Reviews*, **35**, 367-395
- Wright, V.P., Platt, N.H., Marriott, S.B. & Beck, V.H. 1995.** A classification of rhizogenic (root-formed) calcretes, with examples from the Upper Jurassic Lower Cretaceous of Spain and Upper Cretaceous of southern France. *Sedimentary Geology*, **100**, 143-158
- Yousif, S. & Nouman, G. 1997.** Jurassic geology of Kuwait. *GeoArabia*, **2**, 91-110



**Appendix 1: Location of samples and petrographic data**

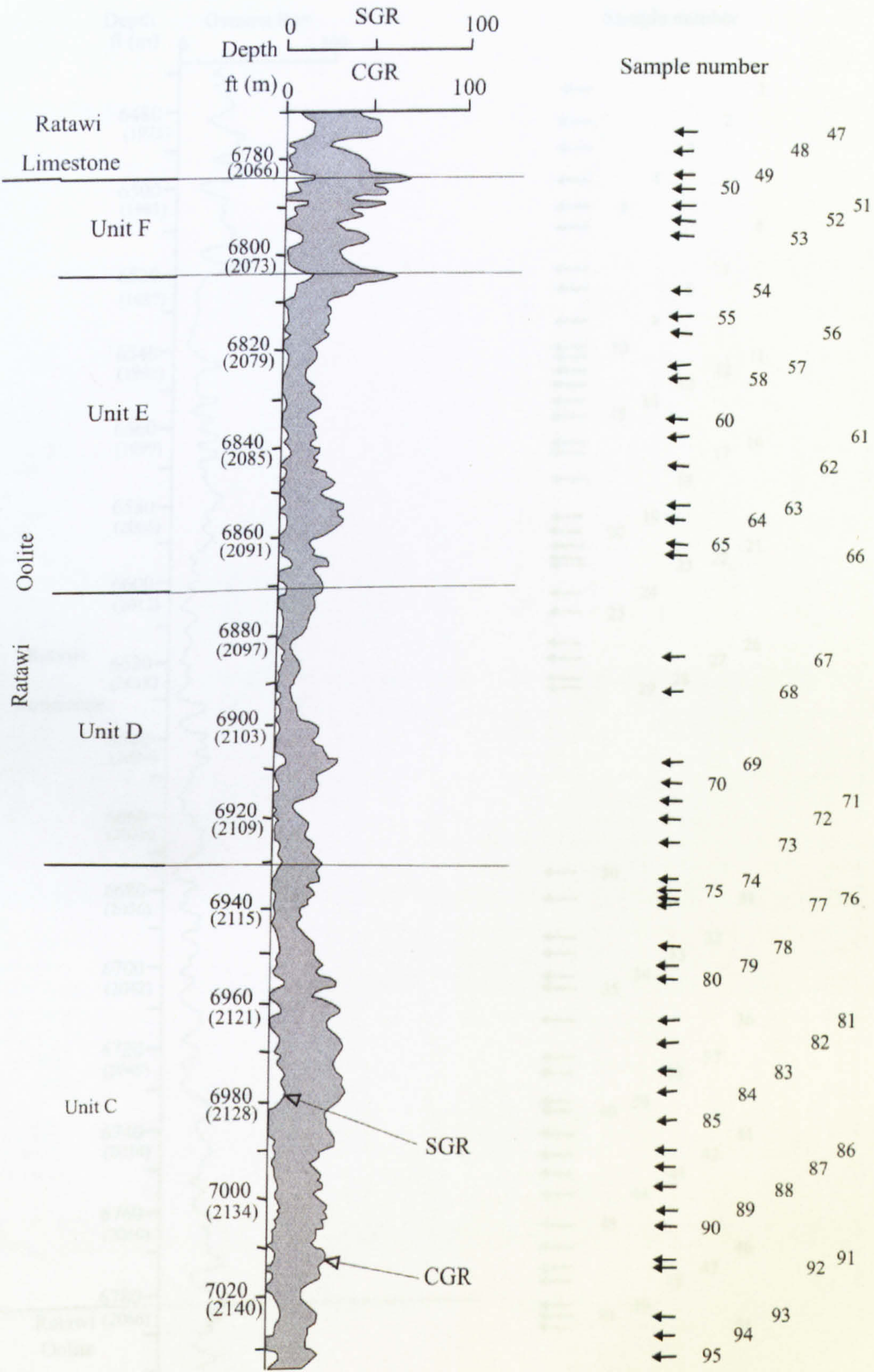
Well R-50.....275

Well R-48.....286

Well R-49.....293

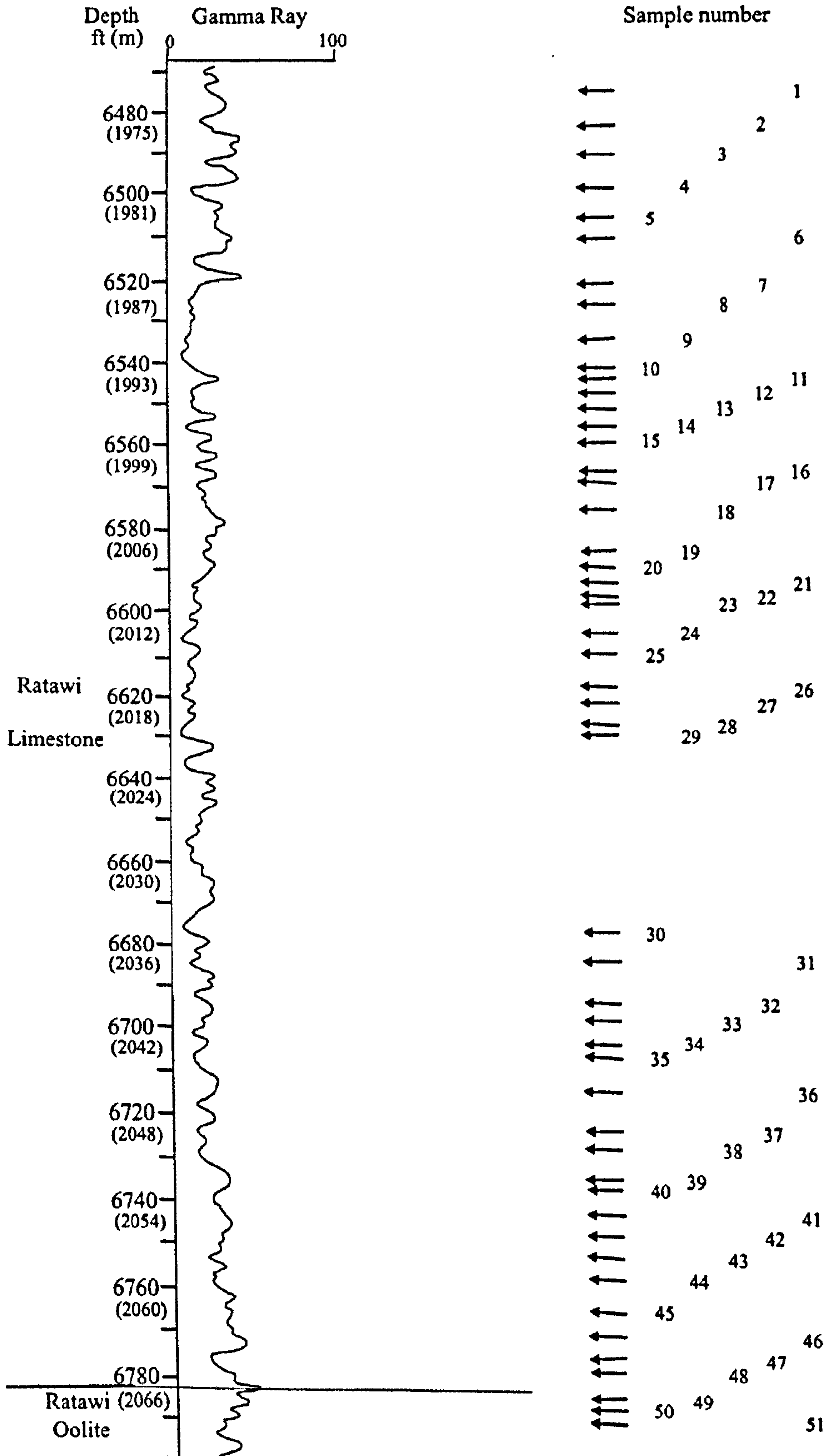


Well R-50





Well R-50





Well R-50										
Sample number	95	94	93	92	91	90	89	88	87	86
Sample depth ( ft )	7032	7028	7024	7015	7013	7006	7002	6998	6994	6990
Sample depth ( m )	2143	2142	2141	2138	2137	2135	2134	2133	2132	2130
Texture	Gs	Rs	Gs	Gs	Rs	Rs	Gs	Gs	Rs	Fs
<b>Non-Skeletal Grains</b>										
Peloids	A	A	A	A	A	B	A	A	A	B
Ooids	E	E	E					E		
Aggregate				E						
Quartz/silt										
Phosphatic										
Black grains										
<b>Skeletal Grains</b>										
Corals	E	D		D	D	B	D	D	D	D
Bivalves	D	D	C	D	E	D	E	D	E	D
Gastropods										
Brachiopods	D	E			E	E	E	E	E	E
Crinoids	D	D	D	D	D	D	D	D	D	D
Ostracods										
Calpionellids										
Sponge spicules										
Green Algae			E	E						D
Forams	E	D	D	D	D	E	E		D	D
Radiolarians										
<b>CEMENT:</b>										
Saddle dolomite		W	W	W	W		W			W
Bladed / granular calcite	W	W	W	W	W	W	W	W	W	W
Granular drusy calcite	W	W	W	W	W	W	W	W	W	W
Syntaxial calcite	W	W	W	W	W	W	W	W	W	W
Poikilotopic calcite	W	W	W	W	W			W		
Columnar calcite										
<b>Porosity:</b>	<b>5 %</b>	<b>5 %</b>	<b>7%</b>	<b>10%</b>	<b>10%</b>	<b>7%</b>	<b>5%</b>	<b>5%</b>	<b>5%</b>	<b>7%</b>
Interparticle	W	W	W	W	W	W	W	W	W	
Vug	W	W	W	W	W	W	W	W	W	W
Mouldic										
Intraparticle										
Fracture	W	W	W	W	W	W	W	W	W	W
Intercrystal										
Rootlet										
Stylolitic										
Burrow										
<b>Sedimentary structures</b>										
Rootlets										
Burrows / Bioturbation										
Cross lamination										
<b>Diagenesis</b>										
Saddle dol. replacement			W							
Micro-euhedral dol. cx.										
Dedolomitization										
Limonite / goethite										
Pyrite										
Vadose compaction	W		W	W	W	W	W	W	W	
Burial compaction	W	W	W	W	W	W	W	W	W	W
Microspar cement	W									
Micrite envelope	W	W	W	W	W	W	W	W	W	W
Grain boring ( marine)	W	W	W	W	W	W	W	W	W	W
Microfacies	SR-4	SR-1	SR-4	SR-3	SR-1	SR-1	SR-1	SR-4	SR-1	DR-1
<p><b>Grain percentage:</b> E = &lt; 1 %  D = 1-20%  C = 21- 40 %  B = 41- 60 %  A = &gt; 61%</p> <p><b>With this feature = W</b></p> <p><b>Texture:</b> Ms = Mudstone  Ws = Wackestone  Ps = Packstone  Gs = Grainstone  Fs = Floatstone  Rs = Rudstone  Cx = Crystalline carbonate</p> <p><b>Matrix =</b> Micrite</p>										



	Well R-50									
Sample number	85	84	83	82	81	80	79	78	77	76
Sample depth ( ft )	6984	6978	6974	6969	6964	6955	6951	6949	6939	6937
Sample depth ( m )	2129	2127	2126	2125	2123	2120	2119	2118	2115	2114
Texture	Ws	Ws	Rs	Ps	Ps	Rs	Ps	Rs	Gs	Ps
<b>Non-Skeletal Grains</b>										
Peloids	A	A	A	A	A	B	A	A	A	A
Ooids									E	
Aggregate				E	E	E			E	E
Quartz/silt										
Phosphatic		E	E				E			
Black grains										
<b>Skeletal Grains</b>										
Corals	D		D	E		D	E	D	E	E
Bivalves		E	E	E	E		E	E		E
Gastropods	E							E		
Brachiopods	E	E	E		E	D	E			
Crinoids	E	D	E	D	D	E	E	E	D	D
Ostracods										
Calpionellids										
Sponge spicules							E			
Green Algae				D	D	D				
Forams	E	E	D	D	D		E	D	D	E
Radiolarians										
<b>CEMENT:</b>										
Saddle dolomite			W	W	W	W			W	
Bladed / granular calcite					W				W	
Granular drusy calcite	W	W	W	W	W	W	W	W	W	W
Syntaxial calcite	W	W	W	W	W	W	W	W	W	W
Poikilotopic calcite									W	W
Columnar calcite										
<b>Porosity:</b>	<b>7%</b>	<b>10%</b>	<b>7%</b>	<b>7%</b>	<b>7%</b>	<b>10%</b>	<b>10%</b>	<b>5%</b>	<b>6%</b>	<b>7%</b>
Interparticle					W				W	
Vug	W	W	W	W	W	W	W	W	W	W
Mouldic		W								W
Intraparticle										
Fracture			W	W			W	W		W
Intercrystal										
Rootlet										
Stylolitic						W				
Burrow										
<b>Sedimentary structures</b>										
Rootlets										
Burrows / Bioturbation										
Cross lamination										
<b>Diagenesis</b>										
Saddle dol. replacement										
Micro-euhedral dol. cx.										
Dedolomitization							W	W	W	W
Limonite / goethite										
Pyrite										
Vadose compaction										
Burial compaction	W	W	W	W	W	W	W	W	W	W
Microspar cement								W	W	W
Micrite envelope	W			W	W		W	W	W	
Grain boring ( marine)	W		W	W				W		W
Microfacies	DR-3	DR-3	SR-1	SR-3	SR-3	SR-1	SR-4	SR-1	SR-3	SR-3
<p><b>Grain percentage:</b> E = &lt; 1 % D = 1-20% C = 21- 40 % B = 41- 60 % A = &gt; 61%</p> <p><b>With this feature = W</b></p> <p><b>Texture:</b> Ms = Mudstone Ws = Wackestone Ps = Packstone Gs = Grainstone Fs = Floatstone Rs = Rudstone Cx = Crystalline carbonate</p> <p><b>Matrix =</b> Micrite</p>										



	Well R-50									
Sample number	75	74	73	72	71	70	69	68	67	66
Sample depth ( ft )	6936	6934	6925	6920	6917	6912	6909	6891	6885	6864
Sample depth ( m )	2114	2113	2110	2109	2108	2107	2106	2100	2098	2092
Texture	Gs	Gs	Gs	Gs	Gs	Gs	Gs	Gs	Fs	Rs
Non-Skeletal Grains										
Peloids	A	A	A	A	A	A	A	A	A	B
Ooids		E	C		E	E	E			
Aggregate	E	E	E		D	E	E		E	E
Quartz/silt										
Phosphatic					E					
Black grains										
Skeletal Grains										
Corals							E	E	D	E
Bivalves	E	D		E	E	D		E	D	E
Gastropods										
Brachiopods			E						E	E
Crinoids	E	E	D	E		E	D	D	D	E
Ostracods										
Calpionellids										
Sponge spicules										
Green Algae						E				
Forams		D	E		E	D	E	E		
Radiolarians										
CEMENT:										
Saddle dolomite	W		W		W		W			W
Bladed / granular calcite	W	W	W	W	W	W	W	W	W	W
Granular drusy calcite	W	W	W	W	W	W	W	W	W	W
Syntaxial calcite	W	W	W	W	W	W	W	W	W	W
Poikilotopic calcite										
Columnar calcite										
Porosity:	7%	7%	16%	16%	16%	16%	16%	16%	16%	16%
Interparticle	W		W	W	W	W	W	W	W	W
Vug	w	W	W	W	W	W	W	W	W	W
Mouldic										
Intraparticle										
Fracture	W	W	W						W	
Intercrystal										
Rootlet									W	W
Stylolitic										
Burrow										
Sedimentary structures										
Rootlets									W	W
Burrows / Bioturbation										
Cross lamination										
Diagenesis										
Saddle dol. replacement										
Micro-euhedral dol. cx.		W								
Dedolomitization	W	W	W	W	W	W	W	W		
Limonite / goethite				W	W	W	W	W		
Pyrite										
Vadose compaction	W	W								W
Burial compaction	W	W	W	W	W	W	W	W	W	W
Microspar cement		W		W					W	W
Micrite envelope	W	W		W		W	W	W		
Grain boring ( marine)										
Microfacies	SR-3	SR-3	SR-3	SR-4	SR-3	SR-3	SR-3	SR-4	DiagCal	DiagCal
<div><div><div>Grain percentage:</div><div>E = &lt; 1 % D =1-20% C =21- 40 % B =41- 60 % A = &gt; 61%</div></div><div><div>With this feature = W</div></div><div><div>Texture:</div><div>Ms = Mudstone Ws = Wackestone Ps = Packstone Gs = Grainstone Fs = Floatstone Rs = Rudstone Cx = Crystalline carbonate</div></div><div><div>Matrrix = Micrite</div></div></div>										



	Well R-50								
Sample number	65	64	63	62	61	60	58	57	56
Sample depth ( ft )	6861	6857	6853	6844	6839	6835	6827	6824	6818
Sample depth ( m )	2091	2090	2089	2086	2084	2083	2081	2080	2078
Texture	Rs	Rs	Gs	FS	Ps	Ps	Gs	Gs	Gs
Non-Skeletal Grains									
Peloids	A	A	A	A	A	A	A	A	A
Ooids									
Aggregate			D		E		E		E
Quartz/silt						E	E	E	
Phosphatic					E				
Black grains					E	D		E	
Skeletal Grains									
Corals	D	D	E	E	E		E		E
Bivalves		E	D	E		E			
Gastropods	D	D		D					
Brachiopods	E	E	E	E	E	E	E	E	E
Crinoids	E	E	D	D	D	D	D	D	D
Ostracods	E		E		E				
Calpionellids									
Sponge spicules									
Green Algae		D	D						E
Forams	E	E			D	D	D	D	D
Radiolarians									
CEMENT:									
Saddle dolomite				W					
Bladed / granular calcite	W		W	W		W	W	W	W
Granular drusy calcite	W	W	W		W		W	W	
Syntaxial calcite		W	W				W	W	W
Poikilotopic calcite			W					W	
Columnar calcite							W		W
Porosity:	4%	7%	7%	3%	3%	2%	7%	16%	16%
Interparticle			W			W	W	W	W
Vug	W	W	W	W	W	W	W	W	W
Mouldic		W		W					
Intraparticle									
Fracture	W	W		W					W
Intercrystal									
Rootlet		W					W	W	W
Stylolitic	W								
Burrow									
Sedimentary structures									
Rootlets		W	W				W	W	W
Burrows / Bioturbation				W					
Cross lamination									
Diagenesis									
Saddle dol. replacement									
Micro-euhedral dol. cx.									W
Dedolomitization								W	W
Limonite / goethite								W	W
Pyrite					W				
Vadose compaction						W	W	W	W
Burial compaction	W	W	W	W	W	W	W	W	W
Microspar cement									
Micrite envelope	W	W	W			W	W	W	W
Grain boring ( marine)	W	W						W	
Microfacies	SR-1	DiagCal	DiagCal	DR-1	SR-5	SR-5	DiagCal	DiagCal	DiagCal
<div><div><div>Grain percentage:</div><div>E = &lt; 1 % D =1-20% C =21- 40 % B =41- 60 % A = &gt; 61%</div></div><div><div>With this feature = W</div></div><div><div>Texture:</div><div>Ms = Mudstone Ws = Wackestone Ps = Packstone Gs = Grainstone Fs = Floatstone Rs = Rudstone Cx = Crystalline carbonate</div></div><div><div>Matrrix = Micrite</div></div></div>									



	Well R-50									
Sample number	55	54	53	52	51	50	49	48	47	46
Sample depth ( ft )	6813	6809	6796	6793	6790	6786	6783	6779	6775	6770
Sample depth ( m )	2077	2075	2071	2071	2070	2068	2067	2066	2065	2063
Texture	Gs	Ps	Gs	Ws	Ws	Ps	Ps	Ws	Ws	Ps
Non-Skeletal Grains										
Peloids	A	A	A	A	A	A	B	A	D	B
Ooids	E									
Aggregate	E	D	D	D	E					
Quartz/silt	E		E	E	E	E	E	E	E	
Phosphatic										
Black grains			E	D	E	D	D	D	D	E
Skeletal Grains										
Corals						E				
Bivalves	D		E	E	D	E		E	D	E
Gastropods										E
Brachiopods	E		E		E	E	E	E	D	
Crinoids	D	D	D	D	D	D	D	D	D	E
Ostracods								E	E	
Calpionellids										
Sponge spicules						E				E
Green Algae										
Forams	D	E	D	D	D	E	E			E
Radiolarians										
CEMENT:										
Saddle dolomite										
Bladed / granular calcite	W	W	W	W	W	W		W		
Granular drusy calcite					W	W	W			W
Syntaxial calcite	W	W	W			W				
Poikilotopic calcite		W								
Columnar calcite										
Porosity:	16%	16%	16%	9%	7%	16%	0%	1%	1%	1%
Interparticle	W	W	W							
Vug	W	W	W	W	W	W		W	W	
Mouldic	W				W	W				
Intraparticle				W						
Fracture	W	W	W	W	W	W		W	W	
Intercrystal										
Rootlet	W	W	W	W		W				
Stylolitic					W		W		W	W
Burrow										
Sedimentary structures										
Rootlets	W	W	W	W		W				
Burrows / Bioturbation				W		W	W			W
Cross lamination										
Diagenesis										
Saddle dol. replacement										
Micro-euhedral dol. cx.	W	W								
Dedolomitization	W									
Limonite / goethite	W									
Pyrite					W	W		W	W	W
Vadose compaction		W								
Burial compaction	W	W	W	W	W	W	W	W	W	
Microspar cement					W	W	W	W		
Micrite envelope	W	W		W						
Grain boring ( marine)	W									
Microfacies	DiagCal	DiagCal	DiagCal	DiagCal	BR-2	BR-1	SR-5	BR-1	BR-1	SR-5
<div><div><div>Grain percentage:</div><div>E = &lt; 1 % D =1-20% C =21- 40 % B =41- 60 % A = &gt; 61%</div></div><div><div>With this feature = W</div></div><div><div>Texture:</div><div>Ms = Mudstone Ws = Wackestone Ps = Packstone Gs = Grainstone Fs = Floatstone Rs = Rudstone Cx = Crystalline carbonate</div></div><div><div>Matrrix = Micrite</div></div></div>										



	Well R-50									
Sample number	45	44	43	42	41	40	39	38	37	36
Sample depth ( ft )	6764	6758	6751	6748	6741	6737	6734	6728	6722	6713
Sample depth ( m )	2062	2060	2058	2057	2055	2053	2052	2051	2049	2046
Texture	Ms	Ws	Ws	Ws	Ws	Ws	Ws	Ws	Ws	Ms
<b>Non-Skeletal Grains</b>										
Peloids										
Ooids										
Aggregate										
Quartz/silt	E	E	E	E	E	E	E	D	D	D
Phosphatic								E	E	E
Black grains	E	E		D	D	D				
<b>Skeletal Grains</b>										
Corals										
Bivalves	D	D	D	E	E		E		D	E
Gastropods								E		
Brachiopods	D	D	E	D	E	E	E	E	D	
Crinoids	E	D	D	D	D	D	D	D	D	E
Ostracods					E	E	E			
Calpionellids										E
Sponge spicules		E	E				E			
Green Algae										
Forams		E		E		E		E		
Radiolarians										
<b>CEMENT:</b>										
Saddle dolomite			W					W		
Bladed / granular calcite						W				
Granular drusy calcite			W	W		W	W	W		W
Syntaxial calcite					W		W	W	W	
Poikilotopic calcite										
Columnar calcite										
<b>Porosity:</b>	<b>2%</b>	<b>16%</b>	<b>16%</b>	<b>8%</b>	<b>5%</b>	<b>3%</b>	<b>7%</b>	<b>3%</b>	<b>3%</b>	<b>3%</b>
Interparticle										
Vug	W	W	W	W		W	W	W	W	W
Mouldic		W	W	W		W	W	W	W	
Intraparticle										
Fracture						W		W		
Intercrystal										
Rootlet										
Stylolitic				W	W	W			W	
Burrow										
<b>Sedimentary structures</b>										
Rootlets										
Burrows / Bioturbation	W	W	W	W	W	W	W	W	W	W
Cross lamination										
<b>Diagenesis</b>										
Saddle dol. replacement										
Micro-euhedral dol. cx.				W					W	W
Dedolomitization										
Limonite / goethite										
Pyrite	W	W	W	W	W	W		W	W	W
Vadose compaction										
Burial compaction	W			W	W	W	W		W	
Microspar cement				W						
Micrite envelope										
Grain boring ( marine)								W		
Microfacies	Br-1	BR-1	DR-3	BR-1	BR-1	BR-1	BR-2	BR-2	DR-2	DR-2
<p><b>Grain percentage:</b> E = &lt; 1 % D = 1-20% C = 21- 40 % B = 41- 60 % A = &gt; 61%</p> <p><b>With this feature = W</b></p> <p><b>Texture:</b> Ms = Mudstone Ws = Wackestone Ps = Packstone Gs = Grainstone Fs = Floatstone Rs = Rudstone Cx = Crystalline carbonate</p> <p><b>Matrix =</b> Micrite</p>										



	Well R-50									
Sample number	35	34	33	32	31	30	29	28	27	26
Sample depth ( ft )	6705	6701	6697	6691	6681	6675	6659	6625	6620	6616
Sample depth ( m )	2044	2042	2041	2039	2036	2034	2030	2029	2018	2017
Texture	Ms	Ps	Ms	Ms	Ms	Ws	Ms	Ms	Ms	Ms
Non-Skeletal Grains										
Peloids		B				D				
Ooids										
Aggregate										
Quartz/silt	D	D	D	D	D	D	D	D	D	D
Phosphatic	E	E	E	E	E	E	E	E		
Black grains		D	E	E	D		E	D	D	D
Skeletal Grains										
Corals					E					
Bivalves	E	E		E	E			E		E
Gastropods		E				E				
Brachiopods	E	E							D	E
Crinoids	E	D	E	D	D	D	D	D	D	D
Ostracods		E			E		E	E	E	E
Calpionellids										
Sponge spicules						E				
Green Algae		E			D					
Forams					E	E	E	E	E	E
Radiolarians										
CEMENT:										
Saddle dolomite		W				W				
Bladed / granular calcite										
Granular drusy calcite		W	W		W	W	W	W		
Syntaxial calcite										
Poikilotopic calcite										
Columnar calcite										
Porosity:	3 %	10%	0%	1 %	0%	3%	0%	3%	2%	2%
Interparticle								W		
Vug	W	W				W				
Mouldic		W								
Intraparticle										
Fracture		W		W		W		W		W
Intercrystal										
Rootlet										
Stylolitic									W	W
Burrow										
Sedimentary structures										
Rootlets										
Burrows / Bioturbation	W	W		W	W			W	W	W
Cross lamination										
Diagenesis										
Saddle dol. replacement										
Micro-euhedral dol. cx.	W		W	W			W	W		
Dedolomitization										
Limonite / goethite										
Pyrite	W		W	W	W	W	W	W	W	
Vadose compaction										
Burial compaction									W	W
Microspar cement					W	W			W	
Micrite envelope										
Grain boring ( marine)										
Microfacies	DR-2	SR-5	BR-1	Br-1	BR-1	DR-3	BR-1	BR-1	BR-1	BR-1
<div><div><div>Grain percentage:</div><div>E = &lt; 1 % D =1-20% C =21- 40 % B =41- 60 % A = &gt; 61%</div></div><div><div>With this feature = W</div></div><div><div>Texture:</div><div>Ms = Mudstone Ws = Wackestone Ps = Packstone Gs = Grainstone Fs = Floatstone Rs = Rudstone Cx = Crystalline carbonate</div></div><div><div>Matrrix =</div><div>Micrite</div></div></div>										



Well R-50										
Sample number	25	24	23	22	21	20	19	18	17	16
Sample depth ( ft )	6609	6603	6598	6595	6591	6588	6583	6574	6567	6565
Sample depth ( m )	2014	2012	2011	2010	2009	2008	2006	2004	2002	2001
Texture	Ws	Ps	Ws	Ws	Ws	Ps	Ps	Ps	Ws	Ws
<b>Non-Skeletal Grains</b>										
Peloids		A		C	A		A	A		C
Ooids										
Aggregate		E								
Quartz/silt	D		E	E	E	E	E	E		
Phosphatic							E			
Black grains			D			C	E		D	E
<b>Skeletal Grains</b>										
Corals	E	E								
Bivalves			E					E	D	
Gastropods		E	E	E						
Brachiopods	E	E	E			E		E	D	E
Crinoids	E		D	D	E	D	D	D	D	D
Ostracods	E			E				E		
Calpionellids										
Sponge spicules	E			D						
Green Algae	D			D	D			E	E	D
Forams	E	D	E	E	E			E		
Radiolarians										
<b>CEMENT:</b>										
Saddle dolomite										
Bladed / granular calcite							W			
Granular drusy calcite	W	W	W	W	W			W	W	
Syntaxial calcite							W			
Poikilotopic calcite										
Columnar calcite										
<b>Porosity:</b>	<b>0%</b>	<b>1%</b>	<b>3%</b>	<b>2%</b>	<b>1%</b>	<b>3%</b>	<b>1%</b>	<b>7%</b>	<b>7%</b>	<b>2%</b>
Interparticle							W			
Vug			W	W			W	W	W	
Mouldic										
Intraparticle										
Fracture			W	W	W	W		W	W	W
Intercrystal										
Rootlet										
Stylolitic		W	W			W		W	W	W
Burrow										
<b>Sedimentary structures</b>										
Rootlets		W			W					
Burrows / Bioturbation			W	W			W		W	W
Cross lamination										
<b>Diagenesis</b>										
Saddle dol. replacement										
Micro-euhedral dol. cx.										
Dedolomitization										
Limonite / goethite										
Pyrite		W		W		W	W	W	W	W
Vadose compaction		W								
Burial compaction		W	W	W	W	W			W	
Microspar cement										
Micrite envelope		W								
Grain boring ( marine)										
Microfacies	BR-2	DiagCal	BR-1	BR-2	DiagCal	SR-5	SR-5	BR-2	BR-1	BR-1
<p><b>Grain percentage:</b> E = &lt; 1 %      <b>With this feature = W</b>      <b>Texture:</b> Ms = Mudstone  D = 1-20%      Ws = Wackestone  C = 21- 40 %      Ps = Packstone  B = 41- 60 %      Gs = Grainstone  A = &gt; 61%      Fs = Floatstone  Rs = Rudstone  Cx = Crystalline carbonate</p> <p><b>Matrix =</b> Micrite</p>										



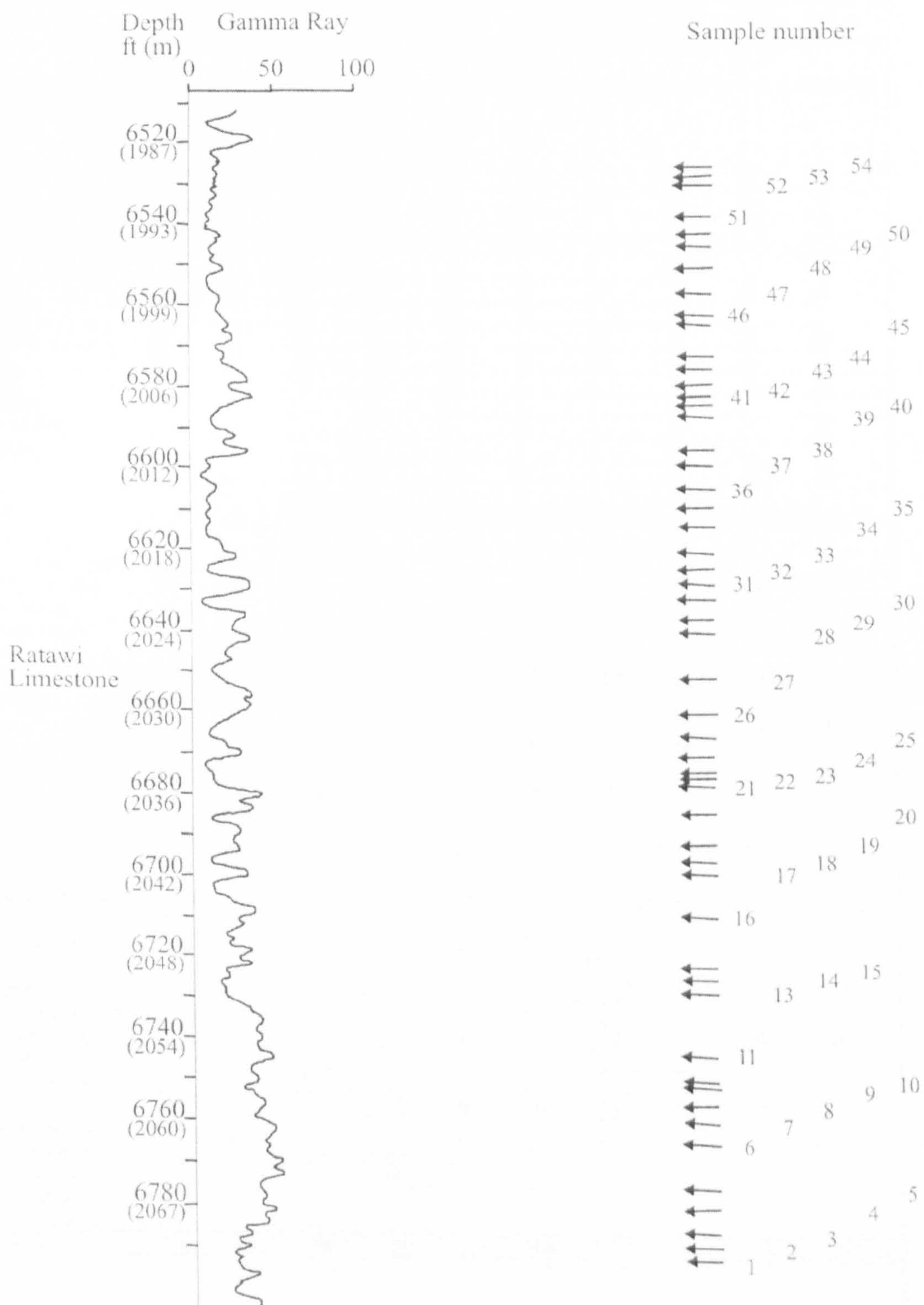
Well R-50										
Sample number	15	14	13	12	11	10	9	8	7	6
Sample depth ( ft )	6559	6554	6550	6546	6542	6540	6533	6525	6520	6510
Sample depth ( m )	1999	1998	1996	1995	1994	1993	1991	1989	1987	1984
Texture	Ms	Ws	Ms	Ws	Ps	Ps	Ps	Ps	Ws	Ms
Non-Skeletal Grains										
Peloids	D	C		C	D	C	B	D		
Ooids										
Aggregate										
Quartz/silt	D	E	E	E	E	D	E	D	E	E
Phosphatic						E	E	E	E	E
Black grains	D	D	E	D	D				E	
Skeletal Grains										
Corals			E					E	E	
Bivalves		E	E						E	
Gastropods			E			E				
Brachiopods	E	D		E	E	E	E	E	E	E
Crinoids	D	D	D	D	D	D	D	D	D	E
Ostracods	E	E	E	E	E				E	E
Calpionellids										
Sponge spicules			E			E				
Green Algae		E	D	E	D	D	D	E	D	
Forams					E		E	E		
Radiolarians										
CEMENT:										
Saddle dolomite										
Bladed / granular calcite										
Granular drusy calcite	W	W	W	W	W	W	W	W	W	
Syntaxial calcite										
Poikilotopic calcite										
Columnar calcite										
Porosity:	3%	3%	3%	0%	2%	0%	0%	3%	3%	1%
Interparticle										
Vug	W	W	W		W			W		W
Mouldic										
Intraparticle										
Fracture	W		W					W		
Intercrystal										
Rootlet										
Stylolitic		W	W		W				W	
Burrow										
Sedimentary structures										
Rootlets										
Burrows / Bioturbation	W		W	W	W					
Cross lamination										
Diagenesis										
Saddle dol. replacement										
Micro-euhedral dol. cx.				W				W		W
Dedolomitization										
Limonite / goethite										
Pyrite	W	W	W	W	W		W	W	W	W
Vadose compaction										
Burial compaction		W	W	W	W	W		W	W	
Microspar cement										
Micrite envelope			W					W		
Grain boring ( marine)										
Microfacies	BR-1	BR-1	BR-1	BR-1	SR-5	SR-4	BR-2	SR-4	BR-1	BR-2
<div><div><div>Grain percentage:</div><div>E = &lt; 1 % D =1-20% C =21- 40 % B =41- 60 % A = &gt; 61%</div></div><div><div>With this feature = W</div></div><div><div>Texture:</div><div>Ms = Mudstone Ws = Wackestone Ps = Packstone Gs = Grainstone Fs = Floatstone Rs = Rudstone Cx = Crystalline carbonate</div></div><div><div>Matrrix =</div><div>Micrite</div></div></div>										



	Well R-50								
Sample number	5	4	3	2	1	..			
Sample depth ( ft )	6505	6499	6490	6481	6475				
Sample depth ( m )	1982	1981	1979	1975	1973				
Texture	Ms	Ms	Ps	Ps	Ms				
Non-Skeletal Grains									
Peloids									
Ooids									
Aggregate									
Quartz/silt	D		D	D	D				
Phosphatic	E								
Black grains	E	E	D	D					
Skeletal Grains									
Corals									
Bivalves	E	E	E	E	E				
Gastropods									
Brachiopods			E						
Crinoids	D	E	D	D	E				
Ostracods	E	E	E	E	E				
Calpionellids									
Sponge spicules									
Green Algae					E				
Forams	E		E						
Radiolarians									
CEMENT:									
Saddle dolomite									
Bladed / granular calcite									
Granular drusy calcite	W		W	W	W				
Syntaxial calcite									
Poikilotopic calcite									
Columnar calcite									
Porosity:	1%	0%	0%	0%	0%	.			
Interparticle									
Vug	W								
Mouldic									
Intraparticle									
Fracture	W								
Intercrystal									
Rootlet									
Stylolitic									
Burrow									
Sedimentary structures									
Rootlets									
Burrows / Bioturbation					W				
Cross lamination									
Diagenesis									
Saddle dol. replacement									
Micro-euhedral dol. cx.	W	W			W				
Dedolomitization									
Limonite / goethite									
Pyrite	W	W	W	W	W				
Vadose compaction									
Burial compaction									
Microspar cement									
Micrite envelope									
Grain boring ( marine)									
Microfacies	BR-1	BR-1	SR-5	SR-5	BR-2				
<div>Grain percentage: E = &lt; 1 % D = 1-20% C = 21- 40 % B = 41- 60 % A = &gt; 61%  Matrix = Micrite</div> <div>With this feature = W</div> <div>Texture: Ms = Mudstone Ws = Wackestone Ps = Packstone Gs = Grainstone Fs = Floatstone Rs = Rudstone Cx = Crystalline carbonate</div>									



## Well R-48





	Well R-48									
Sample number	1	2	3	4	5	6	7	8	9	10
Sample depth ( ft )	6792	6789	6785	6780	6775	6765	6760	6755	6751	6747
Sample depth ( m )	2070	2069	2068	2067	2065	2062	2060	2059	2058	2056
Texture	Ws	Ws	Ws	Ms	Ws	Ws	Ws	Ws	Ws	Ws
<b>Non-Skeletal Grains</b>										
Peloids										
Ooids										
Aggregate										
Quartz/silt		E	D	E	E	E		E	E	E
Phosphatic		E					E	E	E	E
Black grains		D	D	E	E	D		E	E	D
<b>Skeletal Grains</b>										
Corals								E		
Bivalves	D	D	E	D	D	D	D		D	E
Gastropods					E	E				
Brachiopods	D	D		E	D		D	D	D	D
Crinoids	D	D	D	D	D	D	D	D	D	D
Ostracods	E	E	E	E	E			E	E	E
Calpionellids										
Sponge spicules						E		D		E
Green Algae										
Forams	D			E		E		E	E	E
Radiolarians										
<b>CEMENT:</b>										
Saddle dolomite	W		W			W	W	W		
Bladed / granular calcite						W				
Granular drusy calcite	W	W	W	W	W	W	W	W	W	W
Syntaxial calcite										
Poikilotopic calcite										
Columnar calcite		W		W	W	W				
<b>Porosity:</b>	<b>20%</b>	<b>3%</b>	<b>1%</b>	<b>2%</b>	<b>2%</b>	<b>5%</b>	<b>16%</b>	<b>20%</b>	<b>8%</b>	<b>3%</b>
Interparticle						W				
Vug	W				W	W	W	W	W	W
Mouldic					W	W	W	W	W	
Intraparticle										
Fracture					W	W	W		W	
Intercrystal										
Rootlet	W									
Stylolitic		W	W	W	W		W		W	W
Burrow										
<b>Sedimentary structures</b>										
Rootlets	W									
Burrows / Bioturbation					W	W				
Cross lamination										
<b>Diagenesis</b>										
Saddle dol. replacement										
Micro-euhedral dol. cx.					W		W		W	W
Dedolomitization										
Limonite / goethite										
Pyrite	W	W	W	W	W	W	W	W	W	W
Vadose compaction										
Burial compaction			W	W						
Microspar cement	W	W		W						
Micrite envelope										
Grain boring ( marine)										
Microfacies	DiagCal	BR-1	BR-1	BR-1	BR-1	BR-1	DR-3	BR-1	BR-1	BR-1
<p><b>Grain percentage:</b> E = &lt; 1 %      <b>With this feature = W</b>      <b>Texture:</b> Ms = Mudstone  D = 1-20%      Ws = Wackestone  C = 21- 40 %      Ps = Packstone  B = 41- 60 %      Gs = Grainstone  A = &gt; 61%      Fs = Floatstone  Rs = Rudstone  Cx = Crystalline carbonate</p> <p><b>Matrix =</b> Micrite</p>										



	Well R-48									
Sample number	11	13	14	15	16	17	18	19	20	
Sample depth ( ft )	6743	6729	6725	6722	6709	6699	6695	6691	6684	
Sample depth ( m )	2055	2051	2050	2049	2045	2042	2041	2039	2037	
Texture	Ws	Ws	Ws	Ws	Ms	Ws	Ms	Ws	Ms	
Non-Skeletal Grains										
Peloids						E		D		
Ooids										
Aggregate										
Quartz/silt	E	E	E	E	E	E	E	E	E	
Phosphatic	E									
Black grains	E	E	E	E	E	E	E	E	E	
Skeletal Grains										
Corals										
Bivalves	E	E	E	E			E		E	
Gastropods										
Brachiopods	E	D	D			E		E		
Crinoids	D	D	D	D	D	D	D	D	D	
Ostracods	E	E	E	E	E	E	E		E	
Calpionellids										
Sponge spicules	E			E			E			
Green Algae	D	E	E							
Forams	E			E		E		E		
Radiolarians										
CEMENT:										
Saddle dolomite			W					W		
Bladed / granular calcite										
Granular drusy calcite	W	W	W	W	W	W	W	W	W	
Syntaxial calcite										
Poikilotopic calcite										
Columnar calcite										
Porosity:	2%	2%	2%	1%	1%	7%	10%	3%	3%	
Interparticle										
Vug	W	W	W	W	W	W		W		
Mouldic						W		W		
Intraparticle										
Fracture	W		W	W	W		W	W	W	
Intercrystal										
Rootlet										
Stylolitic		W								
Burrow										
Sedimentary structures										
Rootlets										
Burrows / Bioturbation				W			W		W	
Cross lamination										
Diagenesis										
Saddle dol. replacement										
Micro-euhedral dol. cx.		W			W				W	
Dedolomitization										
Limonite / goethite										
Pyrite	W	W	W	W	W	W	W	W	W	
Vadose compaction										
Burial compaction		W		W						
Microspar cement										
Micrite envelope										
Grain boring ( marine)										
Microfacies	BR-1	BR-1	BR-1	BR-1	BR-1	BR-1	BR-1	BR-1	BR-1	BR-1
<div><div>Grain percentage: E = &lt; 1 % D =1-20% C =21- 40 % B =41- 60 % A = &gt; 61%</div><div>With this feature = W</div><div>Texture: Ms = Mudstone Ws = Wackestone Ps = Packstone Gs = Grainstone Fs = Floatstone Rs = Rudstone Cx = Crystalline carbonate</div></div> <div>Matrrix = Micrite</div>										



	Well R-48									
Sample number	21	22	23	24	25	26	27	28	29	30
Sample depth ( ft )	6678	6675	6674	6670	6665	6660	6651	6640	6636	6632
Sample depth ( m )	2036	2035	2034	2033	2031	2030	2027	2024	2023	2021
Texture	Ws	Ms	Ws	Ms	Ms	ws	Ms	Ms	Ms	Ms
<b>Non-Skeletal Grains</b>										
Peloids										
Ooids										
Aggregate										
Quartz/silt	E	E	E	E	E	E	E	E	E	E
Phosphatic			E					E		
Black grains	D	D	D		E	E	E	E	E	E
<b>Skeletal Grains</b>										
Corals										
Bivalves	E			D			E			
Gastropods									E	
Brachiopods	E		E	D	E	D				E
Crinoids	D	D	D	D	D	D	D	D	D	D
Ostracods	E	E			E		E		E	E
Calpionellids		E		E			E			
Sponge spicules					E				E	
Green Algae		E				E	E	E	E	
Forams		E	E	E	E			E	E	E
Radiolarians		E		E						
<b>CEMENT:</b>										
Saddle dolomite										
Bladed / granular calcite										
Granular drusy calcite	W	W	W	W	W	W	W	W	W	W
Syntaxial calcite										
Poikilotopic calcite										
Columnar calcite										
<b>Porosity:</b>	<b>2%</b>	<b>7%</b>	<b>1%</b>	<b>3%</b>	<b>1%</b>	<b>1%</b>	<b>10%</b>	<b>1%</b>	<b>2%</b>	<b>0%</b>
Interparticle										
Vug		W		W		W	W			
Mouldic										
Intraparticle										
Fracture	W	W	W	W	W	W	W	W	W	
Intercrystal										
Rootlet										
Stylolitic										
Burrow										
<b>Sedimentary structures</b>										
Rootlets										
Burrows / Bioturbation	W	W	W				W	W		W
Cross lamination										
<b>Diagenesis</b>										
Saddle dol. replacement										
Micro-euhedral dol. cx.										
Dedolomitization										
Limonite / goethite										
Pyrite	W	W	W	W	W	W	W	W	W	W
Vadose compaction										
Burial compaction				W	W					
Microspar cement										
Micrite envelope										
Grain boring ( marine)										
Microfacies	BR-1	BR-1	BR-1	DR-2	BR-1	BR-1	BR-1	BR-1	BR-1	BR-1
<p><b>Grain percentage:</b> E = &lt; 1 % D = 1-20% C = 21- 40 % B = 41- 60 % A = &gt; 61%</p> <p><b>With this feature = W</b></p> <p><b>Texture:</b> Ms = Mudstone Ws = Wackestone Ps = Packstone Gs = Grainstone Fs = Floatstone Rs = Rudstone Cx = Crystalline carbonate</p> <p><b>Matrix =</b> Micrite</p>										



Well R-48										
Sample number	31	32	33	34	35	36	37	38.	39	40
Sample depth ( ft )	6628	6624	6620	6614	6609	6604	6599	6595	6587	6584
Sample depth ( m )	2020	2029	2018	2016	2014	2013	2011	2010	2008	2006
Texture	Ms	Ms	Ms	Ms	Ws	Ms	Ms	Ws	Ms	Ws
Non-Skeletal Grains										
Peloids										
Ooids										
Aggregate										
Quartz/silt	E	E	E	E	E	E	E	E	E	E
Phosphatic						E				E
Black grains	E	E	D	D			E	E	D	
Skeletal Grains										
Corals					D			E		E
Bivalves	E	E					E		E	
Gastropods										
Brachiopods	E	E	E	E	E	E	E	E	E	D
Crinoids	D	D	D	D		D	D	D	D	D
Ostracods	E	E	E	E			E		E	
Calpionellids		E	E					E		
Sponge spicules					E					
Green Algae					D	D	E	D		D
Forams										
Radiolarians										
CEMENT:										
Saddle dolomite										
Bladed / granular calcite										
Granular drusy calcite	W	W	W	W	W	W	W	W	W	W
Syntaxial calcite										
Poikilotopic calcite										
Columnar calcite										
Porosity:	1%	1%	1%	2%	1%	1%	2%	2%	1%	2%
Interparticle										
Vug		W				W				
Mouldic										
Intraparticle										
Fracture	W	W	W	W	W		W	W	W	W
Intercrystal										
Rootlet										
Stylolitic			W	W	W	W	W	W	W	W
Burrow										
Sedimentary structures										
Rootlets										
Burrows / Bioturbation	W	W	W						W	W
Cross lamination										
Diagenesis										
Saddle dol. replacement										
Micro-euhedral dol. cx.	W									
Dedolomitization										
Limonite / goethite										
Pyrite	W	W	W	W	W	W	W	W	W	W
Vadose compaction										
Burial compaction	W	W	W	W	W		W			
Microspar cement										
Micrite envelope										
Grain boring ( marine)										
Microfacies	BR-1	BR-1	BR-1	BR-1	DR-3	DR-2	BR-1	BR-1	BR-1	DR-3
<div>Grain percentage: E = &lt; 1 % D =1-20% C =21- 40 % B =41- 60 % A = &gt; 61%  Matrix = Micrite</div> <div>With this feature = W</div> <div>Texture: Ms = Mudstone Ws = Wackestone Ps = Packstone Gs = Grainstone Fs = Floatstone Rs = Rudstone Cx = Crystalline carbonate</div>										

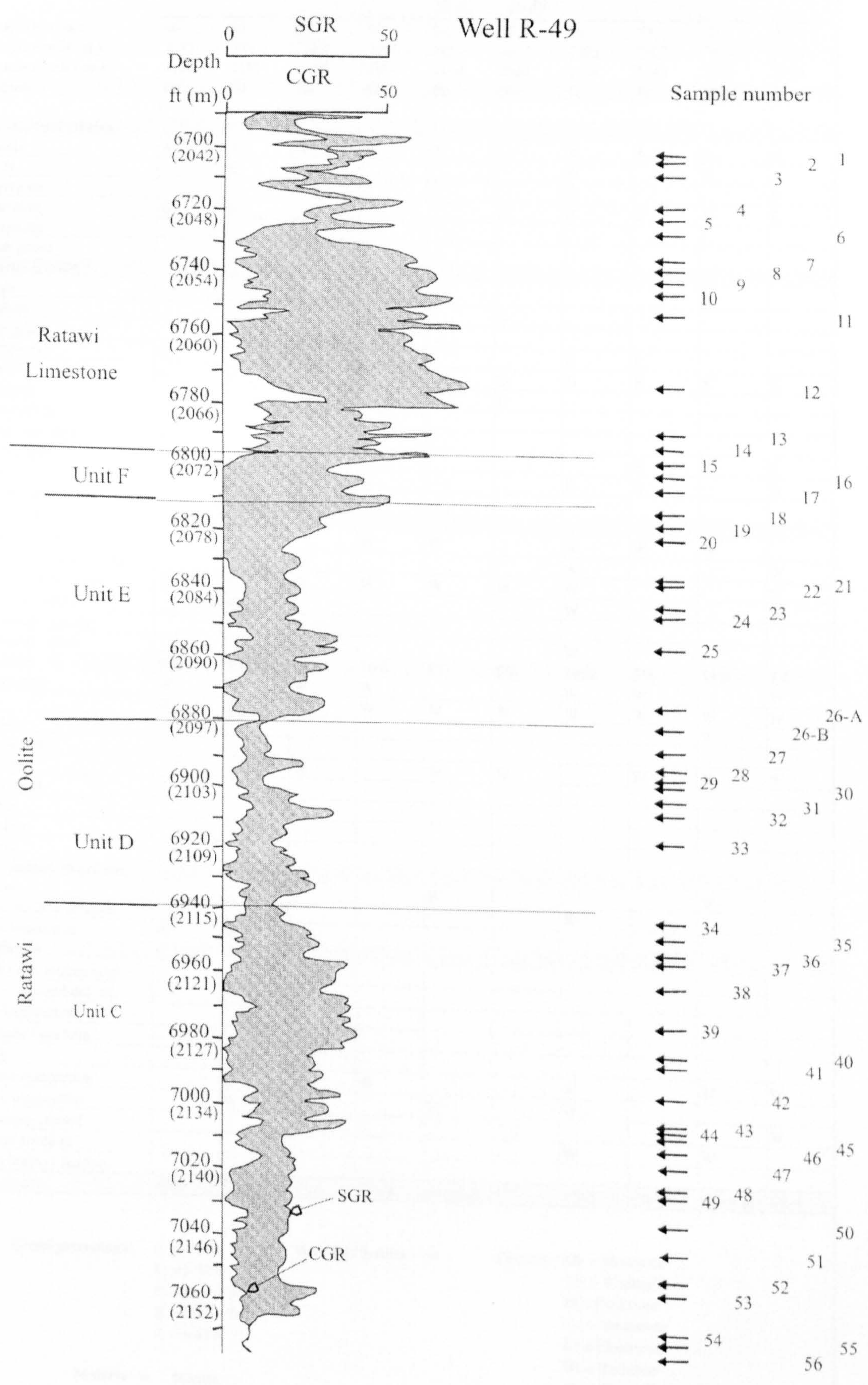


Well R-48										
Sample number	41	42	43	44	45	46	47	48	49	50
Sample depth ( ft )	6582	6579	6575	6572	6564	6561	6556	6550	6545	6542
Sample depth ( m )	2006	2005	2004	2003	2001	2000	1998	1996	1995	1994
Texture	Ps	Ws	Ws	Ws	Ws	Ms	Ws	Ws	Ws	Ws
<b>Non-Skeletal Grains</b>										
Peloids	A									
Ooids										
Aggregate										
Quartz/silt	E	E	E	E		E	E	E	E	E
Phosphatic		E	E					E		E
Black grains	E		E		E	D	D	E	E	
<b>Skeletal Grains</b>										
Corals			E							
Bivalves				E		E				
Gastropods					E					
Brachiopods	D	E	E	D	E		E	D	D	D
Crinoids	D	D	D	D	D	D	D	D	D	D
Ostracods		E	E	E		E	E		E	
Calpionellids										
Sponge spicules		D								
Green Algae			D	D	D	E	D	D	D	D
Forams	E	D	E		E		E		E	E
Radiolarians										
<b>CEMENT:</b>										
Saddle dolomite										
Bladed / granular calcite										
Granular drusy calcite	W	W	W	W	W	W	W	W	W	W
Syntaxial calcite										
Poikilotopic calcite										
Columnar calcite										
<b>Porosity:</b>	<b>1%</b>	<b>3%</b>	<b>2%</b>	<b>1%</b>	<b>2%</b>	<b>7%</b>	<b>3%</b>	<b>2%</b>	<b>3%</b>	<b>1%</b>
Interparticle										
Vug		W	W					W	W	W
Mouldic		W								
Intraparticle										
Fracture	W	W		W	W	W	W	W	W	
Intercrystal										
Rootlet										
Stylolitic			W		W	W	W	W	W	
Burrow										
<b>Sedimentary structures</b>										
Rootlets								W	W	
Burrows / Bioturbation										
Cross lamination										
<b>Diagenesis</b>										
Saddle dol. replacement										
Micro-euhedral dol. cx.						W		W	W	
Dedolomitization										
Limonite / goethite										
Pyrite	W	W	W	W	W	W	W	W	W	W
Vadose compaction	W									
Burial compaction	W		W		W	W	W	W	W	W
Microspar cement										
Micrite envelope	W					W				
Grain boring ( marine)										
Microfacies	SR-5	BR-2	BR-1	DR-3	BR-1	BR-1	BR-1	DiagCal	DiagCal	DR-3
<p><b>Grain percentage:</b> E = &lt; 1 %      <b>With this feature = W</b>      <b>Texture:</b> Ms = Mudstone  D = 1-20%      Ws = Wackestone  C = 21- 40 %      Ps = Packstone  B = 41- 60 %      Gs = Grainstone  A = &gt; 61%      Fs = Floatstone  Rs = Rudstone  Cx = Crystalline carbonate</p> <p><b>Matrix =</b> Micrite</p>										



Well R-48									
Sample number	51	52	53	54					
Sample depth ( ft )	6538	6530	6528	6525					
Sample depth ( m )	1993	1991	1990	1989					
Texture	Ws	Ws	Ws	Ws					
Non-Skeletal Grains									
Peloids									
Ooids									
Aggregate									
Quartz/silt	E	E	E	E					
Phosphatic									
Black grains	E	E		E					
Skeletal Grains									
Corals	E		E	D					
Bivalves									
Gastropods			E						
Brachiopods	D	D	D	D					
Crinoids	D	D	D	D					
Ostracods				E					
Calpionellids									
Sponge spicules									
Green Algae	D	D	D	D					
Forams		E							
Radiolarians									
CEMENT:									
Saddle dolomite									
Bladed / granular calcite	W	W	W						
Granular drusy calcite									
Syntaxial calcite									
Poikilotopic calcite									
Columnar calcite									
Porosity:	3%	5%	2%	2%					
Interparticle									
Vug	W	W	W						
Mouldic									
Intraparticle									
Fracture	W		W	W					
Intercrystal	W								
Rootlet									
Stylolitic	W	W	W	W					
Burrow									
Sedimentary structures									
Rootlets		W							
Burrows / Bioturbation									
Cross lamination									
Diagenesis									
Saddle dol. replacement									
Micro-euhedral dol. cx.	W	W	W						
Dedolomitization									
Limonite / goethite									
Pyrite	W	W	W	W					
Vadose compaction									
Burial compaction	W		W						
Microspar cement									
Micrite envelope									
Grain boring ( marine)									
Microfacies	BR-1	DiagCal	DR-3	BR-1					
<div>Grain percentage: E = &lt; 1 % D =1-20% C =21- 40 % B =41- 60 % A = &gt; 61%  Matrix = Micrite</div> <div>With this feature = W</div> <div>Texture: Ms = Mudstone Ws = Wackestone Ps = Packstone Gs = Grainstone Fs = Floatstone Rs = Rudstone Cx = Crystalline carbonate</div>									







Well R-49										
Sample number	56	55	54	53	52	51	50	49	48	47
Sample depth ( ft )	7073	7071	7069	7057	7051	7043	7035	7027	7024	7018
Sample depth ( m )	2156	2155	2154	2151	2149	2147	2144	2142	2141	2139
Texture	Gs	Gs	Gs	Gs	Ps	Ms	Gs	Ws	Ws	Ps
Non-Skeletal Grains										
Peloids	A	A	A	A	A		A	A	A	A
Ooids		E					D		E	
Aggregate							E			E
Quartz/silt	E	E				E	E	E	E	E
Phosphatic										
Black grains										
Skeletal Grains										
Corals									E	
Bivalves						E				
Gastropods										
Brachiopods	E						E	E		
Crinoids	E	D	E	E	D	D	D	E	E	E
Ostracods						E				
Calpionellids										
Sponge spicules	E									
Green Algae								E	E	E
Forams			E	E			E	E		D
Radiolarians										
CEMENT:										
Saddle dolomite				W	W		W	W	W	
Bladed / granular calcite			W				W			W
Granular drusy calcite	W	W	W	W	W	W	W			W
Syntaxial calcite		W					W			W
Poikilotopic calcite										
Columnar calcite							W			
Porosity:	5%	4%	10%	10%	8%	5%	10%	8%	16%	7%
Interparticle	W	W	W	W			W	W		W
Vug	W	W	W	W	W	W	W	W	W	W
Mouldic									W	
Intraparticle										
Fracture			W		W	W		W	W	W
Intercrystal										
Rootlet										
Stylolitic										
Burrow										
Sedimentary structures										
Rootlets					W				W	
Burrows / Bioturbation							W			
Cross lamination	W	W								
Diagenesis										
Saddle dol. replacement										
Micro-euhedral dol. cx.										
Dedolomitization										
Limonite / goethite										
Pyrite										
Vadose compaction		W	W	W			W		W	W
Burial compaction		W	W		W		W			
Microspar cement										W
Micrite envelope							W		W	
Grain boring ( marine)										
Microfacies	SR-2	SR-2	SR-4	SR=4	DiagCal	BR-2	SR-3	SR-4	DiagCal	SR-4
<div>Grain percentage: E = &lt; 1 % D =1-20% C =21- 40 % B =41- 60 % A = &gt; 61%  Matrrix = Micrite</div> <div>With this feature = W</div> <div>Texture: Ms = Mudstone Ws = Wackestone Ps = Packstone Gs = Grainstone Fs = Floatstone Rs = Rudstone Cx = Crystalline carbonate</div>										



Well R-49										
Sample number	46	45	44	43	42	41	40	39	38	37
Sample depth ( ft )	7012	7009	7006	7005	6997	6987	6983	6975	6964	6956
Sample depth ( m )	2137	2136	2135.5	2135	2133	2130	2128	2126	2123	2020
Texture	Ps	Ps	Gs	Gs	Gs	Ps	Ps	Cx	Ps	Ws
<b>Non-Skeletal Grains</b>										
Peloids		A	A	A	A	A	A		A	A
Ooids										
Aggregate		E								
Quartz/silt	E	E		E		E	E			
Phosphatic										E
Black grains										
<b>Skeletal Grains</b>										
Corals							E			
Bivalves						E	E	E	E	E
Gastropods										
Brachiopods	E		E	E	E	E	E			
Crinoids	D	D	D	D	D		D		D	D
Ostracods										E
Calpionellids										
Sponge spicules										
Green Algae		E				E				
Forams		E		E	D	D	D		D	D
Radiolarians										
<b>CEMENT:</b>										
Saddle dolomite	W	W				W	W	W	W	W
Bladed / granular calcite		W	W	W	W	W	W		W	
Granular drusy calcite	W	W	W	W	W	W	W			
Syntaxial calcite		W	W	W	W	W	W			W
Poikilotopic calcite		W								
Columnar calcite										
<b>Porosity:</b>	<b>25%</b>	<b>10%</b>	<b>7%</b>	<b>8%</b>	<b>7%</b>	<b>6%</b>	<b>5%</b>	<b>3%</b>	<b>5%</b>	<b>3%</b>
Interparticle		W		W	W		W		W	
Vug	W	W	W	W	W	W	W	W	W	W
Mouldic										
Intraparticle							W			
Fracture	W	W	W		W	W	W	W		W
Intercrystal								W		
Rootlet		W			W	W				
Stylolitic										
Burrow										
<b>Sedimentary structures</b>										
Rootlets		W			W	W				
Burrows / Bioturbation										
Cross lamination										
<b>Diagenesis</b>										
Saddle dol. replacement								W		
Micro-euhedral dol. cx.										
Dedolomitization										
Limonite / goethite										
Pyrite										
Vadose compaction	W	W	W	W	W	W	W		W	W
Burial compaction				W	W	W	W		W	
Microspar cement										
Micrite envelope			W		W					
Grain boring ( marine)										
Microfacies	SR-4	DiagCal	SR-4	SR-4	DiagCal	DiagCal	SR-4	DiagDol	SR-4	BR-2
<p><b>Grain percentage:</b> E = &lt; 1 %      <b>With this feature = W</b>      <b>Texture:</b> Ms = Mudstone  D = 1-20%      Ws = Wackestone  C = 21- 40 %      Ps = Packstone  B = 41- 60 %      Gs = Grainstone  A = &gt; 61%      Fs = Floatstone  Rs = Rudstone  Cx = Crystalline carbonate</p> <p><b>Matrix =</b> Micrite</p>										



Well R-49										
Sample number	36	35	34	33	32	31	30	29	28	27
Sample depth ( ft )	6953	6949	6943	6917	6908	6904	6899	6897	6893	6889
Sample depth ( m )	2119	2118	2116	2108	2106	2104	2103	2102	2101	2100
Texture	Ws	Ps	Gs	Gs	Gs	Gs	Gs	Gs	Ps	Fs
<b>Non-Skeletal Grains</b>										
Peloids	B	A	A	A	A	A	A	A	A	A
Ooids										
Aggregate				E	E	E	E			
Quartz/silt	E	E								E
Phosphatic						E				
Black grains										
<b>Skeletal Grains</b>										
Corals	E	E	D	E					E	E
Bivalves	E			D	E		E			D
Gastropods										
Brachiopods	E	E				D		E	E	E
Crinoids	D	D	D	D	D	D	D	D	D	D
Ostracods										
Calpionellids										
Sponge spicules		E								
Green Algae										
Forams		E		E	E	E	E	D	D	E
Radiolarians										
<b>CEMENT:</b>										
Saddle dolomite										
Bladed / granular calcite			W	W			W	W		W
Granular drusy calcite			W	W	W		W	W	W	
Syntaxial calcite	W	W	W	W	W	W	W	W	W	
Poikilotopic calcite										
Columnar calcite										
<b>Porosity:</b>	<b>8%</b>	<b>2%</b>	<b>2%</b>	<b>16%</b>	<b>5%</b>	<b>7%</b>	<b>10%</b>	<b>4%</b>	<b>5%</b>	<b>10%</b>
Interparticle				W	W		W	W	W	
Vug	W	W	W	W	W	W	W	W	W	W
Mouldic		W								W
Intraparticle						W		W	W	
Fracture	W	W					W	W		W
Intercrystal				W						
Rootlet							W			
Stylolitic										
Burrow										
<b>Sedimentary structures</b>										
Rootlets	W			W	W		W			
Burrows / Bioturbation									W	
Cross lamination										
<b>Diagenesis</b>										
Saddle dol. replacement										
Micro-euhedral dol. cx.										
Dedolomitization				W	W	W				
Limonite / goethite				W	W	W				
Pyrite										
Vadose compaction			W	W	W	W	W	W	W	W
Burial compaction	W	W	W	W	W	W		W		
Microspar cement										
Micrite envelope	W		W			W		W		
Grain boring ( marine)	W									W
Microfacies	DiagCal	SR-4	SR-4	DiagCal	DiagCal	SR-3	DiagCal	SR-4	Sr-4	DR-1
<p><b>Grain percentage:</b> E = &lt; 1 % D = 1-20% C = 21- 40 % B = 41- 60 % A = &gt; 61%</p> <p><b>With this feature = W</b></p> <p><b>Texture:</b> Ms = Mudstone Ws = Wackestone Ps = Packstone Gs = Grainstone Fs = Floatstone Rs = Rudstone Cx = Crystalline carbonate</p> <p><b>Matrix =</b> Micrite</p>										



Well R-49										
Sample number	26-B	26-A	25	24	23	22	21	20	19	18
Sample depth ( ft )	6881	6875	6857	6847	6844	6837	6835	6822	6818	6814
Sample depth ( m )	2097	2096	2090	2087	2086	2084	2083	2079	2078	2077
Texture	Gs	Gs	Gs	Gs	Ps	Ps	Gs	Gs	Gs	Gs
Non-Skeletal Grains										
Peloids	A	A	A	A	A	A	A	A	A	A
Ooids										
Aggregate	E		E			E	E	E	E	E
Quartz/silt						E		E		
Phosphatic										
Black grains				E	E	E				
Skeletal Grains										
Corals	E			E					E	
Bivalves					D				E	
Gastropods		E								
Brachiopods	D		D		E	D	E	E	E	E
Crinoids	D	D	D	D	D	D	D	D	D	D
Ostracods										
Calpionellids										
Sponge spicules		E		E						
Green Algae										
Forams	D	D	D	D	E	D	D	E	D	D
Radiolarians										
CEMENT:										
Saddle dolomite	W									
Bladed / granular calcite	W	W	W	W	W	W	W		W	W
Granular drusy calcite	W	W	W	W	W					
Syntaxial calcite	W	W	W	W		W	W		W	W
Poikilotopic calcite										
Columnar calcite										
Porosity:	10%	7%	4%	7%	5%	10%	20%	20%	20%	20%
Interparticle	W	W				W	W	W	W	W
Vug	W	W	W	W	W	W	W	W	W	W
Mouldic										
Intraparticle		W		W	W	W				W
Fracture	W			W		W				
Intercrystal										
Rootlet	W	W					W	W	W	W
Stylolitic										
Burrow										
Sedimentary structures										
Rootlets	W	W					W	W	W	W
Burrows / Bioturbation										
Cross lamination										
Diagenesis										
Saddle dol. replacement										
Micro-euhedral dol. cx.										
Dedolomitization							W			
Limonite / goethite										
Pyrite						W			W	
Vadose compaction	W	W	W	W	W	W	W	W	W	W
Burial compaction	W	W	W	W	W			W	W	W
Microspar cement										
Micrite envelope										
Grain boring ( marine)										
Microfacies	DiagCal	DiagCal	SR-3	SR-5	SR-5	SR-5	DiagCal	DiagCal	DiagCal	DiagCal
<div><div><div>Grain percentage:</div><div>E = &lt; 1 % D = 1-20% C = 21- 40 % B = 41- 60 % A = &gt; 61%</div></div><div><div>With this feature = W</div></div><div><div>Texture:</div><div>Ms = Mudstone Ws = Wackestone Ps = Packstone Gs = Grainstone Fs = Floatstone Rs = Rudstone Cx = Crystalline carbonate</div></div><div><div>Matrix =</div><div>Micrite</div></div></div>										



	Well R-49									
Sample number	17	16	15	14	13	12	11	10	9	8
Sample depth ( ft )	6806	6802	6798	6793	6789	6774	6752	6746	6742	6738
Sample depth ( m )	2074	2073	2072	2071	2069	2065	2058	2056	2055	2054
Texture	Gs	Gs	Ws	Ws	Ws	Ws	Ws	Ws	Ws	Ms
Non-Skeletal Grains										
Peloids	A	A	B	B						
Ooids										
Aggregate		E								
Quartz/silt	E	E	E			E	E	E	E	E
Phosphatic		E								
Black grains										
Skeletal Grains										
Corals					E					
Bivalves	E		E	D	E	E		E	E	D
Gastropods						E				
Brachiopods	E	D				E	D	E		D
Crinoids	D	D	D	D	D	D	D	D	D	D
Ostracods			E			E				
Calpionellids										
Sponge spicules							E	E		
Green Algae										
Forams		D	E	D	D	E	E	E	E	E
Radiolarians										
CEMENT:										
Saddle dolomite							W			W
Bladed / granular calcite	W	W								W
Granular drusy calcite				W						
Syntaxial calcite	W	W								
Poikilotopic calcite							W	W	W	
Columnar calcite										
Porosity:	15%	20%	7%	7%	9%	7%	8%	3%	0%	3%
Interparticle	W	W								
Vug	W	W	W	W	W		W	W		W
Mouldic										W
Intraparticle										
Fracture										W
Intercrystal										
Rootlet	W	W								
Stylolitic										
Burrow						W				
Sedimentary structures										
Rootlets	W	W			W			W		
Burrows / Bioturbation						W		W	W	W
Cross lamination										
Diagenesis										
Saddle dol. replacement										
Micro-euhedral dol. cx.										
Dedolomitization										
Limonite / goethite										
Pyrite		W				W		W	W	W
Vadose compaction	W	W	W							
Burial compaction	W	W								
Microspar cement									W	
Micrite envelope										
Grain boring ( marine)										
Microfacies	DiagCal	DiagCal	BR-2	DR-3	DiagCal	BR-1	DR-3	DiagCal	DR-3	DR-2
<div><div><div>Gain percentage:</div><div>E = &lt; 1 % D =1-20% C =21- 40 % B =41- 60 % A = &gt; 61%</div></div><div><div>With this feature = W</div></div><div><div>Texture:</div><div>Ms = Mudstone Ws = Wackestone Ps = Packstone Gs = Grainstone Fs = Floatstone Rs = Rudstone Cx = Crystalline carbonate</div></div><div><div>Matrrix = Micrite</div></div></div>										



Well R-49							
Sample number	7	6	5	4	3	2	1
Sample depth ( ft )	6735	6727	6722	6719	6709	6704	6702
Sample depth ( m )	2053	2050	2049	2048	2045	2043	2042.5
Texture	Ws	Ms	Ms	Ms	Ms	Ms	Ws
Non-Skeletal Grains							
Peloids						E	D
Ooids							
Aggregate							
Quartz/silt	E	E	E	E	E	E	E
Phosphatic			E				
Black grains				E	D		E
Skeletal Grains							
Corals							
Bivalves	E		E		E	E	
Gastropods	E			E			E
Brachiopods	E		E	E		E	E
Crinoids	C	D	D	D	D	D	D
Ostracods	E				E	E	E
Calpionellids							
Sponge spicules	E	E		E			
Green Algae							
Forams	E	E	E	E		E	E
Radiolarians							
CEMENT:							
Saddle dolomite	W	W	W	W	W	W	W
Bladed / granular calcite							
Granular drusy calcite	W	W		W			
Syntaxial calcite							
Poikilotopic calcite							
Columnar calcite							
Porosity:	5%	5%	5%	3%	1%	1%	2%
Interparticle							
Vug	W	W	W	W	W	W	W
Mouldic	W	W	W	W			
Intraparticle							
Fracture	W	W	W	W	W	W	
Intercrystal							
Rootlet							
Stylolitic							
Burrow							
Sedimentary structures							
Rootlets							
Burrows / Bioturbation	W	W		W	W	W	W
Cross lamination							
Diagenesis							
Saddle dol. replacement							
Micro-euhedral dol. cx.	W				W		
Dedolomitization							
Limonite / goethite							
Pyrite		W	W		W	W	
Vadose compaction							
Burial compaction		W		W			
Microspar cement							
Micrite envelope							
Grain boring ( marine)							
Microfacies	BR-2	DR-2	DR-2	BR-1	BR-1	BR-1	BR-1
<div><div><div>Gain percentage:</div><div>E = &lt; 1 % D = 1-20% C = 21- 40 % B = 41- 60 % A = &gt; 61%</div></div><div><div>With this feature = W</div></div><div><div>Texture:</div><div>Ms = Mudstone Ws = Wackestone Ps = Packstone Gs = Grainstone Fs = Floatstone Rs = Rudstone Cx = Crystalline carbonate</div></div><div><div>Matrix = Micrite</div></div></div>							



**Appendix II: Ratawi parasequence data.....300**



## Appendix 2: Ratawi parasequence data

Two basic surface types are identified by this study (Chapters 3 and 4) from core from wells R-50 and R-48 and used to identify 84 parasequences. Cycle number, surface type and its depth (ft & m) and cycle type and its thickness (ft & m) are listed in this appendix. The two basic surface types are:

### (A) Non-Deposition Subaerial

- (1) Karst = K
- (2) Rootlets = Rot
- (3) Horizontal vein = Hor Ven
- (4) Exposure = Exp

### (B) Non-Deposition Submarine

- (1) Hardground = Had
- (2) Firmground = Frm
- (3) Organic shale Lami = Org-Sh
- (4) Grain size change = Grn Size

### These basic surface types define three basic types of parasequence (cycle):

- (1) Transgressive-Regr = T/R-cycle
- (2) Regressive Cycle = R-cycle
- (3) Aggraded Cycle = A-cycle

The depths of the top and the bottom of these parasequences are used in this study to construct Fischer Plots in depth domain (Section 5.3.2) using the method of Day (1997) that includes the calculation of the cumulative deviation from mean thickness (CDMTi) for each parasequence boundary.

$$\text{CDMTi} = (\text{Do} - (i/N) \cdot T) - \text{Di}$$

**i** = cycle number (cycle number one is for the deepest complete cycle)

**Di** = actual depth of the ith cycle top

**Do** = the depth at the top of cycle number zero (the depth of the base of first cycle)

**N** = the number of cycle in the interval

**T** = the total thickness



Core Well R-48				
Cycle Number	Surface Type and Depth (ft & m)		Cycle Type & Thickness (ft & m)	CDMTI
	6520.6 ft	Exp		0.0.
	(1987.5 m)			
64	6530 ft	K & Frm	R-cycle peritidal	9.6 ft (2.92 m)
	(1990.3 m)			-5.16
63	6540 ft	K & Rot	R-cycle peritidal	10 ft (3.05 m)
	(19993.4 m)			-10.93
62	6541.6 ft	Org-Sh	T/R-cycle peritidal	2 ft (0.61 m)
	(1993.9 m)			
	6542 ft	Rot		-8.69
	(1994 m)			
61	6543 ft	Frm & Org-Sh	T/R-cycle peritidal	1.6 ft (0.49 m)
	(1994.3 m)			
		6543.6 ft		-6.06
		(1994.5 m)		
60	6544.6 ft	Frm	A T/R-cycle subtidal	2.6 ft (0.79 m )
	(1994.8 m)			
	6546 ft	K & Rot		-4.22
	(1995.2 m)			
59	6547.6 ft	Frm	T/R-cycle peritidal	2 ft (0.61 m)
	(1995.7 m)			
		6548 ft		-1.99
		(1995.8 m)		
58	6548.6 ft	Frm	A -cycle subtidal	1 ft (0.30 m)
	(1996 m)			
		6549 ft		1.24
		(1996.1 m)		
57	6550 ft	Frm	A-cycle subtidal	3 ft (0.91 m)
	(1996.5 m)			
		6552 ft		2.47
		(1997 m)		
56	6554.6 ft	Frm	A-cycle subtidal	3.6 ft (1.09 m)
	(1997.8 m)			
		6555.6 ft		3.1
		(1998.2 m)		
55	6556.6 ft	Frm	A-cycle subtidal	4 ft (1.22 m)
	(1998.6 m)			
		6559.6 ft		3.34
		(1999.4 m)		
54	6562.6 ft	Hrd	A T/R-cycle subtidal	5 ft (1.52 m)
	(2000.3 m)			
	6564.6 ft	K		2.57
	(2000.9 m)			
53	6567.6 ft	Hrd	T/R-cycle peritidal	3.6 ft (1.97 m)
	(2002.1 m)			
		6568 ft		3.41
		(2001.9 m)		
52	6568.6 ft	Frm	A-cycle subtidal	1 ft (0.30 m)
	(2002.1 m)			
		6569 ft		6.64
		(2002.2 m)		
51	6569.6 ft	Frm	A-cycle subtidal	1.6 ft (0.49 m)
	(2002.4 m)			
		6570.6 ft		9.28
		(2002.7 m)		
50	6571.6 ft	Frm	A-cycle subtidal	2 ft (0.61 m)
	(2003 m)			
		6572.6 ft		11.51
		(2003.3 m)		
49	6574 ft	Hrd	A T/R-cycle subtidal	7 ft (2.13 m)
	(2003.7 m)			
	6579.6 ft	Rot		8.75
	(2005.5 m)			



Core Well R-48				
Cycle Number	Surface Type and Depth (ft & m)		Cycle Type & Thickness (ft & m)	CDMTI
	6572.6 ft (2003.3 m)			11.51
49	6574 ft Hrd (2003.7 m)	A T/R-cycle subtidal	7 ft (2.13 m)	8.75
	6579.6 ft Rot (2005.5 m)			
48	6581.6 ft Frm (2006 m)	T/R-cycle peritidal	3.6 ft (1.10 m )	9.58
	6583 ft (2006.5 m)			
47	6584.6 ft Hrd (2007 m)	A-cycle subtidal	3.6 ft (1.10 m )	10.21
	6586.6 ft (2007.6 m)			
46	6588.6 ft Org- Sh (2008.2 m)	A-cycle subtidal	3 ft (0.91 m)	11.45
	6589.6 ft (2008.5 m)			
45	6590.6 ft Hrd (2008.8 m)	A-cycle subtidal	4 ft (1.22 m)	11.68
	6593.6 ft (2009.7 m)			
44	6596.6 ft Frm & Rot (2010.6 m)	R-cycle subtidal	3 ft (0.91 m)	12.92
43	6597.6 ft Hrd (2010.9 m)	T/R-cycle peritidal	2 ft (.61 m)	15.15
	6598.6 ft (2011.3 m)			
42	6599 ft Hrd (2011.4 m)	A T/R-cycle subtidal	3 ft (0.91 m)	16.39
	6601.6 ft Rot			
41	6602.6 ft Hrd (2012.5 m)	T/R-cycle peritidal	4.6 ft (1.4 m)	16.22
	6606 ft K (2013.5 m)			
40	6609.6 ft K	R T/R-cycle peritidal	3.6 ft (1.10 m )	16.85
39	6611.6 ft Frm (2015.2 m)	T/R-cycle peritidal	3 ft (0.91 m)	18.09
	6612.6 ft (2015.5 m)			
38	6613.6 ft K & Org Sh 2015.9 m)	R-cycle subtidal	1 ft (0.30 m)	21.32
37	6627.6 ft K & Frm (2020.1 m)	R-cycle peritidal	14 ft (4.27 m)	11.56
36	6628.6 ft Rot (2020.4 m)	R T/R-cycle peritidal	1 ft (0.30 m)	14.79
35	6633 ft K & Rot (2021.7 m)	R T/R-cycle peritidal	4.6 ft (1.40 m)	14.63
34	6661.6 ft Hrd (2030.5 m)	T/R-cycle peritidal	37 ft (11.28 m)	-18.13
	6670 ft Rot (2033 m)			
33	6672.6 ft K	R T/R-cycle peritidal	2.6 ft (0.79 m)	-16.5
32	6673.6 ft Hrd (2034.1 m)	T/R-cycle peritidal	4.6 ft (1.40 m)	-16.66
	6677 ft Grn Size			



Core Well R-48			
Cycle Number	Surface Type and Depth (ft & m)	Cycle Type & Thickness (ft & m)	CDMTi
32	<u>6673.6 ft      Hrd</u> (2034.1 m) <u>6677 ft      Grn Size</u> (2035.1 m)	T/R-cycle peritidal      4.6 ft (1.40 m)	-16.66
31	<u>6680.6 ft      Grn Size</u> (2036.2 m)	R-cycle subtidal      3.6 ft (1.09 m)	-16.03
30	<u>6691.6 ft      Grn Size</u> (2039.6 m)	R-cycle subtidal      11 ft (3.35 m)	-22.79
29	<u>6696.6 ft      Grn Size</u> (2041.1 m)	R-cycle subtidal      5 ft (1.52 m)	-23.56
28	<u>6710 ft      Grn Size</u> (2045.2 m)	R-cycle subtidal      13.6 ft (4.15 m)	-32.27
27	<u>6712 ft      Grn Size</u> (2045.8 m)	R-cycle subtidal      2 ft ( 0.61m)	-30.49
26	<u>6715.6 ft      Grn Size</u> (2047.8 m)	R-cycle subtidal      3.6 ft (1.09 m)	-29.85
25	<u>6718.6 ft      Grn Size</u> (2047.8 m)	R-cycle subtidal      3 ft (0.91 m)	-28.62
24	<u>6722.6 ft      Rot &amp; Hrd</u> (2049 m)	R-cycle subtidal      4 ft (1.22 m)	-28.39
23	<u>6729.6 ft      K</u> (2051.2 m)	<i>R</i> T/R-cycle peritidal      7 ft (2.13 m)	-31.15
22	<u>6732 ft      K</u> (2051.9 m )	<i>R</i> T/R-cycle peritidal      2.6 ft (0.79 m)	-29.32
21	<u>6733 ft      Rot</u> (2052.2 m)	<i>R</i> T/R-cycle peritidal      1 ft (0.30 m)	-26.08
20	<u>6735 ft      K &amp; Rot</u> (2052.8 m)	<i>R</i> T/R-cycle peritidal      2 ft (0.61 m)	-23.85
19	<u>6736 ft      K</u> (2053.1 m)	<i>R</i> T/R-cycle peritidal      1 ft (0.30 m)	-20.61
18	<u>6737 ft      Rot</u> (2053.4 m)	<i>R</i> T/R-cycle peritidal      1 ft (0.30 m)	-17.38
17	<u>6741 ft      Hrd</u> (2054.6 m) <u>6743.6 ft      K</u> (2055.3 m)	T/R-cycle peritidal      6.6 ft (2.01 m)	-19.75
16	<u>6746.6 ft      Hrd</u> (2056.4 m)	T/R-cycle peritidal      4 ft (1.21 m)	-19.5
15	<u>6748.6 ft      Hrd</u> (2057 m) <u>6750 ft      K &amp; Rot</u> (2057.4 m)	<i>P</i> T/R-cycle subtidal      2.6 ft (0.79 m)	-17.68
14	<u>6751.6 ft      Hrd</u> (2057.9 m)	T/R-cycle peritidal      2 ft (0.61 m)	-15.44
13	<u>6752.6 ft      Hrd</u> (2058.2 m)	A-cycle subtidal      5 ft (1.52 m)	-16.21
	<u>6757 ft</u> (2059.5 m)		



Core Well R-48			
Cycle Number	Surface Type and Depth (ft & m)	Cycle Type & Thickness (ft & m)	CDMTI
13	<u>6752.6 ft</u> Hrd (2058.2 m)	A-cycle subtidal      5 ft (1.52 m)	-16.21
	6757 ft (2059.5 m)		
12	<u>6761.6 ft</u> Hrd (2060.9 m)	A-cycle subtidal      5 ft (1.52 m)	-16.97
	6762 ft (2061 m)		
11	<u>6762.6 ft</u> Hrd (2061.2 m)	A-cycle subtidal      1.6 ft (0.49 m)	-14.34
	6763.6 ft (2061.5 m)		
10	<u>6764 ft</u> Hrd (2061.7 m)	A-cycle subtidal      2 ft (0.61 m)	-12.1
	6765.6 ft (2062.2 m)		
9	<u>6766.6 ft</u> Hrd (2062.5 m)	A-cycle subtidal      2 ft (0.61 m)	-9.87
	6767.6 ft (2062.8m)		
8	<u>6768.6 ft</u> Hrd (2063.1m)	A-cycle subtidal      3 ft (0.91 m)	-8.64
	6770.6 ft (2063.7m)		
7	<u>6772.6 ft</u> Frm (2064.3m) 6773.6 ft      K (2064.6 m)	A T/R-cycle subtidal      3 ft (0.91 m)	-7.4
6	6775 ft      Rot (2065 m)	R T/R-cycle peritidal      1.6 ft (0.49 m)	-4.57
5	6778 ft      K & Rot (2065.9 m)	R T/R-cycle peritidal      3 ft (0.91 m)	-3.33
4	<u>6780 ft</u> Hrd (2066.5 m)	T/R-cycle peritidal      4 ft (1.22 m)	-3.1
	6782 ft (2067.2 m)		
3	<u>6783.6 ft</u> Hrd (2067.6 m)	A-cycle subtidal      3 ft (0.91 m)	-1.86
	6785 ft (2068 m)		
2	<u>6786.6 ft</u> Hrd (2068.6 m)	A-cycle subtidal      3.6 ft (1.09 m)	-1.23
	6788.6 ft (2069.2 m)		
1	<u>6790.6 ft</u> Hrd (2069.8 m)	A-cycle subtidal      3 ft (0.91 m)	0
	6791.6 ft (2070.1m)		
0	<u>6792.6 ft</u> Hrd (2070.4 m)		



Core Well R-50			
Cycle Number	Surface Type and Depth (ft & m)	Cycle Type & Thickness (ft & m)	CDMTI
	<u>6776 ft</u> Hrd (2065.3 m)		
		6777.6 ft (2065.8 m)	0
20	<u>6778.6 ft</u> Hrd (2066.1 m)	A-cycle subtidal	3 ft (0.91 m)
		6780.6 ft (2066.7 m)	9.4
19	<u>6782 ft</u> Hrd (2067.2 m)	A T/R-cycle subtidal	4.4 ft (1.34 m)
	6785 ft      K & Frm (2068 m)		17.4
18	6787 ft      Rot & Frm (2068.7 m)	R-cycle peritidal	2 ft (0.61 m)
			27.8
17	<u>6791 ft</u> Frm (2069.3 m)	T/R-cycle peritidal	8 ft (2.44 m)
	<u>6792 ft</u> Org Sh (2069.5 m)		
	<u>6793 ft</u> Org Sh (2069.7 m)		
	<u>6793.6 ft</u> Frm (2069.9 m)		
		6795 ft (2071.1 m)	32.2
16	<u>6796.6 ft</u> Org Sh (2071.6 m)	A-cycle subtidal	3.6 ft (1.09 m)
		6798.6 ft (2072.2 m)	41
15	<u>6800.6 ft</u> Org Sh (2072.6 m)	A-cycle subtidal	27 ft (8.23 m)
		6826 ft (2080.6 m)	26
14	<u>6851 ft</u> Org Sh (2088.2 m)	A-cycle subtidal	26 ft (7.92 m)
		6852 ft (2088.5 m)	12.4
13	<u>6853.6 ft</u> Org Sh (2089 m)	A T/R-cycle subtidal	7 ft (2.13 m)
	6859 ft      Hor Ven (2090.6 m)		17.8
12	6863 ft      Hor Ven (2091.8 m)	R T/R-cycle peritidal	4 ft (1.22 m)
			26.2
11	6887 ft      Hor Ven (2099.2 m)	R T/R-cycle peritidal	24 ft (7.31 m)
			14.6
10	6889.6 ft      Hor Ven & Rot (2100 m)	R T/R-cycle peritidal	2.6 ft (0.79 m)
			24.4
9	6950 ft      K (2118.4 m)	T/R-cycle peritidal	60 ft (18.28 m)
			-23.6
8	6957 ft      Rot (2120.5 m)	R T/R-cycle peritidal	7 ft (2.13 m)
			-18.2
7	6967.6 ft      Hor Ven (2126.2 m)	R T/R-cycle peritidal	10.6 ft (3.23 m)
			-16.4
6	6975.6 ft      Rot & Frm (2126.2 m)	R-cycle peritidal	8 ft (2.44 m)
			-12



Core Well R-50			
Cycle Number	Surface Type and Depth (ft & m)	Cycle Type & Thickness (ft & m)	CDMTI
6	6975.6 ft Rot & Frm (2126.2 m)	R-cycle peritidal 8 ft (2.44 m)	-12
5	6979 ft Rot & Frm (2127.2 m)	R-cycle peritidal 3.6 ft (1.09 m)	-3
4	6988 ft Rot & Frm (2129.9 m)	R-cycle peritidal 9 ft (2.74 m)	0.4
3	6993.6 ft Rot & Frm (2131.6 m)	R-cycle peritidal 5.6 ft (1.71 m)	7.2
2	6999.6 ft Rot & Frm (2133.5 m)	R-cycle peritidal 6 ft (1.82 m)	13.6
1	7007 ft Hrd (2135.7 m)  7025.6 ft Hor Ven (2141.4 m)	T/R-cycle peritidal 26 ft (7.92 m)	0
0	7030 ft Frm (2142.7 m)		

ence data



Appendix 2 B) Ratawi Parasequence Data

Karst	= K
Rootlet	= Rot
Horizontal vein and mudcracks	= Hor Ven
Hardground	= Had
Firmground	= Frm
Organic shale lamina	= Org Sh
Grain size changes	= Grn Size

Fig A.2.1 Log of core R-50 showing depositional texture, core sample number, and microfacies identified in this study (Appendix 1). Also shown are the different surfaces recognized in this study and marked on Core Lab description chart, used in this study to determine the parasequence succession, described in Appendix 2 A and used to construct Fischer Plots (Appendix 3).

Fig A.2.2 Log of core R-48 showing depositional texture, core sample number, and microfacies identified in this study (Appendix 1). Also shown are the different surfaces recognized in this study and marked on Core Lab description chart, used in this study to determine the parasequence succession, described in Appendix 2 A and used to construct Fischer Plots (Appendix 3).

There is no sufficient data to construct log for core R-49

For example of the parasequence in core see Figs A.2.3, A.2.4 and A.2.5.



Core Well R-50

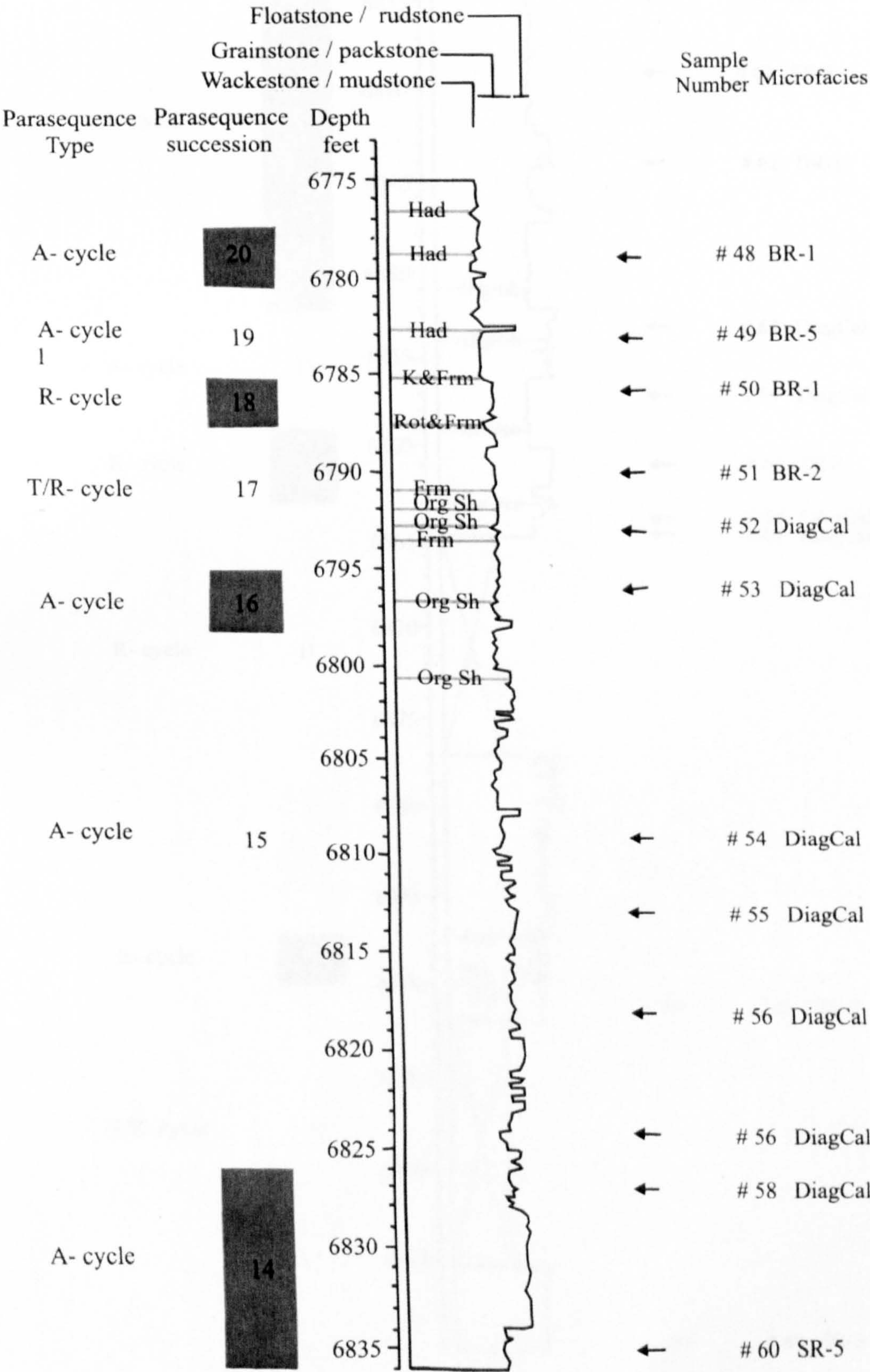


Fig A.2.1



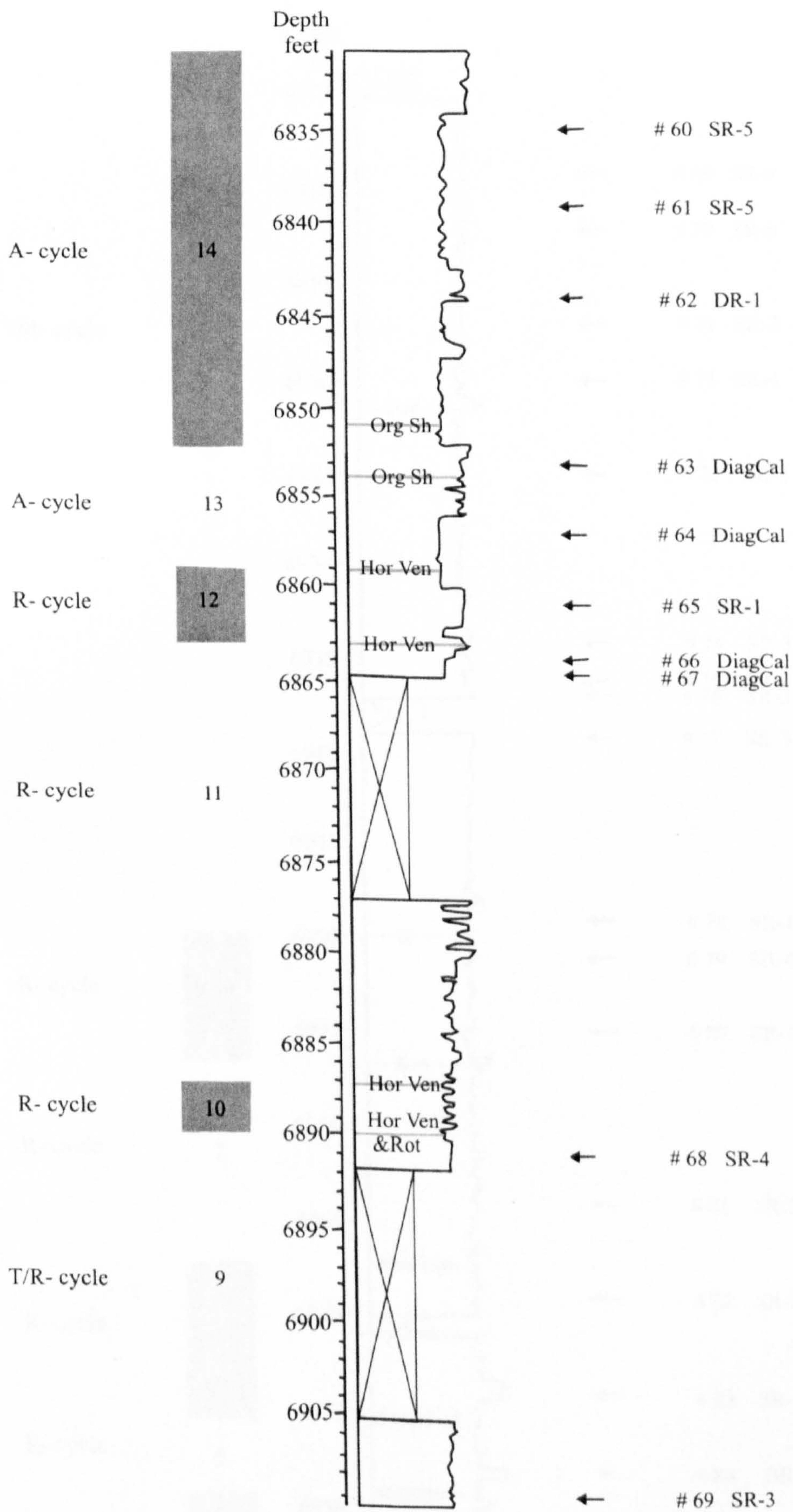


Fig A.2.1 continued



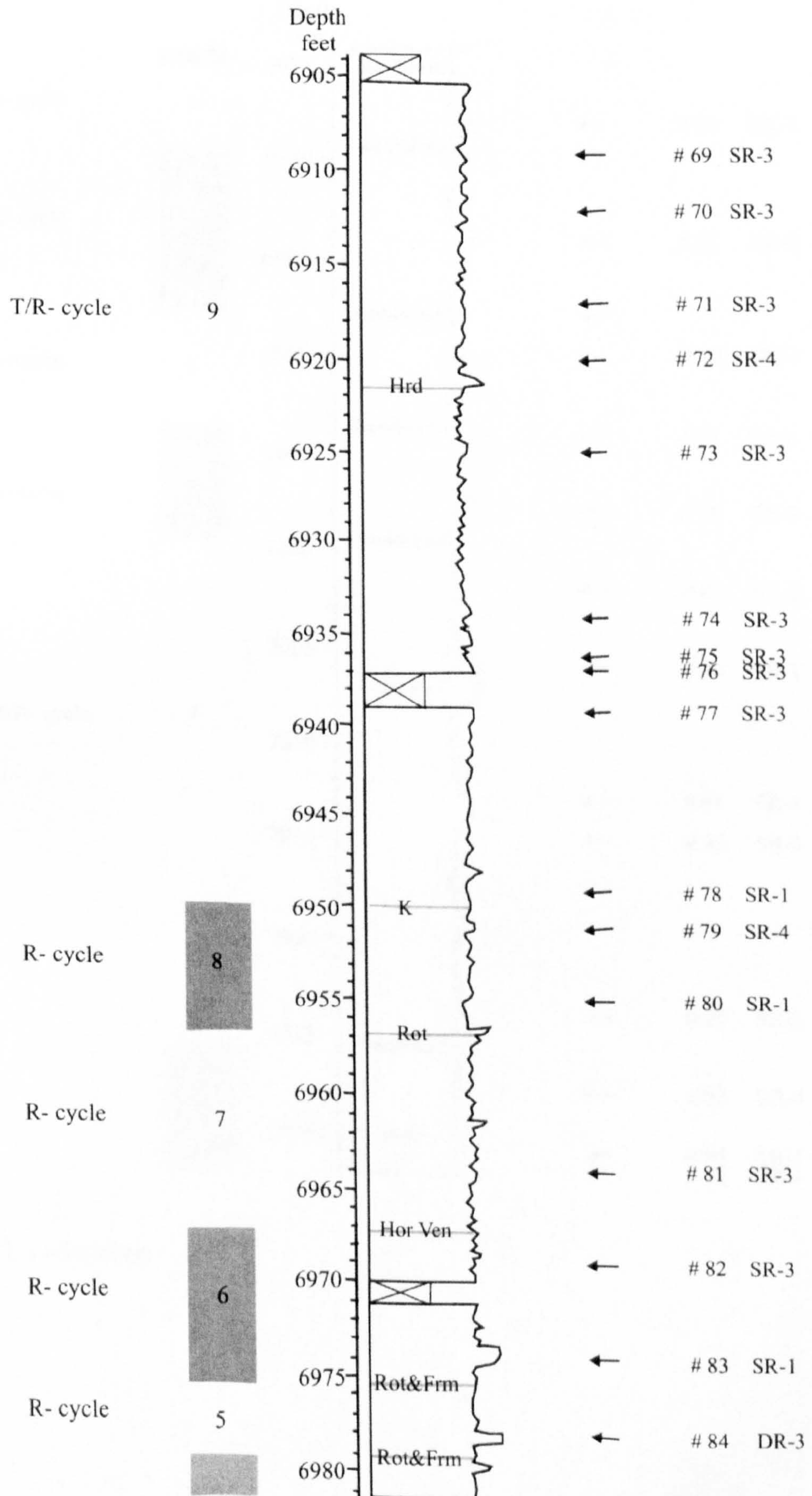


Fig A.2.1 continued



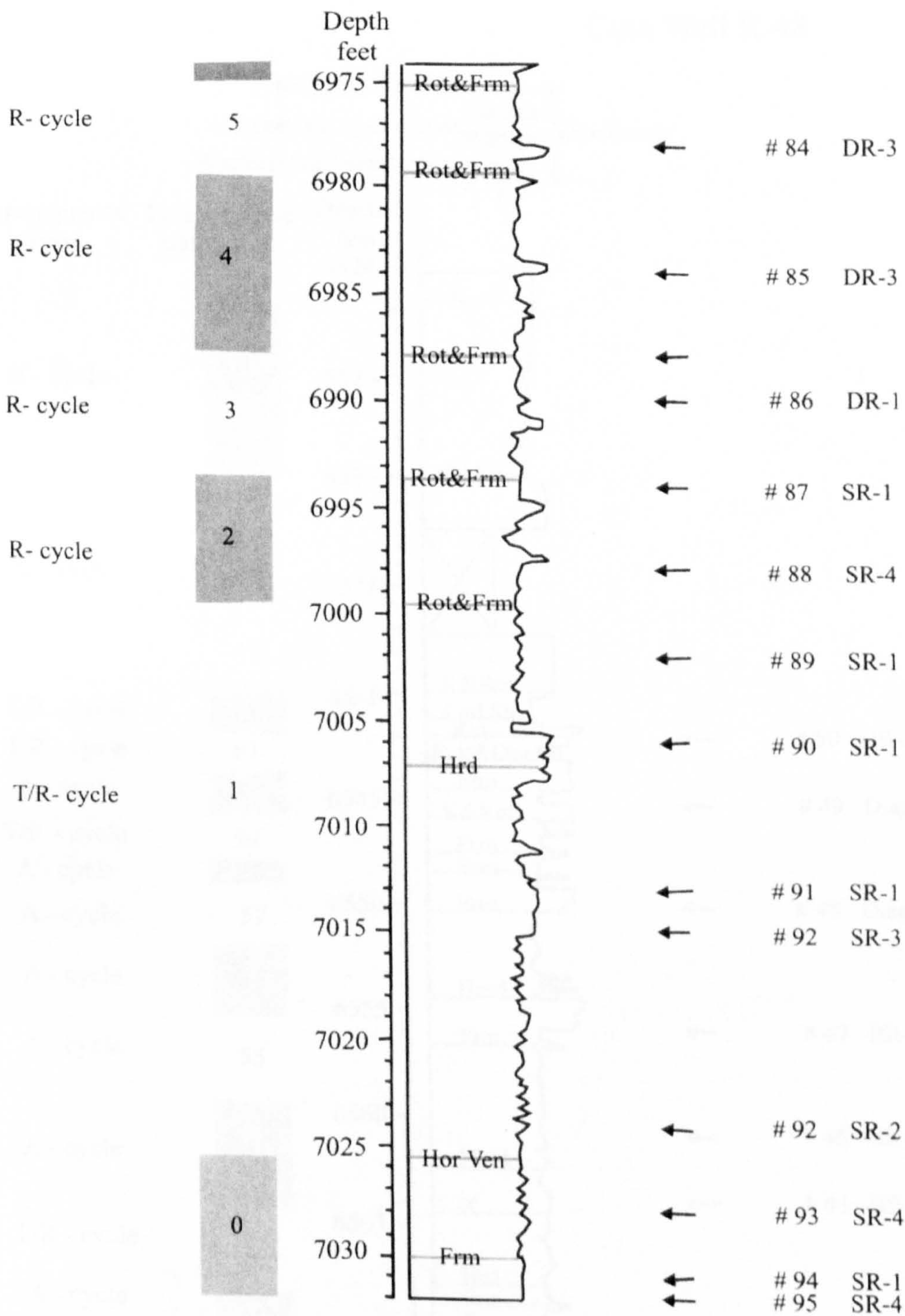


Fig A.2.1 continued



Core Well R-48

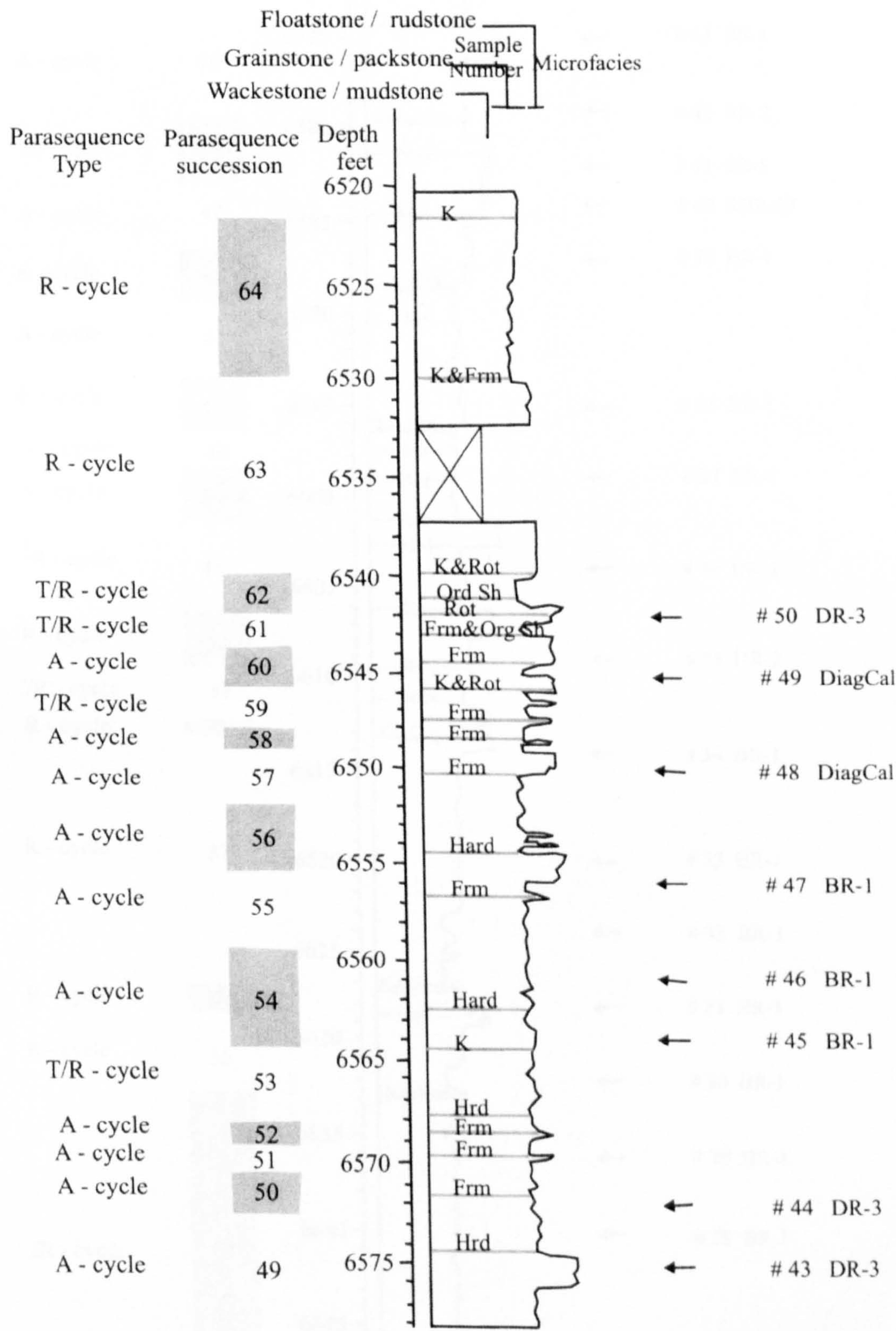


Fig A.2.2



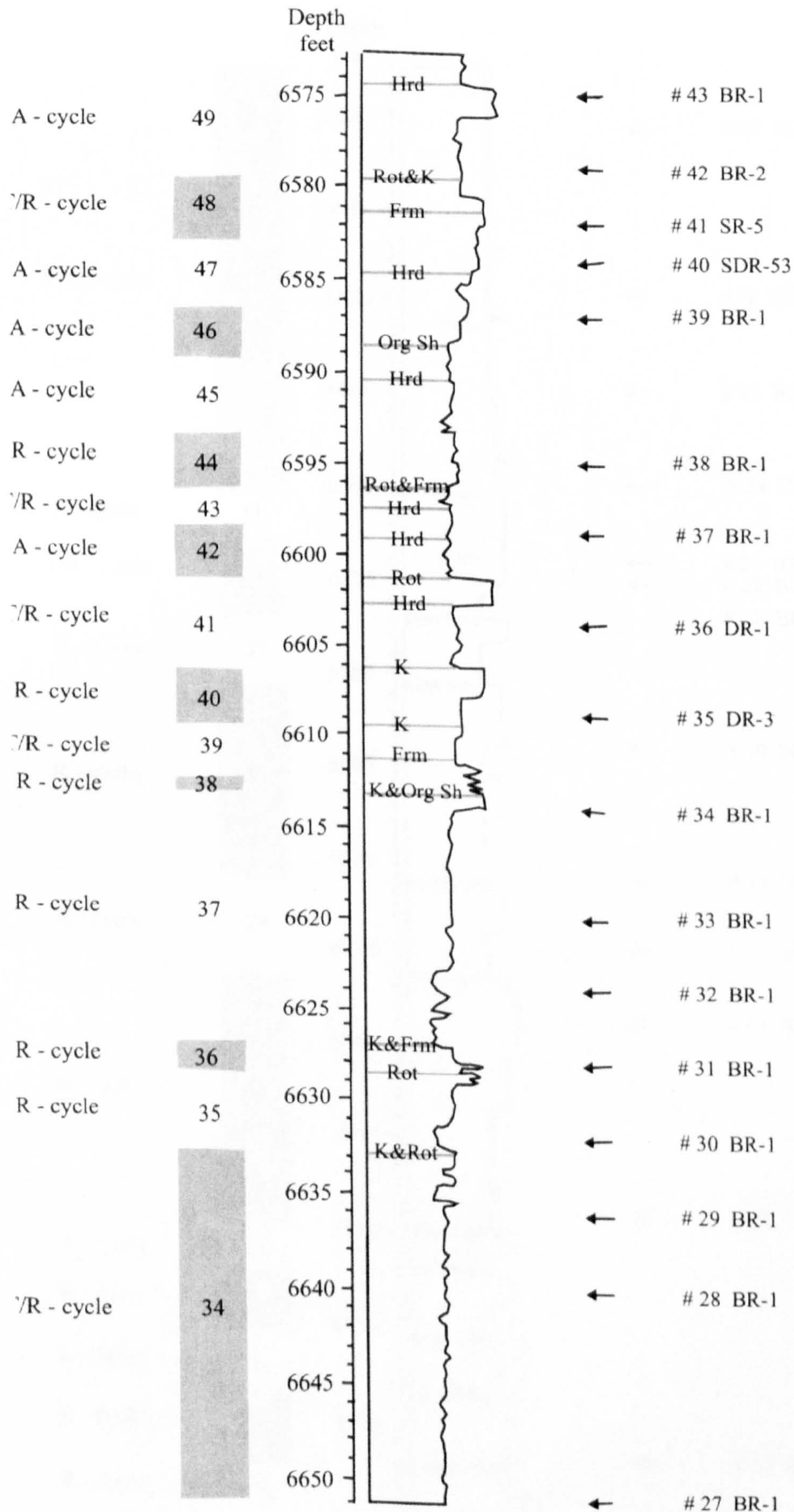


Fig A.2.2 continued



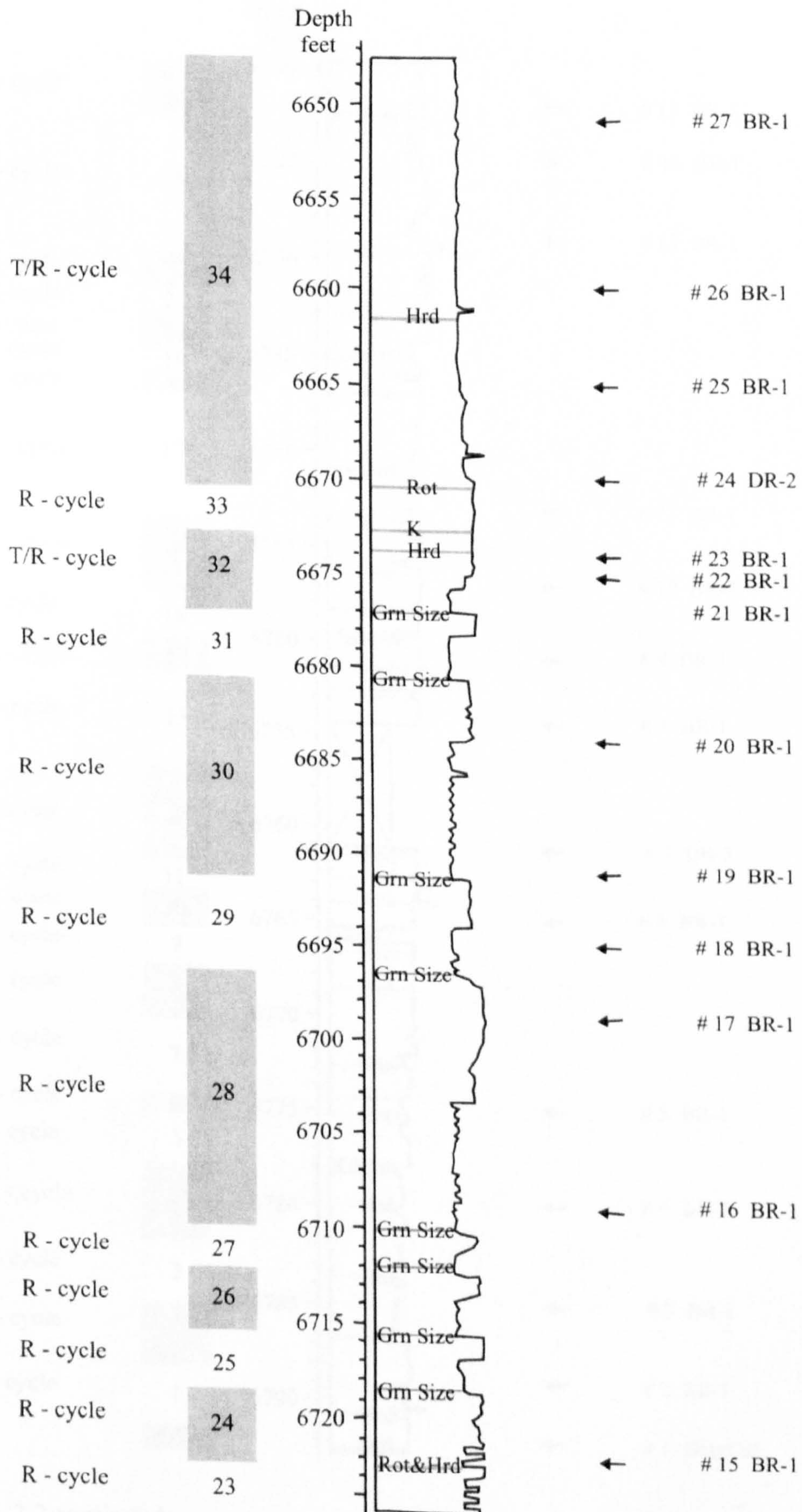


Fig A.2.2 continued



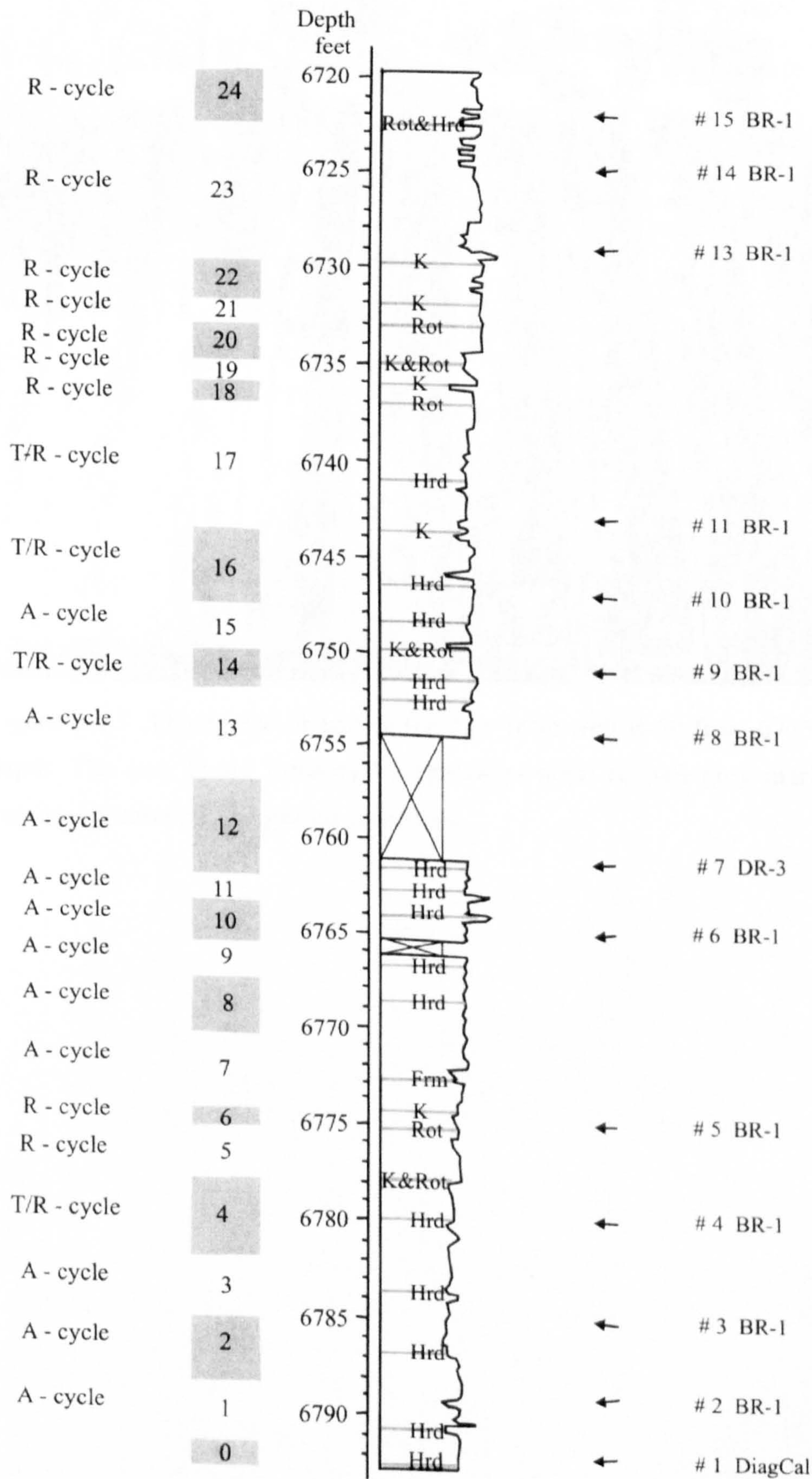


Fig A.2.2 continued





Figure A.2.3 Photograph of part of the core from well R-50 from 6775 to 6805 feet depth. The core shows three cycles (parasequences) of pale-grey marine mudstone passing up into oil impregnated grainstone.

Figure A.2.4 Photograph of core from well R-50, depth 6775 to 6790 feet, showing pale grey fine mudstone at black lamp facies overlying oil impregnated bioclastic mudstone of Foliovermay facies. An exposed surface overprinted by background texture of the mudstone.





Figure A.2.4 Photograph of core from well R-50, depth 6775 to 6790 feet, showing pale grey lime mudstone of back-ramp facies overlying oil impregnated bioclastic grainstone of shallow-ramp facies. An exposure surface overprinted by hardground occurs at the arrows.





Figure A.2.5 Photograph of core from well R-50, depth 7017 to 7032 feet, showing oil impregnated oolitic grainstone of the shallow-ramp facies. A hardground occurs at the arrows.



**Appendix III: Fischer Plots.....307**



## **Appendix 3: Fischer Plots**

Fischer plots were constructed for strata in wells R-48 and R-50 in two domains (Chapter 5:

1. Time domain, in which the cumulative departure from mean parasequence thickness is plotted against cycle number. Excel was used to compute the cumulative deviation from mean thickness (CDMT), the location of different points on the curve, and to draw the plots.
2. Depth domain, in which the cumulative departure from mean parasequence thickness is plotted against cycle depth in the well. This study used the procedure of Day (1997) to compute the CDMT in Appendix 2, whereas the plots are drawn by hand and compared with spectroscopy, computed, 'total' gamma ray, bulk density and neutron porosity logs in addition to reservoir zones.



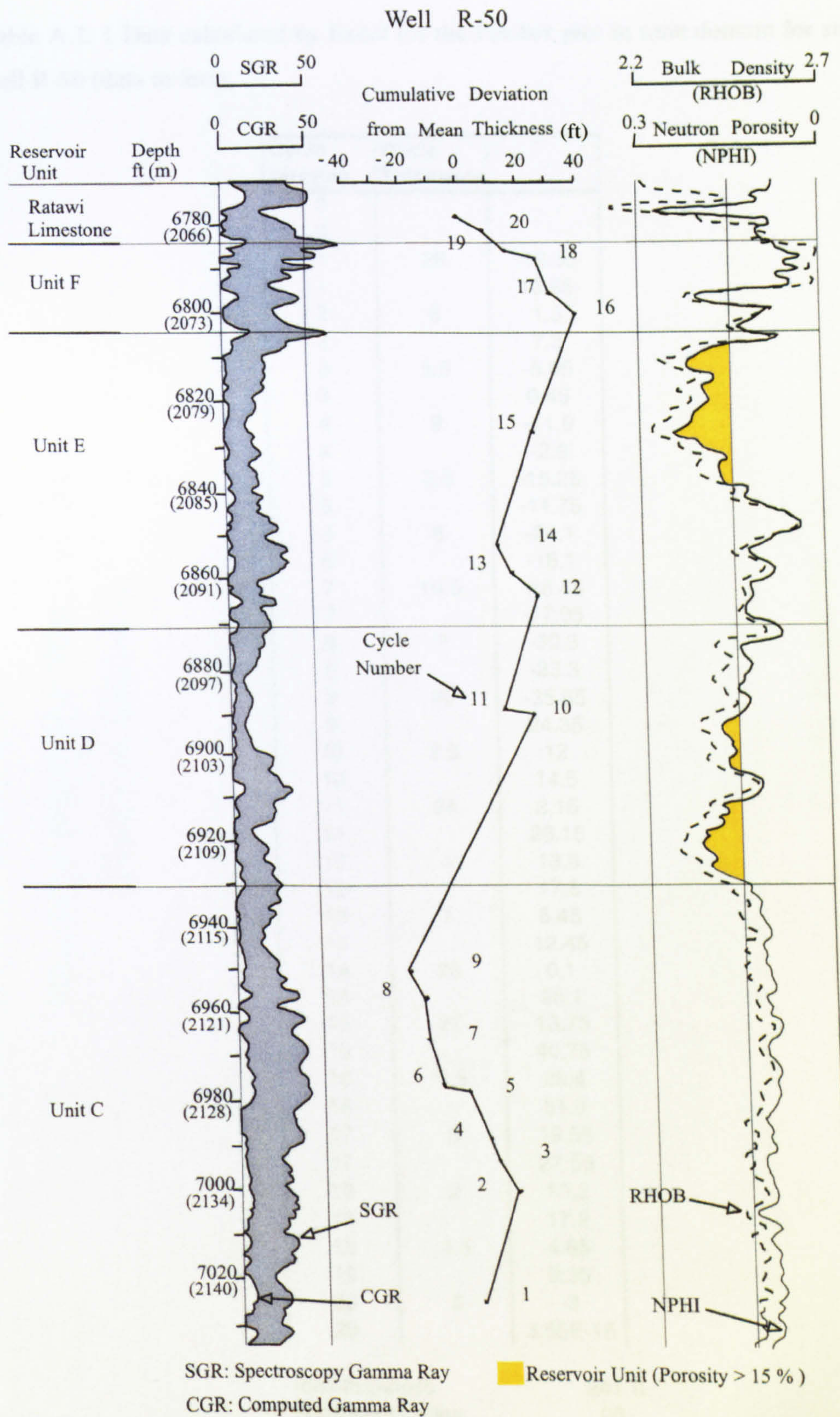


Figure A.3.1 Fischer plot in depth domain for strata in well R-50 compared with log signatures and location of reservoir and non-reservoir units.



Table A.3. 1 Data calculated by Excel for the Fischer plot in time domain for strata in well R-50 (data in feet).

Cycle Number	Cycle Thickness	
0		
0		
1	26	-12.35
1		13.65
2	6	1.3
2		7.3
3	5.5	-5.05
3		0.45
4	9	-11.9
4		-2.9
5	3.5	-15.25
5		-11.75
6	8	-24.1
6		-16.1
7	10.5	-28.45
7		-17.95
8	7	-30.3
8		-23.3
9	60	-35.65
9		24.35
10	2.5	12
10		14.5
11	24	2.15
11		26.15
12	4	13.8
12		17.8
13	7	5.45
13		12.45
14	26	0.1
14		26.1
15	27	13.75
15		40.75
16	3.5	28.4
16		31.9
17	8	19.55
17		27.55
18	2	15.2
18		17.2
19	4.5	4.85
19		9.35
20	3	-3
20		3.55E-15

total thickness 247 ft  
number of cycles 20  
average thickness 12.35 ft

Figure A.3. 1 Fischer plots in time domain for strata in well R-50.



Fischer Plot for Well R-50  
(Ratawi Oolite)

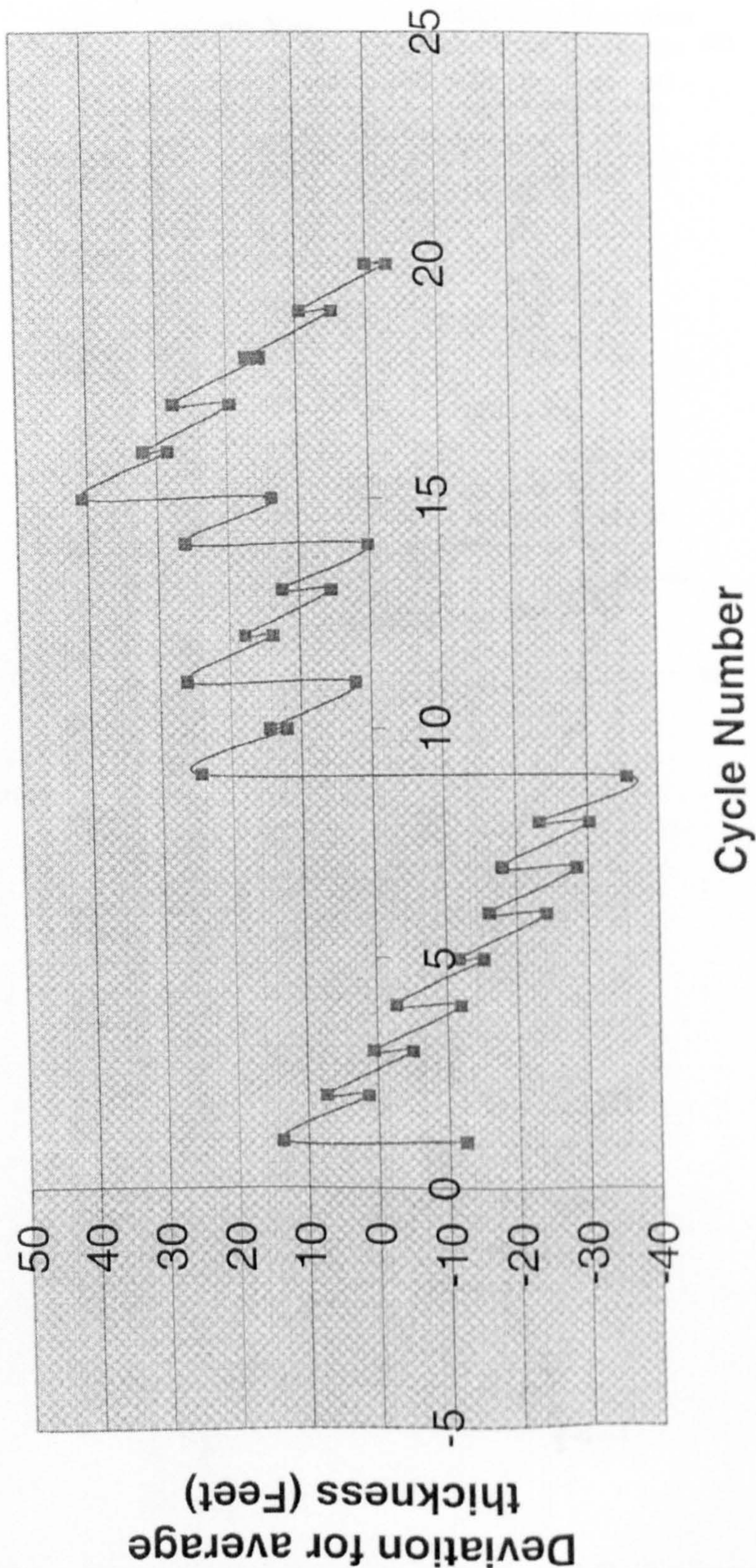


Figure A.3. 2 Fischer plots in time domain for strata in well R-50.



Well R-48

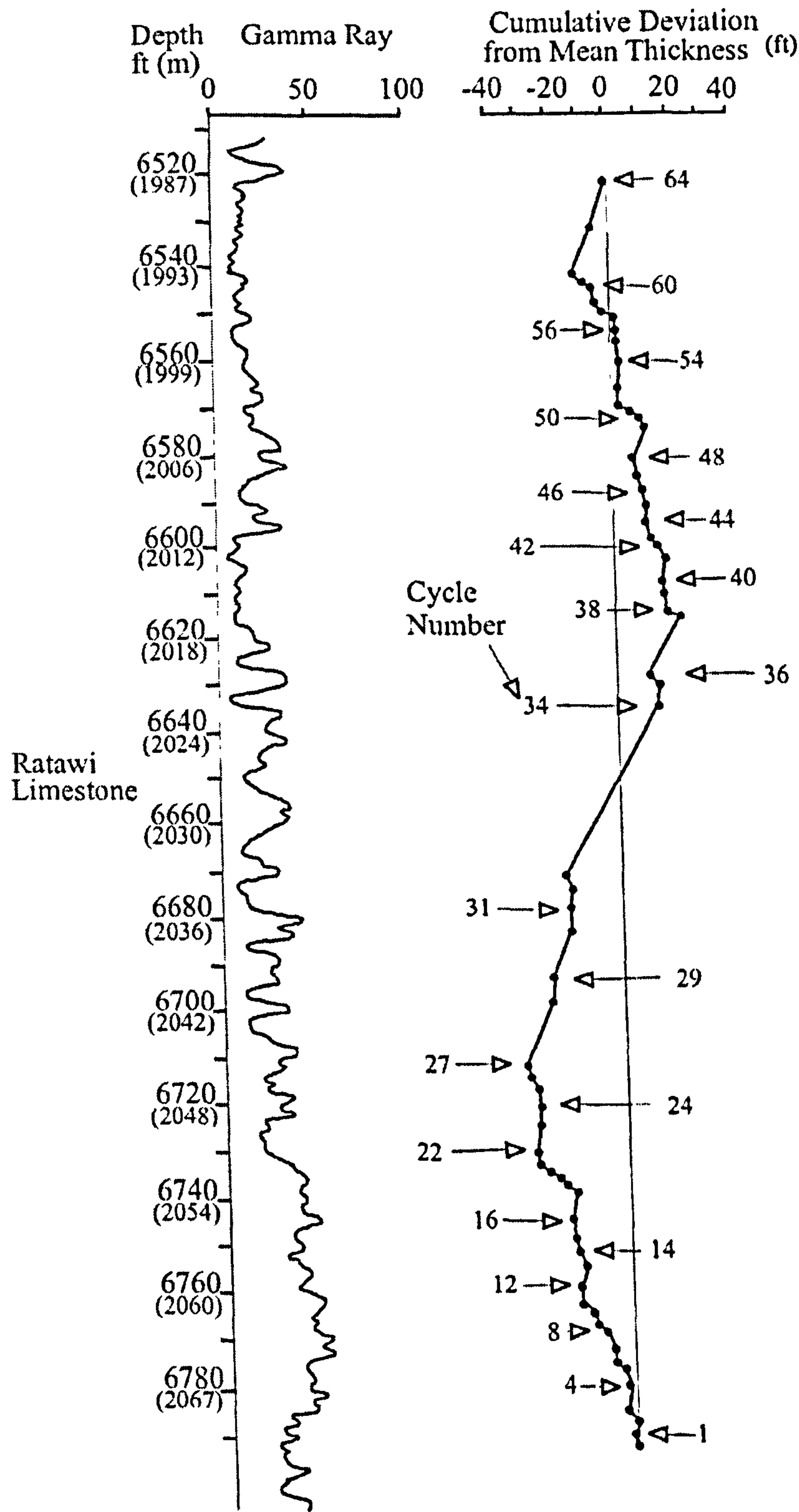


Figure A.3.3 Fischer plots in depth domain for strata in well R-48 compared with 'total' gamma ray signatures in Ratawi Limestone.



Table A.3.2 Data calculated by Excel for the Fischer plot in time domain for strata in well R-48 (data in feet).

Cycle Number	Cycle Thickness		Cycle Number	Cycle Thickness	
0			22		-22.67963
0			23	7	-26.91363
1	3	4.234375	23		-19.91363
1		7.234375	24	4	-24.14763
2	3.5	3.000375	24		-20.14763
2		6.500375	25	3	-24.38163
3	3	2.266375	25		-21.38163
3		5.266375	26	3.5	-25.61563
4	4	1.032375	26		-22.11563
4		5.032375	27	2	-26.34963
5	3	0.798375	27		-24.34963
5		3.798375	28	13.5	-28.58363
6	1.5	-0.435625	28		-15.08363
6		1.064375	29	5	-19.31763
7	3	-3.169625	29		-14.31763
7		-0.169625	30	11	-18.55163
8	3	-4.403625	30		-7.551625
8		-1.403625	31	3.5	-11.78563
9	2	-5.637625	31		-8.285625
9		-3.637625	32	4.5	-12.51963
10	2	-7.871625	32		-8.019625
10		-5.871625	33	2.5	-12.25363
11	1.5	-10.10563	33		-9.753625
11		-8.605625	34	37	-13.98763
12	5	-12.83963	34		23.01238
12		-7.839625	35	4.5	18.77838
13	5	-12.07363	35		23.27838
13		-7.073625	36	1	19.04438
14	2	-11.30763	36		20.04438
14		-9.307625	37	14	15.81038
15	2.5	-13.54163	37		29.81038
15		-11.04163	38	1	25.57638
16	4	-15.27563	38		26.57638
16		-11.27563	39	3	22.34238
17	6.5	-15.50963	39		25.34238
17		-9.009625	40	3.5	21.10838
18	1	-13.24363	40		24.60838
18		-12.24363	41	4.5	20.37438
19	1	-16.47763	41		24.87438
19		-15.47763	42	3	20.64038
20	2	-19.71163	42		23.64038
20		-17.71163	43	2	19.40638
21	1	-21.94563	43		21.40638
21		-20.94563	44	3	17.17238
22	2.5	-25.17963	44		20.17238



Cycle Number	Cycle Thickness	
45	4	15.93838
45		19.93838
46	3	15.70438
46		18.70438
47	3.5	14.47038
47		17.97038
48	3.5	13.73638
48		17.23638
49	7	13.00238
49		20.00238
50	2	15.76838
50		17.76838
51	1.5	13.53438
51		15.03438
52	1	10.80038
52		11.80038
53	3.5	7.566375
53		11.06638
54	5	6.832375
54		11.83238
55	4	7.598375
55		11.59838
56	3.5	7.364375
56		10.86438
57	3	6.630375
57		9.630375
58	1	5.396375
58		6.396375
59	2	2.162375
59		4.162375
60	2.5	-0.071625
60		2.428375
61	1.5	-1.805625
61		-0.305625
62	2	-4.539625
62		-2.539625
63	10	-6.773625
63		3.226375
64	9.5	-1.007625
64		8.492375

Total thickness357.6 ft

Number64

Average thickness4.2 ft



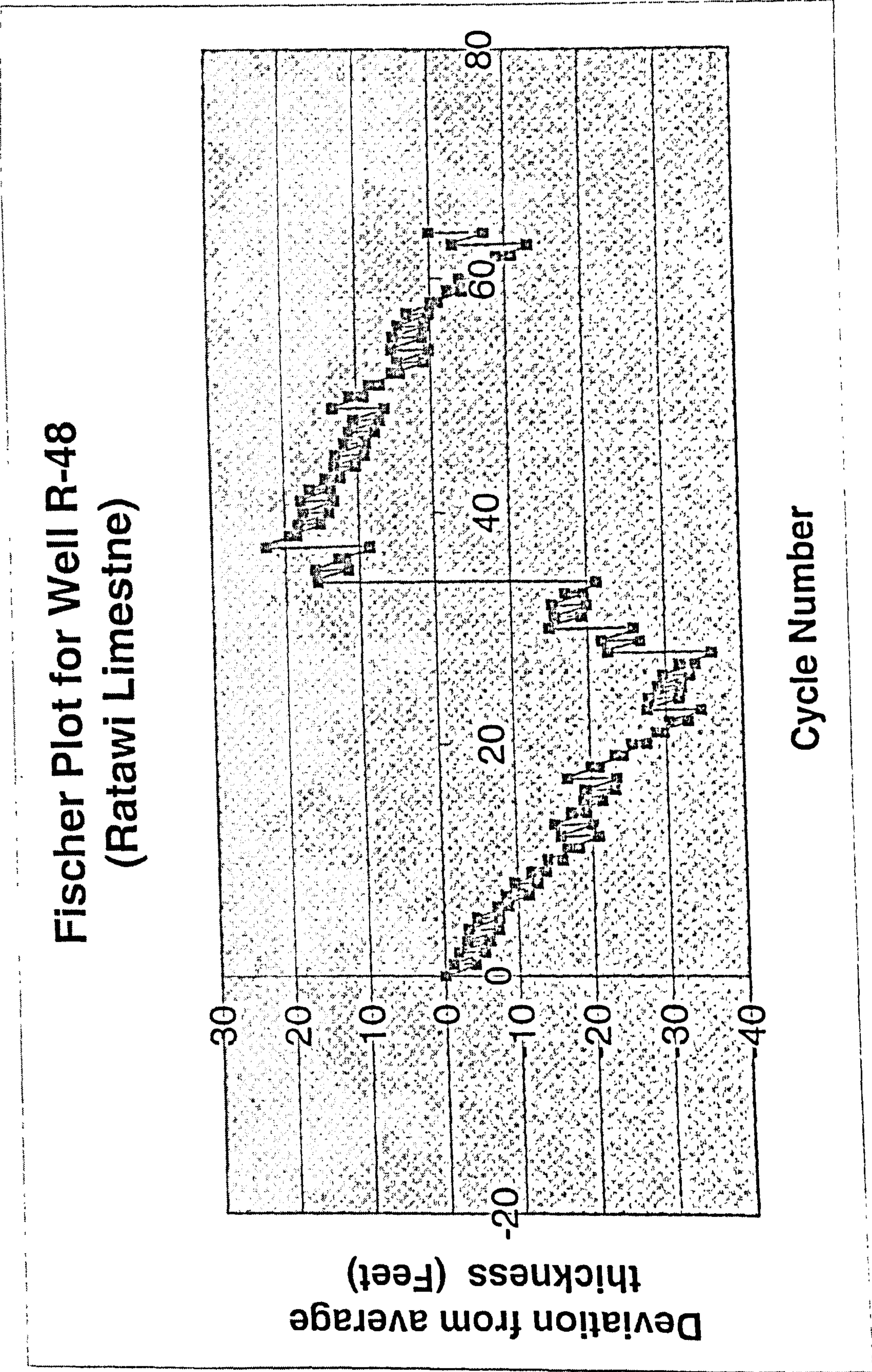


Figure A.3.4 Fischer plots in time domain for strata in well R-48.



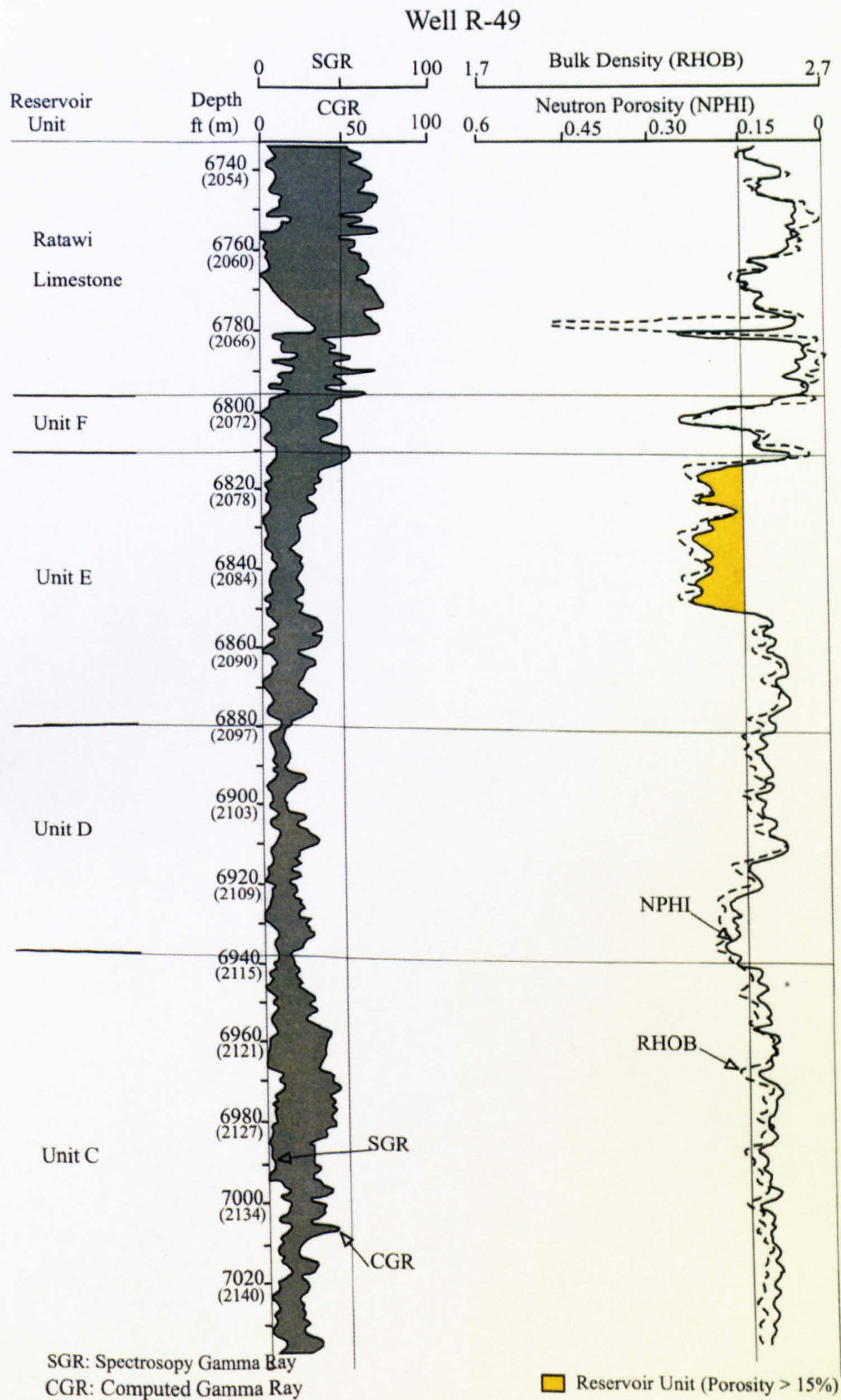


Figure A.3.5 Log signatures for strata in well R-49 and location of reservoir and non-reservoir units.